The role of LKB1 (STK11) in non-small cell lung cancer

Fiona Frances Cahill

St Edmund Hall, University of Oxford

Thesis submitted for the degree of Doctor of Philosophy

Trinity Term 2017

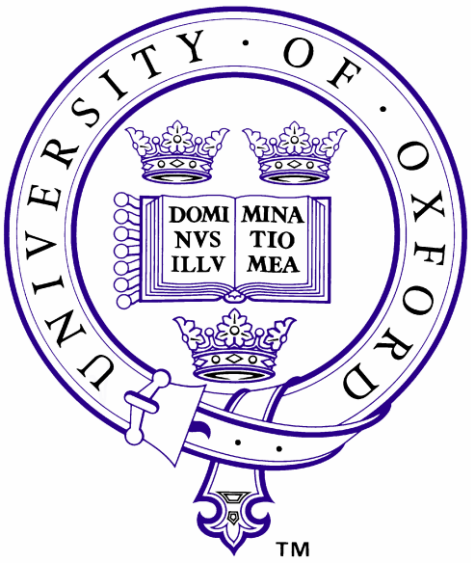

OXFORD INSTITUTE FOR RADIATION ONCOLOGY

The role of LKB1 (STK11) in non-small cell lung cancer

Fiona Frances Cahill
St Edmund Hall, University of Oxford

Thesis submitted for degree of Doctor of Philosophy
Trinity Term 2017

Abstract

LKB1 is the second most commonly altered tumour suppressor gene in lung adenocarcinoma, the most prevalent form of lung cancer. LKB1 is a "master kinase" that has been shown to phosphorylate up to 13 downstream targets. We hypothesised that LKB1 loss is associated with an increased dependency on alternative, targetable pathways. The overall aims of this project were to better understand the role of LKB1 loss in lung cancer and to identify novel approaches to selectively target LKB1 mutated cells.

We generated isogenic cells with or without LKB1 and used these to study the effect of LKB1 on cell proliferation. Importantly, we used a range of models including 2D culture, 3D spheroids and, sub-cutaneous and orthotopic xenograft models. To understand the role of LKB1 loss in lung cancer, the effect of LKB1 on mRNA expression was analysed using whole genome RNA Sequencing. To identify novel approaches to selectively target LKB1 mutated cells, we used biological screening methods and also investigated the effect of several metabolic inhibitors.

We found that loss of LKB1 expression had no effect on cell proliferation in 2D culture, but was associated with increased growth in 3D spheroids, sub-cutaneous and orthotopic xenografts, as well as greater metastasis in a lung orthotopic model. Gene ontology analysis of the transcriptome identified that genes associated with cAMP signalling and cytoskeletal organisation were differentially expressed between LKB1 deficient and proficient cells. We confirmed that cAMP signalling was increased in LKB1 deficient cells, though there was no difference in sensitivity between LKB1 deficient and proficient cells to cAMP signalling modulators. The bioactive small molecule screen showed that LKB1 deficient cells underwent apoptosis more slowly and therefore, were less sensitive to many compounds, compared with LKB1 proficient cells. Screening in 3D spheroids was a novel approach that we used to identify microtubule inhibitors as potentially selective compounds acting in LKB1 deficient cells. Our RNASeq data suggests that there was a metabolic shift from oxidative phosphorylation to aerobic glycolysis in LKB1 deficient cells, although this did not affect sensitivity to complex I inhibitors. Importantly, LKB1 deficient cells were more sensitive to glucose and glutamine deprivation which suggests that targeting these metabolic pathways may hold the greatest promise to selectively inhibit proliferation in LKB1 mutated cells.

Acknowledgments

I would firstly like to thank my supervisor, Dr Anderson Ryan for his guidance, advice, support, encouragement and dedication over the past few years. I would also like to thank him for passing on his overwhelming knowledge on both scientific and non-scientific matters, and I feel very grateful to have had him as my supervisor.

I would also like to offer a special thanks to Dr Agata Patel and Dr John Moore for reading parts of this thesis. I would like to thank all current and previous members of the "Ryan" laboratory including; Agata Patel, Agnes Jung, Amalina Mumin, Anika Weber, Aoife Vaughan, Jennifer Martin, John Moore, Karen Sayal, Luiza Lourenço, Marcus Green, Neele Drobnitzky, Samantha Olyha, Sivan Bokobza, Sophie Ellermann, Sürreyya Çorbacioğlu, Yanyan Jiang and Yasmin Shanneik, for teaching me laboratory skills, for their willingness to offer help and advice when needed and most importantly; for their friendship. I very much enjoyed the time we've spent together including daily lunches, attending conferences, going on lab away days and most of all, marking various milestones in people's lives with cakes, BBQs and dinners.

I would also like to thank the BMS staff for taking care of the animals used in this study on a daily basis and to members the Imaging Core (Sean Smart, Paul Kinchesh, Veerle Kersemans, Ana Da Silva Gomes and Danny Allen) within the University of Oxford, for making the MR imaging possible. I would like to thank Paul Kinchesh for providing all the information I needed to describe the MRI protocol. I am very grateful to Graham Brown for offering unlimited advice on using the microscope and to Thomas Ashton for teaching me how to use the Seahorse XF96 analyser. Furthermore, I would like to thank our course administrator; Katy Higgins for all her help in navigating me through the Oxford system.

I am very grateful to Cancer Research U.K. who have funded my DPhil as it would not have been possible without their help.

Very importantly, I would like to offer an enormous amount of gratitude to my amazing fiancé and best friend, Jason Peevers, whose unconditional love, support and encouragement played a major role in helping me to achieve my best over the past few years. Jason has always made me laugh, smile, kept me calm and encouraged me no matter what and I am so happy that him and I are going to spend the rest of our lives together.

Finally, I would like to sincerely thank my wonderful parents, Tom and Noeleen Cahill and my fabulous sister, Sarah Cahill (recently Sarah Philpott), whose love, support and encouragement has played an immense role in getting me to where I am today.

Some of the work undertaken to generate the data discussed in this thesis was completed by others and is indicated as follows:

- Mycoplasma testing (Section 2.6) – Anderson Ryan
- DNA Sequencing (Section 2.5) – Source BioScience
- RNA Sequencing (Section 2.10.2) – Oxford Gene Technology
- Magnetic resonance imaging (Section 2.9.4) – Imaging Core, University of Oxford (Sean Smart, Paul Kinchesh, Veerle Kersemans, Ana Da Silva Gomes)
- Sample processing and paraffin embedding of cell pellets, spheroids and mouse tissue (Section 2.13) – Neele Drobnitzky, Marcus Green and Richard Stillion
- Generation of A549+LVP cells (Section 2.6) – Yanyan Jiang

Table of contents

1 INTRODUCTION 1
1.1 Discovery of LKB1 and evidence for its tumour suppressive function 1
1.2 LKB1 2
1.2.1 LKB1: DNA and RNA 2
1.2.2 LKB1 protein 2
1.2.3 Subcellular localisation, binding partners and activation 4
1.3 LKB1 downstream signalling 5
1.3.1 Cell cytoskeleton, polarity and adhesion 5
1.3.2 Cell metabolism and growth 6
1.3.3 Cell cycle 7
1.3.4 Cell death and survival 7
1.3.5 Gene expression 8
1.4 LKB1 and cancer 8
1.5 LKB1 loss in lung cancer 9
1.6 Understanding the role of LKB1 loss in lung cancer and targeting LKB1 mutated cells 12
1.6.1 *Lkb1*$^{-/-}$ and *Lkb1*$^{+/-}$ mice 12
1.6.2 Impact of therapies in *Lkb1*$^{+/-}$ mice 13
1.6.3 Genetically engineered mouse models (GEMMs) of lung cancer 13
1.6.4 Impact of therapies in GEMMs of lung cancer 14
1.6.5 Mouse cell lines 16
1.6.6 Human cell lines 16
1.6.7 Impact of therapies in human cell lines 17
1.6.8 *In vivo* models using human lung cancer cells 18
1.6.9 Human lung adenocarcinoma tumours 18
1.7 Hypotheses, aims and objectives 19
2 MATERIALS AND METHODS 21
2.1 Reagents, buffers and compounds used throughout the study 21
2.1.1 Reagents and buffers 21
2.1.2 Compounds 24
2.2 Cell lines 25
2.3 Cell culture, routine passaging and cell seeding 27
2.4 Cryopreservation and thawing 29
2.5 DNA sequencing of LKB1 29
2.5.1 DNA isolation 29
2.5.2 Polymerise chain reaction (PCR) and DNA sequencing 29
2.6 Lentiviral transduction 31
2.6.2 Isolation of clones 34

2.7 Spheroid production, imaging and determination of area 34
2.8 Cell proliferation and viability assays 35
2.8.1 PicoGreen assay in 2D culture and 3D spheroids 35
2.8.2 Resazurin assay in 2D culture and 3D spheroids 36
2.8.3 Data analysis for dose response curve generation, IC_{50} determination and the effect of mutation status/LKB1 expression on the IC_{50} value/cell viability 36
2.9 *In vivo* work 38
2.9.1 Sub-cutaneous xenografts 38
2.9.2 Lung orthotopic model 39
2.9.3 *In vivo* imaging system (IVIS) 40
2.9.4 Magnetic resonance imaging (MRI) 40
2.10 RNA isolation, mRNA sequencing and analysis 42
2.10.1 RNA isolation and purification 42
2.10.2 RNA Sequencing 43
2.10.3 mRNA expression analysis 44
2.11 Bioactive small molecule screen in 2D and 3D models 46
2.11.1 Bioactive small molecule screen in 2D culture 46
2.11.2 Bioactive small molecule screen in 3D spheroids 49
2.12 Protein extraction, SDS-PAGE and western blotting 50
2.12.1 Whole cell protein extract - 2D culture 50
2.12.2 Whole cell protein extract - 3D spheroids 50
2.12.3 Whole cell protein extract - mouse lungs 51
2.12.4 Cytoplasmic and nuclear protein extract - 2D culture 51
2.12.5 SDS-polyacrylamide gel electrophoresis (PAGE) and immunoblotting (western blotting) 52
2.13 Formalin fixation and paraffin embedding (FFPE) 54
2.13.1 FFPE - cell pellets 54
2.13.2 FFPE - 3D spheroids 54
2.13.3 FFPE - mouse tissue (sub-cutaneous xenografts and lungs) 55
2.14 Haematoxylin and Eosin (H and E) staining 56
2.14.1 Haematoxylin staining 56
2.14.2 Eosin staining 56
2.14.3 Mounting 56
2.15 Immunocytochemistry/immunohistochemistry (IHC) 56
2.15.2 Analysis of nuclear and membrane staining 58
2.16 Immunofluorescence 59
2.17 Migration assay 60
2.18 CREB reporter assay 60
2.19 Oxygen consumption rate (OCR) 61
3 CHARACTERISATION OF LKB1 LOSS IN LUNG CANCER CELLS 63
3.1 Introduction 63

3.2 LKB1 expression in lung cancer cell lines 64
3.3 Generation of isogenic cell lines (with or without LKB1) 67
3.4 Characterisation of isogenic cells in 2D culture 67
3.4.1 LKB1 expression, activity and localisation in isogenic cells in 2D culture 67
3.4.2 The effect of LKB1 expression on cell proliferation in 2D culture 70
3.4.3 The effect of LKB1 expression on microtubule and actin cytoskeleton in 2D culture 71
3.4.4 The effect of LKB1 expression on cell migration in 2D culture 71
3.4.5 Summary of 2D data 73
3.5 Characterisation of isogenic cells in 3D spheroids 73
3.5.1 The effect of LKB1 expression on cell proliferation in 3D spheroids 73
3.5.2 The effect of LKB1 expression on spheroid structure 78
3.5.3 The effect of LKB1 expression on microtubule structure and cell contacts in 3D spheroids 80
3.5.4 Summary of spheroid data 84
3.6 Characterisation of isogenic cells *in vivo* 84
3.6.1 Sub-cutaneous xenograft model 84
3.6.2 Lung orthotopic model experiment 1 87
3.6.3 Lung orthotopic model experiment 2 91
3.6.4 Lung orthotopic model experiment 3 98
3.6.5 Summary of *in vivo* data 100
3.7 Discussion 101
4 UNDERSTANDING THE ROLE OF LKB1 LOSS IN LUNG CANCER 105
4.1 Introduction 105
4.2 mRNA sequencing and analysis 105
4.3 Differences in mRNA expression between 2D, 3D and xenograft models 106
4.3.1 Differences in biological processes between models 106
4.3.2 Confirmation of differences in mRNA expression between models 108
4.3.3 Summary of differences in mRNA expression between 2D, 3D and xenograft models 110
4.4 Differences in mRNA expression between LKB1 deficient and proficient cells 111
4.4.1 Identification of pathways different between LKB1 deficient and proficient cells 111
4.4.2 Summary of the differences in mRNA expression between LKB1 deficient and proficient cells 115
4.5 Differential expression of genes involved in cAMP response element (CRE) signalling between LKB1 deficient and proficient cells 115
4.5.1 Confirmation of differences in CRE signalling between LKB1 deficient and proficient cells 115
4.5.2 Summary for CRE signalling in LKB1 deficient and proficient cells 122
4.5.3 Investigation of LKB1 dependent differences on sensitivity to CRE signalling modulators 122
4.6 Discussion 128
5 TARGET IDENTIFICATION FOR LKB1 MUTATED LUNG CANCER CELLS 132
5.1 Introduction 132

5.2 Bioactive small molecule screen in 2D culture 132
5.2.1 Primary screen (2D culture) 134
5.2.2 Secondary screen (2D culture) 139
5.2.3 Tertiary screen (2D culture) 141
5.2.4 Quaternary screen - hit validation (2D culture) 142
5.2.5 Summary of 2D screen 145
5.3 Bioactive small molecule screen in 3D spheroids 146
5.3.2 Summary of 3D screen 153
5.4 The effect of LKB1 expression on sensitivity to microtubule inhibitors 153
5.4.2 Summary of the difference in sensitivity to microtubule inhibitors 159
5.5 Discussion 159
6 EXPLOITATION OF AN ALTERED METABOLIC PHENOTYPE IN LKB1 MUTATED LUNG CANCER CELLS 164
6.1 Introduction 164
6.2 The effect of LKB1 expression on sensitivity to complex I inhibitors 165
6.2.2 Summary of the effect of LKB1 expression on sensitivity to complex I inhibitors 173
6.3 LKB1 loss is associated with a metabolic shift 174
6.3.1 Transcriptomic data for metabolic genes 174
6.3.2 Confirmation of the mRNA differences using western blotting and IHC 177
6.3.3 Summary of the differences in metabolic signalling between LKB1 deficient and proficient cells. 181
6.4 Exploitation of the altered metabolic phenotype in LKB1 deficient cells 181
6.4.1 Metabolic inhibitors 181
6.4.2 Glucose and glutamine deprivation 186
6.4.3 Summary of targeting metabolism in LKB1 deficient cells 192
6.5 Discussion 192
7 GENERAL DISCUSSION AND CONCLUSION 198
7.1 Understanding the role of LKB1 loss in lung cancer 198
7.2 Targeting LKB1 mutated cells 200
7.2.1 Glucose deprivation 202
7.2.2 Glutamine deprivation 203
7.3 Future work 204
7.4 Conclusion 206
BIBLIOGRAPHY 207
APPENDICES 218

List of Figures

Figure 1.1: Human LKB1 protein structure 4
Figure 1.2: Translocation and activation of LKB1, and LKB1 downstream signalling 5
Figure 1.3: LKB1 is the second most commonly altered tumour suppressor gene in lung adenocarcinoma, the most prevalent form of lung cancer 11
Figure 2.1: Lentiviral particles used for restoring functional LKB1 expression and knocking-down LKB1 expression 33
Figure 2.2: Measuring spheroid area using the GELCOUNT and CeligoS 35
Figure 2.3: Schematic showing RNA isolation, mRNA sequencing and analysis 45
Figure 2.4: Hoechst DNA binding live cell assay 46
Figure 2.5: Schematic for the experimental set-up in the bioactive small molecule screen in 2D culture (primary, secondary and tertiary screen) 47
Figure 2.6: Aperio positive pixel count v9 algorithm 58
Figure 2.7: Aperio membrane v9 algorithm 59
Figure 3.1: Mutation status of selected genes and LKB1 expression in NBE1 and 11 lung cancer cell lines used in this study 66
Figure 3.2: LKB1 expression, activity and localisation in isogenic LKB1 deficient and proficient cell lines 69
Figure 3.3: The effect of LKB1 expression on cell proliferation in 2D culture 70
Figure 3.4: Microtubule and actin structure in LKB1 deficient and proficient cells in 2D culture . 71
Figure 3.5: The effect of LKB1 expression on cell migration in 2D culture 72
Figure 3.6: The effect of LKB1 expression on 3D spheroid growth (10 days post seeding) 74
Figure 3.7: The effect of LKB1 expression on long-term spheroid growth (21 days) with or without replenished medium 76
Figure 3.8: Spheroids seeded with equal numbers of LKB1 deficient and proficient cells 77
Figure 3.9: LKB1 deficient and proficient spheroid sections stained with Haematoxylin and Eosin 79
Figure 3.10: LKB1 deficient and proficient spheroid sections stained for cleaved caspase 3 79
Figure 3.11: Schematic showing selected proteins involved in cell cytoskeleton and cell junctions 80
Figure 3.12: Microtubule staining in LKB1 deficient and proficient spheroids 82
Figure 3.13: Integrin-β1 and β-catenin staining in LKB1 deficient and proficient spheroids 83
Figure 3.14: The effect of LKB1 expression on tumour volume of sub-cutaneous xenografts grown in CD1 nude mice 85

Figure 3.15: Haematoxylin and eosin stained sections of LKB1 deficient and proficient sub-cutaneous xenograft tumours from CD1 nude mice 86
Figure 3.16: LKB1 mRNA expression in sub-cutaneous xenografts grown in CD1 nude mice 87
Figure 3.17: Monitoring tumour burden in the lung orthotopic model using IVIS imaging 89
Figure 3.18: The effect of LKB1 on tumour burden in a lung orthotopic model in BALB/c nude mice 90
Figure 3.19: Monitoring the effect of LKB1 expression on tumour burden of a lung orthotopic model in BALB/c nude mice using MRI 93
Figure 3.20: The effect of LKB1 expression on tumour burden in a lung orthotopic model in BALB/c nude mice using MRI and lung weight as endpoints 94
Figure 3.21: Schematic showing the use of western blotting to specifically detect human lung cancer cells in mouse lung 95
Figure 3.22: Western blotting to detect mitochondria, LKB1 and immunoglobulin protein expression in the lung orthotopic model using BALB/c nude mice 96
Figure 3.23: Correlation between MRI, lung weight and western blotting (mitochondrial signal) as methods to measure tumour burden in the lung orthotopic model 97
Figure 3.24: The effect of LKB1 expression on tumour burden in the lung orthotopic model using NOD/SCID gamma mice 99
Figure 4.1: Common differences in gene expression between 2D, 3D and sub-cutaneous xenograft models, in LKB1 deficient and proficient cells 108
Figure 4.2: Genes that have high and low expression in 3D and xenografts compared to 2D culture 109
Figure 4.3: Differences in catabolic, hypoxic and cell cycle protein expression between 2D and 3D models 110
Figure 4.4: Significant differentially expressed genes between LKB1 deficient and proficient samples from 2D culture, 3D spheroids and human lung adenocarcinoma tumours 114
Figure 4.5: Schematic of cyclic AMP response element (CRE) signalling 116
Figure 4.6: Heatmap showing CRE signalling genes that have high or low expression in the LKB1 deficient cells in 2D, 3D and human tumours 117
Figure 4.7: mRNA expression of the known LKB1 targets in LKB1 deficient and proficient cells in 2D and 3D models 118
Figure 4.8: Examining differences in CRE signalling between LKB1 deficient and proficient cells 121
Figure 4.9: Schematic showing modulators of CRE signalling 124
Figure 4.10: Dose response curves for LKB1 deficient and proficient cells treated with modulators of CRE signalling 125

Figure 4.11: Western blotting showing the effect of dexamethasone, HG-9-91-01 and celecoxib on LKB1 and COX2 expression 126
Figure 4.12: LKB1 deficient and proficient spheroids treated with modulators of CRE signalling 127
Figure 5.1: Schematic showing the four stages of the 2D screen 133
Figure 5.2: Correlation between duplicate samples and independent runs within the screen 135
Figure 5.3: Primary screen: identification of positive and negative hits for LKB1 deficient and proficient cells 137
Figure 5.4: Quaternary screen: confirmation of the hits using an apoptosis assay 145
Figure 5.5: 3D bioactive small molecule screen: identification of the positive hits in LKB1 deficient A549 spheroids 148
Figure 5.6: 3D bioactive small molecule screen: identification of the positive hits in LKB1 deficient H1299 spheroids 149
Figure 5.7: LKB1 deficient and proficient spheroids treated with MEK inhibitors 152
Figure 5.8: Potential positive hits for LKB1 deficient A549 spheroids 152
Figure 5.9: Schematic showing that LKB1 phosphorylates MARK, a protein involved in microtubule dynamics 154
Figure 5.10: Microtubule staining in LKB1 deficient and proficient cells after treatment with paclitaxel 156
Figure 5.11: The effect of microtubule inhibitors on cell proliferation in LKB1 deficient and proficient cells in 2D culture 157
Figure 5.12: LKB1 deficient and proficient spheroids treated with paclitaxel 158
Figure 5.13: Phospho-MARK levels after paclitaxel treatment in LKB1 deficient and proficient cells 158
Figure 6.1: Schematic showing the use of the Seahorse XF96 analyser to measure changes in oxygen consumption (oxidative phosphorylation) 165
Figure 6.2: The effect of phenformin and metformin on the oxygen consumption rate in LKB1 deficient and proficient cells in 2D culture 167
Figure 6.3: The effect of LKB1 expression on the dose dependent sensitivity to phenformin and metformin in LKB1 deficient and proficient cells in 2D culture 168
Figure 6.4: The effect of phenformin and metformin on spheroid growth in LKB1 deficient and proficient cells 169
Figure 6.5: The effect of phenformin and metformin on oxygen consumption in 11 LKB1 mutated and wild-type lung cancer cell lines and NBE1 171
Figure 6.6: The effect of LKB1, KRAS, BRAF and TP53 mutation status on determining sensitivity to phenformin and metformin 173

Figure 6.7: Schematic showing that LKB1 loss is associated with a metabolic shift to aerobic glycolysis 176
Figure 6.8: Heatmap showing the difference in mRNA expression levels between LKB1 deficient and proficient cells for the genes involved in glycolysis, carbonic anhydrase signalling, TCA cycle, glutaminolysis and the urea cycle 177
Figure 6.9: Confirmation of PDK4, CA9 and CPS1 mRNA expression differences by western blotting in LKB1 deficient and proficient cells in 2D and 3D culture 179
Figure 6.10: IHC analysis of GLUT1, CA9 and MCT1 protein expression in LKB1 deficient and proficient spheroids 180
Figure 6.11: Schematic showing possible approaches to target metabolism 182
Figure 6.12: The effect of dichloroacetate, AZD3965 and bromopyruvate on cell proliferation in LKB1 deficient and proficient cells in 2D culture..... 183
Figure 6.13: The effect of 2-DG on cell proliferation in LKB1 deficient and proficient cells in 2D culture 184
Figure 6.14: The effect of LKB1, KRAS, BRAF and TP53 mutation status on determining sensitivity to 2-DG 185
Figure 6.15: The effect of glucose deprivation on cell proliferation in LKB1 deficient cells grown in 2D culture 187
Figure 6.16: The effect of glutamine deprivation on cell proliferation in LKB1 deficient cells grown in 2D culture 188
Figure 6.17: The effect of glucose and glutamine deprivation on downstream signalling in LKB1 deficient and proficient cells in 2D culture..... 190
Figure 6.18: The effect of glucose and glutamine deprivation in LKB1 deficient and proficient spheroids 191

List of supplementary Figures (Appendices)

Figure A3.25: E-cadherin, occludin and Zo1 staining in spheroids……..……..……..….236
Figure A5.14: Heatmap showing cytoskeletal, cell junctions and ECM genes expressed and higher or lower levels in the LKB1 deficient cells in 2D, 3D and human tumour samples……..255
Figure A5.15: Microtubule staining in LKB1 deficient and proficient cells after treatment with docetaxel, vincristine and vinorelbine…….....…….256
Figure A5.16: LKB1 deficient and proficient spheroids treated with docetaxel, vincristine and vinorelbine……...……....…...258

Figure A5.17: Correlation between induction of apoptosis and inhibition of proliferation in the primary screen in 2D culture…….258
Figure A6.19: Mitochondrial stress test in LKB1 deficient and proficient A549 and A427 cells using the Seahorse XF96 analyser……..…259

List of Tables

Table 2.1: Reagents and buffers 21
Table 2.2: Compounds 24
Table 2.3: Cell lines 26
Table 2.4: Cell culture reagents 28
Table 2.5: Cell seeding density (no. cells per well of 96-well plate) 28
Table 2.6: Primers for amplification of LKB1 30
Table 2.7: Pre-made lentiviral particles 32
Table 2.8: Antibodies for western blotting 53
Table 2.9: Antibodies for immunohistochemistry 58
Table 2.10: Antibodies for immunofluorescence 60
Table 3.1: Summary of the *in vivo* data 100
Table 5.1: Positive and negative hits from the primary screen 138
Table 5.2: Secondary screen: confirmation of the positive and negative hits identified in the primary screen in the three isogenic pairs 140
Table 5.3: Tertiary screen: confirmation of positive apoptosis and/or proliferation hits identified in two or more isogenic cells in the secondary screen 141
Table 5.4: Quaternary screen: validation of the hits using a proliferation assay 143
Table 5.5: Positive hits identified from the bioactive small molecule screen in 3D spheroids 150

List of supplementary Tables (Appendices)

Table A2.11: Human gene list……..……..……218
Table A4.1: Top 50 GO processes associated with genes that were highly expressed in the complex model……..…….....237
Table A4.2: GO processes associated with genes that were expressed at lower levels in the complex model……...……...…238
Table A4.3: Top 50 GO processes associated with genes that were highly expressed in the 3D and xenografts compared to 2D……..……..…….238
Table A4.4: Top 50 processes associated with genes that were expressed at lower levels in the 3D and xenografts compared to 2D……..……..…….240
Table A4.5: Top 100 GO processes significantly different between LKB1 deficient and proficient cells that were common to 2D and 3D models……..……..….241

Table A4.6: Top 20 pathways associated with genes that were highly expressed in LKB1 deficient spheroids……..……..244
Table A4.7: Top 20 pathways associated with genes that were expressed at lower levels in LKB1 deficient spheroids……...……..…….245
Table A4.8: Pathways associated with highly expressed genes in LKB1 deficient cells common to 2D, 3D and human tumour models …….……..……246
Table A4.9: Pathways associated with genes expressed at lower levels in LKB1 deficient cells common to 2D, 3D and human tumour models …….…….……..……246
Table A5.6a: 326-compound bioactive small molecule library (Selleck L1100)……. ….247
Table A5.6b: Additional compounds tested in the primary screen……..…252
Table A5.7: Additional compounds tested in the secondary screen……..…….……252
Table A5.8: Compounds used in the 3D screen..……. ……..….253
Table A6.1: Observations of the phenotypic differences between LKB1 deficient and proficient isogenic cells ……...……...…260

Abbreviations

2-DG	2-deoxyglucose
4E-BP1	Eukaryotic translation initiation factor 4E-binding protein 1
˚C	Degrees celsius
AAK1	Adaptor associated kinase 1
ABL	Abelson murine leukaemia
ACC	Acetyl coA carboxylase
ADP	Adenosine diphosphate
AICAR	5-aminoimidazole-4-carboxamide ribonucleotide
ALK	Anaplastic lymphoma kinase
AMP	Adenosine monophosphate
AMPK	AMP kinase
ANOVA	Analysis of variance
A-P	Anterior-posterior
APC	Adenomatous polyposis coli
ARK	AMPK related kinase
ATCC	American Type Culture Collection
ATM	Ataxia telangiectasia mutated
ATP	Adenosine triphosphate
bp	Base pair
BRAF	Murine sarcoma viral oncogene homolog B
BRCA	Breast cancer
BrdU	Bromodeoxyuridine
BRSK	Brain-selective kinase
BSA	Bovine serum albumin
C	Cysteine
CA	Carbonic anhydrase
CaMKKβ	Calcium/calmodulin-dependent protein kinase kinase β
cAMP	Cyclic AMP
CC3	Cleaved caspase 3
CCLE	Cancer Cell Line Encyclopaedia
CDC42	Cell division control protein 42
CDK	Cyclin-dependent kinase
Chek1	Checkpoint kinase 1
CHK	Checkpoint kinase
cm	Centimetre
Cmpk1	Cytidine/uridine monophosphate kinase 1
CMV	Cytomegalovirus
CO_2	Carbon dioxide
COSMIC	Catalogue Of Somatic Mutations In Cancer
COX	Cyclooxygenase
CPS1	Carbamoyl phosphate synthetase
CRE	cAMP response element
CREB	CRE binding protein
CRTC	CREB-regulated transcription coactivator 1

CTD	Carboxy terminal domain
D	Aspartate
dH_2O	Distilled water
DMEM	Dulbecco's Modified Eagle Medium
DMSO	Dimethyl sulfoxide
DNA	Deoxyribonucleic acid
DPI	Dots per inch
DPX (mountant)	Distyrene, plasticiser, xylene
dsDNA	Doubled stranded DNA
dTDP	Deoxythymidine diphosphate
dTMP	Deoxythymidine monophosphate
dTTP	Deoxythymidine triphosphate
Dtymk	Deoxythymidylate kinase
ECACC	European Collection of Authenticated Cell Cultures
ECAR	Extracellular acidification rate
ECL	Enhanced chemiluminescence
ECM	Extracellular matrix
EDTA	Ethylenediaminetetraacetic acid
EGFR	Epidermal growth factor receptor
EGTA	Ethylene glycol-tetraacetic acid
Em	Emission
EMT	Epithelial to mesenchymal transition
ER	Estrogen receptor
EV	Empty vector
Ex	Excitation
FAK	Focal adhesion kinase
FBS	Fetal bovine serum
fc	Fold change
FCCP	Carbonyl cyanide-4-phenylhydrazone
FDG	Fluoro-deoxyglucose
FDR	False discovery rate
FFPE	Formalin fixed paraffin embedded
FOXO	Forkhead box O
FPKM	Fragments per kilobase per million mapped reads
fs	frameshift
g	Gram(s)
G (centrifugation)	G force/RCF (relative centrifugal force)
G	Glycine
GATA-6	GATA binding protein 6
GEMM	Genetically engineered mouse models
GIT	Gastrointestinal tract
GLUT1	Glucose transporter
GO	Gene ontology
GOrilla	Gene Ontology enRIchment anaLyses and visuaLisAtion tool
GPNA	L-γ-glutamyl-p-nitroanilide
GSK3β	Glycogen synthase kinase 3 beta

h	Hours(s)
H and E	Haematoxylin and Eosin
HCl	Hydrochloric acid
HCO_3^-	Bicarbonate
HDAC	Histone deacteylase
HEK-293T cells	Human embryonic kidney 293T cells
HEPES	Hydroxyethyl-piperazine-ethanesulfonic acid
HIF	Hypoxia inducible factor
HPV	Human papilloma virus
HR	Homologous recombination
HRP	Horse radish peroxidase
HSP	Heat shock protein
HUVEC	Human umbilical vein endothelial cells
IC_{50}	Inhibitory concentration that reduces cell viability to 50% of the untreated control
IF	Immunofluorescence
Ig	Immunoglobulins
IHC	Immunohistochemistry
ImmTAC	Immune mobilising monoclonal T-cell receptor against cancer
INK4a/ARF	Alternate reading frame
i.p injection	Intraperitoneal injection
IVIS	*In vivo* imaging system
kb	Kilobase(s)
kDa	Kilodalton(s)
KEAP	Kelch-like ECH-associated protein 1
kg	Kilogram(s)
KPA	Key pathway advisor
KRAS	Kirsten rat sarcoma viral oncogene
L	Litre(s)
LEF	Lymphoid enhancer binding factor
Li_2CO_3	Lithium carbonate
LKB1	Liver kinase B 1
LOH	Loss of heterozygosity
LOX	Lysyl oxidase
M	Molar
mAb	Monoclonal antibody
MAP	Microtubule associated protein
MAPK	Mitogen-activated protein kinases
MARK	Microtubule-affinity-regulating-kinase
MCT	Monocarboxylase transporter
MEF	Mouse embryonic fibroblast
MEK	Mitogen-activated protein kinase kinase
µg	Microgram(s)
mg	Milligram(s)
$MgSO_4$	Magnesium sulfate
min	Minutes

µL	Microliter(s)
mL	Millilitre(s)
µM	Micromolar
mM	Millimolar
µm	Micrometre(s)
μm^2	Micrometre squared
mm	Millimetre(s)
mm^3	Millimetre cubed
Mmp2 (MMP2)	Matrix metallopeptidase 2
MO25	Mouse protein 25
MOI	Multiplicity of infection
MRI	Magnetic resonance imaging
mRNA	Messenger ribonucleic acid
µs	Microsecond(s)
mT/m	milliTesla/metre
MTOR	Mammalian target of rapamycin
MYPT1	Myosin phosphatase targeting-1
NaCl	Sodium chloride
$NaHCO_3$	Sodium bicarbonate
NaOH	Sodium hydroxide
NBE1	Normal bronchial epithelium
NEDD9	Neural precursor cell expressed, developmentally down-regulated
NFκB	Nuclear factor kappa B
NF-Y	Nuclear transcription factor y
ng	Nanogram(s)
NH_4	Ammonia
nM	Nanomolar
No.	Number
NOD	Non-obese diabetic
NRF2 (NFE2L2)	Nuclear factor (erythroid-derived 2)-like 2
NSCLC	Non-small cell lung cancer
NSG	NOD/SCID gamma
NTD	Amino terminal domain
NUAK	NUAK family SNF1-like kinase 1
NURR77 (NGFIB)	Nerve growth factor I B
OCR	Oxygen consumption rate
OGT	Oxford Gene Technology
ON	Overnight
pAb	Polyclonal antibody
pACC	Phosphorylated acetyl coA carboxylase
PAK	p21-activating kinases
pAMPK	Phosphorylated AMPK
p/s/cm2/sr	Photon per second per centimetre squared per steradian
PARP	Poly (ADP-ribose) polymerase
PBS	Phosphate buffered saline
PCR	Polymerise chain reaction

PD-1	Programmed death 1
PDE	Phosphodiesterase
PDGF	Platelet derived growth factor
PDH	Pyruvate dehydrogenase
Pdhb	Pyruvate dehydrogenase (lipoamide) β
PDK	Pyruvate dehydrogenase kinase
PD-L1	Programmed death ligand 1
PEA3	Polyoma enhancer activator 3
PET	Positron emission tomography
PFA	Paraformaldehyde
PGE_2	Prostaglandin E2
PI3K	Phosphatidylinositol-4,5-bisphosphate 3-kinase
PIM	Pim-1 Proto-Oncogene, Serine/Threonine Kinase
PJS	Peutz Jeghers Syndrome
PKA	Protein kinase A
PKCζ	Protein kinase C zeta
pM	Picomolar
PPIB	Peptidylprolyl isomerase B
PP1β	Protein phosphatase-1β
PTGS2	Prostaglandin-endoperoxide synthase 2
PTM	Post translational modifications
RCF	Relative centrifugal force
RNA	Ribonucleic acid
RNASeq	RNA Sequencing
RSK	Ribosomal s6 kinase
RT	Room temperature
S6K1	Ribosomal protein S6 kinase beta-1
S	Serine
SCID	Severe combined immunodeficiency
SCLC	Small cell lung cancer
SD	Standard deviation
SDS	Sodium dodecyl sulfate
Sec	Second(s)
SEM	Standard error of the mean
SGC	Structural genomics consortium
shRNA	Short hairpin RNA
SIK	Salk inducible kinase
siRNA	Small interfering RNA
SP1	Specificity protein 1
SPSS	Statistical Package for the Social Sciences
SRC	Rous sarcoma, tyrosine kinase
STK11	Serine threonine kinase 11
STRAD	STE20 related kinase adaptor
T_{50}	Time taken to reduce the OCR by 50% of the baseline OCR
T	Threonine
T (MRI)	Tesla (MRI)

TBE	Tris Borate-EDTA
TBS	Tris buffered saline
TCA cycle	The citric acid cycle
TCF	T-cell-specific transcription factor
TCGA	The Cancer Genome Atlas
TIFF	Tagged image file format
TMPA	Ethyl 2-[2,3,4-trimethoxy-6-(1-octanoyl)phenyl]acetate
TORC1 complex	Target of rapamycin complex 1
TP53	Tumour protein 53
V	Volt(s)
VEGF	Vascular endothelial growth factor
VEGFR	Vascular endothelial growth factor receptor
v/v	Volume/volume
WB	Western blotting
wt	Wild-type
w/v	Weight/volume
Y	Tyrosine
XEEK1	Xenopus egg and embryo kinase
ZEB1	Zinc finger E-box-binding homeobox 1

1 Introduction

1.1 Discovery of LKB1 and evidence for its tumour suppressive function

In 1997, the chromosomal region 19p13.3 was linked to the inherited disease, Peutz-Jeghers syndrome (PJS) (Hemminki et al., 1997). In 1998, the serine threonine kinase 11 (STK11) gene, also known as liver kinase B (LKB1) of 19p13.3 was identified as the gene linked to PJS (Hemminki et al., 1998, Jenne et al., 1998). PJS was first described in 1921 by Johannes Peutz and further characterised in 1949 by Harold Jeghers, as an inherited disease associated with mucocutaneous pigmentation and polyps of the gastrointestinal tract (GIT) (Peutz, 1921, Jeghers et al., 1949). PJS is a rare autosomal dominant disorder (incidence: 1 in 8300-280,000) (Lindor et al., 2008). Mucocutaneous pigmentation is seen around the buccal mucosa, lips, anus, hands and feet. This is observed from childhood and usually becomes less apparent into adulthood (Hemminki, 1999). All PJS individuals develop gastrointestinal hamartomas during or after adolescence. Hamartomas are benign polyps and in PJS are most prevalent in the small intestine (64-90% of patients), but are also seen in the stomach and/or colon (50% of patients). Hamartomas have also been reported in the lungs, nasal mucosa and bladder (Korsse et al., 2013). PJS individuals have an increased risk of developing several forms of cancer including gastrointestinal, breast, gynaecological (ovary, uterus, cervix), lung and testis (by age 70 years, risk = 85% compared to 18% for general population) (Hearle et al., 2006).

A tumour suppressor is characterised by loss-of-function of a specific gene that would normally act as a brake against the initiation and/or progression of cancer. In 1971, Alfred Knudson proposed that expression of both alleles of a tumour suppressor gene are lost in cancer cells. This hypothesis is now known as Knudson “two hit” hypothesis (Chial, 2008) and appears to be the case for carcinomas that develop in PJS patients. In PJS patients, loss

of function germline mutations in one LKB1 allele, termed “haplo-insufficiency”, appears sufficient to lead to hamartoma formation, however, loss of function mutations in the both LKB1 alleles, termed “loss of heterozygosity” (LOH), is found in some polyps and all carcinomas (Entius et al., 2001).

1.2 LKB1

1.2.1 LKB1: DNA and RNA

Human *LKB1* is 23 kilobases long and consists of 10 exons (9 coding and 1 non-coding) (Hemminki et al., 1998). Mouse *Lkb1*, located on chromosome 10, is 15 kb long and also consists of 10 exons. In general, human *LKB1* appears to have longer introns than mouse *Lkb1* (Smith et al., 1999). Human LKB1 messenger ribonucleic acid (mRNA) expression is regulated by specificity protein 1 (SP1), nuclear transcription factor-y (NF-Y) and forkhead box O (FOXO3, FOXO4) transcription factors which bind to cis-acting elements within the LKB1 promoter to activate LKB1 expression (Lützner et al., 2012). Human LKB1 mRNA is alternatively spliced with reports showing a variant without exon 5, 6, 7 and part of exon 8 (Churchman et al., 1999), and a variant which includes intron 4 (Abed et al., 2001).

1.2.2 LKB1 protein

Smith et al observed that human LKB1 protein was conserved compared with Lkb1 protein (mouse) and Xenopus egg and embryo kinase (XEEK1) protein in *Xenopus laevis*, suggesting that these three proteins are orthologs. Human LKB1 shares 89.7% identity with 92.5% overall similarity to mouse Lkb1, and 78.6% identity with 84.5% overall similarity to XEEK1 (Smith et al., 1999). The kinase domain of human LKB1 protein shares 42% amino acid identity to the polarity protein; PAR-4 in *Caenorhabditis elegans* (Watts et al., 2000). PAR-4 is important for the formation of the anterior-posterior (A-P) axis during

embryogenesis in *C. elegans* and is homologous to LKB1 in *Drosophila melanogaster*, which is also important for A-P axis formation (Martin and St Johnston, 2003).

In adult humans, LKB1 is ubiquitously expressed with higher expression observed in the cerebral cortex, ovary, salivary glands, skeletal muscle, testis and tonsils (Sanchez-Cespedes, 2007).

Mouse Lkb1 has 436 amino acids and contains a nuclear localisation signal in its amino terminal domain (NTD) (Smith et al., 1999). Human LKB1 has 433 amino acids, is 48.6 kDa and contains (i) an NTD, (ii) a kinase domain and (iii) a carboxy terminal domain (CTD) with a farnesylation site (Alessi et al., 2006). There are four autophosphorylation sites; threonine 185 (T185), T189, T336, T402, and additionally four phosphorylation sites; serine 31 (S31), S325, T363 and S428, in human LKB1 (Sapkota et al., 2002a). In response to ionising radiation, ataxia telangiectasia mutated (ATM) can phosphorylate T363 (Sapkota et al., 2002b). Also, protein kinase A (PKA) (Collins et al., 2000), ribosomal s6 kinase (RSK) (Sapkota et al., 2001) and protein kinase c zeta (PKCζ) (Song et al., 2008) can phosphorylate S428. Phosphorylation by PKA and RSK has been shown to be important for growth suppression in human malignant melanoma G361 cells (Sapkota et al., 2001). The farnesylation site; cysteine 430 (C430) is important for LKB1 membrane localisation (Collins et al., 2000), however, it plays no role in LKB1 dependent growth suppression (Sapkota et al., 2001).

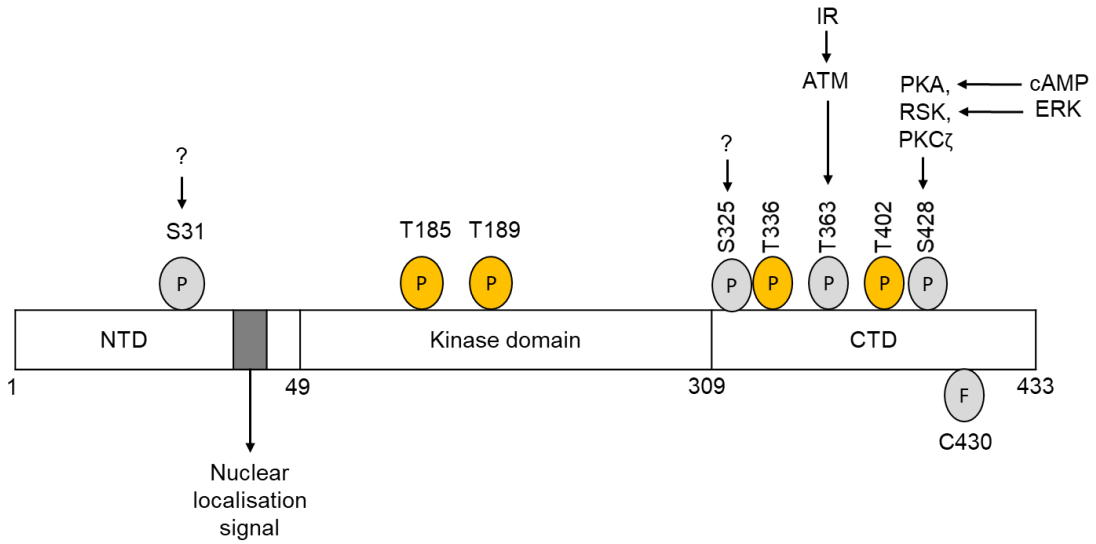

Figure 1.1: Human LKB1 protein structure
Schematic adapted from 2 publications (Alessi et al., 2006, Korsse et al., 2013). Yellow "P" indicates autophosphorylation site, grey "P" - phosphorylation site and "F" - farnesylation site. The phosphorylation sites; T363, T402 and S428 are T366, T404 and S431 in mouse, respectively. The farnesylation site is C433 in mouse.

1.2.3 Subcellular localisation, binding partners and activation

LKB1 is normally localised in the nucleus which is probably due to its nuclear localisation domain (Smith et al., 1999, Nezu et al., 1999). Furthermore, in human fetal hepatocyte LO2 cells, the orphan nuclear receptor; NUR77 (NR4A1) binds and sequesters LKB1 to the nucleus and ethyl 2-[2,3,4-trimethoxy-6-(1-octanoyl)phenyl]acetate (TMPA) inhibits this interaction (Zhan et al., 2012). LKB1 is translocated to the cytoplasm, on forming a heterotrimeric complex with STE20-related adaptor (STRAD) and scaffolding mouse protein 25 (MO25). The kinase domain and amino acids within the CTD of LKB1 are important for binding STRAD. MO25 stabilises the LKB1-STRAD interaction (Boudeau et al., 2003, Baas et al., 2003). As LKB1 lacks a nuclear export domain, STRAD promotes the nuclear export of LKB1 by competitively inhibiting importin-α and by promoting the binding of exportin-7 to LKB1 (Dorfman and Macara, 2008). In the cytoplasm, LKB1 acts as a "master kinase" and phosphorylates the "T"/activation loop of up to 13 downstream proteins which are part of an AMPK (5' adenosine monophosphate-activated protein kinase)

subfamily termed ARK (AMPK related kinases) (Figure 1.2) (Lizcano et al., 2004, Jaleel et al., 2005). One of these proteins is AMPK itself, which is a key enzyme controlling cellular energy homeostasis (Hawley et al., 2003, Woods et al., 2003, Shaw et al., 2004b, Hong et al., 2003). Figure 1.2 shows translocation and activation of LKB1 by the LKB1-STRAD-MO25 complex, schematically.

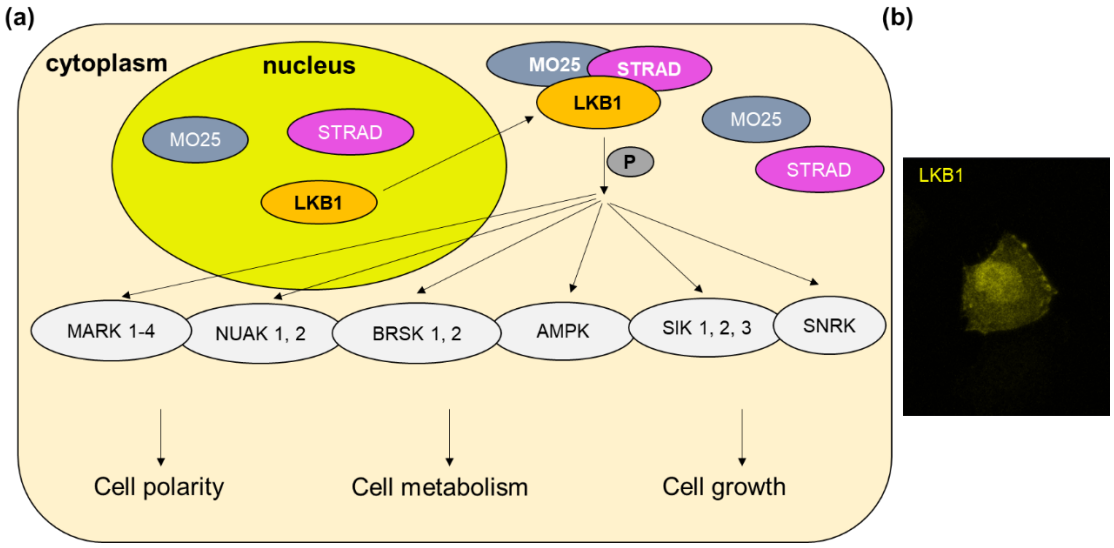

Figure 1.2: Translocation and activation of LKB1, and LKB1 downstream signalling
(a) BRSK 1, 2 are also known as SADKB and SADKA. SIK 2, 3 are also known as QIK and QSK. (b) Immunofluorescence detection of LKB1 protein expression in A549+LKB cells (see Section 2.6 and 2.16) showing nuclear and cytoplasmic distribution.

1.3 LKB1 downstream signalling

LKB1 has been reported to play a role in many processes including cell polarity, cell metabolism and cell growth through activation of ARKs. In addition, LKB1 has been shown to be involved in cell cycle, cell death, anoikis and gene expression.

1.3.1 Cell cytoskeleton, polarity and adhesion

LKB1 phosphorylates MARK, BRSK and NUAK which play roles in cell cytoskeleton, cell polarity and cell adhesion.

Using mouse embryonic fibroblasts (MEFs) with or without LKB1 expression, it was shown that activation of LKB1-MARK (microtubule-affinity-regulating-kinase) signalling stimulates the phosphorylation of the MAP (microtubule associated protein), Tau. Tau is a microtubule stabilising protein. Phosphorylation of Tau causes it to dissociate from the microtubules, thus preventing microtubule polymerisation. Phosphorylation of Tau also triggers it for proteasome dependent degradation (Drewes et al., 1998, Kojima et al., 2007).

In mouse, Lkb1 phosphorylates brain-selective kinase (Brsk) which is important for neuronal polarization at the cerebral cortex. This requires Lkb1 to be phosphorylated at S431 by Pka or Rsk, and to be in a complex with Strad. Phosphorylated Brsk can phosphorylate MAPs like Tau that play a role in the growth and differentiation of axons and dendrites (Barnes et al., 2007).

LKB1 also phosphorylates NUAK family SNF1-like kinase 1 (NUAK), which can stimulate the phosphorylation of myosin phosphatase targeting-1 (MYPT1) protein phosphatase-1β (PP1β) complex and thus cell detachment. This was shown in both MEFs and human HeLa cells with or without LKB1 (Zagorska et al., 2010).

1.3.2 Cell metabolism and growth

LKB1 acts upstream of AMPK, an important sensor and modulator of cellular energy homeostasis. AMPK is a heterotrimeric complex composed of an α catalytic subunit and β and γ regulatory subunits. When ATP levels are low, AMP or ADP bind the γ subunit causing a conformational change. This allows LKB1 or calcium/calmodulin-dependent protein kinase kinase β (CaMKKβ) (Hawley et al., 2005, Hurley et al., 2005, Woods et al., 2005) to phosphorylate AMPK at T172 within the "T" loop of the α subunit (Hardie et al., 2011, Oakhill et al., 2011, Xiao et al., 2011). AMPK restores ATP levels by stimulating catabolism (glycolysis) and inhibiting anabolism (protein synthesis, lipogenesis)

(Mihaylova and Shaw, 2011, Hardie et al., 2012). For example, in MEFs, Lkb1 loss is associated with activated MTOR (mammalian target of rapamycin)-dependent protein synthesis (Shaw et al., 2004a). LKB1 activates AMPK which negatively regulates the TORC1 complex (composed of MTOR and its scaffolding protein, Raptor) (Gwinn et al., 2008). TORC1 activates S6K1 and 4E-BP1 which are key regulators of protein translation and cell growth (Fingar et al., 2004).

1.3.3 Cell cycle

LKB1 was reported to play a role in cell cycle arrest by affecting expression of tumour protein 53 (TP53) and the cyclin dependent kinase (CDK) inhibitors; CDKN1A (p21), CDKN1B (p27) and CDKN2A (p16) (van den Heuvel, 2005). In the G361 cell line, ectopic LKB1 expression increased p21 promoter activity in a TP53 dependent manner, to induce G1 cell cycle arrest (Tiainen et al., 2002). Zeng and Berger confirmed this using MEFs with ectopic LKB1 expression and U2OS human osteosarcoma cells with siRNA targeting LKB1, to show that endogenous and overexpressed LKB1 associates with the p21 promoter (Zeng and Berger, 2006), thereby mediating GATA-dependent (and TP53 independent) gene expression of p21 (Setogawa et al., 2006). In HeLa cells, ectopic LKB1 expression stimulates expression of p27 and induces G1 arrest (Xie et al., 2007). shRNA knock-down of LKB1 in human embryonic kidney 293T cells (HEK-293T cells) and human umbilical vein endothelial cells (HUVECs) led to a decrease in TP53 and p16 stimulated G1/S transition (Liang et al., 2010).

1.3.4 Cell death and survival

LKB1 has been reported to play a role in apoptosis and anoikis.

In the HT1080 human fibrosarcoma cells (TP53 wild-type), ectopic expression of LKB1 can interact with TP53 and stimulate TP53-dependent apoptosis. Karuman et al observed that

the kinase activity of LKB1 is important in stimulating apoptosis following treatment with paclitaxel and vincristine, but not with 5-flurouracil and doxorubicin, suggesting that the effect of LKB1 on apoptosis is compound dependent (Karuman et al., 2001).

LKB1 also plays a role in anoikis, which is apoptosis stimulated by anchorage independent growth. LKB1 activates salt inducible kinase 1 (SIK1) by phosphorylating T182 which stimulates SIK1 autophosphorylation at S186 (Hashimoto et al., 2008). SIK1 is required for TP53 dependent anoikis (Cheng et al., 2009). Ectopic expression of constitutively active SIK1 (T loop mutant T182E) in A549 human lung cancer cells (LKB1 mutated, TP53 wild-type), suppressed matrigel invasion *in vitro* using a Boyden chamber assay, and suppressed lung seeding in NOD/SCID mice after intravenous injection of tumour cells into the tail vein. Ectopic expression of kinase dead SIK1 had no effect on invasion or lung seeding (Cheng et al., 2009).

1.3.5 Gene expression

In MEFs and human lung cancer isogenic cells with or without LKB1, LKB1 phosphorylates and activates SIK2 and SIK3 which can phosphorylate histone deacetylases (HDACs) at conserved motifs. This stimulates the nuclear export of HDAC and thus, stimulates gene expression through reduced HDAC activity. In MEFs, stimulated gene expression was shown to be important for myogenesis (Walkinshaw et al., 2013).

1.4 LKB1 and cancer

LKB1 is mutated in 17% of lung adenocarcinomas (TCGA, 2014) and 20% of human papilloma virus (HPV) positive cervical cancer tumours (Wingo et al., 2009). Somatic LKB1 mutations have also been reported in sporadic malignant melanoma (Guldberg et al., 1999, Rowan et al., 1999), breast cancer (Bignell et al., 1998), head and neck cancer (Qiu et al., 2006), pancreatic (Su et al., 1999) and hepatocellular cancers (Kim et al., 2004).

Nonsense mutations, in-frame deletions, splicing mutations, deletions, point mutations and frameshift mutations in LKB1 gene have been found in both PJS patients and sporadic tumours (Alessi et al., 2006). These mutations can affect LKB1 kinase activity or its ability to interact with STRAD or MO25 (Zeqiraj et al., 2009). In non-small cell lung cancer, LKB1 mutations are generally homozygous and arise somatically (Sanchez-Cespedes, 2007). LKB1 can also be transcriptionally repressed as lung tumours can have a wild-type LKB1 gene sequence but a transcriptomic profile corresponding to LKB1 mutated tumours (Kaufman et al., 2014). LKB1 mRNA expression has been shown to be repressed by promoter methylation in cell lines, primary tumours and polyps from PJS patients (Esteller et al., 2000, Sanchez-Cespedes et al., 2002).

Loss of expression of the LKB1 binding partner; STRAD, causes a genetic disorder called polyhydramnios megalencephaly and symptomatic epilepsy (PMSE) (Puffenberger et al., 2007, Orlova et al., 2010) and STRAD deficiency has been shown to be associated with increased activation of MTOR signalling (Orlova et al., 2010). However, there are no reports that patients with PMSE have an increased risk of developing cancer, therefore, loss of STRAD does not phenocopy loss of LKB1, possibly suggesting that the nuclear role of LKB1 may have the tumour suppressive function.

1.5 LKB1 loss in lung cancer

Lung cancer is the leading cause of cancer related mortality worldwide with approximately 1 million deaths in 2012, exceeding that of breast, prostate, and colorectal cancer combined (Siegel et al., 2012). There are two main histological subtypes of lung cancer; small cell lung cancer (SCLC) (13%) and non-small cell lung cancer (NSCLC) (83%). NSCLC is further divided into 3 main categories; adenocarcinoma, squamous cell carcinoma and large cell carcinoma. Adenocarcinoma is the most common histological subtype of lung cancer (43%)

(Figure 1.3) (Howlader et al., 2015). In lung adenocarcinoma, LKB1 is the second most commonly mutated tumour suppressor gene (Figure 1.3) (TCGA, 2014). Somatic LKB1 mutations are detected in 17.4% of lung adenocarcinoma samples (n=230), in which 6.2% are classed as missense mutations, and 11.2% are classed as truncating mutations that arose from nonsense, non-stop or splice site mutations, or frameshift deletions or frameshift insertions (cBioPortal, TCGA, 2014). Figure 1.3c shows the location of these mutations across the LKB1 amino acid sequence. The missense mutations are located within the kinase domain, possible affecting the kinase activity of LKB1 or the ability of LKB1 to interact with STRAD (as mentioned in Section 1.2.3; the kinase domain and amino acids within the CTD of LKB1 are important for binding STRAD). All other mutations are truncating mutations and thus affecting LKB1 expression or function.

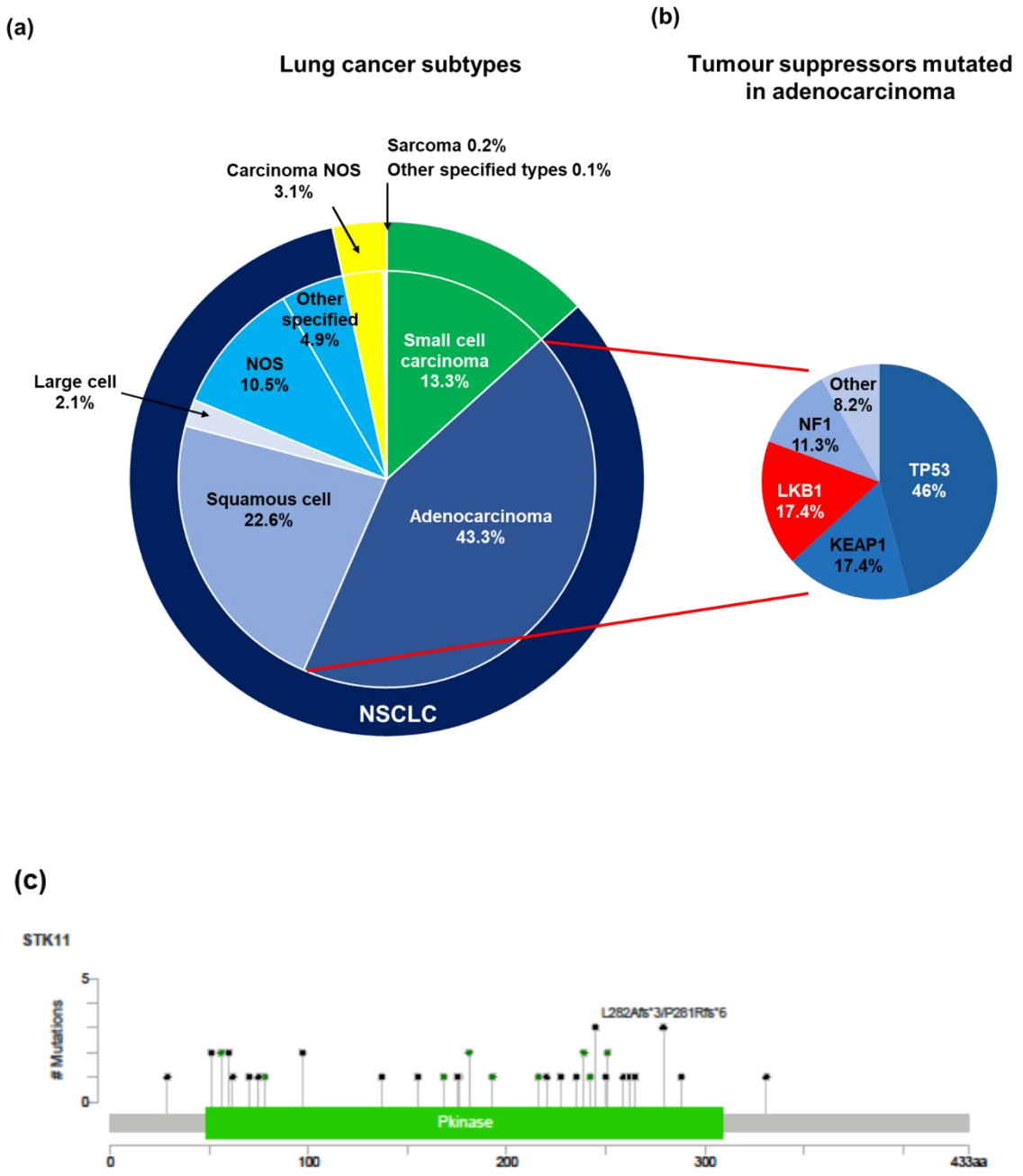

Figure 1.3: LKB1 is the second most commonly altered tumour suppressor gene in lung adenocarcinoma, the most prevalent form of lung cancer
(a) Lung cancer histological subtypes based on data collected between 2008-2012 in USA and includes all race and sexes (Howlader et al., 2015). NOS - not otherwise specified. (b) Frequency of mutations in tumour suppressor genes in lung adenocarcinoma (n = 230 samples) (TCGA, 2014). (c) The location of the missense (green) and truncating (black) mutations within LKB1 (graph was generated using cBioportal to analyse the lung adenocarcinoma dataset described in (b) (TCGA, 2014)).

LKB1 mutations are more prevalent in smokers and are associated with poorly differentiated tumours (Matsumoto et al., 2007). It is believed that LKB1 is a "trunk" mutation occurring early during lung cancer development (Zhang et al., 2014). This finding is supported by

another group that showed that LKB1 protein expression can be lost in severe lung dysplasia on analysis of immunohistochemical staining of lung adenocarcinomas (Ghaffar et al., 2003). LKB1 mutations tend to (i) co-occur with activating KRAS (v-Ki-ras2 Kirsten rat sarcoma viral oncogene homologue) mutations (p-value = 0.003) which are also associated with smoking (TCGA, 2014, Slebos et al., 1991), (ii) be mutually exclusive with TP53 mutations (p-value = 0.006) and (iii) co-occur with KEAP1 mutations (p-value = 0.008) (TCGA, 2014). Furthermore, LKB1 mutations tend to be mutually exclusive with activating mutations in EGFR (epidermal growth factor receptor) (p-value = 0.001) and ALK (anaplastic lymphoma kinase) (p-value = 0.362) (TCGA, 2014) suggesting that LKB1 mutated tumours are unlikely to gain benefit from EGFR and ALK targeted therapies (Lynch et al., 2004, Kwak et al., 2010).

1.6 Understanding the role of LKB1 loss in lung cancer and targeting LKB1 mutated cells

1.6.1 *Lkb1*$^{-/-}$ and *Lkb1*$^{+/-}$ mice

Lkb1$^{-/-}$ mice die 8.5-9.5 days post coitum and *Lkb1*$^{-/-}$ mouse embryos show developmental abnormalities within the neural tube, aorta and placenta (Jishage et al., 2002). *Lkb1*$^{-/-}$ embryos also show elevated vascular endothelial growth factor (Vegf) mRNA and vascular abnormalities (Ylikorkala et al., 2001, Jishage et al., 2002). In heterozygous *Lkb1*$^{+/-}$ mice, polyps, mainly in the glandular stomach are seen at the age of 45 weeks (Jishage et al., 2002). These polyps have been reported to be haplo-insufficient for *Lkb1* (Jishage et al., 2002, Rossi et al., 2002). However, one study reported that the *Lkb1* wild-type allele was not detected in 3 out of 12 mouse polyps and Lkb1 protein was not expressed in 8 out of 14 polyps (Bardeesy et al., 2002).

1.6.2 Impact of therapies in *Lkb1*$^{+/-}$ mice

Previous reports have found that cyclooxygenase 2 (COX2) is also increased in polyps from *Lkb1*$^{+/-}$ mice and from PJS patients (Rossi et al., 2002), suggesting that PJS patients may benefit from the use of COX2 inhbitors. Another study suggested that PJS patients may benefit from the use of MTOR inhibitors as, *Lkb1*$^{+/-}$ mice (9 months old) with PJS like polyps showed reduced tumour burden when treated with rapamycin, an allosteric MTOR inhibitor (Shackelford et al., 2009).

1.6.3 Genetically engineered mouse models (GEMMs) of lung cancer

GEMMs have mainly been used to study the effect of LKB1 loss on lung cancer *in vivo* (Ji et al., 2007, Carretero et al., 2010, Chen et al., 2012, Shackelford et al., 2013). Using these models, conditional genetic alterations in lung cells can be achieved by the inhalation of adenoviruses that express CRE recombinase (Causes Recombination). CRE recombinase recognises DNA sequences flanked by LoxP (floxed sequence) and mediates an alteration of this (i.e. a deletion, insertion, translocation or inversion) (Prost et al., 2001). The disadvantages of GEMMs are that the adenoviruses can cause an inflammatory response which may have a confounding effect. Moreover, adenoviruses only infect dividing cells (Walrath et al., 2010).

Using the approach above, Ji et al induced activating mutations in Kras alone or in combination with, inactivating mutations in *Lkb1* or *p53 in mouse lung cells, to generate lung cancer cells with either of the following genotypes: Kras*^{G12D}, *Kras*^{G12D}*/Lkb1*$^{L/L}$ *or Kras*^{G12D}*/p53*$^{L/L}$. Conditional activating mutations in Kras were also induced in mice with germline mutations in *Ink4a/Arf*$^{-/-}$ or *p16*$^{-/-}$, *generating lung cancer cells with either Kras*^{G12D}*/Ink4a/Arf*$^{-/-}$ *or Kras*^{G12D}*/p16*$^{-/-}$ *genotypes*. In addition, conditional activating mutations in *Kras* were combined with conditional inactivating *Lkb1* mutations in mice heterozygous for *Lkb1* (called *Kras*^{G12D}*/Lkb1*$^{L/-}$ *cancer cells*). In this study,

Kras^{G12D}*/Lkb1*$^{L/L}$ and *Kras*^{G12D}*/Lkb1*$^{L/-}$ (collectively called *Kras*^{G12D}*/Lkb1*$^{-/-}$) driven tumours caused a significant increase in tumour burden and increase in metastasis to the regional lymph nodes and axial skeleton, compared to *Kras*^{G12D} alone or in combination with the *p53*$^{L/L}$, *Ink4a/Arf*$^{-/-}$ or *p16*$^{-/-}$ (Ji et al., 2007). On examination of the tumour tissue, Ji et al observed that Lkb1 deficient tumours had increased expression of Nedd9, Vegfc, Loxl1, Pdgf receptor and Mmp2, which play roles in angiogenesis and metastasis (Ji et al., 2007). The *Kras*^{G12D} and *Kras*^{G12D}*/Lkb1*$^{-/-}$ primary lung tumours and *Kras*^{G12D}*/Lkb1*$^{-/-}$ metastatic tumours were further characterised by Carretero et al using genomic and phosphoproteomic analysis, which revealed that Lkb1 loss is associated with activation of Src in both primary and metastatic tumours (Carretero et al., 2010), identifying Src as a potential target for Lkb1 mutated cells.

Metabolic differences were also observed in *Kras*^{G12D}*/Lkb1*$^{L/L}$ driven mouse lung tumours which had increased uptake of fluoro-deoxyglucose (FDG) during positron emission tomography (PET) imaging, compared to *Kras*^{G12D} and *Kras*^{G12D}*/p53*$^{L/L}$ driven tumours. FDG is a glucose analogue and competitive inhibitor of hexokinase, the first enzyme involved in glycolysis. Therefore, this suggests that Lkb1 deficient mouse lung tumours have increased glycolysis. Supporting evidence came from Chen et al who showed using immunohistochemistry that *Kras*^{G12D}*/Lkb1*$^{L/L}$ driven tumours had higher levels of Glut1 (glucose transporter 1) protein expression (Chen et al., 2012, Shackelford et al., 2013).

1.6.4 Impact of therapies in GEMMs of lung cancer

Several therapies have been investigated in the *Kras*^{G12D}*/Lkb1*$^{-/-}$ or *Kras*^{G12D}*/Lkb1*$^{L/L}$ mouse models of lung cancer including inhibitors of VEGFR, MTOR, SRC, PI3K, MEK and mitochondrial complex I.

Gandhi et al investigated the impact of a VEGFR inhibitor and found that sunitinib (VEGFR1, 2, 3 inhibitor) reduced tumour volume in *Kras*^{G12D}/*Lkb1*$^{L/L}$ driven mouse lung tumours. However, local and distant metastasis formation was not prevented (Gandhi et al., 2009), indicating that inhibitors of angiogenesis might be useful to treat early stage LKB1 mutated primary tumours but not advanced metastatic disease.

The MTOR inhibitor; rapamycin showed potential promise at reducing tumour burden in *Lkb1*$^{+/-}$ mice (Shackelford et al., 2009) (Section 1.6.2). Further work has suggested that MTOR inhibitors in combination with other therapies may prove useful. Carretero et al showed that the *Kras*^{G12D}/*Lkb1*$^{-/-}$ driven tumours were sensitive to the triple combination of dasatinib (SRC inhibitor), BEZ235 (PI3K/MTOR inhibitor) and AZD6244 (MEK inhibitor) (~ 50% reduction in tumour volume) but not to dasatinib alone. The dual combination of BEZ235 and AZD6244 reduced the volume of *Kras*^{G12D} driven tumours by 80% but *Kras*^{G12D}/*Lkb1*$^{-/-}$ driven tumours by only ~ 20% (Carretero et al., 2010). Chen et al further investigated the use of the MEK inhibitor; AZD6244 in combination with docetaxel (microtubule stabiliser), and found that *Kras*^{G12D}/*Lkb1*$^{L/L}$ driven mouse lung tumours were more resistant to the dual combination compared with *Kras*^{G12D} driven tumours (Chen et al., 2012).

As LKB1 was reported to play an important role in metabolism, Shackelford et al examined the effect of phenformin, a complex I inhibitor on tumour burden in *Kras*^{G12D}, *Kras/p53*$^{L/L}$ and *Kras*^{G12D}/*Lkb1*$^{L/L}$ driven lung cancer models. They found that, at 6 weeks post tumour initiation, phenformin treatment reduced tumour burden in *Kras*^{G12D}, *Kras/p53*$^{L/L}$ and *Kras*^{G12D}/*Lkb1*$^{L/L}$ driven lung cancer models and the reduction was statistically significant in the *Kras*^{G12D}/*Lkb1*$^{L/L}$ driven model, for up to 4 weeks post treatment. However, at 6 weeks post treatment, tumour volume increased (Shackelford et al., 2013), thereby suggesting the emergence of resistance.

1.6.5 Mouse cell lines

To identify novel therapeutic strategies to target LKB1 mutated cells, Liu et al completed a shRNA screen using a pooled 40,000 murine shRNA lentiviral library and lung cancer cells derived from *Kras*^{G12D}*/p53*$^{L/L}$ or *Kras*^{G12D}*/p53*$^{L/L}$*/Lkb1*$^{L/L}$ driven mouse lung tumours. They found that, shRNAs targeting Dtymk, Chek1, Pdhb and Cmpk1 caused the greatest effect on growth suppression in *Lkb1* null cell lines. Deoxythymidylate kinase (Dtymk) is an enzyme that catalyses the phosphorylation of dTMP to dTDP, which is important for dTTP and pyrimidine synthesis. Chek1 plays a role in the DNA damage response and cell cycle (Liu et al., 2013).

1.6.6 Human cell lines

Isogenic lung cancer cells with or without LKB1 have been used to study the role of LKB1 loss *in vitro*. These include both ectopic expression of LKB1 and kinase dead LKB1 in LKB1 mutated cells and knock-down of LKB1 in LKB1 wild-type cells (Ji et al., 2007, Shackelford et al., 2013, Kaufman et al., 2014). In human lung cancer cells, LKB1 has been reported to play a role in polarity, migration, invasion and epithelial to mesenchymal transition (EMT), suggesting a possible link between LKB1 loss and metastasis.

As mentioned above, Ji et al observed increased Nedd9 expression in *Kras*^{G12D}*/Lkb1*$^{-/-}$ driven mouse lung tumours (Section 1.6.3). They extended this study to LKB1 mutated A549 and H2126 human lung cancer cells. Ectopic expression of LKB1 in these cells reduced NEDD9 expression further supporting a link between LKB1 and NEDD9 (Ji et al., 2007).

In LKB1 wild-type H1299 lung cancer cells with or without knock-down of LKB1, it was shown that LKB1 associates with actin at the leading edge of motile cancer cells and activates CDC42 (cell division control protein 42) which phosphorylates and activates the polarity protein; PAK (p21-activating kinases) (Zhang et al., 2008).

LKB1 has been reported to play a role in FAK (focal adhesion kinase) signalling in human lung cancer cells. H1299 cells with knock-down of LKB1 have increased FAK phosphorylation/activation and increased cell adhesion. FAK increases focal adhesion site turnover resulting in poor "directional persistence". Treatment of LKB1 deficient cells with the FAK inhibitor; PF-573228 restores the "directional persistence" (Kline et al., 2013).

LKB1 phosphorylates PEA3 (polyoma enhancer activator 3) and increases the proteasome dependent degradation of PEA3. PEA3 is a transcription factor that plays a role in COX2 expression. Knock-down of PEA3 decreases invasion of LKB1 mutated A549 cells through matrigel (Upadhyay et al., 2006), highlighting a possible link between LKB1, COX2 and invasion.

Human immortalized lung epithelial cells and lung adenocarcinoma cells with transient or stable knock-down of LKB1 show increased expression of ZEB1 (zinc finger E-box-binding homeobox 1) (an E-cadherin represser) which stimulates EMT (Roy et al., 2010).

1.6.7 Impact of therapies in human cell lines

Liu et al observed selective inhibition of growth in cells derived from $Kras^{G12D}/p53^{L/L}/Lkb1^{L/L}$ driven tumours compared to $Kras^{G12D}/p53^{L/L}$ cells when transduced with shRNA targeting Dtymk and Chek1 (Section 1.6.5). This finding was recapitulated in human lung cancer cell lines whereby knock-down of DTYMK reduced the survival of LKB1 mutated A549 and H2122 cells compared to LKB1 wild-type H358 and Calu-1 cells (Liu et al., 2013). Furthermore, Liu et al found that inhibition of CHK1/2 using AZD7762 or CHIR124 selectively reduced the survival of LKB1 mutated cells (A549, H2122) compared to LKB1 wild-type cells (H358 and Calu-1) (Liu et al., 2013).

As discussed above (Section 1.6.4), Shackelford et al reported that $Kras^{G12D}/Lkb1^{L/L}$ mutated lung tumours were more sensitive to phenformin than $Kras^{G12D}$ or $Kras^{G12D}/p53^{L/L}$ mutated

tumours. They also studied the effect of phenformin *in vitro* using human lung isogenic cells with or without LKB1. They found that LKB1 mutated cells (A549, H460, H157, A427) had increased expression of proteins involved in apoptosis (cleaved PARP and cleaved caspase 3) on treatment with phenformin compared to cells with ectopic LKB1 expression (Shackelford et al., 2013).

1.6.8 *In vivo* models using human lung cancer cells

Two studies have investigated the effect of human lung cancer cells in the mouse lung by examining the lung seeding potential of A549 cells after injection into the tail vein in SCID (severe combined immunodeficiency) or NOD/SCID mice (Ji et al., 2007, Cheng et al., 2009). Ji et al reported that ectopic expression of LKB1 in LKB1 mutated A549 cells suppressed the development of lung tumours compared with non-transduced A549 cells (Ji et al., 2007). Cheng et al observed a link between loss of LKB1 expression, inactive SIK, anoikis and metastasis (Section 1.3.4).

1.6.9 Human lung adenocarcinoma tumours

Kaufmann et al investigated the effect of LKB1 on the transcriptome in (i) NSCLC cell lines, (ii) isogenic cells with or without LKB1 (A549 and H2122 cells), (iii) $Kras^{G12D}$ and $Kras^{G12D}/Lkb1^{-/-}$ driven mouse tumours and (iv) human lung adenocarcinoma clinical samples (Kaufman et al., 2014). They found that LKB1 loss was associated with a gene expression signature that was similar in the human cell lines and human tumours. However, this gene expression signature was not recapitulated in the $Kras^{G12D}/Lkb1^{-/-}$ driven mouse tumours. The gene expression signature was divided into 4 clusters; mitochondria/MTOR, NRF2, FOX/CREB and downregulated. The mitochondria/MTOR genes included those involved in oxidative phosphorylation and protein translation, and the NRF2 cluster included genes involved in oxidative stress.

1.7 Hypotheses, aims and objectives

Although several studies have utilised GEMMs and mouse cell lines, and some findings have been recapitulated in human lung cancer cell lines, the study by Kaufmann et al (Kaufman et al., 2014) suggests that mouse *Kras^{G12D}/Lkb1$^{-/-}$* lung tumours may not accurately reflect human cell lines or human tumours. This suggests that the role of LKB1 in lung cancer may have some species specific differences and therefore, the current understanding of LKB1 loss in lung cancer is limited. Despite efforts, there are currently no therapies used to selectively target LKB1 mutated cells in the clinic.

Of note, the gene expression profile of LKB1 mutated human cell lines clustered with that of human tumours from the clinic. For our studies, we used human lung cancer cell lines and, generated isogenic cells with or without LKB1 expression. We explored the impact of LKB1 expression on cell growth, gene expression and response to compounds. We also utilised growth in 3D (spheroids) as we hypothesised that the microenvironment (in particular, differences in metabolism and polarity between 2D and 3D) may play an important role in the growth of LKB1 mutated cells. We also extended our studies *in vivo,* including looking at an orthotopic model of metastatic lung cancer, whereby human lung cancer cells were injected into the lung.

We hypothesised that LKB1 mutated cells might be selectively targeted by exploiting vulnerabilities in these cells. This is analogous to “synthetic lethality” where the loss of an individual gene function itself is not lethal but the loss of function of two genes is lethal, as the two genes play essential role in pathways that can compensate for each other. The most advanced example of synthetic lethality in clinical practice is the use of a DNA repair inhibitor targeting PARP to selectively inhibit proliferation and survival of BRCA1/2 deficient cells, which are defective in homologous recombination DNA repair, rendering

them hypersensitive to the S-phase DNA damage induced by PARP inhibitors (Helleday, 2011). We used an approach of "pharmacological synthetic lethality" to selectively target LKB1 mutated cells by identifying compounds that have limited toxicity in LKB1 expressing cells but in the presence of LKB1 loss, are toxic. As LKB1 plays an important role in metabolism, we also tested the effect of metabolic inhibitors.

The overall aims of this project were to understand the role of LKB1 loss in NSCLC and to identify novel strategies to selectively target the LKB1 mutated cells.

To understand the role of LKB1 loss in NSCLC:

1. We generated isogenic human lung cancer cells with or without LKB1 to determine the effect of LKB1 expression alone on cell growth, cell signalling and response to therapy. Differences in cell growth were determined using three models; 2D culture, 3D spheroids and *in vivo*. Two *in vivo* models were used; sub-cutaneous xenografts and lung orthotopic xenografts. In both *in vivo* models, human isogenic cells with or without LKB1 were implanted.

2. We used whole transcriptomic profiling to (i) determine mRNA expression differences between cell growth in 2D culture, 3D spheroids and sub-cutaneous xenografts and (ii) determine the effect of LKB1 loss on differences in the mRNA expression.

To identify novel strategies to selectively target the LKB1 mutated cells:

1. We completed a bioactive small molecule screen in 2D culture and in 3D spheroids to identify compounds that are selectively toxic in LKB1 mutated cells.

2. As LKB1 has been reported to play a role in metabolism, we determined the effect of metabolic inhibitors and nutrient deprivation on cell viability.

2 Materials and Methods

2.1 Reagents, buffers and compounds used throughout the study

2.1.1 Reagents and buffers

Table 2.1: Reagents and buffers

Application	Reagent/buffer	Stock solution or final composition before use	Storage
Bioactive small molecule screen: apoptosis assay	Hoechst 33258	500x stock: 10 mg/mL Hoechst 33258 (Sigma-Aldrich) in dH_2O	- 20°C
Cell culture	1x phosphate buffered saline (PBS)	Dilute 10x PBS (Lonza) in dH_2O and autoclave	4°C
Cell proliferation assay	1x DNA lysis buffer	25 mM EDTA * pH 8.0 (Lonza), 0.1% (v/v) Triton X-100 (VWR) in dH_2O	4°C
Cell proliferation assay	10x DNA lysis buffer	250 mM EDTA pH 8.0 (Lonza), 1% (v/v) Triton X-100 (VWR) in dH_2O	4°C
Cell proliferation assay	PicoGreen®	Dilute 1:200 of Quant-iT™ PicoGreen® dsDNA reagent (Life Technologies) in 1x PBS	- 20°C
Cell viability assay	Resazurin	1000x stock: 12.5 mg/mL resazurin (Sigma-Aldrich) in dH_2O	- 20°C
DNA gel electrophoresis	0.5x Tris Borate-EDTA (TBE) buffer	Dilute 10x TBE (Sigma-Aldrich) in dH_2O	RT
Fixative and stain for cells	Crystal violet solution	0.5% (w/v) crystal violet (Merck), 75% methanol (Sigma-Aldrich), in dH_2O	RT (room temperature)
Fixative for cells and mouse tissue	Paraformaldehyde (PFA)	3% or 4% (w/v) PFA (VWR) dissolved in 1x PBS, pH adjusted to 7.4 with 5 M NaOH (VWR)	4°C
Haematoxylin and Eosin staining	Acid alcohol	1% (v/v) hydrochloric acid (HCl) (Thermo Fisher Scientific) in 70% (v/v) ethanol ** (Thermo Fisher Scientific) in dH_2O	RT
Haematoxylin and Eosin staining	Scott's tap water	41.7 mM sodium bicarbonate ($NaHCO_3$) (Sigma-Aldrich), 81.2 mM magnesium sulfate ($MgSO_4$)	RT

		(Scientific laboratory supplies) in dH_2O	
Haematoxylin and Eosin staining	Lithium carbonate	0.5% (w/v) lithium carbonate (Li_2CO_3) (Sigma-Aldrich) in dH_2O	RT
Immunofluorescence	Permeabilisation and blocking buffer	0.1% (v/v) Triton X-100, 1% (v/v) normal goat serum (Millipore), and 1% (w/v) bovine serum albumin (BSA) (Acros organics) in 1x PBS	4°C (prepared fresh)
Immunofluorescence	Antibody buffer	1% (v/v) normal goat serum and 1% (w/v) BSA in 1x PBS	4°C (prepared fresh)
Immunocytochemistry, Immunohistochemistry, Immunofluorescence	Citrate buffer for antigen retrieval	10 mM citric acid (Sigma-Aldrich), 0.05% (v/v) Tween-20 (Sigma-Aldrich) in dH_2O, adjusted to pH 6 with 1 M sodium hydroxide (NaOH)	RT
Lentiviral transduction	Polybrene	1000x stock: 8 mg/mL polybrene (Sigma-Aldrich) in dH_2O	- 20°C
Oxygen consumption measurements	Hydroxyethyl-piperazine-ethanesulfonic acid (HEPES) buffer	40x stock: 1 M HEPES (Sigma-Aldrich) in dH_2O, pH adjusted to 7.4 with 5 M NaOH (VWR)	4°C
Oxygen consumption measurements	Hoechst 33258	2500x stock: 10 mg/mL Hoechst 33258 in dH_2O	- 20°C
Routine work	1x PBS	5 PBS Tablets (Sigma-Aldrich) dissolved in 1 L dH_2O	RT or 4°C
Routine work	1x PBS-T (tween)	1x PBS with 0.1% (v/v) Tween-20	RT
Western blotting	1x tris buffered saline (TBS)	10x stock solution: dilute 1 pack OmniPur® TBS 20x Ready Pack Powder (Calbiochem) in 2 L dH_2O. Prior to use, 10x TBS was diluted in dH_2O	RT
Western blotting	1x TBS-T	1x TBS with 0.1% (v/v) Tween-20	RT
Western blotting	Protein lysis solution for whole cell extract	50 mM Tris-HCl pH 7.6 (Promega),137 mM NaCl *** (Sigma-Aldrich), 10% (v/v) glycerol (VWR), 0.1% (v/v) Igepal (Sigma-Aldrich), 0.1% (v/v) SDS **** (AppliChem), 50 mM sodium fluoride (Sigma-Aldrich), 1 mM sodium orthovanadate (Sigma-Aldrich) and 1x cOmplete protease inhibitor cocktail (Roche) in dH_2O	Sodium orthovanadate (10x stock solution) and protease inhibitors (25x stock solution) were stored at - 20°C and freshly added before use. The remaining components were stored at 4°C.

Western blotting	Protein lysis solution for cytoplasmic protein extract	10 mM HEPES pH 7.9, 10 mM potassium chloride (Sigma-Aldrich), 0.1 mM EDTA, 0.1 mM egtazic acid (EGTA), 1 mM dithiothreitol (AppliChem), 1 mM sodium orthovanadate and 1x cOmplete protease inhibitor cocktail in dH_2O	4°C (Sodium orthovanadate and protease inhibitors were freshly added before use)
Western blotting	Protein lysis solution for nuclear protein extract	20 mM HEPES pH 7.9, 400 mM KCL, 1 mM EDTA, 1 mM EGTA, 10% (v/v) glycerine (VWR), 1 mM DTT, 1 mM sodium orthovanadate and 1x cOmplete protease inhibitor cocktail (Roche, Switzerland) in dH_2O	4°C (Sodium orthovanadate and protease inhibitors were freshly added before use)
Western blotting	5x sample loading buffer	25 mM tris-base (Sigma-Aldrich) made to pH 6.8 with HCl, 1% (v/v) SDS, 1 mM EDTA, 2.5% (v/v) β-mercaptoethanol (Sigma-Aldrich), 0.25 mg/mL bromophenol blue (Acros organics)	- 20°C
Western blotting	Running buffer	Dilute 10x tris/glycine/SDS running buffer (Bio-Rad) in dH_2O	RT
Western blotting	Transfer buffer	Dilute 10x tris/glycine buffer (Bio-Rad) in dH_2O and make to 20% (v/v) methanol (Sigma-Aldrich)	4°C
Western blotting	Blocking and antibody buffer	For fluorescence: 1:1 mixture of Odyssey® Blocking Buffer (LI-COR) and 1x PBS-T. For chemiluminescence: 5% (w/v) non-fat skimmed milk powder (Sigma-Aldrich) in 1x PBS-T	4°C

* EDTA - Ethylenediaminetetraacetic acid
** 70% ethanol = 70% (v/v) ethanol (Sigma-Aldrich), 30% (v/v) dH_2O
*** NaCl - sodium chloride
**** SDS - sodium dodecyl sulfate

2.1.2 Compounds

Compounds used in the 2D and 3D bioactive small molecule screens (Chapter 5) were from a bioactive small molecule library (Selleck L1100). Compounds in this library were provided as 10 mM stock solutions in DMSO and stored at - 20°C (See Appendices Table A5.6a for the complete list of compounds and their target(s)). For other studies, compounds were either taken from the Selleck L1100 library or acquired separately (Table 2.2):

Table 2.2: Compounds

Compound [1]	Target [2] or mode of action	Source	Stock concentration	Vehicle	Storage
2-DG (2-deoxyglucose)	Hexokinase	Sigma-Aldrich	100 mM	DMEM [3]	- 20˚C
Acetylsalicylic acid (aspirin)	COX	Sigma-Aldrich	10 mg/mL	dH_2O	- 20˚C
Antimycin A	Complex III	Sigma-Aldrich	2.5 mM	DMSO [4]	- 20˚C
AZD0530	SRC, ABL	Selleck Chemicals	10 mM	DMSO	- 20˚C
AZD1208	PIM	Selleck Chemicals	10 mM	DMSO	- 20˚C
AZD3965	MCT1	MedKoo Bioscience	10 mM	DMSO	- 20˚C
AZD6244	MEK	Selleck Chemicals	10 mM	DMSO	- 20˚C
AZD8055	MTOR	Selleck Chemicals	10 mM	DMSO	- 20˚C
Blastocidin	Antibiotic	Invitrogen	10 mg/mL	dH_2O	- 20˚C
Bromopyruvate	Pyruvate and lactic acid analogue	Sigma-Aldrich	20 mM	PBS	- 20˚C
Celecoxib	COX2	Sigma-Aldrich	10 mM	DMSO	- 20˚C
Dexamethasone	Glucocorticoid (anti-inflammatory)	Sigma-Aldrich	10 mM	DMSO	- 20˚C
Dichloroacetate	PDK	Sigma-Aldrich	100 mM	DMEM [3]	- 20˚C
Docetaxel	Microtubule stabiliser	Selleck Chemicals	10 mM	DMSO	- 20˚C
FCCP	Uncouples respiration	Sigma-Aldrich	2.5 mM	DMSO	- 20˚C
Forskolin	Adenylate cyclase	Sigma-Aldrich	10 mM	DMSO	- 20˚C
Ganetespib	HSP90	Selleck Chemicals	10 mM	DMSO	- 20˚C
HG-9-91-01	SIK1, 2, 3	MedChem express	10 mM	DMSO	- 20˚C

JQ1 inhibitor (SGCBD01)	BET bromodomain	SGC	10 mM	DMSO	- 20˚C
LKB1/AAK1/PIM1 inhibitor	LKB1	MedChem express	10 mM	DMSO	- 20˚C
MARK/PAR1 inhibitor	MARK	Calbiochem	10 mM	DMSO	- 20˚C (dark)
Metformin	Complex I	Sigma-Aldrich	100 mM	DMEM [3]	- 20˚C
Oligomycin	ATP synthase	Sigma-Aldrich	2.5 mM	DMSO	- 20˚C
Paclitaxel	Microtubule stabiliser	Selleck Chemicals	10 mM	DMSO	- 20˚C
PF562271	FAK	Selleck Chemicals	10 mM	DMSO	- 20˚C
Phenformin	Complex I	Sigma-Aldrich	100 mM	DMEM [3]	- 20˚C
Phleomycin	Antibiotic	Sigma-Aldrich	10 mg/mL	dH_2O	- 20˚C
PHT-427	AKT, PDPK1	Selleck Chemicals	10 mM	DMSO	- 20˚C
PI-103	PI3K, MTOR	Selleck Chemicals	10 mM	DMSO	- 20˚C
Puromycin	Antibiotic	Calbiochem	1 mg/mL	dH_2O	- 20˚C
Rolipram	PDE4	Sigma-Aldrich	10 mM	DMSO	- 20˚C
Rotenone	Complex I	Sigma-Aldrich	2.5 mM	DMSO	- 20˚C
Selleck library (n = 326) (Appendices Table A5.6a)		Selleck Chemicals	10 mM	DMSO	- 20˚C
Telaprevir	Protease inhibitor (anti-viral)	Selleck Chemicals	10 mM	DMSO	- 20˚C
Vincristine	Microtubule destabiliser	Selleck Chemicals	10 mM	DMSO	- 20˚C
Vinorelbine	Microtubule destabiliser	Selleck Chemicals	10 mM	DMSO	- 20˚C
WZ4003	NUAK	Selleck Chemicals	10 mM	DMSO	- 20˚C
YMU1 thymidylate kinase inhibitor	Thymidylate kinase	Calbiochem	10 mM	DMSO	- 20˚C (dark)

[1] Full name for compounds and targets can be found in the list of abbreviations
[2] Green indicates target activated by compound, orange indicates target inhibited by compound, black describes the mode of action of the compound
[3] DMEM - DMEM with no glucose, glutamine, pyruvate and phenol red (Life Technologies #A14430-01)
[4] DMSO - Dimethyl sulfoxide (Thermo Fisher Scientific)

2.2 Cell lines

Table 2.3 shows the cell lines used including brief information on the histology, origin, LKB1, KRAS, BRAF and TP53 mutation status, and source. NBE1 is a telomerase

immortalized normal bronchial epithelial cell line derived from human lung tissue (Stead et al., 2012). Excluding NBE1, all cell lines are human lung cancer cell lines. Cell lines were authenticated by ATCC or ECACC and were not used beyond passage 25.

Table 2.3: Cell lines

Cell line	Histology	Origin	LKB1 status [1, 2, 3]	Mutations in KRAS, BRAF, and TP53 [1, 4]	Source
A549	Lung carcinoma	58 year old caucasian male	p.Q37*	KRAS (p.G12S)	ATCC #CCL-185
NCI-H2126	Lung adenocarcinoma	65 year old caucasian male	Δ	TP53 (p.E62*)	ATCC #CCL-256
NCI-H23	Lung adenocarcinoma	51 year old black male	p.W332*	KRAS (p.G12C), TP53 (p.M246I)	ATCC #CRL-5800
A427	Lung carcinoma	52 year old caucasian male	Δ	KRAS (p.G12D)	ATCC #HTB-53
NCI-H1395	Lung adenocarcinoma stage II	55 year old caucasian female	p.E57fs	BRAF (p.G468A)	ATCC #CRL-5868
NCI-H460	Large cell lung carcinoma	Male	p.Q37*	KRAS (p.Q61H)	ATCC #HTB-177
NCI-H2030	Lung adenocarcinoma	Male	p.E317*	KRAS (p.G12C) TP53 (p.G262V)	ATCC #CRL-5914
NCI-H1755	Lung adenocarcinoma stage IV	65 year old caucasian female	p.P281fs	BRAF (p.G469A), TP53 (p.C242F)	ATCC #CRL-5892
CORL105	Lung adenocarcinoma	Caucasian male	wt [5]	unconfirmed wt [6]	ECACC #92031918
NCI-H1299	Lung carcinoma (NSCLC)	43 year old caucasian male	wt	TP53 (Δ)	ATCC #CRL-5803
Calu6	Anaplastic carcinoma (probably lung)	61 year old caucasian female	wt	KRAS (p.Q61K), TP53 (p.R196*)	ATCC #HTB-56
NBE1	Telomerase immortalized bronchial epithelium	Stead et al., 2012	wt	unconfirmed wt [7]	Pamela Rabbitts, University of Leeds, UK

[1] p - amino acid position, * - truncation, Δ - deletion, fs - frameshift

Amino acids: A-alanine, C-cysteine, D-aspatic acid, E-glutamic acid, F-phenylalanine, G-glycine, H-histidine, I-isoleucine, K-lysine, M-methionine, P-proline, Q-glutamine, R-arginine, S-serine, V-valine, W-tryptophan
[2] All LKB1 mutations are homozygous
[3, 4] Source for mutation data: LKB1, KRAS, BRAF and TP53 status in 11 NSCLC cell lines (CCLE, COSMIC). Additional LKB1 mutation data: A549 and H23 (Sanchez-Cespedes et al., 2002), A427, H2126, H1395 and H460 (Carretero et al., 2004). KRAS mutation data: A427 (Valenzuela and Groffen, 1986). BRAF mutation data: H1395 (Davies et al., 2002)
[5] wt - wild-type
[6] Not reported as mutated in COSMIC but have not confirmed if it is wild-type
[7] Sequencing has not been completed but assumed wild-type as it is derived from normal bronchial epithelial cells

2.3 Cell culture, routine passaging and cell seeding

Cells were cultured in Advanced DMEM/F12, supplemented with 5% (v/v) Fetal Bovine Serum (FBS), 2 mM GlutaMAX™ and 50 U/mL penicillin/ 50 µg/mL streptomycin, in a humidified incubator at 37˚C with 5% CO_2 (Table 2.4). Cells were passaged using 0.25% Trypsin-EDTA (Life Technologies #25200-056) at sub-confluency approximately twice every week (depending on the cell growth rate). Cell density and viability were determined using an automated cell counter (Invitrogen Countess®). For this, cell suspensions were mixed with an equal volume of 0.4% trypan blue solution (Life Technologies) and added to a Countess® cell counting chamber slide (Invitrogen #C10283). For each experiment, cells were seeded according to the desired cell density/number (Table 2.5). Advanced DMEM/F12 supplemented with 5% (v/v) FBS, 2 mM GlutaMAX™ and 50 U/mL penicillin/ 50 µg/mL streptomycin was used for all experiments unless otherwise stated.

For the bioactive small molecule screen in 2D culture (Chapter 5), phenol red-free DMEM/F12 supplemented with 10% (v/v) FBS, 2 mM GlutaMAX™ and 50 U/mL penicillin/ 50 µg/mL streptomycin was used.

For glucose and glutamine deprivation experiments (Chapter 6), DMEM without glucose, glutamine, sodium pyruvate or phenol red was used, and supplemented with 5% (v/v) dialysed FBS, 50 U/mL penicillin/ 50 µg/mL streptomycin and 1 mM sodium pyruvate. For

glucose deprivation, 2 mM GlutaMAX™ was added together with the desired concentration of glucose. For glutamine deprivation, 17.5 mM glucose was added with the desired concentration of GlutaMAX™. GlutaMAX™/glutamax was referred to as glutamine in experiments (Chapter 6). GlutaMAX™ was used as opposed to glutamine as it is more stable in solution and was used in all other experiments throughout this thesis.

See Table 2.4 for the complete list of cell culture reagents.

Table 2.4: Cell culture reagents

Reagent	Source
Advanced DMEM/F12	Life Technologies #12634-010
Phenol red free DMEM/F12	Life Technologies #11039-021
DMEM with no glucose, glutamine, sodium pyruvate or phenol red	Life Technologies #A14430-01
Penicillin and streptomycin	Life Technologies #15070-063
FBS	Sigma-Aldrich #F7524
Dialysed FBS	Life Technologies #26400-036
GlutaMAX™	Life Technologies #35050-038
D-glucose	Life Technologies #15023-021
Sodium pyruvate	Life Technologies #11360070

Table 2.5: Cell seeding density (no. cells per well of 96-well plate)

Cell line	PicoGreen assay in 2D (experiment duration = 10 days)	Resazurin assay in 2D (experiment duration = 4-7 days)	Bioactive small molecule screen [1]	Seahorse XF96 analyser
A549+EV	$5x10^2$	$1x10^3$	3 or 5 $x10^3$	$1x10^4$
A549+LKB	$5x10^2$	$1x10^3$	3 or 5 $x10^3$	$1x10^4$
A427+EV [2]	$1x10^3$	1 or 2 $x10^3$	3 or 5 $x10^3$	$2x10^4$
A427+LKB [2]	$1x10^3$	1 or 2 $x10^3$	3 or 5 $x10^3$	$2x10^4$
H1299+shLKB	$5x10^2$	$1x10^3$	3 or 5 $x10^3$	
H1299+shEV	$5x10^2$	$1x10^3$	3 or 5 $x10^3$	
A549		$1x10^3$		$1x10^4$
A427		$2x10^3$		$2x10^4$
H1395		$4x10^3$		$4x10^4$
H1755		$3x10^3$		$3x10^4$
H2030		$2x10^3$		$2x10^4$
H2126		$2x10^3$		$2x10^4$
NCI-H23		$3x10^3$		$3x10^4$
H460		$1x10^3$		$1x10^4$
NCI-H1299		$1x10^3$		$1x10^4$
CORL105		$4x10^3$		$4x10^4$
Calu6		$2x10^3$		$2x10^4$
NBE1		$4x10^3$		$4x10^4$

[1] For measuring the time for induction of apoptosis, $3x10^3$ cells were seeded for 48 and 72 h time points and $5x10^3$ cells were seeded for 6, 12 and 24 h time points
[2] For A427+EV and A427+LKB cells, $1x10^3$ cells were seeded for all resazurin experiments except when treated with phenformin, metformin and 2-DG in which $2x10^3$ cells were seeded

2.4 Cryopreservation and thawing

For long-term storage, sub-confluent cells were trypsinised, resuspended in Advanced DMEM/F12 and centrifuged (280x g, 5 min) (MSE Mistral 2000). The cell pellet was resuspended in Advanced DMEM/F12 containing 10% (v/v) DMSO (Thermo Fisher Scientific). Cell lines were stored in cryogenic vials in a Mr. Frosty™ freezing container (Thermo Fisher Scientific), filled with isopropanol, at - 80˚C overnight (freezing rate ~ - 1°C/min). For long-term storage, cryogenic vials were stored in the gaseous phase of a liquid nitrogen storage vessel.

Cell lines were quickly thawed from liquid nitrogen by placing the cryogenic vials in a water bath at 37˚C. Cells were diluted in 10 volumes of Advanced DMEM/F12 and centrifuged (280x g, 5 min). The cell pellet was resuspended in Advanced DMEM/F12 and transferred to a T75 flask and incubated at 37˚C with 5% CO_2.

2.5 DNA sequencing of LKB1

2.5.1 DNA isolation

Cells were seeded in 10 cm plates, incubated until sub-confluent, and harvested by trypsinisation and centrifugation (280x g, 5 min). DNA was isolated using the MasterPure™ DNA Purification Kit (Epicentre Biotechnologies), according to the manufacturer's instructions. DNA concentration was measured using a NanoDrop 1000 spectrophotometer, and purified DNA was stored at - 20˚C.

2.5.2 Polymerise chain reaction (PCR) and DNA sequencing

Exons 1-9 of LKB1 were amplified by PCR. The primers (Sigma-Aldrich) used were as follows:

Table 2.6: Primers for amplification of LKB1

Exon	Sequence
1 - Forward	aacacaaggaaggaccgctc
1 - Reverse	aagacagaaccatcagcacc
2 - Forward	aggtacgccacttccacagg
2 - Reverse	ccattgccacaatggctgac
3 - Forward	ccttttcagaggggtggctgag
3 - Reverse	tatcaggacaagcagtgtgg
4 - Forward	cctggacttctgtgacttcc
4 - Reverse	cgaacgggtgcagtgcctgtg
5 - Forward	caccctcaaaatctccgacc
5 - Reverse	agctgcccaagacgcagagg
6 - Forward	cgtcaaccaccttgactgac
6 - Reverse	ccaaccctacatttctgcac
7 - Forward	aggagcgtccaggtatcac
7 - Reverse	ctagcgcccgctcaaccag
8 - Forward	ctgggtcggaaaactggacc
8 - Reverse	gacgtgggattggccaccag
9 - Forward	ttcaggctggatacacctgg
9 - Reverse	ggtcaccatgactgactagc

PCR reactions were prepared with the following components:

DNA: 25 ng
Forward primer: 0.4 µM
Reverse primer: 0.4 µM
MiFi DNA polymerase (Bioline Reagents, UK): 1 µL
5x MiFi buffer containing dNTPs (Bioline Reagents, UK): 5 µL
dH_2O: to 25 µL

The reactions were performed using a thermal cycler (Applied Biosystems) with conditions:

Hot start: 95°C, 3 min
Denaturation: 94°C, 1 min
Annealing: 60°C, 15 sec } *35 cycles*
Extension: 72°C, 15 sec
Final extension: 72°C, 7 min

To confirm that each PCR product was the expected size, an aliquot of each product was mixed with 6x DNA loading buffer (Thermo Fisher Scientific) and loaded onto a 1.5% agarose (Sigma-Aldrich) gel and submerged in 0.5x TBE buffer (Table 2.1). The GeneRuler 1 kb Plus DNA ladder (Thermo Fisher Scientific) was used. After confirming the size, PCR

products were purified using a MinElute® PCR purification kit (Qiagen), according to the manufacturer's instructions. The purified products were sequenced using Sanger DNA Sequencing (Source BioScience) and the sequences visualised with FinchTV (Geospiza) to identify mutations in the LKB1 gene.

2.6 Lentiviral transduction

Lentiviral particles were used to (i) restore LKB1 expression in LKB1 mutated A549 and A427 cells, (ii) to knock-down LKB1 expression in LKB1 wild-type H1299 cells and (iii) to express firefly luciferase in A549 cells (A549+LVP). A549, A427 and H1299 cells were also transduced with empty vector (EV) lentiviral particles as negative controls (Table 2.7, Figure 2.1). All transductions were performed according to the manufacturer's instructions and lentiviruses were thawed once prior to transductions. For ectopic LKB1 expression, $2.5x10^4$ cells were seeded in each well of a 24-well plate and incubated overnight, and then transduced with 25 µL of lentivirus (approximate MOI = 10), and incubated for 72 h before selection with blastocidin followed by expansion. For LKB1 knock-down, $5x10^5$ cells were seeded in T25 flasks and incubated overnight. Cells were then treated with 8 µg/mL polybrene and transduced with 100 µL of lentivirus (approximate MOI = 5) for 24 h. The following day, the medium was replenished and cells were incubated for a further 24 h before selection with puromycin which was followed by expansion. Cells were selected using either 10 µg/mL of blastocidin or 1 µg/mL of puromycin for 7-14 days and maintained at 2.5 µg/mL of blastocidin or 0.5 µg/mL of puromycin. To minimise any effect of clonal variation from differential transduction efficiency, all LKB1 deficient and proficient A549, A427 and H1299 cells used in this study were from un-cloned populations unless otherwise stated. A549+EV, A427+EV and H1299+shLKB represent LKB1 non-expressing or deficient cells and are colour coded red in graphs throughout this thesis. A549+LKB, A427+LKB and H1299+shEV represent LKB1 expressing or proficient cells and are colour

coded blue in graphs. These cells tested negative for mycoplasma using MycoAlert™ (Lonza). A549 cells transduced with firefly luciferase lentiviral particles were kindly provided by Yanyan Jiang.

Table 2.7: Pre-made lentiviral particles

Source and catalogue number	Description	Vector backbone	Insert	Vector function in mammalian cells	Human cancer cell lines transduced	Selection marker
Amsbio # LVP090	Pre-made lentiviral particles for STK11/LKB1 human gene expression (NCBI acession: NM 000455.4)	HIV-1 derived plasmid	STK11/LKB1	Constitutive expression of STK11/LKB1	A549, A427	Blastocidin
Amsbio # CMV-Null-Bsd	Pre-made negative control lentiviral particles	HIV-1 derived plasmid	Negative control (null spacer sequence 200 bp)	Negative control lentivirus expression particles	A549, A427	Blastocidin
Sigma-Aldrich MISSION transduction particles: pLKO.1-puro-shSTK11 (clone: 04081433MN)	Pre-made lentiviral particles for LKB1 knock-down	TRC1 and TRC1.5 lentiviral plasmid vector: pLKO.1-puro	STK11/LKB1 shRNA	Constitutive knockdown of STK11/LKB1	H1299	Puromycin
Sigma-Aldrich MISSION transduction particles: pLKO.1-puro-empty vector control # SHCLNV	Pre-made negative control lentiviral particles	TRC1 and TRC1.5 lentiviral plasmid vector: pLKO.1-puro	No shRNA insert	Empty vector control	H1299	Puromycin
Amsbio # LVP323	Pre-made lentiviral particles for firefly luciferase gene expression	HIV-1 derived plasmid	Firefly luciferase	Constitutive expression of firefly luciferase	A549	Blastocidin

(a)

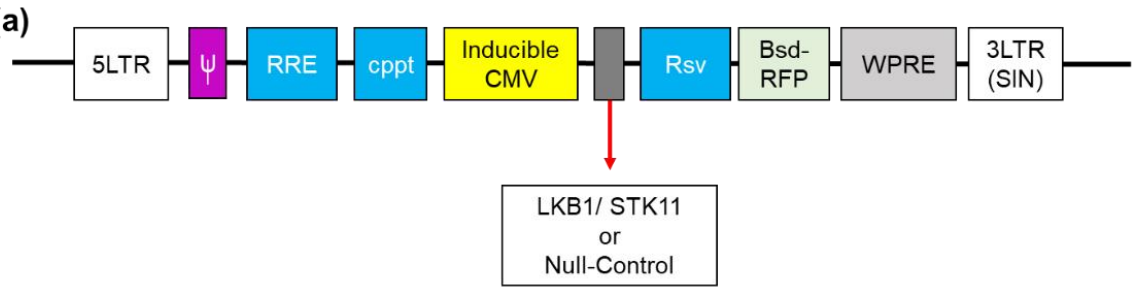

Name	Description
5' LTR	5' long terminal repeat
Ψ	Encapsidation signals
RRE	Rev-response element
cppt	Central polypurine tract (central termination sequence element)
CMV	Cytomegalovirus (promoter)
Rsv	Rous sarcoma virus (promoter)
Bsd-RFP	Blastocidin-Red Fluorescent Protein (selection markers)
WPRE	Woodchuck hepatitis virus post-transcriptional regulatory element
3'LTR (SIN)	3' long terminal repeat (self inactivating)

(b)

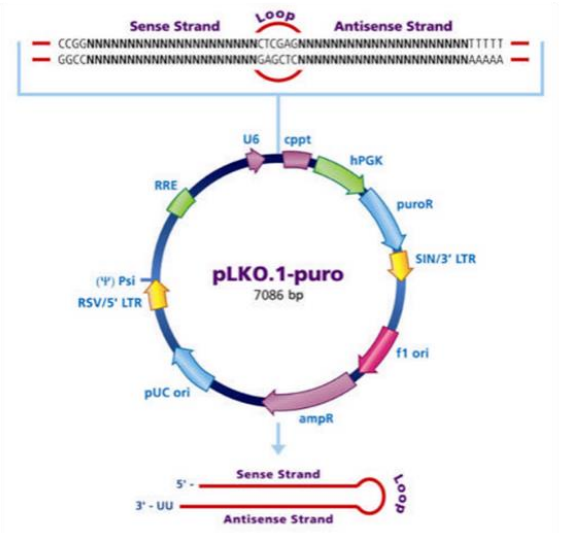

Name	Description
U6	U6 repeat
hPGK	Human phosphoglycerate kinase eukaryotic promoter
puroR	Puromycin resistant gene for mammalian selection
fi ori	f1 origin of replication
ampR	Ampicillin resistance geen for bacterial selection
pUC ori	pUC origin of replication
Psi	RNA packaging signal

Figure 2.1: Lentiviral particles used for restoring functional LKB1 expression and knocking-down LKB1 expression

(a) Amsbio pre-made lentiviral particles for LKB1/STK11 human gene expression or negative control lentiviral particles. (b) Sigma-Aldrich MISSION transduction particles (vector pLKO.1-puro) for either LKB1 knock-down or empty vector (EV) control.

2.6.2 Isolation of clones

Cells were seeded in the presence of blastocidin in a 10 cm petri dish at a low density to allow for distinct colony formation. Independent colonies were isolated using cloning cylinders (Sigma-Aldrich, #C1059) and cells within these colonies were typsinised, resuspended in Advanced DMEM/F12 and transferred to a T25 flask.

2.7 Spheroid production, imaging and determination of area

$1x10^4$ cells in 200 µL of medium were seeded into each well of a low attachment round bottom 96-well plate. For most experiments, lipidure coated plates (Amsbio #AMS.51011610) were used. As this product was discontinued, in later experiments, hydrogel coated plates were used (Corning #7007) (The area of A549+EV spheroids at 5 days post seeding was approximately $5x10^5$ μm^2 in both lipidure and hydrogel coated plates). Immediately post seeding, plates were centrifuged (210x g, 10 min, RT) to form spheroids. Spheroids were incubated at 37˚C with 5% CO_2. Spheroids were imaged using either the CeligoS (NExcelom Bioscience), a Nikon Eclipse TE2000-E microscope or a Nikon Ti-E microscope. To determine changes in spheroid growth, images were acquired at a resolution of 1200 DPI (dots per inch) using a GELCOUNT™ (Oxford Optronix) and area was calculated using a specific spheroid CHARM algorithm. Data was exported to Excel and analysed. In some experiments, CeligoS (tumoursphere migration algorithm) was used to measure area. Figure 2.2 shows that the growth rate of A549+EV spheroids was similar when area was measured using either GELCOUNT™ or CeligoS. The GELCOUNT™ was used to measure spheroid area in all experiments unless otherwise stated. In all experiments, spheroids were seeded in the presence of a compound or in absence of a nutrient, unless otherwise stated.

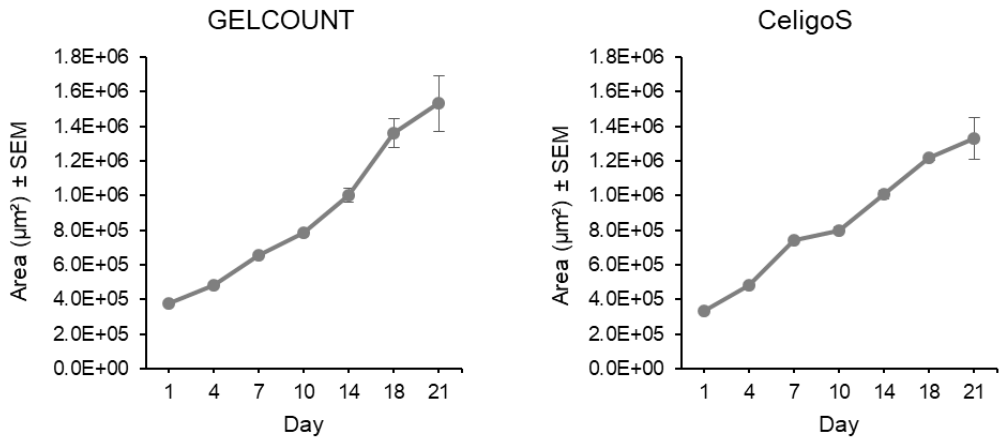

Figure 2.2: Measuring spheroid area using the GELCOUNT and CeligoS
Spheroid area measured in A549+EV cells. Values represent the mean of 12 spheroids.

2.8 Cell proliferation and viability assays

2.8.1 PicoGreen assay in 2D culture and 3D spheroids

PicoGreen is a DNA binding dye that can be used to measure the total amount of dsDNA in cells.

For 2D culture, cell lines were seeded in 96-well plates and incubated at 37˚C overnight (see Table 2.5 for seeding density). At appropriate times, cells were lysed by removing medium and adding 100 µL of 1x DNA lysis buffer (Table 2.1). To determine relative DNA concentration, 100 µL (equal volume) of PicoGreen solution (Table 2.1) was added to the wells and the plates were incubated in the dark at 37˚C for 20 min. Fluorescence intensity (Ex 480nm, Em 520nm) was measured using a plate reader (POLARstar OMEGA BMG Labtech GmbH, Germany). Data was exported to Excel and analysed by subtracting the mean fluorescence value for blank wells (medium with no cells) from the fluorescence value for wells containing cells.

For 3D culture, 10x DNA lysis buffer was added to 100 µL of medium containing spheroids. Spheroids were resuspended by pipetting. 110 µL of PicoGreen solution (Table 2.1) was

added to the wells and the plates were incubated in the dark at 37˚C for 20 min. Fluorescence intensity was measured as described above.

2.8.2 Resazurin assay in 2D culture and 3D spheroids

Resazurin is a sensitive indirect measure of cell viability. Non-fluorescent resazurin is broken down into fluorescent resorufin in metabolically active cells. In particular, resazurin loses an oxygen ion when it is irreversibly reduced by dehydrogenases present within the mitochondria of cells. The oxidized form of resazurin is resorufin. Importantly resorufin can be further broken down into non-fluorescent hydroresorufin, therefore, it is critical to measure fluorescence while it is increasing to avoid underestimating cell viability (O'Brien et al., 2000).

Cell lines were seeded in 96-well plates and incubated at 37˚C (see Table 2.5 for seeding density). Cells in 2D culture were treated one day post seeding, except for the nutrient deprivation experiments where cells were seeded in the absence/lower concentration of the nutrient. At the end of the treatment time, a final concentration of 12.5 µg/mL resazurin (Table 2.1) was added to each well and cells were incubated at 37˚C for 2-3 h (2D culture) or 6-8 h (3D spheroids). Fluorescence intensity (Ex 544 nm, Em 590-610 nm) was measured (POLARstar OMEGA) and the data was exported to Excel and analysed. The mean fluorescence value of blank wells (medium with no cells) was subtracted from the fluorescence value of wells containing cells. Following the assay, cells were fixed and stained with crystal violet (Table 2.1) and the dried plates were stored at RT.

2.8.3 Data analysis for dose response curve generation, IC_{50} determination and the effect of mutation status/LKB1 expression on the IC_{50} value/cell viability

Using the resazurin-based assay described, the effect of the compounds on cell viability was determined by generating a dose response curve and calculating the compound concentration

that reduces viability to 50% of the untreated control (IC_{50}), using curve-fitting software (OriginPro 8.5.1).

2.8.3.1 Dose response curves generation and IC_{50} determination (OriginPro 8.5.1)

Resorufin fluorescence values were normalised to control (untreated) values (%). Non-linear curve fitting (category: growth/sigmoidal, function: dose response) was used with the formula:

$$y = \frac{A1+(A2-A1)}{1+10^{(log_{x0}-x)*p}}$$

where A1 is the top asymptote, A2 is the bottom asymptote, p is the gradient and x is the inflection point

To determine whether IC_{50} values were significantly different between samples, a two sample t-test assuming equal variance was calculated using Microsoft Excel.

2.8.3.2 The effect of mutation status on IC_{50} values (SPSS)

IC_{50} data for the 11 lung cancer cell lines and NBE1 were analysed using factorial ANOVA with LKB1, KRAS, BRAF and TP53 mutation status as factors. The mutation status for each gene is shown in Table 2.3 and Figure 3.1. The mutation status for KRAS, BRAF and TP53 was classified as unknown in CORL105 and NBE1. However, regarding LKB1, CORL105 was confirmed to be LKB1 wild-type and LKB1 protein expression was confirmed in NBE1 (Section 3.2). Using ANOVA, the effect size of each factor was determined using a partial eta squared (η^2) generated and Cohen's rule of thumb (Cohen, 1988) where:

$\eta^2 < 0.02$ - no effect

$\eta^2 \geq 0.02 < 0.13$ - small effect

$\eta^2 \geq 0.13 < 0.26$ - medium effect

$\eta^2 \geq 0.26$ - large effect

η^2 is the proportion of the IC_{50} value that is attributable to the factor. The observed power for the η^2 was computed using a p-value of 0.05. The higher the observed power, the greater the probability that the effect was real (i.e. the mutation status affected the IC_{50} value).

2.8.3.3 The effect of cell line on cell viability using a dose response curve

Cell viability data was analysed using factorial ANOVA with cell line (LKB1 deficient, LKB1 proficient) as a factor. The effect size of each factor was determined using partial eta squared (η^2) and Cohen's rule of thumb, as described above.

2.9 *In vivo* work

All animal procedures were performed under a project license issued by the U.K. Home Office after local ethical committee review and in accordance with the U.K. legal requirements under the Animals Scientific Procedures Act of 1986. All mice were housed in individually ventilated cages within the Biomedical Services (BMS) facility under specific pathogen-free conditions. Food and water was provided *ab libitum*.

2.9.1 Sub-cutaneous xenografts

Female CD1 nude mice were purchased from Charles River Laboratories, U.K. At 6-8 weeks of age, mice were anaesthetised using isoflurane in air/oxygen. Approximately 4% isoflurane was used for induction of anaesthesia and 2-3% for maintenance depending on the breathing rate and depth of anaesthesia. Oxygen was supplied at a rate of 1-2 L/min. 100 µL suspensions containing $5x10^6$ cells in Advanced DMEM/F12 (FBS and antibiotic free) with 50% (v/v) matrigel (Corning, #356234) were injected sub-cutaneously into the back of each anaesthetised mouse. All mice were implanted on the same day except mouse number three in the LKB1 proficient A549 group, which was implanted one day later. Tumour size (length, width and height) was measured using a calliper, three times per week. Tumour volumes were calculated using the formula:

Volume *(mm^3) = ½ x [length (mm) x width (mm) x height (mm)]*

Mice were sacrificed either when their tumour size reached 400 mm^3 or at 48 days post injection of cells. 1 h prior to sacrifice, mice received bromodeoxyuridine (BrdU) (100 mg/kg) (Life Technologies #1448868) by intraperitoneal (i.p.) injection (200 µl per mouse of 10 mg/mL BrdU dissolved in saline, mouse weight approximately 20 g). For RNA isolation, part of the tumour was excised and snap frozen by placing on dry ice and then stored at - 80ºC until RNA extraction. The remaining tumour tissue was fixed in > 10 volumes of 4% PFA (Table 2.1) at 4ºC overnight and then stored in 70% ethanol at 4ºC until further tissue processing and paraffin embedding (Section 2.13.3). To determine if the difference in tumour volume between groups was significant, a two sample t-test assuming equal variance was calculated using Microsoft Excel.

2.9.2 Lung orthotopic model

Female BALB/c nude or NOD/SCID gamma (NSG) mice (6-8 weeks of age) were purchased from Charles River Laboratories, U.K. Mice were anaesthetised using either (i) a combination of domitor (0.5 mg/kg) and ketaset (40 mg/kg) (i.p.) (100 µL per mouse of a solution containing 0.1 mg/mL domitor and 8 mg/mL ketaset in saline, mouse weight approximately 20 g) or (ii) isoflurane in air/oxygen (as described in Section 2.9.1). Mice were then placed in the right lateral decubitus position following the method of Onn et al (Onn et al., 2003). In brief, a 50 µL suspension containing $1x10^6$ cells in Advanced DMEM/F12 (FBS and antibiotic free) with 50% (v/v) matrigel was injected into the left lung of each anaesthetised mouse. Mice were kept in the right lateral decubitus position for a further 5 min. Mice were then turned to the left lateral decubitus position for another 5 min. For mice anaesthetised with domitor/ketaset, animals were awakened using antisedan (2 mg/kg, i.p.) (200 µL per mouse of 0.2 mg/mL in saline, mouse weight approximately 20 g).

IVIS or MRI was used to monitor tumour burden (Section 2.9.3, 2.9.4). On day 14 (orthotopic model 1) or 16 (orthotopic model 2 and 3), mice were sacrificed and the lungs were weighed. Lungs were either fixed in 4% PFA at 4ºC overnight and stored in 70% ethanol at 4ºC until processing and embedding (Section 2.13.3), or lungs were placed in ~ 10 volumes (left lung - 400 µL, right lung - 1 mL) of RNAlater® (Ambion #AM7020) and on ice. Samples in RNAlater were stored at 4ºC overnight and subsequently stored at - 20ºC until protein and RNA extraction (Section 2.12.3). To determine if the tumour burden was significantly different between groups, a two sample t-test assuming equal variance was calculated using Microsoft Excel. To examine the correlation between endpoints, Pearson R was calculated (Microsoft Excel).

2.9.3 *In vivo* imaging system (IVIS)

5 min prior to imaging, mice were injected with luciferin (sc-218662) (150 mg/kg, i.p.) (200 µL per mouse of 15 mg/mL luciferin dissolved in 1x PBS, mouse weight approximately 20 g) and anaesthetised using isoflurane in air/oxygen (as described in Section 2.9.1). Images were acquired using IVIS Spectrum (PerkinElmer) at 5 min intervals for 40 min or until maximum light was collected (i.e. the signal started decreasing). Data was analysed using LivingImage software to calculate the radiance (i.e. photon per second per centimetre squared per steradian (p/s/cm^2/sr)).

2.9.4 Magnetic resonance imaging (MRI)

MRI is a non-ionising imaging technique that can be used to delineate soft tissue by the detection of protons. It exploits the influence of the surrounding proton environment on the precession frequency (also known as the resonance/Larmor frequency) of individual protons. By placing the “object” in a strong magnetic field and delivering an external radiofrequency (RF) pulse (equal to the resonance frequency), protons can be pushed into transient high energy states. This change in energy state alters the net magnetisation vector

of the protons, which generates a maximal imaging signal at an angle to this vector once protons lose the energy. The signal is processed using complex Fourier Transform techniques to convert frequency encoded data to spatially encoded data, which can be used to generate an image.

A method for MR imaging of mice was previously established by the Imaging Core at the University of Oxford. Prior to imaging, mice were anaesthetised using isoflurane in air/oxygen (as described in Section 2.9.1). MRI was performed on a 4.7 Tesla (T), 310 mm horizontal bore Varian Nuclear Magnetic Resonance Spectrometer (VNMRS) preclinical imaging system equipped with a 120 mm bore gradient insert capable of 400 milliTesla/metre (mT/m) in all three axes (Varian Inc, CA). RF transmission and reception was performed with a 30 mm long, 25 mm quadrature birdcage coil (Rapid Biomedical GmbH, Germany). Balanced steady-state free precession (SSFP) scans were acquired with repetition time (TR): 2.684 ms, echo time: (TE) 1.342 ms, flip angle (FA): 20°, field of view (FOV): 48×24×24 mm^3, matrix: 256×96×96 and RF hard pulse duration 16 μs. Prospective cardio-respiratory gating was performed with acquisition of 8 phase encode lines per cardiac R-wave and centric out ordering to align data acquisition to within a 25 ms window starting at the R-wave. Data were acquired with and without phase alternation of the RF transmitter and receiver. A maximum intensity projection (MIP) of the two data sets was performed to minimise banding artefacts in the final image.

MR images were analysed using ITK-SNAP (Yushkevich et al., 2006). Automatic segmentation was used to identify the lungs and manual segmentation was used to identify the tumour. This software gave a 3D reconstruction of the lungs with tumours, and was used to calculate lung and tumour volumes.

2.10 RNA isolation, mRNA sequencing and analysis

2.10.1 RNA isolation and purification

For 2D culture, prior to RNA isolation, cells were grown in Advanced DMEM/F12 on 10 cm petri dishes for 2 days. 24 h prior to RNA isolation, the medium was changed. Immediately prior to isolation, the medium was removed and sub-confluent cells were washed with 1x PBS before the addition of 600 µL of RLT buffer (RNeasy® plus mini kit). Cells were removed from the dish with a cell scraper (Sarstedt) and placed in a 1.5 mL Eppendorf tube.

For 3D spheroids, $1x10^4$ cells per well (200 µL medium) were grown in lipidure coated 96-well plates for 5 days. RNA was extracted on day 5 as spheroids had surpassed their condensation phase and were into their growth phase (Figure 3.7). 24 h prior to isolation, half of the medium in each well was replaced. 15 spheroids per sample were collected into 1.5 mL Eppendorf tubes using a 1 mL tip widened by cutting. Spheroids were centrifuged (100x g, 30 sec) to allow for removal of the medium. Spheroids were washed once with 1x PBS, re-centrifuged and the PBS was discarded. The pellet was resuspended in 350 µL of RLT buffer.

For snap frozen sub-cutaneous xenografts, 600 µL RLT buffer was added to ~ 30 mg of frozen tissue and samples were immediately homogenized by vigorous shaking (50 Hz, 2-10 min) in screw cap tubes (StarLab #E1420 2641), containing a 5 mm stainless steel bead (Qiagen #69989)), using a TissueLyserLT (Qiagen).

All samples were mixed several times using syringes after the addition of RLT buffer and the RNA was extracted using the RNeasy® plus mini kit (Qiagen), according to the manufacturer's instructions.

The concentration and purity of the RNA was measured on a NanoDrop 1000 spectrophotometer. The concentration ranged from 35.8 -1094 ng/µL. The absorbance ratio

(260 nm/280 nm) was between 2.01 - 2.16 indicating sufficiently pure RNA preparations. Purified RNA was stored at – 80ºC until use.

2.10.2 RNA Sequencing

Duplicate samples (1 μg RNA in 30 μL) were analysed by Oxford Gene Technology (OGT) and gene expression quantified using a previously described analysis pipeline (Trapnell et al., 2012). The sequencing libraries were prepared using TruSeq RNA Sample Prep Kit v2 (Illumina). For preparation, the mRNA was isolated (by poly (A) capture), fragmented, randomly primed and reversed transcribed to generate the cDNA. Second strand synthesis was used to generate dsDNA and DNA ends were repaired, phosphorylated and "A" tailed. Adapter ligation and PCR amplification was used to prepare the library for sequencing. Using the HiSeq2000 platform (Illumina), paired-end sequencing was performed over 200 cycles to produce 100 bp reads. Using Bowtie (http://bowtie.cbcb.umd.edu/), an average of 28,215,145 paired end reads per sample were mapped onto the human genome (GRCh37) and using TopHat ((http://tophat.cbcb.umd.edu), splice junctions identified. Using Cufflinks (http://cufflinks.cbcb.umd.edu/), the mapped reads were assembled into transcripts and the fragments per kilobase per million mapped reads (FPKM) was calculated to investigate the gene abundance. Differential gene expression between samples was determined and was expressed as $\log_2$ fold change (fc). This was considered statistically significant when the q-value was < 0.05. Q-value is an adjusted p-value that accounts for the false discovery rate (FDR) within the positivity test. Some gene transcripts were not quantifiable as the expression level was below the detection limit. When comparing differences in gene expression between samples, genes which had a FPKM score of zero in one or more of the samples were excluded from gene ontology analysis.

2.10.3 mRNA expression analysis

Gene ontology (GO) analysis was performed using GOrilla and MetaCore™ KPA (key pathway advisor).

2.10.3.1 GOrilla analysis

GOrilla (Gene Ontology enRIchment anaLyses and visuaLisAtion tool) (http://cbl-gorilla.cs.technion.ac.il) was used for biological process enrichment analysis (Eden et al., 2009, Eden et al., 2007). The unranked target gene list (differentially expressed genes with q-value < 0.05) was compared to a background list of 14,233 human genes (Appendices Table A2.11). This determined enrichment of the target set compared to the background set using hyper geometric statistics:

$$\textbf{\textit{Enrichment}} = \frac{b/n}{B/N}$$

N = total no. of genes (in target and background list that are recognised by GOrilla (any duplicates removed))

B = total no. genes associated with a specific GO term

n = no. of genes in the target set

b = no. of genes in the intersection (in target set associated with a specific GO term)

A p-value for this enrichment was calculated, and additionally an FDR q-value (corrected p-value) which was calculated using the following formula (Benjamini and Hochberg, 1995):

$$\textbf{\textit{FDR q-value}} = \frac{p\text{-}value\ x\ no.\ GO\ terms}{rank\ of\ GO\ term\ according\ to\ p\text{-}value}$$

2.10.3.2 MetaCore™ KPA

To identify pathways that were associated with genes expressed at higher or lower levels in LKB1 deficient cells, MetaCore™ KPA software was used (https://portal.genego.com) (Thomson Reuters, USA). For this, the $\log_2$fc and the q-value for each gene was required.

The significant genes were identified as those with a q-value < 0.05 for 2D and 3D models, or with a q-value ≤ 0.05 for human tumours.

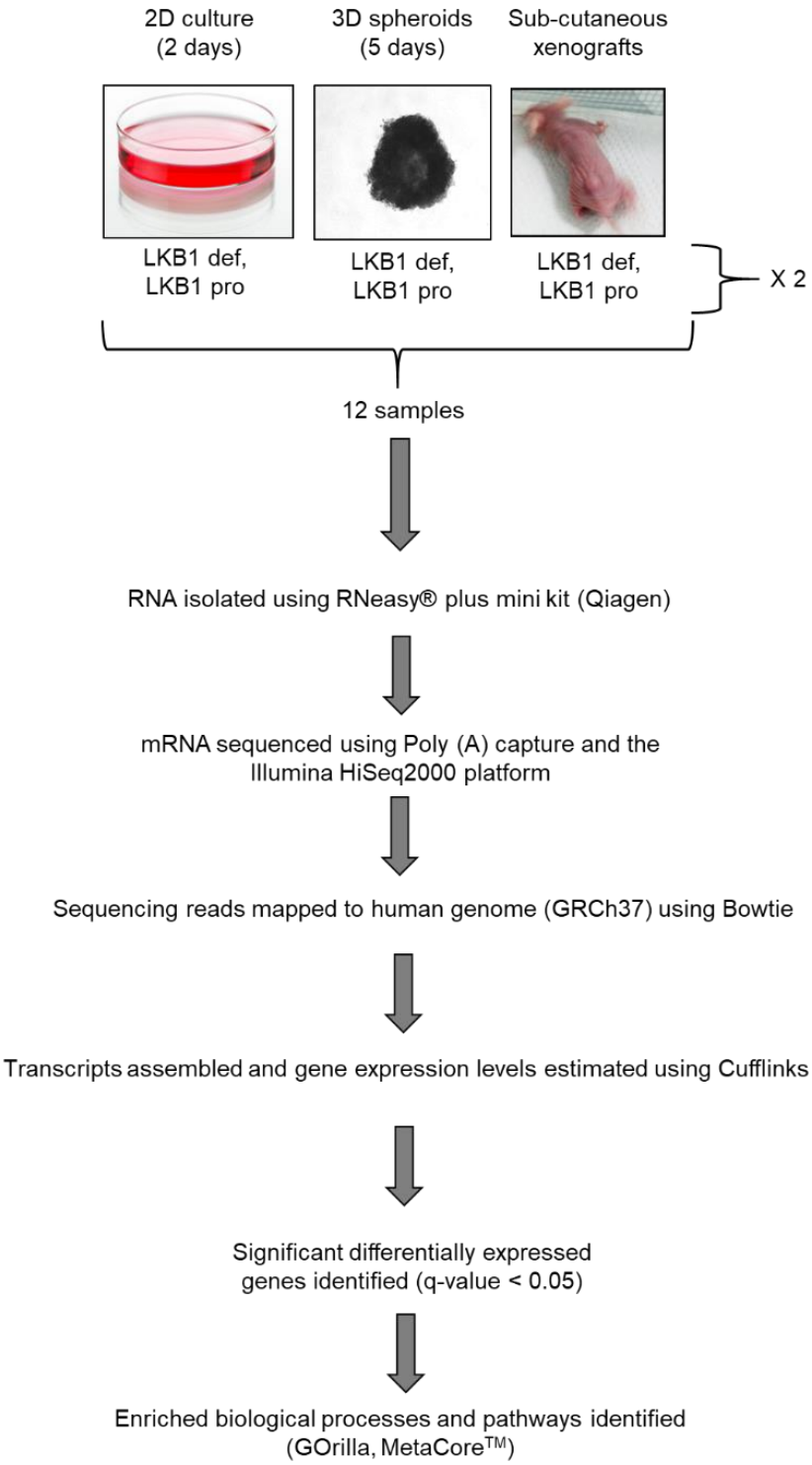

Figure 2.3: Schematic showing RNA isolation, mRNA sequencing and analysis
LKB1 def – LKB1 deficient cells (A549+EV), LKB1 pro – LKB1 proficient cells (A549+LKB). The LKB1 deficient xenografts were from mouse no. 1 and no. 3. The LKB1 proficient xenografts were from mouse no. 3 and no. 4. (see Figure 3.14 for xenograft data).

2.11 Bioactive small molecule screen in 2D and 3D models

2.11.1 Bioactive small molecule screen in 2D culture

2.11.1.1 Endpoints

To measure the efficacy of compounds used in the bioactive small molecule screen; we measured differences in apoptosis and proliferation between the cell lines. Inhibition of proliferation was measured using resazurin (as described in Section 2.8.2). The apoptosis assay used was a Hoechst DNA binding "live" cell assay previously reported by Bokobza et al (Bokobza et al., 2014). Hoechst can be used to distinguish between live and dead cells as Hoechst is taken up faster in dead cells and apoptotic cells have a condensed nucleus. Therefore, the extent of Hoechst signal intensity and the size of the nucleus is dependent on cell viability. Compared to normal, non-apoptotic cells, apoptotic cells have a brighter Hoechst signal and a smaller nuclei. Cells were incubated with Hoechst and imaged using the IN Cell analyser. These images were analysed using the IN Cell automated analysis software which counts the number of bright apoptotic cells and the number of normal cells by quantifying the nuclear Hoechst signal intensity. A threshold was set for nuclear staining intensity (low vs. high Hoechst staining) and condensed nuclei with high Hoechst staining (above set threshold) were scored as apoptotic/dead. The high threshold was set above the signal intensity for mitotic nuclei to reduce the possibility of identifying false positive "hits" as mitotic nuclei are also condensed with a bright Hoechst signal (Figure 2.4).

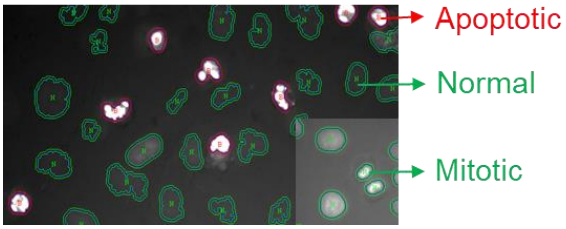

Figure 2.4: Hoechst DNA binding live cell assay
Hoechst can be used to distinguish between live, mitotic cells and apoptotic cells by measuring difference in signal intensity using the IN Cell automated software.

2.11.1.2 Screen set-up and analysis of Hoechst images

Cells were seeded in 96-well plates using phenol red free DMEM/F12 and incubated at 37˚C overnight (see Table 2.5 for seeding density). Phenol red free DMEM/F12 supplemented with 10% FBS was used in this screen to rule out any effect of phenol red on Hoechst fluorescence (Ettinger and Wittmann, 2014). One day post seeding, cells were treated with compounds (1 or 0.1 µM, Selleck Library L1100) for 72 h in the primary, secondary and tertiary screen, and from 6-72 h for confirmation of the hits in the quaternary screen. To investigate apoptosis, the cells were incubated with 20 µg/mL Hoechst 33258 (Table 2.1) for 45 min and images were acquired using the IN Cell Analyser 1000 (GE Healthcare). Following this, inhibition of proliferation was determined using a resazurin assay (as described in Section 2.8.2) (Figure 2.5). Following acquisition, Hoechst images were analysed using IN Cell automated software analysis as described above.

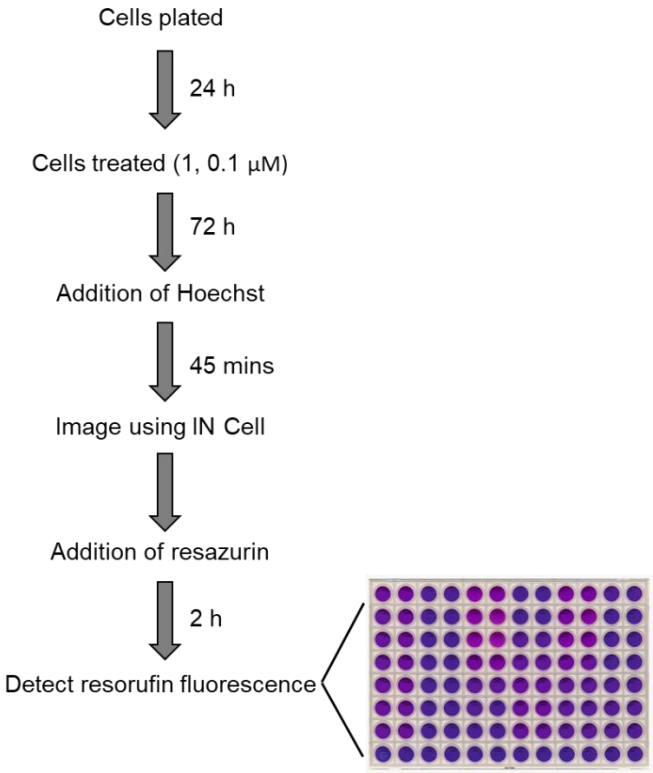

Figure 2.5: Schematic for the experimental set-up in the bioactive small molecule screen in 2D culture (primary, secondary and tertiary screen)

2.11.1.3 Data analysis

To determine the efficacy of the inhibitors, the following calculations were used:

$$\textbf{\textit{Fold change for induction of apoptosis}} = \frac{\%\ apoptotic\ cells\ after\ treatment\ with\ test\ compound}{mean\ \%\ apoptotic\ cells\ in\ DMSO\ treated\ controls}$$

$$\textit{where \% apoptotic cells} = \left(\frac{apoptotic\ cell\ no.}{total\ cell\ no.}\right) \textit{x 100}$$

$$\textbf{\textit{\% inhibition of proliferation}} = \left(\frac{resorufin\ fluorescence\ after\ treatment\ with\ test\ compound}{mean\ resorufin\ fluorescence\ in\ DMSO\ treated\ controls}\right) \textit{x 100}$$

We expected DMSO treated controls to have a value = 1 for fold change induction of apoptosis and a value = 100% when measuring inhibition of proliferation.

To identify compounds with selectivity for either LKB1 deficient or proficient cells, the following calculation was used:

$$\textbf{\textit{Difference in sensitivity between cell lines:}}\ log_{10}\left(\frac{change\ in\ LKB1\ deficient}{change\ in\ LKB1\ proficient}\right)$$

where "change" indicates either:
(i) the fold change for induction of apoptosis or
(ii) the % inhibition of proliferation

A $\log_{10}$ value of 0 indicates no difference in sensitivity to a compound as there was a similar response in both LKB1 deficient and proficient cells ($\log_{10}(1) = 0$). For induction of apoptosis, a positive value indicated greater induction of apoptosis in the LKB1 deficient cells. For proliferation, a negative value indicated selective inhibition of proliferation in LKB1 deficient cells. Potential positive (selective for LKB1 deficient cells) and negative (selective for LKB1 proficient cells) "hit" compounds were identified as having a $log_{10}\left(\frac{change\ in\ LKB1\ deficient}{change\ in\ LKB1\ proficient}\right)$ value $\geq \pm$ 2x standard deviation (SD) from (i) the mean of all samples (DMSO treated controls and test compound treated samples) in the primary screen or (ii) the mean of the DMSO treated controls in the secondary and tertiary screen.

This was because, in the primary screen, active and inactive compounds were tested, therefore, the SD was calculated for all the values (compound treated and DMSO treated). In the secondary screen, only active compounds were used, therefore the SD was calculated for the DMSO treated controls only.

Pearson's correlation was calculated using Microsoft Excel to investigate the reproducibility between duplicates of one experiment and between independent experiments in the primary screen.

2.11.2 Bioactive small molecule screen in 3D spheroids

$1x10^4$ cells per well were seeded in the presence of inhibitor (10 μM), in lipidure coated 96-well plates. Seeding, determination of area (using GELCOUNT™) and imaging (using Nikon Ti-E microscope) was completed as described in Section 2.7.

2.11.2.2 Data analysis

For each cell line on each day, the area of each compound treated spheroid was calculated as a percentage of the area of the DMSO treated spheroids. Positive "hits" (i.e. compounds that selectively reduced the area of LKB1 deficient spheroids) were identified as those that reduced the area of the LKB1 deficient spheroids to a percentage lower than the maximum reduction in area found in a LKB1 proficient spheroid after treatment with any compound on day 8 post seeding.

For each cell line on each day:

$$\textbf{\textit{\% change in spheroid area}} = \left(\frac{spheroid\ area\ after\ treatment\ with\ test\ compound}{mean\ spheroid\ area\ in\ DMSO\ treated\ controls}\right) x\ 100$$

$$\textbf{\textit{Positive hit}} = \frac{\%\ change\ in\ spheroid\ area\ \ of\ LKB1\ deficient}{max\ \%\ change\ in\ spheroid\ area\ \ of\ LKB1\ proficient} < 1, \quad on\ day\ 8$$

Hits were confirmed by manually examining the density and integrity of spheroids using images acquired on the microscope. Final hits were those that selectively reduced the area of LKB1 deficient spheroids on day 8 but did not change the area or density of LKB1 proficient spheroid.

2.12 Protein extraction, SDS-PAGE and western blotting

Whole cell protein was extracted in all experiments unless otherwise stated.

2.12.1 Whole cell protein extract - 2D culture

Cells were seeded in 6-10 cm dishes and incubated at 37°C until sub-confluent. For compound treated cells, cells were incubated overnight before treatment with a compound or alternatively, for glucose or glutamine deprivation experiments, cells were seeded in the absence of these nutrients. Following incubation, cell lysates were prepared on ice by washing twice with ice-cold 1x PBS, followed by the addition of protein lysis buffer for whole cell extract (Table 2.1). Cells were incubated with protein lysis buffer for 10 min and transferred to a 1.5 mL Eppendorf using a cell scraper. Lysates were then homogenized by sonication (2x 10 sec cycles using Bioruptor® Plus, Diagenode) and cell debris was removed by centrifugation (16,100x g, 15 min, 4˚C). Protein concentration was measured using the NanoDrop 1000 spectrophotometer.

2.12.2 Whole cell protein extract - 3D spheroids

$1x10^4$ cells per well were seeded in low attachment round bottom 96-well plates as described in Section 2.7. Spheroids were incubated at 37°C for 5 days. Spheroid protein was extracted on day 5 post seeding as the spheroids had surpassed their condensation phase and were into their growth phase (Figure 3.7). Also, RNA sequencing was performed on 5 day old spheroids.

Spheroids were collected in 1.5 mL Eppendorf tubes using a 1 mL pipette tip with the end widened by cutting. Tubes were centrifuged (100x g, 30 sec) and the medium was removed. 500 µL of ice-cold 1x PBS was added and tubes were centrifuged again before the removal of the PBS. 30 µL of protein lysis buffer for whole cell extract (Table 2.1) was added per 10 spheroids. Lysates were homogenised by sonication (≥ 2x 10 sec cycles), pipetting and vortexing, and cell debris was removed by centrifugation (16,100x g, 15 min, 4˚C). Protein concentration was measured using the NanoDrop 1000 spectrophotometer.

2.12.3 Whole cell protein extract - mouse lungs

As mentioned, lung tissue was placed in ~ 10 volumes of RNAlater® and placed on ice. Samples were stored at 4˚C overnight and then stored at - 20˚C until protein and RNA extraction. Protein was extracted using the PARIS^{TM} kit (Ambion #AM1921). Tissues were placed in the PARIS kit cell disruption buffer with addition of 1 mM sodium orthovanadate and 1x protease inhibitor (Table 2.1) (~ 400 µL per 50 mg of tissue). Tissues were then homogenised by vigorous shaking (50 Hz, 2-5 min) in screw cap tubes containing a 5 mm stainless steel bead and using a TissueLyserLT. Protein and RNA extractions were carried out further according to the manufacturer's instructions. Protein concentration was measured using the NanoDrop 1000 spectrophotometer.

2.12.4 Cytoplasmic and nuclear protein extract - 2D culture

Cells were seeded in 10 cm petri dishes until sub-confluent. Cell lysates were prepared on ice by removal of medium, washing twice with ice-cold 1x PBS followed by the addition of 600 µL of 1x PBS. Cells were transferred into 1.5 mL Eppendorf tubes using a cell scraper. Tubes were centrifuged (100x g, 5 min, 4˚C). The supernatant was removed and the cell pellet was resuspended by vortexing in 400 µL protein lysis buffer for cytoplasmic protein extract (Table 2.1). Lysates were incubated for 30 min at 4˚C with agitation. 0.063 volumes

of 10% (v/v) NP40/IGEPAL was added and samples were vortexed for 10 sec. Lysates were centrifuged (16,100x g, 1 min, 4˚C) and the supernatant contained the cytoplasmic fraction.

For extraction of nuclear protein, the pellet was washed with buffer for extraction of cytoplasmic protein and centrifuged (16,100x g, 1 min, 4˚C). The supernatant was removed and the pellet was resuspended in 80 µL of protein lysis buffer for nuclear protein extract (Table 2.1). Samples were vortexed strongly and incubated for 1 h at 4˚C with agitation, and additional vortexing every 15 min during this time. Lysates were centrifuged (16,100x g, 10 min, 4˚C) and the supernatant contained the nuclear fraction.

2.12.5 SDS-polyacrylamide gel electrophoresis (PAGE) and immunoblotting (western blotting)

Samples were prepared in Laemmli sample loading buffer and protein lysis buffer. For Laemmli sample loading, either 1 volume of 2x sample buffer (Sigma-Aldrich #S3401-AVL) or 0.2 volumes of 5x sample buffer (Table 2.1) was used. Samples were heated at 95˚C for 5 min and then loaded onto 4-15% or 4-20% gradient gels. Electrophoresis was completed in running buffer (Table 2.1) at 220 volts (V) for 22-25 min (Mini-PROTEAN® Precast stain free gels (Bio-Rad Laboratories)) or at 150 V for 50-60 min (Criterion™ TGX stain free gels (Bio-Rad Laboratories)). Protein was transferred to a nitrocellulose membrane (0.45 µm, Bio-Rad #162-0115) in transfer buffer (Table 2.1) at 150 V for 35 min (Mini-PROTEAN® Precast gels) or at 90 V for 1 h (Criterion™ TGX gels).

The nitrocellulose membrane was treated with the appropriate blocking buffer (Table 2.1) for 1 h at RT. Membranes were incubated with primary antibodies (Table 2.8) diluted in the appropriate antibody buffer (Table 2.1) overnight at 4˚C. Following this, membranes were washed 3 times with 1x PBS-T (5 min each) and incubated with secondary antibodies (Table

2.8), diluted in the appropriate antibody buffer (Table 2.1), for 1 h at RT. Membranes were then washed 3 times with 1x PBS-T and 3 times with 1x PBS only (5 min each).

Secondary antibodies were either conjugated to fluorophores (fluorescence detection) or to horse radish peroxidase (HRP) (for enhanced chemiluminescence (ECL) detection). For fluorescence, bands were detected and quantified using Odyssey® Infrared Imaging System (LI-COR Biosciences). For ECL, bands were detected by membrane incubation with luminol (substrate for HRP) (Pierce® ECL Western Blotting Substrate RA226171, Thermo Fisher Scientific #32106) and the signal was detected using a Bio-Rad ChemiDoc Imaging system. Fluorescence detection was generally used, unless otherwise stated.

Bands were quantified using either Odyssey® Image Studio software or Image Studio Lite Ver 5.2. For quantification, band intensities were normalised to the loading control (PPIB (peptidylprolyl isomerase B) or β-actin) for each individual blot. Protein names were colour coded to the loading control used for the same gel. To determine if the difference in signal between samples was significant, a two sample t-test assuming equal variance was calculated using Microsoft Excel.

Table 2.8: Antibodies for western blotting

Antibody name (clone)	Dilution[1]	Source and catalogue number
ACC pAb[2]	1:1000	CST[3] #3662
ACC-phospho[4] S79 (D7D11)	1:1000	CST #11818
AMPKα (F6)	1:1000	CST #2793
AMPKα-phospho T172 (40H9)	1:500	CST #2535
β-actin (AC-15)	1:5000	Sigma-Aldrich #A1978
CA9 pAb	1:1000	Abcam # ab15086
COX2 (D5H5)	1:1000	CST #12282
CPS1 (EPR7494)	1:1000	Abcam #ab128942
Cyclin A2 (6E6)	1:500	Abcam #ab16726
GLUT1 pAb	1:2500	Abcam #ab14683
H3K36ME3 (Mab-183-050)	1:1000	Diagenode #C15200183
Histone H2A.X phospho S139 (JBW3010)	1:1000	Millipore #05-636
LKB1 (27D10)	1:1000	CST #3050
MARK phospho family activation loop pAb	1:500 in TBS	CST #4836

Mitochondria (113-1)	1:1000	Abcam #ab92824
MO25α (C49D8)	1:1000	CST #2716
Mouse conjugated to HRP	1:5000	Thermo Fisher Scientific #31430
Mouse IgG (H + L) conjugated to IRDye® 680RD	1:5000	Odyssey®, LI-COR Biosciences, UK #926-68070
Mouse IgG VeriBlot conjugated to HRP	1:1000	Abcam # ab131368
PARP pAb	1:2000	CST #9542
PDE4B pAb	1:1500	Abcam #ab14612
PDK4 (1C2BG5)	1:500	Abcam #ab110336
PPIB pAb	1:2000	Abcam #ab16045
Rabbit conjugated to HRP	1:5000	Thermo Fisher Scientific #31460
Rabbit IgG (H + L) conjugated to IRDye® 800CW	1:5000	Odyssey®, LI-COR Biosciences, UK #926-32211
SIK1 pAb	1:400	Proteintech #51045-1-ap
STRADα (EPR15603)	1:1000	Abcam #ab192879

[1] All antibodies were diluted in a PBS based solution unless otherwise stated
[2] pAb - polyclonal antibody
[3] CST- Cell Signalling Technology, Inc (Danvers, USA), Abcam - Abcam, plc, Cambridge, UK
[4] phospho - phosphorylated

2.13 Formalin fixation and paraffin embedding (FFPE)

2.13.1 FFPE - cell pellets

Cell lines were grown in T75 flasks until sub-confluent. Cell lines were harvested by trypsinisation and the cell suspension was placed in a 15 mL centrifuge tube. Cell pellets were formed by centrifugation (225x g, 5 min). The cell pellets were fixed in ~ 1 mL of 3% PFA (Table 2.1) at 4ºC overnight. PFA was then removed and cell pellets were stored in 70% ethanol at 4ºC until paraffin embedding. Paraffin embedding was carried out in OIRO IHC Core (Marcus Green) or in the Sir William Dunn School of Pathology (Richard Stillion). For the staining procedure, 5 μm thick sections were cut using a Leica RM2125 microtome and mounted onto charged slides (Thermo Fisher Scientific #J3800AMNZ).

2.13.2 FFPE - 3D spheroids

$1x10^4$ cells were seeded per well on low attachment round bottom 96-well plates as described in Section 2.7. Spheroids were incubated at 37°C for 5 days. Spheroids were fixed

at 5 days for all immunohistochemistry and immunofluorescence images (as the spheroids had surpassed their condensation phase and are into their growth phase (Figure 3.7)). The 96-well spheroid plates were placed on a pre-warmed tray and spheroids were collected using a 1 mL pipette tip with the end widened by cutting. Spheroids were place in a 1.5 mL Eppendorf tube. Tubes were centrifuged (100x g, 30 sec) and the medium was removed. 500 µL of 1x PBS was added and tubes were centrifuged again. The PBS was removed and spheroids were fixed in 10% neutral buffered formalin (Sigma-Aldrich #HT501128-4L) (30 µL per ~10 spheroids) for 30 min at RT. Formalin was removed and spheroids were washed in 1x PBS. The spheroids were carefully placed on a glass slide and excess PBS was removed with a 10 µL tip. 1% (w/v) agarose (Sigma-Aldrich) dissolved in 1x PBS was liquefied by heating and gently placed over the spheroids on the glass slide and left to solidify. The agarose containing the spheroids was placed into a biopsy insert (Thermo Fisher Scientific #12618366) which was placed in a histosette® (Simport® #M490-3) and stored in 70% ethanol at 4ºC until embedding. Paraffin embedding was carried out by Neele Drobnitzky or Marcus Green. For the staining, 5 µm thick sections were cut and mounted onto charged slides.

2.13.3 FFPE - mouse tissue (sub-cutaneous xenografts and lungs)

As mentioned, mouse tissues were immediately placed in > 10 volumes of 4% PFA and stored at 4ºC overnight. The following day, the PFA was removed and the tissue was placed in 70% ethanol at 4ºC until embedding. Paraffin embedding was carried out by Marcus Green or Richard Stillion. For staining, 5 µm thick sections were cut and mounted onto charged slides.

2.14 Haematoxylin and Eosin (H and E) staining

Sections were heated (50˚C, 10 min), dewaxed by immersing twice in citroclear (HD Supplies, UK) and hydrated by immersing twice in 100% ethanol, once in 70% ethanol, once in 50% ethanol (3 min each) and then rinsed in dH_2O.

2.14.1 Haematoxylin staining

Slides were immersed in filtered (filter VWR #516-0820) Harris's hematoxylin (VWR #351945S) for 3-5 min, followed by running tap water for 3 min, and then rinsed in dH_2O. Slides were sequentially dipped (10 times each) in acid alcohol, dH_2O, Scott's tap water, dH_2O, lithium carbonate and finally dH_2O (see Table 2.1 for composition of solutions).

2.14.2 Eosin staining

Slides were sequentially dipped (10 times each) in 50%, 70%, 90% and 90% ethanol. Slides were immersed in alcoholic Eosin (Sigma-Aldrich #HT110132) for 2-3 min. Slides were sequentially dipped (10 times each) in 90% ethanol followed by three more 90% ethanol solutions.

2.14.3 Mounting

Slides were dipped 10 times each in 100% ethanol followed by another 100% ethanol and immersed twice in xylene for 1 min each. Excess liquid was removed and cover slips (Thickness #1, VWR #631-0137) were mounted using DPX mountant. Slides were left to air dry at RT overnight and air dried slides were scanned at 40x magnification using the Aperio ScanScope CS digital slide scanner.

2.15 Immunocytochemistry/immunohistochemistry (IHC)

Sections were heated (50˚C, 10 min), dewaxed by immersing twice in citroclear (HD Supplies, UK) and hydrated by immersing twice in 100% ethanol, once in 70% ethanol, once

in 50% ethanol (3 min each) and then rinsed in dH_2O. For details on the primary antibodies used, dilutions, incubation times and antigen retrieval, see Table 2.9. In brief, antigen retrieval was performed in sodium citrate buffer at pH 6 (Table 2.1) and heat was applied using a Decloaker Chamber (Biocare Medical). Slides were left in citrate buffer at RT for 20 min to cool. Prior to blocking, slides were washed in 1x PBS-T (3 min) and cells/tissue were outlined with a hydrophobic barrier pen. Samples were blocked in peroxidase blocking agent (Dako EnVision™ + Dual Link System-HRP (DAB^+) #K4065) for 15 min to 1 h at RT. Slides were then drained and incubated with the primary antibody diluted in antibody diluent (Abcam #ab64211), either for 1 h at RT or overnight at 4°C (Table 2.9). Slides were washed twice with PBT-T (3 min each). Slides were then incubated with secondary antibody (Polymer/HRP solution - Dako EnVision™ + Dual Link System-HRP (DAB^+) #K4065) for 20 min at RT. Slides were washed twice with 1x PBS-T (3 min each) and incubated with diaminobenzidine DAB+ (Dako EnVision™ + Dual Link System-HRP (DAB^+) #K4065) for 1.5-2 min at RT (Table 2.9). DAB was removed and slides were washed in tap water for 5 min. Slides were then counter stained with aqueous Gill's Haematoxylin solution (Sigma-Aldrich) for 20 sec at RT. Following this, slides were washed with running tap water for 5 min. Slides were dehydrated by sequentially dipping (10 times each) in 50%, 70% and twice in 100% ethanol and immersed twice in xylene for 1 min each. Cover slips (thickness #1, VWR #631-0137) were mounted using DPX mountant and slides were left to air dry at RT overnight. Air dried slides were scanned at 40x magnification using the Aperio ScanScope CS digital slide scanner. Analysis was performed using ScanScope software (Aperio).

Table 2.9: Antibodies for immunohistochemistry

Antibody name (clone)	Antigen retrieval: heating temperature and time [1]	Blocking time	Primary antibody dilution and incubation conditions	DAB incubation time	Source and catalogue number
CA9 (M75)	110˚C, 2 min	1 h	1:800, ON 4˚C	2 min	BioScience Slovakia # AB1001
Cleaved caspase 3-D175 pAb[2]	110˚C, 2 min	15 min	1:600, ON 4˚C	2 min	CST #9661
GLUT1 (EPR3915)	110˚C, 2 min	1 h	1:1000, 1 h RT	2 min	Abcam # ab115730
Integrin-β1 (D2E5)	125˚C, 2 min	15 min	1:100, 1 h RT	2 min	CST #9699
LKB1 (Ley 37D/G6)	125˚C, 2 min	15 min	1:15000, ON 4˚C	2 min	Sigma #L9168
MCT1 pAb	110˚C, 2 min	1 h	1:500, ON 4˚C	1.5 min	Atlas antibodies #HPA003324

[1] All antigen retrieval were carried out in citrate buffer pH 6 (Table 2.1)
[2] pAb - polyclonal antibody

2.15.2 Analysis of nuclear and membrane staining

2.15.2.1 Positive Pixel Count v9

Images were analysed using the Aperio positive pixel count v9 algorithm. This quantifies the number and intensity of DAB positive pixels within a specified region. Positivity was the total number of positive pixels divided by the total number of pixels. To determine if the difference in signal between samples was significant, a two sample t-test assuming equal variance was calculated using Microsoft Excel.

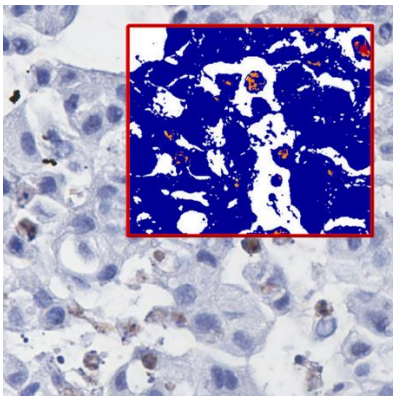

Figure 2.6: Aperio positive pixel count v9 algorithm
Image from LKB1 deficient A549 spheroids stained with cleaved caspase 3 (Figure 3.10)

2.15.2.2 Membrane v9

Images were analysed using Aperio membrane v9 algorithm which quantifies the intensity and completeness of membrane staining. The intensity of staining was categorised as most (3+) to least (1+) intense with 0+ indicating no membrane staining. To determine if the difference in signal between samples was significant, a two sample t-test assuming equal variance was calculated using Microsoft Excel.

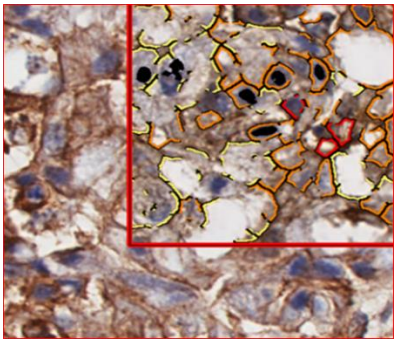

Figure 2.7: Aperio membrane v9 algorithm
Image from LKB1 deficient A549 spheroids stained with integrin-β1 (Figure 3.13)

2.16 Immunofluorescence

Cells in 2D culture were grown on 8-well chamber slides (LAB-TEK® #154534) (1.5-2x10^4 cells/well in 200 µL medium) until sub-confluent or for 4 days (i.e. incubated overnight and treated for 72 h). Cells were then fixed in 100 µL of 3% PFA (Table 2.1) or 10% formalin at RT for 20 min and washed 3 times in 1x PBS prior to permeabilisation and blocking.

FFPE spheroids sections were heated (50˚C, 10 min), dewaxed by immersing twice in citroclear (HD Supplies, UK) and hydrated by immersing twice in 100% ethanol, once in 70% ethanol, once in 50% ethanol (3 min each) and then rinsed in dH_2O. Heat induced antigen retrieval was performed at 110˚C for 30 sec in citrate buffer pH 6 (Table 2.1). Slides were left in citrate buffer to cool at RT for 20 min and washed 3 times in 1x PBS prior to permeabilisation and blocking.

Both 2D and 3D samples were permeabilised and blocked in appropriate buffer (Table 2.1) for 1 h at RT. For details on antibodies and dilutions, please see Table 2.10. Cells were incubated with primary antibodies (β-catenin, α-tubulin) diluted in antibody buffer (Table 2.1) overnight at 4°C. Slides were washed 3 times with 1x PBS and incubated with goat

anti-mouse conjugated to Alexa 488 secondary antibody with or without phalloidin, for 1 h at RT. Slides were washed 3 times with 1x PBS and coverslips (Thickness #1, VWR #631-0137) were mounted using Fluoroshield™ mounting medium containing DAPI (Sigma #F6057). Images were acquired using either the 20x or 63x objective on a confocal microscope (Zeiss LSM 710).

Table 2.10: Antibodies for immunofluorescence

Antibody name (clone)	Dilution	Source and catalogue number
Alexa Fluor® 488 goat anti-rabbit IgG	1:1200	Life Technologies #A11008
Alexa Fluor® 568 phalloidin	1:40	Life Technologies #A12380
α-tubulin (B-5-1-2)	1:5000	Sigma-Aldrich #T6074
β-catenin (D10A8)	1:100	CST #8480
LKB1 (D60C5)	1:4000	CST #3047

2.17 Migration assay

Cells were seeded in 24-well plates ($0.625x10^4$, $1.25x10^4$, $2.5x10^4$, $5x10^4$ cells per well, in 500 µL medium) and incubated at 37°C overnight. Wells containing 50-60% confluent cells were imaged in a controlled environment (37˚C, 5% CO_2). Real time images were acquired using bright field microscopy with a 20x objective at 15 min intervals for 9 h 45 min (Nikon TE- 2000 E microscope). The series of bright field images were exported as TIFF files and imported into the Tracking Tool™ PRO v2.0 software (Gradientech). Individual cell movement was tracked using the automated tracking function.

2.18 CREB reporter assay

To investigate differences in activity of the cAMP response element (CRE), the CREB reporter assay was used. CRE gene expression is under the control of CREB. On use of the CREB reporter assay, cells were transfected with a vector expressing firefly luciferase when

induced by CREB. The CRE reporter was premixed with a constitutively expressing renilla luciferase vector to measure transfection efficiency. A negative control reporter was also used which contained non-inducible firefly luciferase.

$2x10^4$ cells per well were seeded in white 96-well plates (Greiner bio-one #655098) and incubated at 37°C overnight. The following day, cells were transfected with CREB reporter or negative control reporter (BPS Bioscience Inc #60611) according to the manufacturer's instructions. For this, Opti-MEM (Life Technologies #11058-021) and Lipofectamine 2000 (Invitrogen #11668-027) were used. 24 h after transfection, cells were treated with an equal volume of 2x final concentration of forskolin for 24 h. Luciferase activity was measured using a Dual-Glo® Luciferase Assay System (Promega #E2920) according to the manufacturer's instructions. Firefly and renilla luminescence were measured using the plate reader (POLARstar OMEGA). For analysis, the firefly luminescence was normalised to the renilla luminescence and this value was further normalised to that for the negative control reporter.

2.19 Oxygen consumption rate (OCR)

Cells were seeded using Advanced DMEM/F12 in XF96 cell culture plates (Seahorse Bioscience) and incubated at 37˚C overnight (see Table 2.5 for seeding density). 1 h prior to the experiment, the cell medium was buffered by the addition of a final concentration of 25 mM HEPES (Table 2.1). Cells were acutely treated with phenformin or metformin, and the OCR (oxygen consumption rate) was measured for 6 h according to manufacturer's instructions. Briefly, the medium was mixed for 3 min and oxygen consumption was measured for 4 min at 15 min intervals. At the end of the experiment, a mitochondrial stress test was performed by the sequential addition of a final concentration of 1 µM oligomycin, 0.5 µM FCCP and the combined addition of 2 µM antimycin A and 2 µM rotenone. After

the experiment, the cells were fixed in 100% ice-cold methanol (5 min, RT), stained with a final concentration of 4 µg/mL of Hoechst 33258 (Table 2.1) dissolved in 1x PBS (200 µL per well), and fluorescence intensity was measured (Ex 355 nm, Em 460 nm) (POLARstar OMEGA). Data was analysed using the Seahorse software.

For the OCR measurements, the change in OCR was displayed graphically and represented relative values. OCR values were normalized for fluorescence intensity/DNA content (pM/min/ng DNA) and were set to a baseline of 100% at the start of measurements.

3 Characterisation of LKB1 loss in lung cancer cells

3.1 Introduction

We hypothesised that LKB1 loss plays a key role in lung cancer development and that LKB1 loss confers a growth advantage *in vitro* and *in vivo*. In this Chapter, LKB1 expression was examined in a panel of lung cancer cell lines. To determine the effect of LKB1 alone on cell proliferation, isogenic cells with or without wild-type LKB1 expression were generated. The effect of LKB1 expression on cell proliferation was determined in 3 models; 2D culture, 3D spheroids and *in vivo* models. As LKB1 was reported to play an important role in cell polarity (Section 1.3.1), we evaluated differences in cell cytoskeleton organisation and cell migration in 2D culture, as well as differences in spheroid structure and cell-cell/cell-ECM (extracellular matrix) contacts within spheroids.

Although, analysis of 3D spheroids can be challenging, the use of 3D spheroids has several advantages over 2D culture. For example, in 2D culture, oxygen and nutrients tend to be unlimited, however, 3D spheroids have oxygen and nutrient gradients similar to tumours *in situ* (Lin and Chang, 2008). This limited oxygen and nutrient supply can affect response to certain treatments. For instance, Gray et al observed that hypoxic tumours are more resistant to radiation (Gray et al., 1953). This is because oxygen plays a key role in determining the efficacy of radiotherapy as it provides free radicals which assist in DNA damage (Crabtree and Cramer, 1933). As spheroids are more reflective of the tumour microenvironment, they can possibly offer a more clinically relevant model to predict the effect of therapies *in vivo* compared to 2D culture. To my knowledge, there have been a limited number of studies that have used spheroids to investigate the role of LKB1, apart from one study that used spheroids which were embedded in collagen (Gao et al., 2010).

Unlike the widely used GEMMs to study the effect of LKB1 loss *in vivo* (Section 1.6), we determined *in vivo* tumour burden by heterotopic and orthotopic implantation of the isogenic cells. A sub-cutaneous xenograft model was used to determine the effect of LKB1 on tumour growth and a lung orthotopic model was used to determine the effect of LKB1 on growth and metastasis. A wide range of assays were used to examine tumour burden in the orthotopic model including; IVIS, MRI, lung weight, a novel western blotting assay and immunohistochemistry (IHC). The use of the lung orthotopic model was a novel approach for studying the effect of LKB1 on tumour burden *in vivo*.

3.2 LKB1 expression in lung cancer cell lines

Figure 3.1a lists the reported mutations in the LKB1, KRAS, BRAF and TP53 genes in the 12 cell lines used in this study. All cell lines are derived from lung cancer patients except NBE1 (Section 2.2). LKB1 expression was investigated by western blotting in the 12 cell lines. No LKB1 protein expression was detected in 8/8 cell lines with reported LKB1 mutations, and LKB1 expression was confirmed in 3/4 cell lines reported to be LKB1 wild-type (Figure 3.1b). CORL105 has no reported LKB1 mutations, however, LKB1 protein expression was below detection level. PCR amplification and DNA sequencing of exon 1-9 of the LKB1 gene in CORL105 cells did not reveal any LKB1 mutations (Section 2.5). Notably, LKB1 mRNA expression in CORL105 is the second lowest of 1036 human cell lines (CORL105 LKB1 log mRNA expression = 5.23, mean = 6.48, min = 5.2, max = 8.38) (CCLE; accessed February 2017). It was reported that LKB1 gene expression can be silenced epigenetically by promoter hypermethylation (Esteller et al., 2000, Sanchez-Cespedes et al., 2002) (Section 1.4), therefore it is possible that LKB1 is silenced by promoter methylation in CORL105, although this was not investigated.

During activation, LKB1 forms a heterotrimeric complex with STRAD and MO25 (Baas et al., 2003, Boudeau et al., 2003) (Section 1.2.3). Therefore, expression of these proteins was also determined by western blotting. STRADα appeared as 2 bands at approximately 48 and 34 kDa (Figure 3.1b). These 2 bands were also observed in brain tissue by Denison et al (Denison et al., 2009), however, the functional relevance of this is not understood. STRADα contains a potential caspase 1 cleavage site at amino acid position 140 (http://web.expasy.org/peptide_cutter/). The STRADα antibody (EPR15603) used in this study binds a recombinant fragment between amino acids 250 and 400, therefore, EPR15603 should detect both the full length (48 kDa) and cleaved (34 kDa) STRADα, with cleaved STRADα being ~14 kDa lighter. In Figure 3.1b, the upper band of STRADα (48 kDa) was quantified and normalised to PPIB. In the 12 cell lines, STRADα upper band levels were statistically significantly higher in the presence of LKB1 (Figure 3.1c). It is possible that the presence of LKB1 in the complex with STRAD and MO25 stabilises the full length form of STRAD, protecting it from caspase cleavage. MO25α protein levels were generally similar in LKB1 mutated and wild-type cell lines (Figure 3.1b).

(a)

Cell line	LKB1	KRAS	BRAF	TP53
A549	p.Q37*	p.G12S	wt	wt
H2126	Δ	wt	wt	p.E62*
H23	p.W332*	p.G12C	wt	p.M246I
A427	Δ	p.G12D	wt	wt
H1395	p.E57fs	wt	p.G468A	wt
H460	p.Q37*	p.Q61H	wt	wt
H2030	p.E317*	p.G12C	wt	p.G262V
H1755	p.P281fs	wt	p.G469A	p.C242F
CORL105	wt	UC	UC	UC
H1299	wt	wt	wt	Δ
Calu6	wt	p.Q61K	wt	p.R196*
NBE1	wt	UC	UC	UC

(b)

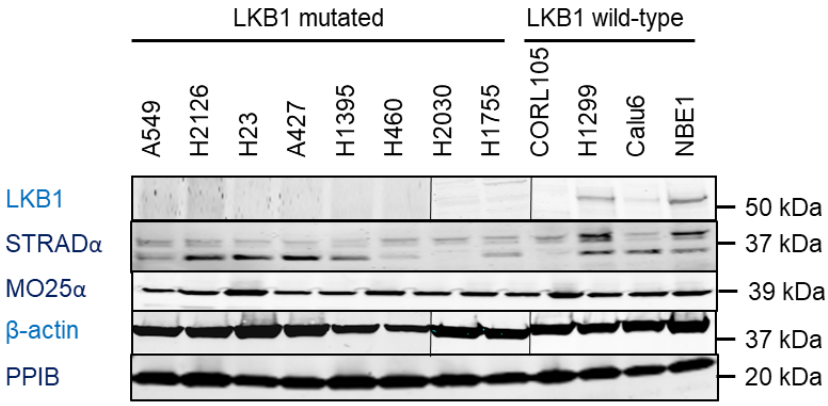

(c)

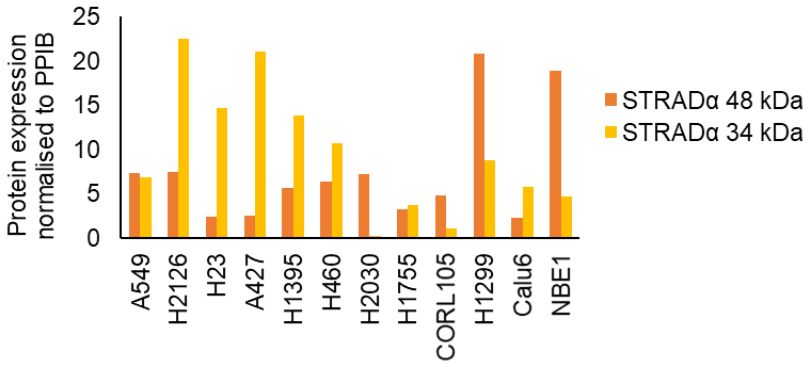

Figure 3.1: Mutation status of selected genes and LKB1 expression in NBE1 and 11 lung cancer cell lines used in this study

(a) Mutation data source: see Table 2.3. UC - unconfirmed. (b) Western blot showing LKB1, STRADα and M025α protein expression. 40 µg of protein was loaded per well. (c) The STRADα bands in (b) were quantified using the Odyssey® Image Studio software, and the values were normalised to PPIB. Mean = 5.25 for LKB1 non-expressing cells including CORL105, mean = 14.03 for LKB1 expressing cells, p-value = 0.02.

3.3 Generation of isogenic cell lines (with or without LKB1)

To understand the effect of LKB1 alone on various phenotypes and response to treatment, isogenic cell lines with or without LKB1 expression were generated (see Section 2.6). In brief, LKB1 expression was restored in the LKB1 mutated A549 and A427 lung cancer cells and knocked-down in the LKB1 wild-type H1299 lung cancer cells. Empty vector (EV) lentiviral particles were used for negative controls.

3.4 Characterisation of isogenic cells in 2D culture

3.4.1 LKB1 expression, activity and localisation in isogenic cells in 2D culture

LKB1 proficient A549 and A427 cells overexpressed LKB1 compared with LKB1 proficient H1299+shEV cells (Figure 3.2b, c). LKB1 appeared as 4 bands around 50 kDa in LKB1 transduced A549 and A427 cells as well as EV transduced H1299 cells suggesting that this was not an artefact of transfection. The bands were estimated to be 54, 50, 48 and 44 kDa. Human LKB1 consists of 433 amino acids and is reported to be 48.6 kDa, however, the antibody we used (27D10) recognised LKB1 at 54 kDa. Denison et al reported long (50 kDa) and short (48 kDa) LKB1 isoforms in mouse testis tissue and concluded that LKB1 was alternatively spliced by the addition of an intron between exon 8 and 9, and that this alternative splicing was conserved between mouse and human (Denison et al., 2009). However, alternative splicing does not explain the 4 bands seen in LKB1 proficient A549 and A427 cells as only the coding region was transduced into these cells. The 4 bands could be a consequence of translation from alternative start sites (considering LKB1 contains many methionine start codons), or post translational modification such as phosphorylation or farnesylation (PTM discussed in Section 1.2.2).

The STRADα 54 kDa band was expressed at a higher level in the presence of LKB1 in the isogenic cells (Figure 3.2b, c). LKB1 kinase activity was demonstrated by an upregulation

of pAMPK (a downstream target of LKB1 (Section 1.3.2)) and phosphorylated acetyl coA carboxylase (pACC) (a downstream target of pAMPK (Munday, 2002)) in LKB1 proficient A549 and A427 cells (Figure 3.2b). In H1299 cells, LKB1 knock-down did not decrease pAMPK nor pACC expression. However, as mentioned in Section 1.3.2, AMPK can also be phosphorylated by CaMKKβ which may play an important role in AMPK regulation in H1299 cells. It remains unknown if there is a LKB1 downstream target that is regulated by LKB1-dependent phosphorylation alone. In further experiments, we primarily focus on A549 and A427 cells, as these cells are more reflective of the biological role of LKB1 in lung cancer because LKB1 loss is intrinsic to these cells and possibly important for tumour development, whereas H1299 cells are naturally LKB1 wild-type and therefore, isolated from a tumour that developed in the presence of LKB1.

LKB1 is reported to be expressed in the nucleus and the cytoplasm (Section 1.2.3). To determine the subcellular localisation of LKB1 in these studies, whole cell protein was fractionated into cytoplasmic and nuclear fractions and analysed by western blotting. H3K36ME3 was used as a control as it is expressed only in the nucleus. We found that LKB1, STRADα and MO25α were expressed in the nucleus and the cytoplasm (Figure 3.2c).

To determine the distribution of LKB1 expression in cells, immunohistochemistry (IHC) of cell pellets was carried out and showed that LKB1 was heterogeneously expressed (Figure 3.2d). We ruled out the possibility that this was a consequence of transfection as LKB1 proficient A549 and A427 clones were also heterogeneous for LKB1 expression (Figure 3.2d). Heterogeneity of LKB1 protein expression was also reported by Calles et al who used the same antibody that was used in our study (Ley 37D/G6) and also used A549 cells transduced with LKB1 expressing lentiviral particles (Calles et al., 2015). The biological significance of this heterogeneity has yet to be determined. The LKB1 antibody used for IHC (Ley 37D/G6) is a mouse monoclonal antibody raised against full length LKB1. It is

possible that the antibody binding to LKB1 could be affected by certain PTMs, like phosphorylation or farnesylation, although this is unknown.

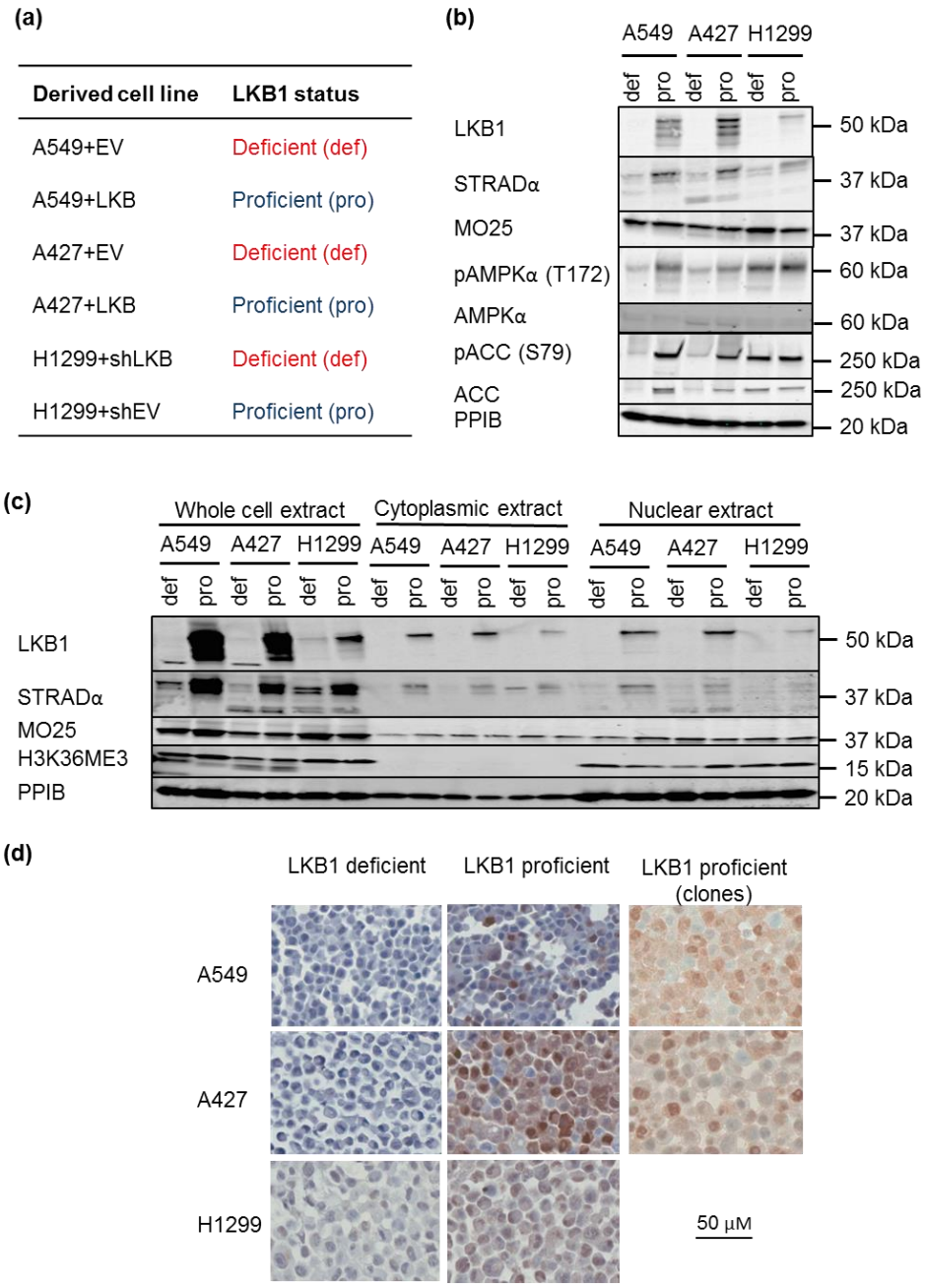

Figure 3.2: LKB1 expression, activity and localisation in isogenic LKB1 deficient and proficient cell lines

(a) Nomenclature for isogenic cells with or without LKB1. LKB1 deficient (def) cells are colour coded red (A549+EV, A427+EV and H1299 shLKB1). LKB1 proficient (pro) cells are colour coded blue (A549+LKB. A427+LKB, H1299 shEV). EV - empty vector. (b) Representative western blotting images showing LKB1 expression and activity in the isogenic cells with or without LKB1. 20 µg of protein was loaded per well. (c) Western blotting images are from a single experiment showing cytoplasmic, nuclear and whole cell extracts. 20 µg of protein was loaded per well. (d) Representative IHC images showing LKB1 expression (brown) and haematoxylin staining (blue) in the isogenic cells with (un-cloned or cloned) or without LKB1.

3.4.2 The effect of LKB1 expression on cell proliferation in 2D culture

The effect of LKB1 expression on the growth rate in 2D culture was determined over 10 days using a PicoGreen assay. In this assay, the medium was replenished to avoid nutrient exhaustion. The results showed that LKB1 caused no difference in the growth rate in 2D culture (Figure 3.3). This result is in contrast to Faubert et al (Faubert et al., 2014), who reported that LKB1 deficient cells had enhanced growth. However, Faubert et al used non-tumour MEFs transduced with MiCD8t for control virus or MiCD8t-Cre to delete stk11-floxed alleles. The role(s) of LKB1 in tumour and non-tumour cells, or the species variation could underlie the differences in these results.

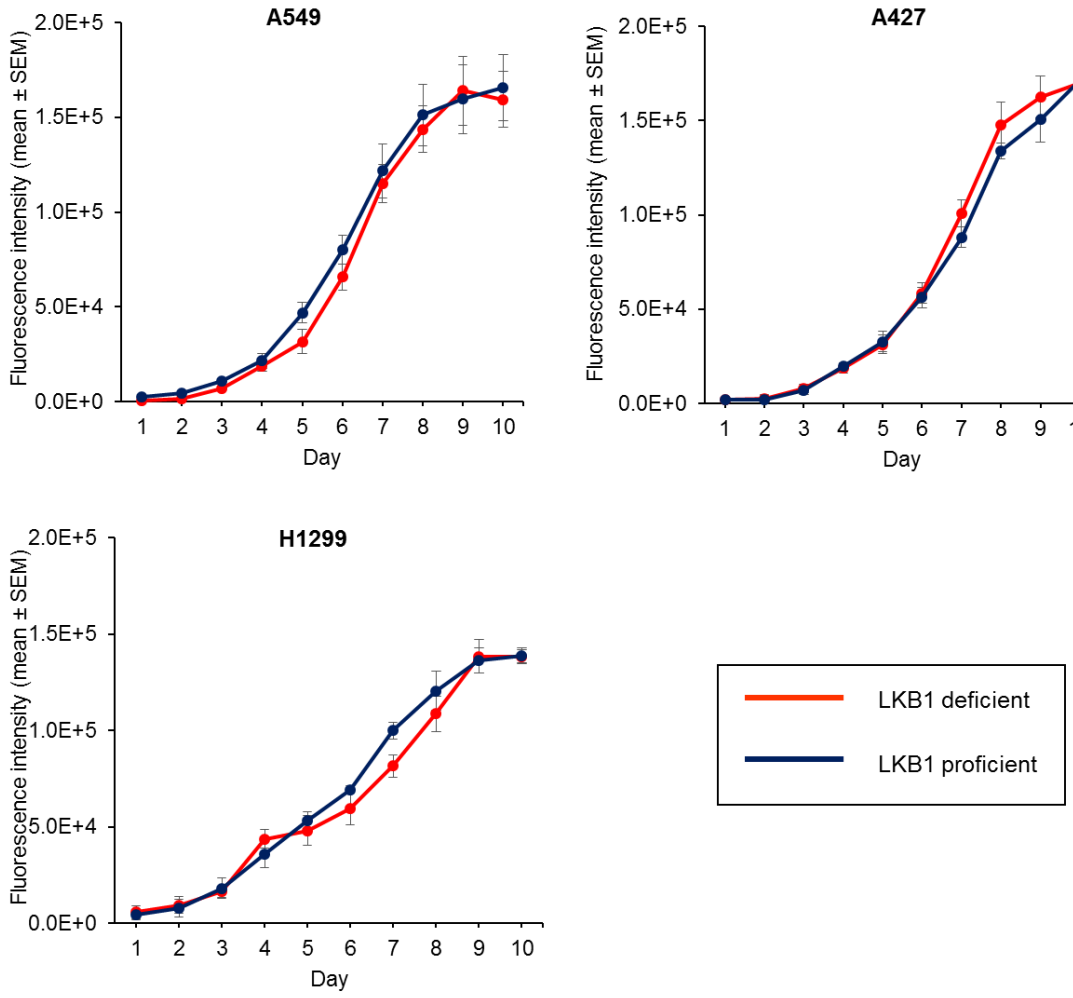

Figure 3.3: The effect of LKB1 expression on cell proliferation in 2D culture
PicoGreen assay showing cell proliferation over 10 days. Medium was replenished on day 7. Data points represent the mean of triplicate values from 2 independent experiments.

3.4.3 The effect of LKB1 expression on microtubule and actin cytoskeleton in 2D culture

Using immunofluorescence (IF), differences in microtubule and actin structure between LKB1 deficient and proficient A549 cells were observed (Figure 3.4). The microtubule cytoskeleton was more organised with distinct microtubule organising centres evident in LKB1 proficient cells. The actin cytoskeleton also appeared more fibrillar in LKB1 proficient cells.

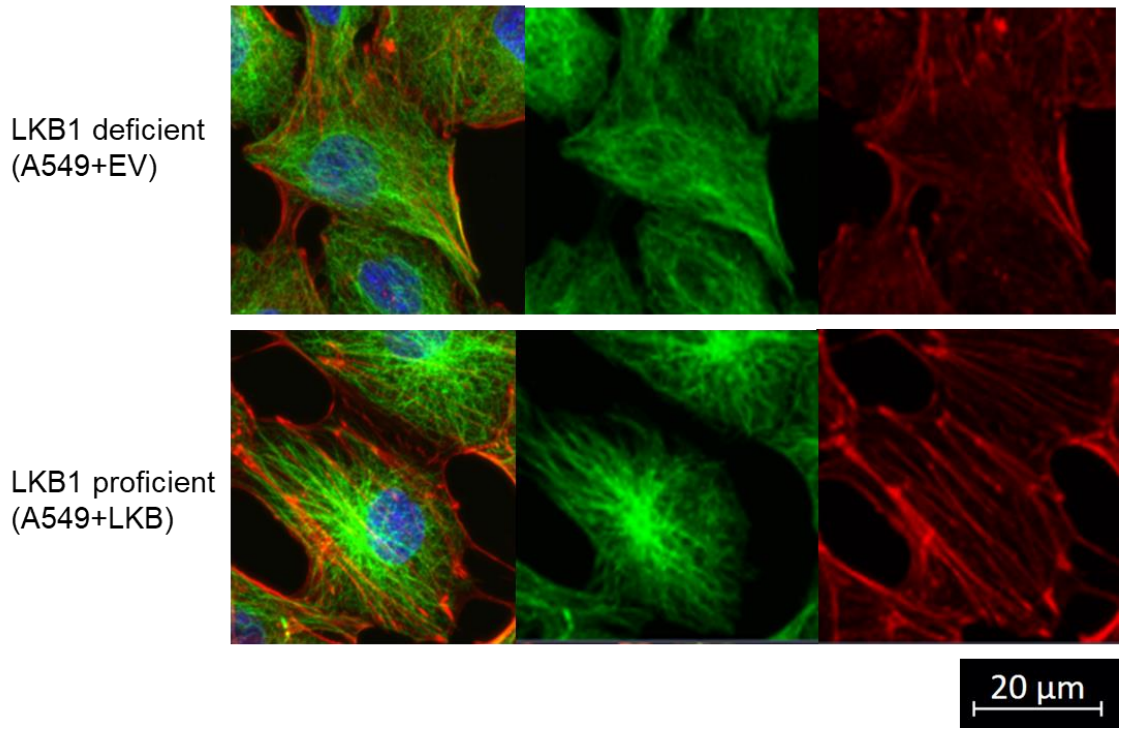

Figure 3.4: Microtubule and actin structure in LKB1 deficient and proficient cells in 2D culture
Representative IF images of cells stained with DAPI (blue), α-tubulin (green) and phalloidin/actin (red). Images were acquired using the 63x objective on a confocal microscopy.

3.4.4 The effect of LKB1 expression on cell migration in 2D culture

Cell migration was assessed using Tracking Tool™ PRO v2.0 software to analyse images acquired with live-cell bright field microscopy. The results showed that LKB1 proficient cells were possibly more migratory as they travelled a greater Euclidean distance and a smaller accumulated distance, indicating that they may have moved in a certain direction

(Figure 3.5). While this work was in progress, Chan et al observed that LKB1 deficient cells were more invasive due to the loss of a dependency on haptotaxis (motility towards ECM bound chemoattractants). They observed that the LKB1 deficient cells lose their ability to respond to ECM inhibitory cues through the lack of MARK activation (Chan et al., 2014). The effect of haptotaxis on cell migration was not determined here. A427 and H1299 cells were relatively static, therefore, it was not possible to assess the impact of LKB1 on motility in these cells.

(a)

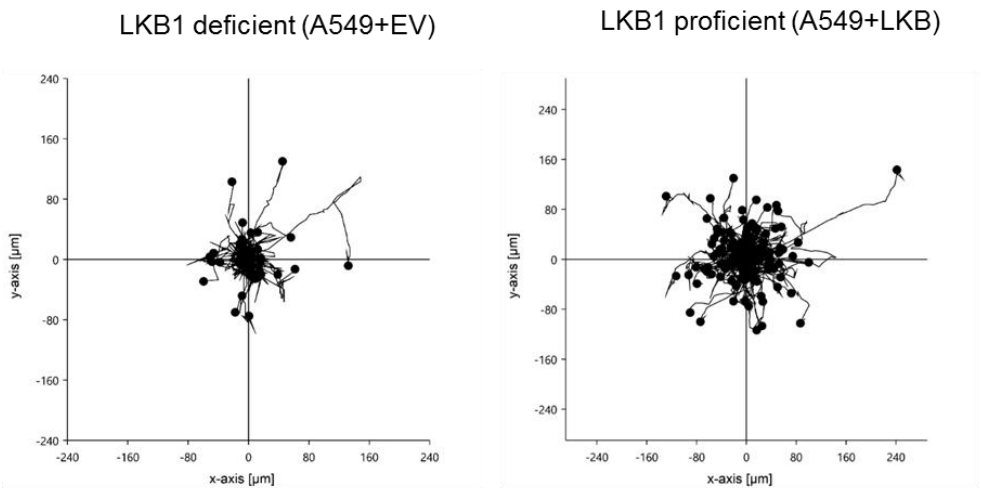

(b)

	LKB1 deficient (A549+EV)	LKB1 proficient (A549+LKB)
No. of tracks	53	137
Accumulated distance (µm) mean ± SD	158 ± 103.3	133.9 ± 91.5
Euclidean distance (µm) mean ± SD	28.8 ± 31.6	48.6 ± 38
Velocity (µm/min) mean ± SD	0.4 ± 0.2	0.5 ± 0.2
Directness	0.28	0.44
Rayleight test p-value	0.77	0.41

Figure 3.5: The effect of LKB1 expression on cell migration in 2D culture
(a) Polar plot showing the tracks of each cell. The starting point for each cells was at position 0,0. (b) Analysed tracking data: Euclidean distance is the straight line distance between 2 points. Directness is the mean of the euclidean distance divided by the accumulated distance for each cell. 0 indicates cells are migrating in a random direction and 1 indicates cells have directionality. Rayleight test p-value was not significant for either cell line indicating that cells have not significantly migrated in a certain direction and the track endpoints are randomly distributed. In this assay, it is important to note that no gradient was present for cells to migrate towards by chemotaxis or haptotaxis.

3.4.5 Summary of 2D data

Isogenic cells were successfully generated and LKB1 activity was demonstrated in both A549 and A427 cells by an upregulation of pAMPK and pACC. LKB1 was present as 4 bands by western blotting and it was heterogeneously expressed in LKB1 proficient A549, A427 and H1299 cells. However, the functional relevance of these observations is not known. There was no difference in cell proliferation between LKB1 deficient and proficient A549, A427 and H1299 cells. However, LKB1 proficient A549 cells had a more organised microtubule and actin cytoskeleton, migrated a greater Euclidean distance and a smaller accumulated distance, possibly suggesting that they moved in a certain direction.

3.5 Characterisation of isogenic cells in 3D spheroids

3.5.1 The effect of LKB1 expression on cell proliferation in 3D spheroids

Unlike A549 and H1299 cells, A427 cells were unable to form stable spheroids. At 10 days post seeding, LKB1 deficient A549 and H1299 cells formed larger spheroids with a less defined edge and a greater amount of dsDNA (Figure 3.6). It was not possible to determine whether these cells were viable as PicoGreen detects dsDNA from both live and dead cells.

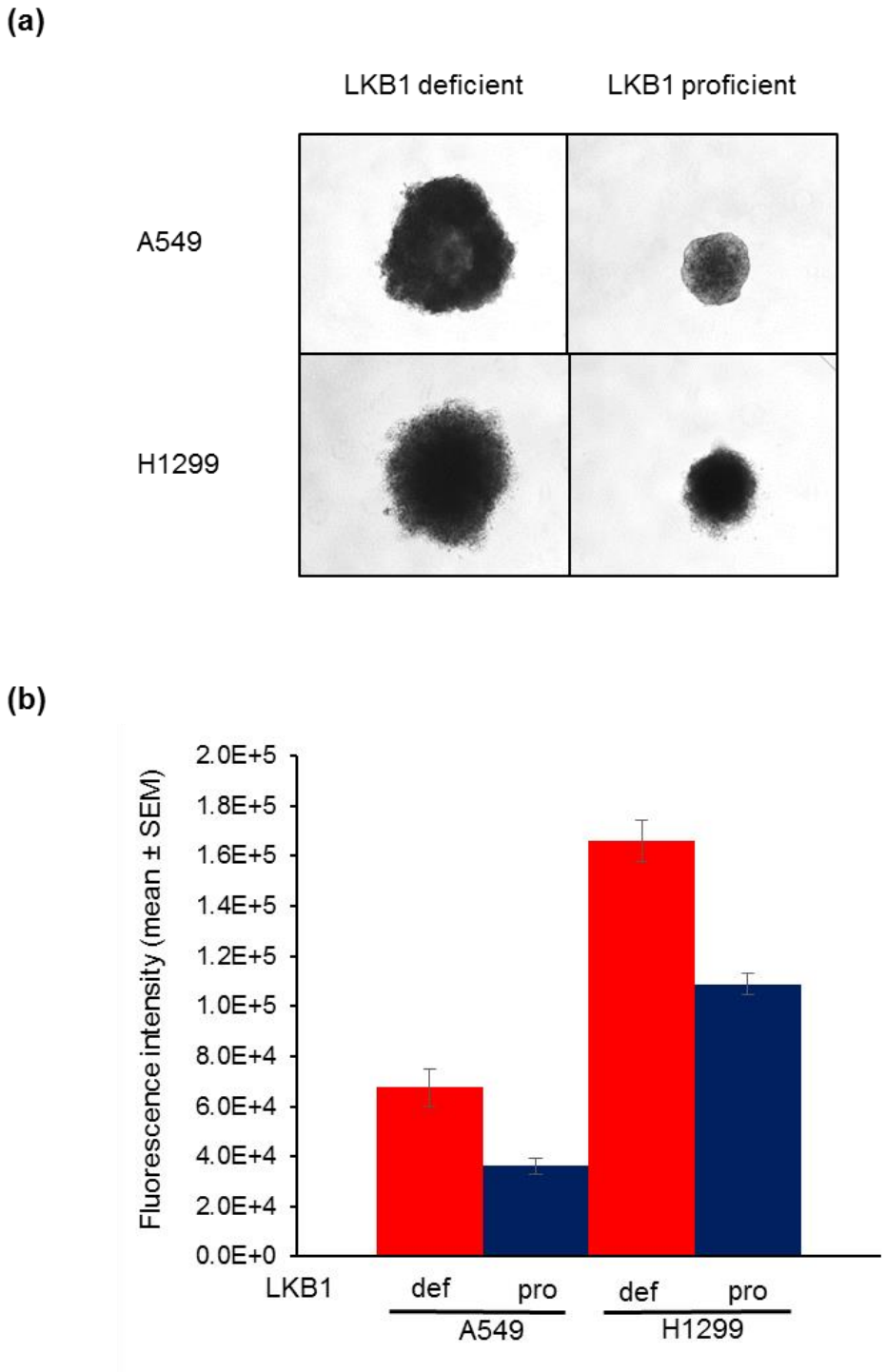

Figure 3.6: The effect of LKB1 expression on 3D spheroid growth (10 days post seeding)

(a) Representative live spheroid images at 40x magnification showing the effect of LKB1 expression on spheroid size. (b) PicoGreen assay showing the effect of LKB1 expression on spheroid cell number. Each value represents the mean of 5 spheroids.

The effect of LKB1 expression on long-term spheroid growth (up to 21 days) was also determined. For this, spheroids were imaged and area was measured every 3-4 days. On day 21, resazurin was used to determine the cell viability (Section 2.8.2). However, the use of the resazurin assay to measure cell viability of spheroids may be limited depending on the spheroid size and whether the cells are tightly or loosely packed, thereby affecting access.

In A549 cells, it was essential to replenish the medium after day 10 post seeding for continued spheroid growth. At 21 days post seeding, LKB1 deficient A549 spheroids were larger with increased resorufin fluorescence (Figure 3.7a, b). In H1299 spheroids, it was also essential to replenish the medium after 10 days for continued spheroid growth. However, at 21 days, LKB1 proficient H1299 spheroids were larger with increased resorufin fluorescence (Figure 3.7a, b). In the spheroid images at day 21, H1299 spheroids appeared looser and possibly breaking apart, particularly in the group with the medium change (Figure 3.7c). Therefore, growing H1299 spheroids beyond 10 days may not accurately represent a spheroid. At 10 days post seeding, LKB1 deficient H1299 spheroids were larger which was in line with the previous result (i.e. that observed in A549 isogenic cells).

To determine if LKB1 loss or expression has the dominant effect in a spheroid co-population, equal numbers of LKB1 deficient and proficient cells were seeded in a single spheroid and the area and resorufin fluorescence was measured. The results demonstrated that A549 spheroids with equal numbers of deficient and proficient cells showed similar characteristics to the LKB1 deficient spheroids in terms of size and resorufin fluorescence, from 4 days post seeding (Figure 3.8). This suggests that LKB1 loss is dominant in a co-population. This was also true for H1299 spheroids with a mixed population of LKB1 deficient and proficient cells up until day 10 post seeding.

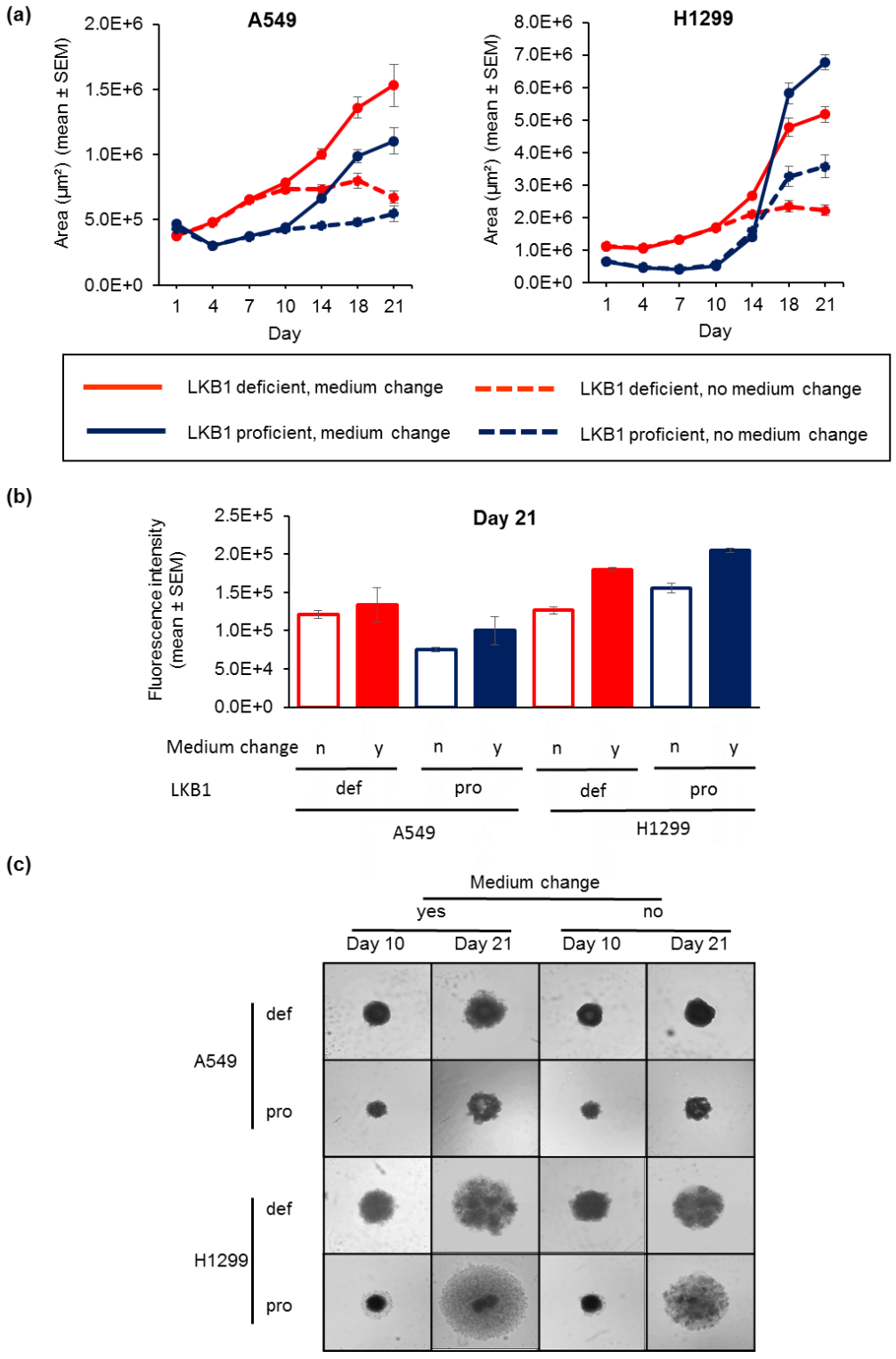

Figure 3.7: The effect of LKB1 expression on long-term spheroid growth (21 days) with or without replenished medium

Medium was replenished every 2-3 days from day 10 post seeding. (a) Spheroid area: data represents the mean of 12 spheroids. (b) Resazurin assay: data represents the mean of 9 spheroids. n - no and y - yes (c) Representative live spheroid images at 15x magnification using the CeligoS.

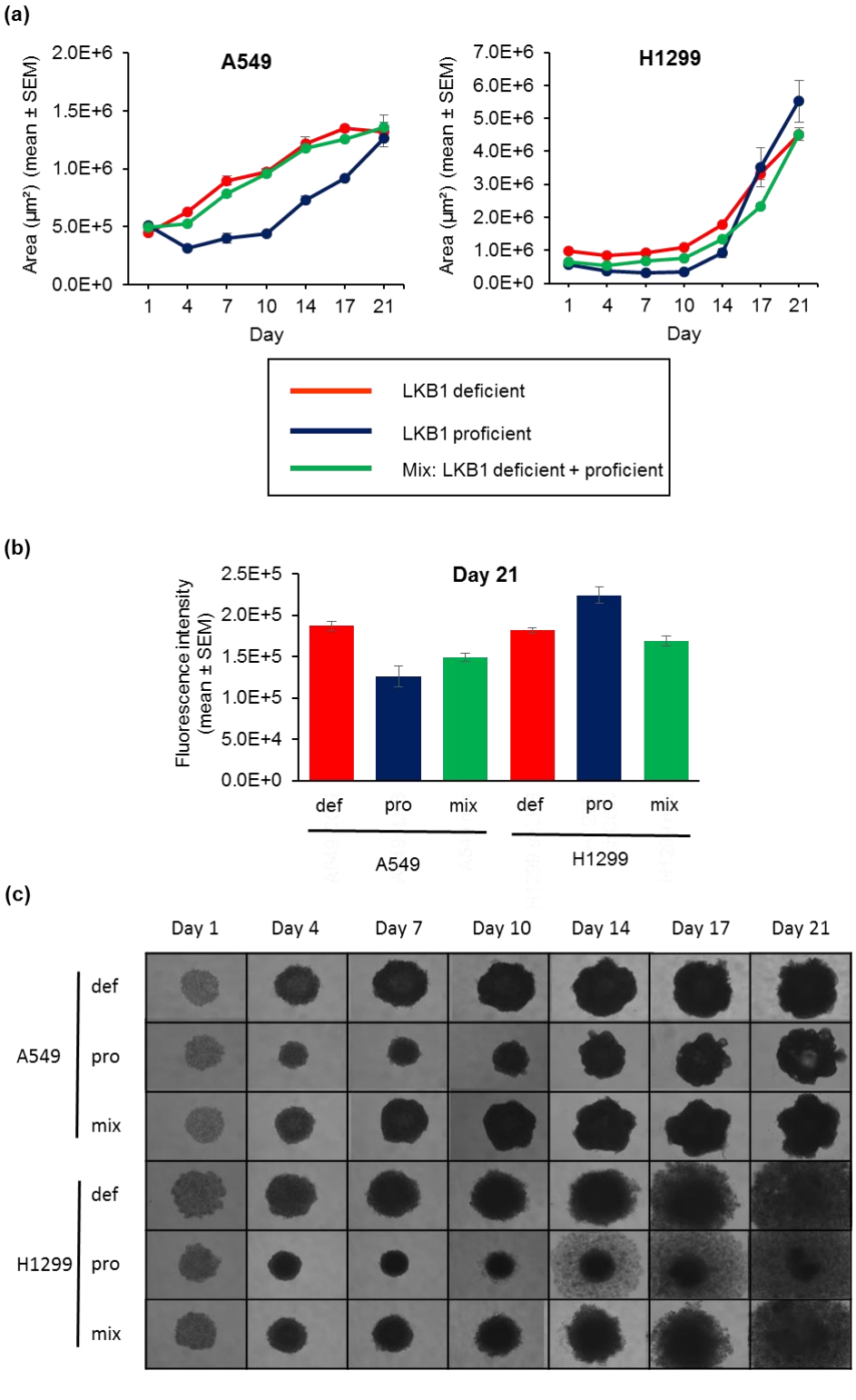

Figure 3.8: Spheroids seeded with equal numbers of LKB1 deficient and proficient cells

Equal numbers of LKB1 deficient and proficient cells were seeded per spheroid ($5x10^3$ def, $5x10^3$ pro cells per well). Medium was changed every 2-3 days from day 10. (a) Spheroid area: data points represent the mean of triplicates. (b) Resazurin assay on day 21: data points represent the mean of triplicates. (c) Representative live spheroid images at 40x magnification using the Nikon Ti-E.

3.5.2 The effect of LKB1 expression on spheroid structure

A possible role for LKB1 loss in lung cancer development may be to promote invasion and thus metastasis. Differences in cell-cell contacts and/or cell-ECM contacts between LKB1 deficient and proficient cells may assist with invasion. In this and next section, LKB1 dependent differences in spheroid structure, cytoskeleton, cell-cell contacts and cell-ECM contacts were determine by IHC and IF.

In haematoxylin and eosin (H and E) stained sections of LKB1 deficient and proficient spheroids, the LKB1 proficient spheroids were more organised as the cells appeared to line up along the outer rim and there were very little gaps evident between cells. In contrast, the LKB1 deficient spheroids appeared more disorganised and there were many acellular gaps throughout the spheroid (Figure 3.9). The material in these gaps were positive for cleaved caspase 3 (CC3) suggesting that they may represent areas of apoptosis (Figure 3.10). This CC3 positive staining was predominantly evident in the acellular gaps and no CC3 positive regions were detected in LKB1 proficient spheroids. Although the data suggests that LKB1 deficient spheroids have apoptotic regions, the proliferation rate clearly outweighs the apoptosis rate as these spheroids were larger with more dsDNA and a higher resorufin fluorescence (Section 3.5.1).

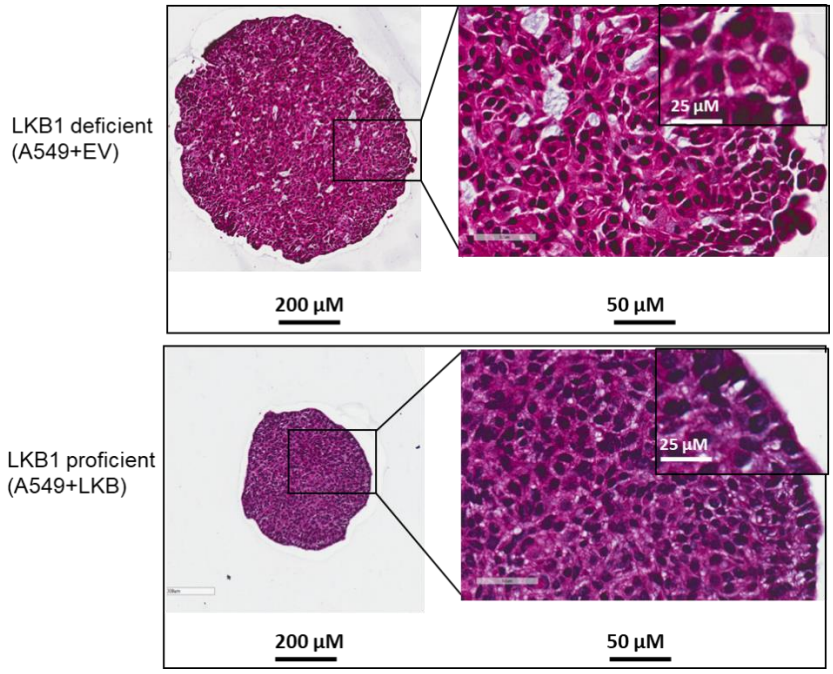

Figure 3.9: LKB1 deficient and proficient spheroid sections stained with Haematoxylin and Eosin
Representative H and E images of spheroid sections. Haematoxylin (purple) stains the nucleus and eosin (pink) stains the cytoplasm.

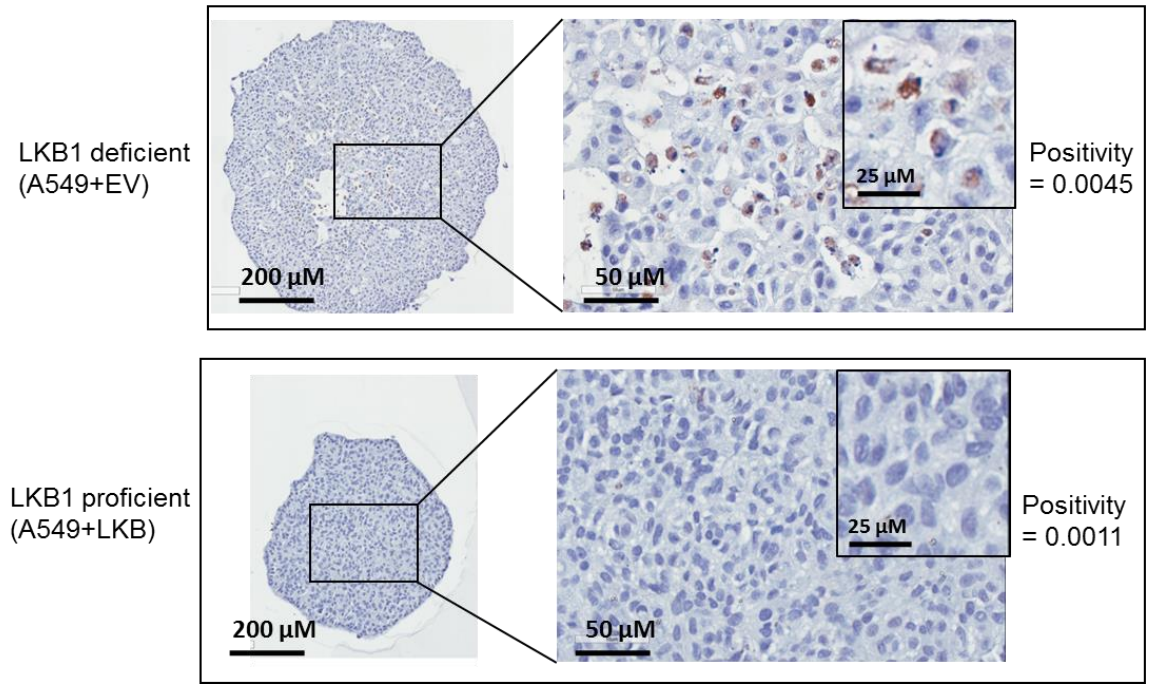

Figure 3.10: LKB1 deficient and proficient spheroid sections stained for cleaved caspase 3
Spheroid sections stained for haematoxylin (blue) and cleaved caspase 3 (brown). Images were analysed using the Aperio Positive Pixel Count v9 algorithm. The values for positivity represent a mean of 3 spheroids (p-value = 0.07).

3.5.3 The effect of LKB1 expression on microtubule structure and cell contacts in 3D spheroids

To investigate potential differences in cell cytoskeleton and cell contacts between LKB1 deficient and proficient cells, proteins involved in cell-cell contacts and cell-ECM contacts were detected by IHC and IF. Selected key proteins are shown schematically in Figure 3.11.

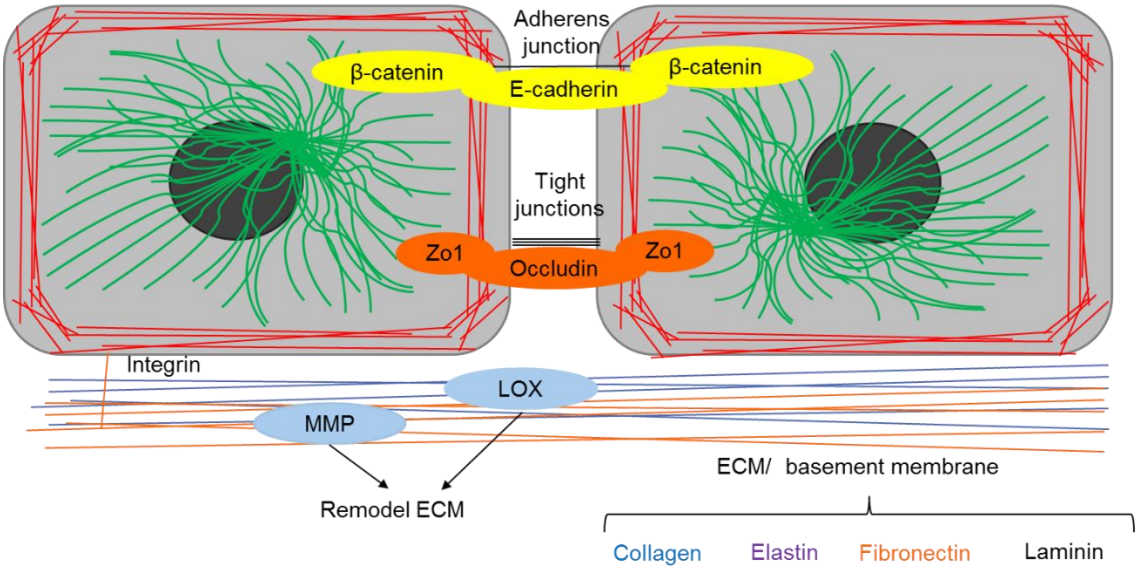

Figure 3.11: Schematic showing selected proteins involved in cell cytoskeleton and cell junctions
Cytoskeleton showing microtubules in green and actin in red. Adherens and tight junctions contribute to cell-cell contacts. The ECM, comprising of collagen, elastin, fibronectin and laminin offers support for the cells. Integrin's interact with the ECM. Cells can release enzymes such as MMP and LOX which remodel the ECM (Lodish et al., 1995).

Figure 3.12 shows that the microtubule cytoskeleton appeared denser in the LKB1 proficient spheroid. Of interest, cells within spheroids were smaller and more rounded compared to cells in 2D culture, and individual microtubules could not be as clearly discerned. IF and IHC images showed differential integrin-β1 and β-catenin staining between the LKB1 deficient and proficient spheroids. Integrin-β1, a protein important for cell attachment to fibronectin in the ECM was expressed at a higher level in LKB1 deficient spheroids (Figure 3.13). β-catenin, a protein important for adherens junctions and cell-cell contacts, was localised to the periphery of cells in LKB1 proficient spheroids. In LKB1 deficient

spheroids, β-catenin signal was less intense and possibly diffused throughout the cell (Figure 3.13). This suggests that in these cells, more β-catenin may be translocated to the nucleus where it can promote the transcription of oncogenes like MYC through LEF/TCF gene transcription (Polakis, 1999). E-cadherin, occludin and ZO1 staining were evaluated using IF in LKB1 deficient and proficient spheroids, however there appeared to be no difference between LKB1 deficient and proficient cells (Appendices Figure A3.25). These data suggest that E-cadherin was localised to the periphery of cells in both LKB1 deficient and proficient spheroids. Occludin and ZO1 protein expression appeared diffused in both LKB1 deficient and proficient spheroids, therefore we could not determine any differences in these proteins and thus differences in tight junctions. Although the adherens junction protein; E-cadherin was localised to the outer rim of the cells in both deficient and proficient spheroids, β-catenin, also involved in adherens junctions was localised to the periphery of cells in the proficient spheroids suggesting that LKB1 proficient spheroids had more adherens junctions, and indicating that there were more cell to cell contacts in these spheroids. As integrin-β1 was mainly localised to the periphery of the LKB1 deficient spheroids, it suggests that perhaps the cells of this spheroid interact more with the ECM rather than each other. This could provide a potential explanation as of why LKB1 deficient cells travelled a smaller Euclidean distance in 2D as they were interacting with the ECM (Figure 3.5).

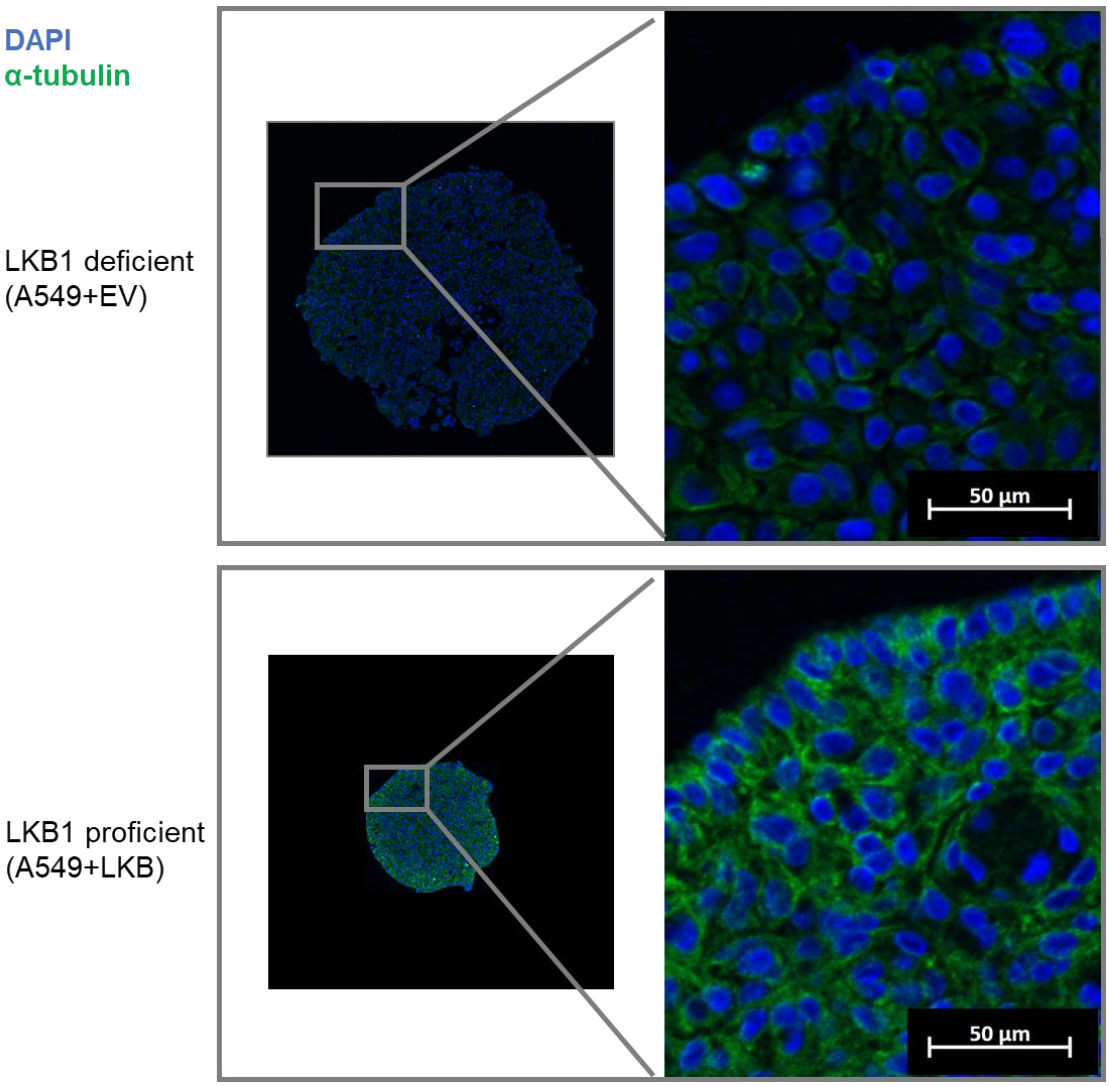

Figure 3.12: Microtubule staining in LKB1 deficient and proficient spheroids
Representative IF images of spheroid sections stained with DAPI (blue) and α-tubulin (green). Images were acquired using the 20x objective on a confocal microscopy.

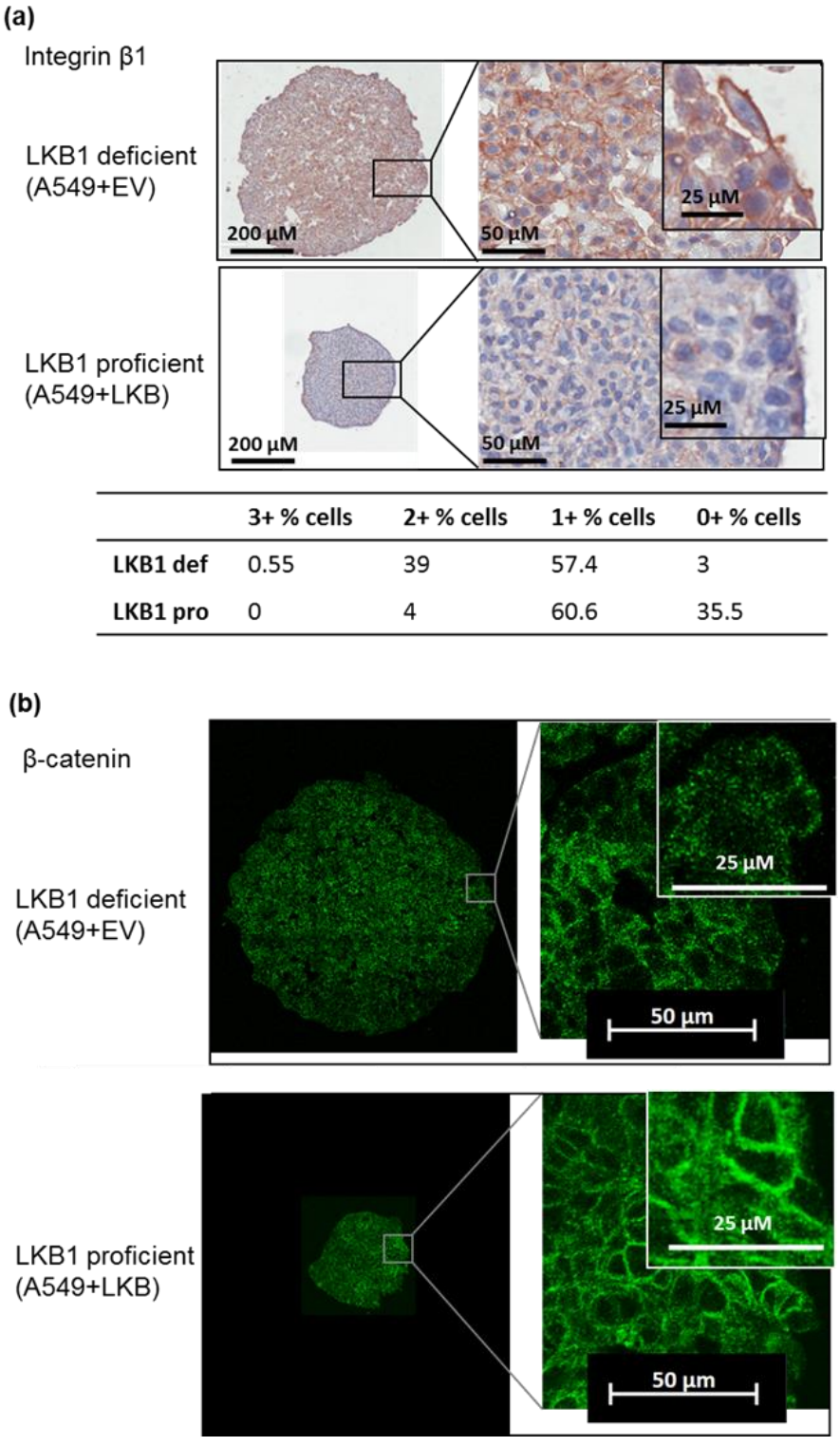

	3+ % cells	2+ % cells	1+ % cells	0+ % cells
LKB1 def	0.55	39	57.4	3
LKB1 pro	0	4	60.6	35.5

Figure 3.13: Integrin-β1 and β-catenin staining in LKB1 deficient and proficient spheroids

(a) Representative IHC images of spheroid sections stained with haematoxylin (blue) and integrin-β1 (brown). Images were analysed using Aperio membrane v9 algorithm. n = 2 spheroids for LKB1 deficient and n = 3 for LKB1 proficient (for 2+ % cells: def = 39, pro = 4, p-value = 0.04) (b) Representative IF images of spheroids fixed and stained with β-catenin (green). Images were acquired using the 20x objective on a confocal microscopy.

3.5.4 Summary of spheroid data

LKB1 loss was associated with larger spheroids containing a greater number of cells. LKB1 deficient cells appeared to be dominant in a spheroid co-population. LKB1 deficient spheroids were less organised, had a less defined edge and contained acellular gaps. Our data suggests that these gaps are where apoptosis had taken place. LKB1 deficient spheroids had less intense microtubule staining. Also, LKB1 deficient spheroids had more diffused β-catenin staining and higher levels of integrin-β1 expression at the periphery of the cells, suggesting that there were less adherens junctions between cells and more cell contacts with the extracellular matrix.

3.6 Characterisation of isogenic cells *in vivo*

3.6.1 Sub-cutaneous xenograft model

The effect of LKB1 on tumour burden was determined by sub-cutaneous injection of LKB1 deficient and proficient A549 cells into the back of CD1 nude mice. LKB1 deficient and proficient H1299 cells were also implanted, however tumours did not establish from either group. LKB1 deficient A549 xenografts grew to a larger size (Figure 3.14). Although the difference in tumour volume between each group did not reach statistical significance, this was likely due to the small sample size. H and E stained tumour sections from xenografts of CD1 nude mice showed that LKB1 proficient tumours appeared to have more stromal tissue throughout the tumour and LKB1 deficient tumours had more acellular gaps (Figure 3.15). These acellular gaps were similar to those seen in LKB1 deficient A549 spheroids which contained material positive for cleaved caspase 3 (Section 3.5.2).

The LKB1 deficient and proficient xenografts from CD1 nude mice were analysed using RNA sequencing (see Section 2.10 for method). On analysis of this data, it was found that increased LKB1 mRNA expression in proficient cells was lost by day 48 post implantation

(Figure 3.16). A possible explanation for this may be negative regulation of the cytomegalovirus (CMV) promoter. This is because A549 cells were transduced with CMV driven LKB1 expressing lentiviral particles and it was reported that the CMV promoter is negatively regulated *in vivo* possibly through an immune response or epigenetic regulation (Morrissey et al., 2013, Papadakis et al., 2004).

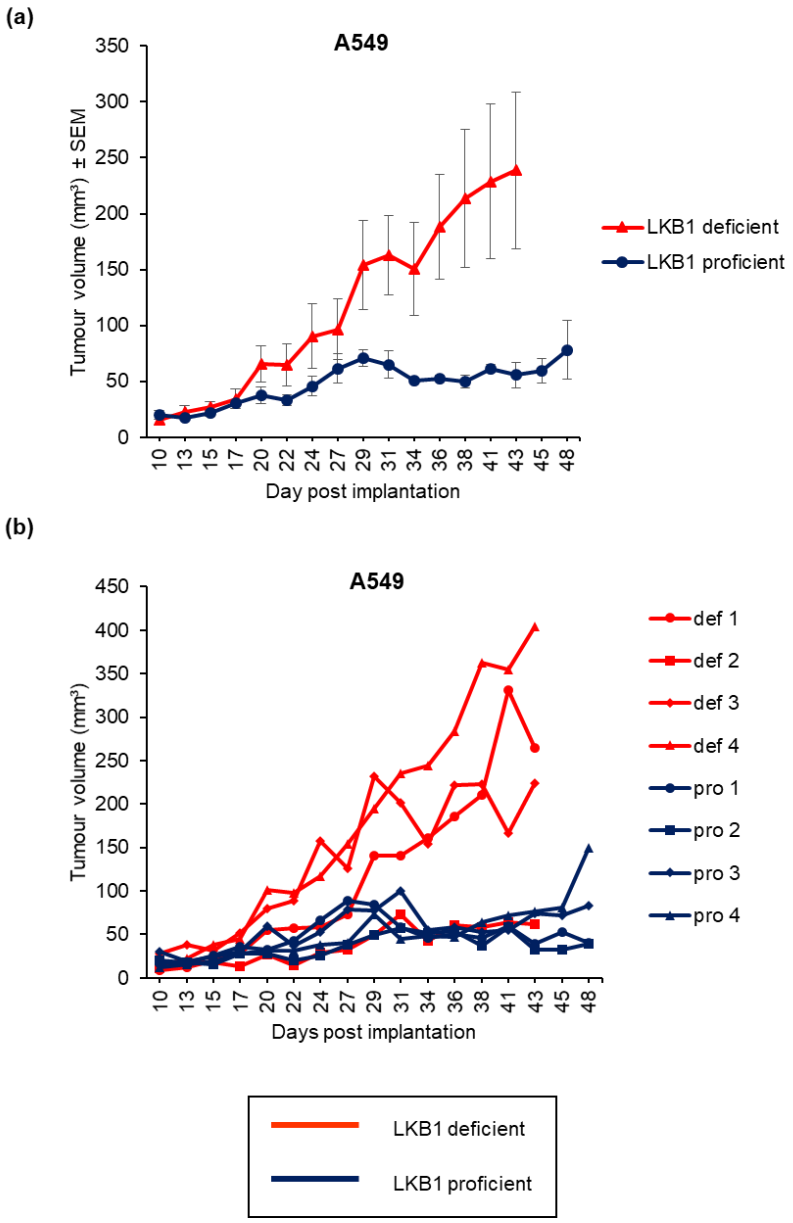

Figure 3.14: The effect of LKB1 expression on tumour volume of sub-cutaneous xenografts grown in CD1 nude mice
(a) Mean tumour volume (n = 4). Final volume (mm^3): def = 238.7, pro = 78.1, p-value = 0.076. (b) Each line represents the tumour volume from 1 mouse.

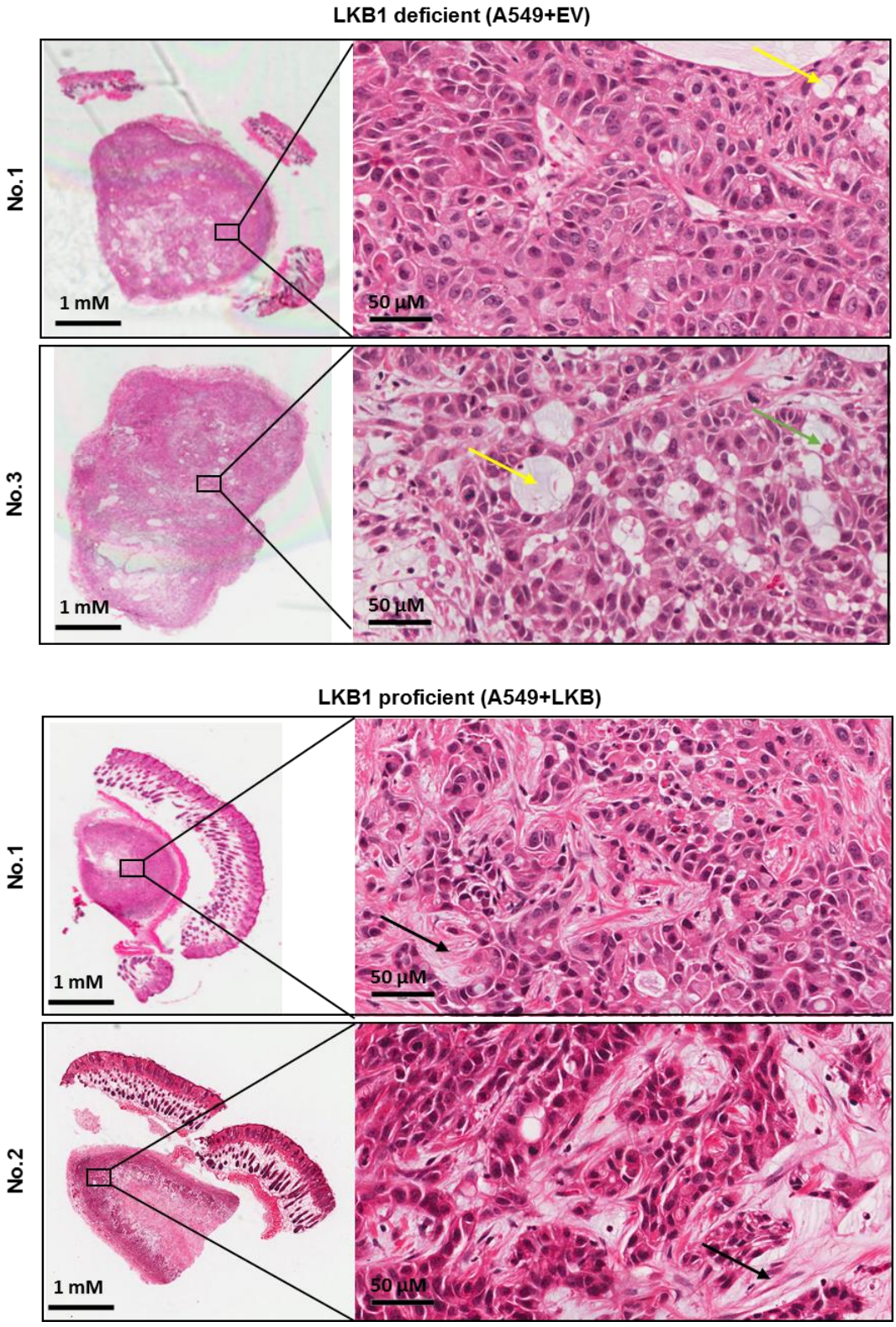

Figure 3.15: Haematoxylin and eosin stained sections of LKB1 deficient and proficient sub-cutaneous xenograft tumours from CD1 nude mice

H and E images at 1x and 40x magnification. Yellow arrows mark acellular gaps in LKB1 deficient tumours, and black arrows mark the stromal tissue in LKB1 proficient tumours respectively. The green arrow shows a possible apoptotic fragment.

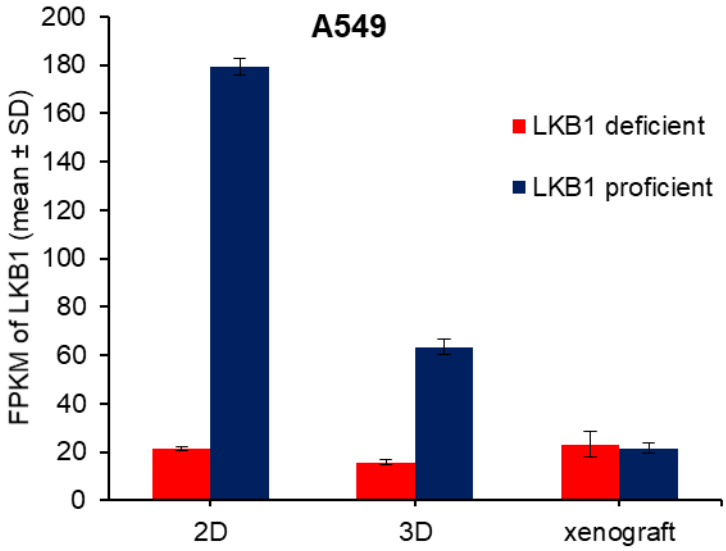

Figure 3.16: LKB1 mRNA expression in sub-cutaneous xenografts grown in CD1 nude mice
mRNA expression data (which will be further discussed in Chapter 4). Data represents the mean of independent duplicate samples. The LKB1 deficient xenografts were from mouse no. 1 and no. 3. The LKB1 proficient xenografts were from mouse no. 3 and no. 4.

3.6.2 Lung orthotopic model experiment 1

Sub-cutaneous xenografts have many advantages including the fact that they are relatively easy to implant. However, sub-cutaneous xenografts are not grown in their organ of origin and the tumours do not usually metastasise. Therefore, the effect of LKB1 expression on tumour burden and metastasis was determined in a lung orthotopic model using LKB1 deficient and proficient A549 cells grown in BALB/c nude mice. In this model, the cells were implanted into the left lung where they can grow and metastasise to the right lung. The development of tumours in this model can occur fast, usually within 2-3 weeks.

We utilised a model that was developed by Onn et al using lung weight as a primary endpoint (Onn et al., 2003). To establish the model, in addition to LKB1 deficient and proficient A549 cells, luciferase expressing A549-LVP cells were used to monitor tumour burden by IVIS. For this, luciferin, a luciferase substrate, was injected into the peritoneal cavity. Luciferase uses luciferin to catalyse the production of oxyluciferin and light (Lembert, 1996), that can be detected by an IVIS Spectrum (PerkinElmer). A549-LVP cells are LKB1 deficient,

therefore, we expected them to have a similar tumour burden to A549+EV cells which caused a greater tumour in the sub-cutaneous xenograft study (Figure 3.14). IVIS was used to detect tumour burden at day 2, 7, 11 and 14 post implantation (Figure 3.17). However, the signal was reduced on day 11 for two mice and on day 14 for another mouse. A possible explanation for this is that LVP was also expressed under the CMV promoter, which may be negatively regulated *in vivo* (see Section 3.6.1).

On day 14 post implantation, LKB1 deficient cells (A549+EV) caused greater tumour burden in the left and right lung by post mortem examination of the whole lung, lung weight and H and E staining of lung sections. Lungs implanted with LKB1 deficient cells appeared to have greater surface lesions (Figure 3.18a). The mean combined left and right lung weight for the LKB1 deficient group was significantly greater (p-value = 0.01) than that of the LKB1 proficient group (Figure 3.18b). Tumour tissue was detected in H and E stained sections from the LKB1 deficient but not the LKB1 proficient groups (Figure 3.18c). The tumour tissue within the LKB1 deficient groups also had acellular gaps consistent with the sub-cutaneous xenografts and spheroids (Figure 3.9 and 3.15).

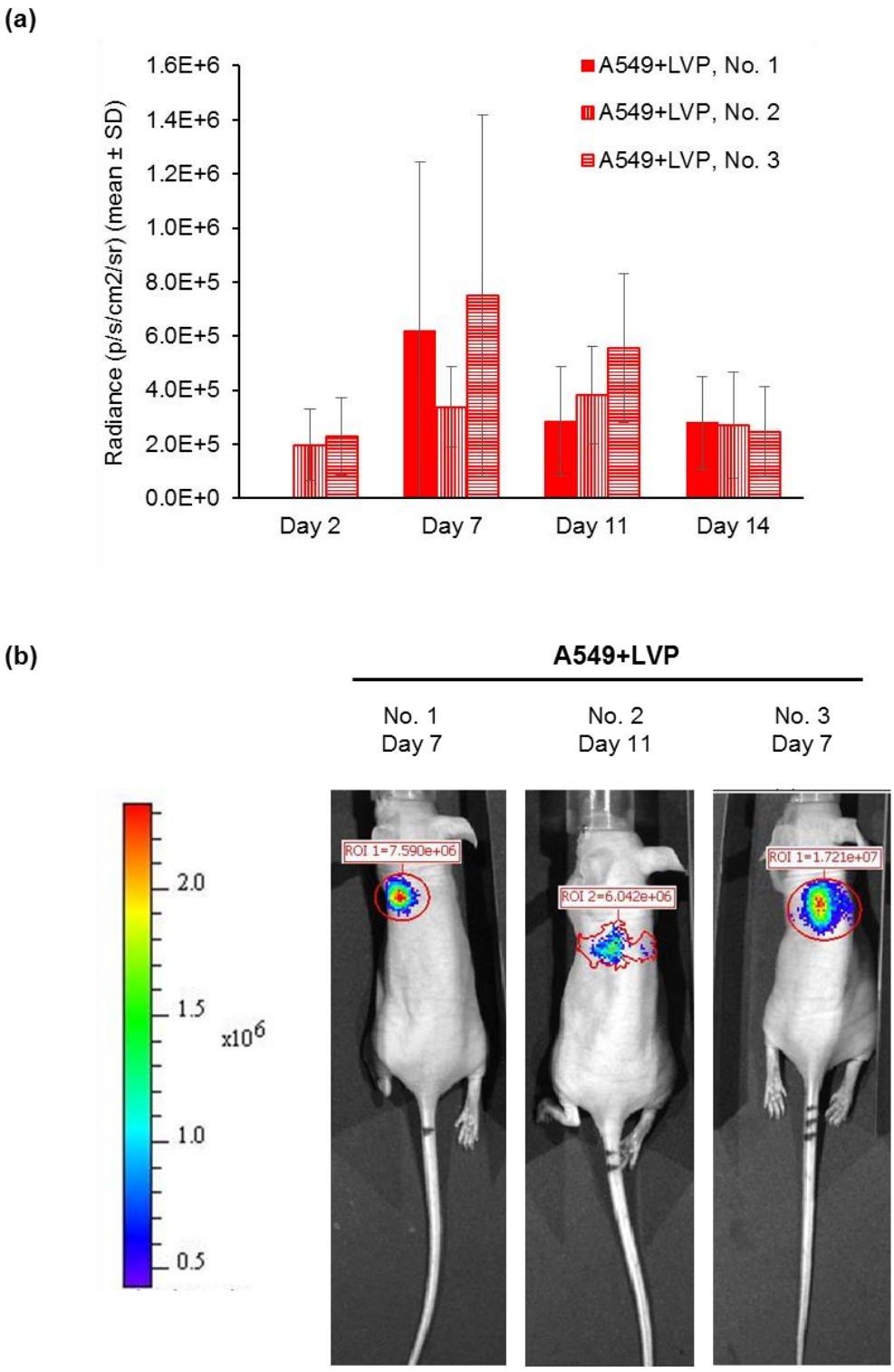

Figure 3.17: Monitoring tumour burden in the lung orthotopic model using IVIS imaging

(a) Each value represents the maximum radiance (p/s/cm^2/sr) collected after i.p. injection of luciferin. No data was collected for mouse no. 1 on day 2 as maximum radiance was achieved before imaging took place for this mouse. (b) The colour chart values indicate the p/s/cm^2/sr (radiance). The mice photos represent those when the maximum radiance signal was collected.

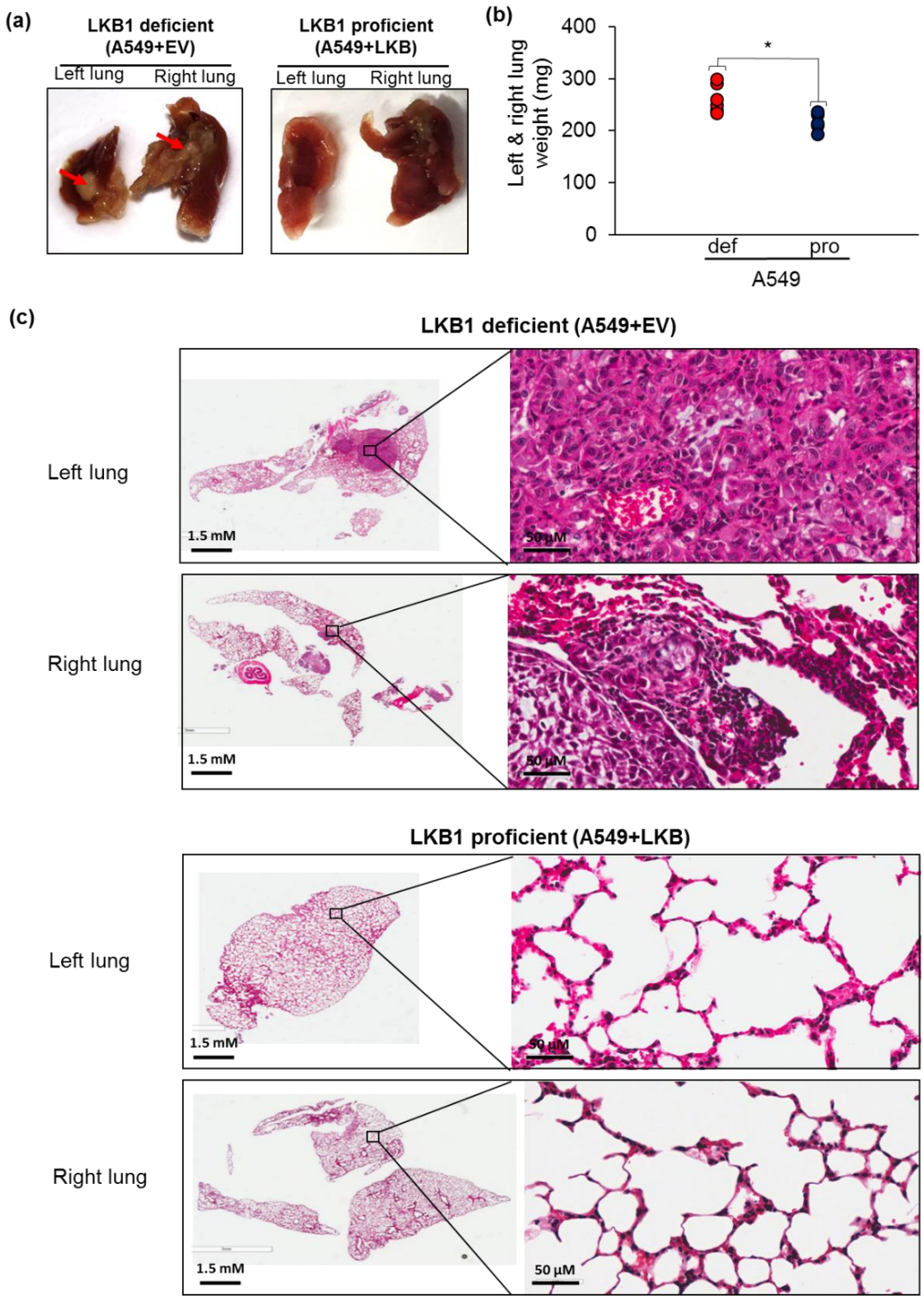

Figure 3.18: The effect of LKB1 on tumour burden in a lung orthotopic model in BALB/c nude mice

(a) Images of 4% PFA fixed lungs from the LKB1 deficient and proficient A549 group. Red arrows represent surface lesions. (b) Combined weight of left and right lung. Mean for LKB1 deficient = 262.3 mg (n = 6), mean for LKB1 proficient = 217.2 mg (n = 5), p-value = 0.01. (c) H and E stained sections of the lungs from the LKB1 deficient and proficient A549 group. Tumour tissue is magnified in the LKB1 deficient group and lung tissue is magnified in the LKB1 proficient group.

3.6.3 Lung orthotopic model experiment 2

Although H and E staining and IHC gives information about the spatial distribution of the tumours, a limitation of using these as endpoints is that tumour burden was determined by a single 5 µM section through the lung, which may not be representative of the whole lung, as serial sections were not analysed. To address this, we completed an additional experiment but used lung weight and western blotting of the whole lung as endpoints. In this experiment, we monitored tumour burden using MRI with images acquired one day prior to tumour cell implantation and at 7 and 16 days post implantation. In the MR images, lungs appeared black (air = no signal) and tumours/tissue was identified as having a white signal (Figure 3.19). However, many biological processes can contribute to the white signal including blood, inflammation, oedema, and fibrosis (Kurihara et al., 2014). Therefore, MRI was combined with lung weight and western blotting to determine tumour burden (Figure 3.19-3.22).

Using the ITK-SNAP software to analyse the MR images, tumour volume was quantified as a percentage of total lung volume. On day 16, the percentage tumour volume was significantly greater (p-value = 0.004) in the LKB1 deficient group compared to the proficient group (Figure 3.20a). Also, the left and right lungs of each group were weighed and the right lungs were significantly heavier in the LKB1 deficient group compared to the proficient group (p-value = 0.0039) (Figure 3.20b).

To measure the total tumour burden of the whole lung, we established a western blotting assay. Anti-mitochondrial antigen antibody (113-1) specifically reacts with the human antigen and does not cross react with mouse antigen (Figure 3.21). While this work was in progress, others reported a similar approach to detect human cells in a mouse xenograft model but using IHC (Thibaudeau et al., 2014). Our results showed that there appeared to be a higher level of mitochondrial protein in the left and right lungs of the LKB1 deficient group (Figure 3.22a). This suggests that lungs implanted with LKB1 deficient cells were

associated with greater tumour burden in the left lung and metastasis to the right lung. This result supported the data from the sub-cutaneous xenograft model that also indicated LKB1 loss was associated with greater tumour burden.

The anti-mitochondrial antigen antibody was raised in mouse. Therefore, the use of an anti-mouse secondary antibody can react with mouse immunoglobulins (Ig) (Figure 3.21). Mitochondrial protein expression is detected at 60 kDa and mouse Ig heavy and light chains are detected at 50 and 25 kDa. The secondary antibody used in Figure 3.22a only reacted with the native form of mouse Ig. As the samples were denatured, only the mitochondrial signal was detected. In Figure 3.22c, we used an anti-mouse secondary antibody that reacts with denatured Ig allowing the Ig heavy and light chains to be seen. It appeared that the presence of human tumour cells may have stimulated a greater systemic immune response as there was no Ig detected in the control lungs (with no tumour cells implanted) and Ig heavy and light chain expression appeared to correlated with mitochondrial signal, in most instances. This could indicate that components of immune response may drive tumour progression. As there was greater mitochondrial signal in the lungs from the LKB1 deficient group, there was also greater Ig expression in this group. It was reported that LKB1 loss is associated with increased neutrophil recruitment and the release of pro-inflammatory cytokines (Koyama et al., 2016) which supports a link between LKB1 expression and immune response in tumours.

The correlation between the use of MRI, lung weight and western blotting for detecting tumour burden was determined (Figure 3.23). There was a strong positive correlation between left lung weight and left lung mitochondrial signal, which decreased when comparing the right lung. Left mouse lung consists of 1 lobe while right mouse lung consists of 4 lobes. At the end of the experiment, the left lung was removed first and then the remaining tissue was removed. Therefore, there was a higher risk of removing non-lung

tissue during removal of the right lung. There was also a positive correlation between the lung weight and MRI but less correlation between MRI and mitochondrial signal (Figure 3.23). These data suggest that correlation between lung weight and mitochondrial signal was best when combining both left and right lung and in particular, when comparing the left lung. However, since each endpoint has limitations, the use of multiple endpoints to assess tumour burden may be required.

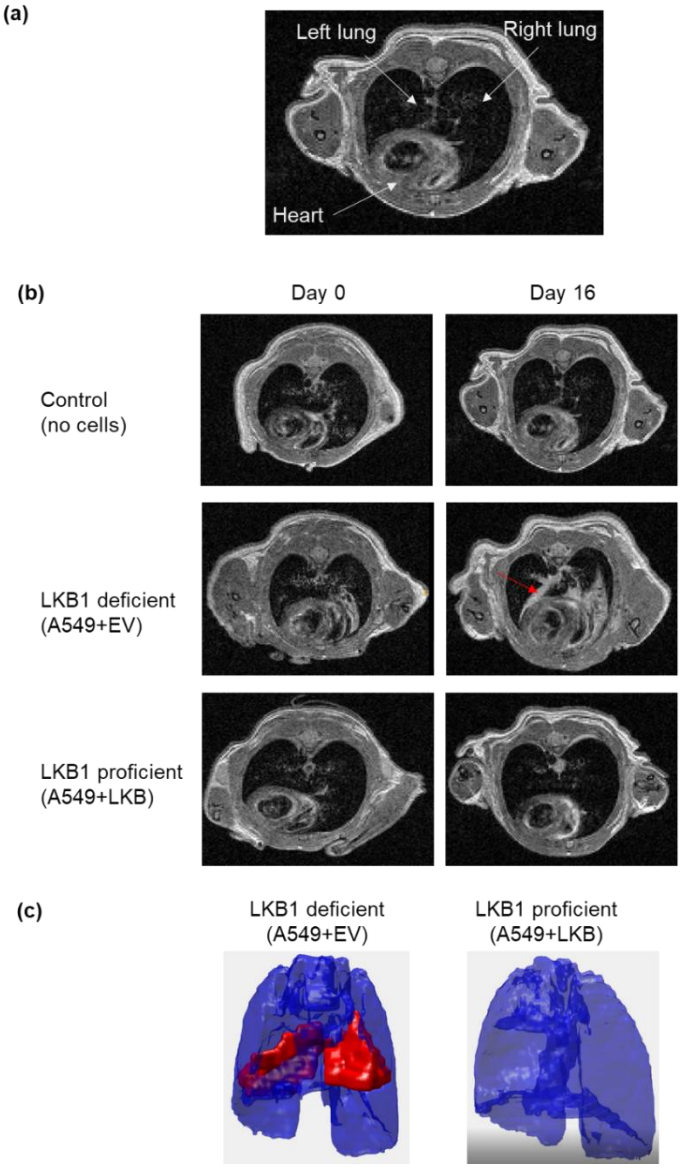

Figure 3.19: Monitoring the effect of LKB1 expression on tumour burden of a lung orthotopic model in BALB/c nude mice using MRI

(a) One section of a MR image showing the heart, left lung and right lung. (b) Representative section of MR images. White signal (possibly tumour) is marked with an arrow. (c) Using ITK-SNAP, the MR images were segmented and the lung and tumour/white signal within the lung were identified. The images represent 3D projections showing the lungs in blue and tumour in red.

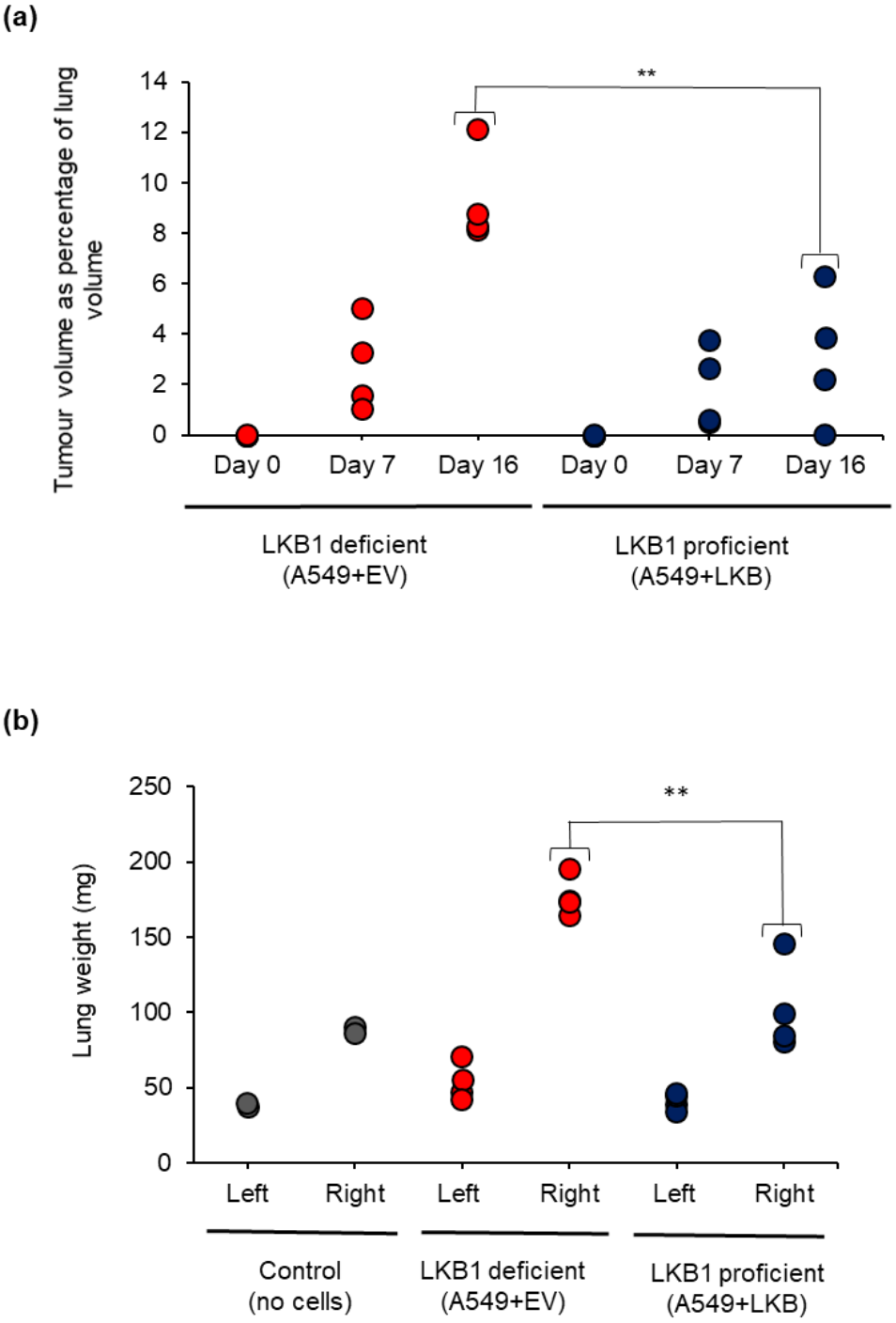

Figure 3.20: The effect of LKB1 expression on tumour burden in a lung orthotopic model in BALB/c nude mice using MRI and lung weight as endpoints

(a) Using ITK-SNAP software, tumour volume was calculated as a percentage of the total lung volume. Each point represents data from 1 of 4 mice. On day 16, the % tumour volume was significantly greater in the deficient group (def 9.31%, pro = 3.08%, p-value = 0.0042). (b) Weight of left and right lungs on day 16. Each point represents data from 1 of 2 mice for control and 1 of 4 mice for LKB1 deficient and proficient groups. The weight of the right lungs with deficient cells were significantly greater than the right lungs with proficient cells (mean weight of right lung; def = 176.75 mg, pro = 102.24 mg, p-value = 0.0039).

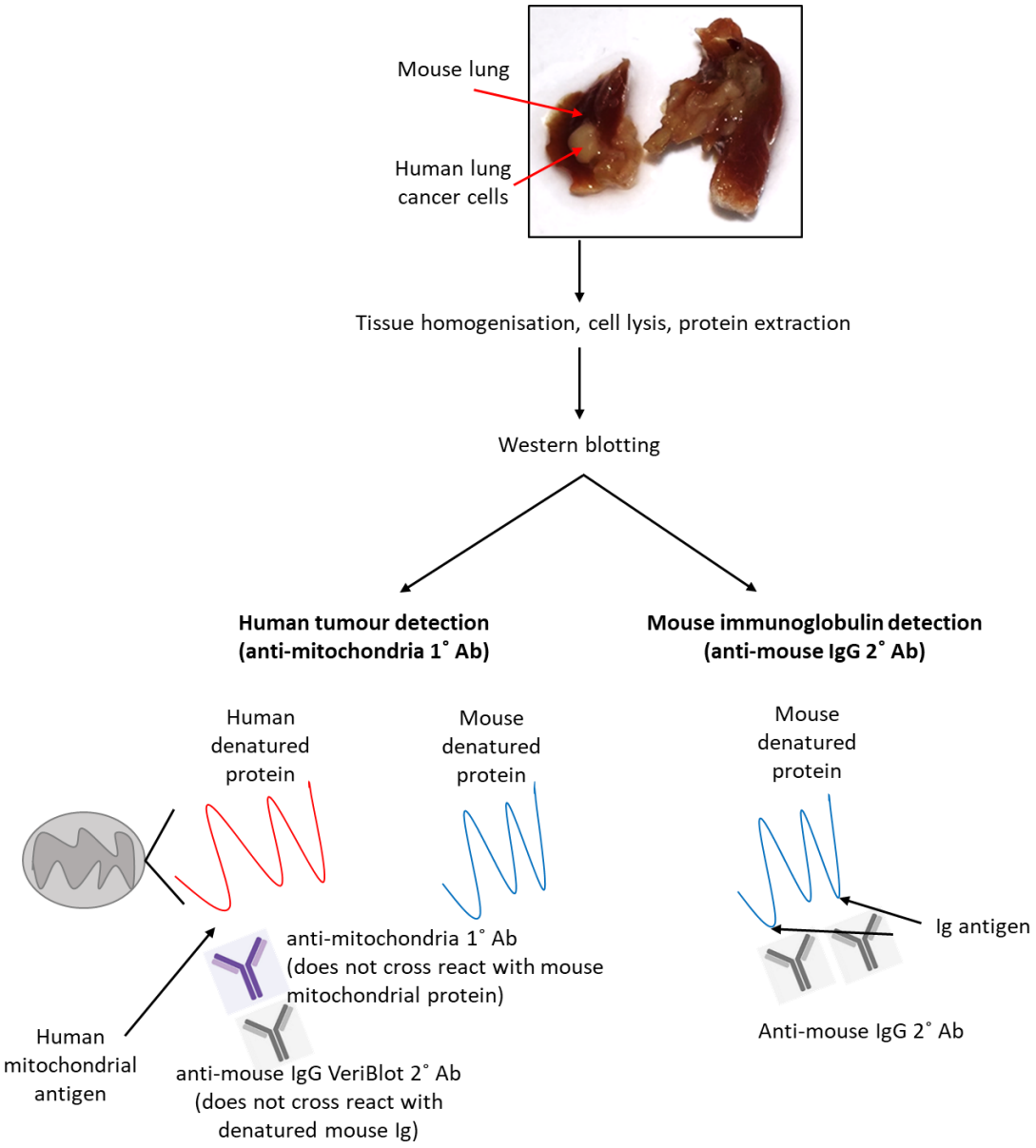

Figure 3.21: Schematic showing the use of western blotting to specifically detect human lung cancer cells in mouse lung

Anti-mitochondrial antigen antibody (113-1) reacts with a human antigen and does not cross react with a mouse antigen. However, it was raised in mouse. Therefore, the use of anti-mouse IgG secondary antibody would also detect mouse immunoglobulins. Anti-mouse IgG VeriBlot is a secondary antibody that only reacts with native forms of Ig. For western blotting, all protein samples were denatured, therefore anti-mouse IgG VeriBlot secondary antibody does not react with the denatured Ig. 1˚ - primary antibody, 2˚ - secondary antibody.

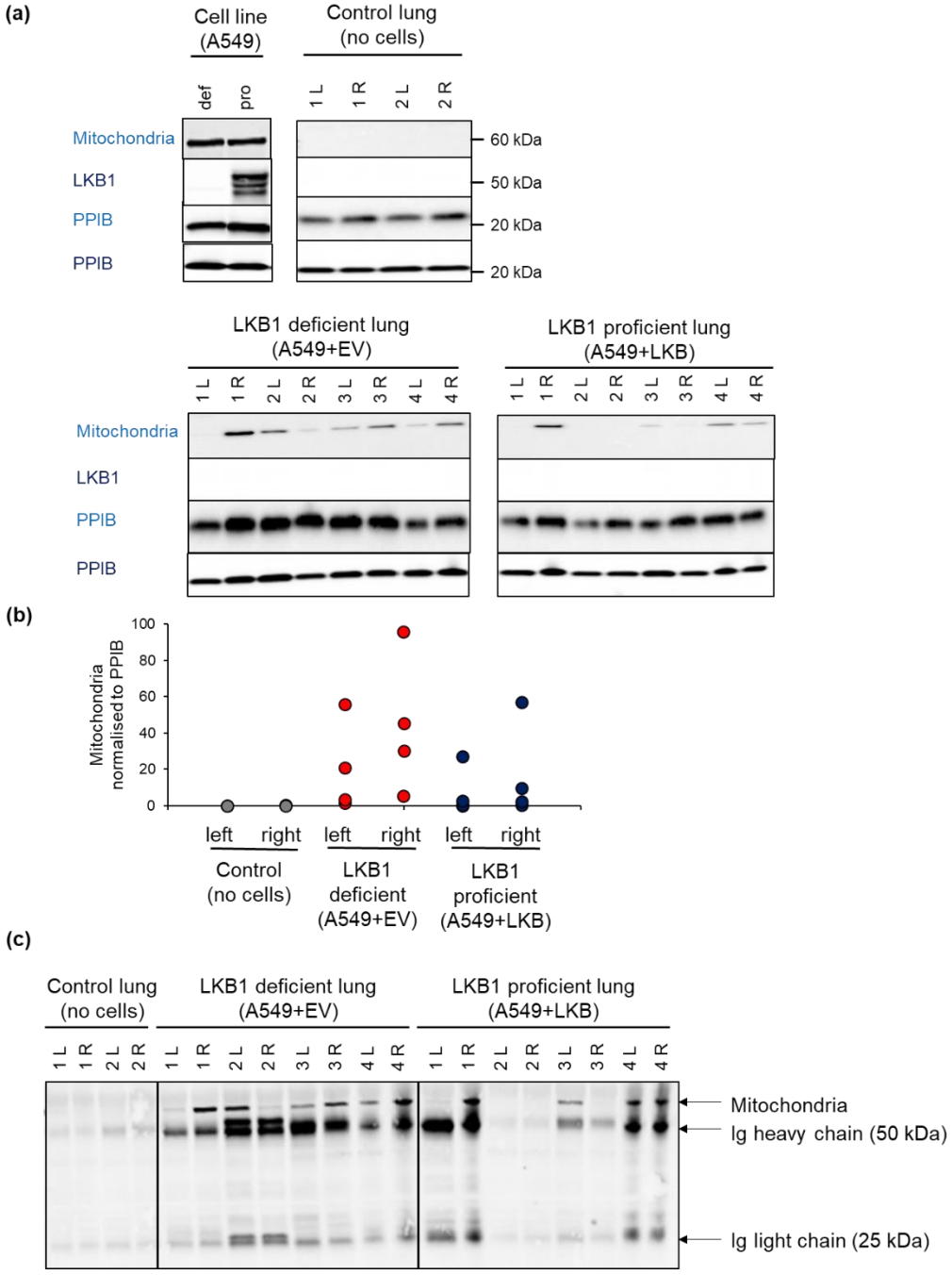

Figure 3.22: Western blotting to detect mitochondrial, LKB1 and immunoglobulin protein expression in the lung orthotopic model using BALB/c nude mice

(a) Western blotting where mitochondria signal was reflective of tumour burden. 50 µg of protein was loaded per well and bands were detected by enhanced chemiluminescence (ECL). "L" represents the left lung and "R" represents the right lung. A549 cells were used as a positive control and control lungs (no cells implanted) were used as a negative control for mitochondrial signal. Western blotting also shows LKB1 expression (a) and Ig expression (c). (b) Mitochondrial signal was quantified using Image Studio Lite software and normalised to PPIB. LKB1 deficient lung - mouse lung with human LKB1 deficient cells, LKB1 proficient lung - mouse lung with human LKB1 proficient cells.

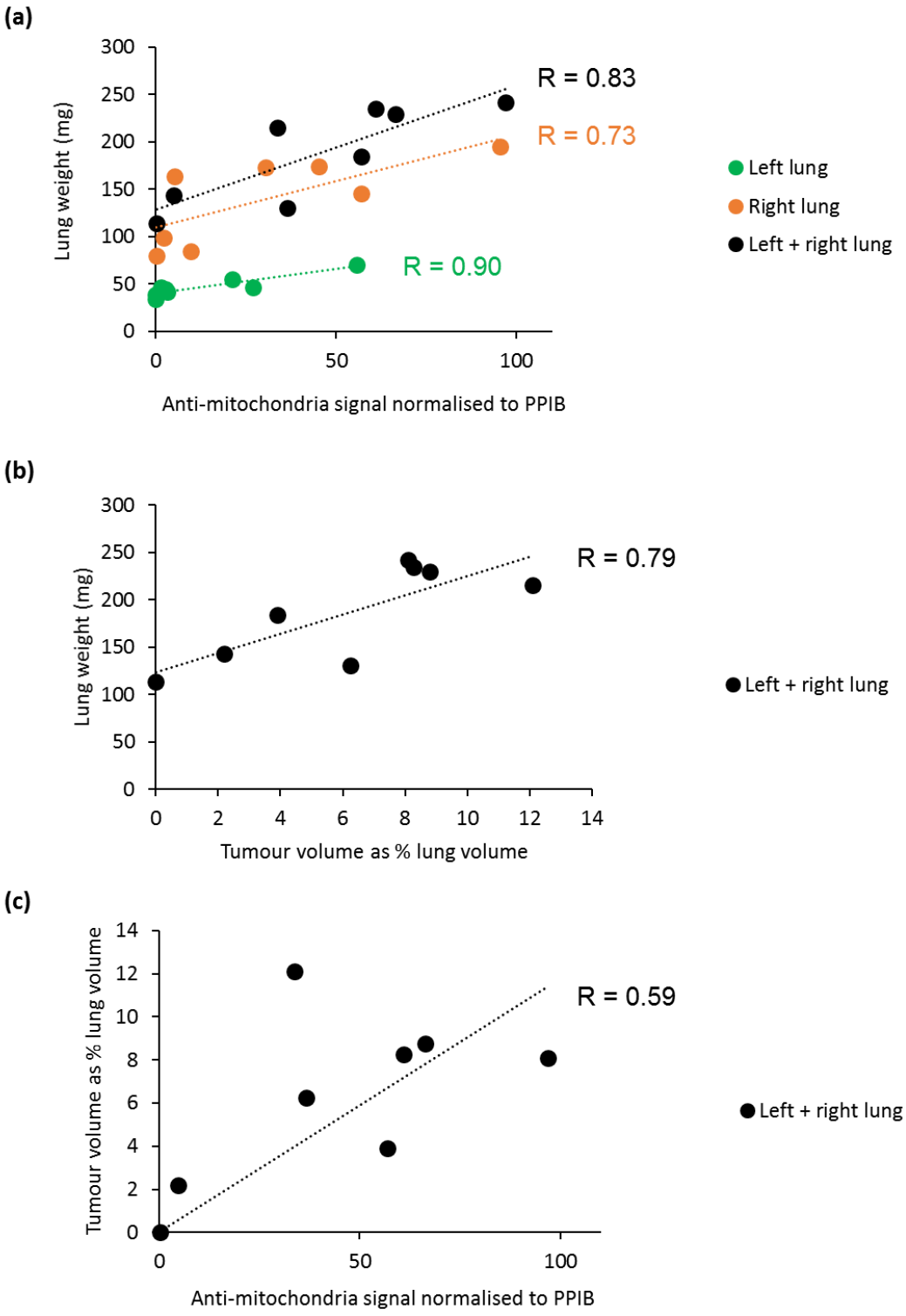

Figure 3.23: Correlation between MRI, lung weight and western blotting (mitochondrial signal) as methods to measure tumour burden in the lung orthotopic model

No.s represent Pearson "R" between (a) lung weight and mitochondrial signal, (b) lung weight and MRI and (c) MRI and mitochondrial signal. (a) n = 4 for either left or right lung and n = 8 for left and right lung. (b, c) n = 4 for left and right lung. p-value < 0.05 for all correlations except (c) which was not significant.

3.6.4 Lung orthotopic model experiment 3

As LKB1 expression was lost in the sub-cutaneous xenografts at 48 days post implantation, we hypothesised that LKB1 would remain expressed in the lung orthotopic model at 16 days post injection. However, western blotting showed that LKB1 expression was below the detectable limit and Ig expression was increased in the presence of mitochondrial protein (Figure 3.22). This suggests that the presence of tumour cells increased mouse inflammation in the lung tissue which may have negatively impacted on the CMV promoter.

To overcome the issue of loss of LKB1 expression, the experiment was extended to NOD/SCID gamma (NSG) mice using lung weight and western blotting as endpoints. Although BALB/c nude mice lack T cells, they have B cells and highly activated natural killer cells. NSG mice have no mature T cells, B cells and no natural killer cells (Belizário, 2009). As NSG mice have a more compromised immune system and as it was suggested that the immune system may play a role in the negative regulation of the CMV promoter *in vivo* (Papadakis et al., 2004), we hypothesised that LKB1 expression would remain high if mice are more immune compromised. At 16 days post injection, there was less tumour burden in the NSG mice compared with the BALB/c nude mice as surface lesions were not evident on the lungs (Figure 3.24a), and compared to the BALB/c nude mice (Section 3.6.2 - 3.6.3), there was a less marked increase in lung weight and mitochondrial protein expression (Figure 3.24b,c). This suggests that the more competent immune system of the BALB/c nude mice could contribute to tumour burden. LKB1 expression was not detected by western blotting, however, this could be due to the low number of cancer cells (Figure 3.24c). Nonetheless, the mitochondrial signal was greater in the LKB1 deficient group compared to the proficient group supporting our hypothesis and the previous results that LKB1 loss is associated with greater tumour burden *in vivo*.

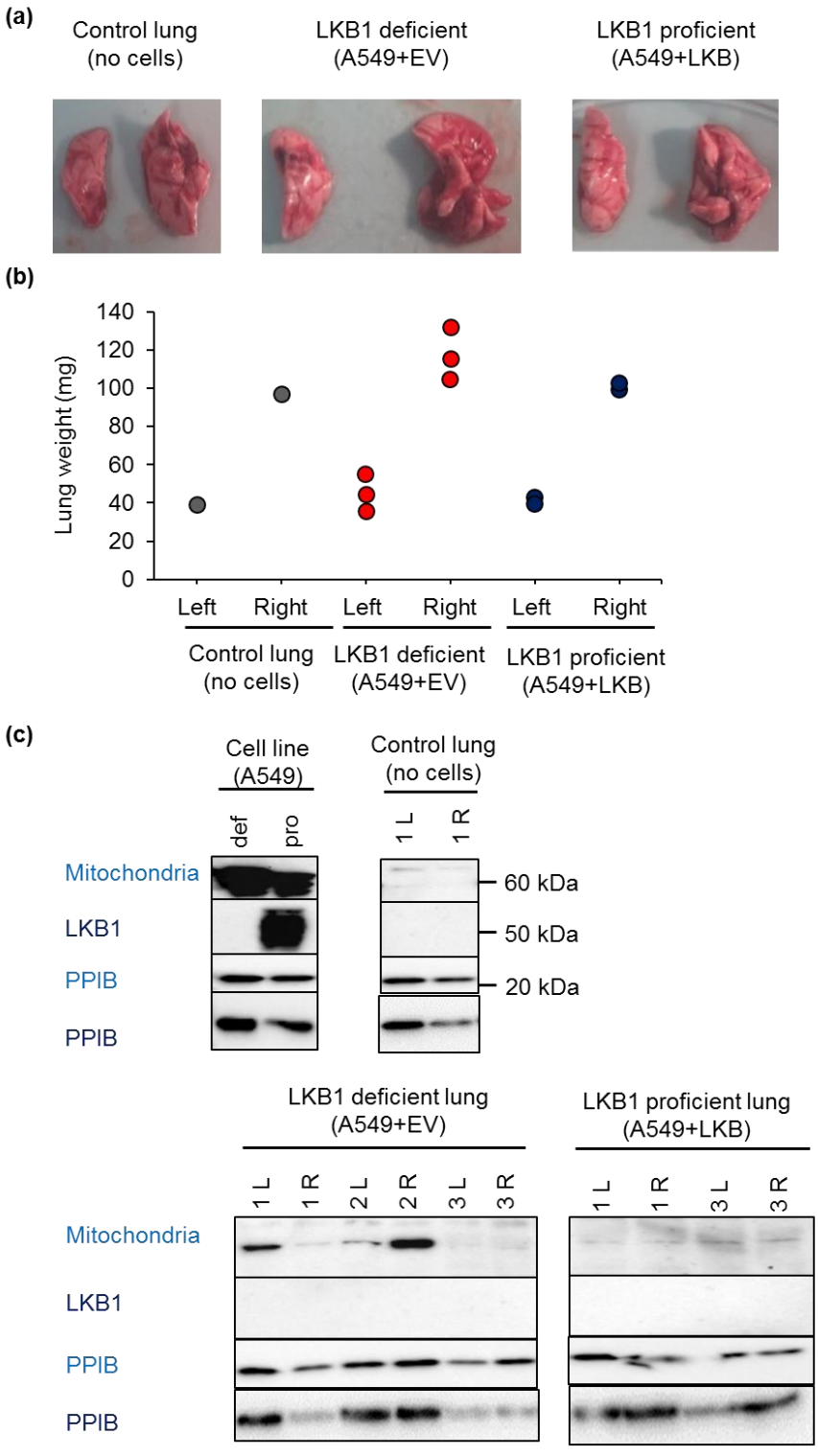

Figure 3.24: The effect of LKB1 expression on tumour burden in the lung orthotopic model using NOD/SCID gamma mice

(a) Representative images of the mouse lungs. (b) Lung weight at 16 days post injection. Each point represents data from 1 mouse. (c) Western blotting showing mitochondria and LKB1 expression. 100 µg of protein was loaded per well and bands were detected using ECL. The secondary antibody used here does not cross react with mouse Ig. "L" – left lung, "R" – right lung. LKB1 deficient lung - mouse lungs with human LKB1 deficient cells, LKB1 proficient lung - mouse lungs with human LKB1 proficient cells.

3.6.5 Summary of *in vivo* data

The LKB1 deficient cells were associated with greater tumour burden in the sub-cutaneous xenografts and lung orthotopic models (Table 3.1). In addition, the LKB1 deficient group had greater metastasis to the right lung in the orthotopic model. Although increased LKB1 mRNA expression in proficient cells was lost *in vivo*, it was reported that LKB1 is lost in the early stages of cancer development (Ghaffar et al., 2003) and is considered a trunk mutation (Zhang et al., 2014), therefore, the difference in LKB1 expression between the deficient and proficient cells may have the greatest impact in the early stages of *in vivo* growth. A possible role of LKB1 loss in early tumour development may be to increase survival in hostile environments. Moreover, the difference in tumour burden between the BALB/c nude mice and the NSG mice suggest that the immune system may play a role in cancer growth as the more immune compromised NSG mice had less tumour burden compared with the BALB/c nude mice.

Table 3.1: Summary of the *in vivo* data

Model	Endpoint	LKB1 deficient	LKB1 proficient
Sub-cutaneous xenograft - CD1 nude	Tumour volume	✓✓✓[1]	✓
	Tumour detected by H and E	✓✓	✓
Orthotopic model 1 - BALB/c nude	Surface lesions on lung	✓✓	✓
	Lung weight	✓✓	✓
	Tumour detected by H and E	✓✓	NF[2]
Orthotopic model 2 - BALB/c nude	"Tumour" [3] detected by MRI	✓✓✓	✓
	Lung weight	✓✓✓	✓
	Tumour detected by western blotting	✓✓✓	✓
Orthotopic model 3 - NSG	Surface lesions on lung	NF	NF
	Lung weight	✓	x[1]
	Tumour detected by western blotting	✓✓	✓

1 ✓ indicates the presence of tumour, x indicates no evidence of tumour
2 NF - not found
3 "Tumour" indicates white signal detected in lung tissue using MRI and assumed tumour

3.7 Discussion

In this Chapter, we aimed to examine LKB1 expression in a range of lung cancer cells, generate isogenic cells and investigate the effect of LKB1 on cell proliferation in 2D, 3D and two *in vivo* models. As LKB1 was reported to play an important role in cell polarity (Section 1.3.1), we evaluated differences in cytoskeletal structure and cell migration in 2D culture, as well as differences in spheroid structure, cytoskeleton and cell-cell/cell-ECM contacts.

The Cancer Genome Atlas (TCGA) showed using DNA sequencing that LKB1 is mutated in 17% of lung adenocarcinoma samples (n = 230) (TCGA, 2014). However, this may be an underestimate as LKB1 mutated tumour cells are co-located with stromal cells with wild-type LKB1. Furthermore, LKB1 can be inactivated by other mechanisms like promoter methylation which may be true for CORL105, a cell line reported to be LKB1 wild-type but does not express LKB1. Other groups have investigated alternative approaches to detect LKB1 loss in tumours including an IHC assay (Calles et al., 2015) and identification of 16 genes whose expression is different between LKB1 expressing and non-expressing cells (Kaufman et al., 2014).

Using isogenic cells with or without LKB1, we found that LKB1 expression caused no marked difference in cell proliferation in 2D culture but LKB1 loss was associated with larger 3D spheroids and greater tumour burden and metastasis *in vivo*. The use of 3D spheroids has proven very useful as they are considered more representative of the tumour microenvironment compared to 2D culture (Lin and Chang, 2008) (Section 3.1). In our study, H and E staining of LKB1 deficient and proficient spheroids was similar to that of the sub-cutaneous xenografts whereby, the LKB1 deficient samples contained acellular gaps and the proficient samples contained more stromal like tissue. LKB1 deficient A549 and

H1299 cells formed larger spheroids with a less defined edge, compared with LKB1 proficient spheroids. The LKB1 deficient spheroids had a greater cell number suggesting that LKB1 loss is important for cell survival in a stressful environment, as in the spheroid assay, nutrients are more limited due to a high cell seeding density. Although LKB1 deficient spheroids had more acellular gaps containing material positive for the apoptosis marker; cleaved caspase 3, the rate of proliferation was greater than the rate of apoptosis. LKB1 deficient cells were dominant in a spheroid co-population, further suggesting that they do have a survival benefit. It has been reported that LKB1 negatively regulates MTOR dependent protein synthesis, therefore LKB1 loss is associated with activated MTOR signalling. Even during energy stress, LKB1 deficient cells have increased pS6 and p4EBP1 expression which are proteins involved in protein translation and cell growth (Shaw et al., 2004a).

In vivo, LKB1 deficient cells have a marked growth advantage. LKB1 loss was associated with greater tumour burden in a sub-cutaneous xenograft and greater tumour burden and metastasis in a lung orthotopic model. This is in line with published data, where they have used GEMMs, however GEMMs have limitations (which were discussed in Section 1.6). The use of the lung orthotopic model is a novel model in the field of LKB1. This model was originally established by Onn et al using lung weight as a primary endpoint (Onn et al., 2003). The use of MRI and western blotting to determine tumour burden in this model is also novel and has proven useful. Western blotting gives the total tumour burden, whilst MRI can give the spatial information. It appeared that the immune system may play a role in tumour burden as we observed greater tumour burden at 16 days post implantation in the BALB/c nude mice compared to the NSG mice, which have a more compromised immune system.

STRAD may help to understand the link between LKB1 and the immune response. STRAD, a protein that forms a complex with LKB1 to translocate it and activate it, was expressed as 2 bands with the upper bands being upregulated in the presence of LKB1. We speculated that STRAD may be cleaved by caspase 1 and LKB1 may be involved in the stabilisation of STRAD by a direct interaction or by negatively regulating caspase 1 (Section 3.2). Future experiments could determine if STRAD is cleaved in LKB1 deficient cells in the presence of a caspase 1 inhibitor and utilise immunoprecipitation to determine if LKB1 or STRAD does interact with caspase 1. Interestingly, caspase 1 was reported to play a role in the maturation of the pro-inflammatory cytokines; IL1β and IL18 (Salvesen and Dixit, 1997). We utilised RNA Sequencing to determine difference in gene expression between LKB1 deficient and proficient A549 cells. This will be discussed further in Chapter 4, however, briefly, we observed that in 2D culture, there was greater IL18 mRNA expression in the LKB1 deficient cells ($log_2fc = 1.38$, q-value = 0.008), suggesting that LKB1 loss increases the activity to caspase 1 which can further increase the maturation of the pro-inflammatory cytokine; IL18. Others have also reported a pro-inflammatory environment in tumours from a $Kras^{G12D}/Lkb1^{-/-}$ driven mouse model of lung cancer (Koyama et al., 2016).

A limitation of our *in vivo* work is that LKB1 expression was lost in LKB1 proficient cells by the end of the experiments. However, as mentioned (Section 3.6.5), LKB1 was reported to be a trunk mutation (Zhang et al., 2014) and the difference between LKB1 deficient and proficient cells may be most prevalent in the early stages of cancer development before the establishment of tumours. Nonetheless, it would be interesting to complete a shorter *in vivo* experiment to determine what day LKB1 expression is lost. We speculated that LKB1 expression was lost through negative regulation of the CMV promoter (which drives LKB1 expression) as it was reported that CMV promoter was negatively regulated *in vivo* by an immune response or epigenetic regulation (Morrissey et al., 2013, Papadakis et al., 2004,

Brooks et al., 2004). Future work could also use alterative eukaryotic/human promoter like EF1A to drive LKB1 expression.

Despite the increased metastatic potential of LKB1 deficient cells, these cells had increased integrin-β1 expression and a smaller Euclidean distance in 2D culture. We hypothesised that LKB1 deficient cells interact more with the ECM through integrin-β1 and interact less with other cells through lack of expression of β-catenin at the periphery of the cell. We speculate that the role of LKB1 loss in lung cancer is analogous to the role of APC loss in colorectal cancer which is found in 90% of tumours. It is known that one of the many roles of APC loss is to cause the re-localisation of β-catenin to the nucleus where it promotes the transcription of several oncogenes including MYC (Morin et al., 1997). Immunofluorescence images of β-catenin suggests a similar effect in LKB1 deficient cells. While this work was in progress, others also reported that LKB1 loss was associated increased WNT/β-catenin signalling in intrahepatic cholangiocarcinoma cells (Wang et al., 2015).

To conclude, the effect of LKB1 on cell proliferation was more apparent in 3D spheroids and *in vivo* models. LKB1 loss was associated with growth of larger 3D spheroids. *In vivo*, LKB1 loss was associated with larger sub-cutaneous xenografts and increased tumour burden and metastasis in the lung orthotopic model.

4 Understanding the role of LKB1 loss in lung cancer

4.1 Introduction

To understand the role of LKB1 loss in lung cancer, other groups have used "omics" approaches by investigating global changes in DNA, RNA and protein expression (Ji et al., 2007, Carretero et al., 2010, Liu et al., 2013, Kaufman et al., 2014) (Section 1.6). Although other groups compared the RNA expression between LKB1 deficient and proficient samples using cell lines, mouse lung tumours and human tumours, to our knowledge, it has not been reported in 3D spheroids. To further understand the role of LKB1 loss in lung cancer, whole transcriptomic profiling was used to determine the differences in mRNA expression between LKB1 deficient and LKB1 proficient A549 cells grown in 2D culture, 3D spheroids, and from human lung adenocarcinoma tumour samples. Differences in mRNA expression between the 3 models; 2D culture, 3D spheroids and sub-cutaneous xenografts, were also determined.

4.2 mRNA sequencing and analysis

RNA was collected from LKB1 deficient (A549+EV) and LKB1 proficient (A549+LKB) cells grown in 2D culture (for 2 days; until sub-confluency), as 3D spheroids (for 5 days) and as sub-cutaneous xenografts (for 43 or 48 days; mean final volume of deficient samples = 244 mm^3, mean final volume of proficient samples = 117 mm^3 (Section 3.6.1)) (Figure 2.3). Independent duplicate samples were prepared, sequenced and analysed. In brief, the mRNA from the 12 samples was isolated by poly (A) capture and sequenced using a Next Generation Sequencing (NGS) platform - Illumina HiSeq2000 platform by Oxford Gene Technology (OGT). An average of 28,215,145 paired end reads per sample were mapped onto the human genome (GRCh37) and assembled into transcripts/genes. For each

sample, more than 13,806 genes were identified. The abundance of each gene was represented as FPKM (fragments per kilobase per million mapped reads). For each gene, differences in the FPKM levels between samples were expressed as $\log_2$(fc) and compared to identify any significant (q-value < 0.05) gene expression differences. The RNA sequencing and analysis was reproducible as there were no significant differences in gene expression between independent duplicates.

4.3 Differences in mRNA expression between 2D, 3D and xenograft models

4.3.1 Differences in biological processes between models

To determine the differences in the gene expression signature between the models, the significant differentially expressed genes between the 2D and 3D (2D-3D), 2D and xenograft (2D-xenograft) or 3D and xenograft (3D-xenograft) models, which were different in both LKB1 deficient and proficient cells, were identified (Figure 4.1). This identified genes differentially expressed between the models that were independent of LKB1 status. The results showed that there were approximately 2000 significant differentially expressed genes when comparing both 2D-3D and 2D-xenograft models. Importantly, there were less differentially expressed genes (approximately 1000) when comparing the 3D-xenograft models, suggesting that 3D spheroids had a more similar gene expression profile to the *in vivo* model, compared to 2D culture (Figure 4.1).

The significant differentially expressed genes between the 2D-3D, 2D-xenograft or 3D-xenograft were divided into 2 groups; higher expression in the more complex model and lower expression in the more complex model. The more complex model was 3D or xenograft when compared to 2D or 3D (i.e. increasing model complexity was 2D < 3D < xenograft). There were 191 genes with higher expression and 56 genes with lower expression in the

more complex model (Figure 4.1). To identify the biological/gene ontology (GO) processes different between the models, GOrilla was used (accessed February 2017) (see Section 2.10.3). There were 153 GO processes associated with the higher gene expression (enrichment p-value ≤ 0.001) and 9 GO processes associated with the lower gene expression (enrichment p-value ≤ 0.001). The top 50 GO processes from each group arranged in order of most to least significant can be found Appendices (Appendices Table A4.1-4.2). A GO process increased in the more complex model was immune response and a GO process decreased in the more complex model was cell division.

To get a broader understanding of the differences in gene signature from 2D culture to 3D spheroids or xenografts, the significant genes with high (n = 1261) and low (n = 1020) expression in 3D or xenograft compared to 2D were also analysed using GOrilla (accessed February 2017). There were 117 GO processes associated with the higher gene expression (enrichment p-value ≤ 0.001) and 488 GO process associated with the lower gene expression (enrichment p-value ≤ 0.001), between the 3D and xenograft models compared with the 2D model. The top 50 GO processes associated with high and low gene expression can be found in the Appendices (Appendices Table A4.3-4.4). There was an increase in expression of genes involved in hypoxia, catabolism and immune response and a decrease in expression of genes involved in cell cycle and DNA repair, in 3D and xenografts compared with 2D (Figure 4.1).

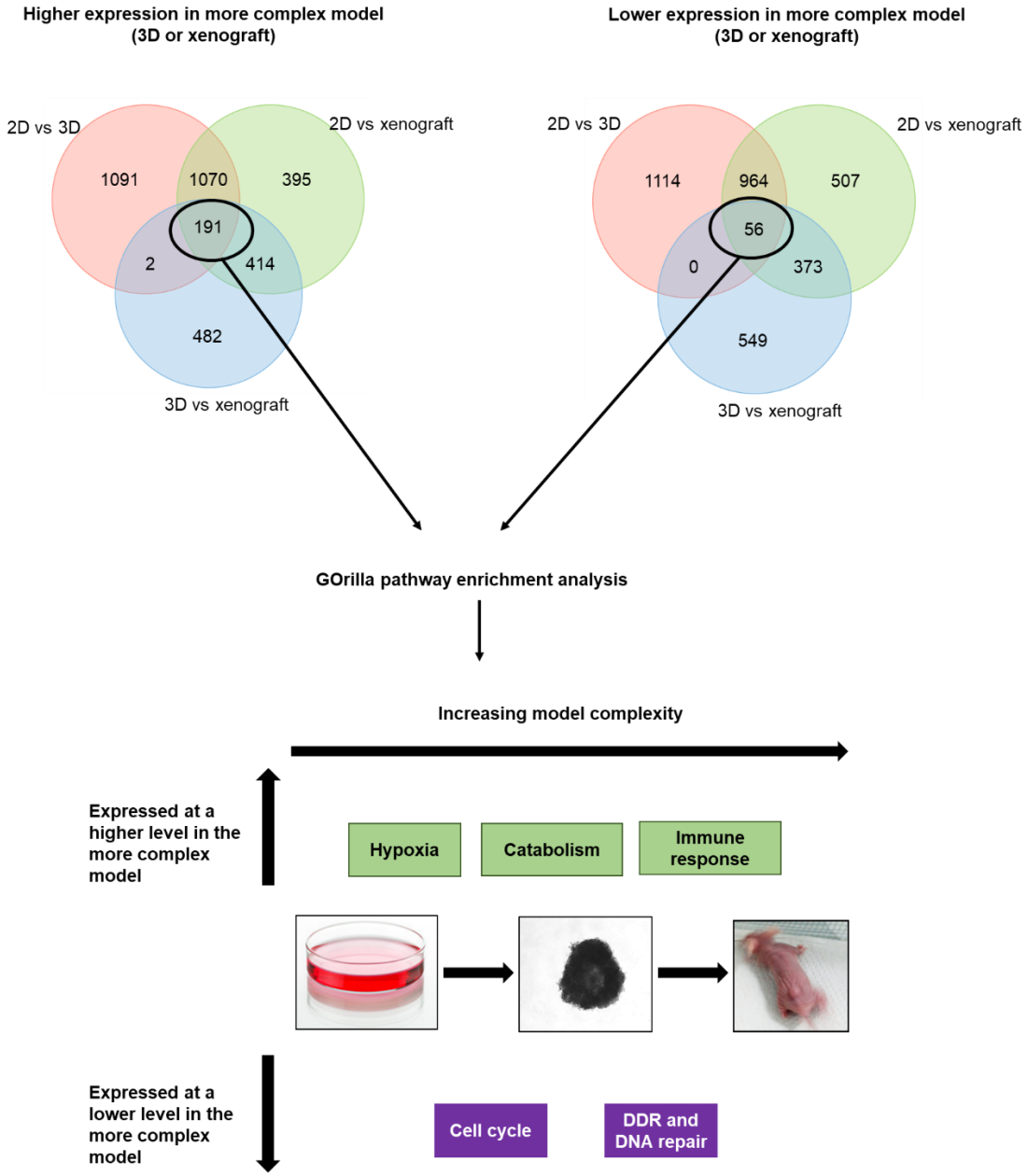

Figure 4.1: Common differences in gene expression between 2D, 3D and sub-cutaneous xenograft models, in LKB1 deficient and proficient cells
The Venn diagrams represent the number of genes expressed at a higher or lower level in 3D and xenograft models compared with 2D or 3D models respectively. These genes were differentially expressed in both LKB1 deficient and proficient cells. The data were overlapped using an online software (Heberle et al., 2015). GOrilla was used to identify biological processes enriched in (i) the more complex model and (ii) both the 3D and xenograft models when compared to the 2D model.

4.3.2 Confirmation of differences in mRNA expression between models

Figure 4.2 shows the abundance of genes involved in catabolism and hypoxia increasing from 2D to 3D or xenograft and the expression genes involved in cell cycle and DNA repair

decreasing from 2D to 3D or xenograft. To determine if the differences in mRNA expression correlated with protein expression, western blotting was used where protein expression for GLUT1 (catabolic), CA9 (hypoxic) and cyclin A (cell cycle), in 2D and 3D models were investigated (Figure 4.3). GLUT1 and CA9 expression were higher and cyclin A expression was lower in 3D spheroids compared to 2D culture.

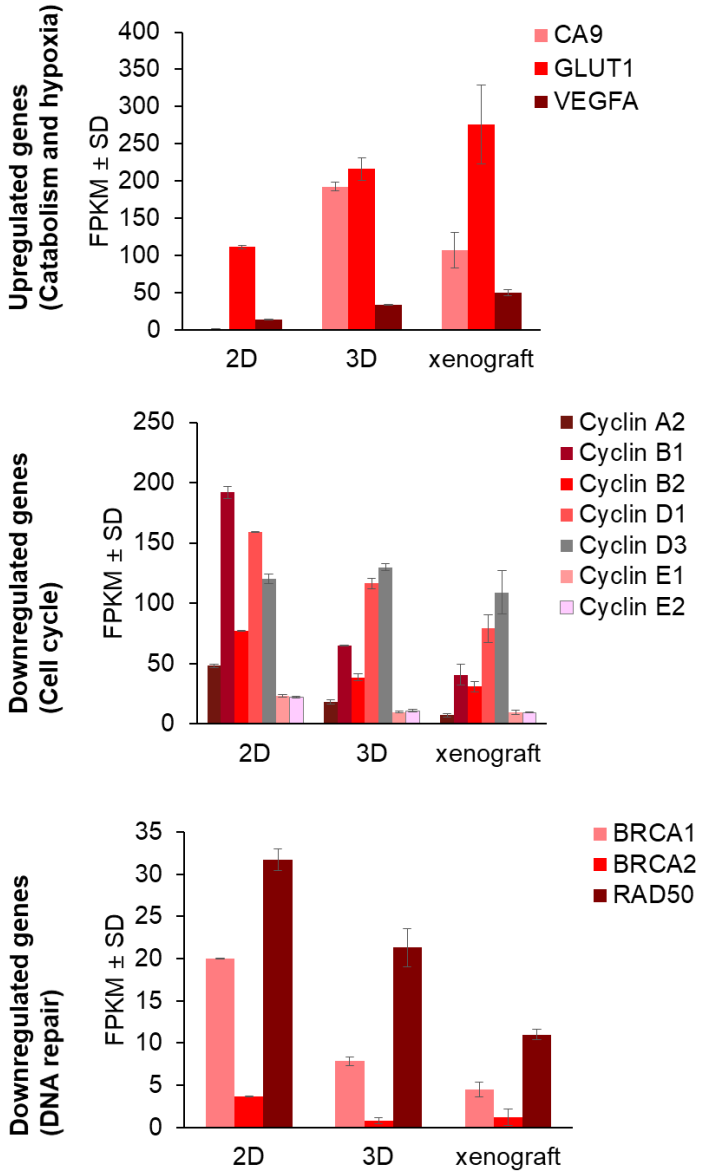

Figure 4.2: Genes that have high and low expression in 3D and xenografts compared to 2D culture

The expression of the genes from the catabolism, hypoxia, cell cycle and DNA repair pathways in LKB1 deficient A549 cells. Data represents the mean of values from independent duplicate samples. SD - standard deviation.

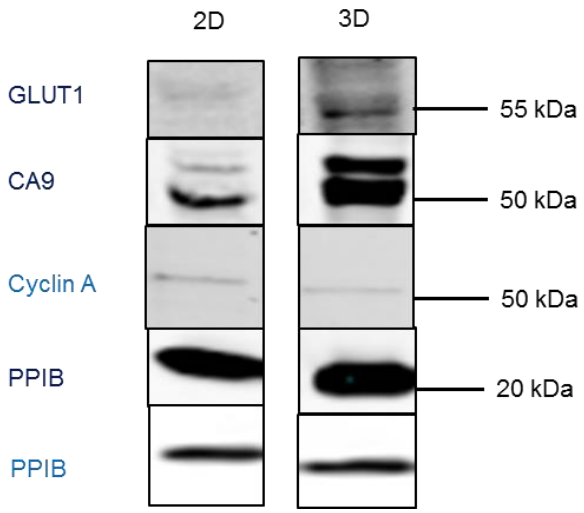

Figure 4.3: Differences in catabolic, hypoxic and cell cycle protein expression between 2D and 3D models
Western blot showing differences in GLUT1, CA9 and cyclin A expression between 2D and 3D models in A549+EV cells. 20 µg of protein per well was loaded.

4.3.3 Summary of differences in mRNA expression between 2D, 3D and xenograft models

There were fewer significant differentially expressed genes between 3D and xenografts than between 2D and 3D or xenografts. This suggests that cells grown as spheroids have a more similar gene expression profile to xenografts compared with cells grown in 2D culture. We expected that genes involved in hypoxia and catabolism would be expressed at a greater level in 3D and xenografts compared to 2D. This is because oxygen and nutrients are more limited in the microenvironment of spheroids and tumours compared with 2D culture. Interestingly, genes involved in cell cycle and DNA repair were expressed at lower levels in spheroids and xenografts compared to 2D. To our surprise, genes involved in immune response were upregulated in spheroids despite the fact that no immune cells were present.

4.4 Differences in mRNA expression between LKB1 deficient and proficient cells

4.4.1 Identification of pathways different between LKB1 deficient and proficient cells

The gene expression profiles of LKB1 deficient and proficient A549 cells grown in 2D culture and 3D spheroids were analysed. As LKB1 expression was lost in the LKB1 proficient sub-cutaneous xenograft samples (Figure 3.16), the LKB1 dependent differences in gene expression was not analysed in this model. However, to include *in vivo* data, a published RNA expression signature from LKB1 mutated vs non-mutated human lung adenocarcinoma tumours (n = 230) was included in our analysis (TCGA, 2014) (Figure 4.4a).

The significant differentially expressed genes between the LKB1 deficient and proficient cells from both 2D and 3D models were identified. These genes were intrinsic for LKB1 loss and not dependent on 2D or 3D growth. There were 710 genes significantly differentially expressed between LKB1 deficient and proficient cells in both 2D and 3D models (Figure 4.4b). To identify differences in biological processes, these genes were analysed using GOrilla (accessed June 2016). 472 GO processes (enrichment p-value ≤ 0.001) were significantly different between LKB1 deficient and proficient cells in both 2D and 3D models. The top 100 processes can be found in the Appendices (Appendices Table A4.5) and include; phosphorylation, cell differentiation, adhesion, motility, cell communication, ECM organisation, cell death, cAMP signalling, response to oxygen and nitrogen containing compounds, MAPK signalling and angiogenesis.

We extended this analysis by investigating LKB1 dependent differences in gene expression in spheroids only. Spheroids were chosen as they were more clinically relevant than 2D culture but a simpler system compared to human tumour samples which contain stromal

components and inflammatory cells. The LKB1 dependent differences in gene expression in spheroids were divided into 2 groups; genes that were expressed at higher or lower levels in LKB1 deficient samples. There were 1091 genes with significant high expression and 1017 genes with significant low expression between LKB1 deficient and proficient cells in 3D spheroids (Figure 4.4b). To identify pathways that had increased or decreased activity between the LKB1 deficient and proficient spheroids, an additional software (MetaCore^{TM} KPA) was used (accessed August 2016), whereby the log_2fc of the top 1000 genes were analysed. 57 pathways were associated with highly expressed genes and 38 pathways were associated with genes expressed at lower levels. The top 20 pathways can be found in the Appendices (Appendices Table A4.6 - 4.7). The pathways associated with the highly expressed genes included; immune response (IL1, IL6, IL17 and IL8), angiogenesis, ECM remodelling, MTOR signalling, AKT-HIF signalling, MAPK signalling and IGF signalling. The pathways associated with genes expressed at lower levels included; CREB signalling, cytoskeleton remodelling and cell death. Some of these pathways were similar to those identified using GOrilla (angiogenesis, ECM organisation, MAPK signalling, cAMP signalling). We speculate that stimulated angiogenesis may assist in cell survival in LKB1 deficient samples within hostile environments. It was reported that VEGFR inhibitors reduce tumour volume in *Kras^{G12D}/Lkb1$^{L/L}$* driven mouse lung tumours but, local and distant metastasis formation was not prevented (Gandhi et al., 2009) (Section 1.6.4). Differences in the localisation of the ECM interacting protein; integrin-β1 between LKB1 deficient and proficient spheroids was previously observed in Figure 3.13. This indicates that the analysis for the differences in gene expression was also observed in a different setting by other groups and may also be recapitulated at a protein level. Interestingly, cAMP signalling is involved in the transcription of cytokines, important in the immune response. In Chapter 3, it was

speculated that the immune system may be important in driving tumour progression. Differences in cAMP signalling will be evaluated further in Section 4.5.

To get a better understanding of the biological processes and pathways most important for survival/growth in LKB1 deficient cells, the significant differentially expressed genes common to 2D, 3D and human tumours were analysed using MetaCore^{TM} (accessed August 2016). As before, the genes were divided into those expressed at higher (n = 72) or lower (n = 75) levels in LKB1 deficient cells (Figure 4.4c). As MetaCore^{TM} only required one log_2fc value and one q-value to analyse the list of genes, the log_2fc and q-value from the 3D data was used. 18 pathways were associated with the highly expressed genes and 6 pathways were associated with genes expressed at lower levels (Appendices Table A4.8-4.9). The pathways associated with the highly expressed genes included IGF signalling and PKA signalling and the pathways associated with genes expressed at lower levels included cytoskeletal remodelling. PKA is involved in cAMP signalling which was identified as being differentially regulated between LKB1 deficient and proficient 2D and 3D samples using GOrilla analysis. Differences in cytoskeletal organisation, in particular microtubule structure were observed in Section 3.4.3 and 3.5.3. The effect of microtubule inhibitors on cell proliferation in 2D and 3D models will be further evaluated in Chapter 5.

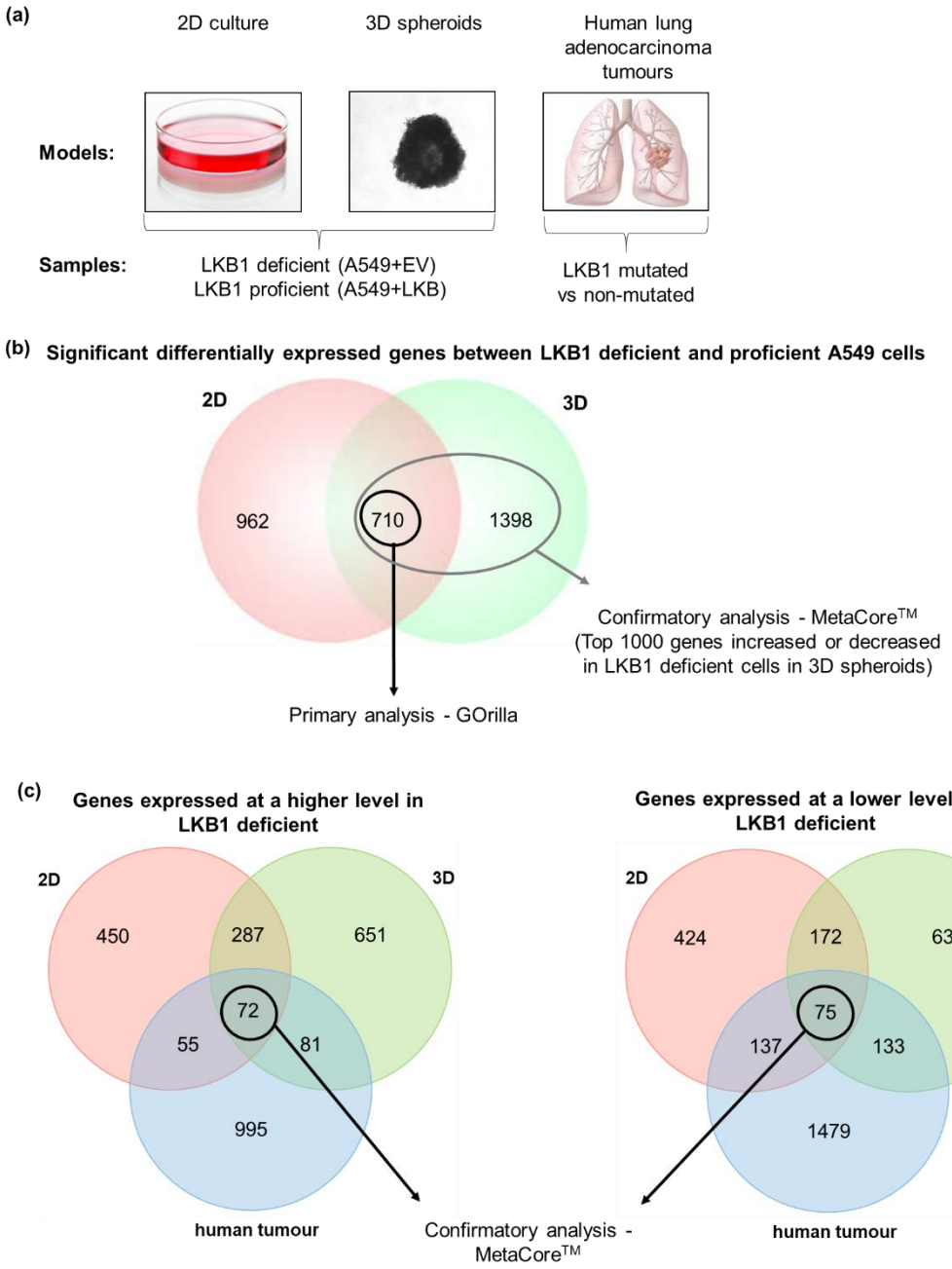

Figure 4.4: Significant differentially expressed genes between LKB1 deficient and proficient samples from 2D culture, 3D spheroids and human lung adenocarcinoma tumours

(a) RNA was extracted from A549+EV and A549+LKB cells grown in 2D and 3D culture. RNA expression in human lung adenocarcinoma tumours was taken from a published dataset (TCGA, 2014). Lung image: http://www.qmedicine.co.in (b) No. of significant differentially expressed genes in 2D and 3D models. GOrilla was used to identify the biological processes significantly different between the LKB1 deficient and proficient cells in both the 2D and 3D models. MetaCore™ was used to identify the key pathways different between the LKB1 deficient and proficient spheroids. (c) No. of genes expressed at a higher or lower level in LKB1 deficient cells from 2D and 3D models and human tumour samples. MetaCore™ was used to identify the key pathways different between the LKB1 deficient and proficient cells in all models. The Venn diagrams data was generated using http://www.bioinformatics.lu/venn.php.

4.4.2 Summary of the differences in mRNA expression between LKB1 deficient and proficient cells

We used the following 3 approaches to determine the biological processes and pathways different between LKB1 deficient and proficient cells; (i) use of GOrilla to analyse the LKB1 dependent differences in gene expression in both 2D and 3D models, (ii) use of MetaCore^{TM} to analyse the genes expressed at higher or lower levels in LKB1 deficient samples in 3D models and (iii) use of MetaCore^{TM} to analyse the genes expressed at higher or lower levels in LKB1 deficient samples common between 2D, 3D and tumour models. LKB1 dependent differences in cAMP signalling was identified using all 3 approaches. Cytoskeletal remodelling was identified as a pathway associated with the genes expressed at lower levels in LKB1 deficient cells in 2D, 3D and human tumours. We previously observed LKB1 dependent differences in the cell cytoskeleton in Section 3.4.3 and 3.5.3. Using the results from the enrichment analysis and observations made in the laboratory, the pathways involved in (i) cAMP response element signalling and (ii) cytoskeleton organisation were studied further in Section 4.5 and Chapter 5.

4.5 Differential expression of genes involved in cAMP response element (CRE) signalling between LKB1 deficient and proficient cells

4.5.1 Confirmation of differences in CRE signalling between LKB1 deficient and proficient cells

As outlined in Figure 4.5, transcription of cAMP response element responsive genes occurs through binding of two transcription factors, phosphorylated CREB and hypophosphorylated CRTC. CREB (cAMP response element binding protein) is phosphorylated by PKA whose activity is dependent on the presence of cAMP. cAMP levels can be reduced by phosphodiesterase (PDE) (Carlezon et al.). LKB1 activates SIK which

phosphorylates CRTC (CREB-regulated transcription coactivator 1), and prevents its translocation to the nucleus, and thus inhibits transcription of cAMP response element (CRE) genes (Cao et al., 2015, Katoh et al., 2006). CRE genes include: COX, NURR77, PDE4D, FOS, JUN, GSK3β, IRS1, VEGF (Impey et al., 2004), IL6 and SIK1 (Fallahi et al., 2014). Figure 4.6 contains a heatmap with data from our transcriptomic analysis which shows the genes involved in CRE signalling, and if they are expressed at higher or lower levels in the LKB1 deficient cells in the 2D, 3D and human tumour models. Many of these genes were expressed at a higher level in LKB1 deficient cells. While this work was in progress, other groups also reported differences in cAMP response element genes; PDE and SIK1 following analysis of transcriptomic data (Kaufman et al., 2014, He et al., 2014, Chen et al., 2016).

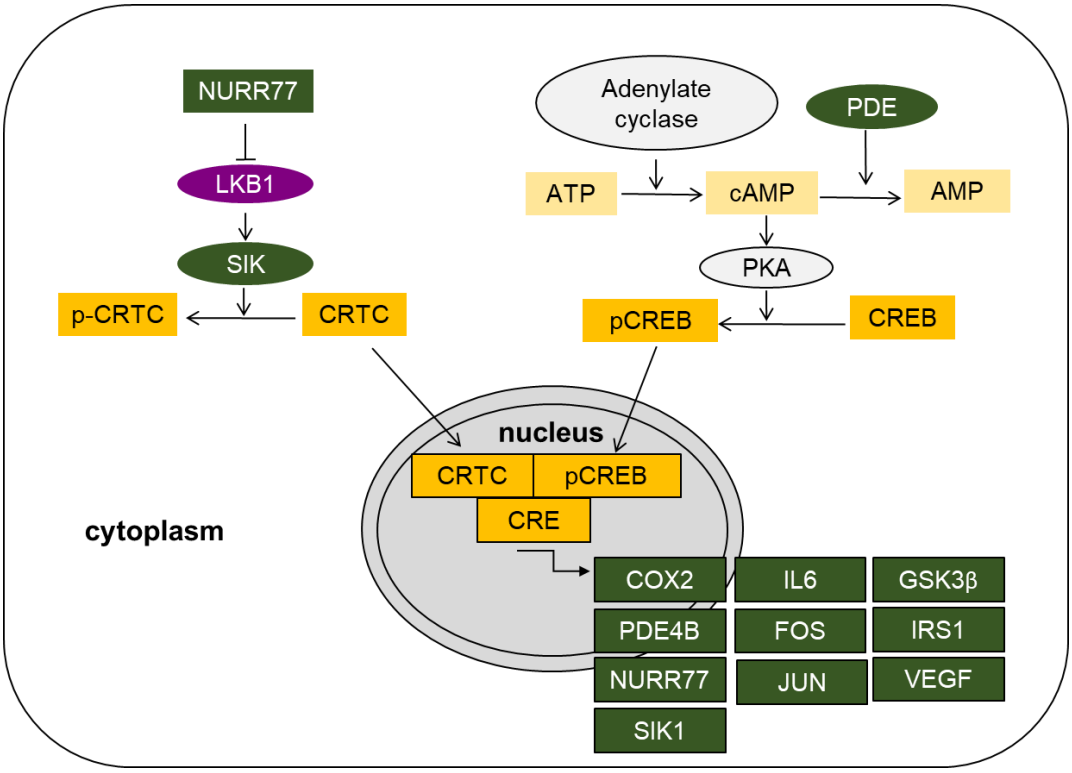

Figure 4.5: Schematic of cyclic AMP response element (CRE) signalling
Schematic showing activation of CRE by hypophosphorylated CRTC and phosphorylated CREB. NURR77 binds LKB1 which prevents formation of the LKB1-STRAD-MO25 heterotrimeric complex (Section 1.2.3). LKB1 complex phosphorylates and activates SIK which prevents activation of CRE. Using our RNASeq dataset, proteins in green were highly expressed in LKB1 deficient cells and proteins in purple expressed at lower levels in LKB1 deficient cells.

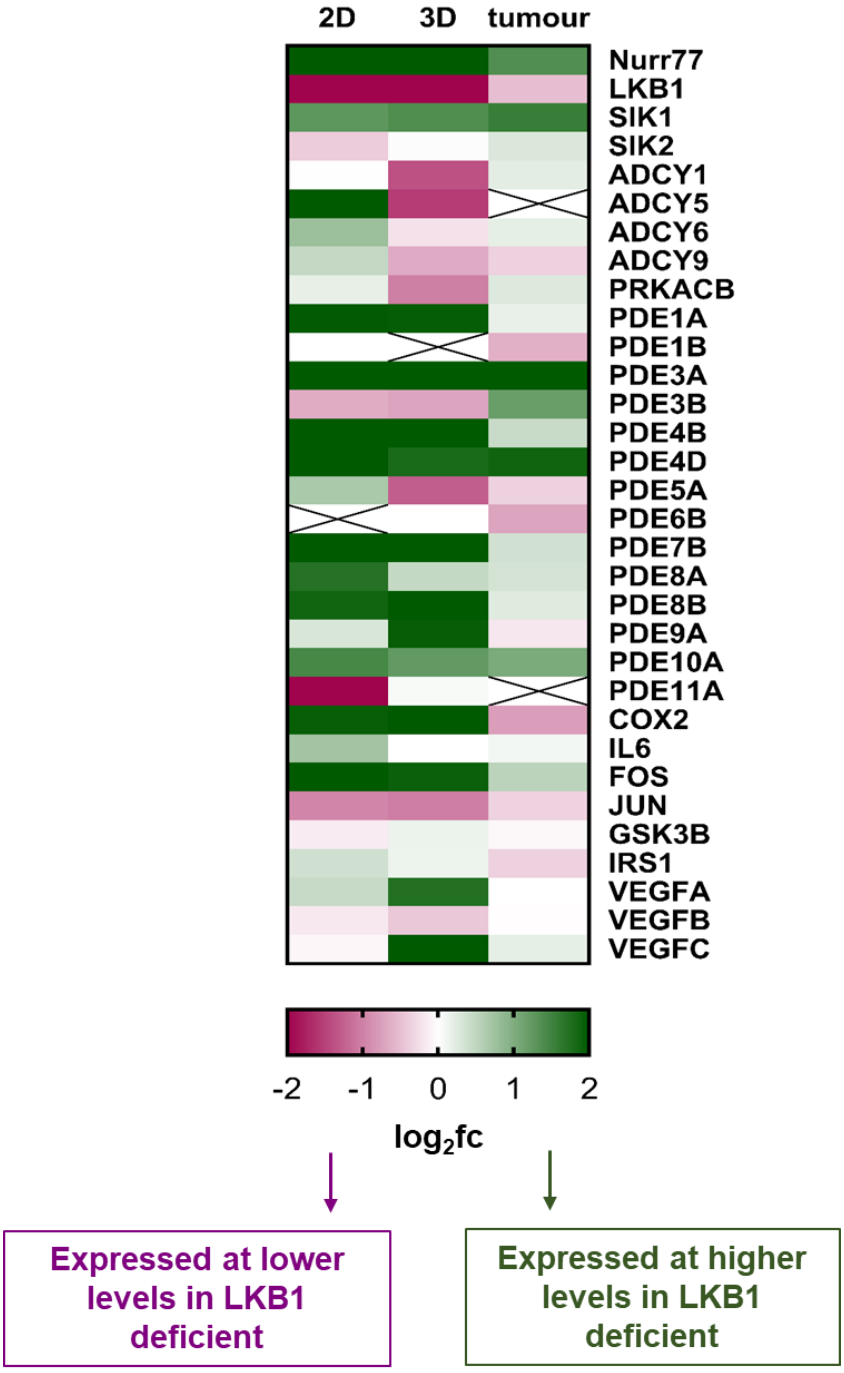

Figure 4.6: Heatmap showing CRE signalling genes that have high or low expression in the LKB1 deficient cells in 2D, 3D and human tumours

Heatmap showing highly expressed genes in green (≥ 2 log_2fc) and genes expressed at lower levels in purple (≤ 2 log_2fc) in LKB1 deficient cells. Heatmap was generated using our RNASeq data for 2D and 3D models and the human lung adenocarcinoma sample dataset (TCGA, 2014). Significant and non-significant differences were included. Genes listed above were (i) those involved in cAMP signalling and (ii) significantly differentially expressed between LKB1 deficient and proficient cells in at least one model. The cross indicates there were no data available for this gene in one or both samples (def and/or pro). Heatmap was produced using GraphPad Prism 7.

Figure 4.5 shows SIK1 involvement in CRE signalling. It was reported that LKB1 phosphorylates SIK1 (Katoh et al., 2006, Hashimoto et al., 2008) which prevents activation of CRE by CRTC. Interestingly, of the 14 reported LKB1 targets (Section 1.2.3), SIK1 was the only target that was significantly differentially expressed between the LKB1 deficient and proficient cells in both 2D and 3D models. This suggests that LKB1 loss may have the greatest impact on SIK1 expression and/or activity in A549 cells, compared to the other known LKB1 targets. Of the other known targets of LKB1; NUAK1 and BRSK1 expression were different in the 2D model and AMPKα2 expression was different in the 3D model (Figure 4.7).

(a)

Gene	Model	log_2fc	q-value
SIK1	**2D**	1.26	< 0.001
NUAK1	**2D**	-1.34	< 0.001
BRSK1	**2D**	1.14	< 0.05
SIK1	**3D**	1.37	< 0.001
AMPKα2	**3D**	0.83	< 0.001

(b)

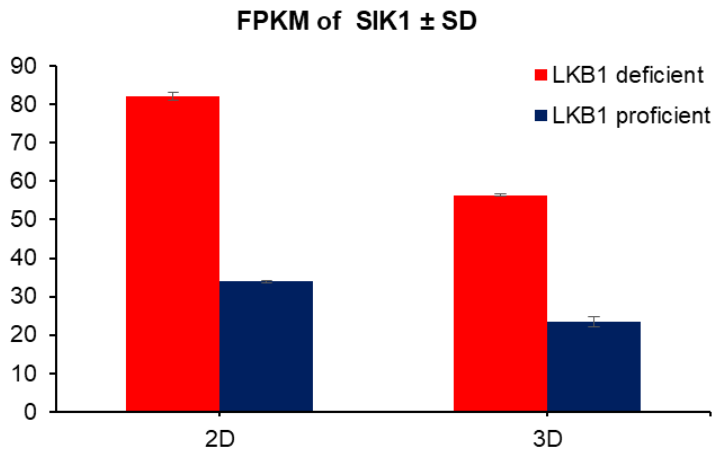

Figure 4.7: mRNA expression of the known LKB1 targets in LKB1 deficient and proficient cells in 2D and 3D models

(a) Log_2fc and q-value for the known LKB1 targets that were significantly different between LKB1 deficient and proficient cells. A positive log_2fc value indicates that the gene was expressed at a higher level in LKB1 deficient cells. (b) FPKM for SIK1 expression. Data represents the mean of independent duplicate samples.

Following this, we aimed to confirm differences in expression of cAMP responsive genes using western blotting. From Figure 4.5 it is difficult to conclude whether CRE dependent transcription was turned on or off in the LKB1 deficient cells. This is because SIK1 and various PDE genes, which negatively regulate CRE transcription, had high expression in LKB1 deficient cells. However, the CRE transcribed genes; COX2, FOS and NURR77 also had high expression in LKB1 deficient cells. Therefore, we measured CRE activity in 2D culture using a CREB luciferase reporter assay (Section 2.18), where, in the presence of pCREB and CRTC, luciferase is transcribed by CRE. Luciferase activity was measured by addition of luciferin and measurement of firefly luminescence. As a positive control, forskolin, (adenylate cyclase activator) was used. CRE activity was increased in both cell lines on treatment with forskolin indicating the assay was viable. In both untreated and forskolin treated samples, CRE activity was higher in LKB1 deficient cells indicating that CRE-dependent transcription was increased in LKB1 deficient cells (Figure 4.8a).

To further determine if the expression of proteins involved in CRE transcription were higher in LKB1 deficient cells; SIK1, PDE4B and COX2 protein levels were measured by western blotting (Figure 4.8b). Interestingly, SIK1 protein levels were lower in 3D compared to 2D in both deficient and proficient cells. PDE4B expression was also different in 3D compared to 2D. The PDE4B antibody (#ab14612) recognised 4 isoforms, however, 3 isoforms were detected in the 2D model and only 1 isoform was detected in the 3D model. However, SIK1 and PDE4B protein levels were similar in LKB1 deficient and proficient A549 cells in both 2D and 3D models showing that mRNA expression did not correlate with the protein expression. Although SIK1 and PDE4B protein expression was not different in an LKB1 dependent manner, COX2 expression was higher in the LKB1 deficient A549 cells in both the 2D and 3D models, which further suggests that CRE dependent gene transcription was increased in LKB1 deficient cells.

We extended this analysis to more cell lines and found that COX2 was also upregulated in LKB1 deficient A427 cells but not LKB1 deficient H1299 cells (Figure 4.8c). However, LKB1 deficient H1299 cells appeared to have higher levels of SIK1 in 2D and 3D models which may negatively impact on COX2 expression in these cells. We also investigated COX2 expression in the 11 lung cancer cells line and NBE1. However, when COX2 protein expression was quantified and normalised to PPIB, the difference in expression between the 8 LKB1 mutated cells and the 4 LKB1 wild-type cells (including CORL105) did not reach statistical significance (Figure 4.8d), therefore the difference may be cell line dependent. Furthermore, COX2 was not different between LKB1 mutated and non-mutated human tumours suggesting that COX2 expression may not play an important role in already established tumours (Figure 4.6).

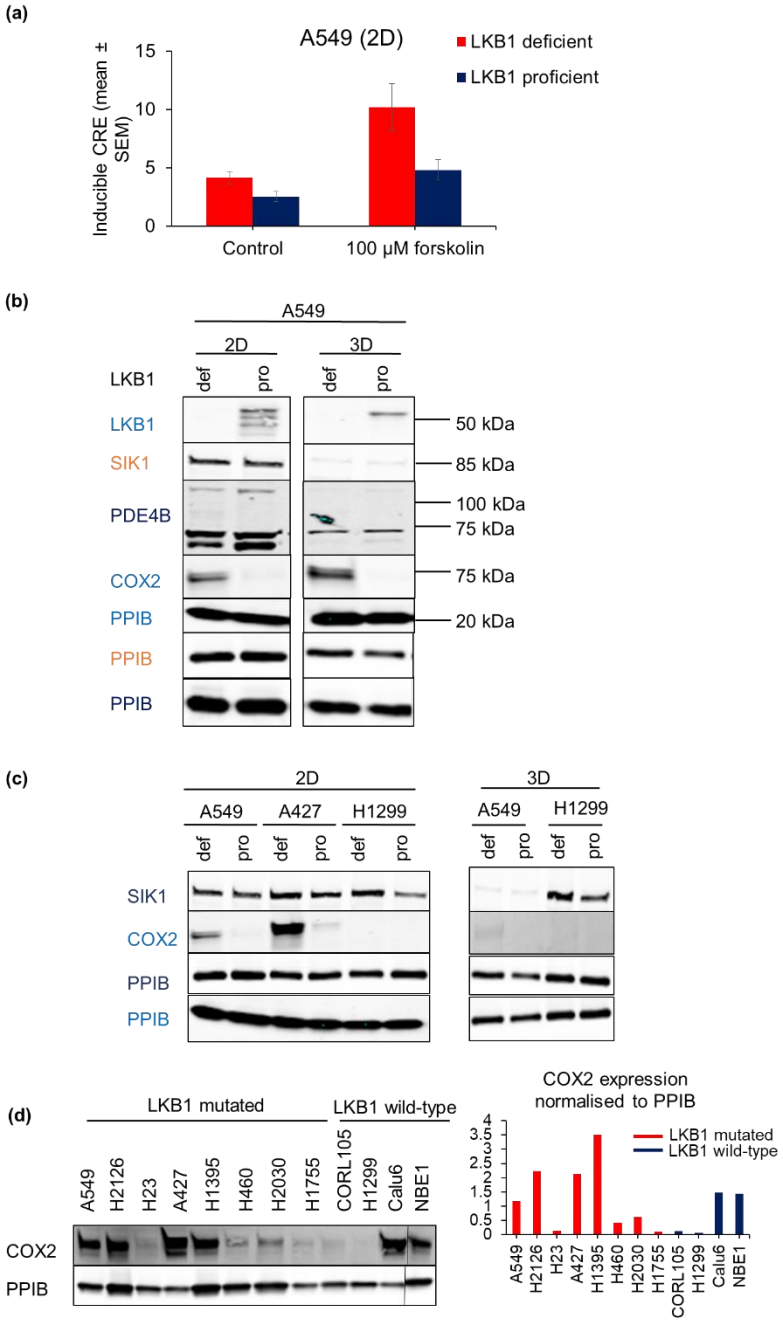

Figure 4.8: Examining differences in CRE signalling between LKB1 deficient and proficient cells

(a) Measuring CRE dependent gene transcription using a CREB luciferase reporter assay. Forskolin was used as a positive control. Data represents the mean of triplicate values from 2 independent experiments. (b) Western blot for LKB1, SIK1 and COX2. 20 µg of protein was loaded per well. For PDE4B western blotting, 40 µg of protein was loaded per well. PDE4B antibody detects 4 isoforms (PDE4B1 = 107 kDa, PDE4B2 = 78 kDa, PDE4B3 = 100 kDa, PDE4B4 = 66 kDa) (c) Western blot showing SIK1 and COX2 expression in isogenic pairs in 2D and 3D. 20 µg of protein was loaded per well. (d) Western blot showing COX2 expression in 11 lung cancer cell lines and NBE1. 40 µg of protein was loaded per well. Graph shows values for COX2 expression normalised to PPIB when quantified using the Odyssey® Image Studio software. The difference in expression between the 8 LKB1 mutated cells and the 4 LKB1 wild-type cells was not significant (mean COX2 expression normalised to PPIB: LKB1 mutated = 1.30, LKB1 wt = 0.78, p-value = 0.464).

4.5.2 Summary for CRE signalling in LKB1 deficient and proficient cells

These data suggest that CRE gene transcription was higher in LKB1 deficient A549 cells in 2D and 3D models. This was also the case for LKB1 deficient A427 cells in 2D culture but not for LKB1 deficient H1299 cells. However, H1299 cells were derived from tumours that developed in the presence of LKB1, whereas, LKB1 loss is intrinsic to A549 and A427 cells. Unlike LKB1 deficient A549 and A427 cells, LKB1 deficient H1299 cells had higher SIK1 expression and did not express COX2, suggesting that LKB1 may not have been completely knocked-down and still phosphorylated SIK1.

Our data suggests that COX2 may play an important role in LKB1 deficient A549 and A427 cells. However, in the broader range of cell lines, COX2 protein expression was not significantly higher in LKB1 mutated cells lines and furthermore, it was not higher in LKB1 mutated human tumours. However, the LKB1 mutated human tumour samples may not be LKB1 deficient, as the LKB1 mutations may be heterozygous, and furthermore, tumour samples with wild-type LKB1 gene sequences may have lost mRNA expression through epigenetic mechanisms (Section 1.4). Therefore, we place more weight on the 2D and 3D data.

4.5.3 Investigation of LKB1 dependent differences on sensitivity to CRE signalling modulators

There are several modulators of CRE signalling; HG-9-91-01 (SIK inhibitor), forskolin (adenylate cyclase activator) and rolipram (PDE inhibitor), which increase CRE signalling, and celecoxib which inhibits COX2 (Figure 4.9). Dexamethasone is a glucocorticoid which was shown to inhibit CRE transcription (Cote-Vélez et al., 2005). We hypothesised that LKB1 deficient and proficient cells may be differentially sensitive to activators and inhibitors of CRE signalling.

The effect of CRE modulators on inhibition of proliferation was determined using a resazurin-based cell viability assay. Despite the increase in CRE signalling in LKB1 deficient cells, the dose response curves show that there were no differences in sensitivity between LKB1 deficient and proficient A549 cells in response to HG-9-91-01, forskolin or rolipram. Furthermore, despite the increased COX2 expression in LKB1 deficient A549 and A427 cells, there were no differences in sensitivity to celecoxib. LKB1 deficient A549 cells were more sensitive to the glucocorticoid; dexamethasone, however, this effect was not recapitulated in the A427 isogenic pair (Figure 4.10).

Western blotting was used to confirm activity of the inhibitors (Figure 4.11). The concentration of inhibitors chosen for western blotting was based on those that inhibited cell proliferation by ≥ 50% (Figure 4.10). After 24 h, dexamethasone normalised the difference in COX2 expression between the two cell lines as it decreased COX2 expression in LKB1 deficient A549 cells and increased COX2 expression in LKB1 proficient A549 cells. Celecoxib decreased COX2 expression in LKB1 deficient A549 cells. HG-9-91-01 increased COX2 expression in both LKB1 deficient and proficient A549 cells. Interestingly, HG-9-91-01 decreased LKB1 expression (Figure 4.11).

As the effect of LKB1 on cell growth was more apparent in 3D, spheroids were treated with the CRE modulators (Figure 4.12). After 5 days of treatment, both LKB1 deficient and proficient A549 spheroids decreased in size in response to HG-9-91-01 and celecoxib which indicated that there were no marked differences in sensitivity between LKB1 deficient and proficient spheroids.

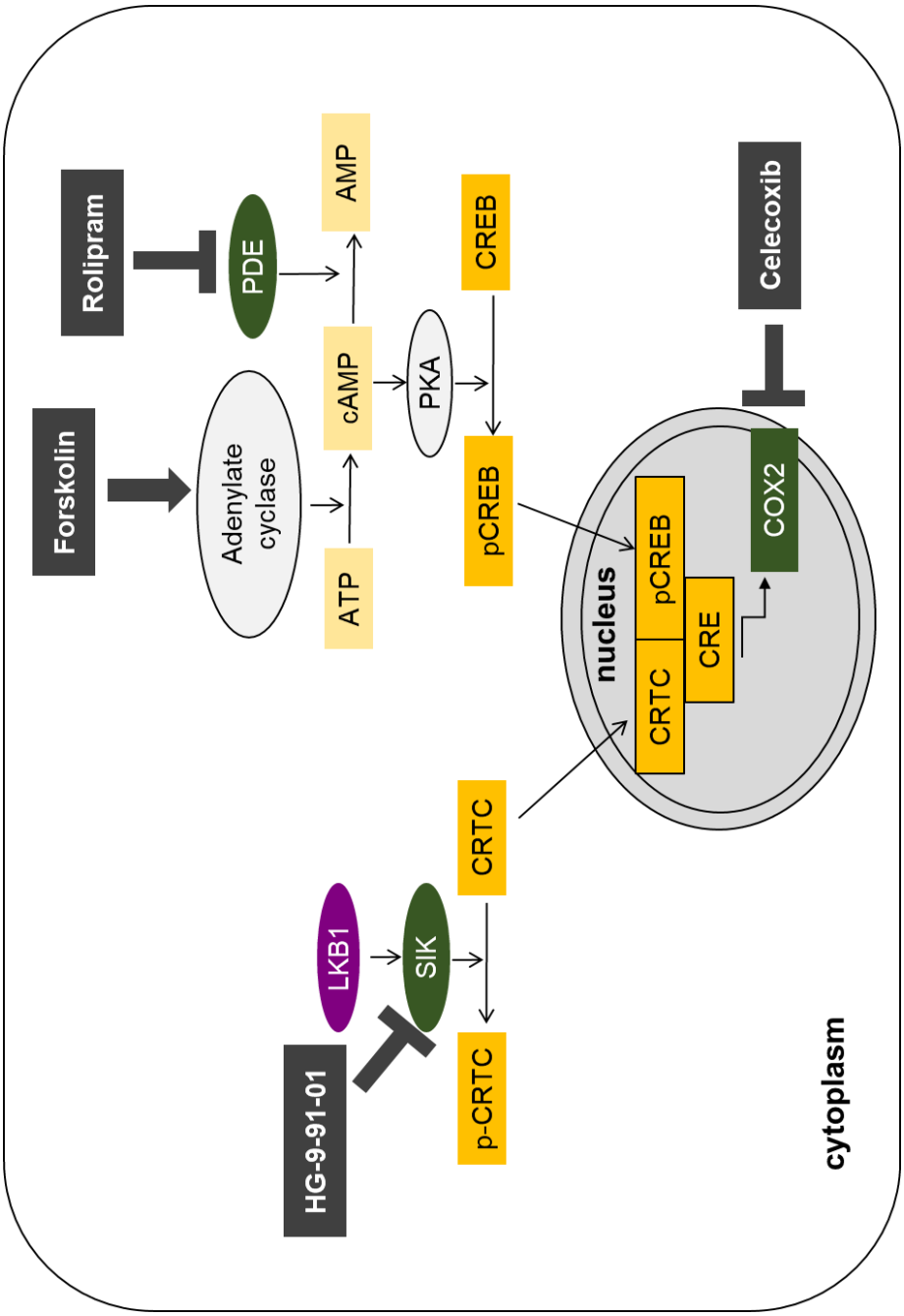

Figure 4.9: Schematic showing modulators of CRE signalling

Using our RNASeq dataset, proteins in green were highly expressed in LKB1 deficient cells and proteins in purple were expressed at lower levels in LKB1 deficient cells. Compounds in grey are modulators of CRE signalling.

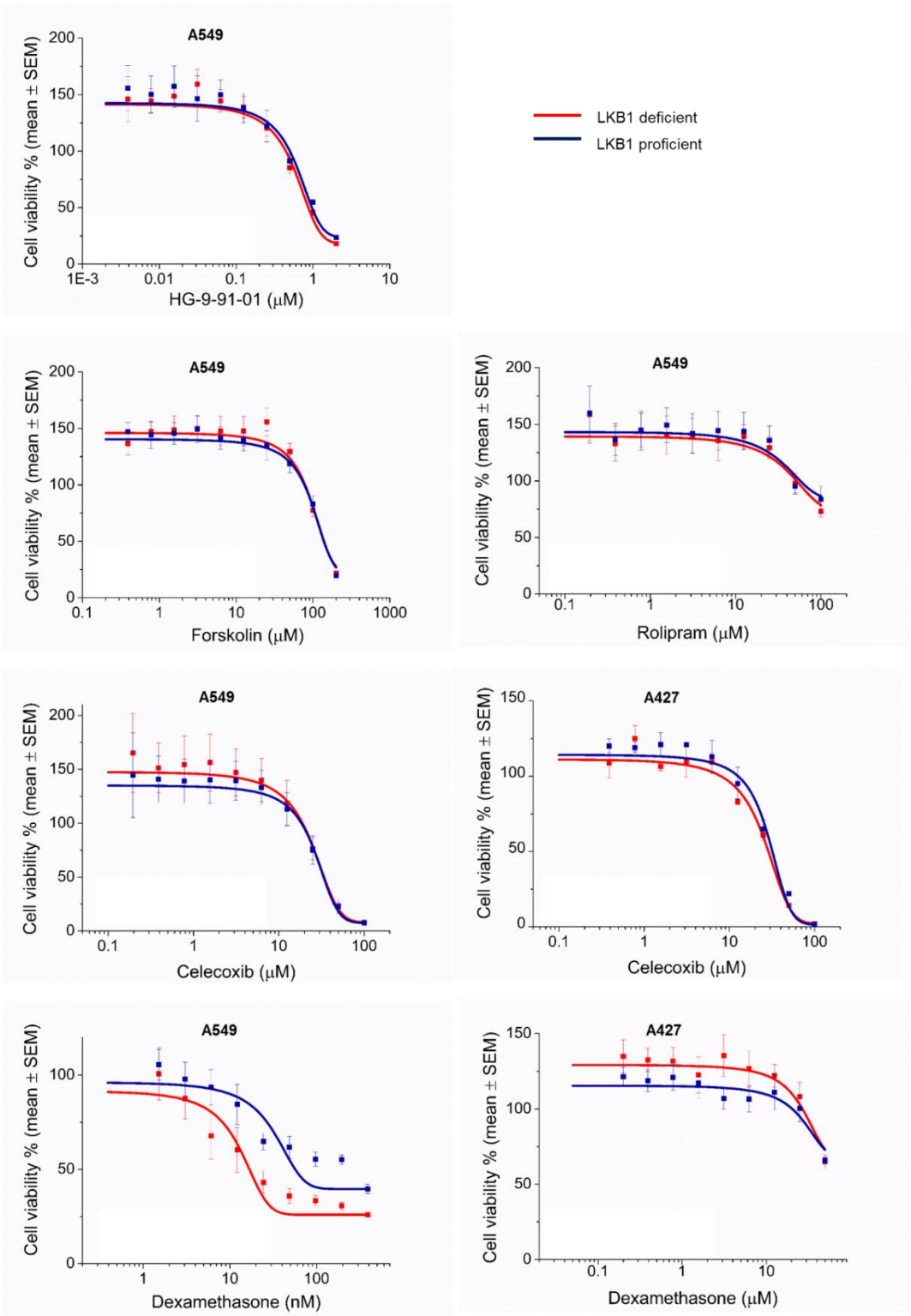

Figure 4.10: Dose response curves for LKB1 deficient and proficient cells treated with modulators of CRE signalling

Cells were exposed to HG-9-91-01, forskolin, rolipram, celecoxib and dexamethasone for 72 h. Cell viability was determined using a resazurin-based assay. Apart from A427 treated with celecoxib, data represents the mean of triplicate values from 2 independent experiments. For A427 treated with celecoxib, data represents the mean of triplicate values.

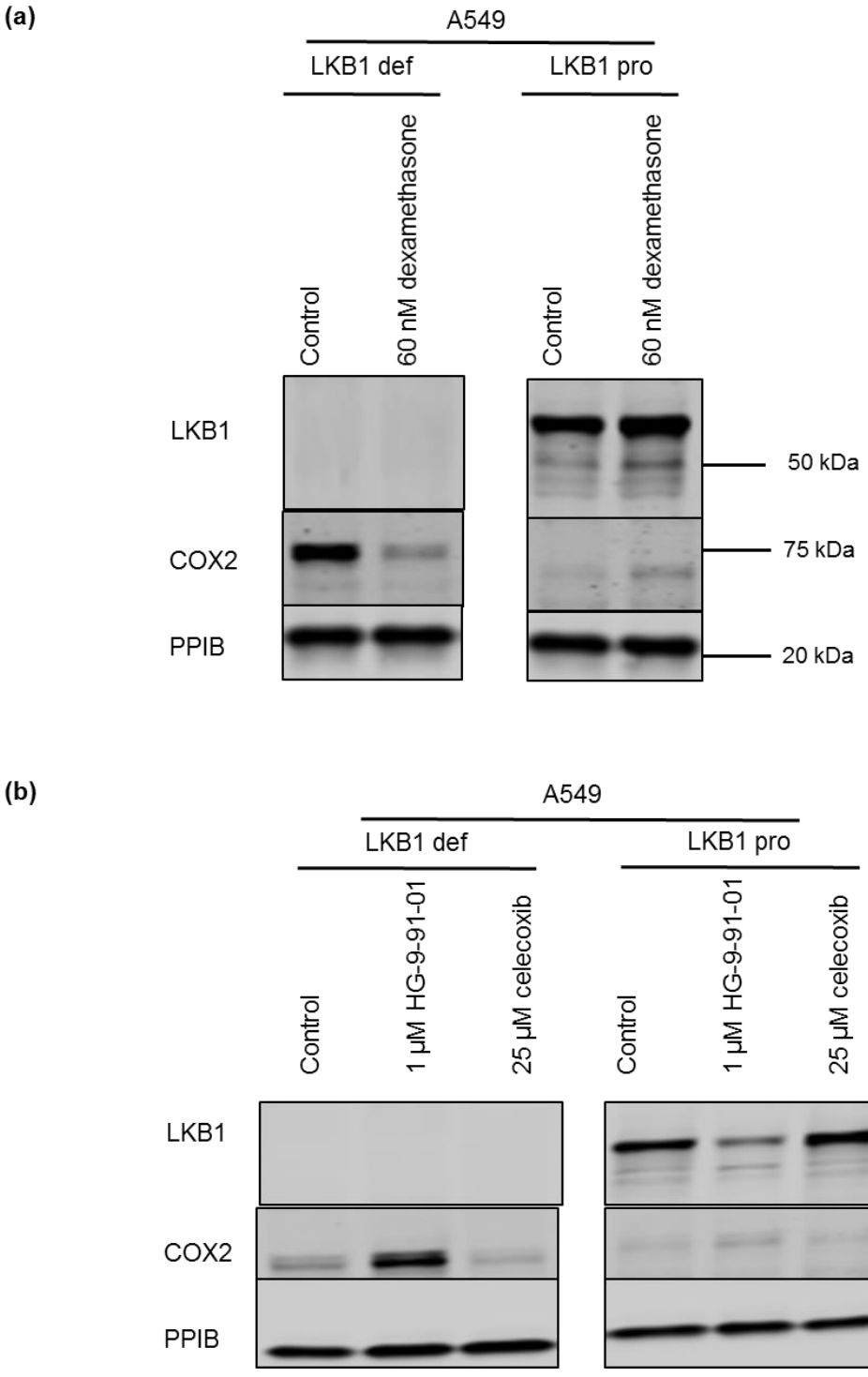

Figure 4.11: Western blotting showing the effect of dexamethasone, HG-9-91-01 and celecoxib on LKB1 and COX2 expression

(a) (b) Cells were grown in 2D culture and treated one day post seeding for 24 h. 15 µg of protein was loaded per well.

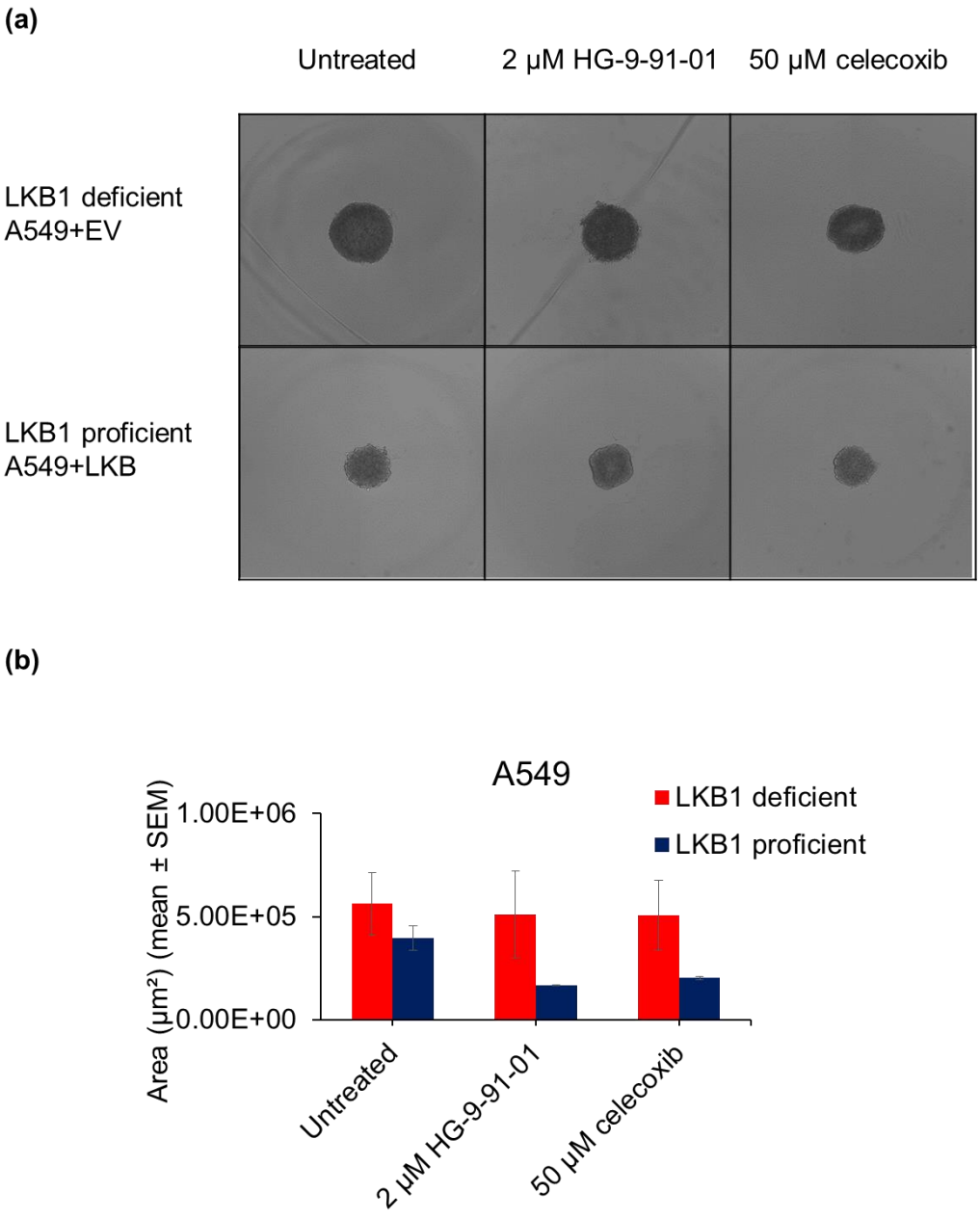

Figure 4.12: LKB1 deficient and proficient spheroids treated with modulators of CRE signalling

Spheroids were treated with inhibitors from seeding for 5 days. Medium was not replenished to avoid any changes in inhibitor concentration. (a) Images were acquired at 15x magnification using the CeligoS. (b) Area was determined using the CeligoS tumoursphere migration analysis. In the graphs, data points represent the mean of 6 independent spheroids for the control and data points represent the mean of 2 independent spheroids for the treated.

4.6 Discussion

In this Chapter, we aimed to understand the role of LKB1 loss in lung cancer using whole transcriptomic profiling. For this, LKB1 deficient and proficient A549 cells were grown in 2D culture, as 3D spheroids and as sub-cutaneous xenografts. Firstly, we aimed to understand the difference in gene expression between the models and to my knowledge, this is the first time the gene signature of spheroids has been analysed and compared to other models. We found that there were fewer differentially expressed genes between the 3D spheroids and xenografts, suggesting that spheroids were more representative of the tumour microenvironment, lending support for the use of 3D models to better predict pre-clinical *in vivo* activity. Although spheroids do not completely represent the *in vivo* microenvironment, as they do not have a blood supply or immune system, they share some similarities such as oxygen and nutrient gradients which are similar to tumours (Lin and Chang, 2008). However, although spheroids lack an immune system, certain metabolic changes can affect the immune response. For example, it has been reported that an acidic microenvironment, caused by increased aerobic glycolysis and lactate production, can inhibit T cell function (reviewed in (Dart, 2016)). We observed an increase in CA9 (carbonic anhydrase 9) expression in 3D and xenografts compared to 2D (Figure 4.1-4.3). CA catalyses the forward and reverse reaction converting protons and bicarbonate to water and carbon dioxide (Lindskog, 1997). Therefore, these enzymes can be reflective of an acidic microenvironment. This further supports the use of spheroids to predict changes in the microenvironment that affect tumour responses. Spheroids were more representative of tumours in terms of cell cycle and DNA repair as genes involved in these pathways were expressed at lower levels in both 3D spheroids and xenografts compared to the 2D model (Figure 4.1-4.3). DNA repair inhibitors are commonly used to treat cancer (reviewed in (Gavande et al., 2016)). Spheroids could be used more widely to support 2D findings before

performing experiments on animals. Furthermore, our dataset can be used to determine the levels of specific genes in 2D, 3D and xenograft models before the commencement of any *in vivo* work.

On understanding some of the differences between 2D, 3D and xenografts, we aimed to determine the LKB1 dependent mRNA changes. As LKB1 expression was lost in sub-cutaneous xenografts (Figure 3.16), we did not use this dataset to determine LKB1 dependent differences in gene expression but used an LKB1 mutated and LKB1 wild-type human lung adenocarcinoma tumour dataset (TCGA, 2014). We identified common differences between LKB1 deficient and proficient cells in 2D, 3D and tumours. The differences in mRNA expression between LKB1 deficient and proficient cells were analysed using gene ontology (GOrilla) and key pathway analysis (MetaCore^{TM}) to identify biological processes and pathways enriched. Pathways involved in cAMP signalling and cytoskeleton organisation were chosen for further investigation (Section 4.4.2).

CRE driven gene expression was upregulated in LKB1 deficient A549 cells. COX2, a CRE gene, was upregulated in LKB1 deficient A549 (2D, 3D) and A427 (2D) cells. LKB1 dependent differences in CRE signalling were also observed by other groups (He et al., 2014, Chen et al., 2016, Cao et al., 2015, Katoh et al., 2006). We did not determine the efficacy of any CRE modulators *in vivo* as the dose response curve for celecoxib was not markedly different between LKB1 deficient and proficient A549 and A427 cells, despite the increased COX2 expression (Figure 4.10). Furthermore, while this work was in progress, Cao et al investigated the effect of COX2 expression on tumour growth *in vivo*. They showed that knock-down of COX2 in A549 cells reduced the tumour burden of sub-cutaneous xenografts in SCID mice (Cao et al., 2015), indicating that COX2 may play a greater role *in vivo*. As COX2 was upregulated in LKB1 deficient A549 and A427 cells and was important for tumour growth in Cao et al's study, but is not upregulated in the established lung

adenocarcinoma samples, we speculate that COX2 expression may be important in tumour initiation but not progression. COX2 and its product, prostaglandin PGE_2, are reported to be involved in evading apoptosis and immune response, and promoting growth signalling, angiogenesis, invasion and metastasis. All of these processes are important in tumour initiation and survival during stress. It has been reported that PGE_2 activates β-catenin signalling (Greenhough et al., 2009) and we observed differences in β-catenin subcellular localisation between LKB1 deficient and proficient cells (Figure 3.13). Also, it was reported that LKB1 dependent COX2 induction may play a role in lung cancer invasion through PEA3 (Upadhyay et al., 2006) (Section 1.6.6). Furthermore, acetylsalicylic acid (aspirin), a COX inhibitor, was shown to be effective at preventing colorectal cancer (Emilsson et al., 2017), highlighting a possible and general role of COX2 in cancer initiation.

SIK1 was the only gene of the 14 known LKB1 downstream targets (Section 1.2.3) that was significantly differentially expressed between LKB1 deficient and proficient cells in both the 2D and 3D models (Figure 4.7). However, changes in mRNA expression did not correlate with the changes in SIK1 or PDE4B protein expression (Figure 4.8b). Although SIK1 protein levels were not different between LKB1 deficient and proficient A549 cells, activated/phosphorylated SIK was not evaluated (Figure 4.8). Unfortunately, there was no phosphorylated-SIK1 antibody available and the polyclonal antibody to total SIK1 showed significant non-specific binding on western blots making it unsuitable for quantitative immunoprecipitation studies. Therefore, it remains possible that SIK1 may be the LKB1 downstream target most affected by LKB1 loss, and that reduced phosphorylated SIK1 may cause the greatest growth advantage. Others have reported that inactive SIK plays a role in anoikis and metastasis (Section 1.3.4). In our work, the SIK inhibitor; HG-9-91-01 reduced LKB1 expression in LKB1 proficient A549 cells (Figure 4.11). HG-9-91-01 turns on CRE transcription of COX2 (Figure 4.9). NURR77 is also a CRE transcribed gene (Impey et al.,

2004) and therefore, is expected to be expressed on treatment with HG-9-91-01. NURR77 sequesters LKB1 to the nucleus (Zhan et al., 2012) and may affect antibody recognition by interacting with a region in the same/similar proximity to where the LKB1 antibody binds, although the precise region where NURR77 interacts with LKB1 is not known.

To conclude, using RNA Sequencing, we observed that genes involved in hypoxia, catabolism and immune response were expressed at higher levels and genes involved in DNA repair and cell cycle were expressed at lower levels in 3D spheroids and xenografts compared to 2D cell culture. Pathways that were differentially expressed between LKB1 deficient and proficient cells included immune response, cell differentiation, cell adhesion, cell motility, cell communication, cytoskeletal remodelling, ECM organisation, cell death, IGF, AKT, MAPK, MTOR signalling, angiogenesis, HIF signalling, response to oxygen and nitrogen containing compounds and cAMP signalling. SIK1 mRNA levels were different between LKB1 deficient and proficient cells in both 2D and 3D models and thus, may be the most important downstream target affected by LKB1 loss. We confirmed differences in cAMP signalling using *in vitro* assays. However, this difference did not appear to be exploitable in our 2D and 3D studies.

5 Target identification for LKB1 mutated lung cancer cells

5.1 Introduction

We hypothesised that LKB1 loss may be associated with an increased dependency on an alternative pathway that could be targeted to selectively kill LKB1 mutated cells (Section 1.7). It was reported that the CHK inhibitors; AZD7762 and CHIR124 and knock-down of deoxythymidylate kinase, were potential approaches to selectively target LKB1 mutated lung cancer cells (Liu et al., 2013) (Section 1.6). Other reported targets for LKB1 mutated lung cancer cells include MTOR, MEK, SRC and PI3K inhibition (Section 1.6). However, there is still no therapy used clinically to selectively target LKB1 mutated cells.

In this Chapter, we test multiple bioactive small molecule compounds in LKB1 deficient and proficient cells in both 2D and 3D cell culture models. A bioactive small molecule screen was used with the aim of identifying compounds that can selectively target LKB1 deficient cells. By identifying the target(s) of hit compounds, we hypothesised that we could better understand the biological role(s) of LKB1 and the consequences of LKB1 loss. For the screen, a bioactive small molecule library containing 326 compounds was used (Selleck L1100 - Appendices Table A5.6a). Compounds in the library are known to inhibit a broad range of cellular targets, most of which are used clinically or are undergoing pre-clinical or clinical trials. Some compounds (atazanavir, AZD0530, AZD6244, AZD7762, flavopiridol, NVP-AUY922) were screened twice and seven additional compounds were included (Appendices Table A5.6b).

5.2 Bioactive small molecule screen in 2D culture

The endpoints used for the whole screen were (i) induction of apoptosis and (ii) inhibition of proliferation (Section 2.11.1). A “hit” was identified as a compound that induced

apoptosis and/or reduced proliferation. A positive "hit" compound was selective for LKB1 deficient cells and a negative "hit" compound was selective for LKB1 proficient cells. In our initial/primary screen, 339 compounds were tested in LKB1 deficient and proficient A549 cells (Figure 5.1). The compounds were distributed over 4x 96-well plates and included 34 DMSO treated controls. For the secondary screen, the positive and negative hits (n = 47) identified in the primary screen, were further tested in the three isogenic pairs (LKB1 deficient and proficient A549, A427 and H1299 cells). In the secondary screen, hits were identified as those compounds that induced apoptosis and/or reduced proliferation in LKB1 deficient cells in at least 2 isogenic pairs. In the tertiary screen, the positive hits from the secondary screen (n = 21) were tested in the 3 isogenic pairs but included a lower dose. Hits were those that induced apoptosis and/or reduced proliferation in LKB1 deficient cells in the 3 isogenic pairs. The hits from the tertiary screen were validated by measuring apoptosis over time and by generating a dose response curve (quaternary screen).

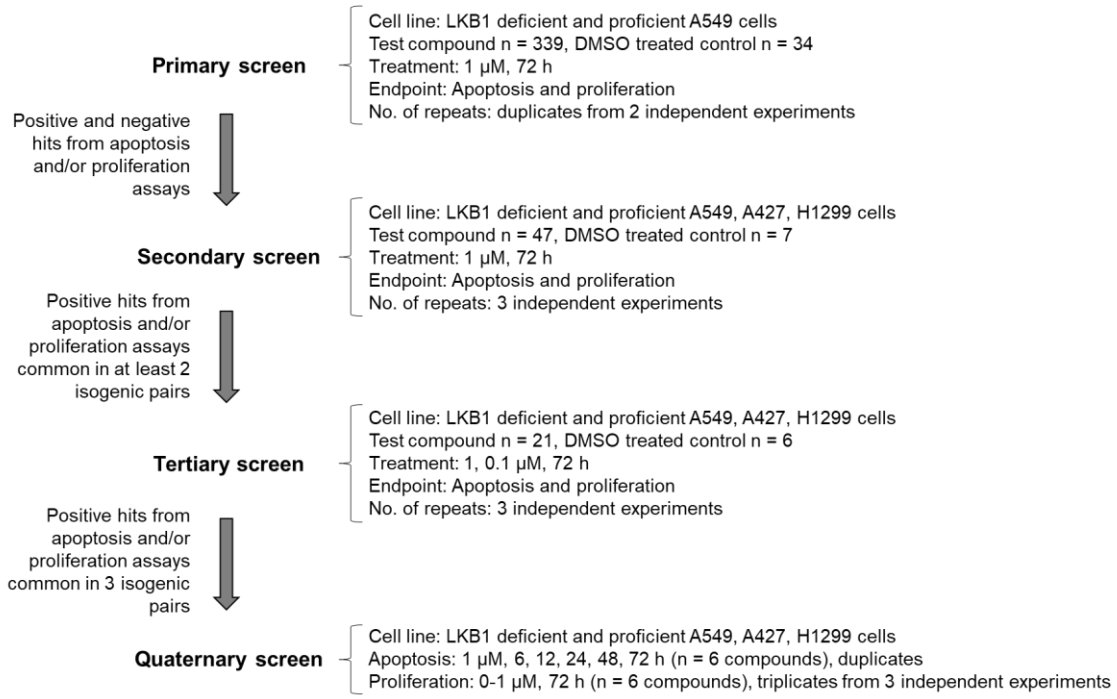

Figure 5.1: Schematic showing the four stages of the 2D screen

5.2.1 Primary screen (2D culture)

For the initial screen, LKB1 deficient and proficient A549 cells were treated for 72 h with test compounds (1 μM) to identify potent hits. Cells were treated for 72 h to allow for at least two cell doublings (Figure 3.3). To determine differences in sensitivity between the 2 cell lines, both induction of apoptosis and inhibition of proliferation were measured (Section 2.11.1, Figure 2.5).

For the primary screen, all data represents duplicate values from 2 independent assays. Figure 5.2 shows the correlations between duplicates within one screen and between the averages of 2 independent screens for each cell line (for both apoptosis and proliferation). There was a strong positive correlation between the duplicates and independent runs for the proliferation assay. For the apoptosis assay, there was also a good positive correlation between duplicates, but more inter-experimental variation. A possible explanation for this may be that cells were more sensitive to inducing apoptosis due to small changes in growth conditions (for example, the frequency of opening and closing the incubator door). Also, when distinguishing the number of apoptotic and normal cells using the IN Cell analyser software, the threshold for Hoechst signal intensity was manually set for some wells on each plate, introducing the potential for intra- and inter-experiment variation.

(a)

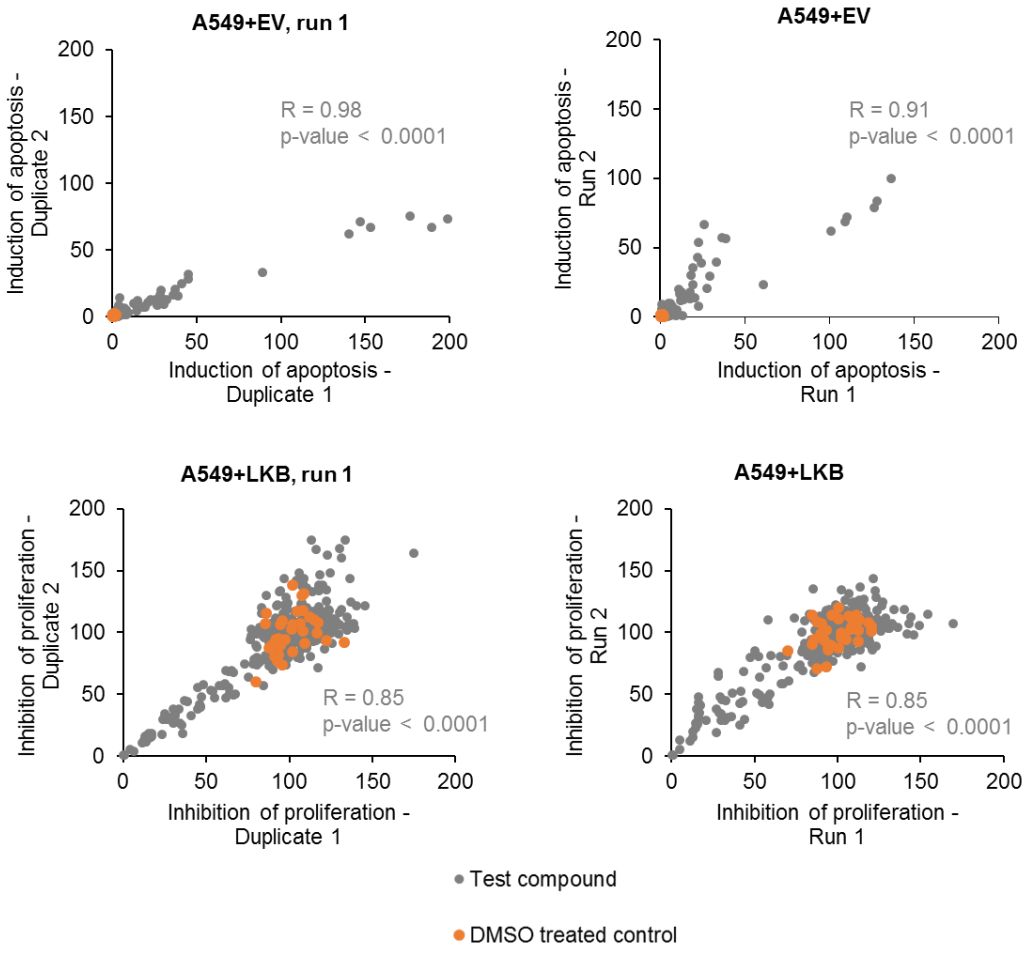

(b)

		Run 1: duplicate 1 vs 2	Run 2: duplicate 1 vs 2	Run 1 vs run 2
Induction of apoptosis	**A549+EV**	0.98	0.66	0.91
	A549+LKB	0.86	0.92	0.52
Inhibition of proliferation	**A549+EV**	0.79	0.82	0.81
	A549+LKB	0.85	0.84	0.85

Figure 5.2: Correlation between duplicate samples and independent runs within the screen

(a) For induction of apoptosis, data points represent the fold change for induction of apoptosis where DMSO treated controls were expected to have a value = 1. For % inhibition of proliferation, the DMSO treated controls were expected to have a value = 100%. R is Pearson's correlation (n = 373). (b) Table shows Pearson's correlation for all duplicates and runs. p-value < 0.0001 for all R values. vs - versus.

To identify compounds with selectivity for either LKB1 deficient or proficient cells, $log_{10}(\frac{change\ in\ LKB1\ deficient}{change\ in\ LKB1\ proficient})$ was calculated (See Section 2.11.1.3). "Hit" compounds were identified as having a value greater than 2x SD away from the mean of all compounds. It was previously reported that LKB1 mutated cells are selectively sensitive to the CHK 1/2 inhibitor; AZD7762 (Liu et al., 2013) (Section 1.6). Therefore, an aim of this screen was to identify any compounds that caused a greater effect than AZD7762. For apoptosis, several positive "hit" compounds (selective for LKB1 deficient cells) including AZD7762 were identified. However, no positive "hit" compounds were identified as selective inhibitors of proliferation in LKB1 deficient cells. Negative "hit" compounds (selective for LKB1 proficient cells) were identified using both endpoints (Figure 5.3). A list of the positive and negative apoptotic and proliferation "hit" compounds are shown in Table 5.1. Surprisingly, some "hit" compounds (panobinostat (LBH-589), BIIB021, topotecan and JNJ-26481585) overlapped as positive apoptosis hits and negative proliferation hits. These hits (Table 5.1) were further tested in LKB1 deficient and proficient A549, A427 and H1299 cells (secondary screen). In addition, hit compounds reported in the literature (Appendices Table A5.7) were also evaluated for comparison.

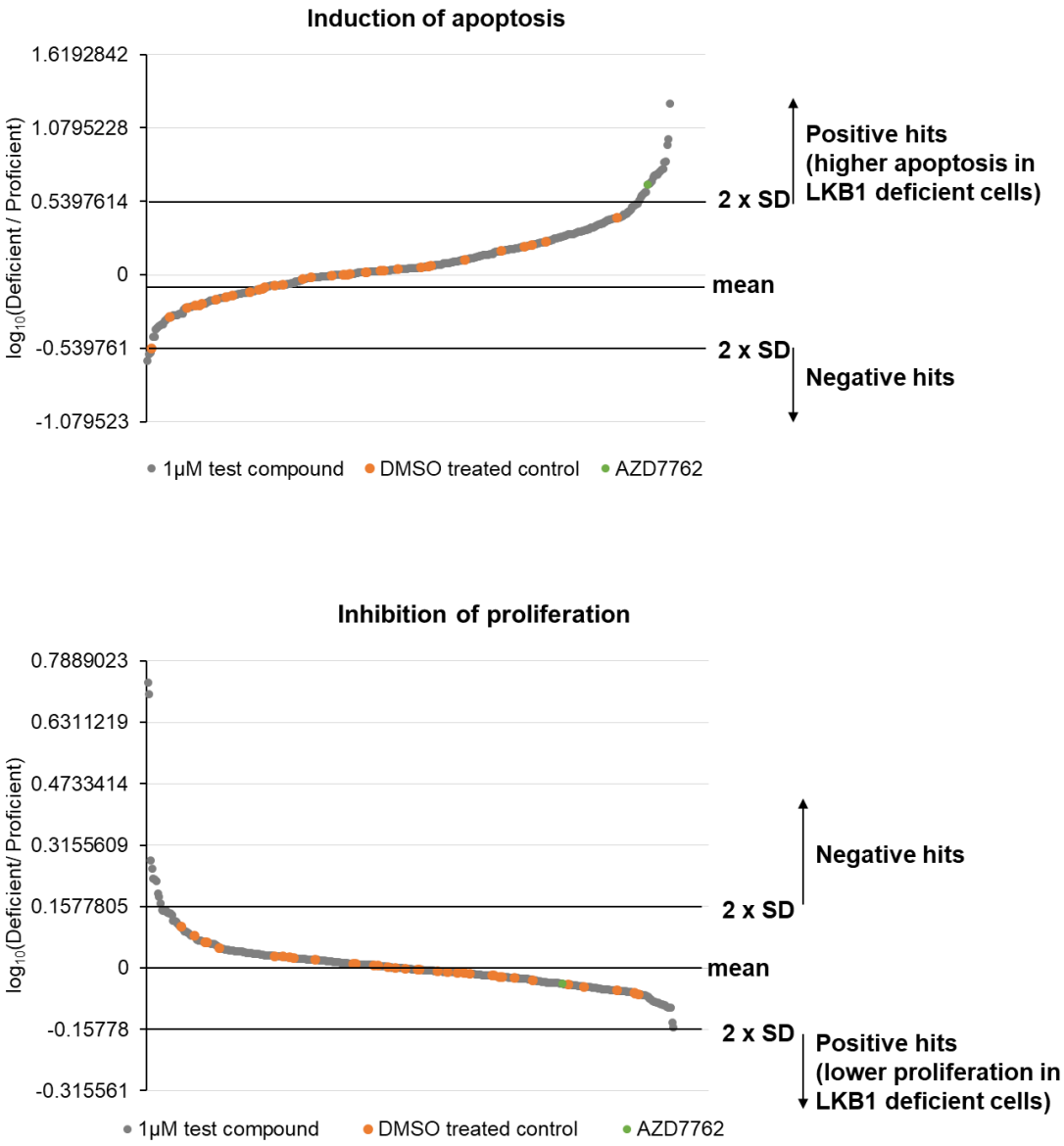

Figure 5.3: Primary screen: identification of positive and negative hits for LKB1 deficient and proficient cells

Each point represents the mean of duplicate values from 2 independent experiments.

Table 5.1: Positive and negative hits from the primary screen

	Compound	Target
Apoptosis: positive hits (> 2x SD (0.5398)) Sorted by inducing most to least apoptosis in LKB1 deficient	Cytarabine (Cytosar-U)	DNA polymerase
	SB 743921	Kinesin spindle protein
	Adriamycin	Topoisomerase
	Belinostat (PXD101)	HDAC
	Ispinesib (SB-715992)	Kinesin spindle protein
	SNS-032 (BMS-387032)	CDK
	Vinorelbine (Navelbine)	p38 MAPK
	Topotecan	Topoisomerase
	17-AAG (Geldanamycin)	HSP90
	PHA-793887	CDK
	AP24534	VEGFR | FGFR | PDGFR | FLT
	CHR-2797	Aminopeptidase N(APN) | LAP
	Sulfamethoxazole	PABA
	Vincristine	Microtubule Formation
	ITF2357	HDAC
	BIIB021	HSP90
	AZD7762	CHK
	Nilotinib	BCR-ABL
	SU11274 (PKI-SU11274)	C-MET
	Camptothecine	Topoisomerase
	Docetaxel	Microtubule Formation
	Imatinib Mesylate	C-KIT | PDGFR
	Panobinostat (LBH-589)	HDAC
Apoptosis: borderline positive hits (> 0.50 SD) Sorted by inducing most to least apoptosis in LKB1 deficient	JNJ-26481585	HDAC
	KU-55933	ATM
	17-DMAG	HSP90
	Cryptotanshinone	STAT
	MK-2206	AKT
Apoptosis: negative hits (> - 2x SD (-0.5398))	CI-1033 (Canertinib)	EGFR | HER2
	TG100-115	PI3K
	Bosutinib (SKI-606)	SRC
Proliferation: borderline positive hits (≥ - 0.14 SD (-2x SD = - 0.1578)) Sorted by causing most to least inhibition of proliferation in LKB1 deficient	PIK-75 Hydrochloride	PI3K | DNA-PK
	YM155	SURVIVIN
Proliferation: negative hits (> 2x SD (0.1578))	Panobinostat (LBH-589)	HDAC
	JNJ-26481585	HDAC
	LAQ824	HDAC
	JNJ-7706621	CDK | Aurora Kinase
	BI 2536	PLK
	Mitoxantrone	Topoisomerase
	Paclitaxel	Microtubule Formation
	BIIB021	HSP90
	GSK461364	PLK
	Topotecan	Topoisomerase
	SB 203580	p38 MAPK

In the initial screen, these positive and negative apoptotic and proliferation hits were identified (See Figure 5.3). All except KU-55933 and SB 203580 were tested further in A549, A427 and H1299 isogenic cells with or without LKB1 in the secondary screen.

5.2.2 Secondary screen (2D culture)

The positive and negative hits identified from the primary screen (Table 5.1) and additional compounds (Appendices Table A5.7) were tested in the 3 isogenic cell lines pairs (LKB1 deficient and proficient A549, A427 and H1299 cell lines). Hits were identified as compounds having a $log_{10}(\frac{change\ in\ LKB1\ deficient}{change\ in\ LKB1\ proficient})$ value greater than 2x SD from the mean of the DMSO treated controls. Interestingly, predominantly hits identified using an apoptosis assay were found in A549 and H1299 cells and hits identified using a proliferation assay were found in A427 cells, suggesting that there are different responses to stress in different cell types (Table 5.2). The positive apoptosis and proliferation hits found in two or more of the isogenic pairs were further tested in the tertiary screen.

Table 5.2: Secondary screen: confirmation of the positive and negative hits identified in the primary screen in the three isogenic pairs

Compound	A549	A427	H1299
17-AAG (Geldanamycin)			
17-DMAG			
Adriamycin			
AP24534			
AZD0530 (Saracatinib)			
AZD6244			
AZD7762			
AZD8055			
Belinostat (PXD101)			
BI 2536			
BIIB021			
Bosutinib (SKI-606)			
Camptothecin			
CHR-2797			
CI-1033 (Canertinib)			
Cryptotanshinone			
Cytarabine (Cytosar-U)			
Docetaxel			
Ganestespib			
GSK461364			
Imatinib Mesylate			
Ispinesib (SB-715992)			
ITF2357			
JNJ-26481585			
JNJ-7706621			
LAQ824			
LBH-589 (Panobinostat)			
LKB1 (AAK1 dual inhibitor)			
Mitoxantrone			
MK-2206			
Nilotinib			
Paclitaxel (Taxol)			
PF562271			
PHA-739358 (Danusertib)			
PI-103			
PIK-75			
SB 743921			
SNS-032 (BMS-387032)			
SU11274 (PKI-SU11274)			
Sulfamethoxazole			
TG100-115			
Thymidylate Kinase Inhibitor, YMU1			
Topotecan			
Vincristine			
Vinorelbine (Navelbine)			
WZ4003			
YM155			

Compounds named above represent positive apoptosis hits (green) or positive proliferation hits (red) or both positive apoptosis and proliferation hits (orange) in each cell line. Hits identified in > 2 isogenic pairs (except docetaxel, PI-103 and PF562271) were further tested in the tertiary screen.

5.2.3 Tertiary screen (2D culture)

The positive apoptosis and/or proliferation hits found in two or more of the isogenic pairs in the secondary screen (Table 5.2) were further tested at 1 and 0.1 µM concentrations. Hits were identified as having a $log_{10}(\frac{change\ in\ LKB1\ deficient}{change\ in\ LKB1\ proficient})$ value greater than 2x SD from the mean of the DMSO treated controls. Table 5.3 shows the positive apoptosis and proliferation hit compounds including their target, found in the 3 isogenic pairs. The compounds in bold were examined further in the quaternary screen.

Table 5.3: Tertiary screen: confirmation of positive apoptosis and/or proliferation hits identified in two or more isogenic cells in the secondary screen

Compound	Target	A549	A427	H1299
17-DMAG	HSP90	+_+_	-_-+	-_-_
AP24534	VEGFR | FGFR | PDGFR | FLT	+_+_	-_+_	+_+_
AZD6244	MEK	-_-_	-_++	-_++
AZD7762	CHK	-_+_	-_+_	-_-+
AZD8055	MTOR	-_-_	+_-_	-_-_
Adriamycin	Topoisomerase	+_-_	-_++	+_++
Belinostat(PXD101)	HDAC	+_+_	-+_-_	+_-_
Camptothecin	Topoisomerase	++_+_	+_++	+_++
ITF2357	HDAC	+_+_	+_-_	+_-_
JNJ-26481585	HDAC	+_++	-_-_	-_+_
LAQ824	HDAC	-_+_	-_-_	-_++
LBH-589(Panobinostat)	HDAC	++_++	-_-_	-_-+
Mitoxantrone	Topoisomerase	+_+_	-_++	++_+_
Nilotinib	BCR-ABL	-_-_	-_-_	+_-_
PIK-75	PI3K | DNA-PK	-_+_	-_-_	-_-+
Paclitaxel	Microtubule Formation	-_-_	-_++	-_-+
SNS-032(BMS-387032)	CDK	+_+_	-_+_	+_+_
Topotecan	Topoisomerase	++_-_	-_++	-_+_
Vincristine	Microtubule Formation	+_+_	-_++	-_-+
Vinorelbine	Microtubule Formation	++_+_	-_++	-_-+
YM155	Survivin	-_++	-_++	-_-_

"+" indicates the compound was identified as a positive hit and "-" indicates the compound was not identified as a positive hit. Green symbol represents hits identified using an apoptosis assay and the red symbol represents hits identified using a proliferation assay. The first large symbol indicates that the cells were treated with 1 µM and the second small symbol indicates that the cells were treated with 0.1 µM. For example, +-+- indicates that the hit was identified at 1 µM using both proliferation and apoptosis endpoints. Targets in blue are those identified as a hit in LKB1 deficient A549, A427 and H1299 cells. The compounds in bold were those further validated in the quaternary screen.

5.2.4 Quaternary screen - hit validation (2D culture)

The compound targets (in bold) from Table 5.3 common to all three isogenic pairs (CHK, topoisomerase, CDK, HDAC and microtubule formation) were investigated further. However, there were some exceptions to this; AP24534 targeting VEGFR/FGFR/PDGFR/FLT was not included as it is a multi-targeted compound, and its effects were unlikely to be limited to effects on a single target. The compounds further studied are marked in bold (Table 5.3) and were chosen for the following reasons; (i) camptothecin and mitoxanthrone were chosen as topoisomerase inhibitors as they caused the greatest effect out of all the topoisomerase inhibitors, (ii) panobinosat was chosen as a HDAC inhibitor as it was highly effective at both inducing apoptosis and inhibiting proliferation in A549 cells, (iii) vinorelbine is a microtubule destabiliser, therefore paclitaxel was additionally included as a microtubule stabiliser, (iv) YM155 was further validated as it was identified as a hit at 0.1 μM in A549 and A427 cells. Although AZD6244 was identified as a hit at 0.1 μM in A427 and H1299 cells, this was not further tested because we placed more weight on data from A549 and A427 isogenic pairs as LKB1 loss is intrinsic to these cells.

These compounds were further validated using (i) a Hoechst DNA binding assay to measure apoptosis over time (0, 6, 12, 24, 48, 72 h) (i.e. to determine if the difference seen in apoptosis levels between cells lines at 72 h was also seen at earlier time points) and (ii) a resazurin assay to generate a dose response curve for each compound in each cell line (i.e. to determine if the difference seen in proliferation between cells lines at 1 and/or 0.1 μM is also seen across a broader dose range).

In the tertiary screen, all hits apart from AZD7762 and YM155 were identified as hits by either the apoptosis assay alone or both the apoptosis and proliferation assays. Therefore, as they are proliferation hits, only the resazurin/proliferation assay was used to confirm

AZD7762 and YM155. The other hits were confirmed by both an apoptosis assay (extended to include the time course) and proliferation assay (extended to generate a dose response curve).

5.2.4.1 Proliferation assay

Table 5.4 shows the IC_{50} values for all inhibitors, except paclitaxel and vinorelbine which will be studied further later in this Chapter (Section 5.4). Apart from AZD7762 and panobinosat, the effect of these inhibitors on cell proliferation was variable between the isogenic pairs (i.e. the IC_{50} value was smaller for LKB1 deficient cells in one isogenic pair and higher for LKB1 deficient cells in another isogenic pair) (Table 5.4). The difference in sensitivity between LKB1 deficient and proficient cells to (i) AZD7762 was consistent with literature, and to (ii) panobinosat was consistent with LKB1 deficient cells being more sensitive, however the effect was small.

Table 5.4: Quaternary screen: validation of the hits using a proliferation assay

	IC_{50} (nM) ± SEM					
Cell line	**AZD7762**	**YM155**	**Camptothecin**	**Mitoxanthrone**	**Panobinosat**	**SNS-052**
A549 def	241.39 ± 74.69	6.23 ± 0.19	19.19 ± 5.02	6.29 ± 4.77	24.06 ± 0.36	315.83 ± 84.55
A549 pro	267.23 ± 99.01	2.97 ± 0.21	14.82 ± 5.53	0.004 ± NC	29.38 ± 2.85	272.54 ± 62.04
A427 def	78.96 ± 19.16	1.04 ± 0.01	17.5 ± 5.43	0.007 ± NC	28.25 ± 1.25	309.71 ± NC
A427 pro	153.63 ± 45.73	1.19 ± 0.02	27.81 ± 7.32	0.016 ± NC	28.67 ± 1.30	261.35 ± NC
H1299 def	202.29 ± NC	4.54 ± NC	33.31 ± 25.58	16.9 ± 4.48	42.51 ± 6.98	394.67 ± 202.67
H1299 pro	297.96 ± 274.02	13 ± 0.66	21.23 ± 9.81	20.49 ± 6.98	65.5 ± 9.13	996.85 ± NC

IC_{50} values ± SEM for cells treated with 0-0.3 μM YM155 and 0-1 μM for all other inhibitors for 72 h. Cell viability was determined using a resazurin assay. Data represents the mean of triplicate values from 3 independent experiments. NC – not calculable.

5.2.4.2 Apoptosis assay

On completion of the apoptosis time course for paclitaxel, vinorelbine, camptothecin, mitoxanthrone and panobinosat, it was found that LKB1 proficient cells underwent more apoptosis at 48 h than 72 h and conversely, LKB1 deficient cells underwent more apoptosis at 72 h than 48 h (Figure 5.4). In response to SNS-052, LKB1 proficient cells underwent greater apoptosis at 12 h and LKB1 deficient cells underwent greater apoptosis at 48 h. Although the hits confirmed at 1 μM and 72 h (i.e. they caused greater induction of apoptosis in LKB1 deficient cells), they were not biologically significant as LKB1 proficient cells had already undergone more apoptosis between 12-48 h. This suggests that LKB1 proficient cells were in a more pro-apoptotic state further suggesting that many pharmacological inhibitors that kill tumour cells via apoptosis may not effectively and selectively target LKB1 mutated tumour cells.

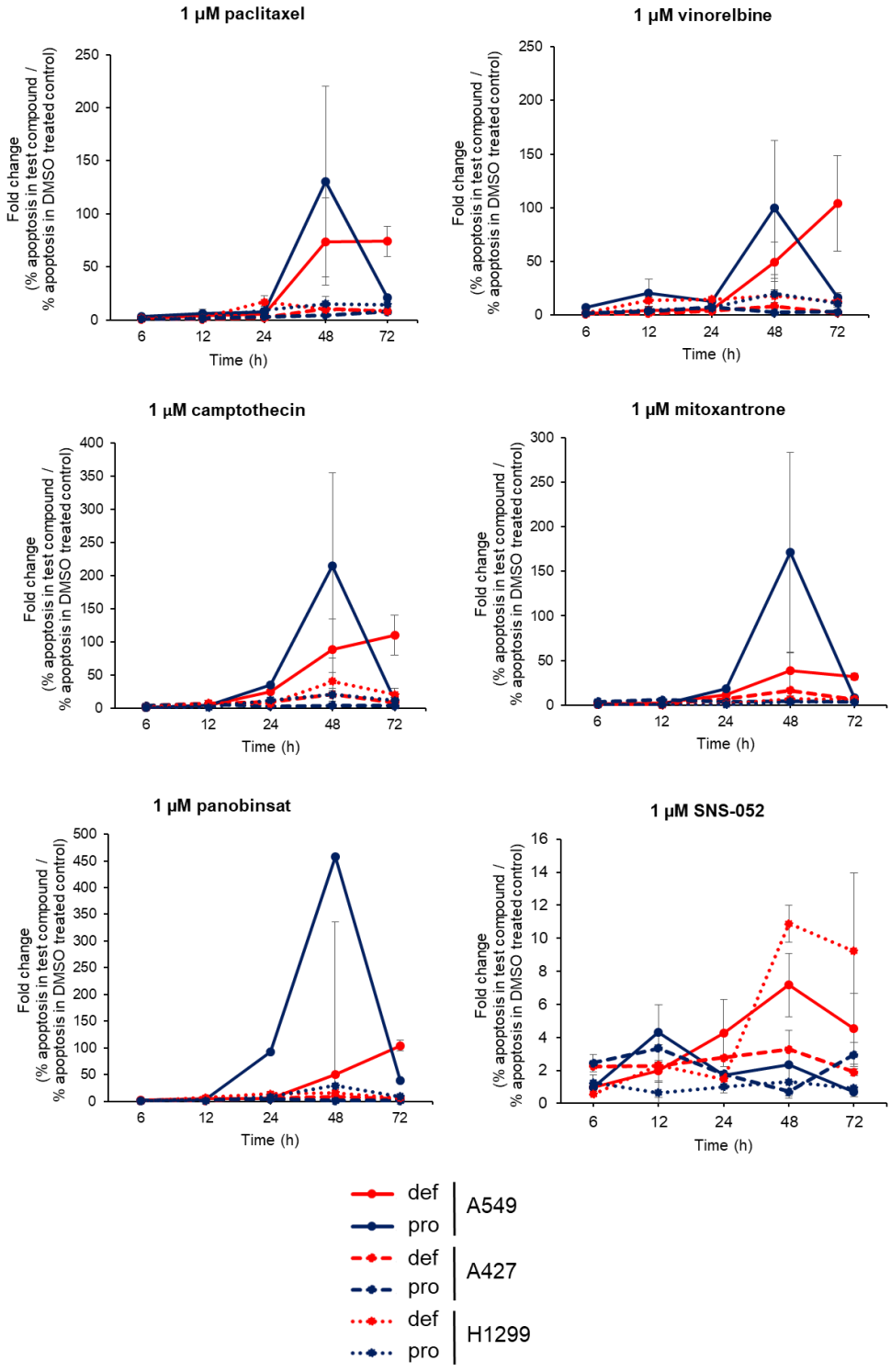

Figure 5.4: Quaternary screen: confirmation of the hits using an apoptosis assay
Apoptosis was measured using a Hoechst DNA binding assay. Time represents treatment time. Data represents the mean of duplicates.

5.2.5 Summary of 2D screen

AZD7762 was previously reported as a compound that had the potential to selectively target LKB1 deficient cells (Liu et al., 2013). Our data was consistent with this earlier work,

although we aimed to identify compound(s) with greater selective effects. Although hits (inhibitors for microtubules, topoisomerase, HDAC or CDK) were identified and confirmed on treatment with a concentration of 1 μM for 72 h, we did not consider them biologically significant as LKB1 proficient cells underwent apoptosis at an earlier time point than that used (72 h) in the primary, secondary and tertiary screens. This finding helps us to understand why many of our hits were identified using an apoptosis assay but not a proliferation assay and furthermore, why some compounds that were identified as both a positive apoptosis hit and a negative proliferation hit (for example, topotecan and adriamycin in A549 cells in the tertiary screen – Table 5.3). This finding highlights the importance of timing to identify hits and the importance of using more than one endpoint. However, compounds that selectively target LKB1 proficient cells were identified, and this provided insight into what compounds LKB1 deficient cells may be more resistant to and therefore, helps us to better understand the biology of LKB1 loss. One of these targets was microtubule inhibitors. A difference in microtubule structure was already observed in Section 3.4.3 and 3.5.3 and cytoskeletal remodelling was identified as a pathway associated with genes that were expressed at lower levels in LKB1 deficient cells (Section 4.4). The effect of microtubule inhibitors on cell proliferation and microtubule structure will be further investigated in Section 5.4.

5.3 Bioactive small molecule screen in 3D spheroids

As the positive hits were not biologically significant in the 2D screen, a smaller screen (74 compounds, 6 DMSO treated controls, 1x 96-well plate) using 3D spheroids was undertaken with the aim of identifying compounds that selectively target LKB1 deficient cells. As discussed in Chapter 3 and 4, spheroids may be a more clinically relevant model than cells in 2D culture. Also, LKB1 expression causes a phenotypic difference in spheroid size that can be easily measured. The compounds chosen include hits from the 2D screen, compounds

inhibiting possible targets identified from the transcriptomic data (PI3K/AKT inhibitors and MAPK pathway inhibitors) (Section 4.4) and suggested targets from the literature (MTOR, VEGF) (Section 1.6). A list of the compounds can be found in the Appendices (Appendices Table A5.8). LKB1 deficient and proficient A549 and H1299 spheroids were formed in the presence of inhibitor (10 μM). A greater concentration than the 2D screen was chosen as there were 10x more cells seeded in the spheroid than 2D culture. Area was measured on day 1, 2, 3 and 8 post seeding. This allowed both the effect on spheroid formation and growth to be determined, without the medium becoming exhausted.

For each cell line on each day, the area of each compound treated spheroid was calculated as a percentage of the area for the DMSO treated spheroids. Positive "hits" (i.e. compounds that selectively reduced the area of LKB1 deficient spheroids) were identified as those that reduced the area of the LKB1 deficient spheroids to a percentage lower than the maximum reduction in area found in a LKB1 proficient spheroid after treatment with a compound (Section 2.11.2). For example, on day 8, PIK93 reduced the area of LKB1 proficient A549 spheroids by 50% compared to the DMSO treated LKB1 proficient controls. This reduction was greater for LKB1 proficient spheroids, than that caused by any other compound used in the screen. Therefore, using day 8 data, hit compounds were selected as those that reduced the area to a value $\geq 50\%$ in LKB1 deficient spheroids compared to the DMSO treated controls. In the case of PIK93, it was identified as a potential positive hit as it reduced the area of the LKB1 deficient A549 spheroids by 65% compared to the DMSO treated LKB1 deficient A549 controls. Figure 5.5-5.6 shows the mean percentage difference in spheroid area after treatment with compounds and DMSO for each cell line on each day. Table 5.5 shows the positive hits (selective for LKB1 deficient spheroids) for both A549 and H1299 spheroids in each of the 3 independent experiments.

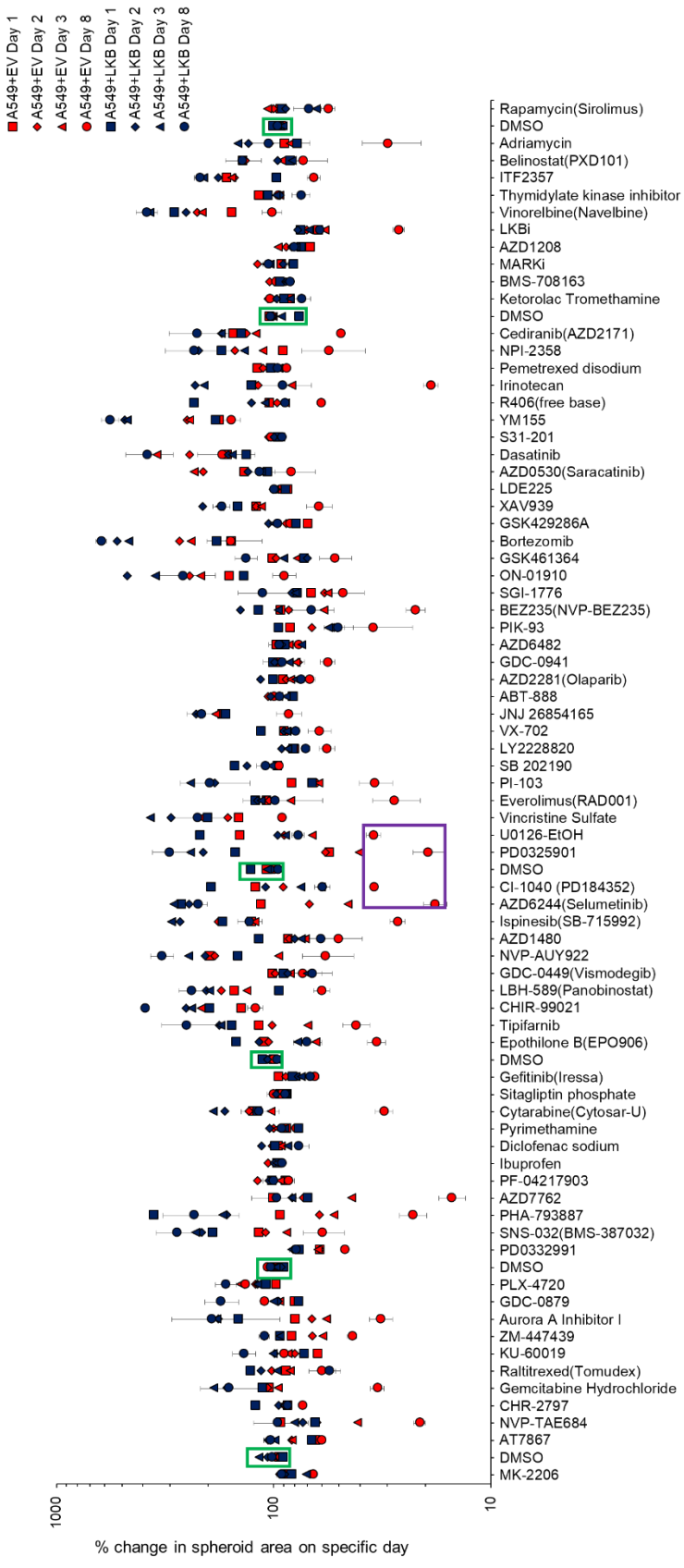

Figure 5.5: 3D bioactive small molecule screen: identification of the positive hits in LKB1 deficient A549 spheroids

Area was measured on day 1, 2, 3 and 8 post seeding using the GelCount. On each day, the area for each spheroid treated with test compounds was calculated as a percentage of the area for the DMSO treated spheroids. Each data point represents the average area of spheroids from 3 independent experiments. Error bars are SEM for LKB1 deficient and proficient spheroids on day 8. Green boxes mark the DMSO treated spheroids which have an approximate value of 100%. Purple box highlights LKB1 deficient spheroids on day 8 treated with four MEK inhibitors.

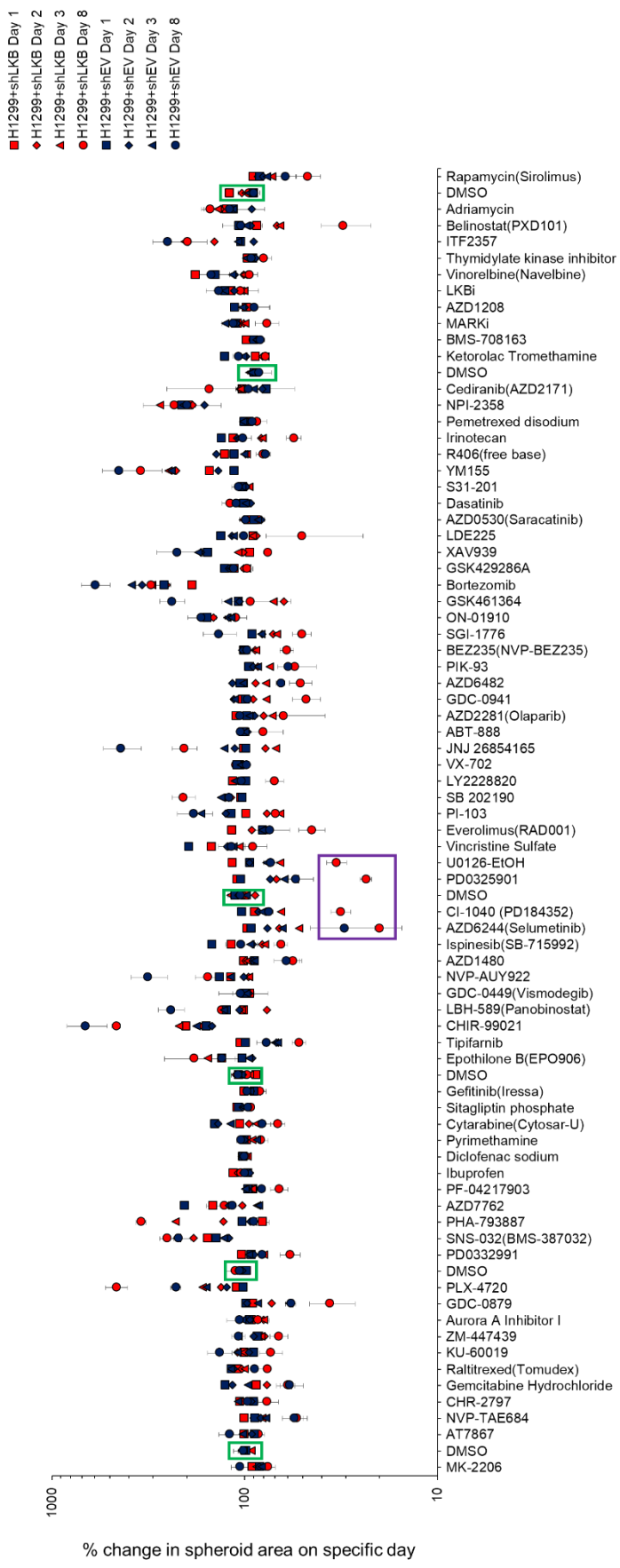

Figure 5.6: 3D bioactive small molecule screen: identification of the positive hits in LKB1 deficient H1299 spheroids

Area was measured on day 1, 2, 3 and 8 post seeding using the GelCount. On each day, the area for each spheroid treated with test compounds was calculated as a percentage of the area for the DMSO treated spheroids. Each data point represents the average area of spheroids from 3 independent experiments. Error bars are SEM for LKB1 deficient and proficient spheroids on day 8. Green boxes mark the DMSO treated spheroids which have an approximate value of 100%. Purple box highlights LKB1 deficient spheroids on day 8 treated with four MEK inhibitors.

Table 5.5: Positive hits identified from the bioactive small molecule screen in 3D spheroids

		Experiment no.		
Compound	**Target**	**1**	**2**	**3**
AZD1480	JAK			
AZD2281 (Olaparib)	PARP			
AZD6244 (Selumetinib)	MEK			
AZD7762	CHK			
Adriamycin	Topoisomerase			
Aurora A Inhibitor I	Aurora Kinase			
Belinostat (PXD101)	HDAC			
BEZ235 (NVP-BEZ235)	MTOR | PI3K			
CI-1040 (PD184352)	MEK			
Cytarabine (Cytosar-U)	DNA polymerase			
Epothilone B (EPO906)	Microtubules			
Everolimus (RAD001)	MTOR			
GDC-0449 (Vismodegib)	Hedgehog			
GDC-0879	B-RAF			
GDC-0941	PI3K			
GSK461364	PLK			
Gemcitabine	Antimetabolites			
Irinotecan	topoisomerase			
Ispinesib (SB-715992)	Kinesin spindle protein			
LKBi	LKB			
NPI-2358	VDA microtubules			
NVP-AUY922	HSP90			
NVP-TAE684	ALK			
PD0325901	CDK			
PHA-793887	CDK			
PI-103	PI3K | MTOR			
PIK-93	PI3K			
Rapamycin (Sirolimus)	MTOR			
SGI-1776	PIM			
SNS-032 (BMS-387032)	CDK			
Tipifarnib	Farnesyltransferase (FTASE)			
U0126-EtOH	MEK			
ZM-447439	Aurora Kinase			

The 3D screen was completed as 3 independent experiments. The inhibitors listed above represent the positive hits on day 8 in each experiment. Yellow indicates the hit was identified in H1299 spheroids, orange indicates the hit was identified in A549 spheroids and red indicates the hit was identified in both A549 and H1299 spheroids.

Table 5.5 shows the positive hits identified in the 3D screen in each of the three independent experiments. Hits were mainly identified in LKB1 deficient A549 spheroids and not H1299 spheroids. Four MEK inhibitors were identified as positive hits for LKB1 deficient A549 and H1299 spheroids in all 3 experiments, thus suggesting that MEK inhibitors may be used to target LKB1 deficient cells. To confirm that the MEK inhibitors were selective for LKB1 deficient spheroids, spheroid images (acquired using the microscope) were investigated to determine the overall spheroid integrity and density. Spheroids with similar areas may not have similar densities and a less dense spheroid could indicate it is falling apart and dying. Figure 5.7 shows images of the spheroids after 8 days treatment with the four MEK inhibitors. The images showed no change in area of LKB1 proficient spheroids treated with AZD6244 and PD325901, however, it is clear that they were less dense, breaking apart and possibly dying. This shows that area does not always correlate with spheroid viability and it is important to investigate both the area and the density/integrity of the spheroid. Using the hits present in one or more of the experiments (Table 5.5), the spheroid images for these hits were manually analysed to ensure proficient spheroids were still intact. Figure 5.8 shows the potential positive hits for LKB1 deficient A549 spheroids. Interestingly, three inhibitors of PI3K (PIK-93, GDC-0941, BEZ235) came up as positive hits suggesting that PI3K signalling may be increased in LKB1 deficient cells, although, we did not further evaluate this as PI3K and MTOR inhibitors have already been studied in the literature (Section 1.6). However, the microtubule inhibitor epothilone, was also identified as a potential positive hit which is in contrast to our 2D screen where it was identified as a negative hit, as paclitaxel and vinorelbine caused a more rapid induction of apoptosis in LKB1 proficient cells than deficient cells (Figure 5.4) (Section 5.2.4).

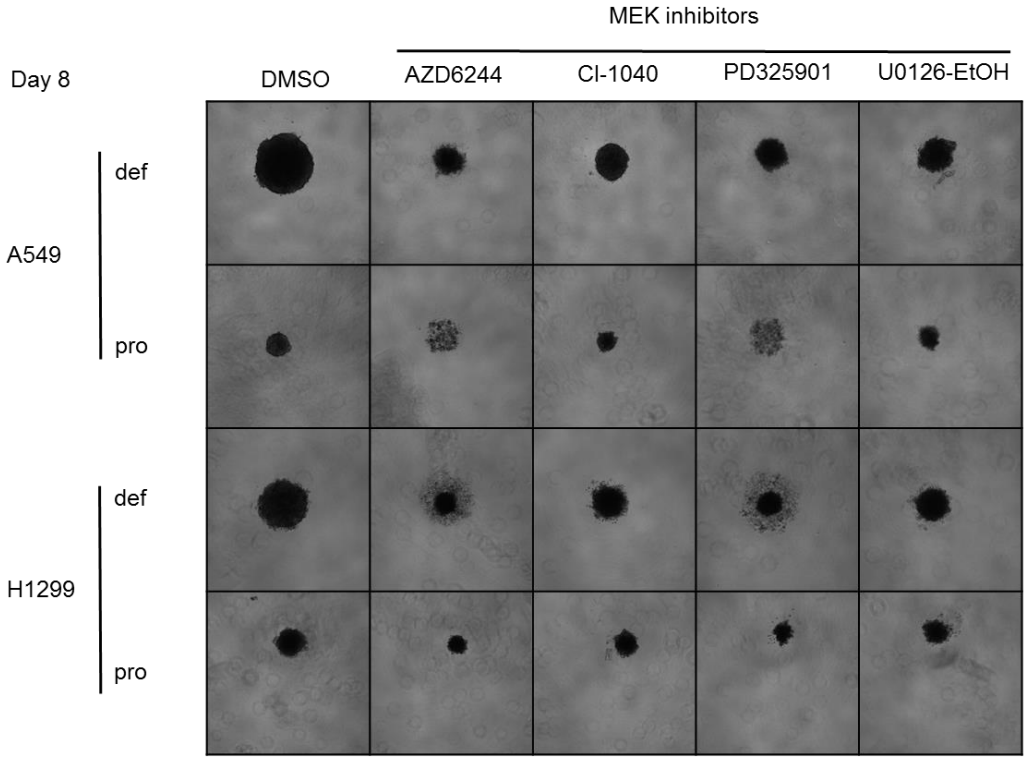

Figure 5.7: LKB1 deficient and proficient spheroids treated with MEK inhibitors
Representative live spheroid images at 40x magnification using the Nikon Ti-E microscope. Spheroids were treated from the point of seeding with 10 μM of MEK inhibitor.

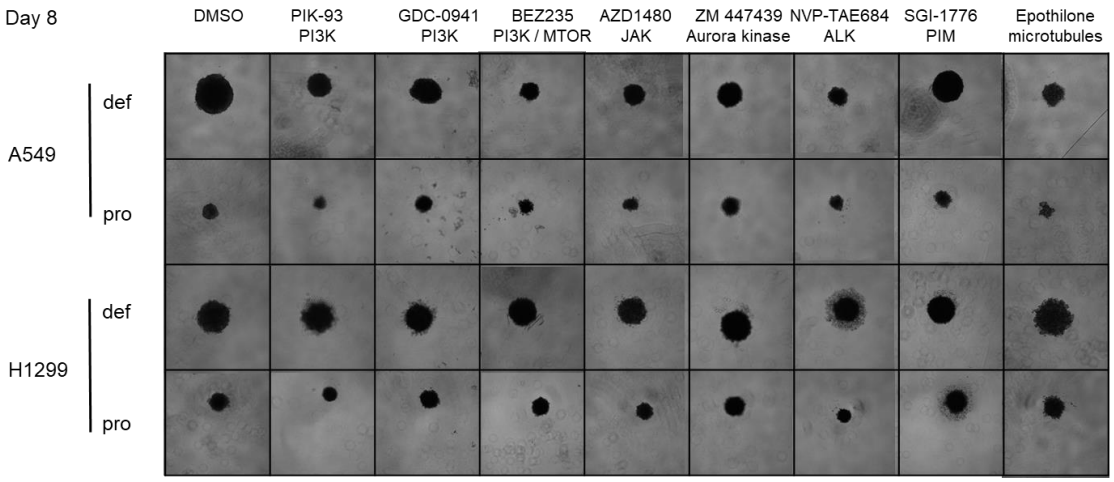

Figure 5.8: Potential positive hits for LKB1 deficient A549 spheroids
Representative live spheroid images at 40x magnification using the Nikon Ti-E microscope. Spheroids were treated from the point of seeding with 10 μM of test compound. The target(s) is/are listed below the test compound.

5.3.2 Summary of 3D screen

There remain technical challenges when performing a compound screen using 3D spheroids. We found that although spheroid area was useful in determining whether or not compounds had an effect on growth, spheroid density was also important. Although four different MEK inhibitors were identified as potential positive hits in both LKB1 deficient A549 and H1299 spheroids, the effect was compound dependent rather than target specific. However, we identified some potential hits including microtubule inhibitors. As we also identified a difference in sensitivity to microtubule inhibitors in our 2D screen, in the next section, we focus on investigating the effect of microtubule stabilisers (paclitaxel and docetaxel) and destabilisers (vincristine and vinorelbine) on microtubule structure, cell proliferation in 2D culture and spheroid area and density in LKB1 deficient and proficient cells.

5.4 The effect of LKB1 expression on sensitivity to microtubule inhibitors

In addition to identifying a difference in sensitivity to microtubule inhibitors in our 2D and 3D screen, reasons to focus our study on these compounds came from (i) microtubule inhibitors are commonly used to treat lung cancer (Ferrara et al., 2016), (ii) on characterisation of the isogenic cells, we observed a difference in the organisation of the microtubule network between LKB1 deficient and proficient cells (Section 3.4.3 and 3.5.3), (iii) the transcriptomic data we generated in Section 4.4 identified cytoskeletal remodelling as a pathway associated with genes that were expressed at lower levels in LKB1 deficient cells in 2D, 3D and human tumours (heatmap showing expression of cytoskeletal genes can be found in the Appendices Figure A5.14). Furthermore, it was reported that MARK (microtubule affinity regulatory kinase) is phosphorylated by LKB1 (Lizcano et al., 2004) (Figure 5.9, Section 1.3.1). MARK phosphorylates the microtubule-binding domain of the microtubule-associated proteins (MAPT, MAP2, and MAP4), causing their dissociation from microtubules and increased microtubule dynamics (Drewes et al., 1997). Therefore,

MARK provides a potential link between LKB1 function, microtubule structure and differences in sensitivity to microtubule inhibitors.

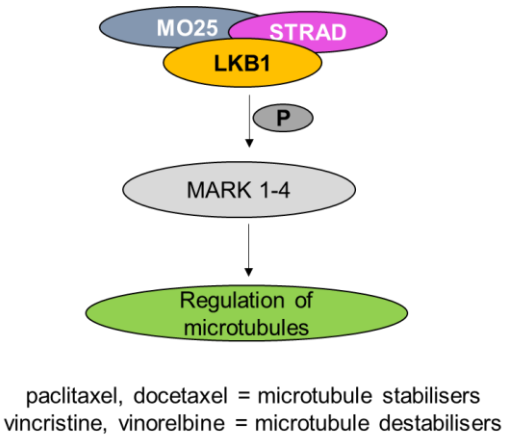

Figure 5.9: Schematic showing that LKB1 phosphorylates MARK, a protein involved in microtubule dynamics

To determine the effect of microtubule inhibitors on the structure of microtubules, LKB1 deficient and proficient A549 cells in 2D culture were treated with microtubule inhibitors (0-100 nM) for 72 h and immunofluorescence was used to visualise the microtubules. Figure 5.10 shows that after 30 nM paclitaxel, LKB1 deficient and proficient cells appeared multi-nucleated suggesting possible issues with cytokinesis. Furthermore, on treatment with 100 nM paclitaxel, LKB1 deficient A549 cells increased in size and LKB1 proficient A549 cells decreased in size and had possibly undergone apoptosis. A similar phenotype was seen from 10 nM docetaxel in both LKB1 deficient and proficient A549 cells (Appendices Figure A5.15). Multi-nucleated LKB1 deficient and proficient cells were seen after 10 nM vincristine treatment. For vinorelbine treated cells, multi-nucleated cells were seen at 10 nM for LKB1 proficient cells and 100 nM for LKB1 deficient cells (Appendices Figure A5.15).

To determine the effect of microtubule inhibitors on cell proliferation in LKB1 deficient and proficient A549, A427 and H1299 cells, a resazurin-based assay was used. Figure 5.11

shows the dose response curves after 72 h of microtubule inhibitor treatment in the cells. LKB1 proficient A549 cells were more sensitive to paclitaxel, docetaxel, vincristine and vinorelbine than LKB1 deficient cells. However, LKB1 proficient A427 cells were less sensitive to paclitaxel, and there was no difference in paclitaxel sensitivity between H1299 cells.

To examine the effect of microtubule inhibitors in 3D spheroids, LKB1 deficient and proficient spheroids were treated with microtubule inhibitors from the point of seeding for 8-10 days. Spheroid area was used as the primary endpoint but spheroids were also imaged to examine their density. Paclitaxel (0-100 nM) reduced the size of LKB1 deficient spheroids and increased the size of LKB1 proficient spheroids. At 30 nM paclitaxel, deficient and proficient spheroids were equal in size (Figure 5.12). A similar effect was seen after 30 nM docetaxel treatment and after 100 nM vincristine treatment and 10 nM vinorelbine treatment (Appendices: Figure A5.16).

We hypothesised that the difference in microtubule organisation and microtubule inhibitor sensitivity between the LKB1 deficient and proficient cells could be dependent on LKB1 phosphorylation and activation of MARK. However, western blotting showed that pMARK was upregulated in both LKB1 deficient and proficient A549 cells in 2D culture after a 24 h treatment with 50 nM paclitaxel (Figure 5.13) suggesting that another protein is involved in the interaction between LKB1 and the microtubules following treatment with microtubule inhibitors. Interestingly, γH2AX expression (marker of DNA double strand breaks and apoptosis) was expressed at higher levels in LKB1 deficient cells after paclitaxel treatment suggesting that these cells may be more sensitive initially at 24 h.

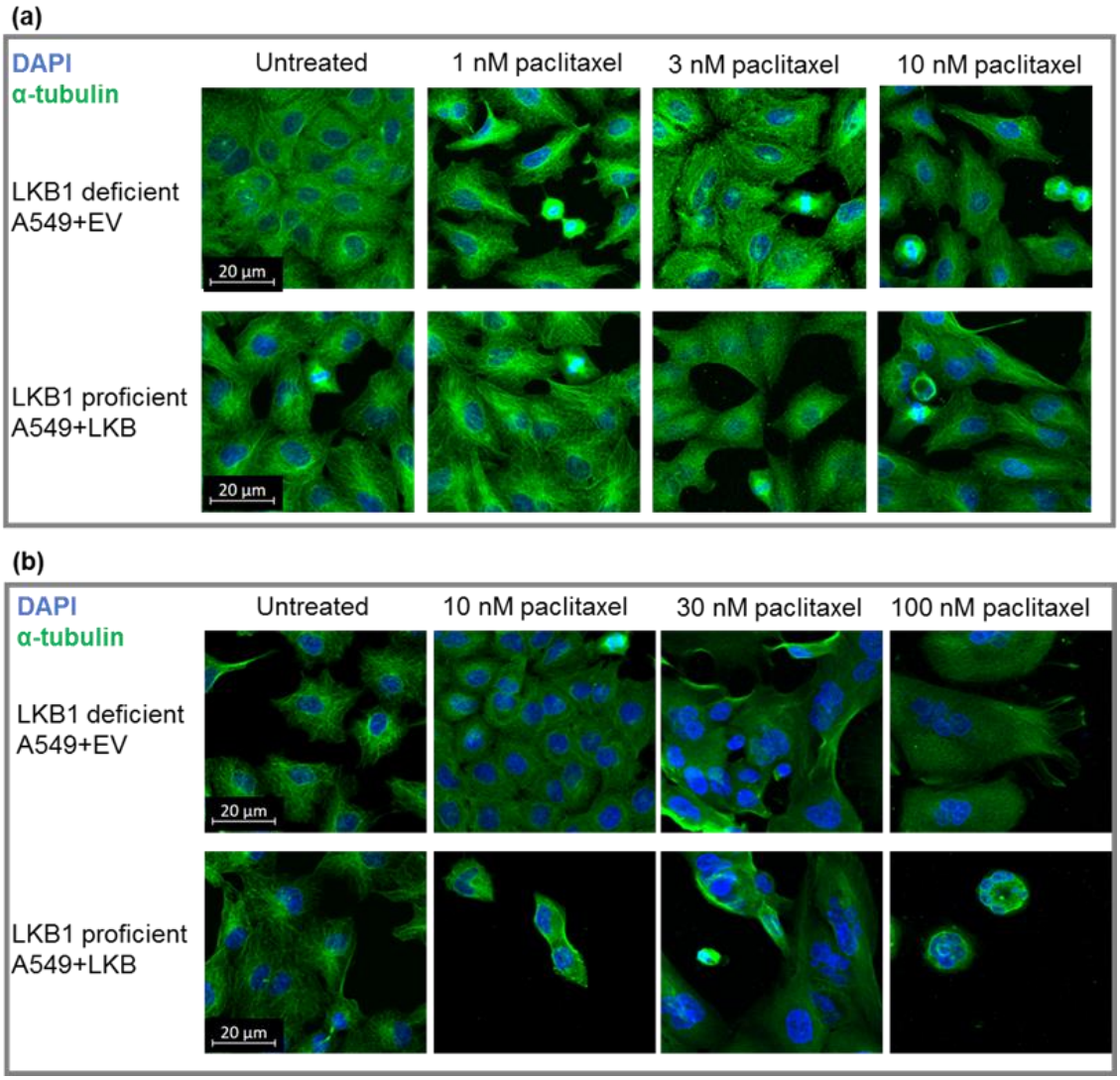

Figure 5.10: Microtubule staining in LKB1 deficient and proficient cells after treatment with paclitaxel

Cells were grown in 2D culture and treated for 72 h before fixing with 10% formalin. Cells were stained with DAPI (blue) and α-tubulin (green). Images were acquired using the 63x objective on a confocal microscopy.

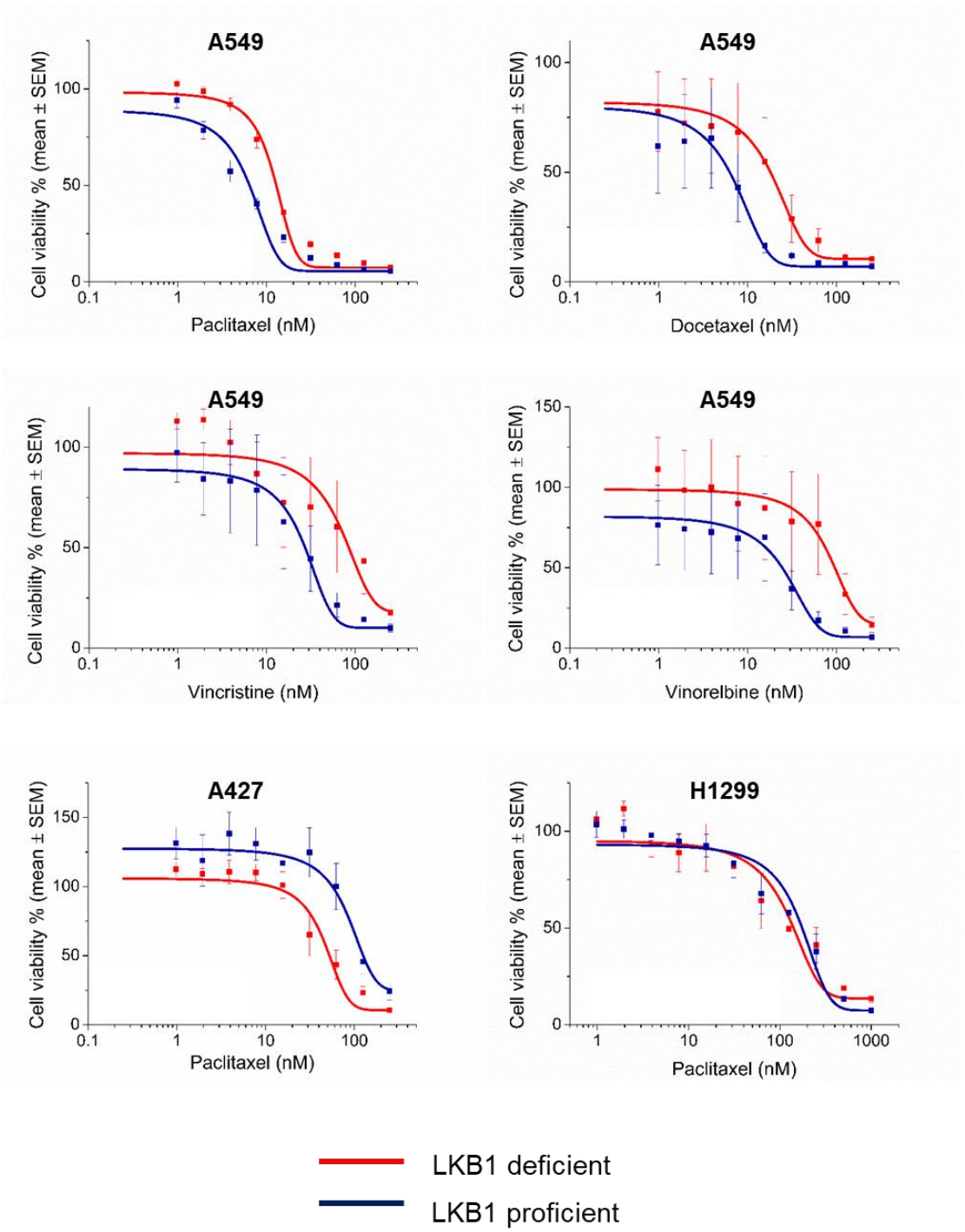

Figure 5.11: The effect of microtubule inhibitors on cell proliferation in LKB1 deficient and proficient cells in 2D culture

LKB1 deficient and proficient A549, A427 and H1299 cells were treated for 72 h. Cell viability was measured using a resazurin-based cell viability assay. Data represents the mean of triplicate values from 2 independent experiments.

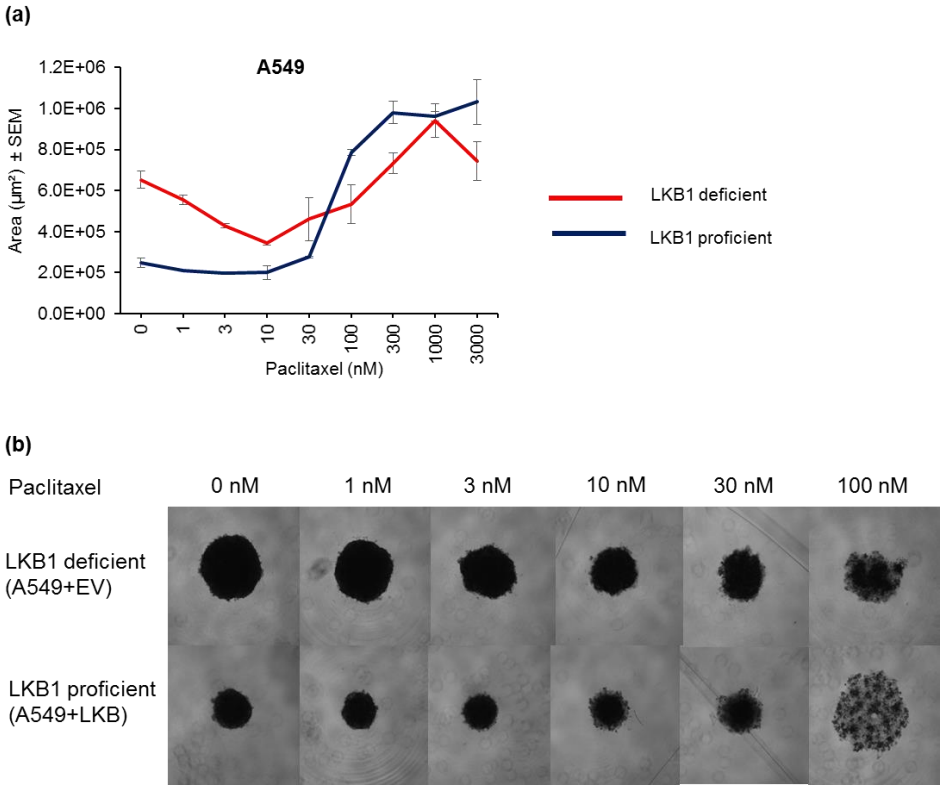

Figure 5.12: LKB1 deficient and proficient spheroids treated with paclitaxel
Spheroids were treated from the point of seeding for 10 days. (a) Data represents the mean of duplicate values form 1 experiment. (b) Representative images at 40x magnification using the Nikon Ti-E microscope.

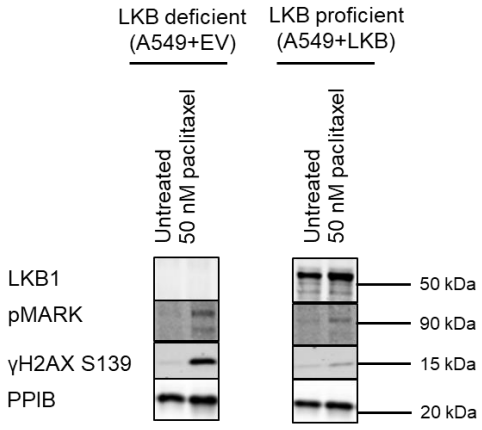

Figure 5.13: Phospho-MARK levels after paclitaxel treatment in LKB1 deficient and proficient cells
Cells in 2D culture were treated for 24 h. Western blotting was carried out and 15 µg of protein was loaded per well.

5.4.2 Summary of the difference in sensitivity to microtubule inhibitors

The difference in response to microtubule inhibitors between LKB1 deficient and proficient cells was complex. In 2D culture, LKB1 proficient A549 and A427 cells were more sensitive to microtubule inhibitors than LKB1 deficient cells, although, MARK does not appear to play a role in determining the difference in sensitivity. LKB1 proficient cells had a more organised microtubule network (Figure 3.4) which may be linked to the enhanced sensitivity. Microtubule inhibitors equalised the size difference between LKB1 deficient and proficient spheroids. As they reduced the size of the LKB1 deficient spheroids and increased the size of LKB1 proficient spheroids, it has yet to be determined if microtubule inhibitors may be used to selectively target LKB1 mutated cells *in vivo*.

5.5 Discussion

AZD7762 was previously reported as a compound that could potentially target LKB1 mutated cells (Liu et al., 2013). Our aim was to identify a novel compound that could selectively target LKB1 deficient cells which had a larger effect than AZD7762. We firstly completed a bioactive small molecule screen in 2D culture using a bioactive small molecule library (n = 326) and then we completed a smaller screen in 3D culture (n = 74 compounds).

Importantly, our 2D data was consistent with the AZD7762 report where Liu et al showed that AZD7762 reduced survival of LKB1 mutated A549 and H2122 cells to a greater degree than LKB1 wild-type Calu-1 and H358 cells. Similar to our approach, Liu et treated cells with 0-1 µM AZD7762 for 72 h (Liu et al., 2013). In our primary screen, AZD7762 was identified as a positive apoptotic hit (Figure 5.3, Table 5.1) and in our quaternary screen, LKB1 deficient A549, A427 and H1299 cell were more sensitive to inhibition of proliferation after 72 h treatment with AZD7762 (0-1 µM) (Table 5.4).

For the 2D screen, two endpoints were used; induction of apoptosis and inhibition of proliferation, although, our data suggests that measuring proliferation using the resazurin assay was more reproducible (Figure 5.2). However, the use of resazurin has limitations. For example, non-fluorescent resazurin is broken down into fluorescent resorufin by metabolically active cells (O'Brien et al., 2000), therefore, mitochondrial defects or inhibitors that increase the metabolic activity of cells could affect the result and provide false positive or false negative hits. Therefore, ideally, a resazurin assay should be confirmed by another assay. Surprisingly, in the primary screen, we identified compounds as both positive hits using the apoptosis assay and negative hits using the proliferation assay. In fact, the apoptosis and proliferation data do not correlate as much as would be expected (Appendices Figure A5.17). Hits were confirmed using a 0-72 h time course measuring induction of apoptosis and also confirmed by interpreting dose response curves. However, the hits did not appear to be biologically significant as LKB1 proficient cells underwent more rapid apoptosis in response to the inhibitors compared with LKB1 deficient cells (Figure 5.4). This suggests that LKB1 proficient A549 cells were in a more pro-apoptotic state than LKB1 deficient cells, which may contribute to resistance towards compounds. It has been reported that LKB1 interacts with TP53 to induce apoptosis in an osteosarcoma cell line (Karuman et al., 2001) which may be a reason for a pro-apoptotic state in LKB1 proficient, TP53 wild-type A549 cells. Interestingly, in the primary 2D screen, three HDAC inhibitors (panobinostat, JNJ-26481585, LAQ824) were identified as negative proliferation hits (Table 5.1), suggesting that LKB1 loss may be associated with epigenetic changes. It was previously reported that SIK2 and SIK3 regulates the subcellular localisation of HDAC (Walkinshaw et al., 2013) (Section 1.3.5) highlighting a possible link with LKB1 and HDAC.

As 3D spheroids may be more clinically relevant and LKB1 expression causes a phenotypic difference in these, a smaller screen was completed using spheroids. To my knowledge, the 3D spheroid screen was a novel method for identifying compounds that selectively target LKB1 mutated cells. However, there are technical issues with screening using spheroids and there is a need to develop a more reproducible, cost effective, high-throughput method for determining spheroid viability that is preferably a continuous assay. Other groups have validated the use of Promega's CellTitre-Glo to measure spheroid viability (Zanoni et al., 2016). Although, CellTitre-Glo is useful for determining spheroid viability, it can only be used as an endpoint assay. Resazurin and PicoGreen were used to determine spheroid viability in Section 3.5 and could be exploited in future experiments, although these are also endpoint assays. In the 3D screen, spheroid area was used as the primary endpoint. Using area, we identified four MEK inhibitors that selectively target LKB1 deficient spheroids in both A549 and H1299 cells. Although two MEK inhibitors (AZD6244 and PD325901) did not disrupt the area of the proficient spheroids, the spheroids appeared looser and less dense, suggesting that the LKB1 dependent differences in sensitivity to MEK inhibitors was compound dependent rather than target specific (Figure, 5.7). Chen et al also reported that, compared to $Kras^{G12D}$ mutated tumours or $Kras^{G12D}/p53^{L/L}$ mutated tumours, $Kras^{G12D}/Lkb1^{L/L}$ mutated tumours were less sensitive to AZD6244 when combined with docetaxel (Chen et al., 2012). Kaufman et al reported that sensitivity to MEK inhibition in LKB1 proficient cells was dependent on LKB1 induced changes in AKT and FOXO3 (Kaufman et al., 2017).

Using the 2D and 3D screens, we also identified a differential response to microtubule inhibitors between LKB1 deficient and proficient cells. Our data discussed in Chapter 3 suggests that LKB1 expression does affect the structure of microtubules as LKB1 proficient cells had a more organised microtubule network and possibly stronger cell-cell contacts. It

is unknown why restoration of LKB1 restores microtubule structure and if microtubule organisation helps with cell-cell contacts or if cell-cell contacts help with microtubule organisation, and if either of these are linked to apoptosis in LKB1 deficient/proficient cells. However, the difference in microtubule organisation could explain the difference in sensitivity to microtubule inhibitors, although the response is complex. LKB1 deficient cells were more resistant to microtubule inhibitors in 2D culture. However, in 3D spheroids, microtubule inhibitors decreased the size of larger LKB1 deficient spheroids and increased the size of the smaller LKB1 proficient spheroids. These data suggest that microtubules were important for spheroid structure as microtubule inhibitors disrupted LKB1 proficient tight spheroids. Considering that the low dose of microtubule inhibitors reduced the size of LKB1 deficient spheroids, it is difficult to predict the response in LKB1 mutated and wild-type tumours. Chen et al showed that docetaxel monotherapy had a smaller effect at reducing tumour burden in $Kras^{G12D}/Lkb1^{L/L}$ driven mouse lung tumours compared with $Kras^{G12D}$ driven tumours (Chen et al., 2012). Conversely, Mao et al reported that re-expression of LKB1 in LKB1 mutated EKVX lung adenocarcinoma cells decreased sensitivity to paclitaxel, due to increased expression of MDR1 (Mao et al., 2015). Our RNA Sequencing data (Chapter 4) showed that MDR1 mRNA levels were not significantly different between the LKB1 deficient and proficient cells in both 2D and 3D models and therefore, MDR1 is unlikely to contribute to the differences in sensitivity observed in our data. However, there could be other factors within each cell line which may affect the way LKB1 responds to inhibitors. We hypothesised that LKB1 dependent MARK phosphorylation (involved in microtubule dynamics) may cause the difference in sensitivity to the microtubule inhibitors. However, MARK was upregulated in response to paclitaxel treatment in both LKB1 deficient and proficient cells. Future experiments could determine changes in LKB1 downstream signalling linked to microtubule organisation.

To conclude, LKB1 deficient A549 cells were less apoptotic and generally more resistant to compounds in the 2D screen. Using the 3D screen, PI3K, MTOR and microtubule inhibitors were identified as a potential targets for LKB1 deficient spheroids. As microtubule inhibitors were identified as a hit in the 2D screen and we observed a difference in microtubule structure between the LKB1 deficient and proficient cells, we investigated the effect of microtubule stabilisers and destabilisers further. In 2D culture, LKB1 deficient cells were less sensitive to microtubule inhibitors. However, microtubule inhibitors equalised the difference in size between large LKB1 deficient A549 spheroids and small LKB1 proficient spheroids. The difference in sensitivity to microtubule inhibitors was not dependent on MARK phosphorylation by LKB1. To identify novel targets for LKB1 mutated cells, future experiments could use a larger library for screening, whole genome siRNA, shRNA or CRISPR.

6 Exploitation of an altered metabolic phenotype in LKB1 mutated lung cancer cells

6.1 Introduction

It has been reported that LKB1 plays a role in metabolism (Section 1.3.2), and thus proposed that LKB1 mutated cells may be selectively sensitive to metabolic inhibitors (Hardie and Alessi, 2013). Shackelford et al investigated this further and found that (i) LKB1 mutated NSCLC cells are more sensitive to phenformin (a complex I/oxidative phosphorylation inhibitor), compared to cells with ectopic expression of LKB1 and (ii) *Kras*^{G12D}*/Lkb1*$^{L/L}$ driven mouse lung tumours were more sensitive to phenformin than *Kras*^{G12D} and *Kras*^{G12D}*/p53*$^{L/L}$ driven tumours (Shackelford et al., 2013) (Section 1.6). In this Chapter, we aimed to broaden the understanding of the difference in sensitivity to complex I inhibitors using (i) LKB1 deficient and proficient isogenic cells and (ii) a broad range of LKB1 mutated and wild-type lung cancer cell lines. As LKB1 has been reported to play an important role in metabolism, we further analysed our RNA Sequencing data to identify any differences in metabolic genes between LKB1 deficient and proficient cells. Using these data, we hypothesised that LKB1 mutated cells were associated with a metabolic shift from oxidative phosphorylation to aerobic glycolysis. To identify potential novel approaches to selectively target LKB1 deficient cells, we also tested other (non-complex I) metabolic inhibitors and nutrient (glucose and glutamine) deprivation on cell proliferation in LKB1 deficient and proficient cells. In the previous Chapter, we used a hypothesis free approach to identify novel strategies to selectively target LKB1 mutated cells. In this Chapter, we used a hypothesis driven approach to identify novel strategies to selectively target LKB1 mutated cells.

6.2 The effect of LKB1 expression on sensitivity to complex I inhibitors

Metformin and phenformin inhibit complex I of the mitochondria (Owen et al., 2000). Complex I plays a role in the electron transport chain of oxidative phosphorylation. Oxidative phosphorylation couples the transfer of electrons produced during the citric acid cycle from complex I to a terminal electron acceptor (oxygen) with the transport of protons from the mitochondrial matrix to the inner mitochondrial space. ATP is produced when, Complex V (an ATP synthase) transports protons from the inner mitochondrial space back to the mitochondrial matrix (Nelson et al., 2008). Therefore, by inhibiting complex I, metformin and phenformin inhibit oxidative phosphorylation and thus, inhibit oxygen consumption. The oxygen consumption rate (OCR) can be determined using a Seahorse XF96 analyser (Seahorse Bioscience) which measures the concentration of dissolved oxygen in the medium using oxygen sensitive fluorophores (Figure 6.1).

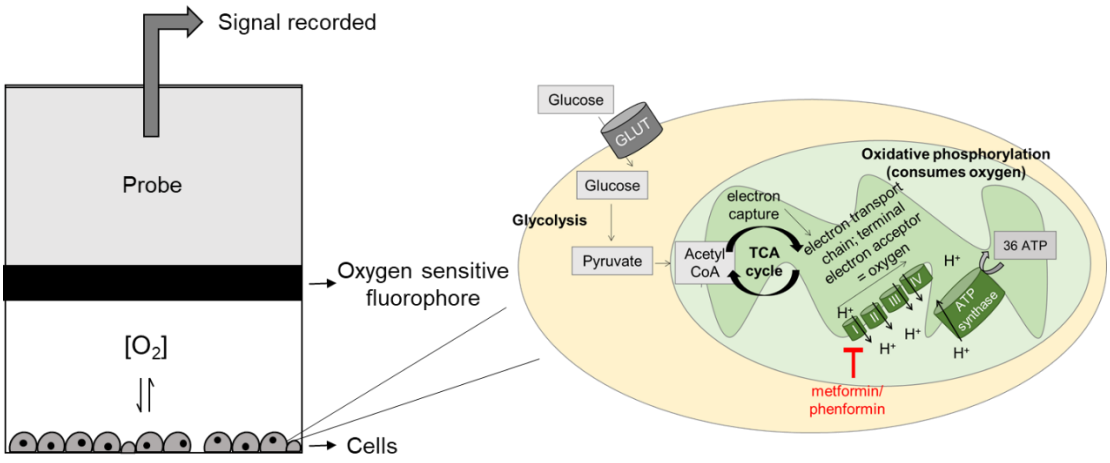

Figure 6.1: Schematic showing the use of the Seahorse XF96 analyser to measure changes in oxygen consumption (oxidative phosphorylation)

We aimed to investigate the effect of phenformin and metformin on the OCR and cell proliferation in isogenic cells with or without LKB1 and in a broad range of lung cancer cell lines (n = 11). Phenformin and metformin reduced the OCR in a dose dependent manner in LKB1 deficient and proficient A549 and A427 cells (Figure 6.2). However, LKB1 expression caused no marked difference on the ability of metformin or phenformin to reduce oxygen consumption. The effect of LKB1 expression on sensitivity to phenformin and metformin was also determined using a resazurin-based cell viability assay (Figure 6.3). LKB1 deficient A549 cells were more sensitive to phenformin and metformin with wild-type LKB1 expression having a modest, but statistically significant effect on increasing the IC_{50} value. Compared to LKB1 proficient cells, LKB1 deficient A427 cells were more sensitive to metformin but not phenformin, and in contrast, LKB1 deficient H1299 cells were modestly more sensitive to phenformin but not metformin. The sensitivity to phenformin or metformin in LKB1 deficient and proficient A549 and H1299 cells was further examined using spheroids. Although phenformin reduced the diameter of the LKB1 deficient A549 spheroids, there was no marked difference in spheroid size after treatment with metformin (Figure 6.4). LKB1 proficient H1299 spheroids appeared more sensitive to phenformin and metformin compared with the LKB1 deficient H1299 spheroids. Together, these data suggest that LKB1 expression was associated with a small and inconsistent effect on determining sensitivity to complex I inhibitors, suggesting that other factors are important for determining sensitivity to these inhibitors.

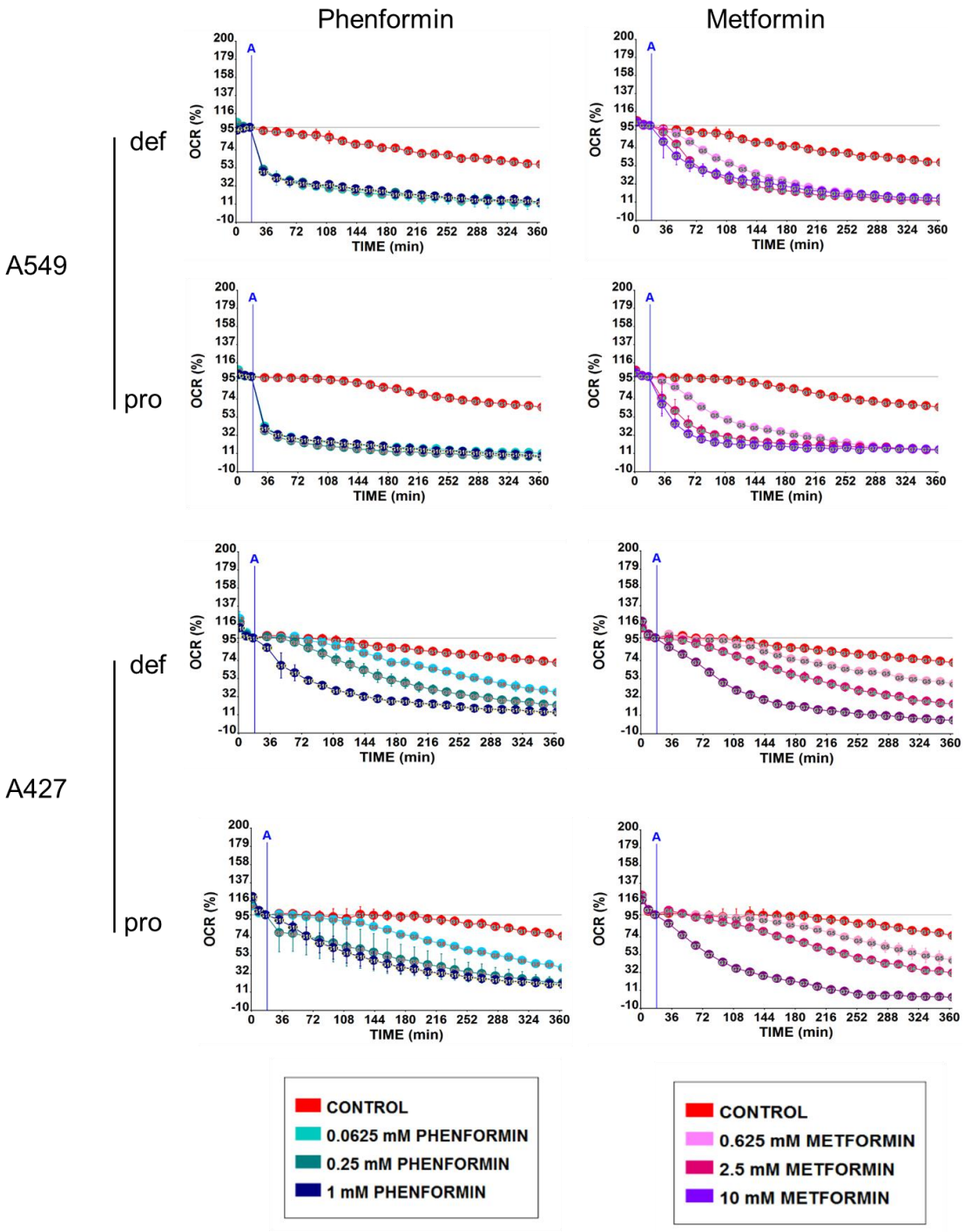

Figure 6.2: The effect of phenformin and metformin on the oxygen consumption rate in LKB1 deficient and proficient cells in 2D culture

Change in oxygen consumption rate (OCR) measured over 6 h post injection with increasing concentrations of phenformin or metformin added at "A". Data points represent the mean of duplicate values. Error bars represent standard deviation.

(a)

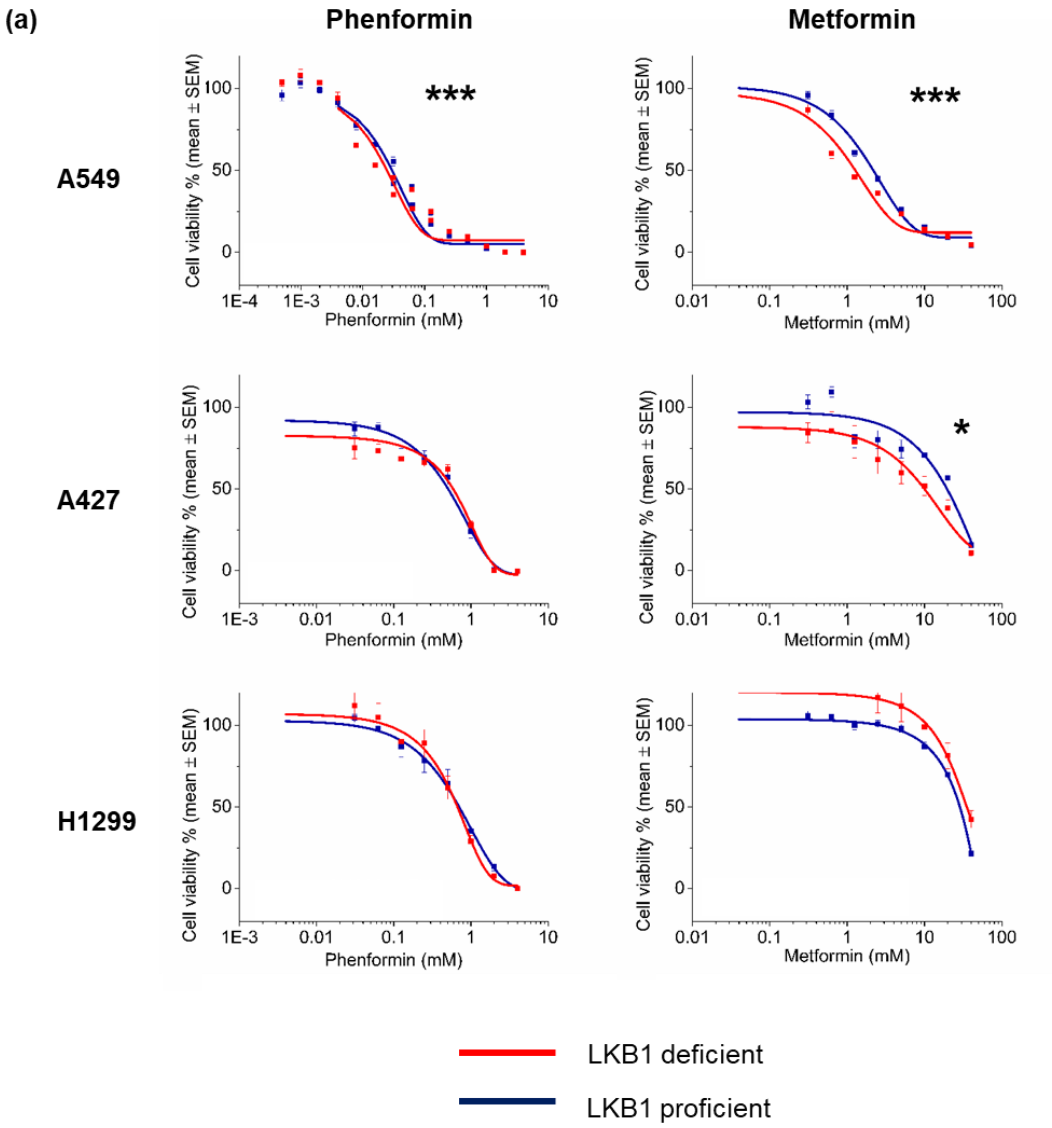

(b)

Cell line	IC_{50} ± SEM	
	Phenformin (mM)	**Metformin (mM)**
A549+EV	0.02 ± 0.0006	1.11 ± 0.08
A549+LKB	0.03 ± 0.0016	1.92 ± 0.10
A427+EV	0.75 ± 0.06	10.31 ± 1.95
A427+LKB	0.58 ± 0.08	17.64 ± 2.80
H1299+shLKB	0.58 ± 0.05	28.20 ± 6
H1299+shEV	0.69 ± 0.14	25.03 ± 1.07

Figure 6.3: The effect of LKB1 expression on the dose dependent sensitivity to phenformin and metformin in LKB1 deficient and proficient cells in 2D culture
Cells were treated for 72 h. Cell viability was determined using resazurin. The dose response curves (a) and IC_{50} values (b) represent the mean of triplicate values from 3 independent experiments. The stars represent the p-value for the difference in IC_{50} values between the LKB1 deficient and proficient cells. * < 0.05, *** < 0.001.

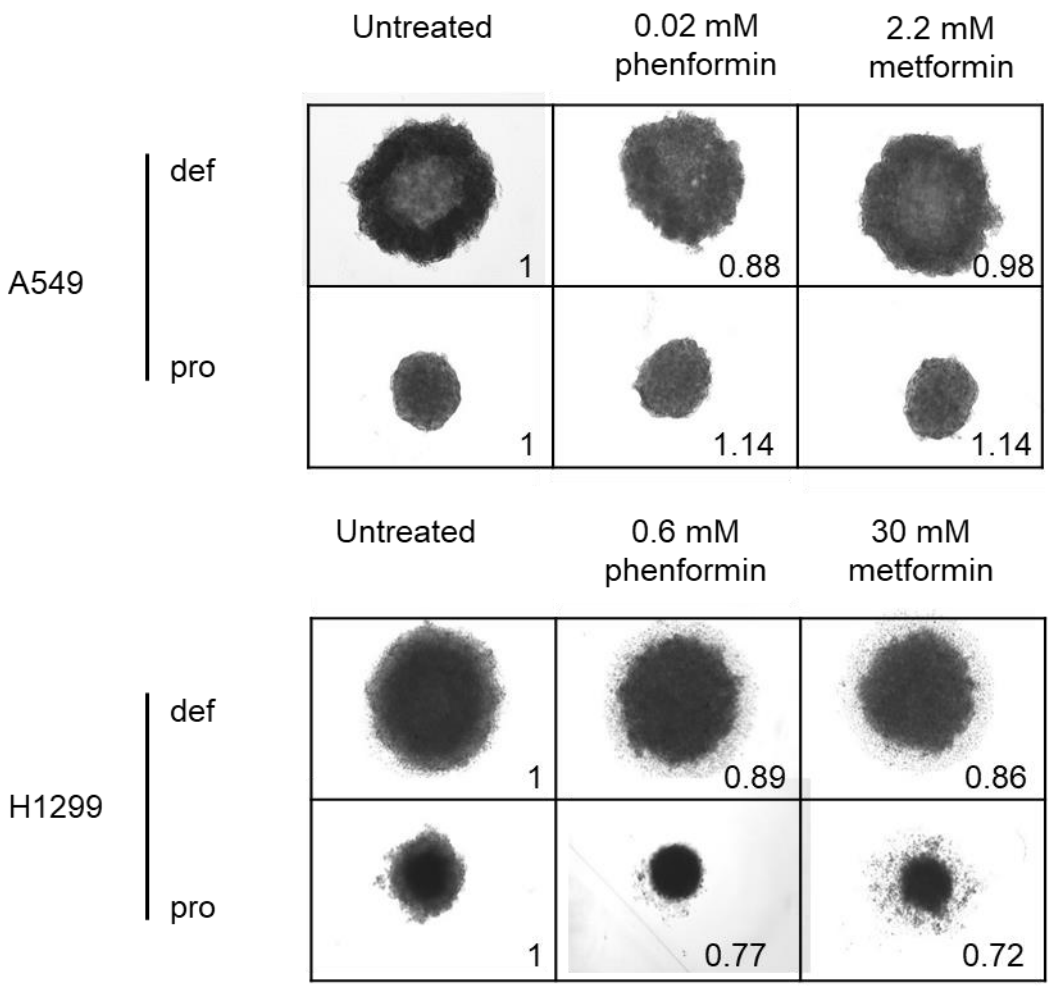

Figure 6.4: The effect of phenformin and metformin on spheroid growth in LKB1 deficient and proficient cells

Spheroids were treated from day 1 post seeding with a concentration similar to the IC_{50} values for the deficient cells. Images were acquired at 40x magnification using the Nikon TE2000 E, at 7 days post treatment. No.s represent the spheroid diameter of the treated normalised to the spheroid diameter of the untreated for each cell line. Spheroid diameter was measured using PowerPoint (line tool) as this experiment was completed before the GELCOUNT or CeligoS were available in our laboratory.

To identify other factors which may be important in determining sensitivity to complex I inhibitors, the effect of phenformin and metformin on oxygen consumption and cell proliferation were determined in 11 lung cancer cell lines and NBE1 (an immortalised normal bronchial epithelial) cell line. To compare the effect of phenformin and metformin on the oxygen consumption rate between the cell lines, we determined the time taken to reduce the OCR by 50% of baseline OCR (T_{50}) (i.e. effective dose) (Figure 6.5). There were a broad range of T_{50} values for phenformin (4.65 - 16.38 min) and metformin (15.40 - 60.13 min) in the 12 cell lines, with the LKB1 wild-type cell lines falling within the range (Figure 6.5). In the 12 cell lines, the effect of phenformin and metformin on cell proliferation was determined using resazurin. Figure 6.6 shows the increasing IC_{50} values (or decreasing sensitivities) for phenformin and metformin in the 12 cell lines. There were also a broad range of IC_{50} values for phenformin (0.01 - 1.39 mM) and metformin (1.22 - 34.37 mM) and the LKB1 wild-type cells fell within the range of IC_{50} values for the LKB1 mutated cells.

These data further suggest that LKB1 expression was not a major determinant of sensitivity to complex I inhibitors. The tables in Figure 6.6 show the mutational status for LKB1, KRAS, BRAF and TP53. The IC_{50} data was analysed using factorial ANOVA with LKB1, KRAS, BRAF and TP53 gene mutation status as factors (Section 2.8.3). This determines the relative contribution of each factor to the IC_{50}. In response to phenformin and metformin, LKB1 mutation status had a small effect in determining the IC_{50}, while TP53 mutation status had a large effect, with wild-type being more sensitive.

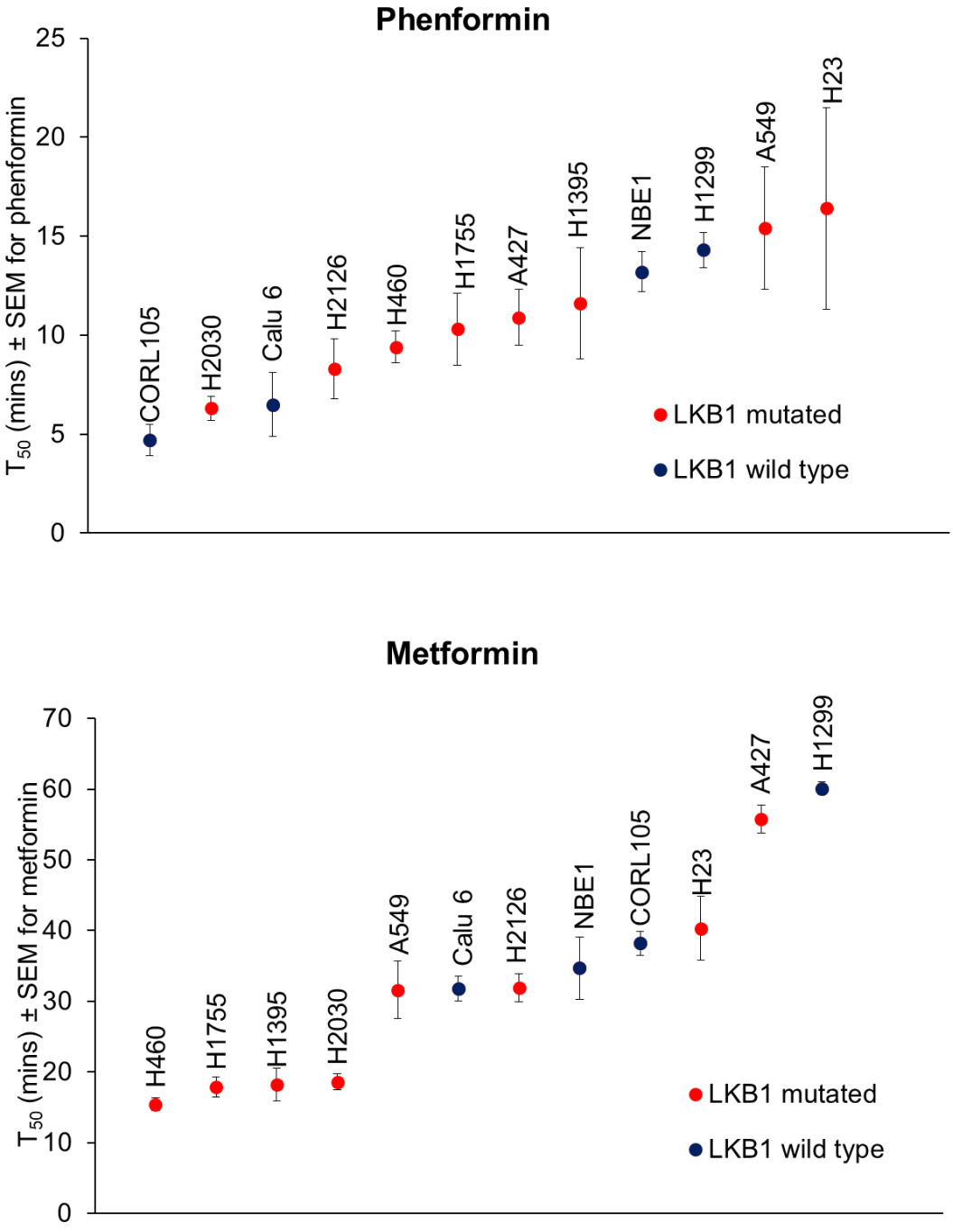

Figure 6.5: The effect of phenformin and metformin on oxygen consumption in 11 LKB1 mutated and wild-type lung cancer cell lines and NBE1

Time to reduce the OCR by 50% (T_{50}) of baseline after treatment with 2 mM phenformin and 20 mM metformin. Values represent the mean of 4 samples.

(a)

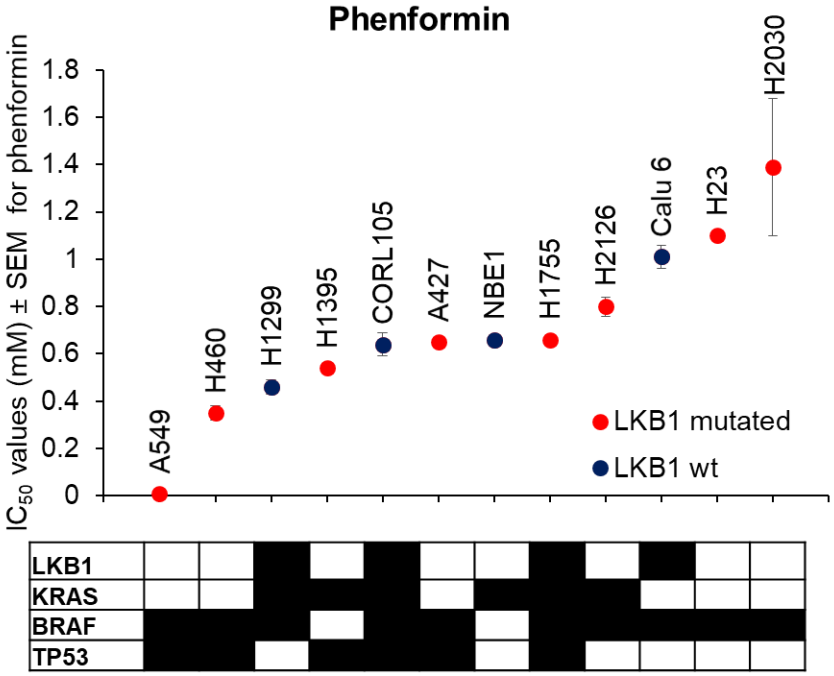
Phenformin
IC50 values (mM) ± SEM for phenformin
1.8
1.6
1.4
1.2
1
0.8
0.6
0.4
0.2
0
A549
H460
H1299
H1395
CORL105
A427
NBE1
H1755
H2126
Calu 6
H23
H2030
LKB1 mutated
LKB1 wt
LKB1
KRAS
BRAF
TP53

(b)

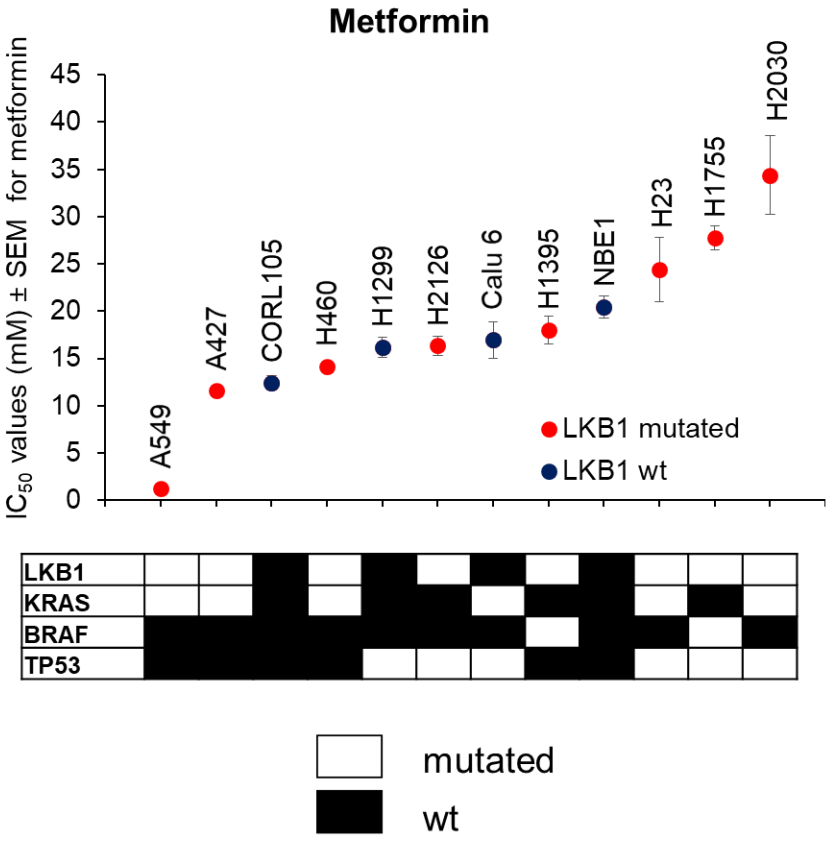
Metformin
IC50 values (mM) ± SEM for metformin
45
40
35
30
25
20
15
10
5
0
A549
A427
CORL105
H460
H1299
H2126
Calu 6
H1395
NBE1
H23
H1755
H2030
LKB1 mutated
LKB1 wt
LKB1
KRAS
BRAF
TP53
mutated
wt

(c)

Treatment	Mutation status			
	LKB1	KRAS	BRAF	TP53
Phenformin				
Partial eta squared (η^2)	0.039	0.104	0.047	0.268
Effect size	Small	Small	Small	Large
Observed power	0.519	0.923	0.603	1.000
Metformin				
Partial eta squared (η^2)	0.029	0.211	0.069	0.431
Effect size	Small	Medium	Small	Large
Observed power	0.405	0.999	0.772	1.000

Figure 6.6: The effect of LKB1, KRAS, BRAF and TP53 mutation status on determining sensitivity to phenformin and metformin
(a,b) Lung cancer cell lines ordered by decreasing sensitivity to phenformin (a) and metformin (b). Cells were treated with 0-4 mM phenformin and 0-40 mM metformin for 72 h. Cell viability was determined using resazurin. Data points represent the mean of triplicates from 3 independent experiments. LKB1, KRAS, BRAF and TP53 status is shown below. (c) Analysis of IC_{50} values using factorial ANOVA with LKB1, KRAS, BRAF and TP53 mutation status as factors (see Section 2.8.3). The darker the green fill indicates a larger effect size.

6.2.2 Summary of the effect of LKB1 expression on sensitivity to complex I inhibitors

Together, these data suggest that there are multiple determinants of sensitivity to complex I inhibitors and although LKB1 contributes to a minor extent, TP53 status may play a bigger role or it may be the combination of LKB1, TP53 and other mutations that contribute towards the sensitivity. We aimed to determine the effect of TP53 expression alone on sensitivity to phenformin and metformin. However, in our laboratory, we have been unsuccessful in our attempts to generate isogenic TP53 cell lines using lung cancer cells (including A549, H1299, H23 and CORL105).

Shackelford et al reported that LKB1 mutated cells are more sensitive to phenformin at 6 weeks post tumour initiation in a GEMM. Phenformin reduced tumour burden in *Kras*^{G12D}, *Kras*^{G12D}/*p53*$^{L/L}$ and *Kras*^{G12D}/*Lkb1*$^{L/L}$ driven lung cancer models and the reduction was statistically significant in the *Kras*^{G12D}/*Lkb1*$^{L/L}$ driven model. Shackelford et al showed that phenformin treatment increased the overall survival of mice with *Kras*^{G12D}/*Lkb1*$^{L/L}$ tumours

to a greater extent than those with *Kras*^{G12D}/*p53*$^{L/L}$ tumours. However, the *Lkb1* mutated model also had a *Kras* mutation and was *p53* wild-type, and the contribution of *p53* to the difference in sensitivity was not determined. Furthermore, at 6 weeks post treatment, tumour volume increased in both models suggesting the emergence of resistance (Shackelford et al., 2013).

6.3 LKB1 loss is associated with a metabolic shift

6.3.1 Transcriptomic data for metabolic genes

As it is reported that LKB1 plays an important role in metabolism (Section 1.3.2), we further analysed the transcriptomic data that we discussed in Section 4.4. In cells, glucose is taken up by the GLUT transporters to the cell cytoplasm (Figure 6.7). Within the cytoplasm, glucose is broken down to pyruvate, resulting in the production of two ATP molecules (glycolysis). The most efficient way for the cell to produce ATP is to convert pyruvate to acetyl CoA, an intermediate of the citric acid (TCA) cycle. TCA cycle produces electrons that are captured by NADH and $FADH_2$. In oxidative phosphorylation, these electrons are passed along the electron transport chain to oxygen, which is coupled to the transfer of protons thus, providing energy for ATP synthase to make 36 molecules of ATP (Nelson et al., 2008) (Figure 6.1, 6.7).

It was reported that compared to normal cells, cancer cell metabolism can be different, resulting in an increase in aerobic glycolysis (the "Warburg effect" (Warburg, 1956)) and glutaminolysis (Dang, 2010). In aerobic glycolysis, even in the presence of oxygen, cells have decreased oxidative phosphorylation (oxygen dependent) and increased glycolysis (oxygen independent). This leads to cells utilising pyruvate to make lactate which is exported via a monocarboxylate transporter (MCT) resulting in extracellular acidification. It was suggested that a possible reason for this was a mitochondrial defect in cancer cells.

However, now it has been proposed that cancer cells utilise aerobic glycolysis to stimulate extracellular acidification, which can be an advantage for cancer cells. For example, extracellular acidification can assist with immune evasion by inhibiting the function of cytotoxic T cells (Choi et al., 2013). Cancer cells can overcome intracellular acidification by upregulating carbonic anhydrase (CA) enzymes, which catalyse the forward and reverse reactions between protons and bicarbonate to water and carbon dioxide (Lindskog, 1997). A possible driver of aerobic glycolysis is PDK (pyruvate dehydrogenase kinase 4) as PDK inhibits pyruvate dehydrogenase (PDH), which catalyses the formation of acetyl CoA from pyruvate (Patel and Korotchkina, 2006) (Figure 6.7).

Glutaminolysis utilises glutamine as a carbon or nitrogen source (Dang, 2010). Glutamine can be broken down into glutamate, which is further broken down into α-ketoglutarate, an intermediate of TCA cycle. Therefore, glutamine can maintain activity of TCA cycle (anaplerosis) during aerobic glycolysis. However, the breakdown of glutamine produces ammonia which must be removed from the cell. Carbamoyl phosphate synthetase 1 (CPS1) is the first rate limiting enzyme of the urea cycle and catalyses the formation of carbamoyl phosphate from ammonia and bicarbonate (Morris Jr, 1992) (Figure 6.7).

Interestingly, the LKB1 dependent differences in gene expression had similarities in 2D and 3D models but the majority of these differences were not observed in human tumours when both LKB1 mutant vs non-mutant and high vs low LKB1 mRNA expression groups were compared (Figure 6.8). As mentioned, the 2D and 3D systems are cleaner systems with LKB1 expression contributing to the only differences between groups. Notably, in LKB1 deficient spheroids, genes involved in aerobic glycolysis, carbonic anhydrase and CPS1 were expressed at higher levels compared with LKB1 proficient spheroids. Importantly, CPS1 was upregulated in LKB1 deficient cells in all three models (2D, spheroids and human

tumours) suggesting this difference is intrinsic to LKB1 loss and independent of the system (Figure 6.7-6.8).

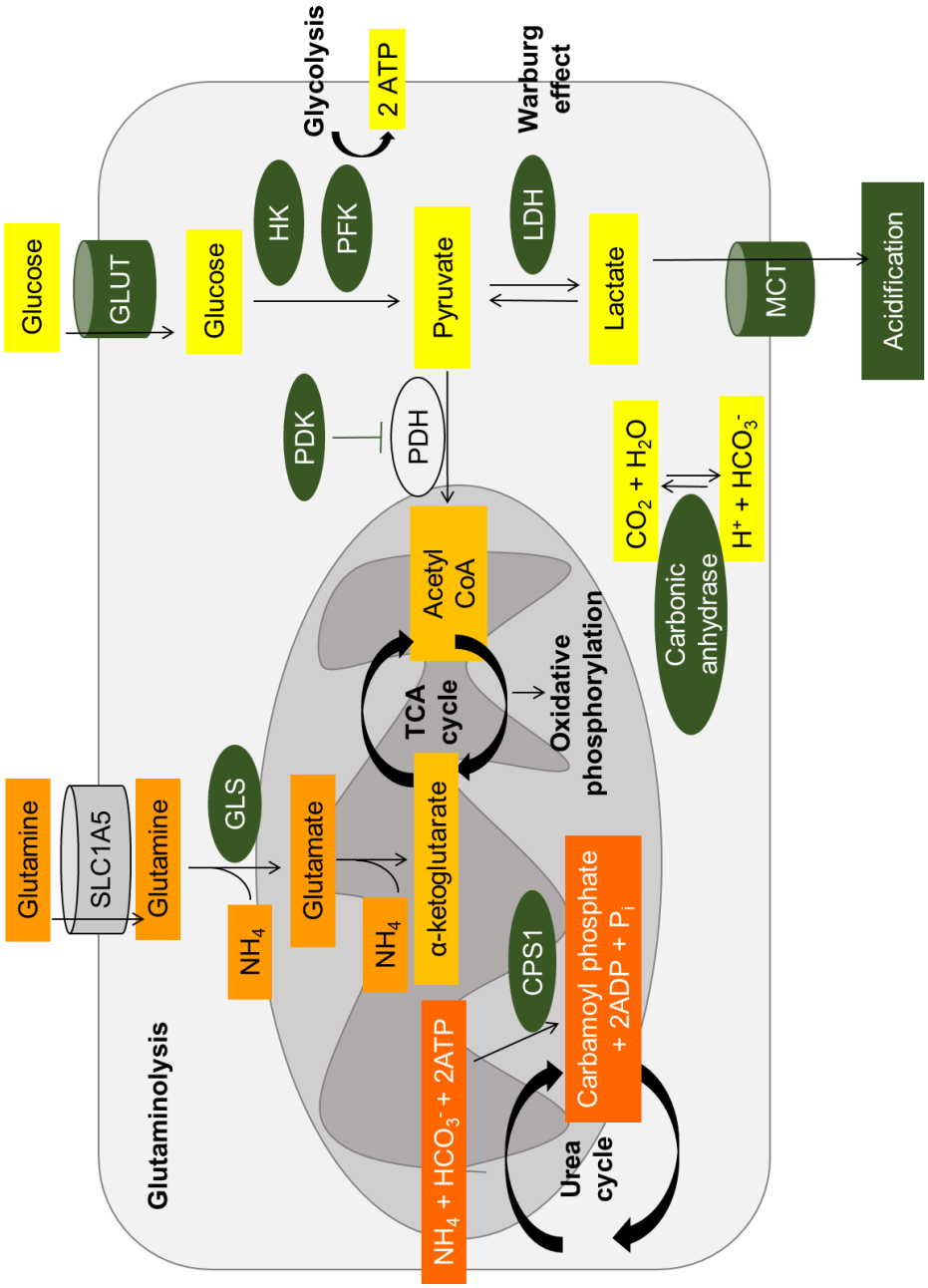

Figure 6.7: Schematic showing that LKB1 loss is associated with a metabolic shift to aerobic glycolysis

Image shows a mitochondrion (grey) within the cell cytoplasm (white). Key pathways are aerobic glycolysis (yellow), TCA cycle (dark yellow), glutaminolysis (orange) and the urea cycle (dark orange). Proteins marked green represent those that are upregulated in LKB1 deficient spheroids using our RNASeq data (Figure 6.8).

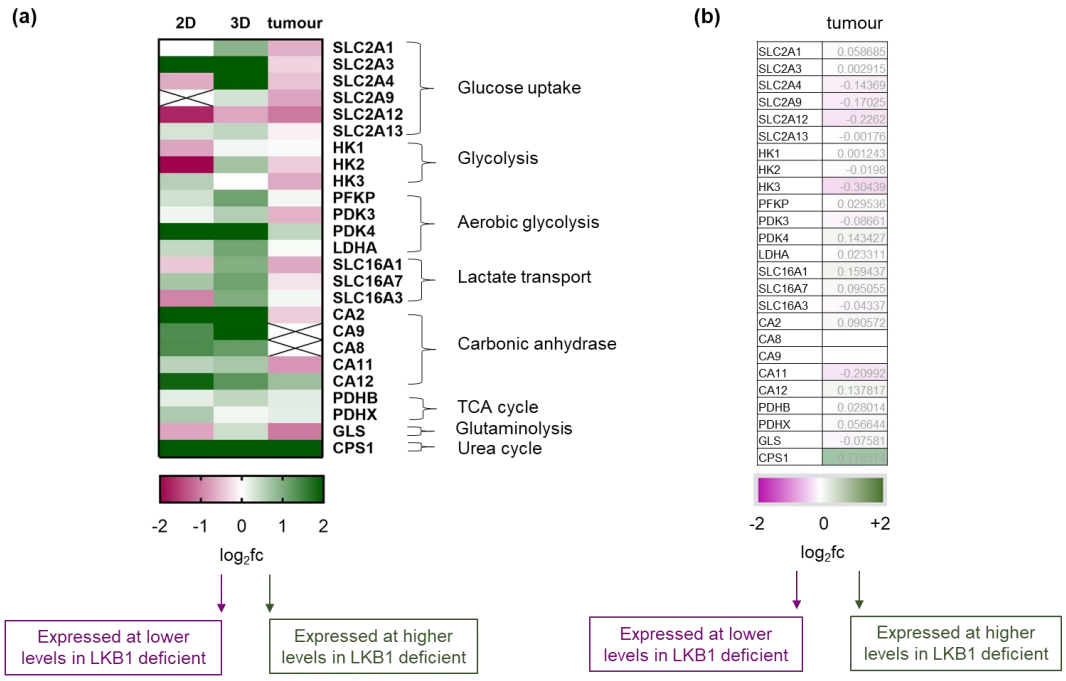

Figure 6.8: Heatmap showing the difference in mRNA expression levels between LKB1 deficient and proficient cells for the genes involved in glycolysis, carbonic anhydrase signalling, TCA cycle, glutaminolysis and the urea cycle
(a) Genes listed above are those significantly different between LKB1 deficient and proficient cells in either 2D or 3D using our RNASeq data, or significantly different between LKB1 mutant vs non-mutant human tumour samples , (TCGA, 2014). Cross implies the FPKM = 0 (i.e. expression was below detectable levels) in the LKB1 deficient and/or proficient sample(s). (b) Differences in mRNA levels between human tumour samples with downregulated/altered LKB1 mRNA levels and unaltered LKB1 mRNA levels (analysis was completed using cBioportal with mRNA expression Z score threshold = ±2. n=227 as opposed to 230 (previously used) to exclude those samples with upregulated LKB1 mRNA levels in the altered group) (TCGA, 2014).

6.3.2 Confirmation of the mRNA differences using western blotting and IHC

For certain genes, the differences in the mRNA expression were confirmed by western blotting and IHC (Figure 6.9-6.10). Figure 6.9 shows that CPS1 expression was higher in LKB1 deficient A549 cells in 2D and 3D culture, compared with LKB1 proficient cells. CPS1 was also higher in LKB1 deficient A427 cells compared with LKB1 proficient cells in 2D culture, but there was no difference in CPS1 expression between LKB1 deficient and proficient H1299 cells. Therefore, this suggests that CPS1 was intrinsic to LKB1 loss in cells that were naturally LKB1 mutated.

PDK4 expression was below the detectable level in A549 cells in 2D culture, however, in 3D spheroids, western blotting suggests that PDK4 was increased in LKB1 deficient spheroids (Figure 6.9). PDK4 was upregulated in LKB1 deficient A427 cells compared with LKB1 proficient A427 cells in 2D culture, suggesting that level of upregulation of PDK4 protein expression may be cell line dependent. In H1299 cells, PDK4 expression was more difficult to determine as there were 2 bands that were slightly higher and lower than the expected size. We confirmed the position of the PDK4 band using a recombinant protein and noted that band is positioned where it can be seen in LKB1 deficient A427 cells.

CA9 was upregulated in LKB1 deficient A549 cells but in a context dependent manner (i.e. only in spheroids and not in 2D). However, CA9 was upregulated in LKB1 deficient H1299 cells in 2D and 3D models. There appears to be no difference in CA9 expression between LKB1 deficient and proficient A427 cells in 2D culture.

These data suggest that high CPS1 levels are intrinsic to LKB1 loss in cells naturally LKB1 mutated but PDK4 and CA9 are cell line and/or context dependent. IHC images show GLUT1, CA9 and MCT1 staining in LKB1 deficient and proficient A549 spheroids (Figure 6.10). For GLUT1, CA9 and MCT1; strong (3+) staining was greater in LKB1 deficient spheroids and for CA9, the difference in staining was statistically significant (p-value < 0.05) (Figure 6.10). This indicates that LKB1 deficient spheroids upregulated expression of proteins involved in aerobic glycolysis.

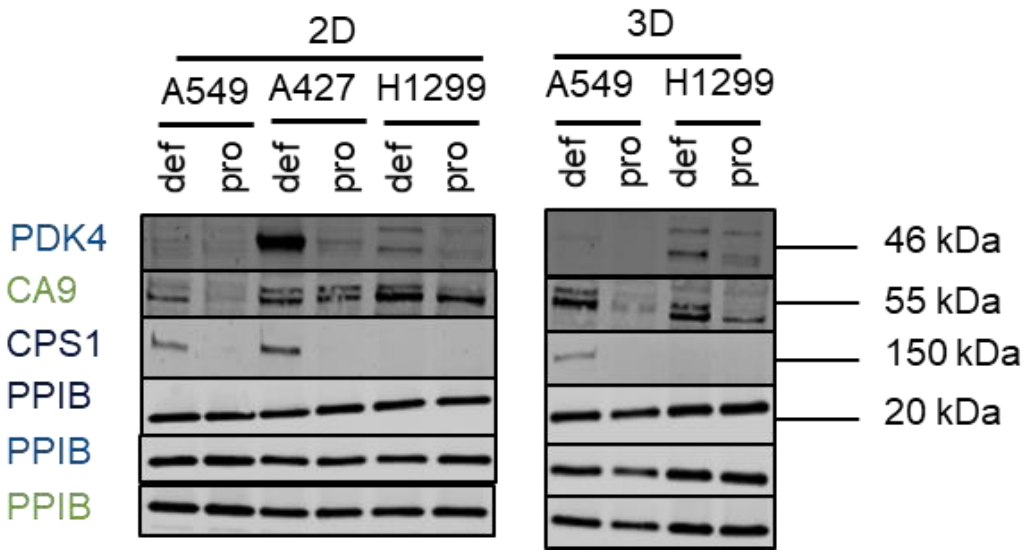

Figure 6.9: Confirmation of PDK4, CA9 and CPS1 mRNA expression differences by western blotting in LKB1 deficient and proficient cells in 2D and 3D culture
Representative western blotting images. Cells in 2D were seeded until sub-confluency and spheroids were grown for 5 days. 20 µg of protein was loaded per well.

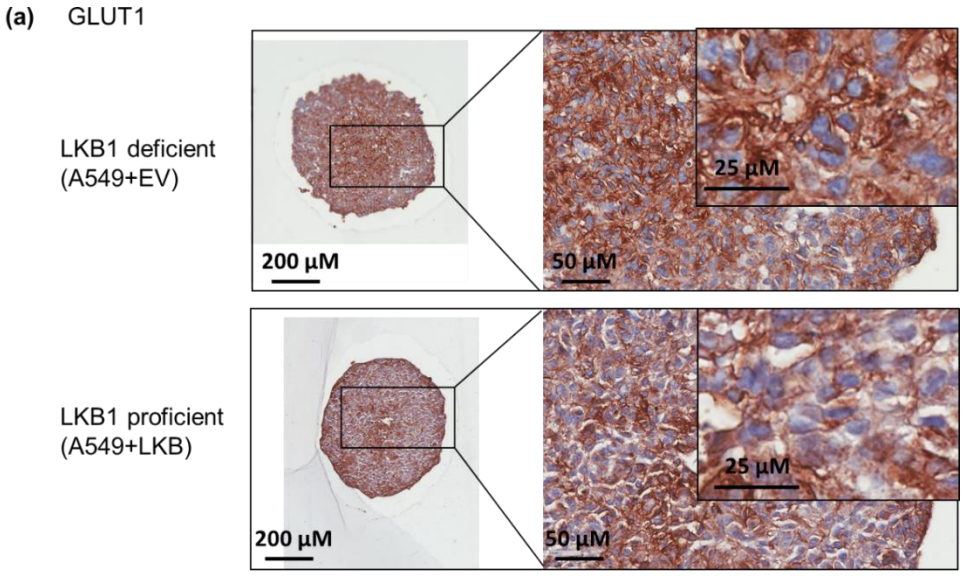

	GLUT1 (mean ± SEM)			
	3+ % cells	2+ % cells	1+ % cells	0+ % cells
LKB1 def	13.45 ± 2.72	62.40 ± 1.60	22.78 ± 2.09	1.38 ± 1.03
LKB1 pro	8.55 ± 2.44	54.52 ± 4.10	36.71 ± 4.26	0.22 ± 0.13

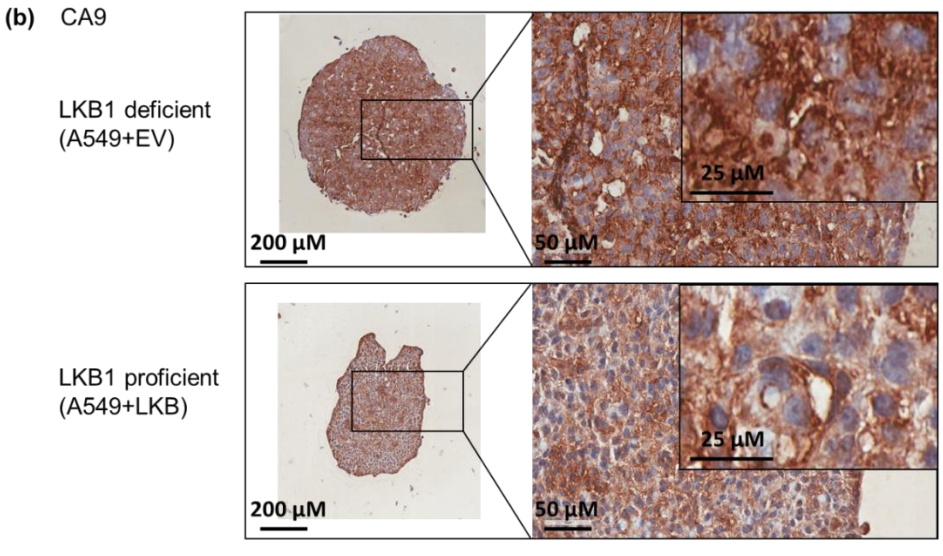

	CA9 (mean ± SEM)			
	3+ % cells	2+ % cells	1+ % cells	0+ % cells
LKB1 def	48.19 ± 2.94	29.67 ± 2.69	22.12 ± 0.64	0.03 ± 0.00
LKB1 pro	9.85 ± 0.99	56.40 ± 3.25	33.72 ± 2.60	0.03 ± 0.02

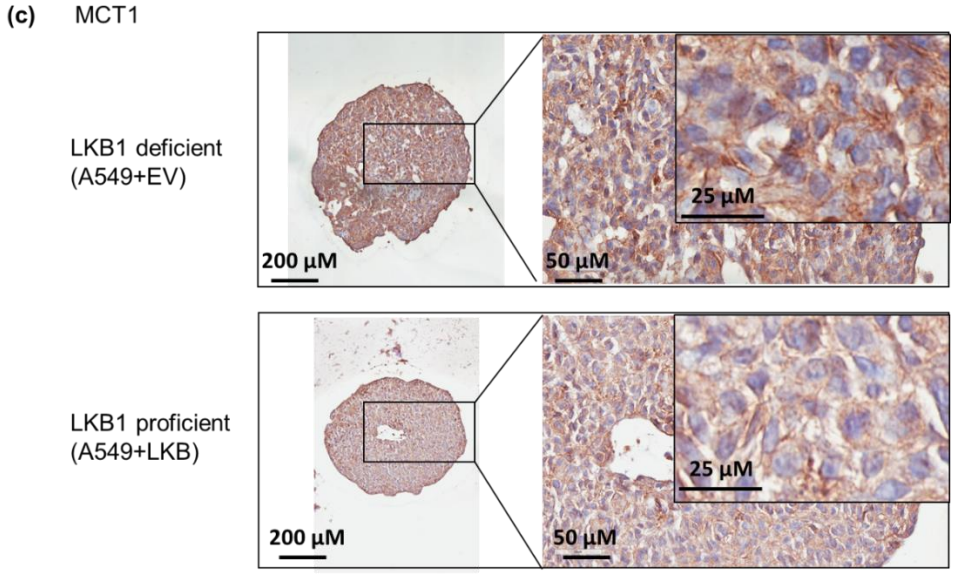

	MCT1 (mean ± SEM)			
	3+ % cells	2+ % cells	1+ % cells	0+ % cells
LKB1 def	0.56 ± 0.08	53.67 ± 12.36	40.20 ± 7.30	5.58 ± 5.07
LKB1 pro	0.23 ± 0.23	22.56 ± 7.51	65.00 ± 4.03	12.20 ± 3.95

Figure 6.10: IHC analysis of GLUT1, CA9 and MCT1 protein expression in LKB1 deficient and proficient spheroids

Spheroid sections were stained with haematoxylin (blue) and GLUT1, CA9 or MCT1 (brown). Images were analysed to calculate the intensity of brown membrane staining using Aperio membrane v9 algorithm. Values represent the mean of 4 spheroids. Unlike GLUT1 or MCT1 which were not significant (p-value < 0.05), the difference between 3+ CA9 membrane staining between the LKB1 deficient and proficient spheroids was significant (mean 3+ CA9; LKB1 deficient = 48.2, LKB1 proficient = 9.9, p-value < 0.001).

6.3.3 Summary of the differences in metabolic signalling between LKB1 deficient and proficient cells

LKB1 deficient A549 spheroids had higher expression of proteins (PDK4, GLUT1, MCT1, and CA9) that play a role in aerobic glycolysis suggesting that LKB1 deficient A549 cells had an increased dependency on aerobic glycolysis in a more stressed environment. However, in 2D culture, higher PDK4 expression was evident in LKB1 deficient A427 cells and higher CA9 expression was evident in LKB1 deficient H1299 cells, suggesting that the increased dependency on aerobic glycolysis is both cell line and context dependent. LKB1 deficient A549 and A427 cells had higher CPS1 expression which was independent of the model. We hypothesised that the increase in CPS1 was due to an increased dependency on glutamine, as CPS1 plays a role in the removal of ammonia which is produced during glutamine utilisation. This will be investigated further in Section 6.4, where we examine the effect of inhibitors of aerobic glycolysis, glucose and glutamine deprivation on cell proliferation in LKB1 deficient and proficient lung cancer cells.

6.4 Exploitation of the altered metabolic phenotype in LKB1 deficient cells

6.4.1 Metabolic inhibitors

Figure 6.11 shows selected approaches to target metabolism. These include inhibition of; PDK by dichloroacetate, glycolysis by 2-DG, MCT1 by AZD3965 and oxidative phosphorylation by metformin or phenformin, or by using bromopyruvate; a pyruvate and lactic acid analogue. Other possible approaches to target metabolism in cell culture include glucose and glutamine deprivation.

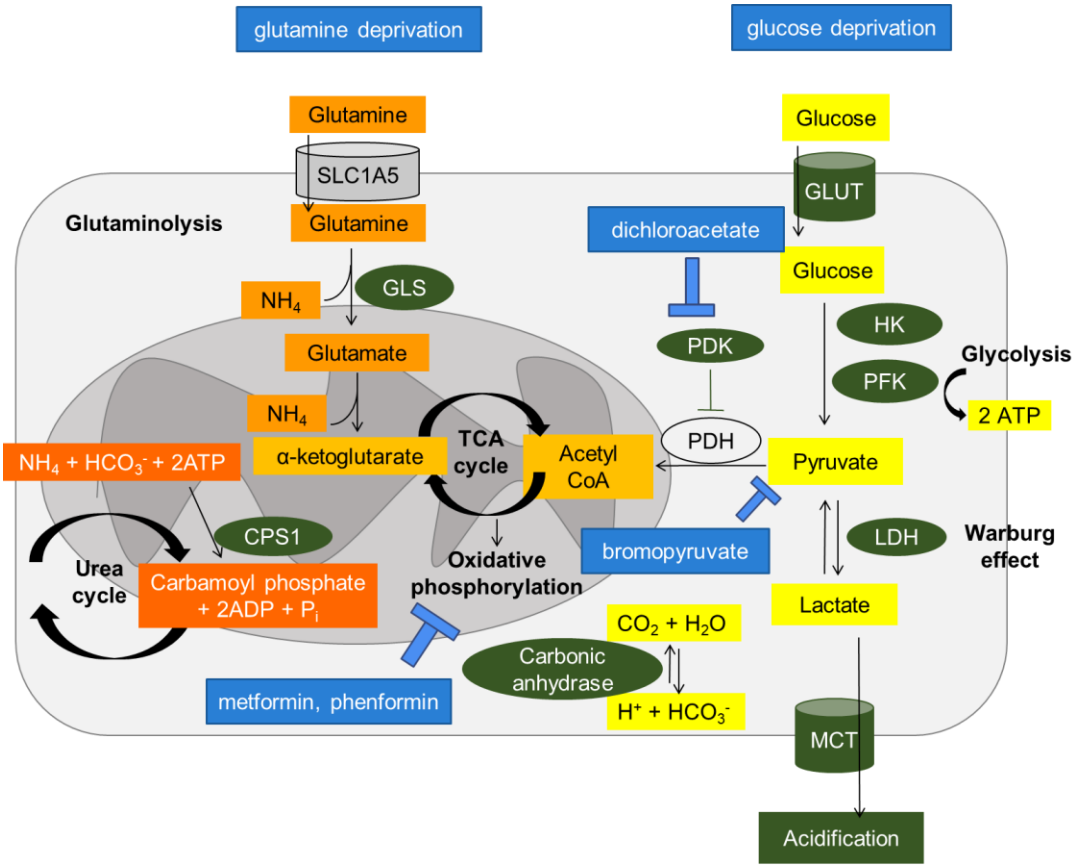

Figure 6.11: Schematic showing possible approaches to target metabolism
Image shows a mitochondria (grey) within the cell cytoplasm (white). Inhibitors of glycolysis, oxidative phosphorylation, PDK and MCT are highlighted in blue.

These approaches were investigated further (Figure 6.12-6.16). Dichloroacetate, AZD3965 and bromopyruvate caused no marked difference in cell proliferation between LKB1 deficient and proficient A549 cells (Figure 6.12). It was reported that bromopyruvate is taken up by cells through the MCT1 transporter, therefore MCT1 positive cells are more sensitive to bromopyruvate treatment (Birsoy et al., 2013). This was not observed in LKB1 deficient A549 cells in 2D culture. However, transcriptomic data showed that in 2D culture, LKB1 deficient cells only upregulated MCT2 (SLC16A7) and the increase in MCT1 (SLC16A1) expression was only observed in LKB1 deficient spheroids (Figure 6.8).

In 2D culture, LKB1 deficient A427 and H1299 cells, but not A549 cells, were more sensitive to 2-DG with LKB1 expression causing a statistically significant increase in the

IC_{50} value (Figure 6.13). The effect of 2-DG on cell proliferation was also determined in the 12 cell lines. Figure 6.14 shows the increasing IC_{50} values (or decreasing sensitivities) for 2-DG in the 12 cell lines. There were a broad range of IC_{50} values (1.86 - 15.18 mM) and although, the LKB1 wild-type cells fell within the range of IC_{50} values for the LKB1 mutated cells, it appeared that a large proportion of LKB1 mutated cells were more sensitive to 2-DG. However, on analysis of the IC_{50} data using factorial ANOVA with LKB1, KRAS, BRAF and TP53 gene mutation status as factors, we found that LKB1 mutation status caused no effect on the IC_{50} value for 2-DG, although, the power was small (0.08) (Figure 6.14).

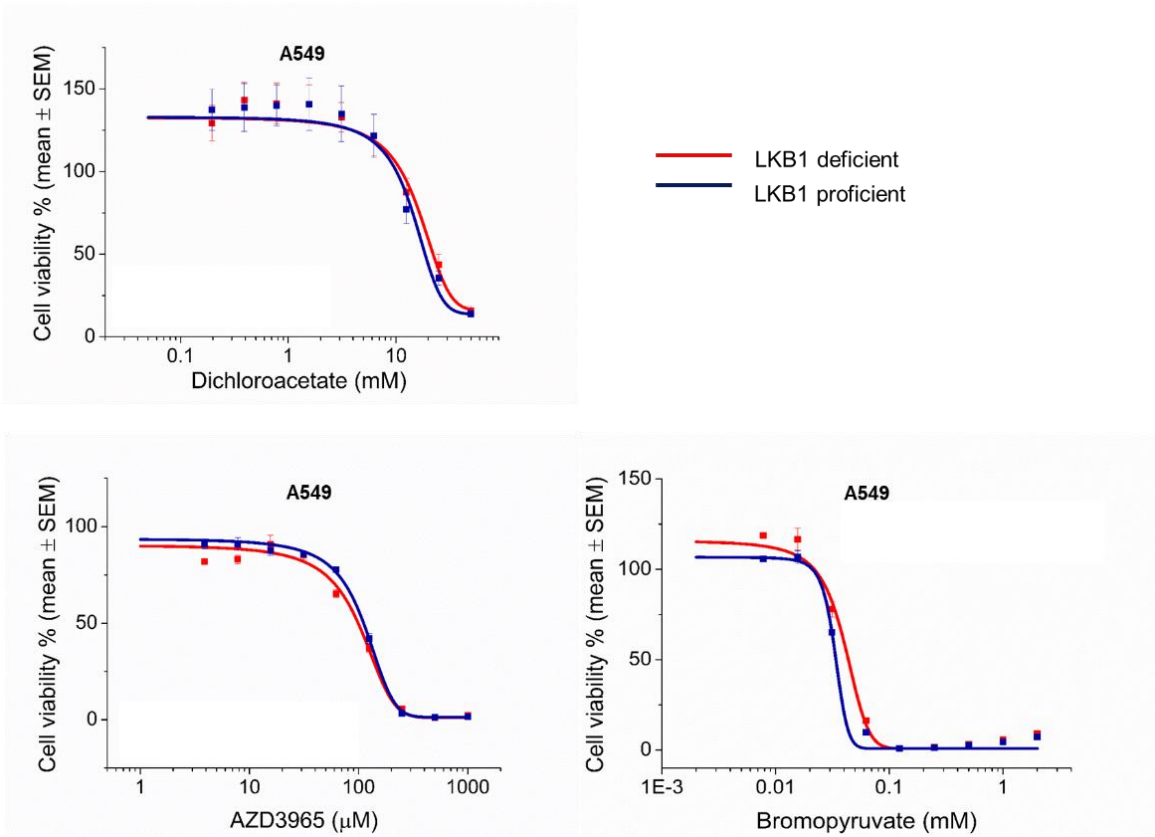

Figure 6.12: The effect of dichloroacetate, AZD3965 and bromopyruvate on cell proliferation in LKB1 deficient and proficient cells in 2D culture
Cells were treated for 72 h. Cell viability was determined using a resazurin assay. Data points represent the mean of triplicates from 2 independent experiments for dichloroacetate. Data points represent the mean of triplicates from a single experiment for AZD3965 and bromopyruvate.

(a)

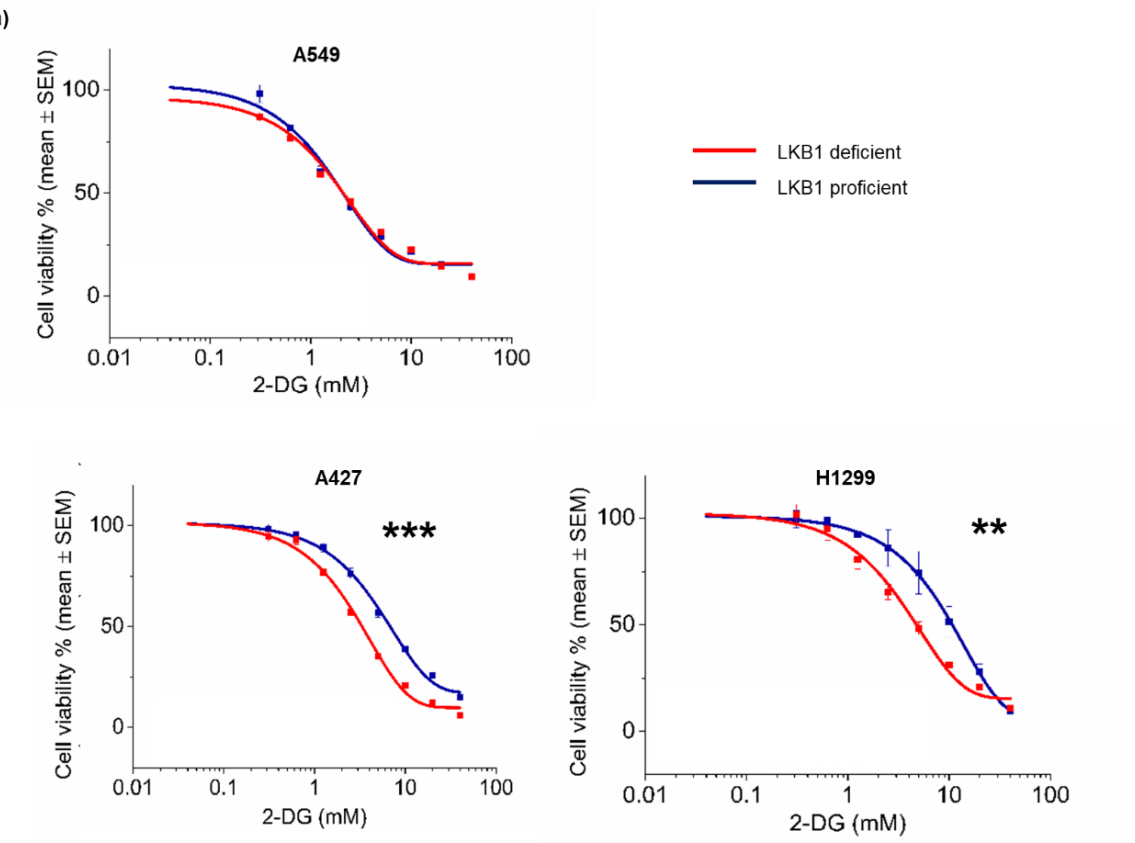

(b)

Cell line	IC_{50} ± SEM
	2-DG (mM)
A549+EV	1.99 ± 0.20
A549+LKB	2.21 ± 0.46
A427+EV	3.06 ± 0.45
A427+LKB	6.50 ± 0.36
H1299+shLKB	4.15 ± 0.39
H1299+shEV	9.77 ± 1.77

Figure 6.13: The effect of 2-DG on cell proliferation in LKB1 deficient and proficient cells in 2D culture

Cells were treated for 72 h. Cell viability was determined using a resazurin assay. Data points represent the mean of triplicates from 3 independent experiments. The stars represent the p-value for the differences in IC_{50} value between the LKB1 deficient and proficient cells. ** < 0.01, *** < 0.001.

(a)

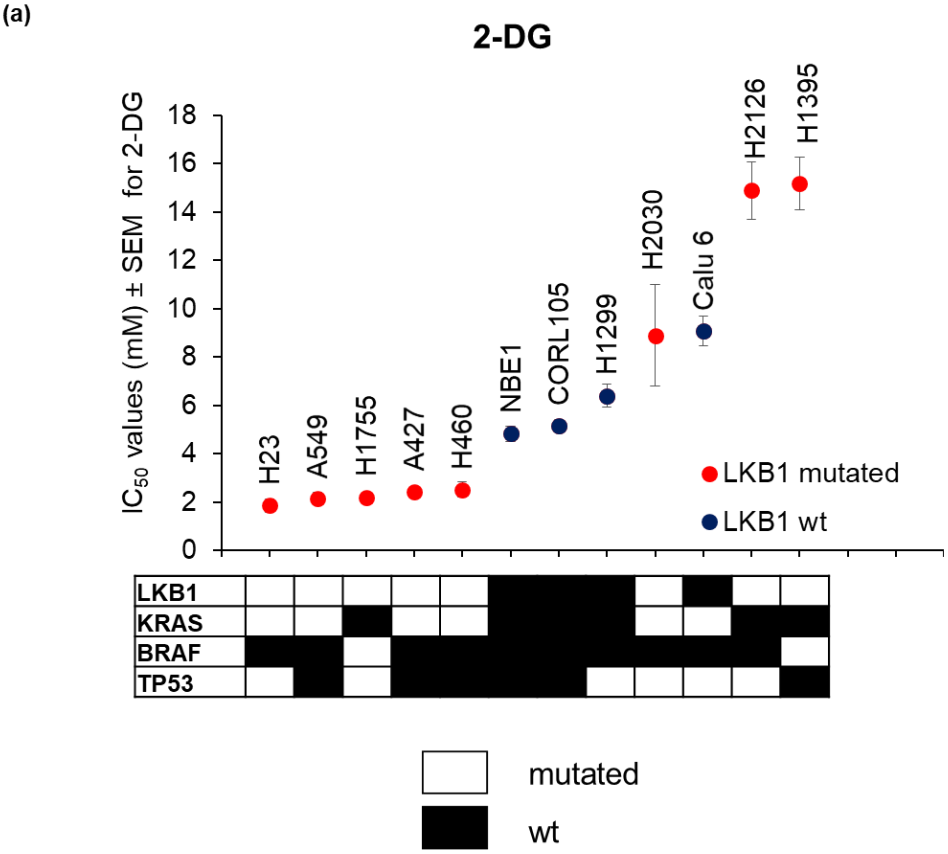

(b)

Treatment		Mutation status			
		LKB1	KRAS	BRAF	TP53
2-DG					
	Partial eta squared (η^2)	0.003	0.001	0.143	0.076
	Effect size	No difference	No difference	Medium	Small
	Observed power	0.080	0.063	0.982	0.813

Figure 6.14: The effect of LKB1, KRAS, BRAF and TP53 mutation status on determining sensitivity to 2-DG

(a) Lung cancer cell lines ordered by decreasing sensitivity to 2-DG. Cells were treated with 0-40 mM 2-DG for 72 h. Cell viability was determined using resazurin. Data points represent the mean of triplicates from 3 independent experiments. LKB1, KRAS, BRAF and TP53 status is shown. (b) Analysis of IC_{50} values using factorial ANOVA with LKB1, KRAS, BRAF and TP53 mutation status as factors (see Section 2.8.3). The darker the green fill indicates a larger effect size.

6.4.2 Glucose and glutamine deprivation

Interestingly, LKB1 deficient A549, A427 and H1299 cells were more sensitive to glucose deprivation, than LKB1 proficient cells (Figure 6.15). Moreover, LKB1 proficient A549, A427 and H1299 cells grew better in low glucose conditions, which may indicate that high glucose (20 mM) was toxic to these cells. ANOVA was used to determine the contribution of LKB1 expression on sensitivity to glucose withdrawal in each isogenic cell line. We found that LKB1 expression had a major role in determining the effect of glucose concentration on cell viability.

We also determined the effect of glutamine deprivation on cell proliferation in LKB1 deficient and proficient cells. For these experiments, glutaMAX^{TM}/glutamax was used as a substitute for glutamine as it is more stable in solution and had been used for all previous experiments. Similar to glucose deprivation in 2D culture, LKB1 deficient A549, A427 and H1299 cells appeared more sensitive to glutamine deprivation in 2D culture (Figure 6.16). LKB1 expression caused a large effect in determining response to glutamine deprivation in A549 cells but a medium effect in A427 and H1299 cells. However, the observed power was ~ 0.5 in A427 and H1299 cells.

(a)

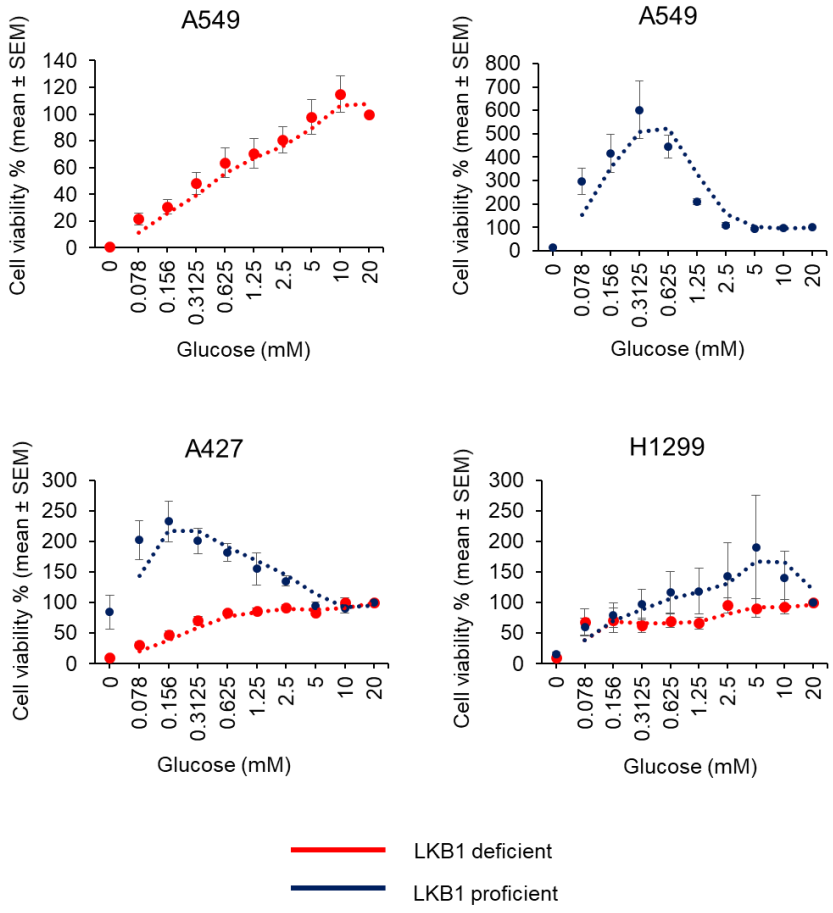

(b)

Deficient vs proficient (glucose deprivation)		
A549	Partial eta squared (η^2)	0.423
	Effect size	Large
	Observed power	1.000
A427	Partial eta squared (η^2)	0.700
	Effect size	Large
	Observed power	1.000
H1299	Partial eta squared (η^2)	0.264
	Effect size	Large
	Observed power	0.722

Figure 6.15: The effect of glucose deprivation on cell proliferation in LKB1 deficient cells grown in 2D culture

Equal cell numbers (1x10^3) were seeded with increasing concentrations of glucose in glucose free DMEM (supplemented with 5% dialysed FBS, 2 mM glutamax and 1 mM pyruvate – see Section 2.3) and incubated for 7 days. Cell viability was determined using resazurin. Resorufin fluorescence was normalised to that for 20 mM glucose. Graphs were produced using Microsoft Excel and moving average trend line was plotted. Data points represent the mean of triplicates from 3 independent experiments for A549 and triplicates from 2 independent experiments for A427 and H1299. (b) Analysis of cell viability values using factorial ANOVA with cell lines (deficient vs proficient) as factors (see Section 2.8.3). The darker the green fill indicates a larger effect size.

(a)

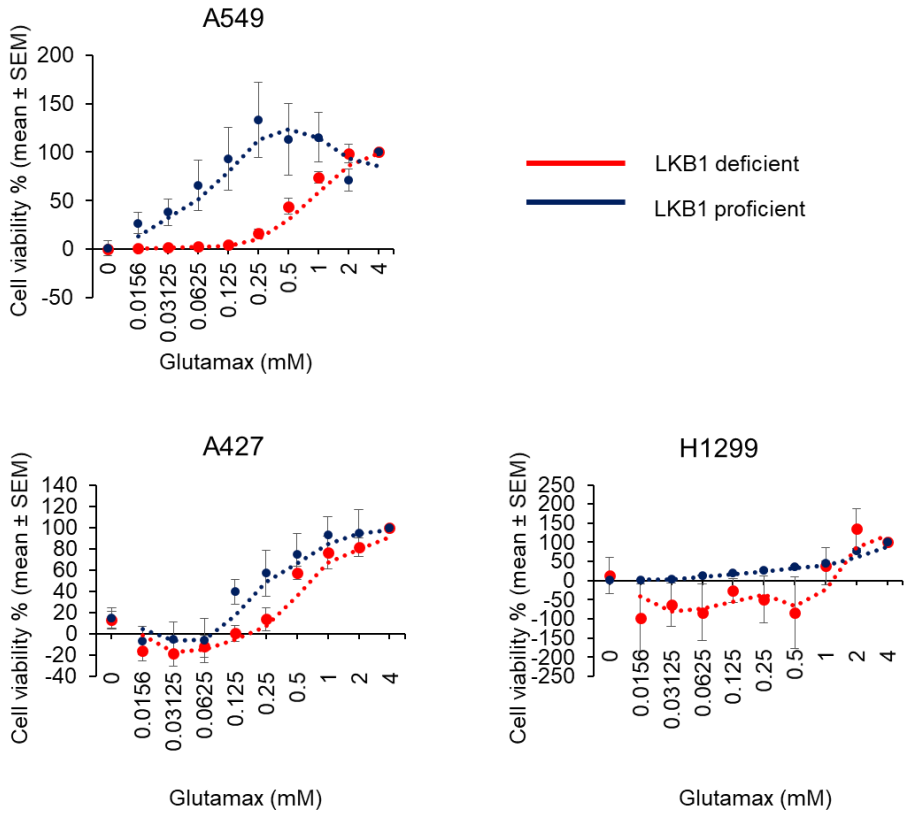

(b)

Deficient vs proficient (glutamax deprivation)		
A549	Partial eta squared (η^2)	0.261
	Effect size	Large
	Observed power	0.956
A427	Partial eta squared (η^2)	0.183
	Effect size	Medium
	Observed power	0.523
H1299	Partial eta squared (η^2)	0.141
	Effect size	Medium
	Observed power	0.407

Figure 6.16: The effect of glutamine deprivation on cell proliferation in LKB1 deficient cells grown in 2D culture

Equal cell numbers ($1x10^3$) were seeded with increasing concentrations of glutamax in DMEM (supplemented with 5% dialysed FBS, 17.5 mM glucose and 1 mM pyruvate – see Section 2.3) and incubated for 7 days. Cell viability was determined using resazurin. Resorufin fluorescence was normalised to that for 4 mM glutamax. Graphs were produced using Microsoft Excel and moving average trend line was plotted. Data points represent the mean of triplicates from 3 independent experiments for A549 and triplicates from 2 independent experiments for A427 and H1299. (b) Analysis of cell viability values using factorial ANOVA with cell lines (deficient vs proficient) as factors (see Section 2.8.3). The darker the green fill indicates a larger effect size.

Western blotting was used to investigate differences in downstream signalling between LKB1 deficient and proficient A549 cells grown in 2D culture after glucose and glutamine deprivation (Figure 6.17). Phospho-AMPK was downregulated in both LKB1 deficient and proficient cells after glucose and glutamine deprivation and pACC was downregulated in both LKB1 deficient and proficient cells after glutamine deprivation. This suggests that LKB1 plays only a limited role in the activation of AMPK. In response to glucose deprivation, both LKB1 deficient and proficient cells upregulated GLUT1, γH2AX and cleaved PARP, suggesting that both cell types responded similarly. COX2 band (normally upregulated in LKB1 deficient cells), was seen at a lower molecular weight upon glucose withdrawal. As it was reported that COX2 is activated by glycosylation (Cao et al., 2015), a possible explanation for our result may be that COX2 was not glycosylated and therefore observed at a lower molecular weight. Western blotting further confirmed that LKB1 deficient A549 cells were more sensitive to glutamine deprivation in 2D culture as they upregulated γH2AX and cleaved PARP which are markers of apoptosis. Moreover, COX2 expression was reduced after glutamine deprivation. There was no change in CA9 expression without glucose or glutamine.

We hypothesised that increased glutaminolysis resulted in increased ammonia production which explained the need for CPS1 in LKB1 deficient cells. However, western blotting analysis showed that CPS1 expression did not decrease after glutamine deprivation, instead CSP1 expression increased after both glucose and glutamine deprivation. The functional significance of CPS1 is not fully understood, however, while this work was in progress, Çeliktaş et al reported an LKB1 dependent difference in CPS1 expression. Similar to our data, they found that restoration of LKB1 in LKB1 deficient lung cancer cells reduced CPS1 expression, however, knock-down of LKB1 in LKB1 wild-type lung cancer cells was not

sufficient to increase CPS1 expression. They concluded that LKB1, in conjunction with other proteins negatively regulates CPS1 (Çeliktaş et al., 2017).

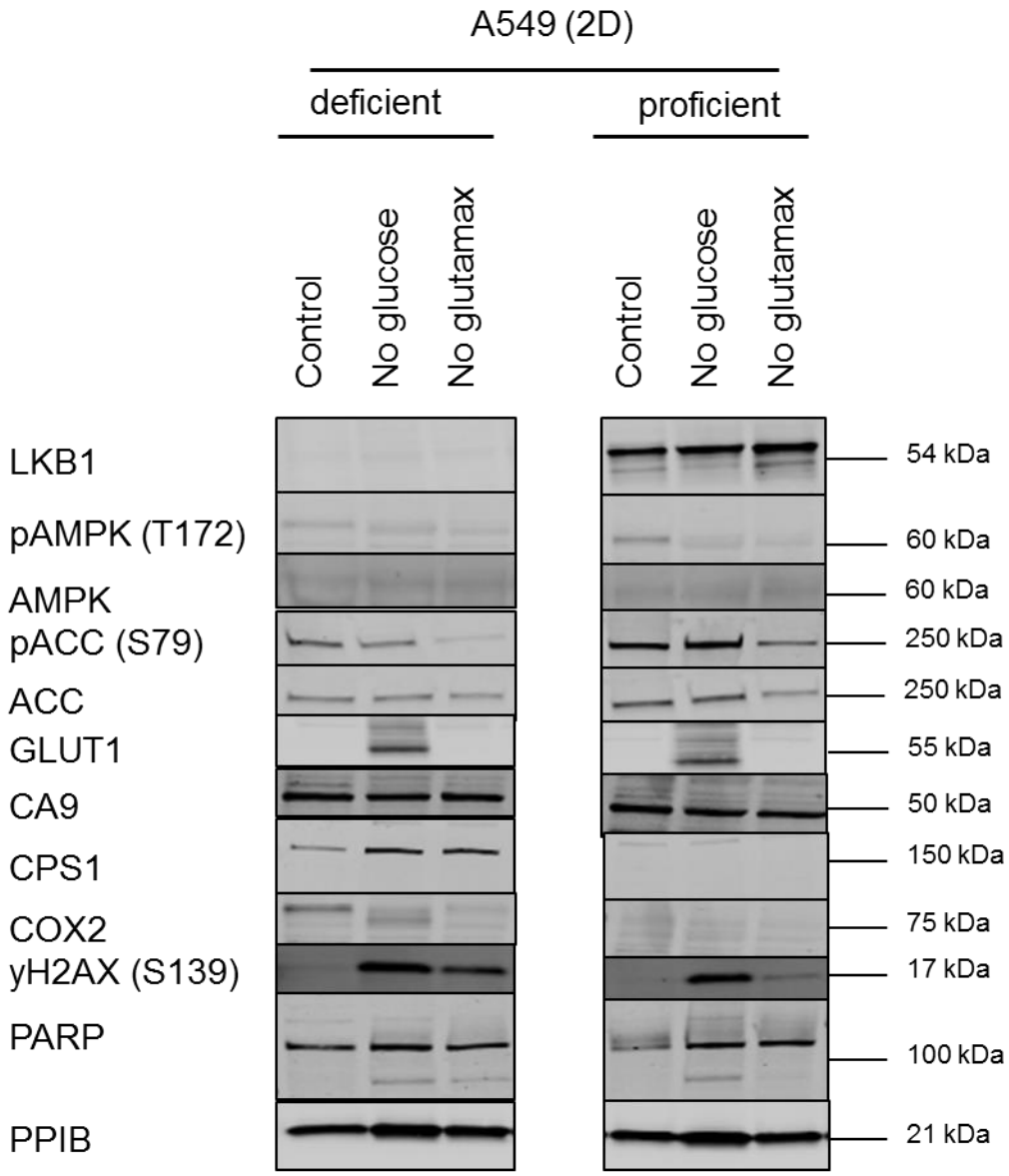

Figure 6.17: The effect of glucose and glutamine deprivation on downstream signalling in LKB1 deficient and proficient cells in 2D culture
For control, cells were seeded in Advanced DMEM/F12 containing 17.5 mM glucose and supplement with 5% FBS and 2 mM glutamax. For glucose and glutamine deprivation conditions, cells were seeded in DMEM supplemented with 5% dialysed FBS and 1 mM pyruvate and either 2 mM glutamax or 17.5 mM glucose. Cell were incubated for 48 h. 20 μg of protein was loaded per well.

We extended the study of glucose and glutamine deprivation to spheroids. Reducing the concentration of glucose caused no marked decrease in the size of LKB1 deficient or

proficient A549 spheroids (Figure 6.18). However, without glutamine, LKB1 deficient A549 spheroids dissociated while the proficient spheroids remained at least partially intact. This suggests that in 2D models, LKB1 deficient cells were sensitive to glucose deprivation, however, in both 2D and 3D models, LKB1 deficient cells were more sensitive to glutamine deprivation. A possible explanation for the reduced sensitivity of LKB1 deficient cells to glucose deprivation in 3D spheroids may be the upregulation of GLUT1, MCT1 and CA9 to overcome the stress (Figure 6.10).

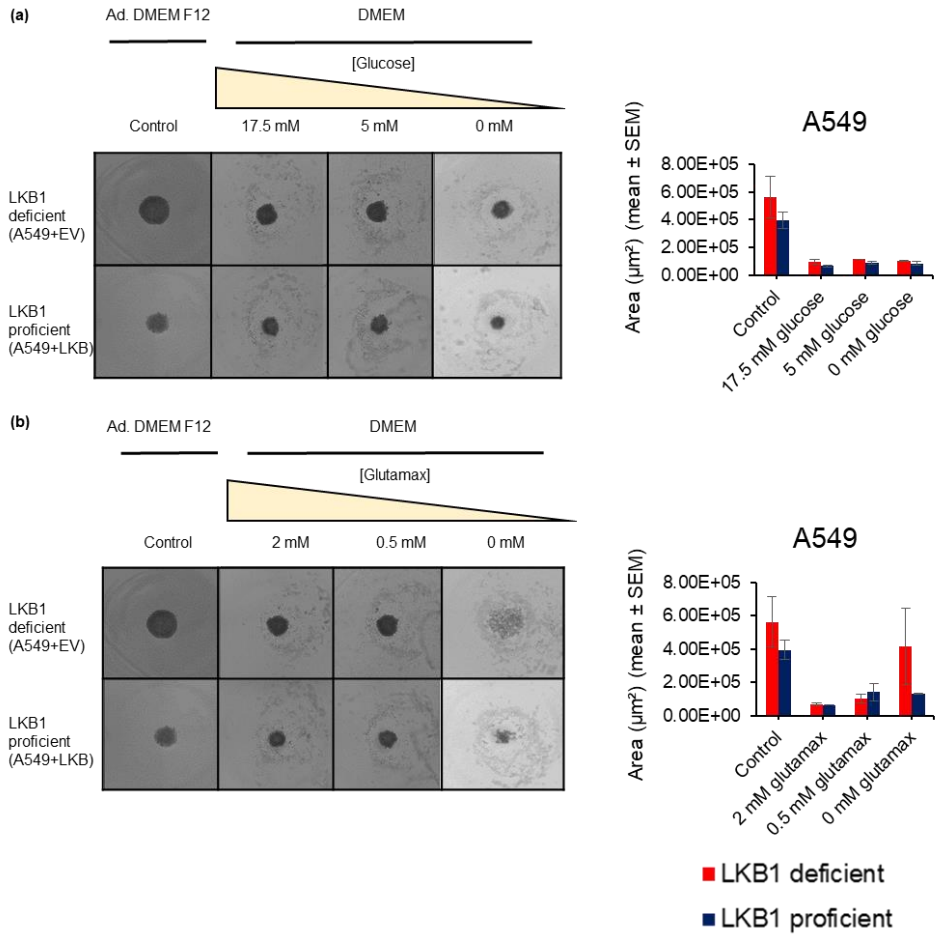

Figure 6.18: The effect of glucose and glutamine deprivation in LKB1 deficient and proficient spheroids

Spheroids were treated from seeding and images were acquired on day 5 post seeding at 15x magnification using the CeligoS. For control, cells were seeded in Advanced DMEM/F12 containing 17.5 mM glucose and supplement with 5% FBS and 2 mM glutamax. For glucose and glutamine deprivation conditions, cells were seeded in DMEM supplemented with 5% dialysed FBS and 1 mM pyruvate and 2 mM glutamax or 17.5 mM glucose. Area was determined using the CeligoS tumoursphere migration analysis. On the graphs, values represent the mean of 6 spheroids (control) or 2 spheroids (treated).

6.4.3 Summary of targeting metabolism in LKB1 deficient cells

LKB1 deficient cells were more sensitive to inhibition of proliferation after glucose deprivation in 2D culture. However, western blotting showed an upregulation of cleaved PARP and γH2AX in both deficient and proficient cells in 2D culture after glucose deprivation. Furthermore, neither LKB1 deficient or proficient spheroids seemed sensitive to glucose deprivation. Treatment of lung cancer cell lines in 2D culture with 2-DG suggests that LKB1 plays a small role in determining sensitivity to 2-DG. LKB1 deficient cells were more sensitive to glutamine deprivation in 2D and 3D culture and western blotting showed an increase in PARP and γH2AX in LKB1 deficient cells.

6.5 Discussion

The aims of this Chapter were to broaden the study of investigating the effect of complex I inhibitors on differences in sensitivity between LKB1 mutated and wild-type lung cancer cells. We also further analysed our RNASeq data to identify any differences in metabolism between LKB1 deficient and proficient cells and tested the effect of other (non-complex I) inhibitors and nutrient deprivation on cell proliferation in LKB1 deficient and proficient cells.

Metformin is a clinically available anti-diabetic drug that is generally well-tolerated in patients although there is a small risk of lactic acidosis (9 events per 100,000 treatment years) (Stang et al., 1999). It was reported that metformin reduced the incidence of cancer in diabetic patients, possibly via a mechanism involving reduced insulin signalling (Evans et al., 2005, Pollak, 2012). Furthermore, prostate cancer patients taking metformin to treat diabetes had an increased reoccurrence free survival (Zannella et al., 2013). Phenformin is approximately 10 times more potent than metformin and has a broader tissue bioavailability but it is less well tolerated in humans due to the higher incidence of lactic acidosis (Hawley

et al., 2010, Huang et al., 2008). The use of complex I inhibitors to selectively target LKB1 mutated cells revealed that although phenformin and metformin reduced oxygen consumption in the isogenic cells and a panel of lung cancer cell lines, there was a small difference in sensitivity between LKB1 deficient and proficient isogenic cells and this difference was not consistent between A549, A427 and H1299 isogenic cells. However, on analysis of the IC_{50} values for lung cancer cell lines, we found that cell lines with wild-type TP53 were more sensitive to phenformin and metformin compared with mutated TP53. Furthermore, it was reported that TP53 plays a role in metabolism by enhancing oxidative phosphorylation, supporting the evidence that TP53 wild-type cells may be more sensitive to complex I inhibitors (Kruiswijk et al., 2015). In lung adenocarcinoma, LKB1 mutations tend to be mutually exclusive from TP53 mutations (p-value = 0.006, n = 230) (TCGA, 2014), therefore it is possible that some LKB1 mutated lung adenocarcinoma patients may benefit from treatment with complex I inhibitors. However, a greater benefit may be seen in combination with other therapies like radiation. It was reported that inhibition of oxygen consumption with metformin reoxygenates tumours and radiosensitises cells (Zannella et al., 2013), as oxygen plays a key role in determining the efficacy of radiotherapy (Gray et al., 1953).

Our RNASeq data suggested that there may be increased glycolysis in LKB1 deficient cells. Furthermore, our data showed that LKB1 deficient cells were more sensitive to glucose deprivation in 2D models but preliminary data suggests that this was not recapitulated in 3D spheroids. Increased glucose uptake in LKB1 mutated tumours was also observed using FDG-PET imaging in a $Kras^{G12D}/Lkb1^{L/L}$ driven mouse lung cancer model (Chen et al., 2012, Shackelford et al., 2013) and in a $Kras^{G12D}/Lkb1^{-/-}$ driven mouse pancreatic cancer model (Kottakis et al., 2016), compared to $Kras^{G12D}$ driven models. We hypothesised that PDK4 was a potential driver of this metabolic shift as PDK4 mRNA levels were higher in LKB1

deficient cells in 2D, 3D and human tumours. Although, PDK4 protein expression was increased in LKB1 deficient A427 cells, PDK4 protein expression was below the detectable level in A549 cells, therefore it was difficult to determine if PDK4 was a driver. Differences in CA9 expression were context dependent for LKB1 deficient A549 cells but increased in LKB1 deficient H1299 cells in 2D and 3D models. The increase in CA9 and other glycolysis proteins (GLUT1, MCT1) in LKB1 deficient A549 spheroids but not 2D culture, may explain the lack of difference in sensitivity to glucose deprivation between LKB1 deficient and proficient cells in 3D culture compared to 2D culture. It was suggested that LKB1 mutated cells may have mitochondrial defects (Shackelford et al., 2013), which could be a possible reason for an increased dependency on glycolysis. We determined differences in mitochondrial function by completing a mitochondrial stress test using the Seahorse XF96 Analyser. For this, oligomycin (ATP synthase inhibitor), FCCP (uncouples respiration, i.e. movement of electrons and protons) and antimycin A (complex III inhibitor) + rotenone (complex I inhibitor) were injected into the medium. The results showed that LKB1 deficient and proficient A549 cells had similar responses for the mitochondrial stress test (Appendices Figure A6.19). Another possible explanation for the increased glycolysis is that it is selected by the cells to confer a growth advantage. As mentioned, increased glycolysis stimulates lactate production and extracellular acidification which was shown to inhibit the function of cytotoxic T cells (Choi et al., 2013).

In 2D culture, LKB1 deficient A549, A427 and H1299 cells appeared more sensitive to glutamine deprivation with LKB1 expression causing a large effect in A549 cells. Although, the effect was moderate in A427 and H1299, the power was small. LKB1 deficient A549 spheroids also appeared more sensitive to glutamine deprivation. In response to glutamine deprivation in 2D culture, LKB1 deficient A549 cells upregulated cleaved PARP and γH2AX (markers of apoptosis) and downregulated COX2 supporting a role for COX2 in

cell survival. Phospho-AMPK and pACC were downregulated in both LKB1 deficient and proficient cells upon glutamine deprivation. This result suggests that LKB1 plays a limited role in phosphorylation and activation of AMPK in these cells. As mentioned in Section 1.3.2, CaMKKβ has also been shown to phosphorylate AMPK (Hurley et al., 2005, Woods et al., 2005). To date, there is no known target which is exclusively phosphorylated by LKB1. Future work should determine the effect of glutaminolysis inhibitors on cell proliferation and downstream signalling in LKB1 deficient and proficient cells. As we do not understand the role of glutamine yet, a glutamine transport inhibitor, like GPNA may hold the greatest promise. However, the use of glutaminolysis inhibitors in the clinic may prove challenging due to the high amounts of glutamine in the blood (plasma glutamine levels in caucasian adults ($n = 280$) ~ 0.53 mM) (Tan and Gajra, 2006). Furthermore, glutamine is a conditionally essential amino acid, meaning that cells can make glutamine but if the need outweighs the supply, the body must obtain glutamine from the blood. Considering glutamine is important for cell proliferation in LKB1 deficient cells and the idea that it may be required for anaplerosis suggests that other amino acids may also be important for cell proliferation/survival in these cells and this could be addressed in future work.

Interestingly, our RNASeq data showed that CPS1, the rate limiting enzyme for the urea cycle was expressed at higher levels in LKB1 deficient samples in 2D, 3D and human tumours models. Furthermore, CPS1 protein was increased in LKB1 deficient A549 cells in 2D and 3D models and in LKB1 deficient A427 cells, suggesting that it is intrinsic to LKB1 loss. Importantly, CPS1 expression was not affected by knock-down of LKB1 in H1299 cells. This phenomenon was also reported in Çeliktaş et al (Çeliktaş et al., 2017). The functional relevance of CPS1 expression in LKB1 mutated cells has yet to be determined. Based on our results, we concluded that glutamine deprivation does not decrease CPS1

expression, ruling out the possibility that CPS1 is required to remove the ammonia produced during glutamine catabolism. However, as CPS1 expression was increased after treatment with glucose and glutamine suggests that CPS1 may be important for survival. Çeliktaş et al have speculated that it may be important for arginine and pyrimidine metabolism (Çeliktaş et al., 2017). Kim et al extended this hypothesis finding that in KRAS/LKB1 mutated NSCLC cells, CPS1 is required for channelling nitrogen from ammonia into the synthesis of pyrimidines which are important in DNA synthesis (Kim et al., 2017). Furthermore, as mentioned in Section 1.6, it was reported that deoxythymidylate kinase (involved in pyrimidine synthesis), was possibly upregulated in LKB1 mutated cells, as knock-down of this gene reduced proliferation in LKB1 mutated A549 and H2122 cells to a greater extent than LKB1 wild-type Calu-1 and H358 cells (Liu et al., 2013). Together, the literature suggests that nucleotide metabolism is different between LKB1 deficient and proficient cells and that CPS1 may be important for maintaining nucleotide pools. As there are no CPS1 inhibitors commercially available to examine the effect of pharmacological inhibition of CPS1, future experiments could aim to investigate the effect of CPS1 knock-down on cell proliferation in 2D, 3D and *in vivo*.

Our data suggests that the metabolic shift to increased glycolysis and glutaminolysis may be driving the differences in CRE signalling and COX2 expression, as glucose and glutamine deprivation affected COX2 expression. However, it has yet to be determined which LKB1 substrate could be responsible for these differences. In Chapter 4, we speculated that SIK may be involved as it was the only LKB1 downstream target different between LKB1 deficient and proficient mRNA samples in 2D, 3D and human tumour models. As mentioned, there is no commercially available pSIK1 antibody and we could not identify a total SIK1 antibody suitable for immunoprecipitation to be able to detect pSIK1. Although

SIK inhibitors are available, LKB1 loss leads to the lack of SIK activation and therefore activators of SIK may be more relevant for targeting LKB1 mutated cells.

To conclude, LKB1 loss only contributed a small effect on determining sensitivity to complex I inhibitors. However, TP53 appeared to be a greater determinant of sensitivity with wild-type cells being more sensitive. We also identified a metabolic shift to an increase in aerobic glycolysis and glutaminolysis in LKB1 deficient cells. To our knowledge, the dependency of LKB1 deficient cells on glutamine for cell proliferation has not been reported before. Future work should aim to expand this observation using more cell lines and glutaminolysis inhibitors. The precise role(s) of CPS1 in LKB1 deficient cells is not fully understood and although we do not understand the importance of CPS1 yet, it was noted that bicarbonate is a substrate of CPS1 and CA9. Future work could also aim to study the interactions bicarbonate and expression of CPS1 and CA9.

7 General discussion and conclusion

The overall aims of this project were to understand the role of LKB1 loss in lung cancer and to identify novel strategies to selectively target LKB1 mutated cells.

7.1 Understanding the role of LKB1 loss in lung cancer

Like others, we generated isogenic cells with or without LKB1 using human lung cancer cells. We restored LKB1 expression in LKB1 mutated cells and knocked-down LKB1 expression in LKB1 wild-type cells. To understand the role of LKB1 loss in lung cancer, we determined the effect of LKB1 expression on cell proliferation in 2D culture, 3D spheroids and *in vivo* models. *In vivo*, we utilised sub-cutaneous xenografts and xenografts grown orthotopically in the mouse lung. Importantly, Kaufmann et al reported that the effect of LKB1 mutations on gene expression is similar between human lung cancer cells and human lung tumours but is not recapitulated in $Kras^{G12D}/Lkb1^{-/-}$ driven mouse tumours (Kaufman et al., 2014). Therefore, the use of LKB1 deficient human lung cancer cells in mouse models may hold greater promise in understanding the role of LKB1 loss in human lung cancer. In our study, we develop a novel western blot assay for determining the tumour burden in whole mouse lungs. We also utilised MRI to monitor tumour growth throughout the experiment which also provided the spatial information for the lung tumours. To include a clinically relevant *in vitro* model, we evaluated the use of spheroids to understand the role of LKB1 loss in lung cancer. Furthermore, we examined the gene expression profile of LKB1 deficient and proficient cells in 2D, 3D and human tumours. The use of 3D spheroids was a novel approach for investigating the effect of LKB1 expression on various processes.

Although there were LKB1 dependent differences in mRNA expression in 2D culture (Figure 4.4), LKB1 expression caused no marked difference in the growth rate in this model

(Figure 3.3). However, LKB1 deficient cells formed larger spheroids (Section 3.5.1) which appeared more apoptotic (Section 3.5.2). However, the overall growth rate exceeded the death rate in these spheroids. *In vivo,* LKB1 deficient A549 cells caused a greater tumour burden in sub-cutaneous xenografts and a greater tumour burden and metastasis in the lung orthotopic model compared with A549 cells transduced with ectopic LKB1 (Section 3.6). This is in agreement with data produced using a GEMM for lung cancer where $Kras^{G12D}/Lkb1^{-/-}$ mutated tumours caused a greater tumour burden than $Kras^{G12D}$ driven tumours (Ji et al., 2007) (Section 1.6.3).

Haematoxylin and Eosin staining of LKB1 deficient and proficient spheroids was remarkably similar to H and E staining of LKB1 deficient and proficient A549 xenografts, in that LKB1 deficient samples had more acellular gaps (Figure 3.9 and 3.15). On characterisation of the spheroids, we observed differences in microtubule cytoskeleton, cell-cell contacts (β-catenin) and cell-ECM contacts (integrin-β1 (Section 3.5.3). The RNA sequencing data also highlighted differences in cytoskeletal and ECM organisation between LKB1 deficient and proficient samples (Appendices Table A4.5-4.9).

Using the RNASeq data, we identified that CRE signalling was different between LKB1 deficient and proficient cells. LKB1 dependent differences in CRE signalling has also been observed by other groups (He et al., 2014, Chen et al., 2016, Cao et al., 2015, Katoh et al., 2006). In our data, COX2 (a CRE transcribed gene) protein was expressed at higher levels in LKB1 deficient cells, however, inhibition of COX2 using celecoxib did not selectively reduce proliferation of LKB1 deficient cells (Section 4.5). We speculated that COX2 has a role in tumour development/initiation as (i) it is not highly expressed in the established human tumours from LKB1 mutated samples, and (ii) Cao et al reported that COX2 expression was important of xenograft tumour development (Cao et al., 2015). Therefore,

COX2 inhibitors, like acetylsalicylic acid (aspirin) may be a useful preventative treatment, although, this has not been demonstrated clinically in lung cancer.

We also compared the mRNA expression profile between 2D culture, 3D spheroids and sub-cutaneous xenografts. To my knowledge, it is the first time that spheroids have been RNA sequenced and compared to other models. Gene ontology analysis revealed that (i) genes involved in hypoxia, catabolism and surprisingly immune response, were expressed at higher levels in 3D and xenografts compared to 2D (Figure 4.1, Appendices Table A4.1, 4.3). This shows that other factors, for example; hypoxia may drive inflammation as it was reported that HIF can activate NFκB which can drive inflammation (Eltzschig and Carmeliet, 2011). Some of the genes involved in cell cycle control and DNA repair were expressed at lower levels in 3D spheroids and in xenografts compared to 2D cell culture (Figure 4.1, Appendices Table A4.2, 4.4). Considering nutrients and growth factors may be more limited in the more complex models, this result is perhaps expected. However, it should be taken into account when testing DNA repair inhibitors as the 2D response may not be recapitulated in 3D or *in vivo*. Our dataset can help researchers predict the expression levels of genes in 3D and *in vivo* compared to 2D, which may be an indicator of the response.

7.2 Targeting LKB1 mutated cells

To identify novel strategies to selectively target LKB1 mutated cells, we used a hypothesis free approach by completing a bioactive small molecular screen in 2D and 3D models and a hypothesis driven approach by determining the effect of LKB1 expression on sensitivity to several metabolic inhibitors.

Although genetic screening has been used to identify strategies to selectively target $Kras^{G12D}/Lkb1^{-/-}$ mouse lung cancer cells (Liu et al., 2013), to my knowledge, it is the first time a bioactive small molecule screen has been used in terms of targeting LKB1 loss. We

observed that, in general, LKB1 deficient cells in 2D culture took more time to undergo apoptosis compared with LKB1 proficient cells and therefore, were less sensitive to a large proportion of the cytotoxic agents used in the bioactive small molecule screen (Figure 5.4). Karuman et al previously reported that LKB1 interacts with TP53 to stimulate apoptosis (Karuman et al., 2001) (Section 1.3.4).

With the aim of identifying novel compounds to selectively target LKB1 mutated cells, we also completed a bioactive small molecule screen in 3D culture. There have been few screens that have used spheroids (Friedrich et al., 2009, Zanoni et al., 2016), and in terms of targeting LKB1, this is the first 3D screen I am aware of. Although this work highlighted the technical challenges with screening in spheroids, we identified MEK, MTOR and PI3K inhibitors as possible approaches to target LKB1 deficient spheroids (Section 5.3). However, MTOR/PI3K inhibitors have been studied previously with mixed results for monotherapy, but with some promise when combined with MEK and SRC inhibitors (Section 1.6). In our gene ontology analysis, MAPK signalling (downstream of MEK) was different between LKB1 deficient and proficient spheroids (Section 4.4, Appendices Table A4.5). As LKB1 and EGFR mutations are mutually exclusive (TCGA, 2014), we speculate that they may share redundant pathways like the MAPK pathway. However, LKB1 mutations tend to co-occur with KRAS mutations, therefore it is likely that oncogenic KRAS is driving MAPK signalling in LKB1 mutated cells. Unfortunately, treatment of spheroids with MEK inhibitors alone showed that LKB1 dependent sensitivity was largely compound dependent rather than target specific, and LKB1 deficient cells were possibly more resistant to AZD6244 (Figure 5.7). This was similar to Chen et al's report, where $Kras^{G12D}/Lkb1^{L/L}$ driven mouse tumours were more resistant to the combination of docetaxel and AZD6244 compared to $Kras^{G12D}$ driven tumours (Chen et al., 2012).

However, by completion of the 2D and 3D screen, we found that microtubule inhibitors caused differential responses between LKB1 deficient and proficient cells. In 2D culture, LKB1 deficient cells were more resistant to microtubule inhibitors. However, microtubule inhibitors reduced the size of LKB1 deficient spheroids and increased the size of LKB1 proficient spheroids (Section 5.4). Therefore, the difference in sensitivity between the two cell lines may be model dependent. Microtubule inhibitors are a widely used chemotherapeutic agent to treat lung cancer (Ferrara et al., 2016), and we speculate that LKB1 loss appears to play a role in determining sensitivity to these inhibitors, although there is currently no data available clinically.

As LKB1 plays a role in metabolism and the RNA sequencing highlighted marked differences in metabolic genes, we investigated the effect of metabolic inhibitors and nutrient deprivation on cell proliferation. We found that LKB1 contributes only a small amount in determining sensitivity to complex I inhibitors and that there are other genetic factors like TP53 which may also play a role (Section 6.2). Therefore, the use of phenformin or metformin to selectively target LKB1 mutated cells may not be beneficial in the clinic. However, LKB1 deficient cells were more dependent on glucose and glutamine (Section 6.4.2) and our data suggests that this may be exploited to selectively target LKB1 mutated cells.

7.2.1 Glucose deprivation

We hypothesised that LKB1 mutated cells were associated with a metabolic shift toward increased aerobic glycolysis. Other groups have also reported increased glucose uptake in $Kras^{G12D}/Lkb1^{L/L}$ driven mouse lung tumours compared with $Kras^{G12D}$ tumours, using FDG-PET (Section 1.6.3) (Chen et al., 2012, Shackelford et al., 2013). While this work was in progress, Faubert et al published that MEFs with knock-out of *Lkb1* using a CRE recombinase system had increased glucose uptake, increased ECAR (extracellular

acidification rate) and increased lactate production (Faubert et al., 2014). A possible advantage of increased aerobic glycolysis in tumour cells may be to increase extracellular lactate, thereby causing acidification. This has been reported to negatively impact on immune cells like T-cells and assist with immune evasion and survival (Choi et al., 2013). Our RNA Sequencing data (Appendices Table A4.6, 4.8) and *in vivo* data (immunoglobulin expression (Figure 3.22)) suggested that there was a difference in inflammation and immune response between LKB1 deficient and proficient cells. Interestingly, LKB1 deficient A549, A427 and H1299 cells were more sensitive to glucose deprivation in 2D culture and surprisingly, LKB1 proficient cells were sensitive to high glucose concentrations (Section 6.4.2).

7.2.2 Glutamine deprivation

LKB1 deficient A549 cells were more sensitive to glutamine deprivation in 2D and 3D models. In addition to being a precursor for glutamate, which is broken down into α-ketoglutarate (TCA cycle intermediate), glutamate is also a precursor for glutathione which is an antioxidant (Hensley et al., 2013). It was reported that LKB1 deficient cells also have increased expression of NRF2 (Kaufman et al., 2014) and LKB1 mutations tend to co-occur with KEAP1 mutations (TCGA, 2014). NRF2 and KEAP1 are genes involved in the oxidative stress response suggesting that LKB1 deficient cells may be under oxidative stress and glutamine is required to make glutathione. Alternatively, glutamine may be utilised for anaplerosis and other amino acids may also be important for this. Although we do not understand the mechanism for increased dependency on glutamine in LKB1 mutated cells, we suggest that glutamine transport inhibitors (like GPNA) may have the potential to selectively target LKB1 mutated cells (Section 6.4.2).

7.3 Future work

Using the bioactive small molecule library, no hits selective for LKB1 mutated cells were identified, as LKB1 proficient cells appeared to be in a more pro-apoptotic state in 2D culture. A larger library of compounds or a genetic screen could be used for future work. Although targeted therapy has many advantages over chemotherapy, including less severe side effects for the patient, one limitation is that it may only target a subset of cells within a tumour, as tumours tend to be heterogeneous (Huang et al., 2014). Therefore, combination therapy may hold the greatest benefit. For example, even though our data suggests reservations about using complex I inhibitors to selectively target LKB1 mutated cells, the use of these in combination with radiation may hold promise (Zannella et al., 2013), especially for LKB1 mutated, TP53 wild-type tumours. Recently, it was reported that complex I inhibitors in combination with MTOR inhibitors could be used to target LKB1 deficient cells, as the $Kras^{G12D}/Lkb1^{L/L}$ driven mouse model of lung adenocarcinoma is sensitive to the combined treatment of phenformin and MLN0128 (inhibitor of MTOR catalytic kinase) (Momcilovic et al., 2015).

Considering, LKB1 deficient and proficient cells have different levels of genes involved in inflammation, (Appendices Table A4.6-4.9), differences in immune response could also be exploited using immunotherapy. It was observed that cancer cells upregulate the immune checkpoint inhibitor; programmed death ligand 1 (PD-L1) and/or its receptor, programmed death 1 (PD-1), to suppress the immune response and evade immune surveillance. In patients, PD1 and PDL1 inhibitors have been used to stimulate immune cells to kill cancer. However these therapies activate the immune system in general and thus, have side effects including GI toxicity and long-term autoimmunity (Michot et al., 2016). Koyama et al reported that, LKB1 deficient mouse and human tumours had reduced expression of PDL1 meaning they may not benefit from this type of therapy. However, Koyama et al observed

that *Kras^{G12D}/Lkb1$^{-/-}$* driven mouse tumours had greater inflammation evident by the increased infiltration of neutrophils that supressed T-cells, and increased expression of T-cell exhaustion markers and tumour promoting cytokines. They went on to show that targeting IL6 with an IL6 neutralising antibody was sufficient to reduce tumour burden in the *Kras^{G12D}/Lkb1$^{-/-}$* model (Koyama et al., 2016). In our RNA sequencing dataset, IL6 was expressed at similar levels between LKB1 deficient and proficient cells in 2D and 3D culture, and IL6R was downregulated in LKB1 deficient spheroids. However, IL8 and IL15 were upregulated in LKB1 deficient cells in 2D and 3D culture. This suggests that increased IL6 may be species specific and that LKB1 deficient human cells may not be sensitive to an IL6 neutralising antibody.

Recently, alternative (non-checkpoint inhibitor) immune therapies have been introduced into clinical trials, including a molecule called "ImmTAC" (Immune mobilising monoclonal T-cell receptor against cancer). This binds a tumour specific antigen and recruits T-cells to stimulate a cytotoxic T-cell response (Oates et al., 2015). As the response is more localised to the tumour, theoretically, it should have less side effects. Also, as the immune cells are recruited to the tumours, it should overcome the heterogeneity issue. However, for LKB1 mutated tumours to benefit from such therapy, a target would still need to be identified. Future experiments could explore the use of genetic screening, especially in 3D spheroids (as this model is more clinically relevant), to identify novel targets. Spheroid screening has technical challenges which were identified in our study. These include a need to develop a low cost, high throughput, continuous spheroid viability assay. However, in addition to genetic screening, our RNA Sequencing dataset could be further analysed to identify possible targets.

A major limitation of any therapy is the emergence of resistance (Komarova and Wodarz, 2005). A long-term spheroid assay in the presence of the therapy of interest, may select for

the resistant population of cells. Future experiments could identify approaches to selectively target these “resistant” cells and a combination of the therapies targeting the sensitive and resistant cells could be further examined.

7.4 Conclusion

The effect of LKB1 expression on cell proliferation was more apparent in 3D and *in vivo*. *In vivo,* LKB1 loss was associated with greater tumour burden and metastasis. Differences in cell cytoskeleton, cell contacts and/or metabolism between LKB1 deficient and proficient cells may play a role in growth. LKB1 expression caused a difference in sensitivity to microtubule inhibitors, glucose deprivation and glutamine deprivation. Future work should aim to further characterise the difference in response to these and in particular to glutamine deprivation due to its novelty. Furthermore, it would be interesting to test the importance of other amino acids for cell growth in LKB1 deficient cells, and further understand the role of CPS1 expression in LKB1 deficient cells.

Bibliography

ABED, A. A., GÜNTHER, K., KRAUS, C., HOHENBERGER, W. & BALLHAUSEN, W. G. 2001. Mutation screening at the RNA level of the STK11/LKB1 gene in Peutz-Jeghers syndrome reveals complex splicing abnormalities and a novel mRNA isoform (STK11 c. 597∕598insIVS4). *Human mutation,* 18**,** 397-410.

ALESSI, D. R., SAKAMOTO, K. & BAYASCAS, J. R. 2006. LKB1-dependent signaling pathways. *Annu. Rev. Biochem.,* 75**,** 137-163.

BAAS, A., BOUDEAU, J., SAPKOTA, G., SMIT, L., MEDEMA, R., MORRICE, N., ALESSI, D. & CLEVERS, H. 2003. Activation of the tumour suppressor kinase LKB1 by the STE20-like pseudokinase STRAD. *The EMBO journal,* 22**,** 3062-3072.

BARDEESY, N., SINHA, M., HEZEL, A. F., SIGNORETTI, S., HATHAWAY, N. A., SHARPLESS, N. E., LODA, M., CARRASCO, D. R. & DEPINHO, R. A. 2002. Loss of the Lkb1 tumour suppressor provokes intestinal polyposis but resistance to transformation. *Nature,* 419**,** 162-167.

BARNES, A. P., LILLEY, B. N., PAN, Y. A., PLUMMER, L. J., POWELL, A. W., RAINES, A. N., SANES, J. R. & POLLEUX, F. 2007. LKB1 and SAD kinases define a pathway required for the polarization of cortical neurons. *Cell,* 129**,** 549-563.

BELIZÁRIO, J. E. 2009. Immunodeficient mouse models: an overview. *Open Immunol J,* 2**,** 79-85.

BENJAMINI, Y. & HOCHBERG, Y. 1995. Controlling the false discovery rate: a practical and powerful approach to multiple testing. *Journal of the royal statistical society. Series B (Methodological)***,** 289-300.

BIGNELL, G. R., BARFOOT, R., SEAL, S., COLLINS, N., WARREN, W. & STRATTON, M. R. 1998. Low frequency of somatic mutations in the LKB1/Peutz-Jeghers syndrome gene in sporadic breast cancer. *Cancer research,* 58**,** 1384-1386.

BIRSOY, K., WANG, T., POSSEMATO, R., YILMAZ, O. H., KOCH, C. E., CHEN, W. W., HUTCHINS, A. W., GULTEKIN, Y., PETERSON, T. R., CARETTE, J. E., BRUMMELKAMP, T. R., CLISH, C. B. & SABATINI, D. M. 2013. MCT1-mediated transport of a toxic molecule is an effective strategy for targeting glycolytic tumors. *Nat Genet,* 45**,** 104-108.

BOKOBZA, S. M., JIANG, Y., WEBER, A. M., DEVERY, A. M. & RYAN, A. J. 2014. Combining AKT inhibition with chloroquine and gefitinib prevents compensatory autophagy and induces cell death in EGFR mutated NSCLC cells. *Oncotarget,* 5**,** 4765.

BOUDEAU, J., BAAS, A. F., DEAK, M., MORRICE, N. A., KIELOCH, A., SCHUTKOWSKI, M., PRESCOTT, A. R., CLEVERS, H. C. & ALESSI, D. R. 2003. MO25α/β interact with STRADα/β enhancing their ability to bind, activate and localize LKB1 in the cytoplasm. *The EMBO journal,* 22**,** 5102-5114.

BROOKS, A. R., HARKINS, R. N., WANG, P., QIAN, H. S., LIU, P. & RUBANYI, G. M. 2004. Transcriptional silencing is associated with extensive methylation of the CMV promoter following adenoviral gene delivery to muscle. *The journal of gene medicine,* 6**,** 395-404.

CALLES, A., SHOLL, L. M., RODIG, S. J., PELTON, A. K., HORNICK, J. L., BUTANEY, M., LYDON, C., DAHLBERG, S. E., OXNARD, G. R. & JACKMAN, D. M. 2015. Immunohistochemical Loss of LKB1 Is a Biomarker for More Aggressive Biology in KRAS-Mutant Lung Adenocarcinoma. *Clinical Cancer Research*.

CAO, C., GAO, R., ZHANG, M., AMELIO, A. L., FALLAHI, M., CHEN, Z., GU, Y., HU, C., WELSH, E. A., ENGEL, B. E., HAURA, E. B., CRESS, W. D., WU, L., ZAJAC-KAYE, M. & KAYE, F. J. 2015. Role of LKB1-CRTC1 on Glycosylated COX-2 and Response to COX-2 Inhibition in Lung Cancer. *Journal of the National Cancer Institute,* 107.

CARLEZON, W. A., JR., DUMAN, R. S. & NESTLER, E. J. The many faces of CREB. *Trends in Neurosciences,* 28**,** 436-445.

CARRETERO, J., MEDINA, P. P., PIO, R., MONTUENGA, L. M. & SANCHEZ-CESPEDES, M. 2004. Novel and natural knockout lung cancer cell lines for the LKB1//STK11 tumor suppressor gene. *Oncogene,* 23**,** 4037-4040.

CARRETERO, J., SHIMAMURA, T., RIKOVA, K., JACKSON, A. L., WILKERSON, M. D., BORGMAN, C. L., BUTTARAZZI, M. S., SANOFSKY, B. A., MCNAMARA, K. L. & BRANDSTETTER, K. A. 2010. Integrative genomic and proteomic analyses identify targets for Lkb1-deficient metastatic lung tumors. *Cancer Cell,* 17**,** 547-559.

ÇELIKTAŞ, M., TANAKA, I., TRIPATHI, S. C., FAHRMANN, J. F., AGUILAR-BONAVIDES, C., VILLALOBOS, P., DELGADO, O., DHILLON, D., DENNISON, J. B. & OSTRIN, E. J. 2017. Role of CPS1 in Cell Growth, Metabolism, and Prognosis in LKB1-Inactivated Lung Adenocarcinoma. *Journal of the National Cancer Institute,* 109**,** djw231.

CHAN, K. T., ASOKAN, S. B., KING, S. J., BO, T., DUBOSE, E. S., LIU, W., BERGINSKI, M. E., SIMON, J. M., DAVIS, I. J. & GOMEZ, S. M. 2014. LKB1 loss in melanoma disrupts directional migration toward extracellular matrix cues. *The Journal of cell biology,* 207**,** 299-315.

CHEN, Z., CHENG, K., WALTON, Z., WANG, Y., EBI, H., SHIMAMURA, T., LIU, Y., TUPPER, T., OUYANG, J. & LI, J. 2012. A murine lung cancer co-clinical trial identifies genetic modifiers of therapeutic response. *Nature,* 483**,** 613-617.

CHEN, Z., LI, J.-L., LIN, S., CAO, C., GIMBRONE, N. T., YANG, R., FU, D. A., CARPER, M. B., HAURA, E. B. & SCHABATH, M. B. 2016. cAMP/CREB-regulated LINC00473 marks LKB1-inactivated lung cancer and mediates tumor growth. *The Journal of clinical investigation,* 126**,** 2267.

CHENG, H., LIU, P., WANG, Z. C., ZOU, L., SANTIAGO, S., GARBITT, V., GJOERUP, O. V., IGLEHART, J. D., MIRON, A. & RICHARDSON, A. L. 2009. SIK1 couples LKB1 to p53-dependent anoikis and suppresses metastasis. *Science signaling,* 2**,** ra35.

CHIAL, H. 2008. Tumor suppressor (TS) genes and the two-hit hypothesis. *Nature Education,* 1**,** 177.

CHOI, S. Y. C., COLLINS, C. C., GOUT, P. W. & WANG, Y. 2013. Cancer-generated lactic acid: a regulatory, immunosuppressive metabolite? *The Journal of pathology,* 230**,** 350-355.

CHURCHMAN, M., DOWLING, B. & TOMLINSON, I. 1999. Identification of a novel mRNA species of the LKB1/STK11 Peutz-Jeghers serine/threonine kinase. *DNA Sequence,* 10**,** 255-261.

COHEN, J. 1988. Statistical power analysis for the behavioral sciences (2nd ed.).

COLLINS, S. P., REOMA, J. L. & UHLER, M. D. 2000. LKB1, a novel serine/threonine protein kinase and potential tumour suppressor, is phosphorylated by cAMP-dependent protein kinase (PKA) and prenylated in vivo. *Biochemical Journal,* 345**,** 673-680.

COTE-VÉLEZ, A., PEREZ-MARTINEZ, L., DIAZ-GALLARDO, M., PÉREZ-MONTER, C., CARREON-RODRIGUEZ, A., CHARLI, J. & JOSEPH-BRAVO, P. 2005. Dexamethasone represses cAMP rapid upregulation of TRH gene transcription: identification of a composite glucocorticoid response element and a cAMP response element in TRH promoter. *Journal of molecular endocrinology,* 34**,** 177-197.

CRABTREE, H. G. & CRAMER, W. 1933. The Action of Radium on Cancer Cells. II.--Some Factors Determining the Susceptibility of Cancer Cells to Radium. *Proceedings of the Royal Society of London. Series B, Containing Papers of a Biological Character,* 113**,** 238.

DANG, C. V. 2010. Glutaminolysis: supplying carbon or nitrogen or both for cancer cells? *Cell Cycle,* 9**,** 3884-6.

DART, A. 2016. Tumour metabolism: Lactic acid: not just a waste product? *Nat Rev Cancer,* 16**,** 676-677.

DAVIES, H., BIGNELL, G. R., COX, C., STEPHENS, P., EDKINS, S., CLEGG, S., TEAGUE, J., WOFFENDIN, H., GARNETT, M. J., BOTTOMLEY, W., DAVIS, N., DICKS, E., EWING, R., FLOYD, Y., GRAY, K., HALL, S., HAWES, R., HUGHES, J., KOSMIDOU, V., MENZIES, A., MOULD, C., PARKER, A., STEVENS, C., WATT, S., HOOPER, S., WILSON, R., JAYATILAKE, H., GUSTERSON, B. A., COOPER, C., SHIPLEY, J., HARGRAVE, D., PRITCHARD-JONES, K., MAITLAND, N., CHENEVIX-TRENCH, G., RIGGINS, G. J., BIGNER, D. D., PALMIERI, G., COSSU, A., FLANAGAN, A.,

NICHOLSON, A., HO, J. W. C., LEUNG, S. Y., YUEN, S. T., WEBER, B. L., SEIGLER, H. F., DARROW, T. L., PATERSON, H., MARAIS, R., MARSHALL, C. J., WOOSTER, R., STRATTON, M. R. & FUTREAL, P. A. 2002. Mutations of the BRAF gene in human cancer. *Nature,* 417**,** 949-954.

DENISON, F. C., HISCOCK, N. J., CARLING, D. & WOODS, A. 2009. Characterization of an alternative splice variant of LKB1. *Journal of Biological Chemistry,* 284**,** 67-76.

DORFMAN, J. & MACARA, I. G. 2008. STRADα regulates LKB1 localization by blocking access to importin-α, and by association with Crm1 and exportin-7. *Molecular biology of the cell,* 19**,** 1614-1626.

DREWES, G., EBNETH, A. & MANDELKOW, E.-M. 1998. MAPs, MARKs and microtubule dynamics. *Trends in biochemical sciences,* 23**,** 307-311.

DREWES, G., EBNETH, A., PREUSS, U., MANDELKOW, E.-M. & MANDELKOW, E. 1997. MARK, a Novel Family of Protein Kinases That Phosphorylate Microtubule-Associated Proteins and Trigger Microtubule Disruption. *Cell,* 89**,** 297-308.

EDEN, E., LIPSON, D., YOGEV, S. & YAKHINI, Z. 2007. Discovering Motifs in Ranked Lists of DNA Sequences. *PLoS Comp Bio,* 3.

EDEN, E., NAVON, R., STEINFELD, I., LIPSON, D. & YAKHINI, Z. 2009. GOrilla: a tool for discovery and visualization of enriched GO terms in ranked gene lists. *BMC bioinformatics,* 10**,** 48.

ELTZSCHIG, H. K. & CARMELIET, P. 2011. Hypoxia and Inflammation. *The New England journal of medicine,* 364**,** 656-665.

EMILSSON, L., HOLME, Ø., BRETTHAUER, M., COOK, N., BURING, J., LØBERG, M., ADAMI, H. O., SESSO, H., GAZIANO, M. & KALAGER, M. 2017. Systematic review with meta-analysis: the comparative effectiveness of aspirin vs. screening for colorectal cancer prevention. *Alimentary pharmacology & therapeutics,* 45**,** 193-204.

ENTIUS, M., KELLER, J., WESTERMAN, A. M., VAN REES, B., VAN VELTHUYSEN, M. F., DE GOEIJ, A., WILSON, J., GIARDIELLO, F. & OFFERHAUS, G. 2001. Molecular genetic alterations in hamartomatous polyps and carcinomas of patients with Peutz-Jeghers syndrome. *Journal of clinical pathology,* 54**,** 126-131.

ESTELLER, M., AVIZIENYTE, E., CORN, P. G., LOTHE, R. A., BAYLIN, S. B., AALTONEN, L. A. & HERMAN, J. G. 2000. Epigenetic inactivation of LKB1 in primary tumors associated with the Peutz-Jeghers syndrome. *Oncogene,* 19**,** 164.

ETTINGER, A. & WITTMANN, T. 2014. Fluorescence Live Cell Imaging. *Methods in cell biology,* 123**,** 77-94.

EVANS, J. M., DONNELLY, L. A., EMSLIE-SMITH, A. M., ALESSI, D. R. & MORRIS, A. D. 2005. Research Pointers: Metformin and reduced risk of cancer in diabetic patients. *BMJ: British Medical Journal,* 330**,** 1304.

FALLAHI, M., AMELIO, A. L., CLEVELAND, J. L. & ROUNBEHLER, R. J. 2014. CREB targets define the gene expression signature of malignancies having reduced levels of the tumor suppressor tristetraprolin. *PloS one* [Online], 9. [Accessed 2014].

FAUBERT, B., VINCENT, E. E., GRISS, T., SAMBORSKA, B., IZREIG, S., SVENSSON, R. U., MAMER, O. A., AVIZONIS, D., SHACKELFORD, D. B. & SHAW, R. J. 2014. Loss of the tumor suppressor LKB1 promotes metabolic reprogramming of cancer cells via HIF-1α. *Proceedings of the National Academy of Sciences,* 111**,** 2554-2559.

FERRARA, R., PILOTTO, S., PERETTI, U., CACCESE, M., KINSPERGHER, S., CARBOGNIN, L., KARACHALIOU, N., ROSELL, R., TORTORA, G. & BRIA, E. 2016. Tubulin inhibitors in non-small cell lung cancer: looking back and forward. *Expert Opinion on Pharmacotherapy,* 17**,** 1113-1129.

FINGAR, D. C., RICHARDSON, C. J., TEE, A. R., CHEATHAM, L., TSOU, C. & BLENIS, J. 2004. mTOR controls cell cycle progression through its cell growth effectors S6K1 and 4E-BP1/eukaryotic translation initiation factor 4E. *Molecular and cellular biology,* 24**,** 200-216.

FRIEDRICH, J., SEIDEL, C., EBNER, R. & KUNZ-SCHUGHART, L. A. 2009. Spheroid-based drug screen: considerations and practical approach. *Nature protocols,* 4**,** 309-324.

GANDHI, L., MCNAMARA, K. L., LI, D., BORGMAN, C. L., MCDERMOTT, U., BRANDSTETTER, K. A., PADERA, R. F., CHIRIEAC, L. R., SETTLEMAN, J. E. & WONG, K.-K. 2009. Sunitinib prolongs survival in genetically engineered mouse models of multistep lung carcinogenesis. *Cancer prevention research,* 2**,** 330-337.

GAO, Y., XIAO, Q., MA, H., LI, L., LIU, J., FENG, Y., FANG, Z., WU, J., HAN, X. & ZHANG, J. 2010. LKB1 inhibits lung cancer progression through lysyl oxidase and extracellular matrix remodeling. *Proceedings of the National Academy of Sciences,* 107**,** 18892-18897.

GAVANDE, N. S., VANDERVERE-CAROZZA, P. S., HINSHAW, H. D., JALAL, S. I., SEARS, C. R., PAWELCZAK, K. S. & TURCHI, J. J. 2016. DNA repair targeted therapy: The past or future of cancer treatment? *Pharmacology & Therapeutics,* 160**,** 65-83.

GHAFFAR, H., SAHIN, F., SANCHEZ-CEPEDES, M., SU, G. H., ZAHURAK, M., SIDRANSKY, D. & WESTRA, W. H. 2003. LKB1 protein expression in the evolution of glandular neoplasia of the lung. *Clinical Cancer Research,* 9**,** 2998-3003.

GRAY, L. H., CONGER, A. D., EBERT, M., HORNSEY, S. & SCOTT, O. 1953. The concentration of oxygen dissolved in tissues at the time of irradiation as a factor in radiotherapy. *The British journal of radiology,* 26**,** 638-648.

GREENHOUGH, A., SMARTT, H. J., MOORE, A. E., ROBERTS, H. R., WILLIAMS, A. C., PARASKEVA, C. & KAIDI, A. 2009. The COX-2/PGE2 pathway: key roles in the hallmarks of cancer and adaptation to the tumour microenvironment. *Carcinogenesis,* 30**,** 377-386.

GULDBERG, P., STRATEN, P. T., AHRENKIEL, V., SEREMET, T., KIRKIN, A. F. & ZEUTHEN, J. 1999. Somatic mutation of the Peutz-Jeghers syndrome gene, LKB 1/STK 11, in malignant melanoma. *Oncogene,* 18**,** 1777-1780.

GWINN, D. M., SHACKELFORD, D. B., EGAN, D. F., MIHAYLOVA, M. M., MERY, A., VASQUEZ, D. S., TURK, B. E. & SHAW, R. J. 2008. AMPK phosphorylation of raptor mediates a metabolic checkpoint. *Molecular cell,* 30**,** 214-226.

HARDIE, D. G. & ALESSI, D. R. 2013. LKB1 and AMPK and the cancer-metabolism link - ten years after. *BMC Biology,* 11**,** 1-11.

HARDIE, D. G., CARLING, D. & GAMBLIN, S. J. 2011. AMP-activated protein kinase: also regulated by ADP? *Trends in biochemical sciences,* 36**,** 470-477.

HARDIE, D. G., ROSS, F. A. & HAWLEY, S. A. 2012. AMPK: a nutrient and energy sensor that maintains energy homeostasis. *Nature Reviews Molecular Cell Biology,* 13**,** 251-262.

HASHIMOTO, Y. K., SATOH, T., OKAMOTO, M. & TAKEMORI, H. 2008. Importance of autophosphorylation at Ser186 in the A-loop of salt inducible kinase 1 for its sustained kinase activity. *Journal of Cellular Biochemistry,* 104**,** 1724-1739.

HAWLEY, S. A., BOUDEAU, J., REID, J. L., MUSTARD, K. J., UDD, L., MAKELA, T. P., ALESSI, D. R. & HARDIE, D. G. 2003. Complexes between the LKB1 tumor suppressor, STRADα/β and MO25α/β are upstream kinases in the AMP-activated protein kinase cascade. *J Biol,* 2.

HAWLEY, S. A., PAN, D. A., MUSTARD, K. J., ROSS, L., BAIN, J., EDELMAN, A. M., FRENGUELLI, B. G. & HARDIE, D. G. 2005. Calmodulin-dependent protein kinase kinase-β is an alternative upstream kinase for AMP-activated protein kinase. *Cell Metabolism,* 2**,** 9-19.

HAWLEY, S. A., ROSS, F. A., CHEVTZOFF, C., GREEN, K. A., EVANS, A., FOGARTY, S., TOWLER, M. C., BROWN, L. J., OGUNBAYO, O. A. & EVANS, A. M. 2010. Use of cells expressing γ subunit variants to identify diverse mechanisms of AMPK activation. *Cell Metabolism,* 11**,** 554-565.

HE, N., KIM, N., SONG, M., PARK, C., KIM, S., PARK, E. Y., YIM, H. Y., KIM, K., PARK, J. H., KIM, K. I., ZHANG, F., MILLS, G. B. & YOON, S. 2014. Integrated Analysis of Transcriptomes of Cancer Cell Lines and Patient Samples Reveals STK11/LKB1–Driven Regulation of cAMP Phosphodiesterase-4D. *American Association for Cancer Research,* 13**,** 2463-2473.

HEARLE, N., SCHUMACHER, V., MENKO, F. H., OLSCHWANG, S., BOARDMAN, L. A., GILLE, J. J., KELLER, J. J., WESTERMAN, A. M., SCOTT, R. J. & LIM, W. 2006. Frequency and spectrum of cancers in the Peutz-Jeghers syndrome. *Clinical Cancer Research,* 12**,** 3209-3215.

HEBERLE, H., MEIRELLES, G. V., DA SILVA, F. R., TELLES, G. P. & MINGHIM, R. 2015. InteractiVenn: a web-based tool for the analysis of sets through Venn diagrams. *BMC bioinformatics,* 16**,** 169.

HELLEDAY, T. 2011. The underlying mechanism for the PARP and BRCA synthetic lethality: Clearing up the misunderstandings. *Molecular Oncology,* 5**,** 387-393.

HEMMINKI, A. 1999. The molecular basis and clinical aspects of Peutz-Jeghers syndrome. *Cellular and Molecular Life Sciences,* 55**,** 735-750.

HEMMINKI, A., MARKIE, D., TOMLINSON, I., AVIZIENYTE, E., ROTH, S., LOUKOLA, A., BIGNELL, G., WARREN, W., AMINOFF, M., HOGLUND, P., JARVINEN, H., KRISTO, P., PELIN, K., RIDANPAA, M., SALOVAARA, R., TORO, T., BODMER, W., OLSCHWANG, S., OLSEN, A. S., STRATTON, M. R., DE LA CHAPELLE, A. & AALTONEN, L. A. 1998. A serine/threonine kinase gene defective in Peutz-Jeghers syndrome. *Nature,* 391.

HEMMINKI, A., TOMLINSON, I., MARKIE, D., JÄRVINEN, H., SISTONEN, P., BJÖRKQVIST, A.-M., KNUUTILA, S., SALOVAARA, R., BODMER, W. & SHIBATA, D. 1997. Localization of a susceptibility locus for Peutz-Jeghers syndrome to 19p using comparative genomic hybridization and targeted linkage analysis. *Nature genetics,* 15**,** 87-90.

HENSLEY, C. T., WASTI, A. T. & DEBERARDINIS, R. J. 2013. Glutamine and cancer: cell biology, physiology, and clinical opportunities. *The Journal of clinical investigation,* 123**,** 3678-3684.

HONG, S.-P., LEIPER, F. C., WOODS, A., CARLING, D. & CARLSON, M. 2003. Activation of yeast Snf1 and mammalian AMP-activated protein kinase by upstream kinases. *Proceedings of the National Academy of Sciences,* 100**,** 8839-8843.

HOWLADER, N., NOONE, A. & KRAPCHO, M. 2015. SEER Cancer Statistics Review, 1975-2012 [seer. cancer. gov/csr. 1975_2012/, based on the November 2014 SEER data submission, posted to the SEER website April 2015]. *Bethesda, MD: National Cancer Institute*.

HUANG, M., SHEN, A., DING, J. & GENG, M. 2014. Molecularly targeted cancer therapy: some lessons from the past decade. *Trends in Pharmacological Sciences,* 35**,** 41-50.

HUANG, X., WULLSCHLEGER, S., SHPIRO, N., MCGUIRE, V., SAKAMOTO, K., WOODS, Y., MCBURNIE, W., FLEMING, S. & ALESSI, D. 2008. Important role of the LKB1-AMPK pathway in suppressing tumorigenesis in PTEN-deficient mice. *Biochem. J,* 412**,** 211-221.

HURLEY, R. L., ANDERSON, K. A., FRANZONE, J. M., KEMP, B. E., MEANS, A. R. & WITTERS, L. A. 2005. The Ca2+/calmodulin-dependent protein kinase kinases are AMP-activated protein kinase kinases. *Journal of Biological Chemistry,* 280**,** 29060-29066.

IMPEY, S., MCCORKLE, S. R., CHA-MOLSTAD, H., DWYER, J. M., YOCHUM, G. S., BOSS, J. M., MCWEENEY, S., DUNN, J. J., MANDEL, G. & GOODMAN, R. H. 2004. Defining the CREB Regulon: A Genome-Wide Analysis of Transcription Factor Regulatory Regions. *Cell,* 119**,** 1041-1054.

JALEEL, M., MCBRIDE, A., LIZCANO, J. M., DEAK, M., TOTH, R., MORRICE, N. A. & ALESSI, D. R. 2005. Identification of the sucrose non-fermenting related kinase SNRK, as a novel LKB1 substrate. *FEBS Lett,* 579.

JEGHERS, H., MCKUSICK, V. A. & KATZ, K. H. 1949. Generalized intestinal polyposis and melanin spots of the oral mucosa, lips and digits: a syndrome of diagnostic significance. *New England Journal of Medicine,* 241**,** 993-1005.

JENNE, D. E., REOMANN, H., NEZU, J.-I., FRIEDEL, W., LOFF, S., JESCHKE, R., MÜLLER, O., BACK, W. & ZIMMER, M. 1998. Peutz-Jeghers syndrome is caused by mutations in a novel serine threoninekinase. *Nature genetics,* 18**,** 38-43.

JI, H., RAMSEY, M. R., HAYES, D. N., FAN, C., MCNAMARA, K., KOZLOWSKI, P., TORRICE, C., WU, M. C., SHIMAMURA, T. & PERERA, S. A. 2007. LKB1 modulates lung cancer differentiation and metastasis. *Nature,* 448**,** 807-810.

JISHAGE, K.-I., NEZU, J.-I., KAWASE, Y., IWATA, T., WATANABE, M., MIYOSHI, A., OSE, A., HABU, K., KAKE, T. & KAMADA, N. 2002. Role of Lkb1, the causative gene of Peutz–Jegher's syndrome, in embryogenesis and polyposis. *Proceedings of the National Academy of Sciences,* 99**,** 8903-8908.

KARUMAN, P., GOZANI, O., ODZE, R. D., ZHOU, X. C., ZHU, H., SHAW, R., BRIEN, T. P., BOZZUTO, C. D., OOI, D. & CANTLEY, L. C. 2001. The Peutz-Jegher gene product LKB1 is a mediator of p53-dependent cell death. *Molecular cell,* 7**,** 1307-1319.

KATOH, Y., TAKEMORI, H., LIN, X. Z., TAMURA, M., MURAOKA, M., SATOH, T., TSUCHIYA, Y., MIN, L., MIYAUCHI, A. & WITTERS, L. A. 2006. Silencing the constitutive active transcription factor CREB by the LKB1-SIK signaling cascade. *Febs Journal,* 273**,** 2730-2748.

KAUFMAN, J. M., AMANN, J. M., PARK, K., ARASADA, R. R., LI, H., SHYR, Y. & CARBONE, D. P. 2014. LKB1 Loss Induces Characteristic Patterns of Gene Expression in Human Tumors Associated with NRF2 Activation and Attenuation of PI3K-AKT. *Journal of Thoracic Oncology,* 9**,** 794-804.

KAUFMAN, J. M., YAMADA, T., PARK, K., TIMMERS, C. D., AMANN, J. M. & CARBONE, D. P. 2017. A transcriptional signature identifies LKB1 functional status as a novel determinant of MEK sensitivity in lung adenocarcinoma. *Cancer research,* 77**,** 153-163.

KIM, C., CHO, Y., PARK, J., KIM, T., LEE, J., KIM, H., LEE, J., SONG, Y., NAM, S. & LEE, S. 2004. Genetic analysis of the LKB1/STK11 gene in hepatocellular carcinomas. *European Journal of Cancer,* 40**,** 136-141.

KIM, J., HU, Z., CAI, L., LI, K., CHOI, E., FAUBERT, B., BEZWADA, D., RODRIGUEZ-CANALES, J., VILLALOBOS, P. & LIN, Y.-F. 2017. CPS1 maintains pyrimidine pools and DNA synthesis in KRAS/LKB1-mutant lung cancer cells. *Nature,* 546**,** 168-172.

KLINE, E. R., SHUPE, J., GILBERT-ROSS, M., ZHOU, W. & MARCUS, A. I. 2013. LKB1 represses focal adhesion kinase (FAK) signaling via a FAK-LKB1 complex to regulate FAK site maturation and directional persistence. *Journal of Biological Chemistry,* 288**,** 17663-17674.

KOJIMA, Y., MIYOSHI, H., CLEVERS, H. C., OSHIMA, M., AOKI, M. & TAKETO, M. M. 2007. Suppression of tubulin polymerization by the LKB1-microtubule-associated protein/microtubule affinity-regulating kinase signaling. *Journal of Biological Chemistry,* 282**,** 23532-23540.

KOMAROVA, N. L. & WODARZ, D. 2005. Drug resistance in cancer: Principles of emergence and prevention. *Proceedings of the National Academy of Sciences of the United States of America,* 102**,** 9714-9719.

KORSSE, S. E., PEPPELENBOSCH, M. P. & VAN VEELEN, W. 2013. Targeting LKB1 signaling in cancer. *Biochimica et Biophysica Acta (BBA) - Reviews on Cancer,* 1835**,** 194-210.

KOTTAKIS, F., NICOLAY, B. N., ROUMANE, A., KARNIK, R., GU, H., NAGLE, J. M., BOUKHALI, M., HAYWARD, M. C., LI, Y. Y. & CHEN, T. 2016. LKB1 loss links serine metabolism to DNA methylation and tumorigenesis. *Nature*.

KOYAMA, S., AKBAY, E. A., LI, Y. Y., AREF, A. R., SKOULIDIS, F., HERTER-SPRIE, G. S., BUCZKOWSKI, K. A., LIU, Y., AWAD, M. M. & DENNING, W. L. 2016. STK11/LKB1 Deficiency Promotes Neutrophil Recruitment and Proinflammatory Cytokine Production to Suppress T-cell Activity in the Lung Tumor Microenvironment. *Cancer research,* 76**,** 999-1008.

KRUISWIJK, F., LABUSCHAGNE, C. F. & VOUSDEN, K. H. 2015. p53 in survival, death and metabolic health: a lifeguard with a licence to kill. *Nature Reviews Molecular Cell Biology,* 16**,** 393-405.

KURIHARA, Y., MATSUOKA, S., YAMASHIRO, T., FUJIKAWA, A., MATSUSHITA, S., YAGIHASHI, K. & NAKAJIMA, Y. 2014. MRI of pulmonary nodules. *American journal of roentgenology,* 202**,** W210-W216.

KWAK, E. L., BANG, Y.-J., CAMIDGE, D. R., SHAW, A. T., SOLOMON, B., MAKI, R. G., OU, S.-H. I., DEZUBE, B. J., JÄNNE, P. A. & COSTA, D. B. 2010. Anaplastic lymphoma kinase inhibition in non–small-cell lung cancer. *New England Journal of Medicine,* 363**,** 1693-1703.

LEMBERT, N. 1996. Firefly luciferase can use L-luciferin to produce light. *Biochemical Journal,* 317**,** 273-277.

LIANG, X., WANG, P., GAO, Q., XIANG, T. & TAO, X. 2010. Endogenous LKB1 knockdown accelerates G1/S transition through p53 and p16 pathways. *Cancer biology & therapy,* 9**,** 156-160.

LIN, R. Z. & CHANG, H. Y. 2008. Recent advances in three-dimensional multicellular spheroid culture for biomedical research. *Biotechnology journal,* 3**,** 1172-1184.

LINDOR, N. M., MCMASTER, M. L., LINDOR, C. J. & GREENE, M. H. 2008. Concise handbook of familial cancer susceptibility syndromes—second edition. *J Natl Cancer Inst Monogr,* 38**,** 1-93.

LINDSKOG, S. 1997. Structure and mechanism of carbonic anhydrase. *Pharmacology & Therapeutics,* 74**,** 1-20.

LIU, Y., MARKS, K., COWLEY, G. S., CARRETERO, J., LIU, Q., NIELAND, T. J., XU, C., COHOON, T. J., GAO, P. & ZHANG, Y. 2013. Metabolic and Functional Genomic Studies Identify Deoxythymidylate Kinase as a target in LKB1 Mutant Lung Cancer. *Cancer discovery*.

LIZCANO, J. M., GÖRANSSON, O., TOTH, R., DEAK, M., MORRICE, N. A., BOUDEAU, J., HAWLEY, S. A., UDD, L., MÄKELÄ, T. P. & HARDIE, D. G. 2004. LKB1 is a master kinase that activates 13 kinases of the AMPK subfamily, including MARK/PAR-1. *The EMBO journal,* 23**,** 833-843.

LODISH, H., BERK, A., ZIPURSKY, S. L., MATSUDAIRA, P., BALTIMORE, D. & DARNELL, J. 1995. *Molecular cell biology (sixth edition)*, Scientific American Books New York.

LÜTZNER, N., ARCE, J. D.-C. & RÖSL, F. 2012. Gene expression of the tumour suppressor LKB1 is mediated by Sp1, NF-Y and FOXO transcription factors. *PloS one,* 7**,** e32590.

LYNCH, T. J., BELL, D. W., SORDELLA, R., GURUBHAGAVATULA, S., OKIMOTO, R. A., BRANNIGAN, B. W., HARRIS, P. L., HASERLAT, S. M., SUPKO, J. G. & HALUSKA, F. G. 2004. Activating mutations in the epidermal growth factor receptor underlying responsiveness of non–small-cell lung cancer to gefitinib. *New England Journal of Medicine,* 350**,** 2129-2139.

MAO, K., LIU, F., LIU, X., KHURI, F. R., MARCUS, A. I., LI, M. & ZHOU, W. 2015. Re-expression of LKB1 in LKB1-mutant EKVX cells leads to resistance to paclitaxel through the up-regulation of MDR1 expression. *Lung Cancer,* 88**,** 131-138.

MARTIN, S. G. & ST JOHNSTON, D. 2003. A role for Drosophila LKB1 in anterior–posterior axis formation and epithelial polarity. *Nature,* 421**,** 379-384.

MATSUMOTO, S., IWAKAWA, R., TAKAHASHI, K., KOHNO, T., NAKANISHI, Y., MATSUNO, Y., SUZUKI, K., NAKAMOTO, M., SHIMIZU, E., MINNA, J. D. & YOKOTA, J. 2007. Prevalence and specificity of LKB1 genetic alterations in lung cancers. *Oncogene,* 26**,** 5911-5918.

MICHOT, J., BIGENWALD, C., CHAMPIAT, S., COLLINS, M., CARBONNEL, F., POSTEL-VINAY, S., BERDELOU, A., VARGA, A., BAHLEDA, R. & HOLLEBECQUE, A. 2016. Immune-related adverse events with immune checkpoint blockade: a comprehensive review. *European Journal of Cancer,* 54**,** 139-148.

MIHAYLOVA, M. M. & SHAW, R. J. 2011. The AMPK signalling pathway coordinates cell growth, autophagy and metabolism. *Nature cell biology,* 13**,** 1016-1023.

MOMCILOVIC, M., MCMICKLE, R., ABT, E., SEKI, A., SIMKO, S. A., MAGYAR, C., STOUT, D. B., FISHBEIN, M. C., WALSER, T. C. & DUBINETT, S. M. 2015. Heightening Energetic Stress Selectively Targets LKB1-Deficient Non–Small Cell Lung Cancers. *Cancer research,* 75**,** 4910-4922.

MORIN, P. J., SPARKS, A. B., KORINEK, V., BARKER, N., CLEVERS, H., VOGELSTEIN, B. & KINZLER, K. W. 1997. Activation of β-catenin-Tcf signaling in colon cancer by mutations in β-catenin or APC. *Science,* 275**,** 1787-1790.

MORRIS JR, S. M. 1992. Regulation of enzymes of urea and arginine synthesis. *Annual review of nutrition,* 12**,** 81-101.

MORRISSEY, D., CASEY, G., O'SULLIVAN, G. C., TANGNEY, M., COLLINS, S. A. & RAJENDERAN, S. 2013. *Plasmid transgene expression in vivo: promoter and tissue variables*, INTECH Open Access Publisher.

MUNDAY, M. 2002. Regulation of mammalian acetyl-CoA carboxylase. Portland Press Limited.

NELSON, D. L., LEHNINGER, A. L. & COX, M. M. 2008. *Lehninger principles of biochemistry*, Macmillan.

NEZU, J.-I., OKU, A. & SHIMANE, M. 1999. Loss of cytoplasmic retention ability of mutant LKB1 found in Peutz-Jeghers syndrome patients. *Biochemical and biophysical research communications,* 261**,** 750-755.

O'BRIEN, J., WILSON, I., ORTON, T. & POGNAN, F. 2000. Investigation of the Alamar Blue (resazurin) fluorescent dye for the assessment of mammalian cell cytotoxicity. *European Journal of Biochemistry,* 267**,** 5421-5426.

OAKHILL, J. S., STEEL, R., CHEN, Z.-P., SCOTT, J. W., LING, N., TAM, S. & KEMP, B. E. 2011. AMPK is a direct adenylate charge-regulated protein kinase. *Science,* 332**,** 1433-1435.

OATES, J., HASSAN, N. J. & JAKOBSEN, B. K. 2015. ImmTACs for targeted cancer therapy: Why, what, how, and which. *Molecular Immunology,* 67**,** 67-74.

ONN, A., ISOBE, T., ITASAKA, S., WU, W., O'REILLY, M. S., HONG, W. K., FIDLER, I. J. & HERBST, R. S. 2003. Development of an orthotopic model to study the biology and therapy of primary human lung cancer in nude mice. *Clinical cancer research,* 9**,** 5532-5539.

ORLOVA, K. A., PARKER, W. E., HEUER, G. G., TSAI, V., YOON, J., BAYBIS, M., FENNING, R. S., STRAUSS, K. & CRINO, P. B. 2010. STRADα deficiency results in aberrant mTORC1 signaling during corticogenesis in humans and mice. *The Journal of clinical investigation,* 120**,** 1591-1602.

OWEN, M., DORAN, E. & HALESTRAP, A. 2000. Evidence that metformin exerts its anti-diabetic effects through inhibition of complex 1 of the mitochondrial respiratory chain. *Biochem. J,* 348**,** 607-614.

PAPADAKIS, E., NICKLIN, S., BAKER, A. & WHITE, S. 2004. Promoters and control elements: designing expression cassettes for gene therapy. *Current gene therapy,* 4**,** 89-113.

PATEL, M. S. & KOROTCHKINA, L. G. 2006. Regulation of the pyruvate dehydrogenase complex. *Biochemical Society Transactions,* 34**,** 217.

PEUTZ, J. 1921. Very remarkable case of familial polyposis of mucous membrane of intestinal tract and nasopharynx accompanied by peculiar pigmentations of skin and mucous membrane. *Ned Tijdschr Geneeskd,* 10**,** 134-146.

POLAKIS, P. 1999. The oncogenic activation of β-catenin. *Current Opinion in Genetics & Development,* 9**,** 15-21.

POLLAK, M. 2012. The insulin and insulin-like growth factor receptor family in neoplasia: an update. *Nature Reviews Cancer,* 12**,** 159-169.

PROST, S., SHEAHAN, S., RANNIE, D. & HARRISON, D. J. 2001. Adenovirus-mediated Cre deletion of floxed sequences in primary mouse cells is an efficient alternative for studies of gene deletion. *Nucleic Acids Research,* 29**,** e80-e80.

PUFFENBERGER, E. G., STRAUSS, K. A., RAMSEY, K. E., CRAIG, D. W., STEPHAN, D. A., ROBINSON, D. L., HENDRICKSON, C. L., GOTTLIEB, S., RAMSAY, D. A. & SIU, V. M. 2007. Polyhydramnios, megalencephaly and symptomatic epilepsy caused by a homozygous 7-kilobase deletion in LYK5. *Brain,* 130**,** 1929-1941.

QIU, W., SCHÖNLEBEN, F., THAKER, H. M., GOGGINS, M. & SU, G. H. 2006. A novel mutation of STK11/LKB1 gene leads to the loss of cell growth inhibition in head and neck squamous cell carcinoma. *Oncogene,* 25**,** 2937-2942.

ROSSI, D. J., YLIKORKALA, A., KORSISAARI, N., SALOVAARA, R., LUUKKO, K., LAUNONEN, V., HENKEMEYER, M., RISTIMÄKI, A., AALTONEN, L. A. & MÄKELÄ, T. P. 2002. Induction of

cyclooxygenase-2 in a mouse model of Peutz–Jeghers polyposis. *Proceedings of the National Academy of Sciences,* 99**,** 12327-12332.

ROWAN, A., TOMLINSON, I., BATAILLE, V., MACKIE, R., HEALY, E., BICKNELL, D. & BODMER, W. 1999. Somatic mutations in the Peutz-Jegners (LKB1/STKII) gene in sporadic malignant melanomas. *Journal of Investigative Dermatology,* 112**,** 509-511.

ROY, B. C., KOHNO, T., IWAKAWA, R., MORIGUCHI, T., KIYONO, T., MORISHITA, K., SANCHEZ-CESPEDES, M., AKIYAMA, T. & YOKOTA, J. 2010. Involvement of LKB1 in epithelial–mesenchymal transition (EMT) of human lung cancer cells. *Lung Cancer,* 70**,** 136-145.

SALVESEN, G. S. & DIXIT, V. M. 1997. Caspases: intracellular signaling by proteolysis. *Cell,* 91**,** 443-446.

SANCHEZ-CESPEDES, M. 2007. A role for LKB1 gene in human cancer beyond the Peutz-Jeghers syndrome. *Oncogene,* 26**,** 7825-7832.

SANCHEZ-CESPEDES, M., PARRELLA, P., ESTELLER, M., NOMOTO, S., TRINK, B., ENGLES, J. M., WESTRA, W. H., HERMAN, J. G. & SIDRANSKY, D. 2002. Inactivation of LKB1/STK11 is a common event in adenocarcinomas of the lung. *Cancer Res,* 62.

SAPKOTA, G. P., BOUDEAU, J., MARIA, D., KIELOCH, A., MORRICE, N. & ALESSI, D. R. 2002a. Identification and characterization of four novel phosphorylation sites (Ser31, Ser325, Thr336 and Thr366) on LKB1/STK11, the protein kinase mutated in Peutz–Jeghers cancer syndrome. *Biochemical Journal,* 362**,** 481-490.

SAPKOTA, G. P., KIELOCH, A., LIZCANO, J. M., LAIN, S., ARTHUR, J. S. C., WILLIAMS, M. R., MORRICE, N., DEAK, M. & ALESSI, D. R. 2001. Phosphorylation of the protein kinase mutated in Peutz-Jeghers cancer syndrome, LKB1/STK11, at Ser431 by p90RSK and cAMP-dependent protein kinase, but not its farnesylation at Cys433, is essential for LKB1 to suppress cell growth. *Journal of Biological Chemistry,* 276**,** 19469-19482.

SAPKOTA, G. P., MARIA, D., KIELOCH, A., MORRICE, N., GOODARZI, A. A., SMYTHE, C., SHILOH, Y., LEES-MILLER, S. P. & ALESSI, D. R. 2002b. Ionizing radiation induces ataxia telangiectasia mutated kinase (ATM)-mediated phosphorylation of LKB1/STK11 at Thr-366. *Biochemical Journal,* 368**,** 507-516.

SETOGAWA, T., SHINOZAKI-YABANA, S., MASUDA, T., MATSUURA, K. & AKIYAMA, T. 2006. The tumor suppressor LKB1 induces p21 expression in collaboration with LMO4, GATA-6, and Ldb1. *Biochemical and biophysical research communications,* 343**,** 1186-1190.

SHACKELFORD, D. B., ABT, E., GERKEN, L., VASQUEZ, D. S., SEKI, A., LEBLANC, M., WEI, L., FISHBEIN, M. C., CZERNIN, J., MISCHEL, P. S. & SHAW, R. J. 2013. LKB1 inactivation dictates therapeutic response of non-small cell lung cancer to the metabolism drug phenformin. *Cancer Cell,* 23.

SHACKELFORD, D. B., VASQUEZ, D. S., CORBEIL, J., WU, S., LEBLANC, M., WU, C. L., VERA, D. R. & SHAW, R. J. 2009. mTOR and HIF-1alpha-mediated tumor metabolism in an LKB1 mouse model of Peutz-Jeghers syndrome. *Proc Natl Acad Sci USA,* 106.

SHAW, R. J., BARDEESY, N., MANNING, B. D., LOPEZ, L., KOSMATKA, M., DEPINHO, R. A. & CANTLEY, L. C. 2004a. The LKB1 tumor suppressor negatively regulates mTOR signaling. *Cancer Cell,* 6**,** 91-99.

SHAW, R. J., KOSMATKA, M., BARDEESY, N., HURLEY, R. L., WITTERS, L. A., DEPINHO, R. A. & CANTLEY, L. C. 2004b. The tumor suppressor LKB1 kinase directly activates AMP-activated kinase and regulates apoptosis in response to energy stress. *Proceedings of the National Academy of Sciences of the United States of America,* 101**,** 3329-3335.

SIEGEL, R., NAISHADHAM, D. & JEMAL, A. 2012. Cancer statistics, 2012. *CA: A Cancer Journal for Clinicians,* 62**,** 10-29.

SLEBOS, R. J., HRUBAN, R. H., DALESIO, O., MOOI, W. J., OFFERHAUS, G. J. A. & RODENHUIS, S. 1991. Relationship between K-ras oncogene activation and smoking in adenocarcinoma of the human lung. *Journal of the National Cancer Institute,* 83**,** 1024-1027.

SMITH, D. P., SPICER, J., SMITH, A., SWIFT, S. & ASHWORTH, A. 1999. The mouse Peutz-Jeghers syndrome gene Lkbl encodes a nuclear protein kinase. *Human molecular genetics,* 8**,** 1479-1485.

SONG, P., XIE, Z., WU, Y., XU, J., DONG, Y. & ZOU, M.-H. 2008. Protein kinase Cζ-dependent LKB1 serine 428 phosphorylation increases LKB1 nucleus export and apoptosis in endothelial cells. *Journal of Biological Chemistry,* 283**,** 12446-12455.

STANG, M., WYSOWSKI, D. K. & BUTLER-JONES, D. 1999. Incidence of lactic acidosis in metformin users. *Diabetes care,* 22**,** 925-927.

STEAD, L. F., BERRI, S., WOOD, H. M., EGAN, P., CONWAY, C., DALY, C., PAPAGIANNOPOULOS, K. & RABBITTS, P. 2012. The transcriptional consequences of somatic amplifications, deletions, and rearrangements in a human lung squamous cell carcinoma. *Neoplasia (New York, N.Y.),* 14**,** 1075-1086.

SU, G. H., HRUBAN, R. H., BANSAL, R. K., BOVA, G. S., TANG, D. J., SHEKHER, M. C., WESTERMAN, A. M., ENTIUS, M. M., GOGGINS, M. & YEO, C. J. 1999. Germline and somatic mutations of the STK11/LKB1 Peutz-Jeghers gene in pancreatic and biliary cancers. *The American Journal of Pathology,* 154**,** 1835-1840.

TAN, I. & GAJRA, B. 2006. Plasma and urine amino acid profiles in a healthy adult population of Singapore. *ANNALS-ACADEMY OF MEDICINE SINGAPORE,* 35**,** 468.

TCGA 2014. Comprehensive molecular profiling of lung adenocarcinoma. *Nature.*

THIBAUDEAU, L., TAUBENBERGER, A. V., HOLZAPFEL, B. M., QUENT, V. M., FUEHRMANN, T., HESAMI, P., BROWN, T. D., DALTON, P. D., POWER, C. A., HOLLIER, B. G. & HUTMACHER, D. W. 2014. A tissue-engineered humanized xenograft model of human breast cancer metastasis to bone. *Disease Models and Mechanisms,* 7**,** 299-309.

TIAINEN, M., VAAHTOMERI, K., YLIKORKALA, A. & MÄKELÄ, T. P. 2002. Growth arrest by the LKB1 tumor suppressor: induction of p21WAF1/CIP1. *Human molecular genetics,* 11**,** 1497-1504.

UPADHYAY, S., LIU, C., CHATTERJEE, A., HOQUE, M. O., KIM, M. S., ENGLES, J., WESTRA, W., TRINK, B., RATOVITSKI, E. & SIDRANSKY, D. 2006. LKB1/STK11 suppresses cyclooxygenase-2 induction and cellular invasion through PEA3 in lung cancer. *Cancer research,* 66**,** 7870-7879.

VALENZUELA, D. M. & GROFFEN, J. 1986. Four human carcinoma cell lines with novel mutations in position 12 of cK-ras oncogene. *Nucleic Acids Research,* 14**,** 843-851.

VAN DEN HEUVEL, S. 2005. Cell-cycle regulation.

WALKINSHAW, D. R., WEIST, R., KIM, G.-W., YOU, L., XIAO, L., NIE, J., LI, C. S., ZHAO, S., XU, M. & YANG, X.-J. 2013. The tumor suppressor kinase LKB1 activates the downstream kinases SIK2 and SIK3 to stimulate nuclear export of class IIa histone deacetylases. *Journal of Biological Chemistry,* 288**,** 9345-9362.

WALRATH, J. C., HAWES, J. J., VAN DYKE, T. & REILLY, K. M. 2010. Genetically Engineered Mouse Models in Cancer Research. *Advances in cancer research,* 106**,** 113-164.

WANG, J., ZHANG, K., WANG, J., WU, X., LIU, X., LI, B., ZHU, Y., YU, Y., CHENG, Q. & HU, Z. 2015. Underexpression of LKB1 tumor suppressor is associated with enhanced Wnt signaling and malignant characteristics of human intrahepatic cholangiocarcinoma. *Oncotarget,* 6**,** 18905.

WARBURG, O. 1956. On respiratory impairment in cancer cells. *Science,* 124**,** 269-270.

WATTS, J. L., MORTON, D. G., BESTMAN, J. & KEMPHUES, K. J. 2000. The C. elegans par-4 gene encodes a putative serine-threonine kinase required for establishing embryonic asymmetry. *Development,* 127**,** 1467-1475.

WINGO, S. N., GALLARDO, T. D., AKBAY, E. A., LIANG, M. C., CONTRERAS, C. M., BOREN, T., SHIMAMURA, T., MILLER, D. S., SHARPLESS, N. E., BARDEESY, N., KWIATKOWSKI, D. J., SCHORGE, J. O., WONG, K. K. & CASTRILLON, D. H. 2009. Somatic LKB1 mutations promote cervical cancer progression. *PloS one,* 4.

WOODS, A., DICKERSON, K., HEATH, R., HONG, S.-P., MOMCILOVIC, M., JOHNSTONE, S. R., CARLSON, M. & CARLING, D. 2005. Ca 2+/calmodulin-dependent protein kinase kinase-β acts upstream of AMP-activated protein kinase in mammalian cells. *Cell Metabolism,* 2**,** 21-33.

WOODS, A., JOHNSTONE, S. R., DICKERSON, K., LEIPER, F. C., FRYER, L. G., NEUMANN, D., SCHLATTNER, U., WALLIMANN, T., CARLSON, M. & CARLING, D. 2003. LKB1 is the upstream kinase in the AMP-activated protein kinase cascade. *Current Biology,* 13**,** 2004-2008.

XIAO, B., SANDERS, M. J., UNDERWOOD, E., HEATH, R., MAYER, F. V., CARMENA, D., JING, C., WALKER, P. A., ECCLESTON, J. F. & HAIRE, L. F. 2011. Structure of mammalian AMPK and its regulation by ADP. *Nature,* 472**,** 230-233.

XIE, X., WANG, Z. & CHEN, Y. 2007. Association of LKB1 with a WD-repeat protein WDR6 is implicated in cell growth arrest and p27Kip1 induction. *Molecular and cellular biochemistry,* 301**,** 115-122.

YLIKORKALA, A., ROSSI, D. J., KORSISAARI, N., LUUKKO, K., ALITALO, K., HENKEMEYER, M. & MÄKELÄ, T. P. 2001. Vascular abnormalities and deregulation of VEGF in Lkb1-deficient mice. *Science,* 293**,** 1323-1326.

YUSHKEVICH, P. A., PIVEN, J., HAZLETT, H. C., SMITH, R. G., HO, S., GEE, J. C. & GERIG, G. 2006. User-guided 3D active contour segmentation of anatomical structures: Significantly improved efficiency and reliability. *NeuroImage,* 31**,** 1116-1128.

ZAGORSKA, A., DEAK, M., CAMPBELL, D. G., BANERJEE, S., HIRANO, M., AIZAWA, S., PRESCOTT, A. R. & ALESSI, D. R. 2010. New roles for the LKB1-NUAK pathway in controlling myosin phosphatase complexes and cell adhesion. *Sci Signal,* 3**,** ra25.

ZANNELLA, V., DAL PRA, A., MUADDI, H., MCKEE, T., STAPLETON, S., SYKES, J., CHAIB, S., GLICKSMAN, R., ZAMIARA, P. & MILOSEVIC, M. 2013. Reprogramming Metabolism with Metformin Improves Tumor Oxygenation and Radiotherapy Response. *Clinical Cancer Research***,** clincanres. 1787.2013.

ZANONI, M., PICCININI, F., ARIENTI, C., ZAMAGNI, A., SANTI, S., POLICO, R., BEVILACQUA, A. & TESEI, A. 2016. 3D tumor spheroid models for in vitro therapeutic screening: a systematic approach to enhance the biological relevance of data obtained. *Scientific Reports,* 6**,** 19103.

ZENG, P.-Y. & BERGER, S. L. 2006. LKB1 is recruited to the p21/WAF1 promoter by p53 to mediate transcriptional activation. *Cancer research,* 66**,** 10701-10708.

ZEQIRAJ, E., FILIPPI, B. M., DEAK, M., ALESSI, D. R. & VAN AALTEN, D. M. 2009. Structure of the LKB1-STRAD-MO25 complex reveals an allosteric mechanism of kinase activation. *Science,* 326**,** 1707-1711.

ZHAN, Y. Y., CHEN, Y., ZHANG, Q., ZHUANG, J. J., TIAN, M., CHEN, H. Z., ZHANG, L. R., ZHANG, H. K., HE, J. P., WANG, W. J., WU, R., WANG, Y., SHI, C., YANG, K., LI, A. Z., XIN, Y. Z., LI, T. Y., YANG, J. Y., ZHENG, Z. H., YU, C. D., LIN, S. C., CHANG, C., HUANG, P. Q., LIN, T. & WU, Q. 2012. The orphan nuclear receptor Nur77 regulates LKB1 localization and activates AMPK. *Nat Chem Biol,* 8**,** 897-904.

ZHANG, J., FUJIMOTO, J., ZHANG, J., WEDGE, D. C., SONG, X., ZHANG, J., SETH, S., CHOW, C.-W., CAO, Y., GUMBS, C., GOLD, K. A., KALHOR, N., LITTLE, L., MAHADESHWAR, H., MORAN, C., PROTOPOPOV, A., SUN, H., TANG, J., WU, X., YE, Y., WILLIAM, W. N., LEE, J. J., HEYMACH, J. V., HONG, W. K., SWISHER, S., WISTUBA, I. I. & FUTREAL, P. A. 2014. Intratumor heterogeneity in localized lung adenocarcinomas delineated by multiregion sequencing. *Science,* 346**,** 256.

ZHANG, S., SCHAFER-HALES, K., KHURI, F. R., ZHOU, W., VERTINO, P. M. & MARCUS, A. I. 2008. The tumor suppressor LKB1 regulates lung cancer cell polarity by mediating cdc42 recruitment and activity. *Cancer research,* 68**,** 740-748.

Appendices

Table A2.11: Human gene list

A1BG	CACNG3	DNMT3L	HDDC3	MCEE	PDIA6	SC5D	TMEM174
A1CF	CACNG4	DNMT3B	HDGF	MCEMP1	PDIK1L	SCAF1	TMEM175
A2M	CACNG5	DNPEP	HDGFL1	MCF2L2	PDILT	SCAF11	TMEM176A
A2ML1	CACUL1	DNPH1	HDHD2	MCFD2	PDK1	SCAF8	TMEM176B
A3GALT2	CACYBP	DNTT	HDHD3	MCHR1	PDK2	SCAI	TMEM177
A4GALT	CADM1	DNTTIP1	HDLBP	MCHR2	PDK4	SCAMP1	TMEM178A
A4GNT	CADM2	DNTTIP2	HEATR3	MCIDAS	PDLIM3	SCAMP2	TMEM179B
AACS	CADM3	DOC2A	HEATR4	MCL1	PDLIM4	SCAMP3	TMEM18
AADAC	CADM4	DOC2B	HEATR5A	MCM10	PDLIM7	SCAMP4	TMEM180
AADACL2	CADPS	DOCK1	HEATR5B	MCM3AP	PDP1	SCAMP5	TMEM181
AADACL3	CADPS	DOCK2	HEATR6	MCM4	PDP2	SCAND1	TMEM182
AADACL4	CADPS	DOCK3	HEATR9	MCM6	PDPN	SCAP	TMEM183A
AADAT	CADPS2	DOCK4	HECA	MCM8	PDPR	SCAPER	TMEM184B
AAED1	CALB1	DOCK5	HECTD3	MCM9	PDRG1	SCARA3	TMEM184C
AAGAB	CALB2	DOCK6	HECW1	MCMBP	PDS5B	SCARA5	TMEM186
AAK1	CALCA	DOCK7	HECW2	MCMDC2	PDSS2	SCARB1	TMEM189
AAMDC	CALCB	DOCK9	HELLS	MCOLN1	PDX1	SCARB2	TMEM19
AAMP	CALCOCO1	DOHH	HELQ	MCOLN2	PDXDC1	SCARF1	TMEM190
AANAT	CALCOCO2	DOK1	HELT	MCOLN3	PDXK	SCCPDH	TMEM194A
AAR2	CALCR	DOK2	HELZ	MCPH1	PDXP	SCD	TMEM196
AARD	CALCRL	DOK3	HELZ2	MCRS1	PDZD3	SCD5	TMEM198
AARS	CALD1	DOK6	HEMGN	MCTP1	PDZD7	SCEL	TMEM199
AARS2	CALHM1	DOK7	HEMK1	MCTP2	PDZD8	SCFD1	TMEM2
AARSD1	CALHM2	DOLK	HENMT1	MCU	PDZD9	SCFD2	TMEM200A
AASDH	CALM2	DOLPP1	HEPACAM	MDC1	PDZK1	SCG2	TMEM200B
AASDHPPT	CALML3	DONSON	HEPACAM2	MDFI	PDZK1IP1	SCG3	TMEM200C
AASS	CALML4	DOPEY1	HEPN1	MDFIC	PDZRN4	SCG5	TMEM201
AATF	CALML5	DOPEY2	HERC1	MDGA2	PEA15	SCGB1A1	TMEM202
AATK	CALML6	DOT1L	HERC2	MDH1B	PEAR1	SCGB1C1	TMEM203
ABAT	CALN1	DPAGT1	HERC3	MDK	PEBP1	SCGB1D1	TMEM204
ABCA1	CALR	DPCR1	HERC4	MDM1	PEBP4	SCGB1D2	TMEM205
ABCA10	CALR3	DPEP1	HERC5	MDM4	PECAM1	SCGB1D4	TMEM206
ABCA12	CALU	DPEP2	HERPUD2	MDP1	PECR	SCGB2A1	TMEM207
ABCA13	CALY	DPEP3	HES2	ME2	PEF1	SCGB2A2	TMEM208
ABCA2	CAMK1	DPF2	HES3	MEAF6	PEG10	SCGB2B2	TMEM209
ABCA3	CAMK1D	DPH1	HES4	MECOM	PELI1	SCGB3A1	TMEM211
ABCA4	CAMK1G	DPH2	HES6	MECOM	PELI3	SCGB3A2	TMEM213
ABCA5	CAMK2A	DPH3	HES7	MECR	PELO	SCIMP	TMEM214
ABCA6	CAMK2B	DPH5	HEXA	MED1	PELP1	SCIN	TMEM215
ABCA7	CAMK2G	DPH6	HEXB	MED10	PEMT	SCLT1	TMEM216
ABCA8	CAMK2N1	DPH7	HEXDC	MED11	PEPD	SCLY	TMEM217
ABCB1	CAMK2N2	DPM1	HEXIM1	MED12L	PER2	SCN10A	TMEM218
ABCB10	CAMK4	DPM2	HEXIM2	MED13	PER3	SCN11A	TMEM219
ABCB11	CAMKK1	DPM3	HEY1	MED15	PERP	SCN1A	TMEM220
ABCB4	CAMKK1	DPP10	HEYL	MED16	PES1	SCN2A	TMEM222
ABCB5	CAMKK1	DPP6	HFE2	MED17	PET100	SCN2B	TMEM225
ABCB6	CAMKK2	DPP7	HFM1	MED18	PEX1	SCN3A	TMEM229A
ABCB8	CAMKMT	DPP8	HGF	MED19	PEX10	SCN3B	TMEM229B
ABCB9	CAMKV	DPPA2	HGH1	MED20	PEX11A	SCN4A	TMEM231
ABCC1	CAMLG	DPPA3	HGNC symbol	MED21	PEX11B	SCN5A	TMEM232
ABCC10	CAMP	DPPA4	HGS	MED22	PEX11G	SCN8A	TMEM233
ABCC11	CAMSAP2	DPPA5	HHAT	MED24	PEX12	SCN9A	TMEM234
ABCC12	CAMTA1	DPRX	HHATL	MED25	PEX13	SCNM1	TMEM235
ABCC2	CAMTA2	DPT	HHIPL2	MED26	PEX16	SCNN1G	TMEM237
ABCC4	CAND1	DPY19L2	HHLA2	MED27	PEX19	SCO1	TMEM238
ABCC5	CANT1	DPY19L3	HIAT1	MED28	PEX2	SCO2	TMEM240
ABCC8	CANX	DPY19L4	HIATL1	MED30	PEX26	SCP2	TMEM241
ABCC9	CAP1	DPY30	HIBADH	MED31	PEX5	SCP2D1	TMEM243
ABCD2	CAPG	DPYD	HIC1	MED4	PEX5L	SCPEP1	TMEM244
ABCD3	CAPN10	DPYS	HID1	MED6	PEX6	SCRG1	TMEM245
ABCD4	CAPN13	DPYSL2	HIF1A	MED7	PEX7	SCRIB	TMEM246
ABCE1	CAPN14	DPYSL3	HIF1AN	MED8	PFDN1	SCRN1	TMEM247
ABCF2	CAPN15	DPYSL5	HIGD1A	MED9	PFDN2	SCRN2	TMEM248
ABCF3	CAPN2	DQX1	HIGD1B	MEDAG	PFDN4	SCRN3	TMEM249
ABCG1	CAPN5	DR1	HIGD1C	MEF2BNB-MEF2B	PFDN6	SCRT1	TMEM25
ABCG2	CAPN7	DRAM1	HIGD2A	MEF2C	PFKFB4	SCRT2	TMEM252
ABCG4	CAPN8	DRAM2	HILPDA	MEF2D	PFKM	SCT	TMEM254
ABCG5	CAPN9	DRAP1	HINFP	MEFV	PFKP	SCUBE1	TMEM255B
ABCG8	CAPNS2	DRAXIN	HINT1	MEGF10	PFN1	SCUBE2	TMEM256
ABHD1	CAPRIN1	DRC1	HINT2	MEGF11	PFN2	SCUBE3	TMEM256-PLSCR3
ABHD10	CAPRIN2	DRC7	HINT3	MEGF6	PFN3	SCYL1	TMEM258
ABHD12	CAPS	DRD1	HIP1	MEGF8	PFN4	SCYL2	TMEM259
ABHD13	CAPSL	DRD2	HIP1R	MEGF9	PGA3	SCYL3	TMEM26
ABHD14A	CAPZA1	DRD4	HIPK1	MEI1	PGA4	SDAD1	TMEM260
ABHD14B	CAPZA2	DRG1	HIPK2	MEIOB	PGA5	SDC1	TMEM261
ABHD15	CAPZA3	DRG2	HIPK3	MEIS1	PGAM1	SDC2	TMEM262
ABHD17A	CARD10	DRICH1	HIPK4	MEIS2	PGAM5	SDC3	TMEM263
ABHD17B	CARD11	DROSHA	HIRA	MELK	PGAP1	SDC4	TMEM30A
ABHD17C	CARD17	DSC1	HIRIP3	MEMO1	PGAP3	SDCBP	TMEM33
ABHD5	CARD18	DSC1	HIST1H1A	MEOX2	PGD	SDCBP2	TMEM37
ABHD6	CARD8	DSC2	HIST1H1B	MEP1A	PGF	SDCCAG3	TMEM38A
ABHD8	CARD9	DSC3	HIST1H1C	MEP1B	PGGT1B	SDCCAG8	TMEM38B
ABI1	CARF	DSC3	HIST1H1D	MESDC1	PGLYRP1	SDE2	TMEM39A
ABI2	CARHSP1	DSCAM	HIST1H1E	MESDC2	PGLYRP2	SDF2	TMEM39B
ABI3	CARKD	DSCAML1	HIST1H1T	MESP1	PGLYRP3	SDF2L1	TMEM40
ABL1	CARNS1	DSCC1	HIST1H2AA	MEST	PGLYRP4	SDF4	TMEM41A
ABL2	CARS	DSCR4	HIST1H2AB	METAP1	PGM1	SDHA	TMEM42
ABLIM2	CARS2	DSE	HIST1H2AC	METAP1D	PGM2	SDHAF1	TMEM43
ABLIM3	CARTPT	DSEL	HIST1H2AD	METAP2	PGM2L1	SDHAF2	TMEM44

ABO
ABRA
ABRACL
ABTB1
ABTB2
ACAA1
ACAA2
ACACA
ACACB
ACAD10
ACAD11
ACAD8
ACAD9
ACADL
ACADS
ACADSB
ACADVL
ACAN
ACAP1
ACAP2
ACAP3
ACAT1
ACAT2
ACBD3
ACBD4
ACBD5
ACCS
ACCSL
ACD
ACER1
ACER3
ACHE
ACIN1
ACKR1
ACKR2
ACKR3
ACKR4
ACLY
ACN9
ACO1
ACO2
ACOT1
ACOT11
ACOT12
ACOT13
ACOT2
ACOT4
ACOT6
ACOT7
ACOX2
ACP2
ACP6
ACPP
ACPT
ACR
ACRBP
ACRV1
ACSBG1
ACSBG2
ACSF2
ACSF3
ACSL1
ACSL3
ACSL5
ACSL6
ACSM1
ACSM2A
ACSM2B
ACSM3
ACSM4
ACSM5
ACSM6
ACSS1
ACSS2
ACSS3
ACTA1
ACTA2
ACTB
ACTBL2
ACTC1
ACTG1
ACTG2
ACTL6A
ACTL6B
ACTL7A
ACTL7B
ACTL8
ACTL9
ACTN1
ACTN2
ACTN3
ACTR1B
ACTR2
ACTR3
ACTR3B
ACTR5
ACTR6
ACTR8
ACTRT2
ACTRT3
ACVR1

CASC1
CASC10
CASC3
CASC4
CASC5
CASD1
CASKIN1
CASKIN2
CASP1
CASP10
CASP12
CASP14
CASP2
CASP3
CASP4
CASP5
CASP6
CASP7
CASP8
CASP8AP2
CASP9
CASQ1
CASQ2
CASR
CASS4
CASZ1
CAT
CATIP
CATSPER1
CATSPER2
CATSPER3
CATSPER4
CATSPERB
CATSPERD
CATSPERG
CAV1
CAV2
CAV3
CBFA2T2
CBFA2T3
CBFB
CBL
CBLB
CBLC
CBLL1
CBLN1
CBLN2
CBLN4
CBR4
CBS
CBWD1
CBWD2
CBWD3
CBWD7
CBX1
CBX2
CBX3
CBX4
CBX5
CBX6
CBX7
CBX8
CBY1
CC2D1A
CC2D1B
CC2D2A
CC2D2B
CCAR1
CCAR2
CCBE1
CCBL2
CCDC101
CCDC102A
CCDC102B
CCDC105
CCDC106
CCDC107
CCDC108
CCDC109B
CCDC110
CCDC112
CCDC113
CCDC114
CCDC115
CCDC116
CCDC117
CCDC12
CCDC121
CCDC122
CCDC124
CCDC125
CCDC126
CCDC127
CCDC129
CCDC13
CCDC130
CCDC132
CCDC134
CCDC136
CCDC138
CCDC14

DSG1
DSG2
DSG3
DSG4
DSN1
DSP
DSPP
DST
DSTN
DSTYK
DTD1
DTD2
DTHD1
DTL
DTNA
DTNB
DTNBP1
DTWD1
DTWD2
DTX3
DTX3L
DTYMK
DUOX1
DUOX2
DUOXA1
DUOXA2
DUS1L
DUS2
DUS3L
DUS4L
DUSP1
DUSP10
DUSP12
DUSP14
DUSP15
DUSP16
DUSP2
DUSP22
DUSP23
DUSP26
DUSP27
DUSP28
DUSP3
DUSP4
DUSP5
DUSP6
DUSP6
DUSP7
DUSP8
DUXA
DVL1
DVL2
DVL3
DYDC1
DYDC2
DYM
DYNAP
DYNC1H1
DYNC1I1
DYNC1I2
DYNC1LI1
DYNC1LI2
DYNC2LI1
DYNLL1
DYNLL2
DYNLRB1
DYNLRB2
DYNLT1
DYRK1A
DYRK1B
DYRK3
DYSF
DYX1C1
DZANK1
DZIP1
DZIP1L
DZIP3
E2F2
E2F4
E2F5
E2F8
E4F1
EAF1
EAF2
EAPP
EBAG9
EBF1
EBF2
EBF3
EBLN1
EBLN2
EBPL
ECD
ECE1
ECE2
ECEL1
ECHDC2
ECHDC3
ECI2
ECM1
ECM2

HIST1H2AE
HIST1H2AG
HIST1H2AH
HIST1H2AI
HIST1H2AJ
HIST1H2AK
HIST1H2AL
HIST1H2AM
HIST1H2BA
HIST1H2BB
HIST1H2BC
HIST1H2BD
HIST1H2BE
HIST1H2BF
HIST1H2BG
HIST1H2BH
HIST1H2BI
HIST1H2BJ
HIST1H2BK
HIST1H2BL
HIST1H2BM
HIST1H2BN
HIST1H2BO
HIST1H3A
HIST1H3B
HIST1H3C
HIST1H3D
HIST1H3E
HIST1H3F
HIST1H3G
HIST1H3H
HIST1H3I
HIST1H3J
HIST1H4A
HIST1H4B
HIST1H4C
HIST1H4D
HIST1H4E
HIST1H4F
HIST1H4G
HIST1H4H
HIST1H4I
HIST1H4J
HIST1H4K
HIST1H4L
HIST2H2AA3
HIST2H2AA4
HIST2H2AA4
HIST2H2AB
HIST2H2AC
HIST2H2BE
HIST2H2BF
HIST2H3C
HIST2H3D
HIST2H4B
HIST3H2A
HIST3H2BB
HIST3H3
HIST4H4
HIVEP1
HIVEP3
HJURP
HK1
HK2
HKDC1
HKR1
HLA-A
HLA-B
HLA-C
HLA-DMA
HLA-DMB
HLA-DOA
HLA-DOB
HLA-DPA1
HLA-DPB1
HLA-DQA1
HLA-DQA2
HLA-DQA2
HLA-DQB1
HLA-DRA
HLA-DRB1
HLA-DRB3
HLA-DRB4
HLA-DRB5
HLA-E
HLA-F
HLA-G
HLF
HLX
HM13
HMBOX1
HMBS
HMCES
HMCES
HMCN1
HMG20A
HMG20B
HMGA1
HMGA2
HMGB1
HMGB2

METRN
METRNL
METTL1
METTL10
METTL11B
METTL12
METTL13
METTL14
METTL15
METTL16
METTL17
METTL18
METTL20
METTL21A
METTL21B
METTL21C
METTL22
METTL23
METTL24
METTL25
METTL2A
METTL2B
METTL3
METTL4
METTL5
METTL6
METTL7A
METTL7B
METTL8
METTL9
MEX3A
MEX3C
MEX3D
MFAP1
MFAP2
MFAP3
MFAP3L
MFAP4
MFAP5
MFF
MFGE8
MFHAS1
MFN2
MFNG
MFRP
MFSD1
MFSD10
MFSD11
MFSD12
MFSD2A
MFSD2B
MFSD3
MFSD4
MFSD5
MFSD6L
MFSD7
MFSD8
MFSD9
MGARP
MGAT1
MGAT2
MGAT3
MGAT4A
MGAT4B
MGAT4C
MGAT5
MGAT5B
MGEA5
MGLL
MGME1
MGMT
MGP
MGST1
MGST2
MGST3
MIA2
MIA3
MIB1
MIB2
MICA
MICAL1
MICAL2
MICALCL
MICALL1
MICALL2
MICB
MICU1
MICU2
MICU3
MIEF1
MIEF2
MIEN1
MIER1
MIER3
MIF
MIF4GD
MIIP
MILR1
MINA
MINK1
MINOS1

PGM3
PGM5
PGPEP1
PGS1
PHACTR2
PHACTR3
PHACTR4
PHAX
PHB
PHC1
PHC2
PHC3
PHF10
PHF12
PHF13
PHF14
PHF2
PHF20
PHF20L1
PHF21A
PHF21B
PHF23
PHF5A
PHF7
PHGDH
PHGR1
PHKG1
PHKG2
PHLDA1
PHLDA2
PHLDA3
PHLDB1
PHLDB2
PHLPP1
PHLPP2
PHOSPHO2
PHOX2A
PHPT1
PHRF1
PHTF1
PHTF2
PHYHD1
PHYHIP
PHYHIPL
PI15
PI16
PI3
PI4K2A
PI4K2B
PI4KA
PI4KB
PIANP
PIAS2
PIAS3
PIAS4
PIBF1
PICALM
PICK1
PID1
PIDD1
PIEZO2
PIF1
PIFO
PIGB
PIGC
PIGF
PIGG
PIGH
PIGK
PIGM
PIGN
PIGO
PIGP
PIGQ
PIGR
PIGS
PIGT
PIGU
PIGV
PIGW
PIGX
PIGZ
PIH1D1
PIH1D2
PIK3AP1
PIK3C2A
PIK3C2B
PIK3C2G
PIK3C3
PIK3CD
PIK3IP1
PIK3R1
PIK3R2
PIK3R3
PIK3R4
PIK3R5
PIK3R6
PIKFYVE
PILRA
PILRB
PIM3

SDHB
SDHC
SDHD
SDK1
SDPR
SDR16C5
SDR42E1
SDR9C7
SDS
SDSL
SEBOX
SEC11A
SEC11C
SEC14L1
SEC14L2
SEC14L3
SEC14L4
SEC16B
SEC22A
SEC22B
SEC22C
SEC31A
SEC31B
SEC61A1
SEC61A2
SEC61B
SEC61G
SEC63
SECISBP2
SECISBP2L
SECTM1
SEH1L
SEL1L
SEL1L3
SELE
SELL
SELP
SEMA3A
SEMA3B
SEMA3C
SEMA3D
SEMA3E
SEMA3F
SEMA3G
SEMA4A
SEMA4B
SEMA4C
SEMA4D
SEMA4F
SEMA5B
SEMA6A
SEMA6B
SEMA6C
SEMA6D
SEMA7A
SEMG1
SEMG2
SENP2
SENP3
SENP5
SENP6
SENP7
SENP8
SEPHS1
SEPHS2
SEPN1
SEPP1
SEPSECS
SEPW1
SERAC1
SERBP1
SERF1A
SERF1B
SERF1B
SERGEF
SERHL2
SERINC1
SERINC2
SERINC3
SERINC5
SERP1
SERP2
SERPINA1
SERPINA10
SERPINA11
SERPINA12
SERPINA2
SERPINA3
SERPINA4
SERPINA5
SERPINA6
SERPINA9
SERPINB10
SERPINB11
SERPINB12
SERPINB13
SERPINB2
SERPINB3
SERPINB5
SERPINB7
SERPINB8

TMEM45A
TMEM45B
TMEM5
TMEM51
TMEM52
TMEM52B
TMEM53
TMEM54
TMEM55A
TMEM55B
TMEM56
TMEM57
TMEM59
TMEM60
TMEM61
TMEM62
TMEM63A
TMEM64
TMEM65
TMEM67
TMEM68
TMEM69
TMEM70
TMEM71
TMEM72
TMEM74
TMEM74B
TMEM79
TMEM80
TMEM81
TMEM82
TMEM86A
TMEM86B
TMEM87A
TMEM87B
TMEM88
TMEM88B
TMEM89
TMEM8A
TMEM8B
TMEM8C
TMEM9
TMEM92
TMEM95
TMEM97
TMEM98
TMEM99
TMF1
TMIE
TMIGD1
TMIGD2
TMOD1
TMPO
TMPPE
TMPRSS11A
TMPRSS11B
TMPRSS11D
TMPRSS11E
TMPRSS11F
TMPRSS12
TMPRSS15
TMPRSS4
TMPRSS5
TMPRSS6
TMPRSS9
TMSB10
TMTC2
TMTC3
TMTC4
TMUB1
TMUB2
TMX1
TMX2
TMX3
TMX4
TNC
TNFAIP1
TNFAIP2
TNFAIP6
TNFAIP8
TNFAIP8L1
TNFAIP8L2
TNFAIP8L3
TNFRSF10A
TNFRSF10B
TNFRSF18
TNFRSF19
TNFRSF1A
TNFRSF1B
TNFRSF21
TNFRSF25
TNFSF12
TNFSF13
TNFSF15
TNFSF18
TNFSF9
TNIP1
TNIP2
TNIP3
TNK1
TNK2

ACVR1B
ACVR1C
ACVR2A
ACVR2B
ACY1
ACY3
ADA
ADAD1
ADAD2
ADAM10
ADAM11
ADAM15
ADAM18
ADAM19
ADAM2
ADAM22
ADAM23
ADAM30
ADAM32
ADAM33
ADAM7
ADAM8
ADAMDEC1
ADAMTS10
ADAMTS12
ADAMTS13
ADAMTS14
ADAMTS15
ADAMTS16
ADAMTS17
ADAMTS19
ADAMTS2
ADAMTS20
ADAMTS4
ADAMTS6
ADAMTS7
ADAMTS8
ADAMTSL2
ADAMTSL3
ADAMTSL4
ADAP1
ADAP2
ADAR
ADARB1
ADARB2
ADAT1
ADAT3
ADCK1
ADCK2
ADCK3
ADCK4
ADCK5
ADCY1
ADCY10
ADCY2
ADCY6
ADCYAP1
ADCYAP1R1
ADD1
ADD2
ADD3
ADGB
ADH1A
ADH1B
ADH1C
ADH4
ADH5
ADH6
ADH7
ADHFE1
ADI1
ADIG
ADIPOQ
ADIPOR1
ADIPOR2
ADIRF
ADK
ADK
ADM
ADM2
ADM5
ADNP
ADNP2
ADO
ADORA1
ADORA2A
ADORA3
ADORA3
ADORA3
ADPGK
ADPRH
ADPRHL1
ADPRHL2
ADPRM
ADRA1A
ADRA1D
ADRA2A
ADRA2C
ADRB2
ADRB3
ADRBK1

CCDC140
CCDC141
CCDC142
CCDC144NL
CCDC146
CCDC148
CCDC149
CCDC15
CCDC150
CCDC151
CCDC154
CCDC155
CCDC157
CCDC158
CCDC159
CCDC166
CCDC167
CCDC168
CCDC169
CCDC170
CCDC171
CCDC172
CCDC173
CCDC174
CCDC175
CCDC176
CCDC177
CCDC178
CCDC179
CCDC18
CCDC180
CCDC181
CCDC184
CCDC185
CCDC186
CCDC23
CCDC24
CCDC25
CCDC27
CCDC28A
CCDC28B
CCDC3
CCDC33
CCDC34
CCDC36
CCDC37
CCDC38
CCDC42
CCDC42B
CCDC43
CCDC47
CCDC50
CCDC51
CCDC53
CCDC54
CCDC57
CCDC58
CCDC59
CCDC6
CCDC60
CCDC63
CCDC64
CCDC65
CCDC66
CCDC67
CCDC68
CCDC69
CCDC7
CCDC70
CCDC71
CCDC71L
CCDC73
CCDC74A
CCDC74B
CCDC77
CCDC8
CCDC80
CCDC81
CCDC82
CCDC83
CCDC84
CCDC85B
CCDC85C
CCDC86
CCDC87
CCDC88B
CCDC89
CCDC9
CCDC90B
CCDC91
CCDC92
CCDC93
CCDC94
CCDC96
CCDC97
CCER1
CCER2
CCHCR1
CCIN
CCK
CCKBR

ECSCR
ECSIT
ECT2
ECT2L
EDARADD
EDC3
EDC4
EDEM1
EDEM2
EDEM3
EDIL3
EDN1
EDN2
EDN3
EDRF1
EEA1
EED
EEF1A1
EEF1A2
EEF1B2
EEF1D
EEF1E1
EEF1G
EEF2
EEF2K
EEF2KMT
EEFSEC
EEPD1
EFCAB1
EFCAB11
EFCAB12
EFCAB13
EFCAB14
EFCAB3
EFCAB5
EFCAB6
EFCAB7
EFCAB9
EFCC1
EFEMP2
EFHB
EFHC1
EFHD1
EFHD2
EFNA1
EFNA2
EFNA3
EFNA4
EFNA5
EFNB2
EFNB3
EFR3A
EFR3B
EFTUD1
EFTUD2
EGFL7
EGFL8
EGFLAM
EGFR
EGLN1
EGR1
EGR2
EGR3
EGR4
EHBP1
EHD1
EHD3
EHD4
EHF
EHMT1
EHMT2
EI24
EID1
EID2
EID2B
EID3
EIF1
EIF1AD
EIF1B
EIF2A
EIF2AK1
EIF2AK2
EIF2AK3
EIF2B1
EIF2B2
EIF2B3
EIF2D
EIF2S1
EIF2S2
EIF3A
EIF3C
EIF3E
EIF3F
EIF3H
EIF3I
EIF3J
EIF3K
EIF3L
EIF3M
EIF4A1
EIF4A2

HMGB4
HMGCL
HMGCS2
HMGN1
HMGN2
HMGN3
HMHB1
HMMR
HMX1
HN1
HN1L
HNF1A
HNF1B
HNF4G
HNRNPA0
HNRNPA1
HNRNPA1L2
HNRNPA2B1
HNRNPA3
HNRNPAB
HNRNPCL1
HNRNPD
HNRNPH1
HNRNPLL
HNRNPR
HNRNPU
HNRNPUL1
HNRNPUL1
HOGA1
HOMER1
HOMEZ
HOOK1
HOOK2
HOOK3
HORMAD1
HORMAD2
HOXB13
HOXC12
HOXD12
HP
HP1BP3
HPCA
HPCAL1
HPCAL4
HPD
HPDL
HPGDS
HPN
HPR
HPS1
HPS1
HPS3
HPS4
HPS5
HPS6
HPSE
HPSE2
HPX
HRAS
HRASLS2
HRASLS5
HRC
HRCT1
HRG
HRH3
HRSP12
HS1BP3
HS2ST1
HS3ST1
HS3ST2
HS3ST3A1
HS3ST3B1
HS3ST4
HS3ST5
HS3ST6
HS6ST1
HS6ST3
HSBP1
HSBP1L1
HSCB
HSD11B1
HSD11B1L
HSD11B2
HSD17B1
HSD17B11
HSD17B13
HSD17B14
HSD17B2
HSD17B3
HSD17B4
HSD17B6
HSD17B7
HSD17B8
HSD3B1
HSD3B2
HSDL1
HSDL2
HSF1
HSF2
HSF2BP
HSF4

MIOS
MIOX
MIP
MIPOL1
MIS12
MIS18A
MISP
MITD1
MITF
MKI67
MKL1
MKL2
MKLN1
MKNK1
MKNK2
MKRN1
MKRN2
MKRN2OS
MKRN3
MKS1
MKX
MLC1
MLEC
MLF1
MLH1
MLH3
MLIP
MLKL
MLLT1
MLLT11
MLLT3
MLLT6
MLNR
MLPH
MLST8
MLX
MLXIP
MLXIPL
MLYCD
MMACHC
MMADHC
MMD2
MME
MMEL1
MMP1
MMP11
MMP12
MMP13
MMP14
MMP15
MMP16
MMP17
MMP19
MMP23B
MMP24
MMP25
MMP26
MMP27
MMP28
MMP3
MMP8
MMRN1
MMRN2
MMS22L
MN1
MNAT1
MND1
MNDA
MNS1
MNT
MOB1A
MOB1B
MOB2
MOB3A
MOB3B
MOB3C
MOB4
MOBP
MOCS1
MOCS3
MOG
MOGAT1
MOGAT2
MOGAT3
MOGS
MON1A
MON1B
MON2
MORC2
MORC3
MORF4L1
MORN1
MORN3
MORN4
MORN5
MOS
MOSPD3
MOV10
MOV10L1
MOXD1
MPC1

PINK1
PINLYP
PINX1
PIP
PIP4K2A
PIP4K2B
PIP4K2C
PIP5K1A
PIP5K1B
PIP5K1C
PIP5KL1
PIPOX
PIRT
PITHD1
PITPNC1
PITPNM1
PITPNM2
PITPNM3
PIWIL3
PIWIL4
PJA2
PKD1L1
PKD1L3
PKD2
PKD2L1
PKD2L2
PKDREJ
PKHD1
PKHD1L1
PKIA
PKLR
PKMYT1
PKN1
PKN1
PKN2
PKN3
PKP1
PKP2
PKP3
PLA2G10
PLA2G12B
PLA2G15
PLA2G16
PLA2G2A
PLA2G2C
PLA2G2E
PLA2G2F
PLA2G3
PLA2G4A
PLA2G4B
PLA2G4D
PLA2G4F
PLA2G5
PLA2G6
PLAA
PLAC8
PLAC9
PLAG1
PLAGL2
PLAT
PLAU
PLAUR
PLBD1
PLBD2
PLCD3
PLCE1
PLCG1
PLCH1
PLCH2
PLCL1
PLCXD1
PLCXD2
PLCZ1
PLD1
PLD2
PLD3
PLD4
PLD5
PLD6
PLEC
PLEK
PLEKHA1
PLEKHA2
PLEKHA3
PLEKHA5
PLEKHA6
PLEKHA7
PLEKHA8
PLEKHB2
PLEKHD1
PLEKHF1
PLEKHF2
PLEKHG2
PLEKHG3
PLEKHG4
PLEKHG4B
PLEKHG5
PLEKHG6
PLEKHG7
PLEKHH2
PLEKHH3

SERPINC1
SERPIND1
SERPINE1
SERPINE2
SERPINE3
SERPINF1
SERPINF2
SERPING1
SERPINI2
SERTAD1
SERTAD2
SERTAD3
SERTAD4
SERTM1
SESN1
SESN3
SESTD1
SET
SETBP1
SETD1A
SETD2
SETD3
SETD4
SETD6
SETD7
SETD8
SETD9
SETDB2
SETMAR
SETSIP
SETX
SEZ6L2
SF1
SF3A1
SF3A3
SF3B3
SF3B4
SF3B5
SF3B6
SFI1
SFMBT1
SFMBT2
SFN
SFPQ
SFR1
SFRP1
SFRP4
SFRP5
SFSWAP
SFT2D1
SFT2D2
SFT2D3
SFTA2
SFTA3
SFTPA1
SFTPA2
SFTPB
SFTPC
SFXN1
SFXN3
SFXN5
SGCA
SGCG
SGCZ
SGIP1
SGMS1
SGMS2
SGOL1
SGOL2
SGPL1
SGPP1
SGSH
SGSM2
SGSM3
SGTA
SGTB
SH2B1
SH2B2
SH2B3
SH2D1B
SH2D2A
SH2D3A
SH2D3C
SH2D4A
SH2D6
SH2D7
SH3BGR
SH3BP1
SH3BP2
SH3BP5
SH3BP5L
SH3D19
SH3D21
SH3GL1
SH3GL2
SH3GL3
SH3GLB1
SH3PXD2A
SH3RF1
SH3RF2
SH3RF3

TNKS
TNKS1BP1
TNKS2
TNNC2
TNNI1
TNNI2
TNNI3K
TNNT1
TNNT2
TNNT3
TNP1
TNP2
TNPO1
TNPO2
TNPO3
TNR
TNRC6C
TNS1
TNS2
TNS3
TNS4
TNXB
TOB2
TOE1
TOLLIP
TOM1
TOM1L1
TOMM20
TOMM20L
TOMM34
TOMM40L
TOMM7
TONSL
TOP1MT
TOP3B
TOPAZ1
TOPBP1
TOPORS
TOR1A
TOR1AIP1
TOR1AIP2
TOR1B
TOR2A
TOR3A
TOR4A
TOX
TOX4
TP53
TP53AIP1
TP53BP2
TP53BP2
TP53I11
TP53I13
TP53I3
TP53INP2
TP53RK
TP53TG3
TP53TG3B
TP53TG3C
TP53TG3D
TP53TG5
TP63
TP73
TPBGL
TPCN1
TPCN2
TPD52
TPD52L3
TPGS1
TPGS2
TPH1
TPH2
TPI1
TPK1
TPM1
TPM2
TPM3
TPM4
TPO
TPPP
TPPP2
TPPP3
TPR
TPRG1
TPRG1L
TPRKB
TPRX1
TPSAB1
TPSB2
TPST1
TPST2
TPTE2
TRA2A
TRA2B
TRABD
TRABD2A
TRABD2B
TRAF1
TRAF2
TRAF3
TRAF3IP1

ADRBK2
ADSL
ADSS
ADTRP
AEBP1
AEBP2
AEN
AES
AFAP1L1
AFAP1L2
AFF1
AFF3
AFF4
AFG3L2
AFTPH
AGA
AGAP1
AGAP2
AGAP3
AGAP4
AGAP6
AGBL1
AGBL2
AGBL3
AGBL4
AGBL5
AGER
AGFG1
AGFG2
AGGF1
AGK
AGL
AGMAT
AGMO
AGO3
AGO4
AGPAT1
AGPAT2
AGPAT3
AGPAT4
AGPAT5
AGPAT6
AGPAT9
AGR2
AGR3
AGRN
AGT
AGTPBP1
AGTRAP
AGXT
AGXT2
AHCTF1
AHCY
AHI1
AHNAK
AHNAK2
AHR
AHRR
AHSA1
AHSA2
AHSG
AHSP
AICDA
AIDA
AIF1L
AIFM2
AIFM3
AIG1
AIM2
AIMP1
AIMP2
AIPL1
AJAP1
AK2
AK3
AK4
AK5
AK8
AK9
AKAP10
AKAP11
AKAP13
AKAP17A
AKAP2
AKAP3
AKAP6
AKAP7
AKAP8
AKAP8L
AKAP9
AKIP1
AKIRIN1
AKIRIN2
AKNA
AKNAD1
AKR1A1
AKR1B1
AKR1B10
AKR1C1
AKR1C2
AKR1C3

CCL1
CCL11
CCL13
CCL14
CCL16
CCL17
CCL18
CCL19
CCL2
CCL20
CCL21
CCL22
CCL23
CCL23
CCL24
CCL25
CCL26
CCL27
CCL28
CCL3
CCL3L3
CCL4
CCL4L1
CCL5
CCL7
CCL8
CCM2
CCM2L
CCNA1
CCNA2
CCNB1
CCNB1IP1
CCNB1IP1
CCNB1IP1
CCNB2
CCNC
CCND1
CCND2
CCND3
CCNDBP1
CCNE1
CCNE2
CCNF
CCNG1
CCNG2
CCNH
CCNI
CCNI2
CCNJ
CCNJL
CCNL1
CCNL2
CCNO
CCNT1
CCNT2
CCNY
CCNYL1
CCP110
CCPG1
CCR1
CCR10
CCR5
CCR8
CCRN4L
CCS
CCSAP
CCSER1
CCSER2
CCT2
CCT3
CCT6A
CCT6B
CCZ1
CCZ1B
CD101
CD109
CD14
CD151
CD160
CD163
CD163
CD163L1
CD164
CD164L2
CD177
CD180
CD1A
CD1B
CD1C
CD1D
CD1E
CD2
CD200R1
CD200R1L
CD207
CD209
CD22
CD226
CD24
CD244
CD247

EIF4A3
EIF4B
EIF4E
EIF4E1B
EIF4E2
EIF4E3
EIF4EBP1
EIF4EBP2
EIF4EBP3
EIF4ENIF1
EIF4G1
EIF4G2
EIF4G3
EIF4H
EIF5
EIF5A
EIF5AL1
EIF5B
EIF6
ELANE
ELAVL1
ELAVL2
ELAVL3
ELAVL4
ELF1
ELF2
ELF3
ELF5
ELFN1
ELFN2
ELK3
ELK4
ELL
ELL2
ELL3
ELMO1
ELMO3
ELMOD1
ELMOD2
ELMOD3
ELMSAN1
ELN
ELOF1
ELOVL1
ELOVL3
ELOVL5
ELOVL6
ELP2
ELP3
ELP4
ELP5
ELTD1
EMB
EMC1
EMC10
EMC2
EMC3
EMC4
EMC6
EMC7
EMC8
EMC9
EMCN
EME1
EMG1
EMID1
EMILIN1
EMILIN2
EML1
EML2
EML3
EML4
EMP1
EMP2
EMP3
EMR3
EMX2
EN2
ENAH
ENAM
ENC1
ENDOD1
ENDOG
ENDOV
ENHO
ENKD1
ENKUR
ENO1
ENO4
ENOPH1
ENOSF1
ENOX1
ENPP6
ENPP7
ENSA
ENTHD1
ENTHD2
ENTPD1
ENTPD2
ENTPD3
ENTPD4

HSH2D
HSP90AA1
HSP90AB1
HSP90B1
HSPA12A
HSPA12B
HSPA14
HSPA4
HSPA4L
HSPA6
HSPA9
HSPB11
HSPB6
HSPB7
HSPB8
HSPB9
HSPBAP1
HSPBP1
HSPD1
HSPE1
HSPG2
HTATIP2
HTN3
HTR1A
HTR1B
HTR1D
HTR1E
HTR1F
HTR2A
HTR2B
HTR3A
HTR3B
HTR3C
HTR3D
HTR3E
HTR4
HTR5A
HTR6
HTR7
HTRA1
HTRA2
HTRA3
HTRA4
HTT
HUNK
HUS1
HUS1B
HVCN1
HYAL2
HYAL3
HYAL4
HYI
HYKK
HYLS1
HYOU1
HYPK
IAH1
IAPP
IARS
IARS2
IBA57
IBTK
ICA1
ICA1L
ICAM4
ICAM5
ICE2
ICK
ICMT
ICOS
ICOSLG
ICT1
ID1
ID2
ID3
ID4
IDE
IDH3A
IDI1
IDI2
IDNK
IDO1
IDO2
IDUA
IER2
IER3IP1
IER5
IFFO1
IFFO2
IFI16
IFI27
IFI27L1
IFI27L2
IFI30
IFI35
IFI44
IFI44L
IFI6
IFIH1
IFIT1
IFIT1B

MPC2
MPDZ
MPEG1
MPHOSPH10
MPHOSPH6
MPHOSPH8
MPL
MPLKIP
MPND
MPP2
MPP3
MPP5
MPP7
MPPE1
MPPED1
MPPED2
MPRIP
MPV17
MPV17L
MPV17L2
MPZ
MPZL1
MPZL2
MPZL3
MR1
MRAP
MRAP2
MRC1
MRE11A
MREG
MRFAP1
MRGBP
MRGPRD
MRGPRF
MRGPRX1
MRGPRX2
MRGPRX3
MRGPRX4
MRI1
MRM1
MRO
MROH1
MROH2B
MROH5
MROH6
MROH8
MROH9
MRPL1
MRPL10
MRPL11
MRPL12
MRPL13
MRPL14
MRPL15
MRPL16
MRPL17
MRPL19
MRPL20
MRPL23
MRPL24
MRPL3
MRPL32
MRPL33
MRPL34
MRPL35
MRPL36
MRPL37
MRPL38
MRPL39
MRPL40
MRPL41
MRPL42
MRPL44
MRPL45
MRPL46
MRPL47
MRPL48
MRPL49
MRPL50
MRPL51
MRPL52
MRPL53
MRPL54
MRPL57
MRPL9
MRPS11
MRPS14
MRPS15
MRPS17
MRPS18A
MRPS21
MRPS22
MRPS23
MRPS24
MRPS25
MRPS26
MRPS27
MRPS28
MRPS30
MRPS33
MRPS34

PLEKHJ1
PLEKHM1
PLEKHM2
PLEKHM3
PLEKHN1
PLEKHO1
PLEKHO2
PLEKHS1
PLET1
PLG
PLGLB2
PLGRKT
PLIN1
PLIN2
PLIN3
PLIN5
PLK1
PLK2
PLK3
PLN
PLOD1
PLOD2
PLRG1
PLS1
PLSCR1
PLSCR2
PLSCR4
PLTP
PLVAP
PLXDC1
PLXDC2
PLXNA1
PLXNA2
PLXNA4
PLXNB1
PLXNB2
PLXND1
PM20D1
PM20D2
PMAIP1
PMCH
PMEL
PMEPA1
PMF1
PMFBP1
PML
PMM1
PMM2
PMP2
PMP22
PMPCA
PMPCB
PMS2
PMVK
PNISR
PNKP
PNLDC1
PNLIP
PNLIPRP1
PNLIPRP2
PNMA1
PNMA2
PNMAL1
PNMAL2
PNMT
PNN
PNO1
PNOC
PNPLA1
PNPLA2
PNPLA3
PNPLA5
PNPLA6
PNPLA7
PNPLA8
PNPO
PNPT1
PNRC1
PNRC2
POC1A
POC1B
POC5
PODN
PODNL1
PODXL
PODXL2
POFUT1
POFUT2
POGK
POGLUT1
POGZ
POLA2
POLB
POLD2
POLD3
POLD4
POLDIP2
POLDIP3
POLE
POLE2
POLE3

SH3TC1
SH3TC2
SH3YL1
SHANK1
SHANK2
SHARPIN
SHBG
SHC1
SHC3
SHC4
SHCBP1
SHCBP1L
SHD
SHE
SHF
SHFM1
SHFM1
SHH
SHISA2
SHISA3
SHISA4
SHISA5
SHISA6
SHISA7
SHISA8
SHISA9
SHKBP1
SHMT1
SHMT2
SHOC2
SHOX
SHPRH
SHQ1
SHROOM1
SHROOM3
SI
SIAE
SIAH2
SIAH3
SIDT1
SIGIRR
SIGLEC1
SIGLEC10
SIGLEC11
SIGLEC12
SIGLEC14
SIGLEC15
SIGLEC5
SIGLEC6
SIGLEC7
SIGLEC8
SIGLEC9
SIGLECL1
SIGMAR1
SIK1
SIK2
SIK3
SIKE1
SIL1
SIM1
SIM2
SIMC1
SIN3A
SIN3B
SIPA1
SIPA1L1
SIRPA
SIRPB1
SIRPD
SIRPG
SIRT4
SIRT7
SIT1
SIVA1
SIX3
SIX5
SKA1
SKA2
SKA3
SKAP1
SKI
SKIDA1
SKIL
SKOR2
SKP1
SKP2
SLA2
SLAIN1
SLAIN2
SLAMF6
SLAMF7
SLAMF8
SLAMF9
SLBP
SLC10A4
SLC10A6
SLC10A7
SLC11A1
SLC12A2
SLC12A4
SLC12A6

TRAF5
TRAF6
TRAF7
TRAFD1
TRAIP
TRAK1
TRAK2
TRAM1
TRAM1L1
TRAM2
TRANK1
TRAP1
TRAPPC1
TRAPPC10
TRAPPC11
TRAPPC12
TRAPPC13
TRAPPC2L
TRAPPC3
TRAPPC4
TRAPPC6A
TRAPPC6B
TRAPPC8
TRAPPC9
TRAT1
TRDMT1
TREH
TREM1
TREM2
TREML1
TREML2
TRERF1
TREX1
TRH
TRHDE
TRIAP1
TRIB1
TRIB2
TRIB3
TRIL
TRIM11
TRIM13
TRIM14
TRIM15
TRIM16
TRIM16L
TRIM17
TRIM21
TRIM22
TRIM23
TRIM24
TRIM25
TRIM26
TRIM28
TRIM29
TRIM3
TRIM32
TRIM33
TRIM34
TRIM35
TRIM36
TRIM37
TRIM39
TRIM4
TRIM41
TRIM42
TRIM43
TRIM44
TRIM45
TRIM46
TRIM49
TRIM49C
TRIM49D1
TRIM49D2
TRIM5
TRIM50
TRIM51
TRIM52
TRIM54
TRIM55
TRIM56
TRIM58
TRIM59
TRIM6
TRIM60
TRIM62
TRIM63
TRIM65
TRIM67
TRIM68
TRIM6-TRIM34
TRIM7
TRIM71
TRIM72
TRIM74
TRIM77
TRIM8
TRIM9
TRIML1
TRIML2
TRIO

AKR1C4
AKR1D1
AKR7A2
AKR7A3
AKT1
AKT1S1
AKT2
AKT3
AKTIP
ALB
ALCAM
ALDH16A1
ALDH18A1
ALDH1L1
ALDH2
ALDH3A1
ALDH3B1
ALDH3B2
ALDH7A1
ALDOA
ALG1
ALG10
ALG10B
ALG11
ALG12
ALG14
ALG1L
ALG1L2
ALG2
ALG3
ALG5
ALG6
ALG8
ALG9
ALK
ALKBH1
ALKBH2
ALKBH3
ALKBH4
ALKBH5
ALKBH6
ALKBH7
ALKBH8
ALMS1
ALOX5AP
ALPI
ALPK1
ALPK2
ALPK3
ALPL
ALPP
ALPPL2
ALS2
ALS2CL
ALS2CR11
ALS2CR12
ALX1
ALX3
ALYREF
AMACR
AMBN
AMBP
AMBRA1
AMDHD1
AMDHD2
AMER2
AMER3
AMH
AMHR2
AMICA1
AMIGO1
AMIGO2
AMIGO3
AMMECR1L
AMOTL1
AMOTL2
AMPD3
AMPH
AMT
AMTN
AMY1A
AMY1B
AMY1C
AMY2A
AMY2B
AMZ1
AMZ2
ANAPC1
ANAPC10
ANAPC11
ANAPC13
ANAPC15
ANAPC16
ANAPC2
ANAPC4
ANAPC7
ANG
ANGEL1
ANGEL2
ANGPT1
ANGPT2
CD248
CD274
CD276
CD28
CD2BP2
CD300A
CD300C
CD300E
CD300LB
CD300LD
CD300LF
CD300LG
CD302
CD320
CD33
CD34
CD36
CD38
CD3D
CD3E
CD3EAP
CD3G
CD4
CD40
CD44
CD46
CD47
CD48
CD5
CD52
CD53
CD55
CD58
CD59
CD5L
CD6
CD68
CD7
CD72
CD74
CD80
CD81
CD84
CD86
CD8A
CD93
CD97
CD99
CDA
CDADC1
CDC123
CDC14A
CDC14B
CDC16
CDC20
CDC20B
CDC25A
CDC26
CDC34
CDC37
CDC37L1
CDC40
CDC42
CDC42BPA
CDC42BPB
CDC42EP1
CDC42EP2
CDC42EP3
CDC42EP4
CDC42EP5
CDC42SE1
CDC42SE2
CDC45
CDC7
CDC73
CDCA2
CDCA3
CDCA4
CDCA5
CDCA7
CDCA7L
CDCA8
CDCP1
CDCP2
CDH1
CDH10
CDH12
CDH13
CDH15
CDH16
CDH17
CDH18
CDH19
CDH2
CDH20
CDH22
CDH23
CDH24
CDH26
CDH3
CDH4
ENTPD5
ENTPD7
ENTPD8
ENY2
EOGT
EOMES
EP300
EP400
EPAS1
EPB41
EPB41L1
EPB41L3
EPB41L4B
EPB41L5
EPB42
EPC2
EPDR1
EPG5
EPHA10
EPHA2
EPHA3
EPHA5
EPHA6
EPHA8
EPHB1
EPHB2
EPHB3
EPHB4
EPHX1
EPHX3
EPHX4
EPM2AIP1
EPN1
EPN2
EPN3
EPO
EPPK1
EPRS
EPS15
EPS15L1
EPS8L1
EPS8L2
EPS8L3
EPSTI1
EPX
EPYC
EQTN
ERAP1
ERAP2
ERBB2
ERBB2IP
ERBB3
ERBB4
ERC2
ERCC1
ERCC2
ERCC3
ERCC4
ERCC6
ERCC6L2
ERCC8
ERF
ERG
ERGIC2
ERGIC3
ERH
ERI1
ERI2
ERI3
ERICH1
ERICH3
ERICH4
ERICH5
ERICH6
ERICH6B
ERLEC1
ERLIN1
ERLIN2
ERMAP
ERMARD
ERMN
ERMP1
ERN1
ERO1L
ERO1LB
ERP27
ERRFI1
ERV3-1
ERVFRD-1
ERVMER34-1
ERVV-1
ERVV-2
ERVW-1
ESAM
ESCO1
ESCO2
ESF1
ESM1
ESPL1
ESPN
ESPNL
IFIT2
IFIT3
IFIT5
IFITM1
IFITM10
IFITM2
IFITM3
IFITM5
IFNA1
IFNA10
IFNA13
IFNA14
IFNA16
IFNA17
IFNA2
IFNA21
IFNA4
IFNA5
IFNA6
IFNA7
IFNA8
IFNB1
IFNE
IFNK
IFNL1
IFNL2
IFNL3
IFNL4
IFNLR1
IFNW1
IFRD1
IFRD2
IFT122
IFT140
IFT172
IFT20
IFT22
IFT27
IFT43
IFT46
IFT52
IFT57
IFT74
IFT80
IFT81
IFT88
IGDCC3
IGDCC4
IGF1
IGF1R
IGF2
IGF2BP1
IGF2BP2
IGF2BP3
IGF2R
IGFBP1
IGFBP2
IGFBP3
IGFBP4
IGFBP5
IGFL1
IGFL2
IGFL3
IGFL4
IGFLR1
IGHMBP2
IGIP
IGJ
IGLL1
IGLL5
IGLON5
IGSF10
IGSF21
IGSF22
IGSF23
IGSF3
IGSF5
IGSF8
IGSF9
IHH
IK
IKBIP
IKZF1
IKZF2
IKZF3
IKZF4
IL10
IL11
IL11RA
IL12A
IL12B
IL12RB2
IL13
IL15
IL15RA
IL15RA
IL16
IL17A
IL17B
IL17C
IL17D
MRPS35
MRPS36
MRPS5
MRPS6
MRPS7
MRPS9
MRRF
MRTO4
MRVI1
MS4A10
MS4A13
MSANTD2
MSANTD3
MSANTD4
MSC
MSH3
MSH4
MSH6
MSI1
MSL1
MSL2
MSMB
MSMB
MSMO1
MSMP
MSRA
MSRB1
MSRB2
MSRB3
MST1
MSTN
MSTO1
MT1A
MT1B
MT1E
MT1F
MT1G
MT1H
MT1M
MT1X
MT2A
MT3
MT4
MTA2
MTA3
MTAP
MTBP
MTCH1
MTCH2
MTCL1
MTERF1
MTERF2
MTERF3
MTERF4
MTF1
MTF2
MTFMT
MTFP1
MTFR1
MTFR1L
MTFR2
MTG1
MTG2
MTHFD1L
MTHFR
MTHFS
MTHFSD
MTIF2
MTIF3
MTL5
MTMR10
MTMR11
MTMR14
MTMR2
MTMR3
MTMR4
MTMR6
MTMR7
MTMR9
MTO1
MTOR
MTPAP
MTPN
MTR
MTRF1
MTRF1L
MTRNR2L1
MTRNR2L12
MTRNR2L3
MTRNR2L4
MTRNR2L5
MTRNR2L6
MTRNR2L7
MTRNR2L8
MTSS1
MTSS1L
MTURN
MTX1
MTX2
MUC1
MUC13
POLE4
POLG
POLG2
POLH
POLI
POLK
POLL
POLM
POLN
POLQ
POLR1A
POLR1B
POLR1D
POLR1D
POLR1E
POLR2A
POLR2B
POLR2C
POLR2D
POLR2E
POLR2F
POLR2G
POLR2H
POLR2I
POLR2J
POLR2J3
POLR2K
POLR2L
POLR3A
POLR3B
POLR3C
POLR3D
POLR3E
POLR3F
POLR3G
POLR3GL
POLR3H
POLR3K
POLRMT
POM121C
POM121L12
POM121L2
POMC
POMGNT1
POMGNT2
POMK
POMP
POMT1
POMT2
POMZP3
PON1
PON2
PON3
POP1
POP4
POP5
POP7
POPDC2
POPDC3
POR
POSTN
POTEB3
POTED
POTEE
POTEF
POTEG
POTEH
POTEM
POU1F1
POU2AF1
POU2F1
POU3F1
POU4F2
POU4F3
POU5F1
POU5F1B
POU5F2
POU6F1
POU6F2
PPA1
PPA2
PPAN
PPAN-P2RY11
PPAP2B
PPAPDC1B
PPAPDC2
PPAPDC3
PPARA
PPARD
PPARG
PPARGC1A
PPARGC1B
PPAT
PPBP
PPCDC
PPCS
PPEF2
PPFIA1
PPFIA3
PPFIA4
PPFIBP1
SLC12A7
SLC12A8
SLC12A9
SLC13A1
SLC13A2
SLC13A4
SLC13A5
SLC14A1
SLC15A1
SLC15A2
SLC15A3
SLC15A4
SLC16A1
SLC16A11
SLC16A12
SLC16A14
SLC16A3
SLC16A4
SLC16A5
SLC16A6
SLC16A7
SLC16A8
SLC16A9
SLC17A6
SLC17A8
SLC17A9
SLC18A2
SLC18A3
SLC18B1
SLC19A2
SLC1A2
SLC1A3
SLC1A4
SLC1A6
SLC1A7
SLC20A1
SLC22A10
SLC22A11
SLC22A12
SLC22A13
SLC22A14
SLC22A15
SLC22A16
SLC22A17
SLC22A18
SLC22A2
SLC22A23
SLC22A24
SLC22A25
SLC22A3
SLC22A31
SLC22A4
SLC22A5
SLC22A6
SLC22A8
SLC22A9
SLC23A1
SLC23A3
SLC24A1
SLC24A2
SLC24A3
SLC24A4
SLC24A5
SLC25A1
SLC25A11
SLC25A12
SLC25A13
SLC25A15
SLC25A17
SLC25A18
SLC25A19
SLC25A2
SLC25A20
SLC25A21
SLC25A23
SLC25A24
SLC25A25
SLC25A26
SLC25A27
SLC25A28
SLC25A3
SLC25A31
SLC25A32
SLC25A33
SLC25A34
SLC25A35
SLC25A36
SLC25A37
SLC25A38
SLC25A39
SLC25A4
SLC25A40
SLC25A41
SLC25A42
SLC25A44
SLC25A45
SLC25A46
SLC25A48
SLC25A51
SLC25A6
SLC26A1
TRIP12
TRIP13
TRIP4
TRIP6
TRIQK
TRIT1
TRMT1
TRMT10A
TRMT10B
TRMT10C
TRMT112
TRMT12
TRMT13
TRMT1L
TRMT2A
TRMT44
TRMT61A
TRMT61B
TRMU
TRNAU1AP
TRNP1
TROAP
TROVE2
TRPA1
TRPC1
TRPC3
TRPC4
TRPC4AP
TRPC6
TRPC7
TRPM1
TRPM2
TRPM3
TRPM4
TRPM5
TRPM6
TRPM7
TRPM8
TRPS1
TRPT1
TRPV1
TRPV2
TRPV3
TRPV4
TRPV5
TRRAP
TRUB1
TRUB2
TSACC
TSC2
TSC22D1
TSC22D2
TSC22D4
TSEN2
TSEN34
TSEN54
TSFM
TSG101
TSGA10
TSGA10IP
TSGA13
TSHB
TSHR
TSHZ1
TSHZ2
TSHZ3
TSKS
TSKU
TSLP
TSN
TSNARE1
TSNAX
TSNAXIP1
TSPAN1
TSPAN10
TSPAN12
TSPAN13
TSPAN14
TSPAN15
TSPAN16
TSPAN18
TSPAN19
TSPAN2
TSPAN3
TSPAN33
TSPAN5
TSPAN8
TSPAN9
TSPEAR
TSPYL5
TSR1
TSR3
TSSC1
TSSC4
TSSK1B
TSSK4
TSSK6
TSTA3
TSTD1
TSTD2
TTBK2

ANGPT4
ANGPTL1
ANGPTL2
ANGPTL3
ANGPTL4
ANGPTL5
ANGPTL6
ANGPTL7
ANK1
ANK2
ANK3
ANKAR
ANKDD1A
ANKEF1
ANKFN1
ANKFY1
ANKH
ANKHD1
ANKHD1-EIF4EBP3
ANKK1
ANKLE1
ANKMY1
ANKMY2
ANKRA2
ANKRD1
ANKRD11
ANKRD12
ANKRD13A
ANKRD13B
ANKRD13C
ANKRD13D
ANKRD17
ANKRD20A2
ANKRD20A4
ANKRD22
ANKRD23
ANKRD27
ANKRD28
ANKRD29
ANKRD30A
ANKRD30B
ANKRD31
ANKRD32
ANKRD33
ANKRD34B
ANKRD34C
ANKRD35
ANKRD36B
ANKRD37
ANKRD39
ANKRD40
ANKRD42
ANKRD44
ANKRD45
ANKRD46
ANKRD49
ANKRD50
ANKRD52
ANKRD53
ANKRD54
ANKRD55
ANKRD66
ANKS1B
ANKS3
ANKS4B
ANKS6
ANKUB1
ANKZF1
ANLN
ANO1
ANO10
ANO3
ANO4
ANO5
ANO7
ANO9
ANP32B
ANP32D
ANP32E
ANTXR1
ANTXR2
ANXA1
ANXA10
ANXA11
ANXA13
ANXA2
ANXA2R
ANXA3
ANXA4
ANXA5
ANXA6
ANXA7
ANXA8
ANXA9
AOAH
AOC1
AOC2
AOC2
AOC3
AOX1

CDH5
CDH6
CDH7
CDH8
CDH9
CDHR1
CDHR2
CDHR3
CDHR4
CDHR5
CDIP1
CDIPT
CDK1
CDK11A
CDK11B
CDK12
CDK13
CDK14
CDK17
CDK18
CDK19
CDK20
CDK2AP1
CDK2AP2
CDK4
CDK5R1
CDK5R2
CDK5RAP1
CDK5RAP2
CDK5RAP3
CDK7
CDKAL1
CDKL2
CDKL3
CDKN1A
CDKN1B
CDKN1C
CDKN2A
CDKN2AIP
CDKN2AIPNL
CDKN2B
CDKN2C
CDKN2D
CDNF
CDO1
CDON
CDPF1
CDR2L
CDRT1
CDRT15
CDT1
CDV3
CDX1
CDYL
CDYL2
CEACAM1
CEACAM19
CEACAM21
CEACAM3
CEACAM4
CEACAM5
CEACAM7
CEBPA
CEBPB
CEBPD
CEBPE
CEBPG
CEBPZ
CECR2
CECR5
CECR6
CELA1
CELA2A
CELA2B
CELA3A
CELA3B
CELF1
CELF3
CELF4
CELF5
CELF6
CELSR1
CELSR2
CELSR3
CEMIP
CEMP1
CEND1
CENPA
CENPB
CENPBD1
CENPF
CENPJ
CENPK
CENPL
CENPM
CENPN
CENPO
CENPP
CENPQ
CENPT

ESRP1
ESRP2
ESRRA
ESRRG
ESYT1
ESYT2
ESYT3
ETAA1
ETF1
ETFA
ETHE1
ETNK1
ETNK2
ETNPPL
ETS1
ETV1
ETV3
ETV3L
ETV4
ETV5
ETV6
ETV7
EVA1A
EVA1B
EVA1C
EVC2
EVI2A
EVI2B
EVI5
EVI5L
EVPL
EVPLL
EWSR1
EXD1
EXD3
EXO1
EXO5
EXOC1
EXOC2
EXOC3
EXOC3L1
EXOC3L2
EXOC4
EXOC5
EXOC6
EXOC7
EXOC8
EXOG
EXOSC10
EXOSC2
EXOSC3
EXOSC4
EXOSC5
EXOSC6
EXOSC7
EXOSC8
EXOSC9
EXPH5
EXT1
EXT2
EXTL1
EXTL2
EXTL3
EYA1
EYA1
EYA2
EYA3
EYA4
EZH1
EZH2
EZR
F11R
F13A1
F13B
F3
F5
F7
FA2H
FAAH
FABP1
FABP12
FABP2
FABP3
FABP4
FABP5
FABP6
FABP7
FABP9
FADD
FADS1
FADS2
FAF1
FAF2
FAHD1
FAHD2A
FAHD2B
FAIM
FAIM2
FAIM3
FAM101A

IL17F
IL17RA
IL17RC
IL17RD
IL17RE
IL17REL
IL18
IL18BP
IL18R1
IL18RAP
IL19
IL1A
IL1B
IL1F10
IL1R2
IL1RAP
IL1RL1
IL1RL2
IL1RN
IL20
IL20RA
IL20RB
IL21
IL21R
IL22
IL23A
IL23R
IL24
IL26
IL27
IL27RA
IL2RA
IL3
IL31
IL31RA
IL32
IL33
IL34
IL36A
IL36B
IL36G
IL36RN
IL37
IL4
IL5
IL6
IL6R
IL6ST
IL9
IL9R
ILDR1
ILDR2
ILF2
ILK
ILKAP
ILVBL
IMMP1L
IMMP2L
IMMT
IMP3
IMP4
IMPACT
IMPAD1
IMPDH1
IMPG1
INA
INAFM1
INCA1
INCENP
INF2
ING1
ING2
ING3
ING5
INHBC
INHBE
INIP
INMT
INO80
INO80B
INO80C
INO80D
INO80E
INPP4A
INPP4B
INPP5A
INPP5B
INPP5D
INPP5E
INPP5F
INPP5J
INPPL1
INS
INSC
INSIG1
INSIG2
INSL3
INSL4
INSL5
INSL6

MUC15
MUC16
MUC17
MUC2
MUC20
MUC21
MUC22
MUC4
MUC7
MUCL1
MUL1
MUM1
MURC
MUS81
MUTYH
MVB12A
MVD
MVK
MVP
MX2
MXD1
MXD4
MXI1
MXRA7
MXRA8
MYADM
MYBBP1A
MYBL2
MYBPC2
MYBPH
MYBPHL
MYCBP
MYCBP2
MYCBPAP
MYCL
MYCN
MYCT1
MYD88
MYDGF
MYEF2
MYEOV2
MYF5
MYF6
MYH1
MYH11
MYH13
MYH14
MYH2
MYH3
MYH4
MYH7
MYH7B
MYH8
MYH9
MYL1
MYL10
MYL12A
MYL12B
MYL2
MYL3
MYL4
MYL5
MYL6B
MYL7
MYL9
MYLIP
MYLK
MYLK2
MYLK3
MYLK4
MYLPF
MYNN
MYO10
MYO15A
MYO16
MYO18A
MYO18B
MYO19
MYO1A
MYO1B
MYO1E
MYO3A
MYO5A
MYO5C
MYO6
MYO7A
MYO9A
MYOC
MYOCD
MYOD1
MYOF
MYOG
MYOM1
MYOM2
MYOM3
MYOT
MYOZ3
MYPN
MYPOP
MYRF

PPFIBP2
PPHLN1
PPIA
PPIAL4A
PPIAL4B
PPIAL4B
PPIAL4C
PPIAL4D
PPIAL4E
PPIAL4F
PPIAL4G
PPIC
PPID
PPIE
PPIF
PPIH
PPIP5K1
PPIP5K2
PPL
PPM1A
PPM1B
PPM1D
PPM1E
PPM1F
PPM1H
PPM1J
PPM1K
PPM1L
PPM1M
PPM1N
PPME1
PPOX
PPP1CA
PPP1R10
PPP1R11
PPP1R12A
PPP1R12C
PPP1R13B
PPP1R13L
PPP1R14A
PPP1R14B
PPP1R14C
PPP1R14D
PPP1R15A
PPP1R15B
PPP1R16A
PPP1R16B
PPP1R17
PPP1R18
PPP1R1A
PPP1R1B
PPP1R1C
PPP1R2
PPP1R21
PPP1R26
PPP1R27
PPP1R32
PPP1R35
PPP1R36
PPP1R3A
PPP1R3B
PPP1R3C
PPP1R3D
PPP1R3G
PPP1R42
PPP1R7
PPP1R8
PPP1R9A
PPP1R9B
PPP2CA
PPP2CB
PPP2R1A
PPP2R1B
PPP2R2A
PPP2R2B
PPP2R2C
PPP2R2D
PPP2R3A
PPP2R3B
PPP2R3C
PPP2R4
PPP2R5A
PPP2R5B
PPP2R5C
PPP2R5D
PPP2R5E
PPP3CA
PPP3CB
PPP3CC
PPP3R1
PPP3R2
PPP4C
PPP4R1
PPP4R2
PPP4R4
PPP5C
PPP5D1
PPP6R1
PPP6R2
PPP6R3

SLC26A1
SLC26A2
SLC26A3
SLC26A4
SLC26A5
SLC26A6
SLC26A9
SLC27A1
SLC27A2
SLC27A3
SLC27A5
SLC27A6
SLC28A2
SLC28A3
SLC29A2
SLC29A3
SLC29A4
SLC2A1
SLC2A11
SLC2A14
SLC2A2
SLC2A3
SLC2A4RG
SLC2A5
SLC2A6
SLC2A7
SLC2A8
SLC30A10
SLC30A2
SLC30A7
SLC30A8
SLC31A1
SLC31A2
SLC32A1
SLC33A1
SLC34A1
SLC34A2
SLC34A3
SLC35A3
SLC35A4
SLC35A5
SLC35B1
SLC35B3
SLC35B4
SLC35C1
SLC35C2
SLC35D1
SLC35E1
SLC35E3
SLC35F2
SLC35F3
SLC35F5
SLC35F6
SLC35G1
SLC35G2
SLC35G3
SLC35G5
SLC35G6
SLC36A1
SLC36A3
SLC37A3
SLC37A4
SLC38A10
SLC38A11
SLC38A3
SLC38A7
SLC38A8
SLC38A9
SLC39A1
SLC39A12
SLC39A12
SLC39A13
SLC39A2
SLC39A5
SLC39A7
SLC39A8
SLC39A9
SLC3A1
SLC41A2
SLC41A3
SLC43A1
SLC43A2
SLC43A3
SLC44A1
SLC44A3
SLC44A5
SLC45A2
SLC45A3
SLC46A1
SLC46A2
SLC46A3
SLC47A1
SLC47A2
SLC48A1
SLC4A1
SLC4A10
SLC4A1AP
SLC4A2
SLC4A3
SLC4A4

TTC1
TTC12
TTC13
TTC14
TTC16
TTC17
TTC19
TTC21A
TTC21B
TTC22
TTC23L
TTC25
TTC26
TTC27
TTC29
TTC30A
TTC30B
TTC31
TTC32
TTC33
TTC36
TTC37
TTC38
TTC39B
TTC39C
TTC4
TTC5
TTC8
TTC9B
TTC9C
TTF1
TTI1
TTI2
TTL
TTLL1
TTLL10
TTLL12
TTLL2
TTLL4
TTLL5
TTLL6
TTLL7
TTLL9
TTN
TTPA
TTPAL
TTR
TUB
TUBA1A
TUBA1B
TUBA1C
TUBA3C
TUBA3D
TUBA3E
TUBA4A
TUBA8
TUBAL3
TUBB
TUBB1
TUBB2A
TUBB2B
TUBB3
TUBB4A
TUBB4B
TUBB6
TUBB8
TUBD1
TUBE1
TUBG1
TUBG2
TUBGCP3
TUBGCP4
TUBGCP5
TUBGCP6
TUFM
TUFT1
TULP2
TULP3
TULP4
TUSC1
TUSC2
TUSC3
TUSC5
TUT1
TVP23A
TVP23B
TVP23C
TWF1
TWIST1
TXK
TXLNA
TXLNB
TXN2
TXNDC11
TXNDC12
TXNDC15
TXNDC17
TXNDC5
TXNDC8
TXNDC9

AP1AR
AP1B1
AP1G2
AP1M1
AP1S1
AP2A2
AP2M1
AP4B1
AP4M1
AP5B1
AP5M1
AP5S1
APBA1
APBA2
APBB1
APBB1IP
APBB2
APBB3
APC
APC2
APCDD1
APCDD1L
APCS
APEX1
APH1A
APH1B
API5
APIP
APITD1
APLF
APLNR
APLP1
APLP2
APMAP
APOA1
APOA1BP
APOA2
APOA4
APOBEC1
APOBEC2
APOBEC3A
APOBEC3A
APOBEC3B
APOBEC3C
APOBEC3D
APOBEC3F
APOBEC3G
APOBEC3H
APOBEC4
APOC3
APOC4
APOC4-APOC2
APOD
APOE
APOH
APOL1
APOL2
APOL3
APOL4
APOL5
APOL6
APOLD1
APOM
APOPT1
APP
APPBP2
APPL1
APPL2
APRT
AQP10
AQP11
AQP12A
AQP2
AQP3
AQP4
AQP4
AQP5
AQP6
AQP7
AQP8
AQP9
AQR
ARAP1
ARAP2
ARAP3
ARF1
ARF3
ARF4
ARF5
ARF6
ARFGAP1
ARFGAP2
ARFGAP3
ARFGEF1
ARFGEF2
ARFIP1
ARFIP2
ARG2
ARGFX
ARGLU1
ARHGAP1

CENPU
CENPV
CEP104
CEP112
CEP120
CEP128
CEP131
CEP135
CEP152
CEP162
CEP164
CEP170
CEP170B
CEP19
CEP192
CEP250
CEP290
CEP295
CEP350
CEP41
CEP55
CEP57
CEP57L1
CEP63
CEP68
CEP70
CEP72
CEP76
CEP83
CEP85
CEP85L
CEP89
CEP95
CEP97
CEPT1
CER1
CERCAM
CERK
CERS1
CERS2
CERS3
CERS4
CERS5
CERS6
CES1
CES2
CES3
CES4A
CES5A
CETN1
CETN3
CETP
CFAP126
CFAP20
CFAP36
CFAP43
CFAP44
CFAP45
CFAP46
CFAP52
CFAP53
CFAP57
CFAP58
CFAP61
CFAP69
CFAP70
CFAP99
CFB
CFC1
CFC1B
CFD
CFDP1
CFH
CFHR1
CFHR2
CFHR3
CFHR4
CFHR5
CFI
CFL1
CFL2
CFLAR
CFTR
CGA
CGB
CGB1
CGB2
CGB5
CGB7
CGB8
CGGBP1
CGN
CGNL1
CGREF1
CGRRF1
CH25H
CHAC1
CHAC2
CHAD
CHADL
CHAF1A

FAM101B
FAM102B
FAM103A1
FAM104A
FAM105A
FAM107A
FAM107B
FAM109A
FAM109B
FAM110A
FAM110B
FAM110C
FAM110D
FAM111A
FAM111B
FAM114A1
FAM114A2
FAM117A
FAM117B
FAM118A
FAM118B
FAM120A
FAM120B
FAM122A
FAM124A
FAM124B
FAM126A
FAM126B
FAM129B
FAM129C
FAM131A
FAM131B
FAM131C
FAM133B
FAM134A
FAM134B
FAM134C
FAM135A
FAM135B
FAM136A
FAM149A
FAM149B1
FAM150A
FAM150B
FAM151A
FAM151B
FAM153A
FAM154A
FAM154B
FAM155A
FAM159A
FAM160A1
FAM160A2
FAM161A
FAM161B
FAM162A
FAM163A
FAM163B
FAM166A
FAM166B
FAM167B
FAM168A
FAM168B
FAM169B
FAM170A
FAM171A2
FAM171B
FAM172A
FAM173A
FAM173B
FAM174A
FAM174B
FAM175A
FAM175B
FAM177A1
FAM177B
FAM178B
FAM179A
FAM180A
FAM181A
FAM181B
FAM183A
FAM184A
FAM184B
FAM185A
FAM186B
FAM187A
FAM187B
FAM188A
FAM188B
FAM189A1
FAM189A2
FAM189B
FAM192A
FAM193A
FAM195A
FAM195B
FAM196A
FAM196B
FAM198A
FAM198B

INSM1
INSRR
INTS10
INTS12
INTS2
INTS3
INTS4
INTS5
INTS6
INTS7
INTS8
INTS9
INVS
IP6K1
IP6K2
IP6K3
IPCEF1
IPMK
IPO11
IPO13
IPO4
IPO5
IPO7
IPO8
IPO9
IPP
IPPK
IQCA1
IQCC
IQCD
IQCE
IQCF1
IQCF2
IQCF3
IQCG
IQCH
IQCJ-SCHIP1
IQCJ-SCHIP1
IQCK
IQGAP1
IQGAP2
IQGAP3
IQSEC1
IQUB
IREB2
IRF1
IRF2BP1
IRF2BP2
IRF2BPL
IRF3
IRF5
IRF6
IRF7
IRF8
IRGC
IRGM
IRGQ
IRS1
IRS2
IRX1
IRX4
IRX6
ISCA1
ISCA2
ISCU
ISG15
ISG20
ISG20L2
ISL1
ISLR
ISLR2
ISM2
ISOC1
ISOC2
ISPD
IST1
ISX
ISY1
ISYNA1
ITFG1
ITFG2
ITFG3
ITGA1
ITGA10
ITGA2
ITGA3
ITGA7
ITGA8
ITGA9
ITGAD
ITGAE
ITGAM
ITGAV
ITGAX
ITGB1
ITGB1BP1
ITGB1BP1
ITGB2
ITGB3
ITGB3BP
ITGB5

MYRIP
MYT1
MYT1L
MYZAP
MZB1
MZF1
MZT1
MZT2B
N4BP2
N4BP2L1
N4BP2L2
N4BP3
N6AMT1
N6AMT2
NAA15
NAA16
NAA20
NAA25
NAA30
NAA35
NAA38
NAA40
NAA50
NAA60
NAALAD2
NAALADL1
NAALADL2
NAB1
NAB2
NABP2
NACA2
NACAD
NACC1
NACC2
NADK
NADK2
NADSYN1
NAE1
NAF1
NAGLU
NAGPA
NAGS
NAIF1
NAIP
NALCN
NANOG
NANP
NANS
NAP1L1
NAP1L4
NAP1L5
NAPA
NAPB
NAPEPLD
NAPG
NAPRT
NAPSA
NARF
NARFL
NARS
NARS2
NASP
NAT1
NAT10
NAT14
NAT16
NAT2
NAT6
NAT8
NAT8L
NAT9
NATD1
NAV1
NAV2
NAV3
NBAS
NBEA
NBL1
NBPF1
NBPF10
NBPF11
NBPF14
NBPF15
NBPF3
NBPF9
NBR1
NCAM1
NCAM2
NCAN
NCAPD2
NCAPD3
NCAPG
NCAPG2
NCAPH
NCAPH2
NCBP1
NCBP2
NCCRP1
NCDN
NCEH1
NCF1

PPRC1
PPT1
PPT2
PPTC7
PPWD1
PPY
PQLC1
PQLC2
PQLC2L
PQLC3
PRAC1
PRADC1
PRAM1
PRAME
PRAMEF1
PRAMEF17
PRAMEF17
PRAMEF18
PRAMEF18
PRAMEF2
PRAMEF20
PRAMEF25
PRAMEF4
PRAMEF5
PRAMEF6
PRAMEF7
PRAMEF8
PRAMEF9
PRAP1
PRB1
PRB2
PRB3
PRB4
PRB4
PRC1
PRCC
PRCP
PRDM10
PRDM12
PRDM15
PRDM16
PRDM2
PRDM4
PRDM9
PRDX1
PRDX2
PRDX3
PRDX5
PRDX6
PREB
PRELID1
PRELID2
PRELP
PREPL
PREX1
PRF1
PRG2
PRG3
PRG4
PRH1
PRH2
PRICKLE2
PRICKLE4
PRIM1
PRIM2
PRIMA1
PRIMPOL
PRKAA1
PRKAA2
PRKAB1
PRKAB2
PRKACA
PRKACB
PRKAG1
PRKAG2
PRKCB
PRKCDBP
PRKCG
PRKCH
PRKCI
PRKCQ
PRKCZ
PRKD1
PRKD2
PRKD3
PRKDC
PRKG2
PRKRA
PRKRIP1
PRKRIR
PRL
PRLH
PRLHR
PRMT1
PRMT2
PRMT3
PRMT6
PRMT7
PRMT8
PRND
PRNP

SLC4A7
SLC4A9
SLC50A1
SLC51A
SLC51B
SLC52A1
SLC52A2
SLC52A3
SLC5A1
SLC5A10
SLC5A11
SLC5A12
SLC5A4
SLC5A6
SLC5A8
SLC6A1
SLC6A11
SLC6A12
SLC6A13
SLC6A15
SLC6A15
SLC6A16
SLC6A18
SLC6A20
SLC6A3
SLC6A4
SLC6A5
SLC6A6
SLC6A7
SLC6A9
SLC7A1
SLC7A10
SLC7A13
SLC7A14
SLC7A2
SLC7A4
SLC7A5
SLC7A6
SLC7A6OS
SLC8A1
SLC8B1
SLC9A1
SLC9A3
SLC9A9
SLC9B1
SLC9B2
SLC9C1
SLC9C2
SLCO1A2
SLCO1B1
SLCO1B3
SLCO1B7
SLCO1C1
SLCO2A1
SLCO2B1
SLCO3A1
SLCO4A1
SLCO4C1
SLCO5A1
SLCO6A1
SLFN11
SLFN12
SLFN13
SLFN14
SLFN5
SLFNL1
SLIRP
SLIT1
SLIT3
SLITRK1
SLITRK3
SLITRK6
SLK
SLMAP
SLMO1
SLMO2
SLN
SLTM
SLU7
SLURP1
SLX1A
SLX1B
SLX4
SLX4IP
SMAD1
SMAD2
SMAD3
SMAD4
SMAD5
SMAD6
SMAD7
SMAD9
SMAP1
SMAP2
SMARCA2
SMARCA4
SMARCAD1
SMARCB1
SMARCD1
SMARCD2
SMARCD3

TXNIP
TXNL4A
TXNL4B
TXNRD1
TXNRD2
TXNRD3
TYMP
TYMS
TYR
TYRP1
TYSND1
TYW1
TYW1B
TYW3
TYW5
U2AF1
U2AF1L4
U2AF2
U2SURP
UAP1
UBA2
UBA3
UBA5
UBA52
UBA6
UBA7
UBAC1
UBAC2
UBALD1
UBALD2
UBAP1L
UBAP2
UBAP2L
UBASH3A
UBASH3B
UBB
UBC
UBE2B
UBE2C
UBE2D1
UBE2D2
UBE2D3
UBE2D4
UBE2E1
UBE2E2
UBE2E3
UBE2F
UBE2G1
UBE2G2
UBE2H
UBE2I
UBE2J1
UBE2J2
UBE2K
UBE2L6
UBE2M
UBE2N
UBE2O
UBE2Q1
UBE2Q2
UBE2Q2L
UBE2QL1
UBE2R2
UBE2S
UBE2T
UBE2U
UBE2V1
UBE2V2
UBE2W
UBE2Z
UBE3A
UBE3B
UBE3C
UBE3D
UBE4A
UBE4B
UBFD1
UBIAD1
UBL3
UBL4B
UBL5
UBL7
UBL7
UBLCP1
UBN2
UBOX5
UBP1
UBQLN1
UBQLN3
UBQLN4
UBQLNL
UBR1
UBR2
UBR3
UBR4
UBR5
UBR7
UBTD1
UBTD2
UBTF
UBTFL1

ARHGAP10
ARHGAP11A
ARHGAP11B
ARHGAP15
ARHGAP17
ARHGAP18
ARHGAP19
ARHGAP20
ARHGAP21
ARHGAP22
ARHGAP24
ARHGAP25
ARHGAP26
ARHGAP27
ARHGAP29
ARHGAP30
ARHGAP32
ARHGAP33
ARHGAP35
ARHGAP42
ARHGAP44
ARHGAP5
ARHGAP9
ARHGDIA
ARHGDIB
ARHGEF1
ARHGEF10L
ARHGEF11
ARHGEF12
ARHGEF15
ARHGEF16
ARHGEF17
ARHGEF18
ARHGEF19
ARHGEF2
ARHGEF26
ARHGEF3
ARHGEF33
ARHGEF35
ARHGEF37
ARHGEF38
ARHGEF39
ARHGEF5
ARHGEF7
ARID1A
ARID1B
ARID3A
ARID3B
ARID4A
ARID4B
ARID5A
ARIH1
ARIH2
ARIH2OS
ARL1
ARL10
ARL11
ARL13B
ARL14
ARL14EP
ARL14EPL
ARL15
ARL17A
ARL17B
ARL2
ARL2BP
ARL3
ARL4A
ARL4D
ARL5B
ARL5C
ARL6
ARL6IP1
ARL6IP4
ARL6IP5
ARL6IP6
ARL8A
ARL8B
ARL9
ARMC1
ARMC10
ARMC12
ARMC2
ARMC3
ARMC4
ARMC5
ARMC6
ARMC7
ARMC8
ARMC9
ARNTL
ARNTL2
ARPC1A
ARPC1B
ARPC2
ARPC4
ARPC5
ARPC5L
ARPIN
ARPP19
CHAF1B
CHAMP1
CHAT
CHCHD10
CHCHD2
CHCHD3
CHCHD4
CHCHD5
CHCHD6
CHCHD7
CHD1
CHD1L
CHD2
CHD3
CHD4
CHD5
CHD8
CHD9
CHDH
CHEK1
CHEK2
CHERP
CHGA
CHGB
CHI3L1
CHI3L2
CHID1
CHIT1
CHKA
CHKB
CHL1
CHML
CHMP1A
CHMP1B
CHMP2A
CHMP2B
CHMP3
CHMP4A
CHMP4C
CHMP5
CHMP6
CHMP7
CHN1
CHN2
CHODL
CHORDC1
CHP1
CHP2
CHPF
CHPF2
CHPT1
CHRAC1
CHRD
CHRFAM7A
CHRM1
CHRM3
CHRM4
CHRNB2
CHRNG
CHST1
CHST10
CHST11
CHST12
CHST13
CHST14
CHST15
CHST2
CHST3
CHST4
CHST6
CHST8
CHST9
CHSY1
CHSY3
CHTF18
CHTOP
CHUK
CHURC1
CIAO1
CIAPIN1
CIART
CIB2
CIB3
CIDEA
CIDEC
CIITA
CILP
CILP2
CINP
CIPC
CIR1
CIRBP
CIRH1A
CISD1
CISD2
CISH
CIT
CITED4
CIZ1
CKAP2L
FAM198B
FAM19A1
FAM19A2
FAM19A3
FAM19A4
FAM19A5
FAM200A
FAM200B
FAM204A
FAM205A
FAM206A
FAM207A
FAM208A
FAM208B
FAM20A
FAM20B
FAM20C
FAM210A
FAM210B
FAM212A
FAM212B
FAM213B
FAM214A
FAM214B
FAM216A
FAM216B
FAM217A
FAM217B
FAM218A
FAM219A
FAM219B
FAM21A
FAM220A
FAM221A
FAM221B
FAM222A
FAM222B
FAM227A
FAM227B
FAM228A
FAM228B
FAM229B
FAM231A
FAM24B
FAM25G
FAM26D
FAM26E
FAM26F
FAM32A
FAM35A
FAM3B
FAM3C
FAM3D
FAM43A
FAM43B
FAM45A
FAM46B
FAM46C
FAM47E
FAM47E-STBD1
FAM49A
FAM49B
FAM50B
FAM53A
FAM53B
FAM53C
FAM57A
FAM57B
FAM60A
FAM63A
FAM64A
FAM65A
FAM69A
FAM69B
FAM71A
FAM71B
FAM71C
FAM71D
FAM71E2
FAM71F1
FAM73A
FAM73B
FAM76A
FAM76B
FAM78A
FAM78B
FAM81A
FAM81B
FAM83A
FAM83E
FAM83F
FAM83H
FAM84A
FAM84B
FAM86C1
FAM89A
FAM89B
FAM90A1
FAM91A1
FAM92A1
ITGB6
ITGB8
ITGBL1
ITIH1
ITIH2
ITIH3
ITIH4
ITIH5
ITLN1
ITLN2
ITM2B
ITM2C
ITPK1
ITPKA
ITPKB
ITPKC
ITPR1
ITPR2
ITPR3
ITPRIP
ITPRIPL1
ITPRIPL2
ITSN1
ITSN2
IVL
IVNS1ABP
IWS1
IYD
IZUMO1
IZUMO2
IZUMO3
JADE1
JADE2
JAG1
JAGN1
JAK1
JAK3
JAKMIP1
JAKMIP2
JAM3
JARID2
JAZF1
JDP2
JKAMP
JMJD4
JMJD6
JMJD7
JMJD8
JMY
JOSD1
JOSD2
JPH4
JRK
JRKL
JSRP1
JTB
JUN
JUNB
JUND
KALRN
KANK1
KANK2
KANK3
KANK4
KANSL1
KANSL1L
KANSL2
KARS
KAT2A
KAT2B
KAT5
KAT6A
KAT6B
KAT7
KAT8
KATNA1
KATNAL1
KATNAL2
KATNBL1
KAZALD1
KAZN
KBTBD11
KBTBD12
KBTBD13
KBTBD3
KBTBD4
KBTBD6
KBTBD7
KBTBD8
KCMF1
KCNA1
KCNA10
KCNA2
KCNA3
KCNA4
KCNA5
KCNA7
KCNAB1
KCNAB2
KCNAB3
NCF2
NCF4
NCK1
NCK2
NCKAP1
NCKAP1L
NCKAP5
NCKIPSD
NCL
NCLN
NCMAP
NCOA1
NCOA3
NCOA4
NCOA5
NCOA6
NCOR1
NCOR2
NCR3LG1
NCS1
NCSTN
NDC1
NDC80
NDE1
NDEL1
NDFIP1
NDN
NDNF
NDNL2
NDOR1
NDST1
NDST2
NDST3
NDST4
NDUFA10
NDUFA11
NDUFA12
NDUFA13
NDUFA2
NDUFA3
NDUFA4
NDUFA4L2
NDUFA5
NDUFA6
NDUFA7
NDUFA8
NDUFA9
NDUFAB1
NDUFAF1
NDUFAF2
NDUFAF3
NDUFAF4
NDUFAF5
NDUFAF6
NDUFAF7
NDUFB1
NDUFB10
NDUFB2
NDUFB3
NDUFB4
NDUFB5
NDUFB6
NDUFB7
NDUFB8
NDUFB9
NDUFC1
NDUFC2
NDUFS1
NDUFS2
NDUFS3
NDUFS4
NDUFS5
NDUFS6
NDUFS7
NDUFS8
NDUFV1
NDUFV2
NEB
NEBL
NECAB1
NECAB2
NECAP1
NECAP2
NEDD4
NEDD8
NEDD9
NEFH
NEFL
NEFM
NEGR1
NEIL1
NEIL2
NEIL3
NEK11
NEK2
NEK4
NEK5
NEK6
NEK7
NEK9
PROB1
PROC
PROCA1
PRODH
PRODH2
PROK1
PROK2
PROKR2
PROL1
PROM1
PROM2
PROP1
PROS1
PROSC
PROSER1
PROSER2
PROX1
PROZ
PRPF19
PRPF3
PRPF38A
PRPF38B
PRPF4
PRPF40B
PRPF6
PRPH
PRPH2
PRPS1L1
PRPSAP1
PRPSAP2
PRR11
PRR12
PRR13
PRR14
PRR14L
PRR15
PRR15L
PRR16
PRR18
PRR19
PRR20A
PRR20B
PRR20C
PRR20D
PRR20E
PRR21
PRR23A
PRR23B
PRR23C
PRR25
PRR27
PRR29
PRR3
PRR30
PRR34
PRR35
PRR36
PRR4
PRR4
PRR5
PRR5-ARHGAP8
PRR5L
PRR7
PRRC1
PRRC2A
PRRC2C
PRRG2
PRRG4
PRRT1
PRRT2
PRRT3
PRRT4
PRRX1
PRRX2
PRSS21
PRSS22
PRSS23
PRSS27
PRSS3
PRSS3
PRSS33
PRSS35
PRSS36
PRSS37
PRSS38
PRSS42
PRSS45
PRSS48
PRSS54
PRSS55
PRSS56
PRSS57
PRSS58
PRSS8
PRTFDC1
PRTG
PRTN3
PRUNE
PRX
PSAP
SMARCE1
SMC1B
SMC3
SMC5
SMC6
SMCO2
SMCO3
SMCO4
SMCP
SMCR8
SMDT1
SMEK2
SMG1
SMG5
SMG8
SMG9
SMIM1
SMIM11
SMIM12
SMIM13
SMIM14
SMIM15
SMIM17
SMIM18
SMIM19
SMIM20
SMIM21
SMIM24
SMIM3
SMIM4
SMIM5
SMIM6
SMIM7
SMIM8
SMKR1
SMLR1
SMN1
SMN2
SMN2
SMNDC1
SMO
SMOX
SMPD1
SMPD3
SMPD4
SMPDL3A
SMPDL3B
SMR3A
SMR3B
SMTN
SMTNL2
SMU1
SMUG1
SMURF1
SMURF2
SMYD2
SMYD3
SMYD5
SNAI2
SNAP23
SNAP25
SNAP29
SNAP47
SNAPC1
SNAPC2
SNAPC3
SNAPC4
SNAPIN
SNCB
SND1
SNF8
SNIP1
SNN
SNPH
SNRK
SNRNP200
SNRNP25
SNRNP27
SNRNP40
SNRNP48
SNRNP70
SNRPA
SNRPA1
SNRPB2
SNRPC
SNRPD1
SNRPD2
SNRPD3
SNRPE
SNRPF
SNRPN
SNTA1
SNTB1
SNTG2
SNTN
SNUPN
SNURF
SNW1
SNX1
SNX13
UBXN1
UBXN10
UBXN11
UBXN2A
UBXN2B
UBXN4
UBXN6
UBXN8
UCHL1
UCHL3
UCHL5
UCK1
UCK2
UCKL1
UCMA
UCN
UCN2
UCN3
UCP2
UCP3
UEVLD
UFC1
UFL1
UFM1
UFSP1
UFSP2
UGCG
UGDH
UGGT1
UGGT2
UGP2
UGT1A10
UGT1A3
UGT1A4
UGT1A5
UGT1A6
UGT1A7
UGT1A8
UGT1A9
UGT2A1
UGT2A3
UGT2B10
UGT2B11
UGT2B15
UGT2B17
UGT2B28
UGT2B4
UGT2B7
UGT3A1
UGT3A2
UGT8
UHMK1
UHRF1
UHRF1BP1
UHRF1BP1L
UIMC1
ULK2
UMPS
UNC119B
UNC13A
UNC13B
UNC45A
UNC45B
UNC50
UNC5B
UNC5C
UNC5CL
UNC80
UNC93A
UNC93B1
UNCX
UNG
UNK
UNKL
UPF1
UPK2
UPK3A
UPK3B
UPK3BL
UPP1
UPP2
UQCC1
UQCC2
UQCC3
UQCR10
UQCR11
UQCRB
UQCRC1
UQCRC2
UQCRFS1
UQCRH
UQCRQ
URB2
URGCP
URM1
UROC1
UROD
UROS
USB1
USE1

ARPP21
ARRB1
ARRB2
ARRDC1
ARRDC2
ARRDC3
ARRDC4
ARSA
ARSB
ARSG
ARSI
ARSJ
ARSK
ART1
ART3
ART4
ART5
ARTN
ARV1
ARVCF
AS3MT
ASAH1
ASAH2
ASAP1
ASAP2
ASAP3
ASB1
ASB10
ASB17
ASB18
ASB4
ASB6
ASB7
ASCC2
ASCC3
ASCL2
ASCL4
ASF1A
ASF1B
ASGR1
ASGR2
ASH1L
ASH2L
ASIC1
ASIC2
ASIC2
ASIC3
ASL
ASMT
ASMTL
ASNA1
ASNS
ASNS
ASNSD1
ASPA
ASPDH
ASPG
ASPH
ASPHD1
ASPHD2
ASPM
ASPN
ASPRV1
ASPSCR1
ASRGL1
ASS1
ASTE1
ASTN1
ASTN2
ASUN
ASXL1
ASXL2
ASZ1
ATAD1
ATAD2
ATAD2B
ATAD3A
ATAD3B
ATAD3C
ATAD5
ATAT1
ATE1
ATF1
ATF2
ATF3
ATF4
ATF6
ATF7IP
ATF7IP2
ATG10
ATG101
ATG12
ATG13
ATG14
ATG16L1
ATG16L2
ATG2A
ATG2B
ATG3
ATG4B

CKAP5
CKLF
CKMT1B
CKMT2
CKS1B
CKS2
CLASP1
CLASP2
CLASRP
CLC
CLCA1
CLCA2
CLCA4
CLCC1
CLCF1
CLCN1
CLCN6
CLCN7
CLCNKB
CLDN1
CLDN10
CLDN11
CLDN12
CLDN14
CLDN15
CLDN16
CLDN17
CLDN18
CLDN19
CLDN20
CLDN23
CLDN25
CLDN3
CLDN4
CLDN5
CLDN6
CLDN7
CLDN8
CLDN9
CLDND1
CLDND2
CLEC10A
CLEC11A
CLEC12A
CLEC12B
CLEC14A
CLEC16A
CLEC17A
CLEC18A
CLEC18B
CLEC18C
CLEC1A
CLEC1B
CLEC2A
CLEC2B
CLEC2D
CLEC2L
CLEC3A
CLEC3B
CLEC4A
CLEC4C
CLEC4D
CLEC4E
CLEC4F
CLEC4G
CLEC4M
CLEC5A
CLEC6A
CLEC7A
CLEC9A
CLECL1
CLGN
CLHC1
CLIC1
CLIC3
CLIC4
CLINT1
CLIP1
CLIP2
CLIP3
CLIP4
CLK2
CLLU1
CLMP
CLN5
CLN6
CLN8
CLNK
CLNS1A
CLOCK
CLP1
CLPB
CLPP
CLPS
CLPSL1
CLPSL2
CLPTM1
CLPTM1L
CLPX
CLRN2

FAM92B
FAM96A
FAM96B
FAM98A
FAM98B
FAM98C
FAN1
FANCC
FANCD2OS
FANCF
FANCG
FANCI
FANCL
FANK1
FAR1
FAR2
FARP1
FARS2
FARSA
FARSB
FASN
FASTK
FASTKD1
FASTKD2
FASTKD3
FASTKD5
FAT1
FAT2
FAT3
FAT4
FAU
FAXC
FAXDC2
FBF1
FBL
FBLIM1
FBLN1
FBLN2
FBLN7
FBN2
FBN3
FBP1
FBP2
FBXL12
FBXL13
FBXL14
FBXL16
FBXL18
FBXL2
FBXL20
FBXL21
FBXL22
FBXL6
FBXL7
FBXO11
FBXO15
FBXO16
FBXO17
FBXO18
FBXO2
FBXO21
FBXO22
FBXO25
FBXO28
FBXO3
FBXO31
FBXO36
FBXO38
FBXO39
FBXO40
FBXO44
FBXO47
FBXO48
FBXO6
FBXO8
FBXW11
FBXW12
FBXW4
FBXW5
FBXW8
FBXW9
FCAMR
FCAR
FCER1A
FCER1G
FCER2
FCF1
FCGBP
FCGR1A
FCGR2A
FCGR2A
FCGR2B
FCGR3A
FCGR3B
FCHO1
FCHSD1
FCHSD2
FCN1
FCN2
FCRL1

KCNB1
KCNB2
KCNC1
KCNC2
KCNC3
KCNC4
KCND2
KCND3
KCNE3
KCNE4
KCNF1
KCNG1
KCNG2
KCNG3
KCNG4
KCNH1
KCNH2
KCNH3
KCNH4
KCNH5
KCNH6
KCNH7
KCNH8
KCNIP1
KCNIP3
KCNIP4
KCNJ1
KCNJ10
KCNJ11
KCNJ12
KCNJ13
KCNJ14
KCNJ15
KCNJ16
KCNJ18
KCNJ2
KCNJ3
KCNJ4
KCNJ5
KCNJ6
KCNJ8
KCNJ9
KCNK1
KCNK10
KCNK12
KCNK13
KCNK15
KCNK16
KCNK17
KCNK18
KCNK2
KCNK3
KCNK5
KCNK6
KCNK7
KCNMA1
KCNMB2
KCNMB4
KCNN1
KCNN2
KCNN3
KCNN4
KCNQ1
KCNQ2
KCNQ3
KCNQ4
KCNQ5
KCNS1
KCNS2
KCNS3
KCNT1
KCNT2
KCNU1
KCNV1
KCNV2
KCTD10
KCTD11
KCTD12
KCTD13
KCTD14
KCTD15
KCTD17
KCTD18
KCTD20
KCTD21
KCTD3
KCTD5
KCTD6
KCTD7
KCTD9
KDELC2
KDF1
KDM1A
KDM1B
KDM2A
KDM2B
KDM3A
KDM3B
KDM4A
KDM4B

NELFA
NELFB
NELFCD
NELL1
NELL2
NEMF
NENF
NEO1
NES
NET1
NETO1
NETO2
NEU2
NEU3
NEU4
NEURL4
NEUROD1
NEUROD2
NEUROD6
NEUROG1
NEUROG2
NEUROG3
NEXN
NF1
NF2
NFAM1
NFASC
NFAT5
NFATC1
NFATC2
NFATC2IP
NFATC3
NFATC4
NFE2
NFE2L1
NFE2L2
NFIA
NFIB
NFIC
NFIL3
NFIX
NFKB1
NFKBIA
NFKBIB
NFKBIL1
NFKBIZ
NFRKB
NFS1
NFU1
NFXL1
NFYC
NGB
NGDN
NGF
NHEJ1
NHLH1
NHLH2
NHLRC2
NHLRC3
NHLRC4
NHP2
NHP2L1
NICN1
NID1
NIF3L1
NIFK
NIM1K
NIN
NINJ1
NINJ2
NINL
NIP7
NIPA1
NIPA2
NIPAL1
NIPAL2
NIPAL3
NIPAL4
NIPBL
NIPSNAP3A
NIPSNAP3B
NISCH
NIT2
NKAIN1
NKAIN2
NKAIN3
NKAIN4
NKD2
NKG7
NKIRAS1
NKIRAS2
NKPD1
NKTR
NKX2-1
NKX2-6
NKX6-1
NKX6-3
NLE1
NLGN1
NLGN2

PSAT1
PSCA
PSD2
PSD3
PSD4
PSEN1
PSEN2
PSENEN
PSG11
PSG2
PSG3
PSG4
PSG5
PSG6
PSG7
PSG9
PSIP1
PSKH1
PSKH2
PSMA1
PSMA2
PSMA3
PSMA4
PSMA5
PSMA7
PSMA8
PSMB1
PSMB10
PSMB11
PSMB2
PSMB3
PSMB4
PSMB5
PSMB6
PSMB7
PSMB8
PSMB9
PSMC1
PSMC2
PSMC3
PSMC3IP
PSMC4
PSMC5
PSMC6
PSMD11
PSMD12
PSMD12
PSMD13
PSMD14
PSMD2
PSMD3
PSMD4
PSMD5
PSMD6
PSMD7
PSMD8
PSMD9
PSME1
PSME2
PSME3
PSMF1
PSMG1
PSMG2
PSMG3
PSORS1C1
PSPH
PSPN
PSRC1
PSTK
PSTPIP1
PTAFR
PTAR1
PTBP1
PTCD1
PTCD2
PTCD3
PTCH1
PTCH2
PTCHD4
PTCRA
PTEN
PTER
PTF1A
PTGDR
PTGDR2
PTGDS
PTGER4
PTGES
PTGES3
PTGES3L
PTGES3L-AARSD1
PTGFR
PTGFRN
PTGS2
PTH
PTH1R
PTH2
PTH2R
PTHLH
PTK2

SNX14
SNX16
SNX17
SNX19
SNX2
SNX20
SNX21
SNX22
SNX24
SNX25
SNX27
SNX31
SNX32
SNX33
SNX4
SOAT1
SOBP
SOD1
SOD2
SOGA1
SOGA3
SOHLH1
SOHLH2
SON
SORBS2
SORBS3
SORCS1
SORCS2
SORCS3
SORL1
SORT1
SOS1
SOST
SOSTDC1
SOWAHA
SOWAHB
SOWAHC
SOX1
SOX10
SOX11
SOX12
SOX13
SOX14
SOX15
SOX2
SOX21
SOX30
SOX4
SOX5
SOX6
SOX9
SP100
SP110
SP140
SP140L
SP2
SP3
SP4
SP6
SP9
SPA17
SPACA3
SPACA4
SPACA7
SPAG1
SPAG11A
SPAG11B
SPAG11B
SPAG11B
SPAG11B
SPAG11B
SPAG11B
SPAG16
SPAG17
SPAG4
SPAG5
SPAG7
SPAG9
SPARC
SPAST
SPATA12
SPATA13
SPATA16
SPATA17
SPATA18
SPATA19
SPATA2
SPATA20
SPATA21
SPATA22
SPATA24
SPATA2L
SPATA3
SPATA31A1
SPATA31A3
SPATA31A5
SPATA31A6
SPATA31A7
SPATA31D1

USF1
USF2
USH1C
USH1G
USH2A
USHBP1
USMG5
USO1
USP1
USP12
USP14
USP15
USP17L1
USP17L10
USP17L11
USP17L12
USP17L13
USP17L15
USP17L17
USP17L18
USP17L19
USP17L2
USP17L20
USP17L21
USP17L22
USP17L24
USP17L25
USP17L26
USP17L27
USP17L28
USP17L29
USP17L3
USP17L30
USP17L4
USP17L5
USP17L7
USP17L8
USP19
USP2
USP30
USP31
USP32
USP33
USP36
USP37
USP38
USP39
USP4
USP43
USP44
USP46
USP47
USP48
USP49
USP54
USP6
USP6NL
USP8
USPL1
UST
UTP11L
UTP14C
UTP15
UTP18
UTP20
UTP23
UTP3
UTP6
UTS2
UTS2B
UTS2R
UVRAG
UVSSA
VAC14
VAMP3
VAMP4
VAMP5
VAMP7
VAMP8
VANGL2
VARS
VARS2
VASH1
VASH2
VASN
VAT1
VAT1L
VAV3
VCAM1
VCAN
VCL
VCL
VCP
VCPKMT
VDAC2
VEGFA
VEGFB
VEGFC
VENTX
VEPH1

ATG4C
ATG4D
ATG5
ATG7
ATG9A
ATG9B
ATHL1
ATIC
ATL2
ATL3
ATM
ATMIN
ATN1
ATOH1
ATOH8
ATOX1
ATP10A
ATP10B
ATP10D
ATP11A
ATP11AUN
ATP11B
ATP12A
ATP13A1
ATP13A2
ATP13A3
ATP13A4
ATP13A5
ATP1A1
ATP1A2
ATP1A3
ATP1A4
ATP1B2
ATP1B3
ATP2A1
ATP2A2
ATP2A3
ATP2B1
ATP2B2
ATP2B4
ATP2C1
ATP2C2
ATP4A
ATP4B
ATP5A1
ATP5B
ATP5C1
ATP5D
ATP5F1
ATP5G1
ATP5G2
ATP5G3
ATP5H
ATP5J
ATP5J2
ATP5L
ATP5L2
ATP5O
ATP5S
ATP5SL
ATP6AP1L
ATP6V0A1
ATP6V0A2
ATP6V0A4
ATP6V0B
ATP6V0C
ATP6V0D1
ATP6V0D2
ATP6V0E1
ATP6V0E2
ATP6V1A
ATP6V1B1
ATP6V1B2
ATP6V1C1
ATP6V1C2
ATP6V1D
ATP6V1E1
ATP6V1E2
ATP6V1F
ATP6V1G1
ATP6V1G2
ATP6V1G3
ATP6V1H
ATP7B
ATP8A1
ATP8A2
ATP8B1
ATP8B2
ATP8B3
ATP8B4
ATP9A
ATP9B
ATPAF1
ATPAF2
ATPIF1
ATR
ATRAID
ATRIP
ATRN
ATXN1
ATXN10
CLRN3
CLSPN
CLSTN2
CLSTN3
CLTA
CLTC
CLTCL1
CLU
CLUAP1
CLUH
CLVS1
CLVS2
CMAS
CMBL
CMC1
CMC2
CMIP
CMPK1
CMPK2
CMSS1
CMTM1
CMTM3
CMTM8
CMTR1
CMTR2
CMYA5
CNBD1
CNBD2
CNBP
CNDP1
CNDP2
CNEP1R1
CNFN
CNGA1
CNGA3
CNGA4
CNGB1
CNGB3
CNIH1
CNIH2
CNIH3
CNIH4
CNKSR1
CNKSR3
CNN1
CNN2
CNN3
CNNM1
CNNM2
CNNM3
CNNM4
CNOT1
CNOT10
CNOT11
CNOT3
CNOT4
CNOT6
CNOT7
CNOT8
CNPPD1
CNPY2
CNPY3
CNPY4
CNR2
CNRIP1
CNST
CNTD1
CNTD2
CNTF
CNTLN
CNTN1
CNTN2
CNTN3
CNTN5
CNTN6
CNTNAP1
CNTNAP3
CNTNAP4
CNTRL
CNTROB
COA1
COA4
COA5
COA6
COA7
COASY
COBL
COBLL1
COCH
COG2
COG8
COL11A1
COL12A1
COL14A1
COL15A1
COL16A1
COL17A1
COL1A2
COL20A1
COL23A1
COL24A1
FCRL2
FCRL3
FCRL4
FCRL5
FCRL6
FCRLA
FDCSP
FDPS
FDX1
FDXACB1
FDXR
FEM1C
FEN1
FER
FER1L6
FERMT1
FERMT2
FERMT3
FES
FETUB
FEZ1
FEZF1
FEZF2
FFAR1
FFAR2
FFAR3
FFAR4
FGA
FGB
FGD2
FGD3
FGD4
FGD5
FGD6
FGF1
FGF10
FGF11
FGF12
FGF17
FGF18
FGF19
FGF2
FGF3
FGF4
FGF6
FGF7
FGF8
FGF8
FGFBP1
FGFBP2
FGFBP3
FGFR1OP
FGFR1OP2
FGFR2
FGFR3
FGFRL1
FGG
FGGY
FGL1
FGL2
FGR
FH
FHAD1
FHDC1
FHIT
FHL3
FHL5
FIBCD1
FIBIN
FIBP
FICD
FIG4
FIGLA
FIGN
FIGNL1
FILIP1L
FIP1L1
FIS1
FITM1
FIZ1
FJX1
FKBP10
FKBP11
FKBP14
FKBP15
FKBP1B
FKBP2
FKBP3
FKBP6
FKBP7
FKBP8
FKBP9
FKRP
FKTN
FLAD1
FLCN
FLG
FLG2
FLI1
FLII
FLNB
KDM4C
KDM4D
KDM4E
KDM5B
KDM7A
KDM8
KEAP1
KEL
KERA
KHDC1
KHDC1L
KHDC3L
KHDRBS1
KHDRBS2
KIAA0020
KIAA0040
KIAA0100
KIAA0101
KIAA0141
KIAA0195
KIAA0196
KIAA0226L
KIAA0232
KIAA0319
KIAA0319L
KIAA0355
KIAA0391
KIAA0408
KIAA0430
KIAA0513
KIAA0556
KIAA0586
KIAA0753
KIAA0825
KIAA0895
KIAA0895L
KIAA0907
KIAA0922
KIAA0930
KIAA1024
KIAA1024L
KIAA1033
KIAA1143
KIAA1191
KIAA1211
KIAA1211L
KIAA1217
KIAA1244
KIAA1257
KIAA1279
KIAA1324
KIAA1324L
KIAA1328
KIAA1377
KIAA1407
KIAA1429
KIAA1456
KIAA1462
KIAA1467
KIAA1468
KIAA1524
KIAA1549L
KIAA1551
KIAA1586
KIAA1598
KIAA1644
KIAA1671
KIAA1755
KIAA1841
KIAA1919
KIAA1958
KIAA2012
KIAA2013
KIAA2018
KIAA2026
KIDINS220
KIF11
KIF12
KIF14
KIF17
KIF18A
KIF19
KIF20A
KIF20B
KIF21A
KIF27
KIF2A
KIF2B
KIF2C
KIF3A
KIF3B
KIF5A
KIF5B
KIF5C
KIF6
KIF7
KIFAP3
KIFC1
KIFC2
KIFC3
KIN
NLK
NLRC3
NLRC4
NLRC5
NLRP1
NLRP10
NLRP11
NLRP12
NLRP13
NLRP14
NLRP2
NLRP3
NLRP4
NLRP5
NLRP6
NLRP7
NLRP8
NLRP9
NMB
NMD3
NME1
NME1-NME2
NME3
NME4
NME5
NME6
NME7
NME8
NME9
NMI
NMNAT3
NMRAL1
NMRK1
NMRK2
NMS
NMT1
NMT2
NMUR1
NMUR2
NNAT
NNMT
NNT
NOA1
NOB1
NOC2L
NOC3L
NOC4L
NOD2
NODAL
NOG
NOL10
NOL11
NOL12
NOL4
NOL4L
NOL6
NOL7
NOL8
NOL9
NOLC1
NOM1
NOMO2
NOMO3
NOP10
NOP14
NOP16
NOP2
NOP56
NOP58
NOS1AP
NOS2
NOS3
NOSTRIN
NOTCH1
NOTCH2
NOTCH2NL
NOTCH3
NOTUM
NOV
NOVA1
NOVA2
NOX4
NOX5
NPAP1
NPAS1
NPAS4
NPAT
NPB
NPBWR1
NPBWR2
NPC1
NPC1L1
NPC2
NPDC1
NPEPL1
NPEPPS
NPFF
NPFFR1
NPFFR2
NPHP1
NPHP3
PTK2B
PTK7
PTN
PTOV1
PTP4A2
PTP4A3
PTPDC1
PTPDC1
PTPLA
PTPLAD1
PTPLAD2
PTPLB
PTPN14
PTPN2
PTPN2
PTPN2
PTPN20A
PTPN22
PTPN23
PTPN5
PTPN6
PTPN7
PTPRC
PTPRCAP
PTPRG
PTPRQ
PTPRR
PTPRZ1
PTRF
PTRH1
PTRH2
PTRHD1
PTS
PTTG1
PTX3
PTX4
PUF60
PUM2
PURA
PURB
PURG
PUS1
PUS10
PUS3
PUS7
PUS7L
PUSL1
PVALB
PVR
PVRIG
PVRL2
PVRL3
PVRL4
PWP1
PWP2
PWWP2B
PXDC1
PXDN
PXDNL
PXK
PXMP2
PXMP4
PXN
PXT1
PXYLP1
PYCARD
PYCR2
PYCRL
PYDC1
PYDC2
PYGB
PYGL
PYGM
PYGO1
PYGO2
PYHIN1
PYROXD1
PYROXD2
PYURF
PYY
PZP
QARS
QDPR
QKI
QPCTL
QPRT
QRFP
QRFPR
QRICH1
QRICH2
QRSL1
QSOX1
QSOX2
QTRT1
QTRTD1
R3HCC1
R3HCC1L
R3HDM1
R3HDM2
R3HDM4
R3HDML
SPATA31E1
SPATA32
SPATA33
SPATA4
SPATA45
SPATA5
SPATA5L1
SPATA6
SPATA8
SPATA9
SPATC1
SPATC1L
SPATS1
SPATS2
SPATS2L
SPC24
SPC25
SPCS1
SPCS2
SPCS3
SPDEF
SPDL1
SPDYA
SPDYC
SPDYE1
SPDYE2
SPDYE3
SPDYE4
SPDYE5
SPDYE6
SPECC1
SPECC1L
SPEF2
SPEG
SPEM1
SPEN
SPERT
SPESP1
SPG21
SPG7
SPHAR
SPHK1
SPHK1
SPHKAP
SPI1
SPIB
SPIC
SPICE1
SPIDR
SPIN1
SPINK1
SPINK14
SPINK2
SPINK4
SPINK5
SPINK6
SPINK7
SPINK8
SPINK9
SPINT1
SPINT3
SPNS1
SPNS3
SPO11
SPOCD1
SPOCK1
SPOP
SPP2
SPPL2A
SPPL2C
SPPL3
SPRN
SPRR1A
SPRR1B
SPRR2A
SPRR3
SPRR4
SPRTN
SPRY3
SPRYD3
SPRYD4
SPRYD7
SPSB1
SPSB2
SPSB3
SPSB4
SPTA1
SPTAN1
SPTBN2
SPTBN5
SPTLC1
SPTLC2
SPTLC3
SPTSSA
SPTY2D1
SPX
SPZ1
SQLE
SRBD1
SRC
SRCAP
VEZT
VGF
VGLL2
VGLL3
VGLL4
VHL
VHLL
VIL1
VILL
VIM
VIMP
VIPAS39
VIPR1
VIPR2
VKORC1
VKORC1L1
VLDLR
VMAC
VMO1
VMP1
VN1R1
VN1R2
VN1R4
VOPP1
VPRBP
VPREB3
VPS11
VPS13A
VPS13C
VPS13D
VPS16
VPS25
VPS26A
VPS26B
VPS33B
VPS37A
VPS37B
VPS37C
VPS39
VPS45
VPS4A
VPS4B
VPS51
VPS52
VPS53
VPS54
VPS72
VPS8
VPS9D1
VRK1
VRK2
VRK3
VRTN
VSIG10
VSIG10L
VSIG2
VSIG8
VSNL1
VSTM1
VSTM2A
VSTM2B
VSTM4
VSTM5
VSX2
VTA1
VTCN1
VTN
VWA1
VWA3B
VWA5A
VWA7
VWA8
VWC2
VWC2L
VWCE
VWF
WAC
WAPAL
WARS
WARS2
WASF1
WASF2
WASH1
WASL
WBP1
WBP11
WBP1L
WBP2
WBP2NL
WBP4
WBSCR16
WBSCR17
WBSCR27
WBSCR28
WDFY1
WDFY2
WDFY3
WDHD1
WDPCP
WDR12
WDR20

ATXN2	COL25A1	FLOT2	KIR2DL2	NPIPA1	RAB10	SRCIN1	WDR24
ATXN2L	COL26A1	FLRT1	KIR2DL5A	NPIPB4	RAB11B	SRD5A1	WDR25
ATXN3	COL27A1	FLRT3	KIR2DL5A	NPIPB5	RAB11FIP1	SRD5A2	WDR26
ATXN7	COL28A1	FLT1	KIR2DL5B	NPL	RAB11FIP2	SRD5A3	WDR27
ATXN7L2	COL2A1	FLVCR1	KIR2DS1	NPM1	RAB11FIP3	SREBF1	WDR3
ATXN7L3	COL3A1	FLVCR2	KIR2DS2	NPM2	RAB11FIP4	SREBF2	WDR31
ATXN7L3B	COL4A2	FLYWCH1	KIR2DS3	NPM3	RAB11FIP5	SREK1	WDR33
AUNIP	COL4A3	FLYWCH2	KIR2DS4	NPPA	RAB13	SREK1IP1	WDR34
AUP1	COL4A3BP	FMN1	KIR2DS5	NPPB	RAB14	SRF	WDR35
AURKA	COL4A4	FMNL1	KIR3DL1	NPPC	RAB15	SRFBP1	WDR36
AURKAIP1	COL5A1	FMNL2	KIR3DL3	NPR1	RAB18	SRGAP2	WDR37
AURKB	COL5A2	FMNL3	KIR3DS1	NPR3	RAB1A	SRGAP2B	WDR38
AURKC	COL5A3	FMO1	KIR3DS1	NPRL2	RAB1B	SRGN	WDR41
AVEN	COL6A1	FMO2	KIRREL	NPRL3	RAB20	SRI	WDR45B
AVIL	COL6A3	FMO3	KIRREL2	NPS	RAB24	SRM	WDR46
AVL9	COL6A5	FMO4	KIRREL3	NPSR1	RAB27A	SRMS	WDR47
AVP	COL6A6	FMO5	KISS1	NPTN	RAB27A	SRP14	WDR48
AVPI1	COL7A1	FMOD	KISS1R	NPTX2	RAB27B	SRP19	WDR49
AVPR1B	COL8A1	FN1	KITLG	NPTXR	RAB28	SRP54	WDR5
AXDND1	COL8A2	FN3K	KIZ	NPVF	RAB29	SRP68	WDR53
AXIN2	COL9A2	FN3KRP	KLB	NPW	RAB30	SRP9	WDR54
AZGP1	COL9A3	FNBP1L	KLC1	NPY	RAB32	SRPK1	WDR55
AZU1	COLCA2	FNDC1	KLC2	NPY2R	RAB33B	SRPK2	WDR59
B2M	COLEC11	FNDC3A	KLC4	NPY5R	RAB34	SRPR	WDR5B
B3GALNT1	COLGALT1	FNDC3B	KLF1	NR1H4	RAB36	SRR	WDR60
B3GALNT2	COLGALT2	FNDC4	KLF11	NR2C1	RAB37	SRRD	WDR61
B3GALT1	COLQ	FNDC5	KLF12	NR2C2	RAB39A	SRRM1	WDR63
B3GALT2	COMMD1	FNDC8	KLF13	NR2C2AP	RAB3A	SRRM3	WDR64
B3GALT5	COMMD10	FNDC9	KLF14	NR2E3	RAB3B	SRRM4	WDR66
B3GALT6	COMMD2	FNIP1	KLF15	NR2F1	RAB3C	SRRM5	WDR70
B3GALTL	COMMD3	FNIP2	KLF17	NR5A1	RAB3D	SRRT	WDR72
B3GAT1	COMMD4	FNTA	KLF4	NRAP	RAB3GAP1	SRSF1	WDR73
B3GAT2	COMMD5	FNTB	KLF7	NRARP	RAB3GAP2	SRSF10	WDR74
B3GAT3	COMMD7	FOCAD	KLF9	NRAS	RAB3IL1	SRSF11	WDR75
B3GNT2	COMMD8	FOLH1	KLHDC1	NRBF2	RAB3IP	SRSF12	WDR76
B3GNT3	COMMD9	FOLR1	KLHDC3	NRBP1	RAB40C	SRSF2	WDR77
B3GNT4	COMP	FOLR2	KLHDC4	NRBP2	RAB42	SRSF3	WDR78
B3GNT5	COMT	FOLR3	KLHDC7A	NRCAM	RAB4A	SRSF4	WDR81
B3GNT6	COMTD1	FOPNL	KLHDC7B	NRD1	RAB4B	SRSF5	WDR82
B3GNT7	COPA	FOS	KLHDC8A	NRDE2	RAB5A	SRSF6	WDR83
B3GNT8	COPB1	FOSB	KLHDC8B	NREP	RAB5C	SRSF7	WDR83OS
B3GNT9	COPB2	FOSL1	KLHDC9	NRF1	RAB6C	SRSF8	WDR86
B3GNTL1	COPE	FOSL2	KLHL1	NRG2	RAB7B	SRSF9	WDR88
B4GALNT1	COPG1	FOXB2	KLHL10	NRG4	RAB8A	SRXN1	WDR89
B4GALNT2	COPG2	FOXC2	KLHL11	NRGN	RAB8B	SS18L2	WDR90
B4GALNT3	COPRS	FOXD1	KLHL12	NRIP1	RABAC1	SSB	WDR91
B4GALNT4	COPS2	FOXD2	KLHL17	NRIP2	RABEP1	SSBP1	WDR92
B4GALT1	COPS6	FOXD4	KLHL18	NRIP3	RABEP2	SSBP2	WDR93
B4GALT2	COPS7B	FOXD4L1	KLHL20	NRN1L	RABEPK	SSBP3	WDSUB1
B4GALT3	COPS8	FOXD4L5	KLHL21	NRROS	RABGAP1	SSBP4	WDTC1
B4GALT4	COPZ1	FOXD4L6	KLHL22	NRSN1	RABGAP1	SSC4D	WDYHV1
B4GALT5	COPZ2	FOXE3	KLHL23	NRSN2	RABGAP1L	SSFA2	WEE1
B4GALT6	COQ10A	FOXF1	KLHL24	NRTN	RABGEF1	SSH1	WEE2
B4GALT7	COQ10B	FOXI1	KLHL25	NRXN1	RABGGTA	SSH2	WFIKKN1
B4GAT1	COQ2	FOXI1	KLHL26	NRXN2	RABGGTB	SSMEM1	WFIKKN2
B9D1	COQ3	FOXI2	KLHL29	NRXN3	RABL2B	SSNA1	WHSC1
B9D2	COQ4	FOXI3	KLHL30	NSA2	RABL3	SSPN	WHSC1L1
BAAT	COQ5	FOXJ1	KLHL31	NSD1	RABL6	SSR2	WIBG
BABAM1	COQ7	FOXJ2	KLHL32	NSF	RAC1	SSR3	WIPF1
BACH1	COQ9	FOXJ3	KLHL40	NSFL1C	RACGAP1	SSRP1	WIPF2
BACH2	CORO1A	FOXL1	KLHL41	NSL1	RAD1	SSSCA1	WIPI1
BAD	CORO1B	FOXL2NB	KLHL42	NSMAF	RAD17	SST	WIPI2
BAG1	CORO1C	FOXM1	KLHL6	NSMCE1	RAD18	SSU72	WISP1
BAG3	CORO2A	FOXN2	KLHL7	NSMCE2	RAD21	SSUH2	WISP2
BAG4	CORO2B	FOXN3	KLHL9	NSMCE4A	RAD23A	SSX2IP	WISP3
BAG6	CORO6	FOXO1	KLK1	NSMF	RAD23B	ST13	WIZ
BAHD1	CORO7	FOXP1	KLK10	NSRP1	RAD50	ST3GAL1	WLS
BAI1	CORO7	FOXP2	KLK11	NSUN2	RAD51	ST3GAL2	WNK1
BAI2	CORO7	FOXP4	KLK12	NSUN3	RAD51	ST3GAL3	WNK2
BAIAP2L1	CORO7-PAM16	FOXQ1	KLK13	NSUN4	RAD51AP1	ST3GAL4	WNT10A
BAIAP2L2	CORO7-PAM16	FOXR1	KLK14	NSUN5	RAD51AP2	ST3GAL5	WNT10B
BAK1	CORO7-PAM16	FOXRED1	KLK15	NSUN6	RAD51C	ST3GAL6	WNT11
BAMBI	CORT	FOXRED2	KLK4	NSUN7	RAD51D	ST5	WNT16
BANF1	COTL1	FOXS1	KLK5	NT5C1A	RAD52	ST6GAL1	WNT2
BANF2	COX10	FPR1	KLK6	NT5C2	RAD54B	ST6GAL2	WNT2B
BANK1	COX11	FPR2	KLK7	NT5C3A	RAD54L	ST6GALNAC1	WNT3
BANP	COX14	FPR3	KLK8	NT5C3B	RAD54L2	ST6GALNAC2	WNT3A
BARD1	COX16	FRA10AC1	KLK9	NT5DC1	RAD9A	ST6GALNAC3	WNT5A
BARX2	COX17	FRAT1	KLKB1	NT5DC2	RAD9B	ST6GALNAC4	WNT6
BATF	COX18	FRAT2	KLLN	NTAN1	RADIL	ST6GALNAC5	WNT7A
BATF2	COX19	FREM1	KLRB1	NTF4	RAET1E	ST6GALNAC6	WNT7B
BATF3	COX20	FREM2	KLRC1	NTHL1	RAET1L	ST7	WNT8A
BAX	COX4I1	FRG1	KLRC2	NTM	RAF1	ST8SIA1	WNT8B
BAZ1B	COX4I2	FRG2	KLRC3	NTMT1	RAG1	ST8SIA2	WNT9A
BAZ2A	COX5A	FRG2B	KLRC4	NTN3	RAG2	ST8SIA3	WNT9B
BBC3	COX5B	FRK	KLRD1	NTN4	RAI1	ST8SIA4	WRAP53
BBOX1	COX6A1	FRMD1	KLRF1	NTN5	RAI14	ST8SIA5	WRNIP1
BBS10	COX6A2	FRMD3	KLRF2	NTNG1	RALA	ST8SIA6	WSB1
BBS12	COX6B1	FRMD4A	KLRG1	NTNG2	RALB	STAB1	WSB2
BBS2	COX6B2	FRMD5	KLRG2	NTPCR	RALBP1	STAC	WSCD1
BBS4	COX6C	FRMD6	KLRK1	NTRK1	RALGAPA2	STAC2	WSCD2
BBS5	COX7A1	FRMD8	KMO	NUAK1	RALGAPB	STAC3	WT1
BBX	COX7A2	FRMPD1	KMT2A	NUAK2	RALGDS	STAG1	WTAP
BCAM	COX7A2L	FRRS1	KMT2B	NUB1	RALGPS1	STAG3	WWC1
BCAN	COX7B2	FRRS1L	KNDC1	NUBP1	RALGPS2	STAM	WWC2
BCAP29	COX7C	FRS2	KNG1	NUBP2	RAMP1	STAM2	WWP1
BCAR1	COX8A	FRS3	KNOP1	NUBPL	RAMP2	STAMBP	WWP2
BCAS1	COX8C	FRY	KNSTRN	NUCB1	RAMP3	STAMBPL1	WWTR1

BCAS2
BCAS3
BCAS4
BCAT1
BCDIN3D
BCKDHA
BCKDHB
BCKDK
BCL10
BCL11A
BCL11B
BCL2
BCL2
BCL2A1
BCL2L1
BCL2L13
BCL2L14
BCL2L15
BCL2L2
BCL3
BCL6
BCL6B
BCL7B
BCL7C
BCL9
BCL9L
BCLAF1
BCO1
BCO2
BCR
BCS1L
BDH1
BDH2
BDNF
BDP1
BEAN1
BECN1
BEGAIN
BEND4
BEND5
BEND6
BEND7
BEST1
BEST2
BEST3
BEST4
BET1
BET1L
BFAR
BFSP1
BGLAP
BHLHA15
BHLHE22
BHLHE23
BHLHE40
BHLHE41
BHMT
BHMT2
BICD1
BICD2
BID
BIK
BIN1
BIRC2
BIRC3
BIRC5
BIRC6
BIRC7
BIRC8
BIVM-ERCC5
BLCAP
BLID
BLMH
BLNK
BLOC1S1
BLOC1S2
BLOC1S3
BLOC1S4
BLOC1S5
BLOC1S6
BLVRA
BLVRB
BLZF1
BMF
BMI1
BMP10
BMP2K
BMP3
BMP4
BMP6
BMP7
BMP8A
BMP8B
BMPER
BMPR1A
BMPR1B
BMPR2
BMS1
BNC1
BNC2
BNIP1

CP
CPA1
CPA2
CPA3
CPA4
CPA5
CPA6
CPAMD8
CPB1
CPB2
CPD
CPE
CPEB1
CPEB3
CPEB4
CPED1
CPLX3
CPLX4
CPM
CPN1
CPN2
CPNE2
CPNE4
CPNE5
CPNE8
CPO
CPOX
CPPED1
CPQ
CPSF1
CPSF3
CPSF3L
CPSF4L
CPSF6
CPSF7
CPT1A
CPT1B
CPT1C
CPT2
CPTP
CPVL
CPXM1
CPXM2
CPZ
CR1
CR2
CRABP1
CRABP2
CRACR2A
CRACR2B
CRADD
CRB1
CRB2
CRBN
CRCP
CRCT1
CREB1
CREB3
CREB3L1
CREB3L2
CREB3L3
CREB3L4
CREB5
CREBBP
CREBL2
CREBRF
CREBZF
CREG1
CREG2
CRELD1
CRELD2
CREM
CRH
CRHBP
CRIM1
CRIP1
CRIP2
CRIPAK
CRIPT
CRISP1
CRISP2
CRISP3
CRISPLD1
CRISPLD2
CRK
CRKL
CRLF2
CRLS1
CRMP1
CRNN
CROCC
CROT
CRP
CRTAC1
CRTAM
CRTC2
CRTC3
CRX
CRY1
CRY2
CRYBA1

FRZB
FSBP
FSCB
FSCN1
FSCN2
FSCN3
FSD1
FSD2
FSHB
FSIP1
FSIP2
FST
FSTL1
FSTL3
FSTL5
FTCD
FTH1
FTL
FTMT
FTO
FTSJ2
FUBP1
FUCA1
FUCA2
FUK
FUOM
FURIN
FUS
FUT1
FUT10
FUT11
FUT2
FUT3
FUT4
FUT5
FUT6
FUT7
FUT8
FUT9
FUZ
FXN
FXYD1
FXYD2
FXYD3
FXYD4
FXYD5
FXYD6
FXYD7
FYB
FYCO1
FYTTD1
FZD1
FZD2
FZD3
FZD4
FZD5
FZD6
FZD7
FZD8
FZR1
G0S2
G2E3
G3BP1
G3BP2
G6PC
G6PC2
G6PC3
GAB1
GAB2
GABARAPL2
GABPA
GABPB2
GABRD
GABRG1
GABRP
GAD2
GADD45A
GADD45B
GADD45G
GADD45GIP1
GADL1
GAK
GAL3ST1
GAL3ST2
GAL3ST3
GAL3ST4
GALE
GALM
GALNT1
GALNT10
GALNT11
GALNT12
GALNT13
GALNT14
GALNT15
GALNT16
GALNT18
GALNT2
GALNT3
GALNT4
GALNT5

KPNA1
KPNA2
KPNA3
KPNA4
KPNA5
KPNA6
KPNA7
KPNB1
KPRP
KRAS
KRBA1
KRBA2
KRBOX1
KRCC1
KRI1
KRR1
KRT1
KRT10
KRT12
KRT13
KRT14
KRT15
KRT16
KRT17
KRT18
KRT19
KRT2
KRT222
KRT24
KRT25
KRT26
KRT27
KRT28
KRT3
KRT31
KRT32
KRT33A
KRT33B
KRT34
KRT35
KRT36
KRT37
KRT38
KRT39
KRT4
KRT40
KRT6A
KRT6B
KRT6C
KRT7
KRT71
KRT72
KRT73
KRT74
KRT75
KRT76
KRT77
KRT78
KRT79
KRT8
KRT80
KRT81
KRT82
KRT83
KRT84
KRT85
KRT86
KRT9
KRTAP10-10
KRTAP10-11
KRTAP10-12
KRTAP10-4
KRTAP10-6
KRTAP10-7
KRTAP10-8
KRTAP1-1
KRTAP12-1
KRTAP12-2
KRTAP16-1
KRTAP19-8
KRTAP20-3
KRTAP2-3
KRTAP2-4
KRTAP24-1
KRTAP25-1
KRTAP26-1
KRTAP27-1
KRTAP4-1
KRTAP4-8
KRTAP4-9
KRTAP5-1
KRTAP5-11
KRTAP5-2
KRTAP5-4
KRTAP5-8
KRTAP6-1
KRTAP6-3
KRTAP7-1
KRTAP9-9
KRTCAP2
KRTCAP3

NUCB2
NUCKS1
NUDCD1
NUDCD2
NUDCD3
NUDT1
NUDT12
NUDT13
NUDT14
NUDT15
NUDT16
NUDT16L1
NUDT18
NUDT2
NUDT21
NUDT22
NUDT4
NUDT6
NUDT8
NUF2
NUFIP1
NUFIP2
NUGGC
NUMBL
NUP107
NUP133
NUP155
NUP155
NUP160
NUP210
NUP210L
NUP214
NUP35
NUP37
NUP43
NUP62
NUP85
NUP88
NUP93
NUP98
NUPL2
NUPR1
NUPR1L
NUS1
NUSAP1
NUTM1
NUTM2A
NUTM2F
NUTM2G
NVL
NWD1
NWD2
NXF1
NXNL1
NXNL2
NXPE1
NXPE2
NXPE3
NXPE4
NXPH1
NXPH4
NXT1
NYAP1
NYAP2
OAF
OARD1
OASL
OAT
OAZ1
OAZ2
OAZ3
OBFC1
OBP2A
OBP2B
OBSCN
OC90
OCA2
OCEL1
OCIAD1
OCIAD2
OCLM
OCLN
OCM
OCM2
ODAM
ODF3L1
ODF3L2
OGDHL
OGFOD1
OGFOD2
OGFOD3
OGFRL1
OGG1
OIP5
OIT3
OLA1
OLAH
OLFM1
OLFM4
OLFML1
OLFML2A

RAN
RANBP1
RANBP10
RANBP17
RANBP2
RANBP3
RANBP3L
RANBP6
RANGAP1
RANGRF
RAP1A
RAP1B
RAP1GAP
RAP1GDS1
RAP2B
RAPGEF1
RAPGEF2
RAPGEF3
RAPGEF4
RAPGEF5
RAPGEF6
RAPGEFL1
RARB
RARB
RARG
RARS
RARS2
RASA1
RASA2
RASA3
RASA4
RASAL1
RASAL2
RASAL3
RASD1
RASD2
RASEF
RASGEF1A
RASGEF1B
RASGEF1C
RASGRF1
RASGRF2
RASGRP1
RASGRP2
RASGRP3
RASGRP4
RASIP1
RASL10B
RASL11A
RASL11B
RASL12
RASSF10
RASSF2
RASSF4
RASSF6
RASSF7
RASSF8
RAVER1
RAVER2
RAX2
RB1
RB1CC1
RBAK
RBBP4
RBBP5
RBBP6
RBBP8
RBBP8NL
RBBP9
RBCK1
RBFA
RBFOX1
RBFOX3
RBKS
RBL1
RBL2
RBM11
RBM12
RBM12B
RBM14
RBM15
RBM15B
RBM17
RBM18
RBM19
RBM20
RBM22
RBM24
RBM26
RBM28
RBM34
RBM38
RBM4
RBM42
RBM43
RBM44
RBM45
RBM46
RBM47
RBM48
RBM4B

STAP1
STAP2
STAR
STARD4
STARD6
STAT1
STAT2
STAT3
STAT3
STAT4
STAT5A
STAT5B
STAT6
STATH
STAU1
STAU2
STC2
STEAP1
STEAP2
STEAP3
STEAP4
STIL
STIM1
STIM2
STIP1
STK10
STK11
STK11IP
STK17A
STK24
STK25
STK3
STK31
STK32A
STK32B
STK32C
STK33
STK35
STK38
STK38L
STK39
STK4
STK40
STKLD1
STMN1
STMN2
STMN3
STMN4
STMND1
STOM
STOML1
STOML2
STON1
STON2
STOX1
STOX2
STPG1
STPG2
STRA13
STRA8
STRADB
STRAP
STRC
STRIP1
STRIP2
STRN3
STT3A
STT3B
STUB1
STX10
STX12
STX16
STX17
STX19
STX1A
STX2
STX3
STX4
STX5
STX6
STX8
STXBP1
STXBP2
STXBP3
STXBP4
STYK1
STYX
STYXL1
SUB1
SUCLG1
SUCLG2
SUCNR1
SUCO
SUDS3
SUFU
SUGCT
SUGP2
SULF1
SULF2
SULT1A1
SULT1A2

XAB2
XAF1
XBP1
XCL1
XCL2
XDH
XIRP2
XKR3
XKR4
XKR5
XKR6
XKR7
XKR8
XKR9
XPA
XPC
XPNPEP3
XPO1
XPO4
XPO5
XPO7
XPOT
XPR1
XRCC1
XRCC2
XRCC3
XRCC4
XRCC5
XRCC6
XRCC6BP1
XRN1
XRN2
XRRA1
XXYLT1
XYLB
XYLT1
XYLT2
YAE1D1
YAP1
YARS
YBEY
YBX1
YBX2
YBX3
YEATS2
YEATS4
YES1
YIF1A
YIF1B
YIPF1
YIPF2
YIPF3
YIPF4
YIPF5
YIPF7
YJEFN3
YKT6
YLPM1
YME1L1
YOD1
YPEL1
YPEL3
YPEL4
YPEL5
YRDC
YTHDC1
YTHDC2
YTHDF1
YTHDF2
YTHDF3
YWHAB
YWHAE
YWHAG
YWHAH
YWHAQ
YWHAZ
YY1
YY1AP1
ZACN
ZADH2
ZAN
ZBBX
ZBED1
ZBED2
ZBED3
ZBED4
ZBED5
ZBED6
ZBED6CL
ZBED8
ZBED9
ZBP1
ZBTB10
ZBTB11
ZBTB12
ZBTB14
ZBTB16
ZBTB17
ZBTB18
ZBTB2
ZBTB20

BNIP2
BNIP3L
BOC
BOD1
BOD1L1
BOD1L2
BOK
BOLA1
BOLA2
BOLA2B
BOLA3
BOLL
BOP1
BORA
BPGM
BPI
BPIFA1
BPIFA2
BPIFA3
BPIFB1
BPIFB2
BPIFB3
BPIFB4
BPIFB6
BPIFC
BPNT1
BPTF
BPTF
BRAF
BRAT1
BRCA1
BRCA2
BRD1
BRD3
BRD4
BRD7
BRD8
BRD9
BRDT
BRF1
BRF2
BRI3
BRI3BP
BRICD5
BRINP1
BRINP2
BRINP3
BRIP1
BRIX1
BRK1
BRMS1
BRMS1L
BROX
BRPF1
BRPF3
BRSK1
BRSK2
BRWD1
BSCL2
BSDC1
BSG
BSN
BSND
BSPH1
BSPRY
BST1
BST2
BSX
BTAF1
BTBD10
BTBD16
BTBD17
BTBD18
BTBD19
BTBD7
BTBD8
BTBD9
BTD
BTF3
BTF3L4
BTG2
BTG3
BTG4
BTLA
BTN1A1
BTN2A1
BTN3A3
BTNL2
BTNL3
BTNL8
BTNL9
BTRC
BUB1
BUD13
BUD31
BVES
BZRAP1
BZW1
BZW2

CRYBA2
CRYBA4
CRYBB1
CRYBB2
CRYBB3
CRYBG3
CRYGA
CRYGB
CRYGC
CRYGD
CRYGS
CRYL1
CRYZL1
CS
CSAD
CSDC2
CSDE1
CSE1L
CSF1
CSF1R
CSF2
CSF2RB
CSF3
CSF3R
CSGALNACT1
CSGALNACT2
CSH1
CSH2
CSHL1
CSK
CSMD1
CSMD2
CSMD3
CSN3
CSNK1A1
CSNK1A1L
CSNK1D
CSNK1E
CSNK1G1
CSNK1G2
CSNK1G3
CSNK2A1
CSNK2A2
CSNK2A3
CSNK2B
CSPG4
CSPG5
CSPP1
CSRNP1
CSRNP3
CSRP1
CSRP2
CSRP2BP
CSRP3
CST1
CST11
CST3
CST4
CST5
CST6
CST7
CST9L
CSTA
CSTB
CSTF1
CSTF2T
CSTF3
CT62
CTAGE1
CTAGE15
CTAGE4
CTAGE5
CTAGE6
CTAGE9
CTBP1
CTBP2
CTBS
CTC1
CTCF
CTCFL
CTDNEP1
CTDP1
CTDSP1
CTDSP1
CTDSP2
CTDSPL
CTDSPL2
CTF1
CTGF
CTH
CTHRC1
CTIF
CTLA4
CTNNA1
CTNNA2
CTNNA3
CTNNAL1
CTNNB1
CTNNBIP1

GALNT6
GALNT7
GALNT8
GALNT8
GALNT9
GALNTL5
GALNTL6
GALP
GALT
GAMT
GANAB
GANC
GAP43
GAPDH
GAPDHS
GAPT
GAREM
GAREML
GARNL3
GARS
GART
GAS1
GAS2
GAS2L1
GAS2L2
GAS2L3
GAS6
GAS7
GAS7
GAS7
GATA2
GATA3
GATA4
GATA5
GATA6
GATAD1
GATAD2A
GATAD2B
GATC
GATM
GATS
GATSL2
GATSL3
GBA
GBA2
GBAS
GBGT1
GBP1
GBP2
GBP3
GBP4
GBP5
GBP6
GBP7
GBX2
GCA
GCC1
GCFC2
GCG
GCGR
GCHFR
GCKR
GCLM
GCNT1
GCNT2
GCNT3
GCNT4
GCNT7
GCOM1
GCSAM
GCSAML
GCSH
GDAP1
GDAP1L1
GDAP2
GDE1
GDF10
GDF15
GDF2
GDF6
GDF7
GDF9
GDI2
GDNF
GDPD1
GDPD3
GDPD4
GDPD5
GDPGP1
GEM
GEMIN4
GEN1
GET4
GFAP
GFER
GFI1
GFI1B
GFM1
GFM2

KSR1
KSR2
KTI12
KXD1
KY
KYNU
L1TD1
L2HGDH
L3HYPDH
L3MBTL1
L3MBTL2
L3MBTL4
LACC1
LACE1
LACRT
LACTB
LACTB2
LAD1
LALBA
LAMA1
LAMA3
LAMA3
LAMA4
LAMA5
LAMB1
LAMB2
LAMB3
LAMC1
LAMC2
LAMC3
LAMP5
LAMTOR1
LAMTOR2
LAMTOR3
LAMTOR4
LAMTOR5
LANCL1
LANCL2
LAPTM4A
LAPTM5
LARGE
LARP1B
LARP4
LARP4B
LARP6
LARP7
LARS
LARS2
LASP1
LATS1
LAX1
LAYN
LBH
LBHD1
LBP
LBR
LBX1
LBX2
LCA5
LCA5L
LCE1A
LCE1B
LCE1C
LCE1D
LCE1E
LCE1F
LCE2A
LCE2B
LCE2C
LCE2D
LCE3A
LCE3B
LCE3C
LCE3D
LCE3E
LCE4A
LCE5A
LCK
LCLAT1
LCMT1
LCMT2
LCN1
LCN10
LCN12
LCN15
LCN2
LCN6
LCN8
LCN9
LCNL1
LCORL
LCP1
LCP2
LCT
LCTL
LDB1
LDHA
LDHAL6A
LDHAL6B

OLFML2B
OLFML3
OLIG1
OLIG2
OLIG3
OLR1
OMA1
OMD
OMG
OMP
OOEP
OOSP2
OPA1
OPALIN
OPCML
OPLAH
OPN1SW
OPN3
OPN4
OPN5
OPRD1
OPRL1
OPRM1
OPTC
OPTN
OR10A2
OR10A3
OR10A4
OR10A5
OR10A6
OR10AG1
OR10G4
OR10G7
OR10G8
OR10G9
OR10J1
OR10J5
OR10K2
OR10Q1
OR10R2
OR10S1
OR10T2
OR10V1
OR10W1
OR10X1
OR10Z1
OR11H1
OR11H12
OR11H2
OR11L1
OR13A1
OR13C2
OR13C5
OR13G1
OR14A16
OR14C36
OR14I1
OR1A1
OR1A2
OR1B1
OR1D2
OR1D5
OR1E1
OR1S1
OR1S2
OR2A4
OR2AG1
OR2AG2
OR2AK2
OR2AT4
OR2B11
OR2C3
OR2D2
OR2D3
OR2K2
OR2L13
OR2L2
OR2L3
OR2M2
OR2M3
OR2M4
OR2M5
OR2M7
OR2S2
OR2T10
OR2T11
OR2T12
OR2T2
OR2T27
OR2T29
OR2T3
OR2T33
OR2T34
OR2T35
OR2T4
OR2T5
OR2T6
OR2T8
OR2W3

RBM5
RBM6
RBM7
RBM8A
RBMS1
RBMS2
RBMS3
RBMXL1
RBMXL2
RBP1
RBP2
RBP3
RBP4
RBP5
RBP7
RBPJ
RBPJL
RBSN
RBX1
RC3H1
RC3H2
RCBTB1
RCBTB2
RCC1
RCC2
RCCD1
RCE1
RCHY1
RCL1
RCN1
RCN2
RCN3
RCOR1
RCOR2
RCOR3
RCSD1
RCVRN
RD3
RD3L
RDH13
RDH16
RDH5
RDM1
RDX
REC114
REC8
RECQL
RECQL4
RECQL5
REEP1
REEP2
REEP3
REEP4
REEP5
REEP6
REG1A
REG1B
REG3A
REG3G
REG4
REL
RELA
RELL1
RELL2
RELN
RELT
REM1
REM2
REN
REP15
REPIN1
RERG
RERGL
RESP18
REST
RET
RETN
RETSAT
REV1
REV3L
REXO1
REXO2
RFC1
RFC2
RFC3
RFC4
RFC5
RFESD
RFK
RFNG
RFPL1
RFPL2
RFPL3
RFPL4B
RFT1
RFTN1
RFTN2
RFWD2
RFWD3

SULT1B1
SULT1C2
SULT1C3
SULT1C4
SULT1E1
SULT2A1
SULT2B1
SULT4A1
SULT6B1
SUMF1
SUMF2
SUMO1
SUMO2
SUN1
SUN3
SUN5
SUOX
SUPT20H
SUPT3H
SUPT4H1
SUPT5H
SUPT6H
SUPT7L
SUPV3L1
SURF1
SURF2
SURF4
SURF6
SUSD1
SUSD2
SUSD3
SUSD4
SUSD6
SUV39H2
SUV420H1
SUV420H2
SUZ12
SV2B
SVIP
SVOP
SVOPL
SWAP70
SWI5
SWSAP1
SWT1
SYBU
SYCE1L
SYCE3
SYCP1
SYCP2
SYCP3
SYDE1
SYF2
SYMPK
SYN2
SYNC
SYNCRIP
SYNDIG1
SYNE1
SYNE2
SYNE3
SYNE4
SYNGR1
SYNJ2BP
SYNM
SYNPO
SYNPO2L
SYNRG
SYS1
SYT1
SYT10
SYT11
SYT12
SYT13
SYT14
SYT15
SYT16
SYT17
SYT2
SYT3
SYT4
SYT5
SYT6
SYT7
SYT9
SYTL1
SYVN1
SZT2
T
TAAR1
TAAR2
TAAR5
TAAR6
TAAR8
TAAR9
TAB1
TAC1
TAC4
TACC1

ZBTB21
ZBTB24
ZBTB25
ZBTB26
ZBTB3
ZBTB32
ZBTB34
ZBTB37
ZBTB39
ZBTB4
ZBTB40
ZBTB41
ZBTB43
ZBTB44
ZBTB45
ZBTB46
ZBTB47
ZBTB48
ZBTB49
ZBTB5
ZBTB6
ZBTB7A
ZBTB7C
ZBTB8B
ZBTB8OS
ZBTB9
ZC2HC1A
ZC2HC1B
ZC2HC1C
ZC3H10
ZC3H11A
ZC3H12A
ZC3H12C
ZC3H12D
ZC3H13
ZC3H14
ZC3H15
ZC3H18
ZC3H3
ZC3H6
ZC3H7A
ZC3H7B
ZC3H8
ZC3HAV1
ZC3HAV1L
ZC3HC1
ZCCHC10
ZCCHC14
ZCCHC17
ZCCHC2
ZCCHC24
ZCCHC6
ZCCHC7
ZCCHC8
ZCCHC9
ZCRB1
ZCWPW1
ZDBF2
ZDHHC1
ZDHHC11
ZDHHC12
ZDHHC13
ZDHHC14
ZDHHC16
ZDHHC17
ZDHHC18
ZDHHC2
ZDHHC20
ZDHHC21
ZDHHC22
ZDHHC23
ZDHHC24
ZDHHC3
ZDHHC4
ZDHHC5
ZDHHC6
ZDHHC7
ZDHHC8
ZEB1
ZEB2
ZER1
ZFAND1
ZFAND2A
ZFAND2B
ZFAND3
ZFAND4
ZFAND6
ZFAT
ZFC3H1
ZFHX3
ZFHX4
ZFP1
ZFP14
ZFP2
ZFP28
ZFP3
ZFP30
ZFP36L2
ZFP37

C10orf10
C10orf105
C10orf107
C10orf11
C10orf113
C10orf12
C10orf120
C10orf126
C10orf128
C10orf131
C10orf2
C10orf32
C10orf35
C10orf53
C10orf54
C10orf55
C10orf62
C10orf67
C10orf76
C10orf82
C10orf88
C10orf90
C10orf99
C11orf1
C11orf16
C11orf21
C11orf24
C11orf30
C11orf31
C11orf40
C11orf42
C11orf45
C11orf49
C11orf52
C11orf53
C11orf54
C11orf57
C11orf58
C11orf63
C11orf65
C11orf68
C11orf70
C11orf71
C11orf73
C11orf74
C11orf80
C11orf84
C11orf85
C11orf86
C11orf87
C11orf88
C11orf94
C11orf95
C11orf96
C11orf98
C12orf10
C12orf29
C12orf4
C12orf42
C12orf43
C12orf45
C12orf49
C12orf5
C12orf50
C12orf54
C12orf56
C12orf57
C12orf60
C12orf65
C12orf66
C12orf71
C12orf73
C12orf74
C12orf75
C12orf76
C14orf1
C14orf105
C14orf119
C14orf142
C14orf159
C14orf166
C14orf169
C14orf177
C14orf178
C14orf180
C14orf2
C14orf28
C14orf37
C14orf39
C14orf79
C14orf80
C14orf93
C15orf26
C15orf27
C15orf39
C15orf40
C15orf41
C15orf43
C15orf48
C15orf52
C15orf53
CTNNBL1
CTNND1
CTNND2
CTNS
CTPS1
CTR9
CTRB1
CTRB2
CTRC
CTSA
CTSB
CTSC
CTSD
CTSE
CTSF
CTSG
CTSH
CTSK
CTSL
CTSO
CTSS
CTSV
CTSW
CTSZ
CTTN
CTTNBP2
CTTNBP2NL
CTU1
CTU2
CUBN
CUEDC2
CUL1
CUL2
CUL4A
CUL7
CUL9
CUTA
CUTC
CUX1
CUX2
CUZD1
CWC15
CWC22
CWC25
CWC27
CWF19L1
CWF19L2
CWH43
CX3CL1
CX3CR1
CXCL12
CXCL14
CXCL16
CXCL2
CXCL5
CXCL6
CXCL8
CXCR1
CXCR2
CXCR5
CXXC1
CXXC4
CXXC5
CYB561
CYB561A3
CYB561D1
CYB561D2
CYB5A
CYB5A
CYB5B
CYB5D1
CYB5D2
CYB5R1
CYB5R2
CYB5R4
CYB5RL
CYBA
CYBRD1
CYC1
CYFIP1
CYFIP2
CYGB
CYHR1
CYLC2
CYP17A1
CYP1A1
CYP1A2
CYP1B1
CYP21A2
CYP26B1
CYP26C1
CYP27B1
CYP27C1
CYP2A13
CYP2A6
CYP2A7
CYP2B6
CYP2C18
CYP2C19
CYP2C8
CYP2C9
GFOD1
GFOD2
GFPT2
GFRA1
GFRA2
GFRA3
GFRA4
GFRAL
GFY
GGA1
GGA3
GGACT
GGCT
GGCX
GGN
GGNBP2
GGT1
GGT5
GGT6
GGT7
GGTLC2
GH1
GH2
GHDC
GHITM
GHR
GHRL
GHSR
GID4
GID8
GIF
GIGYF1
GIGYF2
GIMAP1
GIMAP2
GIMAP4
GIMAP5
GIMAP6
GIMAP7
GIMAP8
GIN1
GINM1
GINS1
GINS2
GINS3
GINS4
GIP
GIPC2
GIPC3
GIT1
GIT2
GJA1
GJA10
GJA3
GJA4
GJA5
GJA8
GJA9
GJB3
GJB4
GJB5
GJC1
GJC2
GJC3
GJD3
GJD4
GK2
GK5
GKAP1
GKN1
GKN2
GLB1
GLB1L
GLB1L2
GLCCI1
GLCE
GLDC
GLDN
GLE1
GLG1
GLI1
GLI2
GLI3
GLIPR1
GLIPR1L1
GLIPR1L2
GLIPR2
GLIS1
GLIS2
GLIS3
GLMP
GLO1
GLOD4
GLRB
GLRX
GLRX2
GLRX3
GLS2
GLT1D1
GLT6D1
GLT8D1
LDHB
LDHC
LDHD
LDLRAD1
LDLRAD2
LDLRAD3
LDLRAD4
LDLRAP1
LDOC1L
LEAP2
LECT2
LEFTY1
LEFTY2
LEKR1
LELP1
LEMD1
LENEP
LENG1
LENG8
LENG9
LEO1
LEPR
LEPROT
LETM2
LETMD1
LFNG
LGALS1
LGALS12
LGALS13
LGALS14
LGALS2
LGALS3
LGALS3BP
LGALS4
LGALS7
LGALS8
LGALS9
LGALS9B
LGALS9C
LGALSL
LGI1
LGMN
LGR4
LGR5
LGR6
LGSN
LHB
LHFP
LHFPL2
LHFPL3
LHFPL4
LHFPL5
LHPP
LHX1
LHX4
LHX4-AS1
LHX5
LHX6
LHX8
LHX9
LIAS
LIF
LIFR
LIG1
LIG3
LIG4
LILRA1
LILRA4
LILRA5
LILRA6
LILRA6
LILRB3
LIM2
LIMA1
LIMCH1
LIMD1
LIMD2
LIME1
LIMK1
LIMK2
LIMS1
LIMS2
LIMS3
LIMS3L
LIN28A
LIN28B
LIN37
LIN54
LIN7B
LIN7C
LIN9
LINGO1
LINGO2
LINGO3
LIPA
LIPE
LIPG
LIPI
LIPT1
LIPT2
LITAF
OR4A15
OR4A16
OR4A47
OR4A5
OR4B1
OR4C11
OR4C12
OR4C13
OR4C15
OR4C16
OR4C3
OR4C46
OR4C6
OR4D10
OR4D11
OR4D5
OR4D6
OR4D9
OR4F15
OR4F16
OR4F29
OR4F4
OR4F5
OR4K5
OR4P4
OR4S1
OR4S2
OR4X1
OR4X2
OR51A2
OR51A4
OR51A7
OR51B2
OR51B4
OR51B5
OR51B6
OR51D1
OR51E1
OR51E2
OR51F1
OR51F2
OR51G1
OR51G2
OR51I1
OR51I2
OR51L1
OR51M1
OR51Q1
OR51S1
OR51T1
OR51V1
OR52A1
OR52A5
OR52B2
OR52B4
OR52B6
OR52D1
OR52E2
OR52E4
OR52E6
OR52E8
OR52H1
OR52I1
OR52I2
OR52J3
OR52K1
OR52K2
OR52L1
OR52M1
OR52N1
OR52N2
OR52N4
OR52N5
OR52R1
OR52W1
OR56A1
OR56A3
OR56A4
OR56B1
OR56B4
OR5A1
OR5A2
OR5AK2
OR5AN1
OR5AP2
OR5AR1
OR5AS1
OR5B12
OR5B17
OR5B2
OR5B21
OR5B3
OR5D13
OR5D14
OR5D16
OR5D18
OR5F1
OR5H1
OR5I1
OR5J2
OR5L1
RFX1
RFX2
RFX3
RFX4
RFX5
RFX6
RFX7
RFX8
RFXANK
RFXAP
RGCC
RGL1
RGL4
RGMA
RGPD1
RGPD2
RGPD5
RGPD6
RGR
RGS1
RGS10
RGS12
RGS13
RGS14
RGS16
RGS18
RGS19
RGS2
RGS22
RGS3
RGS4
RGS5
RGS7
RGS7BP
RGS8
RGS9
RGS9BP
RHBDD3
RHBDF1
RHBDF2
RHBDL2
RHBDL3
RHBG
RHCE
RHCG
RHD
RHEB
RHEBL1
RHO
RHOA
RHOB
RHOBTB3
RHOC
RHOD
RHOG
RHOH
RHOQ
RHOT1
RHOT2
RHOU
RHPN2
RIBC2
RIC3
RIC8A
RIC8B
RICTOR
RIIAD1
RILP
RILPL1
RILPL2
RIMBP2
RIMBP3
RIMKLA
RIMKLB
RIMS1
RIMS2
RIMS3
RIMS4
RIN1
RINL
RINT1
RIOK1
RIOK2
RIOK3
RIPK1
RIPK3
RIPK4
RIPPLY2
RIT1
RIT2
RITA1
RLBP1
RLF
RLN2
RLTPR
RMDN1
RMDN2
RMDN3
RMI1
RMI2
RMND1
TACO1
TACR1
TACR3
TACSTD2
TADA1
TADA2A
TADA2B
TAF10
TAF11
TAF12
TAF13
TAF15
TAF1A
TAF1B
TAF1C
TAF1D
TAF2
TAF3
TAF4
TAF4B
TAF5L
TAF6
TAF6L
TAF7
TAF8
TAF9
TAF9
TAGAP
TAGLN
TAGLN2
TAGLN3
TAL1
TAL2
TALDO1
TAMM41
TANGO2
TANK
TAOK1
TAOK2
TAOK3
TAP1
TAP2
TAPBPL
TAPT1
TARBP1
TARDBP
TARM1
TARS
TARS2
TARSL2
TAS2R14
TAS2R16
TAS2R19
TAS2R20
TAS2R30
TAS2R31
TAS2R38
TAS2R39
TAS2R42
TAS2R43
TAS2R46
TAS2R50
TASP1
TATDN1
TAX1BP1
TAX1BP3
TBATA
TBC1D1
TBC1D10A
TBC1D10B
TBC1D10C
TBC1D13
TBC1D14
TBC1D15
TBC1D16
TBC1D17
TBC1D19
TBC1D2
TBC1D20
TBC1D21
TBC1D22A
TBC1D22B
TBC1D23
TBC1D24
TBC1D28
TBC1D29
TBC1D2B
TBC1D3
TBC1D31
TBC1D32
TBC1D3B
TBC1D3C
TBC1D3E
TBC1D3G
TBC1D3I
TBC1D4
TBC1D5
TBC1D7
TBC1D9
TBC1D9B
TBCA
ZFP41
ZFP42
ZFP62
ZFP64
ZFP69
ZFP69B
ZFP82
ZFP91
ZFPL1
ZFR2
ZFYVE1
ZFYVE16
ZFYVE19
ZFYVE21
ZFYVE26
ZFYVE27
ZFYVE9
ZG16
ZG16B
ZGLP1
ZGRF1
ZHX2
ZHX3
ZIC1
ZIC2
ZIC5
ZIK1
ZKSCAN1
ZKSCAN2
ZKSCAN3
ZKSCAN4
ZKSCAN5
ZKSCAN7
ZMAT2
ZMAT3
ZMAT4
ZMAT5
ZMIZ1
ZMIZ2
ZMYM1
ZMYM2
ZMYM4
ZMYM6
ZMYND10
ZMYND11
ZMYND12
ZMYND15
ZMYND19
ZMYND8
ZNF10
ZNF100
ZNF101
ZNF106
ZNF107
ZNF112
ZNF114
ZNF12
ZNF121
ZNF124
ZNF131
ZNF132
ZNF133
ZNF134
ZNF135
ZNF136
ZNF138
ZNF14
ZNF140
ZNF141
ZNF143
ZNF146
ZNF148
ZNF155
ZNF16
ZNF160
ZNF165
ZNF169
ZNF17
ZNF174
ZNF175
ZNF177
ZNF180
ZNF181
ZNF184
ZNF189
ZNF19
ZNF197
ZNF2
ZNF20
ZNF202
ZNF205
ZNF208
ZNF212
ZNF213
ZNF217
ZNF22
ZNF224
ZNF227
ZNF229
ZNF23
ZNF232

C15orf57
C15orf59
C15orf61
C15orf62
C16orf13
C16orf45
C16orf46
C16orf52
C16orf54
C16orf58
C16orf59
C16orf62
C16orf70
C16orf71
C16orf72
C16orf74
C16orf78
C16orf86
C16orf87
C16orf89
C16orf90
C16orf92
C16orf93
C16orf95
C16orf96
C17orf100
C17orf104
C17orf105
C17orf107
C17orf47
C17orf49
C17orf50
C17orf51
C17orf53
C17orf58
C17orf59
C17orf62
C17orf64
C17orf67
C17orf70
C17orf74
C17orf75
C17orf78
C17orf80
C17orf89
C17orf96
C17orf97
C17orf98
C17orf99
C18orf21
C18orf25
C18orf32
C18orf42
C18orf54
C18orf63
C18orf65
C18orf8
C19orf12
C19orf18
C19orf24
C19orf25
C19orf26
C19orf33
C19orf35
C19orf38
C19orf40
C19orf43
C19orf44
C19orf45
C19orf52
C19orf53
C19orf54
C19orf57
C19orf66
C19orf70
C19orf71
C19orf73
C19orf80
C19orf81
C19orf84
C1D
C1GALT1
C1orf100
C1orf101
C1orf105
C1orf106
C1orf109
C1orf110
C1orf111
C1orf112
C1orf115
C1orf122
C1orf123
C1orf131
C1orf137
C1orf146
C1orf158
C1orf159
C1orf162
C1orf168
C1orf174

CYP2E1
CYP2J2
CYP2R1
CYP2U1
CYP2W1
CYP4A11
CYP4B1
CYP4F11
CYP4F2
CYP4F22
CYP4F3
CYP4F8
CYP4X1
CYP4Z1
CYP7A1
CYP8B1
CYR61
CYSRT1
CYSTM1
CYTH1
CYTH2
CYTH3
CYTIP
CYTL1
CYYR1
D2HGDH
DAAM1
DAB1
DAB2
DAB2IP
DACH1
DACT1
DACT3
DAD1
DAGLA
DAGLB
DAK
DALRD3
DAND5
DAOA
DAP
DAP3
DAPK1
DAPK2
DAPK3
DAPL1
DARS
DARS2
DAW1
DAZAP1
DAZAP2
DAZL
DBF4
DBF4B
DBH
DBI
DBN1
DBNDD1
DBNDD2
DBNL
DBP
DBT
DBX1
DBX2
DCAF10
DCAF12
DCAF13
DCAF15
DCAF16
DCAF17
DCAF4
DCAF4L1
DCAF4L2
DCAF5
DCAF6
DCAF7
DCAF8
DCAKD
DCANP1
DCBLD1
DCBLD2
DCC
DCD
DCDC1
DCDC2
DCHS1
DCHS2
DCLK1
DCLK2
DCLRE1A
DCLRE1B
DCLRE1C
DCN
DCP1A
DCP1B
DCP2
DCPS
DCST1
DCST2
DCSTAMP
DCTN1

GLT8D2
GLTP
GLTPD2
GLTSCR1
GLTSCR1L
GLTSCR2
GLUD1
GLUL
GLYAT
GLYATL1
GLYATL2
GLYATL3
GLYCTK
GLYR1
GM2A
GMCL1
GMEB1
GMEB2
GMFB
GMIP
GML
GMNC
GMNN
GMPPA
GMPPB
GMPR2
GNA11
GNA12
GNA13
GNA15
GNAI1
GNAI2
GNAI3
GNAL
GNAO1
GNAQ
GNAS
GNAT1
GNAT2
GNAZ
GNB1
GNB2
GNB2L1
GNB3
GNB4
GNE
GNG11
GNG13
GNG3
GNG4
GNG5
GNG7
GNGT1
GNGT2
GNL2
GNL3
GNLY
GNMT
GNPDA1
GNPDA2
GNPTG
GNRH1
GNRH2
GOLGA1
GOLGA2
GOLGA3
GOLGA4
GOLGA6B
GOLGA6C
GOLGA6D
GOLGA6L1
GOLGA6L1
GOLGA6L10
GOLGA6L22
GOLGA6L4
GOLGA6L6
GOLGA6L9
GOLGA7
GOLGA7B
GOLGA8B
GOLGA8N
GOLGA8R
GOLGB1
GOLM1
GOLPH3
GOLPH3L
GOLT1A
GOLT1B
GON4L
GOPC
GORAB
GOT1
GOT1L1
GP5
GPA33
GPAA1
GPALPP1
GPAM
GPANK1
GPAT2
GPATCH1

LIX1
LIX1L
LKAAEAR1
LLGL2
LLPH
LMAN1
LMAN2
LMAN2L
LMBR1
LMBR1L
LMBRD1
LMBRD2
LMCD1
LMF1
LMF2
LMLN
LMNA
LMNB1
LMNB2
LMNTD1
LMNTD2
LMO1
LMO2
LMO3
LMO4
LMO7
LMO7DN
LMTK2
LMX1A
LNPEP
LONP1
LONP2
LONRF1
LONRF2
LOR
LOXHD1
LOXL1
LOXL3
LOXL4
LPA
LPAR1
LPAR2
LPAR3
LPAR5
LPAR6
LPCAT1
LPCAT2
LPCAT3
LPCAT4
LPGAT1
LPHN1
LPHN2
LPIN1
LPIN2
LPIN3
LPP
LPXN
LRAT
LRCH1
LRCH3
LRCH4
LRCOL1
LRFN1
LRFN3
LRFN4
LRFN5
LRG1
LRGUK
LRIF1
LRIG1
LRIG2
LRIG3
LRIT1
LRIT3
LRMP
LRP1
LRP11
LRP12
LRP1B
LRP2
LRP2BP
LRP4
LRP5
LRP5L
LRP8
LRPPRC
LRR1
LRRC10
LRRC10B
LRRC14
LRRC14B
LRRC16A
LRRC16B
LRRC17
LRRC18
LRRC19
LRRC20
LRRC23
LRRC24
LRRC25
LRRC26

OR5L2
OR5M1
OR5M10
OR5M11
OR5M3
OR5M8
OR5M9
OR5P2
OR5P3
OR5R1
OR5T1
OR5T2
OR5T3
OR5W2
OR6A2
OR6B2
OR6C1
OR6C2
OR6C76
OR6F1
OR6K2
OR6K6
OR6M1
OR6N1
OR6Q1
OR6T1
OR6X1
OR6Y1
OR7A10
OR7A17
OR7A5
OR8A1
OR8B2
OR8B3
OR8B4
OR8B8
OR8D1
OR8D2
OR8D4
OR8G1
OR8G5
OR8H1
OR8H2
OR8H3
OR8I2
OR8J1
OR8J3
OR8K1
OR8K3
OR8K5
OR8U1
OR8U1
OR8U8
OR9A4
OR9G1
OR9G4
OR9G9
OR9I1
OR9Q1
OR9Q2
ORAI1
ORAI2
ORAI3
ORAOV1
ORC1
ORC2
ORC4
ORC5
ORM2
ORMDL1
ORMDL2
ORMDL3
OS9
OSBP2
OSBPL11
OSBPL1A
OSBPL2
OSBPL6
OSBPL8
OSCAR
OSCP1
OSER1
OSGEP
OSGEPL1
OSGIN2
OSM
OSMR
OSR1
OSR2
OST4
OSTC
OSTF1
OSTM1
OSTN
OTOGL
OTOL1
OTOP1
OTOP2
OTOP3
OTOS
OTUB1

RMND5A
RMND5B
RNASE11
RNASE3
RNASE7
RNASE8
RNASE9
RNASEH2A
RNASEH2B
RNASEH2C
RNASEK
RNASEL
RNASET2
RND1
RND2
RND3
RNF103
RNF11
RNF111
RNF112
RNF113B
RNF114
RNF115
RNF121
RNF122
RNF123
RNF125
RNF130
RNF133
RNF135
RNF138
RNF139
RNF14
RNF141
RNF144A
RNF145
RNF146
RNF148
RNF149
RNF151
RNF152
RNF165
RNF166
RNF167
RNF168
RNF170
RNF175
RNF180
RNF181
RNF182
RNF183
RNF185
RNF186
RNF187
RNF19A
RNF19B
RNF2
RNF20
RNF207
RNF208
RNF212
RNF214
RNF215
RNF216
RNF217
RNF219
RNF220
RNF223
RNF224
RNF25
RNF26
RNF31
RNF32
RNF34
RNF38
RNF39
RNF4
RNF40
RNF41
RNF43
RNF5
RNF6
RNF7
RNFT1
RNFT2
RNGTT
RNH1
RNLS
RNMT
RNMTL1
RNPC3
RNPEP
RNPEPL1
RNPS1
ROBO1
ROBO4
ROCK1
ROGDI
ROM1
ROMO1
ROPN1

TBCB
TBCC
TBCCD1
TBCD
TBCE
TBCEL
TBCK
TBK1
TBKBP1
TBL1XR1
TBL2
TBL3
TBP
TBPL2
TBR1
TBRG1
TBRG4
TBX1
TBX10
TBX15
TBX18
TBX19
TBX2
TBX21
TBX3
TBX3
TBX4
TBX5
TBX6
TC2N
TCAF1
TCAF2
TCAIM
TCAP
TCEA1
TCEA2
TCEA3
TCEANC2
TCEB1
TCEB2
TCEB3
TCEB3B
TCEB3C
TCERG1
TCERG1L
TCF12
TCF15
TCF19
TCF20
TCF21
TCF23
TCF24
TCF25
TCF3
TCF4
TCF7
TCF7L1
TCF7L2
TCFL5
TCHH
TCHP
TCIRG1
TCN1
TCN2
TCP1
TCP10
TCP10L
TCP11
TCP11L1
TCP11L2
TCTA
TCTE1
TCTE3
TCTEX1D1
TCTEX1D2
TCTEX1D4
TCTN1
TCTN2
TCTN3
TDGF1
TDO2
TDP1
TDRD10
TDRD3
TDRD5
TDRD7
TDRD9
TDRKH
TDRP
TEAD1
TEAD2
TEAD4
TECPR1
TECPR2
TECR
TECRL
TECTA
TECTB
TEDDM1
TEF
TEFM

ZNF233
ZNF24
ZNF248
ZNF25
ZNF250
ZNF251
ZNF253
ZNF26
ZNF260
ZNF267
ZNF268
ZNF274
ZNF276
ZNF277
ZNF28
ZNF280A
ZNF280B
ZNF281
ZNF282
ZNF283
ZNF284
ZNF285
ZNF286A
ZNF286A
ZNF292
ZNF296
ZNF3
ZNF30
ZNF300
ZNF316
ZNF317
ZNF318
ZNF32
ZNF320
ZNF321P
ZNF322
ZNF324
ZNF324B
ZNF329
ZNF330
ZNF331
ZNF333
ZNF335
ZNF33A
ZNF33B
ZNF34
ZNF343
ZNF346
ZNF347
ZNF35
ZNF350
ZNF354A
ZNF354B
ZNF362
ZNF365
ZNF37A
ZNF382
ZNF383
ZNF385A
ZNF385B
ZNF385D
ZNF391
ZNF394
ZNF396
ZNF397
ZNF404
ZNF407
ZNF408
ZNF410
ZNF414
ZNF415
ZNF416
ZNF417
ZNF418
ZNF419
ZNF420
ZNF423
ZNF426
ZNF428
ZNF429
ZNF43
ZNF430
ZNF432
ZNF436
ZNF438
ZNF44
ZNF440
ZNF441
ZNF442
ZNF443
ZNF444
ZNF445
ZNF446
ZNF45
ZNF451
ZNF460
ZNF461
ZNF462
ZNF467
ZNF468
ZNF470

C1orf177
C1orf185
C1orf186
C1orf189
C1orf194
C1orf195
C1orf198
C1orf204
C1orf21
C1orf210
C1orf216
C1orf226
C1orf228
C1orf233
C1orf27
C1orf35
C1orf43
C1orf50
C1orf52
C1orf53
C1orf54
C1orf56
C1orf61
C1orf64
C1orf68
C1orf74
C1orf86
C1orf87
C1orf94
C1orf95
C1QA
C1QB
C1QBP
C1QC
C1QL1
C1QL2
C1QL4
C1QTNF1
C1QTNF3
C1QTNF4
C1QTNF5
C1QTNF5
C1QTNF6
C1QTNF9
C1QTNF9B
C1R
C1RL
C1S
C20orf141
C20orf144
C20orf173
C20orf194
C20orf195
C20orf196
C20orf202
C20orf24
C20orf27
C20orf85
C20orf96
C21orf2
C21orf33
C21orf58
C21orf59
C21orf62
C21orf91
C22orf15
C22orf23
C22orf29
C22orf31
C22orf39
C22orf42
C2CD2
C2CD2L
C2CD3
C2CD4A
C2CD4B
C2CD4D
C2CD5
C2orf15
C2orf16
C2orf40
C2orf42
C2orf43
C2orf44
C2orf47
C2orf49
C2orf50
C2orf54
C2orf54
C2orf57
C2orf61
C2orf66
C2orf68
C2orf69
C2orf70
C2orf71
C2orf72
C2orf73
C2orf74
C2orf76
C2orf78

DCTN2
DCTN5
DCTN6
DCTPP1
DCUN1D1
DCUN1D3
DCUN1D4
DCUN1D5
DDA1
DDB1
DDB2
DDI1
DDI2
DDIAS
DDIT3
DDIT4
DDIT4L
DDOST
DDR1
DDR2
DDRGK1
DDT
DDTL
DDX1
DDX10
DDX11
DDX18
DDX19A
DDX19B
DDX20
DDX21
DDX23
DDX24
DDX25
DDX28
DDX31
DDX39B
DDX4
DDX41
DDX42
DDX43
DDX46
DDX47
DDX49
DDX5
DDX50
DDX51
DDX54
DDX56
DDX58
DDX6
DDX60
DDX60L
DEAF1
DECR2
DEDD2
DEF6
DEF8
DEFA1
DEFA1B
DEFA3
DEFA4
DEFA5
DEFA6
DEFB1
DEFB103A
DEFB103B
DEFB104A
DEFB105A
DEFB106A
DEFB108B
DEFB110
DEFB112
DEFB113
DEFB114
DEFB115
DEFB116
DEFB118
DEFB119
DEFB121
DEFB123
DEFB124
DEFB125
DEFB126
DEFB127
DEFB128
DEFB129
DEFB130
DEFB131
DEFB132
DEFB133
DEFB134
DEFB135
DEFB136
DEFB4A
DEGS2
DENND1A
DENND1B
DENND1C
DENND2A
DENND2C

GPATCH11
GPATCH2
GPATCH2L
GPATCH3
GPATCH8
GPBAR1
GPBP1
GPBP1L1
GPC1
GPC2
GPC5
GPC6
GPCPD1
GPD1L
GPER1
GPHA2
GPHB5
GPHN
GPIHBP1
GPLD1
GPN1
GPN2
GPN3
GPNMB
GPR1
GPR110
GPR111
GPR113
GPR114
GPR115
GPR116
GPR132
GPR133
GPR135
GPR137
GPR137B
GPR139
GPR141
GPR142
GPR146
GPR151
GPR155
GPR156
GPR157
GPR160
GPR162
GPR171
GPR176
GPR180
GPR182
GPR183
GPR19
GPR20
GPR25
GPR27
GPR3
GPR31
GPR33
GPR35
GPR37
GPR37L1
GPR4
GPR45
GPR52
GPR55
GPR75-ASB3
GPR83
GPR88
GPR89A
GPR89B
GPR97
GPR98
GPRC5A
GPRIN1
GPRIN2
GPRIN3
GPS1
GPS2
GPSM1
GPSM2
GPSM3
GPX1
GPX4
GPX7
GPX8
GRAMD1A
GRAMD1C
GRAMD2
GRAMD3
GRAMD4
GRAP
GRAP2
GRAPL
GRB7
GREB1
GREM1
GREM2
GRHL2
GRHL3
GRHPR
GRIK3

LRRC28
LRRC29
LRRC31
LRRC32
LRRC34
LRRC36
LRRC37A
LRRC37A2
LRRC37A3
LRRC37B
LRRC39
LRRC3B
LRRC4
LRRC40
LRRC41
LRRC42
LRRC43
LRRC45
LRRC46
LRRC47
LRRC48
LRRC49
LRRC4B
LRRC4C
LRRC52
LRRC55
LRRC56
LRRC57
LRRC59
LRRC6
LRRC61
LRRC66
LRRC69
LRRC7
LRRC71
LRRC73
LRRC74A
LRRC75A
LRRC75B
LRRC8A
LRRC8B
LRRC8C
LRRC8D
LRRC8E
LRRCC1
LRRFIP1
LRRFIP2
LRRIQ4
LRRK1
LRRN1
LRRN2
LRRN3
LRRN4
LRRN4CL
LRRTM1
LRRTM3
LRRTM4
LRSAM1
LRTM1
LRTOMT
LRWD1
LSAMP
LSG1
LSM1
LSM10
LSM11
LSM12
LSM14A
LSM14B
LSM2
LSM3
LSMEM1
LSMEM2
LSP1
LSR
LTA4H
LTBP1
LTBP2
LTBP3
LTBP4
LTF
LTN1
LTV1
LUC7L3
LUM
LURAP1
LURAP1L
LUZP1
LUZP2
LUZP6
LXN
LY6D
LY6E
LY6G6F
LY6K
LY9
LY96
LYAR
LYG1
LYG2
LYL1

OTUD4
OTUD6B
OTUD7A
OTUD7B
OTULIN
OVCA2
OVCH1
OVCH2
OVGP1
OVOL1
OVOL2
OXA1L
OXCT1
OXCT2
OXER1
OXGR1
OXLD1
OXNAD1
OXR1
OXSM
OXSR1
OXT
P2RX1
P2RX3
P2RX5
P2RX5
P2RX6
P2RX7
P2RY1
P2RY11
P2RY14
P2RY2
P2RY8
P3H1
P3H2
P3H3
P4HA1
P4HA2
P4HA3
P4HB
P4HTM
PA2G4
PAAF1
PABPC1
PABPC3
PABPC4
PABPC4L
PABPN1
PABPN1L
PACRG
PACRGL
PACS1
PACSIN2
PACSIN3
PADI1
PADI4
PADI6
PAEP
PAF1
PAFAH1B1
PAFAH1B2
PAFAH1B3
PAFAH2
PAG1
PAGR1
PAICS
PAIP1
PAIP2
PAK1
PAK1IP1
PAK2
PALB2
PALD1
PALLD
PALM
PALM2
PALM3
PALMD
PAM
PAM16
PAMR1
PAN2
PAN3
PANK2
PANK3
PANO1
PANX1
PANX2
PAOX
PAPD4
PAPD7
PAPLN
PAPOLB
PAPOLG
PAPPA
PAQR4
PAQR5
PAQR6
PAQR7
PAQR8
PAQR9

ROPN1B
ROPN1L
ROR1
RORA
RP1
RP9
RPA1
RPA2
RPA3
RPAIN
RPAP1
RPAP2
RPAP3
RPE
RPE65
RPEL1
RPF1
RPF2
RPGRIP1
RPGRIP1L
RPH3A
RPH3AL
RPL10A
RPL11
RPL13
RPL14
RPL15
RPL17
RPL18
RPL18A
RPL19
RPL21
RPL22
RPL23
RPL23A
RPL24
RPL26
RPL26L1
RPL27
RPL27A
RPL28
RPL29
RPL3
RPL31
RPL32
RPL34
RPL34
RPL35
RPL35A
RPL36
RPL37
RPL37A
RPL38
RPL39L
RPL3L
RPL4
RPL5
RPL7
RPL7A
RPL8
RPLP0
RPLP1
RPLP2
RPN1
RPN2
RPP14
RPP21
RPP25
RPP25L
RPP30
RPP38
RPP40
RPRD1A
RPRD1B
RPRD2
RPRM
RPRML
RPS11
RPS12
RPS13
RPS14
RPS15
RPS15A
RPS16
RPS17
RPS19
RPS19BP1
RPS2
RPS20
RPS21
RPS23
RPS24
RPS25
RPS26
RPS27
RPS27L
RPS28
RPS29
RPS3
RPS5
RPS6

TEKT1
TEKT2
TEKT3
TEKT4
TEKT5
TELO2
TEN1
TEN1-CDK3
TENM2
TEP1
TEPP
TERF1
TERF2IP
TES
TESC
TESK1
TESK2
TESPA1
TET1
TET2
TEX10
TEX101
TEX19
TEX2
TEX26
TEX261
TEX264
TEX29
TEX30
TEX33
TEX35
TEX36
TEX37
TEX38
TEX43
TEX9
TF
TFAM
TFAP2A
TFAP2B
TFAP2C
TFAP2D
TFAP2E
TFAP4
TFB2M
TFCP2
TFCP2L1
TFDP1
TFDP2
TFEC
TFF1
TFF2
TFF3
TFG
TFIP11
TFPI
TFPI2
TFPT
TFR2
TG
TGDS
TGFB2
TGFB3
TGFBR3
TGFBR3L
TGFBRAP1
TGIF1
TGIF2
TGM1
TGM3
TGM4
TGM5
TGM6
TGM7
TGOLN2
TGS1
TH
THADA
THAP1
THAP10
THAP11
THAP2
THAP3
THAP4
THAP5
THAP6
THAP7
THAP8
THAP9
THBS1
THBS2
THBS3
THEGL
THEM4
THEM5
THEM6
THEMIS
THEMIS2
THG1L
THNSL1
THNSL2

ZNF471
ZNF474
ZNF48
ZNF480
ZNF485
ZNF486
ZNF488
ZNF490
ZNF491
ZNF492
ZNF493
ZNF496
ZNF497
ZNF501
ZNF502
ZNF503
ZNF507
ZNF510
ZNF511
ZNF512
ZNF512B
ZNF513
ZNF514
ZNF516
ZNF518A
ZNF518B
ZNF519
ZNF521
ZNF524
ZNF527
ZNF528
ZNF529
ZNF530
ZNF532
ZNF536
ZNF540
ZNF544
ZNF546
ZNF547
ZNF548
ZNF549
ZNF551
ZNF552
ZNF555
ZNF556
ZNF557
ZNF558
ZNF559
ZNF560
ZNF561
ZNF562
ZNF563
ZNF564
ZNF565
ZNF566
ZNF567
ZNF568
ZNF569
ZNF57
ZNF570
ZNF571
ZNF572
ZNF573
ZNF574
ZNF575
ZNF576
ZNF577
ZNF579
ZNF580
ZNF581
ZNF582
ZNF583
ZNF584
ZNF585A
ZNF585B
ZNF586
ZNF587
ZNF587B
ZNF589
ZNF592
ZNF593
ZNF595
ZNF596
ZNF597
ZNF598
ZNF600
ZNF605
ZNF606
ZNF607
ZNF610
ZNF611
ZNF613
ZNF614
ZNF615
ZNF621
ZNF622
ZNF623
ZNF625
ZNF626
ZNF627
ZNF638

C2orf80
C2orf81
C2orf82
C2orf83
C2orf88
C2orf91
C3
C3AR1
C3orf14
C3orf17
C3orf18
C3orf20
C3orf22
C3orf30
C3orf33
C3orf36
C3orf38
C3orf52
C3orf56
C3orf58
C3orf62
C3orf67
C3orf70
C4A
C4B
C4B_2
C4BPB
C4orf17
C4orf19
C4orf22
C4orf26
C4orf27
C4orf29
C4orf3
C4orf32
C4orf33
C4orf36
C4orf45
C4orf46
C4orf47
C4orf48
C4orf51
C5
C5AR1
C5AR2
C5orf15
C5orf22
C5orf24
C5orf28
C5orf30
C5orf34
C5orf38
C5orf42
C5orf45
C5orf46
C5orf47
C5orf49
C5orf51
C5orf52
C5orf58
C5orf60
C5orf63
C6orf1
C6orf10
C6orf106
C6orf118
C6orf120
C6orf132
C6orf136
C6orf15
C6orf163
C6orf201
C6orf203
C6orf211
C6orf222
C6orf223
C6orf226
C6orf229
C6orf25
C6orf47
C6orf48
C6orf52
C6orf57
C6orf58
C6orf62
C6orf89
C7orf25
C7orf26
C7orf31
C7orf33
C7orf34
C7orf43
C7orf49
C7orf50
C7orf55
C7orf55-LUC7L2
C7orf57
C7orf60
C7orf61
C7orf62
C7orf72

DENND2D
DENND3
DENND4A
DENND4C
DENND5A
DENND5B
DENND6A
DENND6B
DENR
DEPDC1
DEPDC1B
DEPDC4
DEPDC5
DEPDC7
DEPTOR
DERA
DERL1
DERL2
DERL3
DES
DESI1
DESI2
DET1
DEXI
DFFA
DFFB
DFNA5
DFNB31
DGAT1
DGAT2
DGCR2
DGCR6
DGCR6L
DGKB
DGKD
DGKE
DGKH
DGKI
DGKZ
DHCR24
DHCR7
DHDDS
DHDH
DHFR
DHFRL1
DHH
DHODH
DHPS
DHRS1
DHRS11
DHRS12
DHRS13
DHRS2
DHRS3
DHRS7
DHRS7B
DHRS9
DHRSX
DHTKD1
DHX15
DHX16
DHX29
DHX30
DHX32
DHX33
DHX34
DHX35
DHX36
DHX37
DHX38
DHX40
DHX58
DIABLO
DIAPH1
DIAPH3
DIDO1
DIEXF
DIMT1
DIO3
DIP2A
DIP2B
DIP2C
DIRAS3
DIRC1
DIRC2
DIS3
DIS3L
DIS3L2
DISC1
DISP1
DISP2
DIXDC1
DKK3
DKKL1
DLAT
DLC1
DLC1
DLD
DLEC1
DLEU7
DLG1

GRIK4
GRIN1
GRINA
GRIP2
GRK4
GRK5
GRK6
GRK7
GRM5
GRM7
GRN
GRP
GRPEL1
GRPEL2
GRSF1
GRTP1
GRWD1
GRXCR1
GSAP
GSC2
GSDMA
GSDMB
GSDMD
GSE1
GSG1
GSG1L
GSG2
GSKIP
GSN
GSPT1
GSTA2
GSTA4
GSTA5
GSTCD
GSTK1
GSTM1
GSTM2
GSTM3
GSTM4
GSTM5
GSTO1
GSTO2
GSTP1
GSTT1
GSTT2
GSTT2B
GSTZ1
GSX1
GSX2
GTDC1
GTF2A1
GTF2A1L
GTF2A2
GTF2B
GTF2E1
GTF2E2
GTF2F1
GTF2F2
GTF2H1
GTF2H2
GTF2H2
GTF2H2C
GTF2H2C_2
GTF2H3
GTF2H4
GTF2H5
GTF2I
GTF2IRD1
GTF2IRD2
GTF2IRD2B
GTF3A
GTF3C1
GTF3C5
GTF3C6
GTPBP1
GTPBP10
GTPBP3
GTPBP4
GTPBP6
GTPBP8
GTSE1
GTSF1
GTSF1L
GUCA1B
GUCA1C
GUCA2A
GUCA2B
GUCD1
GUCY1A2
GUCY2C
GUCY2D
GUF1
GUK1
GULP1
GUSB
GXYLT2
GYG1
GYLTL1B
GYPA
GYPB
GYPC

LYN
LYNX1
LYPD1
LYPD2
LYPD3
LYPD4
LYPD5
LYPD6
LYPD6B
LYPD8
LYPLAL1
LYRM1
LYRM2
LYRM4
LYRM5
LYRM7
LYRM9
LYSMD1
LYSMD2
LYSMD4
LYZ
LYZL1
LYZL2
LYZL4
LYZL6
LZIC
LZTFL1
LZTR1
LZTS1
M1AP
MAATS1
MAB21L1
MAB21L2
MAB21L3
MACC1
MACF1
MACROD1
MACROD2
MAD1L1
MAD2L1BP
MAD2L2
MADCAM1
MAEA
MAEL
MAF1
MAFA
MAFF
MAFG
MAFK
MAG
MAGEF1
MAGEL2
MAGI1
MAGI2
MAGI3
MAGOH
MAGOHB
MAK
MAK16
MAL
MAL2
MALL
MALSU1
MAMDC2
MAMDC4
MAML1
MAMSTR
MAN1A1
MAN1A2
MAN1B1
MAN1C1
MAN2A2
MAN2B2
MANBAL
MANEA
MANEAL
MANF
MANSC1
MAP10
MAP1A
MAP1B
MAP1LC3A
MAP1LC3B2
MAP1LC3C
MAP1S
MAP2
MAP2K3
MAP2K6
MAP3K10
MAP3K12
MAP3K13
MAP3K14
MAP3K19
MAP3K2
MAP3K3
MAP3K6
MAP3K7
MAP3K7CL
MAP3K8
MAP4
MAP4K1

PARD3
PARD3B
PARD6A
PARD6B
PARD6G
PARG
PARK7
PARL
PARM1
PARN
PARP1
PARP10
PARP12
PARP14
PARP15
PARP16
PARP4
PARP6
PARP8
PARP9
PARPBP
PARS2
PARVA
PARVB
PARVG
PASK
PATE1
PATE2
PATE3
PATE4
PATL1
PATL2
PATZ1
PAWR
PAX6
PAX7
PAXBP1
PAXIP1
PBK
PBLD
PBOV1
PBX1
PBXIP1
PC
PCBD1
PCBD2
PCBP1
PCBP2
PCBP4
PCDH1
PCDH10
PCDH12
PCDH15
PCDH17
PCDH18
PCDH20
PCDH7
PCDH7
PCDH8
PCDH9
PCDHA1
PCDHA10
PCDHA11
PCDHA12
PCDHA13
PCDHA2
PCDHA3
PCDHA4
PCDHA5
PCDHA6
PCDHA7
PCDHA8
PCDHA9
PCDHAC1
PCDHAC2
PCDHB1
PCDHB10
PCDHB11
PCDHB12
PCDHB13
PCDHB14
PCDHB15
PCDHB16
PCDHB2
PCDHB3
PCDHB4
PCDHB5
PCDHB6
PCDHB7
PCDHB8
PCDHB9
PCDHGA1
PCDHGA10
PCDHGA11
PCDHGA12
PCDHGA2
PCDHGA3
PCDHGA4
PCDHGA5
PCDHGA6
PCDHGA7

RPS6KA1
RPS6KA2
RPS6KA4
RPS6KA5
RPS6KB1
RPS6KB2
RPS6KC1
RPS7
RPS8
RPS9
RPSA
RPTOR
RPUSD1
RPUSD2
RPUSD3
RPUSD4
RQCD1
RRAD
RRAGA
RRAGC
RRAGD
RRAS
RRAS2
RRBP1
RRH
RRM1
RRN3
RRNAD1
RRP1
RRP12
RRP15
RRP1B
RRP36
RRP7A
RRP8
RRP9
RRS1
RSAD1
RSAD2
RSBN1
RSBN1L
RSC1A1
RSF1
RSG1
RSL1D1
RSL24D1
RSPH10B
RSPH10B2
RSPH14
RSPH3
RSPH4A
RSPH9
RSPO2
RSPO3
RSPRY1
RSRC1
RSRC2
RSRP1
RSU1
RSU1
RTBDN
RTCB
RTEL1
RTF1
RTFDC1
RTKN
RTKN2
RTL1
RTN2
RTN3
RTN4RL1
RTN4RL2
RTP1
RTP2
RTP3
RTP4
RTP5
RTTN
RUFY1
RUFY2
RUFY3
RUFY4
RUNDC1
RUNDC3A
RUNDC3B
RUNX1T1
RUNX1T1
RUNX3
RWDD1
RWDD2A
RWDD3
RWDD4
RXFP1
RXFP2
RXFP3
RXFP4
RXRA
RXRB
RXRG
RYBP
RYK

THOC1
THOC5
THOC6
THOC7
THPO
THRAP3
THRB
THRSP
THSD4
THUMPD1
THUMPD2
THUMPD3
THY1
THYN1
TIA1
TIAF1
TIAL1
TIAM1
TIAM2
TICAM2
TICRR
TIE1
TIFA
TIFAB
TIGD1
TIGD2
TIGD3
TIGD4
TIGD5
TIGD6
TIGD7
TIGIT
TIMD4
TIMELESS
TIMM10
TIMM10B
TIMM17A
TIMM21
TIMM22
TIMM50
TIMM8B
TIMMDC1
TIMP2
TIMP3
TIMP4
TINAG
TINAGL1
TIPARP
TIPIN
TIPRL
TIRAP
TJAP1
TJP1
TJP2
TK1
TKTL2
TLCD1
TLCD2
TLDC1
TLDC2
TLE1
TLE2
TLE3
TLE6
TLK1
TLK2
TLN1
TLR4
TLR5
TLX1
TLX1NB
TM2D1
TM2D2
TM2D3
TM4SF18
TM4SF19
TM4SF20
TM6SF1
TM7SF2
TM7SF3
TM9SF1
TM9SF3
TM9SF4
TMA16
TMA7
TMBIM1
TMBIM4
TMBIM6
TMC5
TMC7
TMCC2
TMCC3
TMCO1
TMCO2
TMCO3
TMCO4
TMCO5A
TMCO6
TMED1
TMED10
TMED2

ZNF639
ZNF641
ZNF644
ZNF646
ZNF649
ZNF652
ZNF653
ZNF654
ZNF655
ZNF658
ZNF660
ZNF662
ZNF664
ZNF665
ZNF667
ZNF668
ZNF669
ZNF670
ZNF671
ZNF672
ZNF675
ZNF676
ZNF677
ZNF678
ZNF679
ZNF680
ZNF681
ZNF682
ZNF683
ZNF684
ZNF687
ZNF688
ZNF689
ZNF69
ZNF691
ZNF692
ZNF695
ZNF696
ZNF699
ZNF7
ZNF70
ZNF700
ZNF701
ZNF703
ZNF704
ZNF705A
ZNF705B
ZNF705D
ZNF706
ZNF707
ZNF708
ZNF709
ZNF71
ZNF710
ZNF713
ZNF714
ZNF716
ZNF718
ZNF721
ZNF727
ZNF728
ZNF732
ZNF736
ZNF74
ZNF740
ZNF746
ZNF747
ZNF749
ZNF750
ZNF75A
ZNF76
ZNF761
ZNF763
ZNF764
ZNF766
ZNF768
ZNF77
ZNF770
ZNF771
ZNF772
ZNF773
ZNF774
ZNF775
ZNF776
ZNF777
ZNF778
ZNF780A
ZNF780B
ZNF781
ZNF782
ZNF783
ZNF784
ZNF785
ZNF786
ZNF787
ZNF789
ZNF79
ZNF790
ZNF791
ZNF792
ZNF793

C7orf73
C8A
C8orf22
C8orf31
C8orf33
C8orf34
C8orf37
C8orf4
C8orf44
C8orf46
C8orf48
C8orf58
C8orf59
C8orf74
C8orf76
C8orf82
C8orf86
C8orf89
C9orf114
C9orf116
C9orf117
C9orf129
C9orf131
C9orf135
C9orf142
C9orf152
C9orf156
C9orf16
C9orf171
C9orf172
C9orf173
C9orf24
C9orf3
C9orf40
C9orf41
C9orf43
C9orf50
C9orf57
C9orf64
C9orf66
C9orf69
C9orf72
C9orf78
C9orf84
C9orf85
C9orf89
C9orf9
C9orf91
CA1
CA10
CA11
CA12
CA13
CA14
CA2
CA3
CA4
CA5A
CA9
CAAP1
CAB39
CAB39L
CABIN1
CABLES1
CABP1
CABP5
CABP7
CABS1
CABYR
CACFD1
CACHD1
CACNA1A
CACNA1B
CACNA1C
CACNA1D
CACNA1E
CACNA1G
CACNA1H
CACNA1I
CACNA1S
CACNA2D2
CACNB2
DLG2
DLG4
DLG5
DLGAP2
DLGAP4
DLGAP5
DLK2
DLX1
DLX6
DMAP1
DMBT1
DMC1
DMGDH
DMKN
DMPK
DMRT1
DMRT2
DMRT3
DMRTA2
DMRTC2
DMTF1
DMTN
DMWD
DMXL1
DMXL2
DNAAF1
DNAAF3
DNAAF5
DNAH1
DNAH12
DNAH17
DNAH2
DNAH3
DNAH5
DNAH6
DNAH7
DNAH8
DNAH9
DNAI2
DNAJA4
DNAJB1
DNAJB13
DNAJB7
DNAJB8
DNAJC1
DNAJC10
DNAJC11
DNAJC12
DNAJC13
DNAJC14
DNAJC15
DNAJC16
DNAJC17
DNAJC18
DNAJC19
DNAJC21
DNAJC22
DNAJC24
DNAJC25
DNAJC27
DNAJC5
DNAJC5B
DNAJC5G
DNAJC8
DNAJC9
DNAL1
DNAL4
DNALI1
DNASE1L2
DNASE1L3
DNASE2B
DND1
DNER
DNHD1
DNLZ
DNM1
DNM1L
DNM2
DNM3
DNMBP
DNMT1
DNMT3A
GYPE
GYS1
GYS2
GZF1
GZMA
GZMB
GZMH
GZMK
GZMM
H1F0
H1FNT
H1FOO
H1FX
H2AFJ
H2AFV
H2AFX
H2AFY
H2AFY2
H2AFZ
H3F3A
H3F3B
H3F3C
H6PD
HABP2
HABP4
HACL1
HADH
HADHA
HADHB
HAGH
HAGHL
HAMP
HAND1
HAO2
HAPLN1
HAPLN2
HAPLN3
HAPLN4
HARBI1
HARS
HARS2
HAS1
HAS2
HAS3
HAT1
HAUS1
HAUS2
HAUS3
HAUS6
HAUS8
HAX1
HBA1
HBA2
HBB
HBD
HBE1
HBEGF
HBG1
HBG2
HBM
HBP1
HBQ1
HBZ
HCAR2
HCAR3
HCFC1R1
HCFC2
HCLS1
HCN1
HCN2
HCN3
HCN4
HCRT
HCRTR1
HCST
HDAC1
HDAC10
HDAC11
HDAC3
HDAC4
HDAC5
HDDC2
MAP4K2
MAP4K3
MAP4K4
MAP4K5
MAP6
MAP6D1
MAP7
MAP7D1
MAP9
MAPK12
MAPK14
MAPK15
MAPK1IP1L
MAPK4
MAPK6
MAPK7
MAPK8IP1
MAPK8IP2
MAPK8IP3
MAPKAPK2
MAPKAPK3
MAPKAPK5
MAPKBP1
MAPRE1
MAPRE2
MAPRE3
MAPT
MARCKS
MARCKSL1
MARCO
MARK2
MARK3
MARK4
MARS
MARS2
MARVELD1
MARVELD3
MAS1
MAS1L
MASP1
MASP2
MAST1
MAST2
MASTL
MAT1A
MAT2A
MAT2B
MATK
MATN1
MATN3
MATR3
MAU2
MAVS
MAX
MAZ
MB
MB21D1
MB21D2
MBD1
MBD2
MBD3L1
MBD3L2
MBD3L3
MBD3L4
MBD3L5
MBD4
MBIP
MBL2
MBLAC1
MBLAC2
MBNL1
MBNL2
MBOAT2
MBOAT7
MBP
MBTPS1
MC1R
MC4R
MC5R
MCAT
MCC
MCCC1
PCDHGA8
PCDHGA9
PCDHGB1
PCDHGB2
PCDHGB3
PCDHGB4
PCDHGB5
PCDHGB6
PCDHGB7
PCDHGC3
PCDHGC4
PCDHGC5
PCED1A
PCED1B
PCF11
PCGF1
PCGF2
PCGF3
PCGF5
PCGF6
PCID2
PCIF1
PCK2
PCLO
PCM1
PCMTD1
PCMTD2
PCNP
PCNT
PCNX
PCNXL2
PCNXL3
PCNXL4
PCOLCE
PCOLCE2
PCP4
PCSK1
PCSK2
PCSK4
PCSK6
PCSK7
PCSK9
PCTP
PCYOX1
PCYOX1L
PCYT1A
PCYT2
PDAP1
PDCD1
PDCD10
PDCD1LG2
PDCD2
PDCD2L
PDCD4
PDCD5
PDCD6
PDCD7
PDCL
PDCL2
PDCL3
PDDC1
PDE12
PDE2A
PDE3B
PDE4B
PDE4DIP
PDE5A
PDE6B
PDE6C
PDE8A
PDE8B
PDF
PDGFB
PDGFD
PDGFRA
PDGFRB
PDGFRL
PDHX
PDIA2
PDIA3
PDIA4
PDIA5
RYR2
S100A1
S100A10
S100A11
S100A12
S100A13
S100A14
S100A16
S100A2
S100A3
S100A4
S100A5
S100A6
S100A7
S100A7A
S100A7L2
S100A8
S100A9
S100B
S100P
S100PBP
S100Z
S1PR1
S1PR2
S1PR3
S1PR4
S1PR5
SAA1
SAA2
SAA4
SAAL1
SAC3D1
SACM1L
SACS
SAE1
SAFB2
SAG
SALL1
SALL2
SALL3
SAMD1
SAMD10
SAMD11
SAMD12
SAMD13
SAMD14
SAMD15
SAMD4A
SAMD4B
SAMD5
SAMD7
SAMD8
SAMD9
SAMD9L
SAMHD1
SAMM50
SAP130
SAP18
SAP30
SAP30BP
SAP30L
SAPCD1
SAPCD2
SAR1B
SARAF
SARM1
SARNP
SARS
SARS2
SASH1
SASS6
SAT2
SATB1
SATB2
SAYSD1
SBDS
SBF2
SBK2
SBNO1
SBNO2
SBSN
SBSPON
TMED3
TMED4
TMED5
TMED6
TMED7
TMED7-TICAM2
TMED8
TMED9
TMEFF1
TMEFF2
TMEM100
TMEM101
TMEM102
TMEM104
TMEM105
TMEM106A
TMEM106B
TMEM106C
TMEM107
TMEM108
TMEM109
TMEM11
TMEM110
TMEM110-MUSTN1
TMEM114
TMEM115
TMEM116
TMEM117
TMEM119
TMEM120A
TMEM120B
TMEM121
TMEM123
TMEM125
TMEM126A
TMEM126B
TMEM127
TMEM128
TMEM129
TMEM130
TMEM132A
TMEM132B
TMEM132D
TMEM132E
TMEM133
TMEM134
TMEM135
TMEM136
TMEM138
TMEM139
TMEM140
TMEM141
TMEM143
TMEM144
TMEM145
TMEM147
TMEM14A
TMEM14B
TMEM14C
TMEM14E
TMEM150B
TMEM150C
TMEM151A
TMEM154
TMEM155
TMEM156
TMEM158
TMEM159
TMEM160
TMEM161A
TMEM161B
TMEM163
TMEM165
TMEM167A
TMEM167B
TMEM168
TMEM169
TMEM17
TMEM170A
TMEM170B
TMEM171
TMEM173
ZNF799
ZNF8
ZNF80
ZNF800
ZNF804A
ZNF804B
ZNF805
ZNF808
ZNF813
ZNF816
ZNF821
ZNF823
ZNF827
ZNF829
ZNF83
ZNF830
ZNF831
ZNF835
ZNF836
ZNF837
ZNF839
ZNF84
ZNF843
ZNF846
ZNF85
ZNF853
ZNF862
ZNF865
ZNF878
ZNF879
ZNF880
ZNF90
ZNF91
ZNF92
ZNF93
ZNF98
ZNFX1
ZNHIT1
ZNHIT2
ZNHIT3
ZNHIT6
ZNRF2
ZNRF4
ZP1
ZPBP
ZPBP2
ZPLD1
ZPR1
ZRANB1
ZRANB2
ZRANB3
ZSCAN1
ZSCAN10
ZSCAN16
ZSCAN18
ZSCAN2
ZSCAN20
ZSCAN21
ZSCAN22
ZSCAN25
ZSCAN29
ZSCAN30
ZSCAN31
ZSCAN32
ZSCAN4
ZSCAN5A
ZSCAN5B
ZSCAN9
ZSWIM1
ZSWIM2
ZSWIM3
ZSWIM6
ZSWIM7
ZSWIM8
ZUFSP
ZW10
ZWILCH
ZXDC
ZYG11A
ZYG11B
ZYX
ZZEF1
ZZZ3

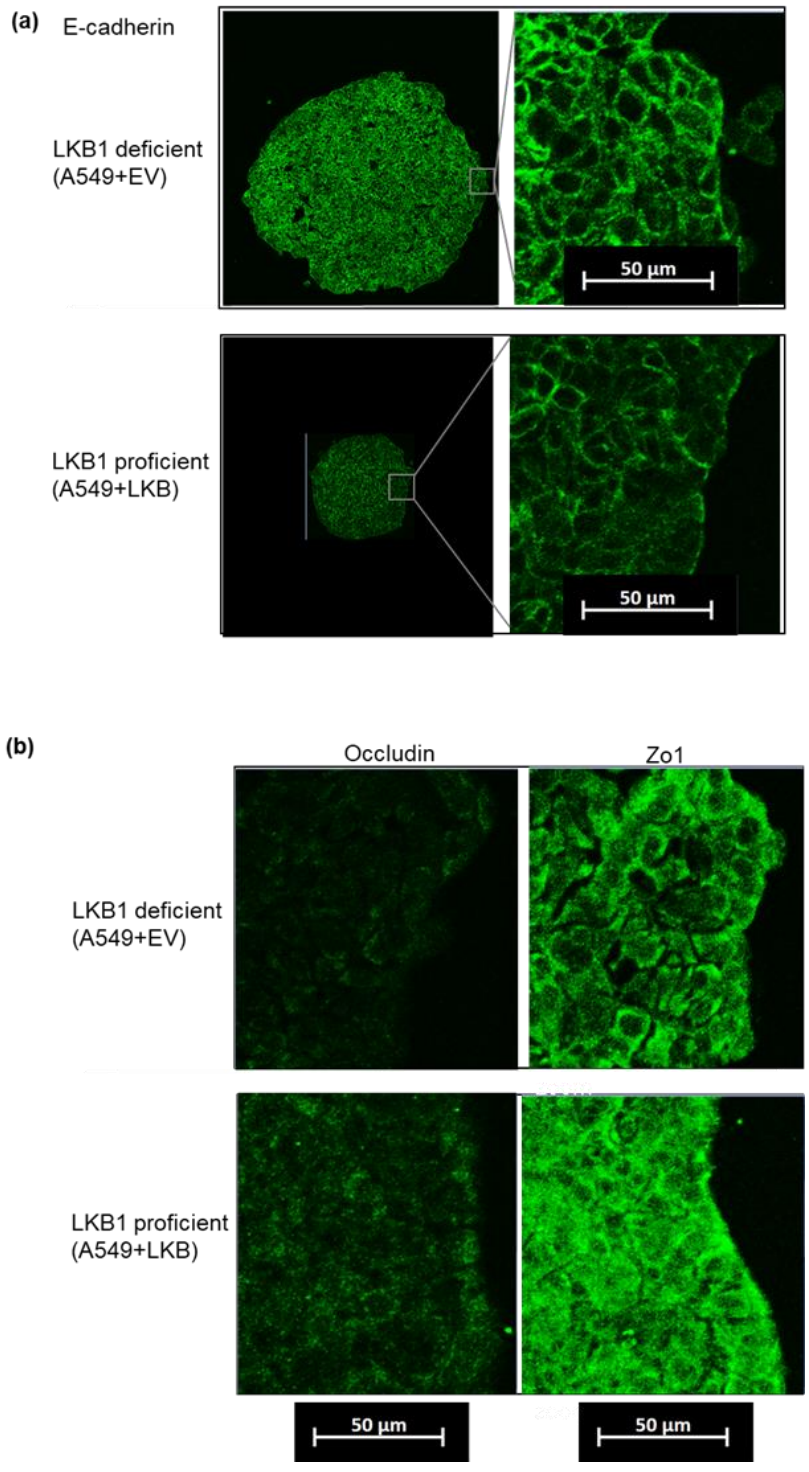

Figure A3.25: E-cadherin, occludin and Zo1 staining in spheroids
(a) (b) Representative IF images of spheroids fixed and stained with E-cadherin, occludin and ZO1. Images were acquired using the 20x objective on a confocal microscope. IF was carried out as described in Section 2.16. E-cadherin (CST #14472) was used at a concentration of 1:50, occludin (Abcam #ab31721) at 1:2000, and Zo1 (CST #13663) at 1:200.

Table A4.1: Top 50 GO processes associated with genes that were highly expressed in the complex model

GO Term	Description	P-value	FDR q-value	Enrichment	N	B	n2	b3
GO:0002376	immune system process	4.15E-11	5.71E-07	2.58	13523	1496	186	53
GO:0060337	type I interferon signalling pathway	4.53E-08	3.11E-04	12.12	13523	54	186	9
GO:0002252	immune effector process	1.12E-07	5.12E-04	3.07	13523	664	186	28
GO:0045055	regulated exocytosis	2.24E-07	7.68E-04	3.33	13523	524	186	24
GO:0001775	cell activation	2.26E-07	6.20E-04	2.96	13523	687	186	28
GO:0002682	regulation of immune system process	3.21E-07	7.36E-04	2.56	13523	966	186	34
GO:0030155	regulation of cell adhesion	3.33E-07	6.54E-04	3.49	13523	458	186	22
GO:0006950	response to stress	7.09E-07	1.22E-03	1.9	13523	2146	186	56
GO:0006887	exocytosis	1.02E-06	1.56E-03	3.06	13523	570	186	24
GO:0051239	regulation of multicellular organismal process	1.25E-06	1.72E-03	1.95	13523	1904	186	51
GO:0044699	single-organism process	1.46E-06	1.82E-03	1.29	13523	7700	186	137
GO:0042221	response to chemical	1.56E-06	1.79E-03	2.03	13523	1646	186	46
GO:0050776	regulation of immune response	2.13E-06	2.25E-03	2.85	13523	637	186	25
GO:0002480	antigen processing and presentation of exogenous peptide antigen via MHC class I, TAP-independent	2.32E-06	2.28E-03	36.35	13523	8	186	4
GO:0050896	response to stimulus	3.31E-06	3.03E-03	1.58	13523	3588	186	78
GO:0032940	secretion by cell	3.89E-06	3.34E-03	2.69	13523	703	186	26
GO:1901700	response to oxygen-containing compound	4.86E-06	3.93E-03	2.43	13523	896	186	30
GO:0034097	response to cytokine	5.30E-06	4.05E-03	4.01	13523	272	186	15
GO:0042981	regulation of apoptotic process	5.32E-06	3.85E-03	2.34	13523	996	186	32
GO:0072376	protein activation cascade	5.78E-06	3.97E-03	9.98	13523	51	186	7
GO:0043067	regulation of programmed cell death	6.02E-06	3.94E-03	2.32	13523	1002	186	32
GO:0009719	response to endogenous stimulus	6.13E-06	3.83E-03	2.62	13523	721	186	26
GO:0043299	leukocyte degranulation	6.30E-06	3.77E-03	3.39	13523	386	186	18
GO:0002275	myeloid cell activation involved in immune response	6.53E-06	3.74E-03	3.38	13523	387	186	18
GO:0044763	single-organism cellular process	9.16E-06	5.04E-03	1.33	13523	6516	186	119
GO:0070887	cellular response to chemical stimulus	1.06E-05	5.58E-03	2.34	13523	932	186	30
GO:0010033	response to organic substance	1.21E-05	6.17E-03	2.08	13523	1291	186	37
GO:0002366	leukocyte activation involved in immune response	1.56E-05	7.65E-03	3.05	13523	453	186	19
GO:0043312	neutrophil degranulation	1.61E-05	7.62E-03	3.3	13523	374	186	17
GO:0002283	neutrophil activation involved in immune response	1.61E-05	7.36E-03	3.3	13523	374	186	17
GO:0002263	cell activation involved in immune response	1.61E-05	7.13E-03	3.04	13523	454	186	19
GO:0042119	neutrophil activation	1.78E-05	7.65E-03	3.28	13523	377	186	17
GO:0016477	cell migration	1.85E-05	7.73E-03	2.81	13523	543	186	21
GO:0036230	granulocyte activation	1.91E-05	7.71E-03	3.26	13523	379	186	17
GO:1901342	regulation of vasculature development	1.94E-05	7.63E-03	4.79	13523	167	186	11
GO:0002274	myeloid leukocyte activation	2.05E-05	7.81E-03	3.11	13523	421	186	18
GO:1902578	single-organism localization	2.33E-05	8.65E-03	1.84	13523	1821	186	46

GO:2001233	regulation of apoptotic signalling pathway	2.39E-05	8.64E-03	3.74	13523	272	186	14
GO:0046903	secretion	2.49E-05	8.76E-03	2.42	13523	781	186	26
GO:0048870	cell motility	2.50E-05	8.59E-03	2.67	13523	598	186	22
GO:0006952	defence response	2.71E-05	9.10E-03	2.41	13523	785	186	26
GO:0009725	response to hormone	2.84E-05	9.28E-03	3.16	13523	391	186	17
GO:0002684	positive regulation of immune system process	2.84E-05	9.09E-03	2.58	13523	648	186	23
GO:0045321	leukocyte activation	2.98E-05	9.32E-03	2.64	13523	605	186	22
GO:0010941	regulation of cell death	3.00E-05	9.17E-03	2.14	13523	1085	186	32
GO:0032879	regulation of localization	3.46E-05	1.03E-02	1.82	13523	1793	186	45
GO:0045765	regulation of angiogenesis	3.76E-05	1.10E-02	4.91	13523	148	186	10
GO:2000145	regulation of cell motility	3.77E-05	1.08E-02	2.76	13523	526	186	20
GO:0009607	response to biotic stimulus	3.79E-05	1.06E-02	2.68	13523	570	186	21
GO:0051270	regulation of cellular component movement	3.99E-05	1.10E-02	2.67	13523	572	186	21

Table A4.2: GO processes associated with genes that were expressed at lower levels in the complex model

GO Term	Description	P-value	FDR q-value	Enrichment	N	B	n2	b3
GO:0051782	negative regulation of cell division	6.69E-04	1.00E+00	50.87	13481	10	53	2
GO:0034613	cellular protein localization	7.11E-04	1.00E+00	3.63	13481	631	53	9
GO:0070727	cellular macromolecule localization	7.78E-04	1.00E+00	3.58	13481	639	53	9
GO:0071428	rRNA-containing ribonucleoprotein complex export from nucleus	8.15E-04	1.00E+00	46.25	13481	11	53	2
GO:0033750	ribosome localization	8.15E-04	1.00E+00	46.25	13481	11	53	2
GO:0033753	establishment of ribosome localization	8.15E-04	1.00E+00	46.25	13481	11	53	2
GO:0000054	ribosomal subunit export from nucleus	8.15E-04	1.00E+00	46.25	13481	11	53	2
GO:0033365	protein localization to organelle	8.35E-04	1.00E+00	4.52	13481	394	53	7
GO:0071426	ribonucleoprotein complex export from nucleus	9.76E-04	1.00E+00	42.39	13481	12	53	2

Table A4.3: Top 50 GO processes associated with genes that were highly expressed in the 3D and xenografts compared to 2D

GO Term	Description	P-value	FDR q-value	Enrichment	N	B	n2	b3
GO:0055114	oxidation-reduction process	4.92E-17	6.79E-13	2.3	13723	654	1005	110
GO:0044710	single-organism metabolic process	1.88E-15	1.30E-11	1.53	13723	2522	1005	283
GO:0006810	transport	2.10E-11	9.65E-08	1.39	13723	3055	1005	311
GO:0051234	establishment of localization	6.36E-11	2.19E-07	1.37	13723	3156	1005	317
GO:0044281	small molecule metabolic process	9.77E-11	2.69E-07	1.67	13723	1238	1005	151
GO:0044712	single-organism catabolic process	9.89E-11	2.27E-07	2.13	13723	499	1005	78
GO:1901575	organic substance catabolic process	1.53E-10	3.02E-07	1.71	13723	1085	1005	136

GO:0009056	**catabolic process**	3.69E-10	6.37E-07	1.66	13723	1174	1005	143
GO:0051179	localization	6.50E-10	9.96E-07	1.33	13723	3428	1005	334
GO:1901564	organonitrogen compound metabolic process	1.07E-09	1.48E-06	1.63	13723	1203	1005	144
GO:0044282	small molecule catabolic process	3.56E-09	4.46E-06	2.63	13723	223	1005	43
GO:0043312	neutrophil degranulation	2.55E-08	2.93E-05	2.11	13723	389	1005	60
GO:0002283	neutrophil activation involved in immune response	2.55E-08	2.70E-05	2.11	13723	389	1005	60
GO:0005996	monosaccharide metabolic process	3.02E-08	2.97E-05	2.91	13723	150	1005	32
GO:0042119	neutrophil activation	3.39E-08	3.12E-05	2.09	13723	392	1005	60
GO:0036230	granulocyte activation	4.09E-08	3.52E-05	2.08	13723	394	1005	60
GO:0044248	cellular catabolic process	5.75E-08	4.67E-05	1.64	13723	948	1005	114
GO:0044765	single-organism transport	5.82E-08	4.46E-05	1.45	13723	1747	1005	185
GO:0006629	lipid metabolic process	6.72E-08	4.88E-05	1.66	13723	897	1005	109
GO:0043299	leukocyte degranulation	7.78E-08	5.37E-05	2.04	13723	401	1005	60
GO:1902578	single-organism localization	8.34E-08	5.48E-05	1.42	13723	1861	1005	194
GO:0002275	myeloid cell activation involved in immune response	8.52E-08	5.34E-05	2.04	13723	402	1005	60
GO:0044699	single-organism process	1.06E-07	6.35E-05	1.14	13723	7821	1005	651
GO:0002274	myeloid leukocyte activation	1.60E-07	9.19E-05	1.96	13723	438	1005	63
GO:0045055	regulated exocytosis	1.79E-07	9.90E-05	1.85	13723	538	1005	73
GO:0016192	vesicle-mediated transport	1.95E-07	1.04E-04	1.56	13723	1113	1005	127
GO:0006887	exocytosis	2.69E-07	1.37E-04	1.8	13723	584	1005	77
GO:0044723	single-organism carbohydrate metabolic process	2.91E-07	1.43E-04	2.25	13723	267	1005	44
GO:0006082	organic acid metabolic process	3.05E-07	1.45E-04	1.71	13723	710	1005	89
GO:0043436	oxoacid metabolic process	6.03E-07	2.77E-04	1.7	13723	700	1005	87
GO:0072329	monocarboxylic acid catabolic process	6.43E-07	2.86E-04	3.6	13723	72	1005	19
GO:0002366	leukocyte activation involved in immune response	7.95E-07	3.43E-04	1.87	13723	468	1005	64
GO:0002263	cell activation involved in immune response	8.57E-07	3.58E-04	1.86	13723	469	1005	64
GO:0005975	carbohydrate metabolic process	1.16E-06	4.70E-04	1.98	13723	365	1005	53
GO:0019752	carboxylic acid metabolic process	1.83E-06	7.23E-04	1.72	13723	613	1005	77
GO:0044255	cellular lipid metabolic process	2.94E-06	1.13E-03	1.63	13723	727	1005	87
GO:0019318	hexose metabolic process	5.15E-06	1.92E-03	2.8	13723	112	1005	23
GO:0032787	monocarboxylic acid metabolic process	6.74E-06	2.45E-03	1.88	13723	377	1005	52
GO:0044711	single-organism biosynthetic process	7.15E-06	2.53E-03	1.55	13723	853	1005	97
GO:0046903	secretion	7.55E-06	2.60E-03	1.57	13723	799	1005	92
GO:0002252	immune effector process	8.70E-06	2.93E-03	1.62	13723	682	1005	81
GO:0010561	negative regulation of glycoprotein biosynthetic process	1.05E-05	3.46E-03	9.1	13723	9	1005	6
GO:0019852	L-ascorbic acid metabolic process	1.05E-05	3.38E-03	9.1	13723	9	1005	6
GO:1901135	carbohydrate derivative metabolic process	1.22E-05	3.83E-03	1.65	13723	613	1005	74
GO:0045321	leukocyte activation	1.32E-05	4.04E-03	1.64	13723	625	1005	75
GO:0044763	single-organism cellular process	1.34E-05	4.01E-03	1.13	13723	6615	1005	549
GO:0016054	organic acid catabolic process	2.19E-05	6.43E-03	2.42	13723	147	1005	26

GO:0046395	carboxylic acid catabolic process	2.19E-05	6.30E-03	2.42	13723	147	1005	26
GO:0070972	protein localization to endoplasmic reticulum	2.30E-05	6.48E-03	2.79	13723	98	1005	20
GO:1901615	organic hydroxy compound metabolic process	2.76E-05	7.60E-03	1.95	13723	287	1005	41

Table A4.4: Top 50 processes associated with genes that were expressed at lower levels in the 3D and xenografts compared to 2D

GO Term	Description	P-value	FDR q-value	Enrichment	N	B	n2	b3
GO:0022402	**cell cycle process**	2.22E-84	3.06E-80	3.96	13676	889	917	236
GO:1903047	mitotic cell cycle process	1.25E-82	8.62E-79	4.61	13676	640	917	198
GO:0051276	chromosome organization	1.99E-52	9.16E-49	5.04	13676	346	917	117
GO:0006259	DNA metabolic process	8.17E-45	2.82E-41	3.49	13676	646	917	151
GO:0090304	nucleic acid metabolic process	1.32E-44	3.65E-41	1.9	13676	2999	917	383
GO:0006139	nucleobase-containing compound metabolic process	3.66E-42	8.40E-39	1.82	13676	3311	917	403
GO:0006996	organelle organization	2.08E-41	4.10E-38	2.26	13676	1740	917	264
GO:0006725	cellular aromatic compound metabolic process	1.29E-39	2.22E-36	1.76	13676	3462	917	409
GO:0046483	heterocycle metabolic process	2.47E-39	3.79E-36	1.76	13676	3433	917	406
GO:0051301	cell division	8.79E-39	1.21E-35	4.66	13676	301	917	94
GO:0071840	cellular component organization or biogenesis	1.20E-37	1.50E-34	1.7	13676	3728	917	425
GO:1901360	organic cyclic compound metabolic process	1.79E-35	2.05E-32	1.7	13676	3607	917	410
GO:0016043	cellular component organization	7.89E-35	8.37E-32	1.68	13676	3680	917	414
GO:0044770	cell cycle phase transition	1.03E-34	1.01E-31	5.2	13676	215	917	75
GO:0034641	cellular nitrogen compound metabolic process	1.18E-34	1.08E-31	1.68	13676	3673	917	413
GO:0051726	regulation of cell cycle	4.70E-34	4.05E-31	2.88	13676	777	917	150
GO:0044772	mitotic cell cycle phase transition	1.08E-33	8.76E-31	5.18	13676	210	917	73
GO:0044260	cellular macromolecule metabolic process	1.18E-32	9.06E-30	1.51	13676	5013	917	507
GO:0007062	sister chromatid cohesion	4.19E-31	3.04E-28	7.46	13676	96	917	48
GO:0006260	DNA replication	1.46E-30	1.00E-27	5.92	13676	146	917	58
GO:0006396	RNA processing	5.79E-29	3.80E-26	2.84	13676	689	917	131
GO:0010564	regulation of cell cycle process	2.41E-28	1.51E-25	3.33	13676	457	917	102
GO:0006807	nitrogen compound metabolic process	2.48E-28	1.49E-25	1.56	13676	4035	917	423
GO:0006974	cellular response to DNA damage stimulus	9.29E-27	5.34E-24	2.95	13676	576	917	114
GO:0051052	regulation of DNA metabolic process	3.77E-26	2.08E-23	3.85	13676	302	917	78
GO:0000280	nuclear division	1.47E-25	7.79E-23	4.24	13676	239	917	68
GO:0044843	cell cycle G1/S phase transition	4.10E-25	2.09E-22	6.74	13676	93	917	42
GO:0043170	macromolecule metabolic process	6.88E-25	3.39E-22	1.4	13676	5532	917	520
GO:0034470	ncRNA processing	8.88E-25	4.22E-22	3.57	13676	338	917	81
GO:0048285	organelle fission	1.03E-24	4.75E-22	4.02	13676	260	917	70
GO:0007067	mitotic nuclear division	1.87E-24	8.32E-22	4.7	13676	184	917	58
GO:0000082	G1/S transition of mitotic cell cycle	2.87E-24	1.24E-21	6.65	13676	92	917	41

GO:0033044	regulation of chromosome organization	3.83E-24	1.60E-21	4.14	13676	238	917	66
GO:0007346	regulation of mitotic cell cycle	9.55E-24	3.87E-21	3.28	13676	396	917	87
GO:0006281	**DNA repair**	3.37E-23	1.33E- 20	3.25	13676	395	917	86
GO:0034660	ncRNA metabolic process	3.09E-22	1.18E-19	2.98	13676	465	917	93
GO:0006270	DNA replication initiation	3.52E-21	1.31E-18	10.53	13676	34	917	24
GO:0007059	chromosome segregation	5.05E-21	1.83E-18	6.69	13676	78	917	35
GO:0044237	cellular metabolic process	1.62E- 20	5.75E-18	1.31	13676	6386	917	563
GO:0009987	cellular process	1.31E-19	4.51E-17	1.14	13676	10628	917	815
GO:0071103	DNA conformation change	1.87E-19	6.28E-17	5.61	13676	101	917	38
GO:0006364	rRNA processing	1.97E-18	6.47E-16	3.8	13676	216	917	55
GO:0007017	microtubule-based process	2.50E-18	8.01E-16	2.91	13676	405	917	79
GO:1901990	regulation of mitotic cell cycle phase transition	6.94E-18	2.17E-15	3.51	13676	251	917	59
GO:0044238	primary metabolic process	7.07E-18	2.17E-15	1.29	13676	6383	917	553
GO:1901987	regulation of cell cycle phase transition	8.30E-18	2.49E-15	3.41	13676	267	917	61
GO:0051054	positive regulation of DNA metabolic process	1.83E-17	5.37E-15	4.12	13676	170	917	47
GO:0016072	rRNA metabolic process	2.06E-17	5.91E-15	3.57	13676	234	917	56
GO:0016070	RNA metabolic process	2.51E-17	7.08E-15	1.59	13676	2581	917	275

Table A4.5: Top 100 GO processes significantly different between LKB1 deficient and proficient cells that were common to 2D and 3D models

GO Term	Description	P-value	FDR q-value	Enrichment	N	B	n2	b3
GO:0051239	regulation of multicellular organismal process	4.09E-27	5.46E-23	2.12	13612	1892	667	197
GO:0032502	**developmental process**	6.04E-24	4.03E- 20	1.77	13612	2966	667	257
GO:0044767	single-organism developmental process	4.32E-21	1.92E-17	1.79	13612	2579	667	226
GO:0048856	anatomical structure development	1.00E- 20	3.34E-17	1.86	13612	2239	667	204
GO:0050793	regulation of developmental process	1.97E- 20	5.26E-17	2.1	13612	1516	667	156
GO:0044699	single-organism process	1.06E-19	2.36E-16	1.29	13612	7687	667	487
GO:2000026	regulation of multicellular organismal development	1.82E-19	3.47E-16	2.22	13612	1233	667	134
GO:0048519	negative regulation of biological process	2.07E-19	3.45E-16	1.63	13612	3288	667	263
GO:0048523	negative regulation of cellular process	4.12E-19	6.11E-16	1.66	13612	3061	667	249
GO:0051240	positive regulation of multicellular organismal process	4.37E-18	5.83E-15	2.31	13612	1027	667	116
GO:0044763	single-organism cellular process	5.80E-18	7.03E-15	1.33	13612	6578	667	430
GO:0051094	positive regulation of developmental process	2.08E-17	2.31E-14	2.52	13612	768	667	95
GO:0048518	positive regulation of biological process	3.20E-17	3.29E-14	1.54	13612	3712	667	280
GO:0048583	regulation of response to stimulus	7.77E-17	7.40E-14	1.68	13612	2634	667	217
GO:0045595	**regulation of cell differentiation**	2.17E-16	1.93E-13	2.18	13612	1095	667	117
GO:0023051	regulation of signalling	1.09E-15	9.08E-13	1.74	13612	2211	667	188
GO:1901700	**response to oxygen-containing compound**	1.21E-15	9.48E-13	2.27	13612	925	667	103
GO:0042221	response to chemical	3.29E-15	2.44E-12	1.86	13612	1675	667	153

GO:0033993	**response to lipid**	3.39E-15	2.38E-12	2.74	13612	536	667	72
GO:0010646	**regulation of cell communication**	4.85E-15	3.24E-12	1.72	13612	2178	667	184
GO:0048522	positive regulation of cellular process	6.46E-15	4.10E-12	1.53	13612	3367	667	253
GO:0009725	response to hormone	9.32E-15	5.65E-12	2.99	13612	416	667	61
GO:0051241	negative regulation of multicellular organismal process	1.41E-14	8.17E-12	2.42	13612	716	667	85
GO:0045597	positive regulation of cell differentiation	1.52E-14	8.46E-12	2.56	13612	614	667	77
GO:0022603	regulation of anatomical structure morphogenesis	4.92E-14	2.62E-11	2.36	13612	745	667	86
GO:0010033	response to organic substance	9.20E-14	4.72E-11	1.94	13612	1324	667	126
GO:0009966	regulation of signal transduction	1.62E-13	8.01E-11	1.73	13612	1962	667	166
GO:0048513	animal organ development	3.35E-13	1.60E-10	2.21	13612	839	667	91
GO:0009719	response to endogenous stimulus	4.15E-13	1.91E-10	2.31	13612	733	667	83
GO:0032870	cellular response to hormone stimulus	6.65E-13	2.96E-10	3.82	13612	203	667	38
GO:0060284	regulation of cell development	8.38E-13	3.61E-10	2.44	13612	610	667	73
GO:0007165	signal transduction	1.23E-12	5.11E-10	1.5	13612	3192	667	235
GO:0010769	**regulation of cell morphogenesis involved in differentiation**	2.02E-12	8.18E-10	3.41	13612	251	667	42
GO:0045664	regulation of neuron differentiation	3.00E-12	1.18E-09	2.77	13612	412	667	56
GO:0032879	regulation of localization	5.99E-12	2.28E-09	1.72	13612	1784	667	150
GO:1902531	regulation of intracellular signal transduction	6.35E-12	2.35E-09	1.91	13612	1221	667	114
GO:0048584	positive regulation of response to stimulus	6.41E-12	2.31E-09	1.84	13612	1374	667	124
GO:0051270	regulation of cellular component movement	7.40E-12	2.60E-09	2.43	13612	572	667	68
GO:0001525	**angiogenesis**	1.41E-11	4.83E-09	3.7	13612	193	667	35
GO:0071495	cellular response to endogenous stimulus	1.44E-11	4.79E-09	2.7	13612	416	667	55
GO:0048585	negative regulation of response to stimulus	1.55E-11	5.03E-09	2	13612	999	667	98
GO:0010975	regulation of neuron projection development	1.79E-11	5.68E-09	3.05	13612	301	667	45
GO:0010941	**regulation of cell death**	2.08E-11	6.45E-09	1.95	13612	1078	667	103
GO:0040012	regulation of locomotion	2.10E-11	6.35E-09	2.43	13612	546	667	65
GO:0042127	regulation of cell proliferation	2.47E-11	7.31E-09	1.94	13612	1096	667	104
GO:0023057	negative regulation of signalling	3.43E-11	9.94E-09	2.06	13612	882	667	89
GO:0042981	**regulation of apoptotic process**	3.58E-11	1.02E-08	1.98	13612	999	667	97
GO:0030334	**regulation of cell migration**	4.13E-11	1.15E-08	2.5	13612	490	667	60
GO:0040011	locomotion	4.24E-11	1.15E-08	2.27	13612	648	667	72
GO:0065007	biological regulation	4.25E-11	1.13E-08	1.2	13612	8120	667	477
GO:0016477	**cell migration**	4.30E-11	1.12E-08	2.43	13612	529	667	63
GO:0060548	**negative regulation of cell death**	4.39E-11	1.13E-08	2.28	13612	635	667	71
GO:0048646	anatomical structure formation involved in morphogenesis	4.52E-11	1.14E-08	2.35	13612	582	667	67
GO:0043067	**regulation of programmed cell death**	5.02E-11	1.24E-08	1.97	13612	1005	667	97
GO:0044707	single-multicellular organism process	5.48E-11	1.33E-08	1.69	13612	1722	667	143
GO:0010648	**negative regulation of cell communication**	6.42E-11	1.53E-08	2.05	13612	878	667	88
GO:0030155	**regulation of cell adhesion**	7.50E-11	1.76E-08	2.53	13612	459	667	57

GO:2000145	**regulation of cell motility**	8.14E-11	1.87E-08	2.41	13612	524	667	62
GO:0043066	**negative regulation of apoptotic process**	8.44E-11	1.91E-08	2.33	13612	577	667	66
GO:0050767	regulation of neurogenesis	9.34E-11	2.08E-08	2.47	13612	487	667	59
GO:0032501	multicellular organismal process	9.96E-11	2.18E-08	1.57	13612	2270	667	175
GO:0070887	cellular response to chemical stimulus	1.12E-10	2.40E-08	1.99	13612	931	667	91
GO:0071310	cellular response to organic substance	1.13E-10	2.39E-08	2.15	13612	731	667	77
GO:0030198	**extracellular matrix organization**	1.16E-10	2.43E-08	3.37	13612	218	667	36
GO:0043062	**extracellular structure organization**	1.16E-10	2.39E-08	3.37	13612	218	667	36
GO:0010647	**positive regulation of cell communication**	1.29E-10	2.61E-08	1.9	13612	1097	667	102
GO:0014070	response to organic cyclic compound	1.35E-10	2.69E-08	2.33	13612	570	667	65
GO:0043069	**negative regulation of programmed cell death**	1.42E-10	2.79E-08	2.31	13612	584	667	66
GO:0023056	positive regulation of signalling	1.59E-10	3.07E-08	1.89	13612	1101	667	102
GO:0051093	negative regulation of developmental process	1.80E-10	3.43E-08	2.41	13612	508	667	60
GO:0048869	cellular developmental process	2.26E-10	4.25E-08	1.65	13612	1822	667	147
GO:0051960	regulation of nervous system development	2.38E-10	4.41E-08	2.33	13612	551	667	63
GO:0006198	**cAMP catabolic process**	2.75E-10	5.02E-08	18.14	13612	9	667	8
GO:0001932	**regulation of protein phosphorylation**	2.87E-10	5.17E-08	1.97	13612	933	667	90
GO:0050789	regulation of biological process	3.05E-10	5.42E-08	1.2	13612	7679	667	453
GO:0009968	negative regulation of signal transduction	3.17E-10	5.56E-08	2.06	13612	804	667	81
GO:1901698	**response to nitrogen compound**	5.33E-10	9.24E-08	2.35	13612	522	667	60
GO:0010770	**positive regulation of cell morphogenesis involved in differentiation**	5.89E-10	1.01E-07	4.25	13612	120	667	25
GO:0048870	**cell motility**	8.55E-10	1.44E-07	2.24	13612	582	667	64
GO:0010243	**response to organonitrogen compound**	8.75E-10	1.46E-07	2.4	13612	476	667	56
GO:0042325	**regulation of phosphorylation**	1.01E-09	1.66E-07	1.9	13612	1001	667	93
GO:0009991	response to extracellular stimulus	1.05E-09	1.71E-07	2.82	13612	304	667	42
GO:0045765	**regulation of angiogenesis**	1.10E-09	1.76E-07	3.76	13612	152	667	28
GO:1901701	**cellular response to oxygen-containing compound**	1.20E-09	1.90E-07	2.38	13612	480	667	56
GO:0031344	regulation of cell projection organization	1.20E-09	1.88E-07	2.53	13612	403	667	50
GO:0043408	**regulation of MAPK cascade**	1.20E-09	1.86E-07	2.4	13612	467	667	55
GO:0009214	cyclic nucleotide catabolic process	1.32E-09	2.02E-07	16.33	13612	10	667	8
GO:0019220	regulation of phosphate metabolic process	1.53E-09	2.32E-07	1.81	13612	1162	667	103
GO:0051174	regulation of phosphorus metabolic process	1.60E-09	2.40E-07	1.81	13612	1163	667	103
GO:1903522	regulation of blood circulation	1.78E-09	2.64E-07	3.25	13612	207	667	33
GO:0048545	**response to steroid hormone**	2.23E-09	3.26E-07	3.46	13612	177	667	30
GO:1901342	**regulation of vasculature development**	3.54E-09	5.13E-07	3.48	13612	170	667	29
GO:0009967	positive regulation of signal transduction	3.60E-09	5.17E-07	1.86	13612	1011	667	92
GO:0007155	**cell adhesion**	4.59E-09	6.52E-07	2.01	13612	763	667	75
GO:0010720	positive regulation of cell development	5.07E-09	7.11E-07	2.57	13612	357	667	45
GO:0022610	**biological adhesion**	5.45E-09	7.58E-07	2	13612	766	667	75

GO:0030154	**cell differentiation**	7.45E-09	1.02E-06	1.74	13612	1228	667	105
GO:0032101	regulation of response to external stimulus	9.96E-09	1.35E-06	2.14	13612	591	667	62
GO:0022604	regulation of cell morphogenesis	1.07E-08	1.45E-06	2.42	13612	404	667	48
GO:0007166	cell surface receptor signalling pathway	1.13E-08	1.50E-06	1.67	13612	1446	667	118

Table A4.6: Top 20 pathways associated with genes that were highly expressed in LKB1 deficient spheroids

Key Pathway Maps Details [57 processes]				
#	Name	Input Objects ▲ p-value	Key Hubs p-value	Union Objects p-value
1	Signal transduction_mTORC1 downstream signaling	2.168E-10	5.461E-7	6.428E-13
2	Transcription_Sirtuin6 regulation and functions	5.053E-8	3.878E-4	8.669E-9
3	Immune response_IL-6-induced acute-phase response in hepatocytes	2.563E-6	1.011E-4	3.59E-8
4	Transcription_Role of Akt in hypoxia induced HIF1 activation	6.055E-6	1.691E-6	7.527E-10
5	Regulation of lipid metabolism_Regulation of lipid metabolism via LXR, NF-Y and SREBP	9.385E-6	0.0053	1.45E-6
6	Immune response_Human NKG2D signaling	7.997E-5	0.04277	6.347E-5
7	Development_Leptin signaling via JAK/STAT and MAPK cascades	1.748E-4	0.001535	5.311E-6
8	IGF family signaling in colorectal cancer	4.561E-4	8.703E-13	2.427E-13
9	Immune response_IL-17 signaling pathways	4.561E-4	2.004E-4	3.08E-5
10	Development_Role of IL-8 in angiogenesis	5.378E-4	1.988E-7	4.454E-12
11	Transcription_Ligand-dependent activation of the ESR1/SP pathway	6.973E-4	4.394E-7	3.491E-8
12	Development_Differentiation of white adipocytes	7.608E-4	5.785E-9	2.13E-10
13	Glucocorticoid-induced elevation of intraocular pressure as glaucoma risk factor	8.598E-4	2.9E-9	5.825E-11
14	Development_Glucocorticoid receptor signaling	0.0011	3.757E-4	5.311E-6
15	Immune response_Oncostatin M signaling via JAK-Stat in human cells	0.001696	1.246E-6	1.529E-7
16	Cell adhesion_ECM remodeling	0.002065	1.448E-9	4.734E-12
17	Development_Insulin, IGF-1 and TNF-alpha in brown adipocyte differentiation	0.002065	3.734E-11	4.734E-12
18	Cell adhesion_Chemokines and adhesion	0.002073	1.735E-14	5.378E-17
19	Development_Beta adrenergic receptors in brown adipocyte differentiation	0.002506	1.077E-6	2.281E-7
20	Immune response_IL-1 signaling pathway	0.002522	2.896E-7	2.671E-8

Table A4.7: Top 20 pathways associated with genes that were expressed at lower levels in LKB1 deficient spheroids

Key Pathway Maps Details [38 processes]				
#	Name	Input Objects p-value ▲	Key Hubs p-value	Union Objects p-value
1	Colorectal cancer (general schema)	1.548E-5	0.04391	8.895E-6
2	Immune response_TLR2 and TLR4 signaling pathways	6.976E-4	6.19E-5	8.779E-8
3	Nociception_Nociceptin receptor signaling	0.001001	0.001831	5.08E-6
4	Development_Transcription regulation of granulocyte development	0.001158	0.004063	2.076E-5
5	Immune response_Platelet activating factor/ PTAFR pathway signaling	0.001228	5.295E-7	7.669E-9
6	Development_Adenosine A1 receptor signaling	0.003307	0.01212	0.002052
7	Muscle contraction_Regulation of eNOS activity in endothelial cells	0.003495	9.063E-5	3.708E-6
8	Development_Oligodendrocyte differentiation from adult stem cells	0.004292	0.01538	9.796E-4
9	Cytoskeleton remodeling_TGF, WNT and cytoskeletal remodeling	0.004699	7.63E-5	7.41E-7
10	Mucin expression in CF airways	0.006731	9.357E-4	1.934E-5
11	Reproduction_Gonadotropin-releasing hormone (GnRH) signaling	0.009033	0.03302	0.001204
12	Development_TGF-beta-dependent induction of EMT via SMADs	0.009206	3.234E-4	1.234E-5
13	Transcription_CREB signaling pathway	0.009757	0.02928	0.001342
14	Immune response_C5a signaling	0.01096	0.03253	0.005099
15	Development_Gastrin in cell growth and proliferation	0.01174	0.004684	6.428E-4
16	Immune response_PIP3 signaling in B lymphocytes	0.01207	0.03202	0.001986
17	Immune response_Function of MEF2 in T lymphocytes	0.01227	0.01212	0.002052
18	G-protein signaling_Proinsulin C-peptide signaling	0.01227	0.03601	0.006114
19	Immune response_Innate immune response to RNA viral infection	0.01439	0.001796	6.477E-4
20	Development_Growth factors in regulation of oligodendrocyte precursor cell proliferation	0.01562	0.049	0.008369

Table A4.8: Pathways associated with highly expressed genes in LKB1 deficient cells common to 2D, 3D and human tumour models

Key Pathway Maps Details [18 processes]				
#	Name	Input Objects p-value ▲	Key Hubs p-value	Union Objects p-value
1	Immune response_Function of MEF2 in T lymphocytes	0.00405	5.921E-6	4.678E-7
2	Development_Insulin, IGF-1 and TNF-alpha in brown adipocyte differentiation	0.004808	0.009432	2.436E-4
3	Reproduction_Gonadotropin-releasing hormone (GnRH) signaling	0.01068	1.396E-4	2.283E-5
4	Putative pathways for stimulation of fat cell differentiation by Bisphenol A	0.01724	0.02141	0.001367
5	G-protein signaling_RhoA regulation pathway	0.02186	6.094E-15	3.494E-15
6	Immune response_IL-4 signaling pathway	0.02193	0.01431	0.001238
7	Immune response_IL-3 signaling via JAK/STAT, p38, JNK and NF-kB	0.02391	4.253E-4	2.774E-5
8	Immune response_IL-6-induced acute-phase response in hepatocytes	0.02434	0.008731	6.538E-4
9	Development_Beta adrenergic receptors in brown adipocyte differentiation	0.02434	0.001597	1.001E-4
10	Possible pathway of TGF-beta 1-dependent inhibition of CFTR expression	0.02692	0.002132	9.192E-4
11	Development_Growth hormone signaling via PI3K/AKT and MAPK cascades	0.03101	5.63E-4	4.072E-5
12	Signal transduction_PTMs in IL-17-induced CIKS-independent signaling pathways	0.03532	0.004555	4.368E-4
13	Neurophysiological process_Corticoliberin signaling via CRHR1	0.03831	1.99E-4	1.063E-4
14	Development_Beta-adrenergic receptors signaling via Cyclic AMP	0.03985	0.02585	0.003309
15	Signal transduction_PKA signaling	0.04298	0.03034	0.004205
16	Signal transduction_Activation of PKC via G-Protein coupled receptor	0.04458	0.001899	0.001061
17	Development_Role of HDAC and calcium/calmodulin-dependent kinase (CaMK) in control of skeletal myogenesis	0.04621	0.002135	2.436E-4
18	Development_Differentiation of white adipocytes	0.04952	0.01133	0.00157

Table A4.9: Pathways associated with genes expressed at lower levels in LKB1 deficient cells common to 2D, 3D and human tumour models

Key Pathway Maps Details [6 processes]				
#	Name	Input Objects p-value ▲	Key Hubs p-value	Union Objects p-value
1	Development_Regulation of epithelial-to-mesenchymal transition (EMT)	0.00419	0.01797	1.825E-4
2	Immune response_Role of integrins in NK cells cytotoxicity	0.01606	0.006595	2.66E-4
3	Cytoskeleton remodeling_TGF, WNT and cytoskeletal remodeling	0.01803	2.146E-5	2.982E-6
4	Development_TGF-beta-dependent induction of EMT via RhoA, PI3K and ILK.	0.02211	3.886E-4	3.303E-5
5	Stimulation of TGF-beta signaling in lung cancer	0.02399	0.009962	6.077E-4
6	Immune response_IL-2 activation and signaling pathway	0.02495	0.01038	6.588E-4

Table A5.6a: 326-compound bioactive small molecule library (Selleck L1100)

Compound	Target(s)
17-AAG(Geldanamycin)	HSP90
17-DMAG	HSP90
2-Methoxyestradiol	HIF
ABT-263(Navitoclax)	BCL-2
ABT-737	BCL-2
ABT-751	Microtubule Formation
ABT-869	RTK | VEGFR | PDGFR | FGFR
ABT-888	PARP
AC-220	FLT
Acetaminophen(Tylenol)	COX
Adriamycin	Topoisomerase
AEE788	EGFR | HER1/2 | VEGFR | FGFR
AG-014699	PARP
AG14361	PARP
AG-490	JAK | EGFR
Alendronate Sodium	farnesyl diphosphate synthase
Allopurinol	xanthine oxidase
Amfebutamone hcl	norepinephrine-dopamine reuptake
Amisulpride	Dopamine Receptor
Amlodipine besylate	calcium channel
Anastrozole(Arimidex)	Aromatase
AP24534	VEGFR | FGFR | PDGFR | FLT
Apigenin	P450
Apixaban	Factor Xa
AS-605240	PI3K
AS703026	MEK
Asenapine maleate	5-HT | adrenergic receptor
AT7519	CDK
AT7867	Akt | S6 kinase
AT9283	Bcr-Abl| JAK | Aurora Kinase
Atazanavir(BMS-232632)	Proteasome
Atropine sulfate monohydrate	mAChRs
Aurora A Inhibitor I	Aurora Kinase
AV-951(Tivozanib)	VEGFR | c-Kit | PDGFR
Axitinib	VEGFR
AZD0530(Saracatinib)	SRC | Abl
AZD1152-HQPA(Barasertib)	Aurora Kinase
AZD1480	JAK
AZD2281(Olaparib)	PARP
AZD6244(Selumetinib)	MEK
AZD6482	PI3K
AZD7762	CHK
AZD8055	MTOR
AZD8330	MEK
Baicalin	prolyl endopeptidase |GABA receptor
BAY 73-4506(Regorafenib)	C-KIT | B-RAF | VEGFR
Belinostat(PXD101)	HDAC
Benazepril hydrochloride	RAAS
Benserazide hcl	Dopamine | AAAD
BEZ235(NVP-BEZ235)	MTOR | PI3K
BI 2536	PLK
BIBF1120(Vargatef)	VEGFR | PDGFR | FGFR
BIBR 953	thrombin
BIBR-1048	thrombin
BIBR1532	Telomerase
BIBW2992(Tovok)	EGFR | HER2
Bicalutamide(Casodex)	androgen receptor
BIIB021	HSP90

BIRB 796	p38 MAPK
Bisoprolol Fumarate	Adrenergic receptors
BIX 02188	MEK
BIX 02189	MEK
BMS 777607	C-MET
BMS 794833	c-MET | VEGFR | MET | AXL | FLT
BMS-599626	EGFR | HER2
BMS-707035	HIV-1 Integrase(IN)
BMS-708163	γ-secretase
BMS-790052	HCV protease
Bortezomib	proteasome
Bosutinib(SKI-606)	Src
BS-181 hydrochloride	CDK
BSI- 201	PARP
Camptothecin	Topoisomerase
Capecitabine(Xeloda)	Antimetabolites
Carbamazepine(Carbatrol)	sodium channel
Carbidopa	aromatic-L-amino-acid decarboxylase
CCT129202	Aurora kinase
Cediranib(AZD2171)	VEGFR | FGFR
CHIR-99021	GSK-3
Chlorpromazine hcl	Dopamine | potassium channel
Chlorprothixene	5-HT | Dopamine receptor
CHR-2797	Aminopeptidase N(APN) | LAP
CI-1033(Canertinib)	EGFR | HER2
CI-1040 (PD184352)	MEK
Cilnidipine	calcium channe
Cilomilast(SB- 207499)	PDE
Cilostazol	PDE
Cladribine	Antimetabolites
Clemastine fumarate	histamine H1 antagonist
Clofarabine	ribonucleotide reductase
Clopidogrel bisulfate	NULL
Clozapine	5-HT1C receptor
CP-724714	HER2
Cryptotanshinone	Stat
CUDC-101	HDAC | EGFR | HER2
CYC116	Aurora Kinase | VEGFR
Cyclopamine	Hedgehog
Cytarabine(Cytosar-U)	DNA polymerase
Danoprevir(ITMN-191)	Proteasome
Dasatinib	SRC | Abl
Decitabine	Antimetabolites
Deforolimus(MK-8669)	MTOR
Diclofenac sodium	COX
Diphenhydramine hcl	histamine H1
Dipyridamole	PDE
Docetaxel	Microtubule Formation
Donepezil hydrochloride	mAChRs
Dorzolamide HCL	carbonic anhydrase(CA)
Doxazosin mesylate	adrenergic receptor
Droxinostat	HDAC
Dutasteride(Avodart)	5α-reductase
Elvitegravir	HIV Integrase
Emtricitabine	nucleoside reverse transcriptase
Enalapril maleate	RAAS
Enalaprilat	RAAS
ENMD- 2076	Flt | Aurora Kinase | Src | VEGFR
Enzastaurin	PKC
Eplerenone	RAAS

Epothilone A	Microtubule Formation
Epothilone B(EPO906)	Epothilone B
Erlotinib Hydrochloride	EGFR
Etoposide(Etopophos)	Topoisomerase
Everolimus(RAD001)	MTOR
EX 527	Sirtuin
Exemestane	aromatase enzyme
Fasudil HCl	ROCK
Febuxostat	XAO
Felodipine	calcium channel
Finasteride	5α-reductase
Flavopiridol(Alvocidib)	CDK
Flucytosine(Ancobon)	DNA/RNA synthesis
Fludarabine Phosphate	Antimetabolites
Fludarabine(Fludara)	Antimetabolites
Fluoxetine hydrochloride	5-HT
Fluvastatin Sodium	HMG-CoA reductase
Fulvestrant	estrogen receptor
GDC-0449(Vismodegib)	Hedgehog
GDC-0879	B-RAF
GDC-0941	PI3K
Gefitinib(Iressa)	EGFR | Akt
Gemcitabine Hydrochloride	Antimetabolites
Granisetron Hydrochloride	5-HT receptor
GSK1059615	PI3K | MTOR
GSK429286A	ROCK
GSK461364	PLK
Hesperadin	Aurora kinase
HMN-214	PLK
Ibuprofen	COX
IC-87114	PI3K
Icariin	PDE
Imatinib Mesylate	c-Kit | PDGFR
Imatinib(STI571)	PDGFR | c-Kit
Indirubin	CDK | GSK-3
INO-1001	PARP
Irbesartan(Avapro)	RAAS
Irinotecan	topoisomerase
Ispinesib(SB-715992)	Kinesin spindle protein
ITF2357	HDAC
JNJ 26854165	p53
JNJ-26481585	HDAC
JNJ-38877605	C-MET
JNJ-7706621	CDK | Aurora Kinase
Ketoprofen(Actron)	COX
Ketorolac Tromethamine	COX
Ki8751	VEGFR | C-KIT | PDGFR | FGFR
KRN 633	VEGFR | PDGFR | C-KIT
KU-0063794	MTOR
KU-55933	ATM
KU-60019	ATM
KW 2449	FLT | ABL | AURORA KINASE
Lapatinib Ditosylate	EGFR | HER2
LAQ824	HDAC
LBH-589(Panobinostat)	HDAC
LDE225	SMO
Lenalidomide	TNF-alpha
Letrozole	Aromatase
Linezolid	NULL
Luteolin(Luteolol)	PDE | Interleukin 6

LY2228820	p38 MAPK
LY2784544	JAK
LY294002	PI3K
LY500307	ERβ
Manidipine	calcium channel
Maraviroc(Selzentry)	CCR5(cellular coreceptor 5)
Masitinib(AB1010)	c-KIT | PDGFR | FGFR | VEGFR
MC1568	HDAC
MGCD0103(Mocetinostat)	HDAC
MGCD-265	C-MET | VEGFR | TIE-2
Mitoxantrone	Topoisomerase
Mizoribine	DNA/RNA synthesis
MK 3207 hydrochloride	CGRP
MK-2206	AKT
MLN2238	Proteasome
MLN8237	Aurora
MLN9708	Proteasome
Motesanib Diphosphate	VEGFR | PDGFR | C-KIT | SRC
MP-470	C-MET | C-KIT | PDGFR | FLT3 | SRC
MS-275	HDAC
Naftopidil	α1-adrenergic receptor
Naftopidil Dihydrochloride	adrenergic receptor
Nebivolol HCl	adrenergic receptor
Neratinib	HER2 | EGFR
Nilotinib	BCR-ABL
Nisoldipine	calcium channel
Nizatidine	histamine H2-receptor
NPI-2358	VDA
NVP-ADW742	IGF-1R
NVP-AUY922	HSP90
NVP-BEP800	HSP90
NVP-TAE684	ALK
Obatoclax Mesylate	Bcl-2
ON-01910	PLK
OSI-930	c-KIT | VEGFR
Ozagrel	thromboxane A2 synthetase
Paclitaxel(Taxol)	Microtubule Formation
Pancuronium bromide	mAChRs
Pazopanib Hydrochloride	VEGFR
PD0325901	MEK
PD0332991	CDK
PD153035 hydrochloride	EGFR
PD318088	MEK
PD98059	MEK
Pelitinib	EGFR
Pemetrexed disodium	TS | DHFR | GARFT
Perindopril Erbumine	RAAS
PF-04217903	C-MET
PF-2341066	C-MET | ALK
PHA-680632	Aurora Kinase
PHA-739358(Danusertib)	Aurora Kinase | BCR-ABL
PHA-793887	CDK
PI-103	PI3K | MTOR
PIK-293	PI3K
PIK-75 Hydrochloride	PI3K | DNA-PK
PIK-90	PI3K
PIK-93	PI3K
Pimobendan(Vetmedin)	PDE
Piroxicam	COX
PLX-4720	B-RAF

Pomalidomide	TNF-alpha
Pramipexole dihydrochloride monohydrate	NULL
Pyrimethamine	dihydrofolate reductase(DHFR)
Quercetin(Sophoretin)	PI3K | PKC | SRC
R406	SYK
R406(free base)	SYK
RAF265	RAF | VEGFR
Raltegravir	HIV Integrase
Raltitrexed(Tomudex)	Antimetabolites
Ramipril	RAAS
Ranitidine Hydrochloride	histamine H2-receptor
Rapamycin(Sirolimus)	MTOR
Ritonavir	HIV protease
Rivaroxaban(Xarelto)	Factor Xa
RO4929097	Y-Secretase
Roscovitine(CYC202)	CDK
S-(+)-Rolipram	PDE
S31- 201	STAT3
SB 202190	p38 MAPK
SB 203580	p38 MAPK
SB 216763	GSK-3
SB 431542	ALK
SB 525334	ALK
SB 743921	Kinesin spindle protein
SB939	HDAC
Selegiline hydrochloride	monoamine oxidase
Semagacestat	Y-Secretase
SGI-1776	PIM
SGX-523	C-MET | VEGFR
Sitagliptin phosphate	DPP-4
SNS-032(BMS-387032)	CDK
SNS-314 Mesylate	Aurora Kinase
Sodium valproate	HDAC
Sorafenib Tosylate	VEGFR | PDGFR | RAF | MEK
Sotalol hydrochloride	Beta-1 adrenergic receptor
SP600125	JNK
Stavudine	NART
SU11274(PKI-SU11274)	c-Met
Sulfamethoxazole	PABA
Sulfanilamide	PABA
Sunitinib Malate	FLT3 | PDGFR | VEGFR | Kit
Tadalafil(Cialis)	PDE
Tamoxifen Citrate	Estrogen receptor
Tamsulosin hydrochloride	hydroxysteroid dehydrogenase
Tandutinib (MLN518)	FLT-3 | PDGFR | KIT
Telmisartan	RAAS
Temsirolimus	MTOR
Tenofovir	NART
Terbinafine hydrochloride	COX
TG100-115	PI3K
TGX-221	PI3K
Tipifarnib	farnesyltransferase(Ftase)
Topotecan Hydrochloride	Topoisomerase
Trichostatin A	HDAC
Trilostane	hydroxysteroid dehydrogenase
Tropisetron hcl	5-HT receptor
TSU-68	VEGFR | PDGFR | FGFR
TW-37	BCL-2
U0126-EtOH	MEK

Valsartan	RAAS
Vandetanib	VEGFR | EGFR | Src
Vardenafil(Vivanza)	PDE
Vatalanib	VEGFR | c-Kit | Flk | Flt | FGFR
Venlafaxine hcl	5-HT receptor
Vicriviroc Malate	CCR5(cellular coreceptor 5)
Vincristine Sulfate	Microtubule Formation
Vinorelbine(Navelbine)	p38 MAPK
Vorinostat	HDAC
VX-222	HCV protease
VX-680	Aurora Kinase
VX-702	p38 MAPK | IL-6 | IL-1β | TNFα
VX-745	p38 MAPK
VX-770	CFTR
WYE-354	MTOR
WZ3146	EGFR
WZ4002	EGFR
WZ8040	EGFR
XAV-939	WNT
XL147	PI3K
XL184	VEGFR | C-MET | FLT | TIE-2 | C-KIT
XL765	PI3K | MTOR
XL880(GSK1363089)	C-MET | VEGFR | FGFR
YM155	Survivin
Yohimbine hydrochloride	alpha 2-adrenergic receptors
Zalcitabine	NART
Zibotentan(ZD4054)	ETA-receptor
ZM-447439	Aurora Kinase
ZSTK474	PI3K

Table A5.6b: Additional compounds tested in the primary screen

Compound	Target(s)
Acetylsalicylic acid (aspirin)	COX
Compound 1	Unknown
JQ1 inhibitor	BET bromodomain
PF562271	FAK
Phleomycin	Antibiotic
PHT-427	AKT and PDPK1
Telaprevir	Anti-viral, protease inhibitor

Information on the source, stock concentration, vehicle and storage can be found in Table 2.2.

Table A5.7: Additional compounds tested in the secondary screen

Compound	Target
AZD8055	MTOR
AZD0530 (Saracatinib)	SRC | ABL
PI-103	PI3K | MTOR
AZD6244	MEK
PF562271	FAK
LKB1 (AAK1 dual inhibitor)	LKB1
Thymidylate Kinase Inhibitor, YMU1	Thymidylate kinase
WZ4003	NUAK
Ganetespib	HSP90

These targets (MTOR, SRC, PI3K, MEK, FAK, thymidylate kinase) were identified as possible hits in the literature (Section 1.6). NUAK is a downstream target of LKB1 (Section 1.3). HSP90 was identified as a target in our primary 2D screen (Table 5.1). These compounds and the compounds in Table 5.1 were confirmed in A549, A427 and H1299 isogenic cells with or without LKB1.

Table A5.8: Compounds used in the 3D screen

Inhibitor	Target
ABT-888	PARP
Adriamycin	Topoisomerase
AT7867	Akt | S6 kinase
Aurora A Inhibitor I	Aurora Kinase
AZD0530(Saracatinib)	SRC | Abl
AZD1208	PIM
AZD1480	JAK
AZD2281(Olaparib)	PARP
AZD6244(Selumetinib)	MEK
AZD6482	PI3K
AZD7762	CHK
Belinostat(PXD101)	HDAC
BEZ235(NVP-BEZ235)	MTOR | PI3K
BMS-708163	γ-secretase
Bortezomib	proteasome
Cediranib(AZD2171)	VEGFR | FGFR
CHIR-99021	GSK-3
CHR-2797	Aminopeptidase N(APN) | LAP
CI-1040 (PD184352)	MEK
Cytarabine(Cytosar-U)	DNA polymerase
Dasatinib	SRC | Abl
Diclofenac sodium	COX
Epothilone B(EPO906)	Microtubules
Everolimus(RAD001)	MTOR
GDC-0449(Vismodegib)	Hedgehog
GDC-0879	B-RAF
GDC-0941	PI3K
Gefitinib(Iressa)	EGFR | Akt
Gemcitabine Hydrochloride	Antimetabolites
GSK429286A	ROCK
GSK461364	PLK
Ibuprofen	COX
Irinotecan	topoisomerase
Ispinesib(SB-715992)	Kinesin spindle protein
ITF2357	HDAC
JNJ 26854165	p53
Ketorolac Tromethamine	COX
KU-60019	ATM
LBH-589(Panobinostat)	HDAC
LDE225	Smo
LKBi	LKB
LY2228820	p38 MAPK
MARKi	MARK
MK-2206	Akt
NPI-2358	VDA, microtubules
NVP-AUY922	HSP90
NVP-TAE684	ALK
ON-01910	PLK
PD0325901	MEK
PD0332991	CDK
Pemetrexed disodium	TS | DHFR | GARFT
PF-04217903	c-Met
PHA-793887	CDK

PI-103	PI3K | MTOR
PIK-93	PI3K
PLX-4720	B-Raf
Pyrimethamine	dihydrofolate reductase (DHFR)
R406(free base)	Syk
Raltitrexed(Tomudex)	Antimetabolites
Rapamycin(Sirolimus)	MTOR
S31- 201	STAT3
SB 202190	p38 MAPK
SGI-1776	Pim
Sitagliptin phosphate	DPP-4
SNS-032(BMS-387032)	CDK
Thymidylate kinase inhibitor	TK
Tipifarnib	farnesyltransferase(Ftase)
U0126-EtOH	MEK
Vincristine Sulfate	Microtubule Formation
Vinorelbine(Navelbine)	Microtubule Formation
VX-702	p38 MAPK | IL-6 | IL-1β | TNFα
XAV939	Wnt
YM155	Survivin
ZM-447439	Aurora Kinase

Compounds in bold indicate that they were identified as a hit in the 2D screen

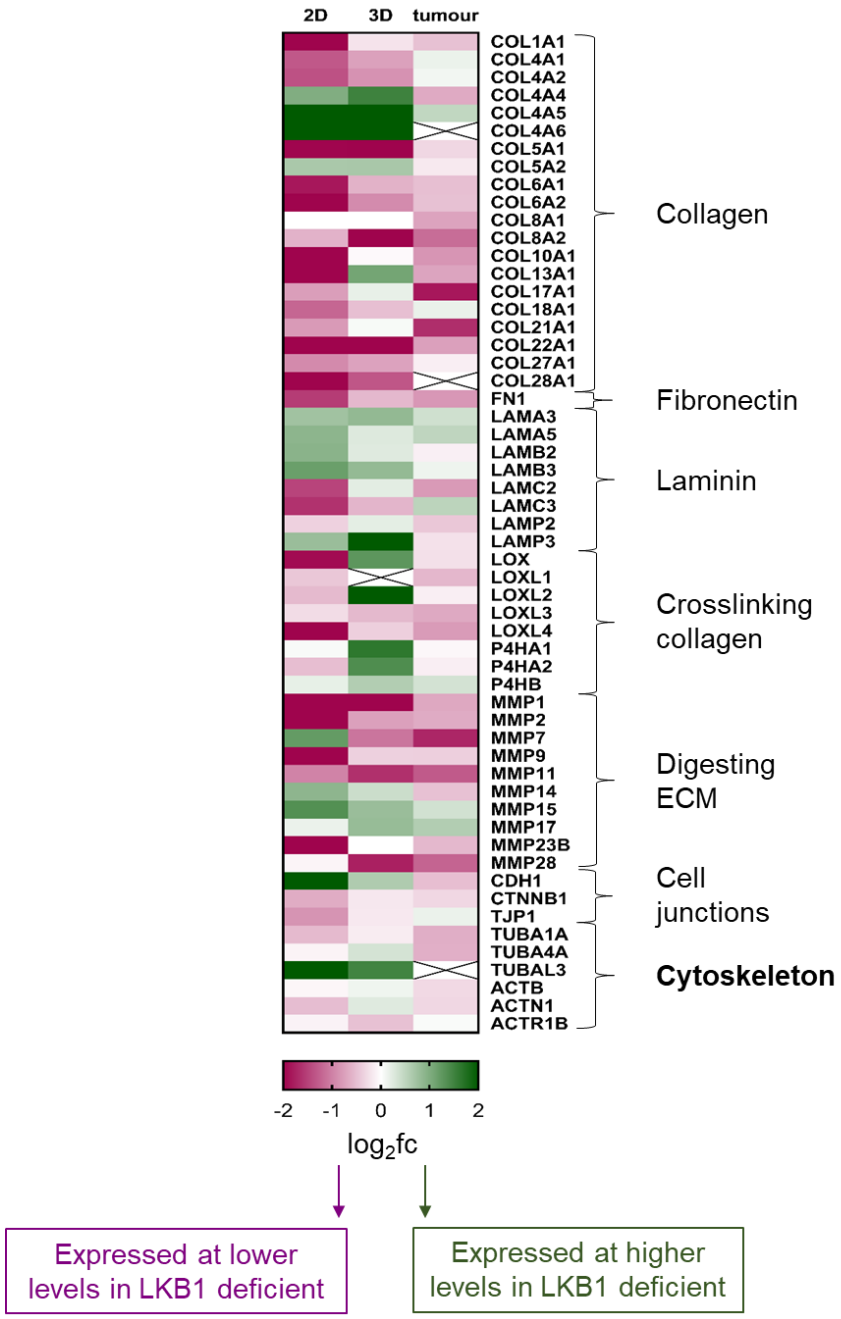

Figure A5.14: Heatmap showing cytoskeletal, cell junctions and ECM genes expressed and higher or lower levels in the LKB1 deficient cells in 2D, 3D and human tumour samples

Heatmap showing genes expressed at higher levels in green (≥ 2 log_2fc (fold change)) and genes expressed at lower levels in purple (≤ 2 log_2fc). Significant and non-significant differences are included. The cross implies there is no data available on this gene. Heatmap was produced using GraphPad Prism 7, with the RNASeq data analysed in Chapter 4 (2D and 3D) and the human lung adenocarcinoma dataset (TCGA, 2014).

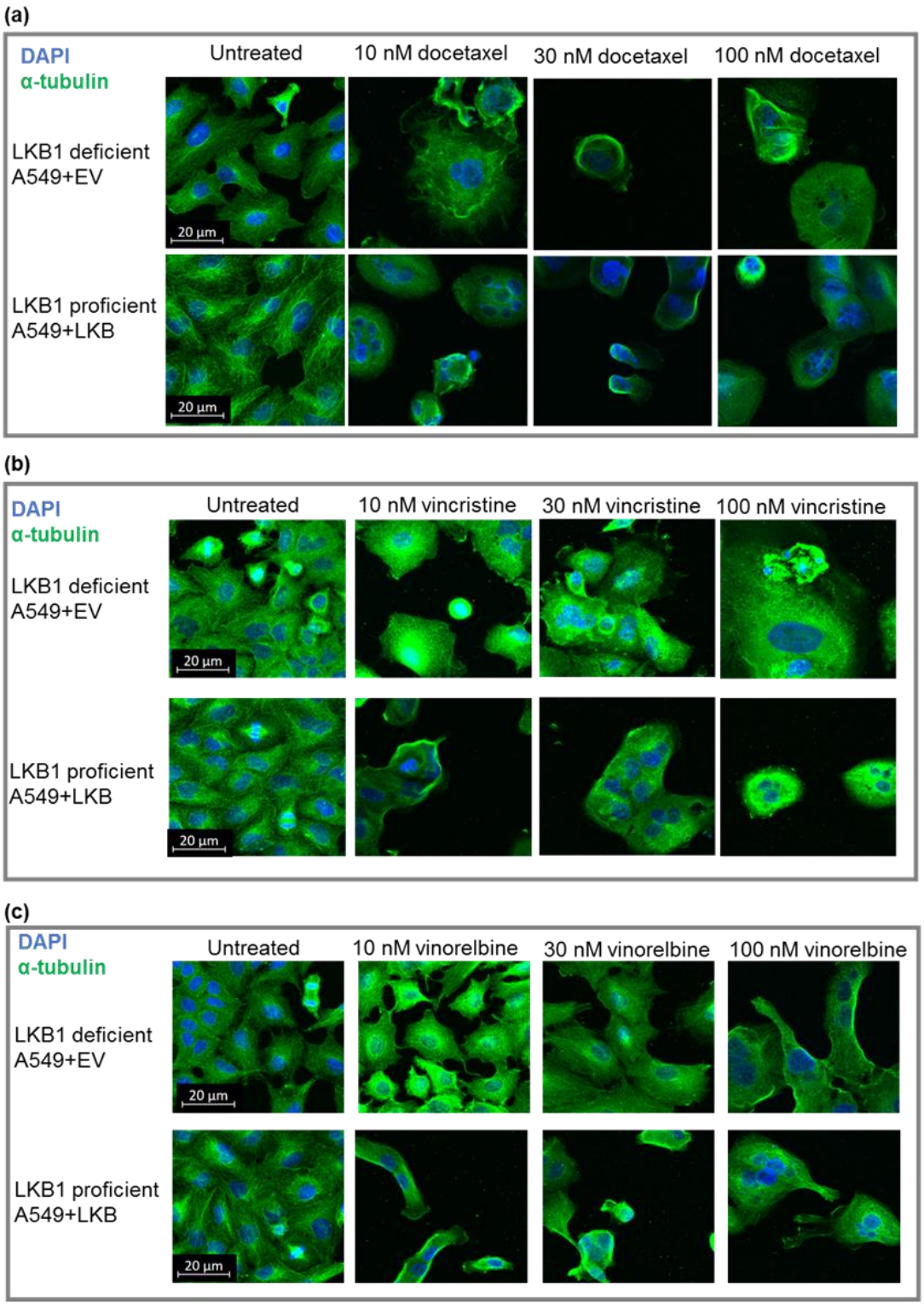

Figure A5.15: Microtubule staining in LKB1 deficient and proficient cells after treatment with docetaxel, vincristine and vinorelbine

Cells were grown in 2D culture and treated for 72 h before fixing with 10% formalin. Cells were stained with DAPI (blue) and α-tubulin (green). Images were acquired using the 63x objective on a confocal microscope.

(a)

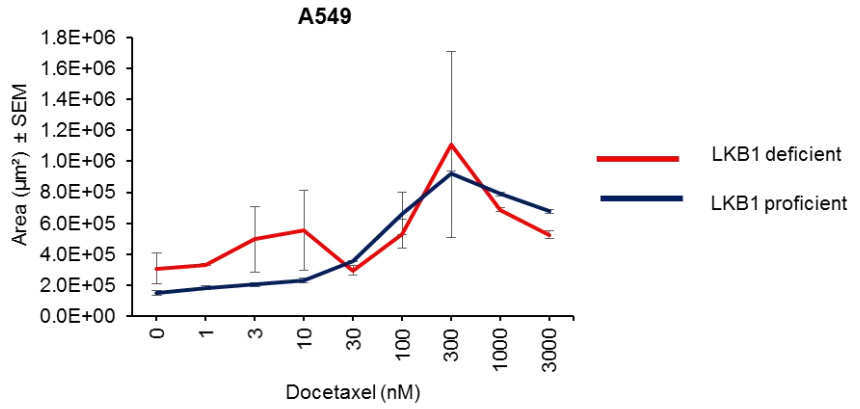
A549
Area (µm²) ± SEM
1.8E+06
1.6E+06
1.4E+06
1.2E+06
1.0E+06
8.0E+05
6.0E+05
4.0E+05
2.0E+05
0.0E+00
0
1
3
10
30
100
300
1000
3000
Docetaxel (nM)
LKB1 deficient
LKB1 proficient

(b)

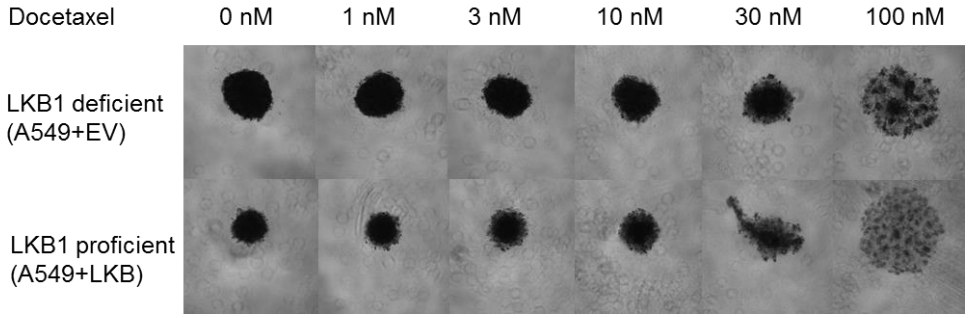
Docetaxel
0 nM
1 nM
3 nM
10 nM
30 nM
100 nM
LKB1 deficient
(A549+EV)
LKB1 proficient
(A549+LKB)

(c)

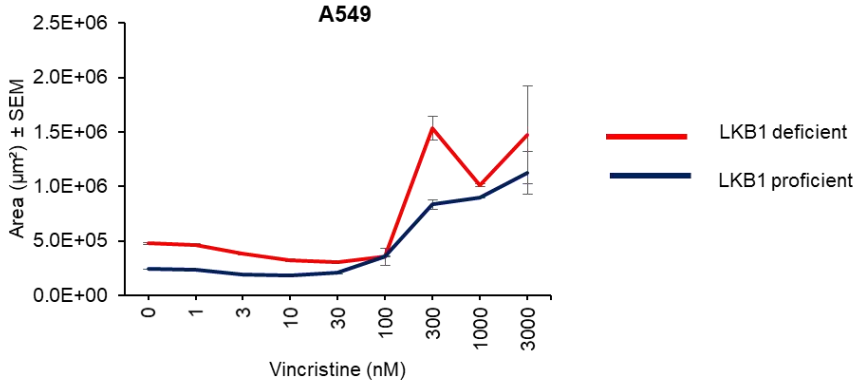
A549
Area (µm²) ± SEM
2.5E+06
2.0E+06
1.5E+06
1.0E+06
5.0E+05
0.0E+00
0
1
3
10
30
100
300
1000
3000
Vincristine (nM)
LKB1 deficient
LKB1 proficient

(d)

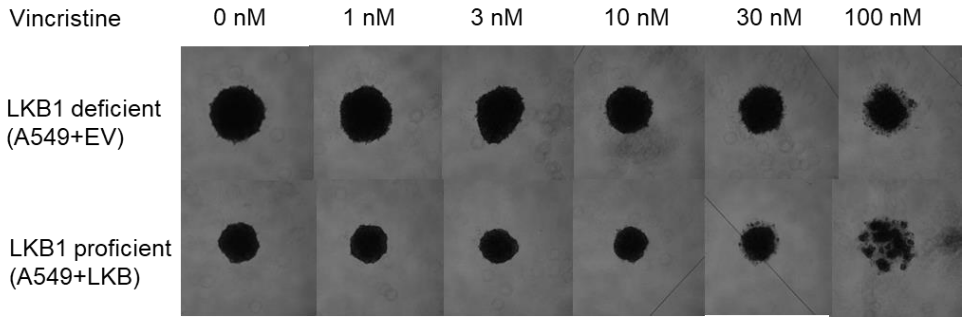
Vincristine
0 nM
1 nM
3 nM
10 nM
30 nM
100 nM
LKB1 deficient
(A549+EV)
LKB1 proficient
(A549+LKB)

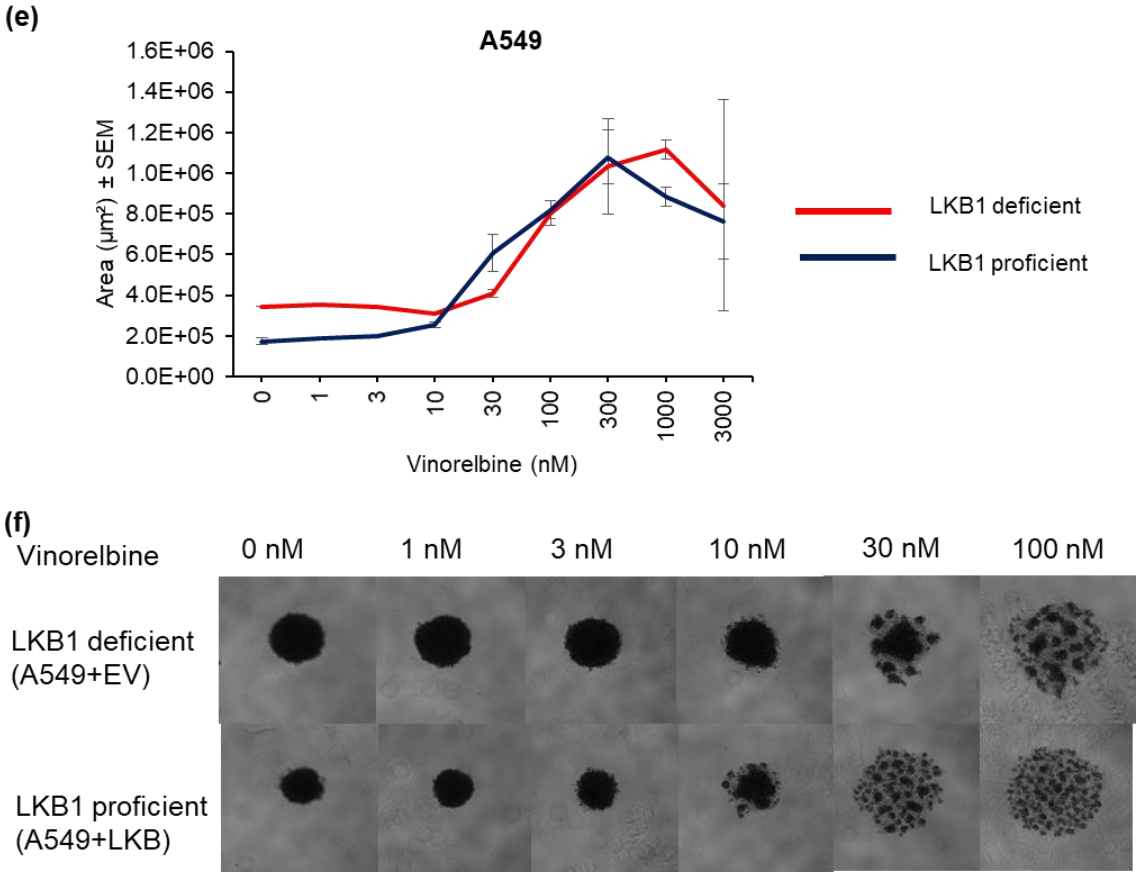

Figure A5.16: LKB1 deficient and proficient spheroids treated with docetaxel, vincristine and vinorelbine
Spheroids were treated from the point of seeding for 10 days (docetaxel) or 8 days (vincristine, vinorelbine). Data represents the mean of duplicate values (a, c, e). Representative images at 40x magnification using the Nikon Ti-E microscope (b, d, f).

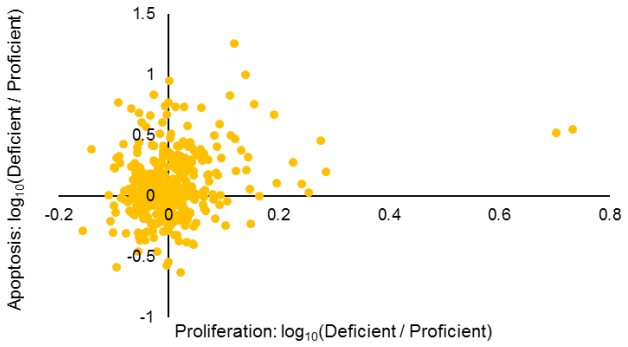

Figure A5.17: Correlation between induction of apoptosis and inhibition of proliferation in the primary screen in 2D culture
Pearson's correlation is 0.22 with a p-value < 0.00005 (n = 373).

(a)

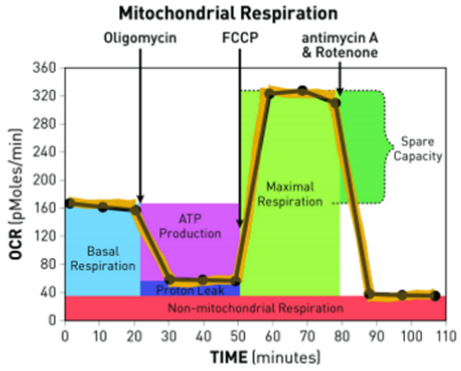

(b)

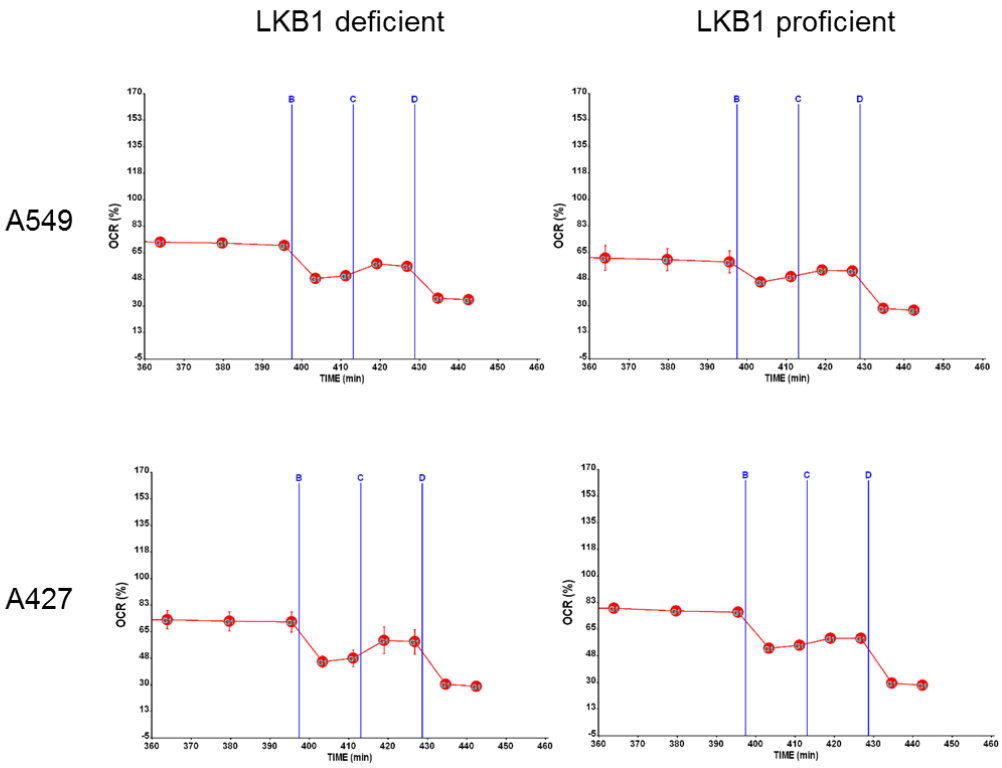

Figure A6.19: Mitochondrial stress test in LKB1 deficient and proficient A549 and A427 cells using the Seahorse XF96 analyser

(a) Mitochondrial stress test explanation from the Seahorse Analyser manual. (b) The OCR was measured for 6 h and then the mitochondrial stress test was performed. For this, oligomycin was injected at “B”, FCCP was injected at “C” and antimycin A + rotenone were injected at “D”. Data represents the mean of duplicate samples.

Table A6.1: Observations of the phenotypic differences between LKB1 deficient and proficient isogenic cells

Phenotype (model)	LKB1 deficient (cell line)	LKB1 proficient (cell line)
LKB1 expression by western blotting (2D)		LKB1 appeared as 4 bands at and below 54 kDa (A549, A427 and H1299)
LKB1 expression by IHC (2D)		Heterogeneous staining (A549, A427 and H1299)
LKB1 expression *in vivo*		Lost by day 16 post implantation (A549)
STRAD expression (2D)		More upper (48 kDa) STRAD (A549, A427 and H1299)
2D growth over 10 days in replenished medium	No difference (A549, A427 and H1299 cells)	
3D spheroid growth	Larger spheroids with a less defined edge (A549, H1299)	
3D spheroid co-population	Dominant in spheroid co-population (A549, H1299)	
***In vivo* growth**	Greater tumour burden in sub-cutaneous xenografts and greater tumour burden and metastasis in a lung orthotopic model (A549)	
***In vivo* immune response**	Greater immune response (IgG heavy and light chains) (A549)	
Integrin-β1 expression (3D)	Higher expression	
β-catenin expression (3D)	Diffused throughout a cell	Localised to the periphery of cells
Cell migration (2D)		Possibly more migratory
SIK1 mRNA (2D and 3D)	Upregulated (A549)	
COX2 protein expression (2D and 3D)	Upregulated (A549, A427)	
Apoptosis (2D)		Pro-apoptotic state (A549)
Apoptosis (3D)	Greater cleaved caspase 3 (A549)	
Sensitivity to microtubule inhibitors (2D)		More sensitive (A549, A427)
Sensitivity to microtubule inhibitors (3D)	Reduced spheroid size (A549)	Increased spheroid size (A549)
Sensitivity to complex I inhibitors (2D and 3D)	No marked difference (A549, A427, H1299)	
GLUT1, CA9 and MCT1 protein expression (3D)	Higher (A549)	
CPS1 protein expression (2D and 3D)	Higher (A549, A427)	
Glucose deprivation (2D)	More sensitive (A549, A427, H1299)	Grow better at lower concentrations of glucose
GlutaMAX^{TM} deprivation (2D and 3D)	More sensitive (A549)	